THÈSE

En vue de l'obtention du

DOCTORAT DE L'UNIVERSITÉ DE TOULOUSE

Délivré par :

Institut National Polytechnique de Toulouse (INP Toulouse)

Discipline ou spécialité :

Hydrologie, Hydrochimie, Sols, Environnement

Présentée et soutenue par :

M. LEONARD BERNARD JANNIN

le lundi 25 janvier 2016

Titre :

MODELISATION DU PROCESSUS DE DENITRIFICATION DANS LES EAUX SOUTERRAINES DES PLAINES ALLUVIALES

Ecole doctorale :

Sciences de l'Univers de l'Environnement et de l'Espace (SDUEE)

Unité de recherche :

Laboratoire Ecologie Fonctionnelle et Environnement (ECOLAB)

Directeur(s) de Thèse :

M. JOSE-MIGUEL SANCHEZ-PEREZ

MME SABINE SAUVAGE

Rapporteurs :

M. OLIVIER ATTEIA, UNIVERSITE BORDEAUX 3

M. PHILIPPE ACKERER, UNIVERSITE STRASBOURG 1

Membre(s) du jury :

M. PHILIPPE BEHRA, INP TOULOUSE, Président

M. JOSE-MIGUEL SANCHEZ-PEREZ, INP TOULOUSE, Membre

Mme JOSETTE GARNIER, UNIVERSITE PARIS 6, Membre

Mme SABINE SAUVAGE, UNIVERSITE TOULOUSE 3, Membre

M. RAMIRO NEVES, UNIVERSIDADE TECNICA DE LISBONNE, Membre

Remerciements

Je remercie tout d'abord mes directeurs de thèse, José-Miguel Sánchez-Pérez et Sabine Sauvage de m'avoir proposé ce sujet de thèse et de m'avoir accueilli au sein du laboratoire ECOLAB. Merci également à eux pour m'avoir encadré, conseillé et encouragé au cours de ces trois années de thèse.

Je remercie également les rapporteurs de cette thèse Philippe Ackerer et Olivier Atteia, ainsi que les membres du jury, Philippe Behra, Josette Garnier, Mélanie Bardeau et Ramiro Neves pour avoir accepté d'évaluer ce travail.

Merci à Ramiro Neves de m'avoir accueilli lors de deux séjours de deux mois au sein de l'équipe MARETEC de l'Institut Supérieur Technique de Lisbonne et merci à David et Eduardo de m'avoir guidé dans les méandres de MOHID. Merci à Cristina et Lucian de m'avoir fait découvrir Lisbonne.

Je remercie toutes les personnes qui ont fait que ce travail ait été possible. Merci à mes collègues modélisateurs : Youen, Xiaoling, Laurie, Grégory ; à tous les participants du projet ATTENAGUA et particulièrement à l'équipe de Toulouse coordonnée de main de maître par Samuel. Merci également aux jeunes chercheurs de l'ANR ADAPT'EAU.

Merci à tous mes collègues et amis pour les bons moments passés à Toulouse. Merci surtout à Youen, Xiaoling, Pierre-Alexis, Vincent, Adrien, Antoine, Théo, Cyril, Julie, Ane, Joana, Allison, Samuel, Sophia, Ousama, Laurie, Laure, Sylvain, Christophe, Mélodie, Anthony, Jingmei, Tian-Tian, Danielle, Hugo, Simon et à la RCTM.

Enfin, je souhaite remercier ma famille pour leur support et encouragements malgré toutes ces années passées loin du cocon familial.

Table des matières

Liste des figures

Liste des tables

Liste des abréviations

ACP : Analyse en Composantes Principales

Alk : Alkalinity (alcalinité)

BR : Bacterial Richness (richesse bactérienne)

BV : Bassin Versant

COD : Carbone Organique Dissous

COP : Carbone Organique Particulaire

CIZI : Carte Informative des Zones Inondables

CV : Coefficient de variation

DEA : Dénitrification Enzyme Activity (activité enzymatique dénitrifiante)

DO : Dissolved Oxygen (oxygène dissous)

DOC : Dissolved Organic Carbon (carbone organique dissous)

DREAL : Direction Régionale de l'Environnement, de l'Aménagement et du Logement

DTM : Digital terrain model (modèle numérique de terrain)

EC : Electrical conductivity (conductivité électrique)

FPC : Flood Pulse Concept

GPL : Général Publique Licence (licence publique générale)

GW : Groundwater (eaux souterraines)

HBH : High bankfull height (berges hautes)

IC : Initial Conditions (conditions initiales)

IDW : Inverse Distance Weight (ponderation inverse à la distance)

IGN : Insitut Géographiqe National

IST : Instituto Superior Técnico

LBH : Low Bankfull Height (berges hautes)

LOO : Leave-One-Out

MNT : Modèle numérique de terrain

MO : Matière Organique

MOHID : Modelo Hydrodynâmico

NGF : Nivellement Général de la France

NS : Nash-Sutcliff coefficient

OC : Organic Carbon (carbone organique)

OM : Organic Matter (matière organique)

ORP : Oxygen Reduction Potential (potentiel redox)

OTU : Operational Taxonomic Unit (unité taxonomique opérationnelle)

PBIAS : Percent Bias

PCR : Polymerase Chain Reaction (réaction en chaîne par polymérase)

PLSR : Partial Least Square Regression (régression des moindres carrés partiels)

PM : Porous Media (milieu poreux)

POC : Particulate Organic Carbon (carbone organique particulaire)

RMSE : Root mean square error (erreur des moindres carrés)

RMSECV : Root mean square error of cross validation (erreur des moindres carrés de validation croisée)

RZWQM : Root Zone Water Quality Model

SUDOE : SUd-Ouest Européen

SW : Surface Water (eaux de surface)

SWAT : Soil and Water Assessment Tool

SWAT-LUD : Soil and Water Assessment Tool - Landscape Unit Darcy

SWIM : Soil and Water Integrated Model

T : Température

WD : Water Depth (profondeur de l'eau, distance sol – toit de la nappe)

Introduction générale

L'utilisation excessive de fertilisants azotés et l'irrigation soutenue initiées lors du siècle dernier contribuent à entrainer un transfert important des nitrates vers les eaux souterraines (Bijay-Singh et al., 1995; Billen and Garnier, 1999; Galloway et al., 2003). L'augmentation des quantités de nitrates dans les eaux souterraines pose à la fois un problème de santé et un problème pour l'environnement. En effet, la consommation d'une eau chargée en nitrates peut entrainer un syndrome de méthémoglobinémie chez les jeunes enfants (blue baby syndrom) et augmente les risque d'apparition de certains cancers (Fan and Steinberg, 1996; Höring and Chapman, 2002). Les nitrates présents dans les eaux souterraines peuvent également être transférés dans les autres compartiments du cycle hydrologique, notamment les masses d'eau libres. En milieu marin (zones côtières et estuaires), les nitrates constituent le un facteur limitant du phénomène d'eutrophisation. L'eutrophisation des masses d'eau entraine une dégradation des écosystèmes aquatiques avec notamment l'apparition de bloom algaux, une augmentation de la turbidité et une diminution de la biodiversité.

Au sein de l'Union Européenne, la directive cadre sur l'eau (2000/60/CE) a établi des règles pour mettre fin à la détérioration de l'état des masses d'eau avec comme objectif l'atteinte du bon état des masses d'eau pour 2015. Dans ce contexte, la directive sur la protection des eaux souterraines contre la pollution et la détérioration (2006/118/EEC) impose le seuil à ne pas dépasser pour considérer les masses d'eau souterraines en bon état à 50 mg-NO_3^-.L^{-1}. Cette valeur est également la limite de potabilité de l'eau (98/83/CE). En outre, la directive nitrate (91/676/EEC) encadre les pratiques agricoles afin de limiter la contamination des eaux par les nitrates. Au niveau mondial, l'organisation mondiale pour la santé (OMS) recommande une teneur en nitrates maximale de 50 mg-NO_3^-.L^{-1} dans l'eau destinée à la consommation (World Health Organization, 2004).

Les plaines alluviales dont les surfaces sont majoritairement cultivées (Tockner and Stanford, 2002) sont particulièrement touchées par la contamination en nitrates. En effet, les activités agricoles combinées à une nappe d'eau peu profonde, une forte perméabilité du milieu et une connexion importante entre les eaux de surface et les eaux souterraines, font des aquifères alluviaux des zones particulièrement vulnérable à la pollution aux nitrates (Jégo, 2008; Arauzo et al., 2011).

Cependant, les environnements de plaines alluviales fournissent de nombreux services écosystémiques dont l'un des plus importants est l'élimination de l'azote (Tockner and Stanford, 2002). Ce service est particulièrement important dans les zones situées à l'interface

entre l'aquifère et la rivière (zones ripariennes) où les nitrates sont transformés en azote gazeux à travers le processus de dénitrification (Hill et al., 2000; Seitzinger et al., 2006; Mayer et al., 2007).

La dénitrification est un processus complexe qui est influencé par de nombreux facteurs comme la présence de nitrates, de carbone organique et de bactéries dénitrifiantes ainsi que des conditions environnementales favorables (Rivett et al., 2008). La dynamique hydrologique au sein des plaines alluviales ainsi que leurs caractéristiques géomorphologiques ont également été identifiées comme étant des facteurs contrôlant la capacité de dénitrification des zones ripariennes (Vidon and Hill, 2005; Ranalli and Macalady, 2010). Aussi, la dénitrification dans les zones ripariennes est caractérisée par une forte variabilité spatiale (*hots spots*) et temporelle (*hots moments*) (McClain et al., 2003; Groffman et al., 2009).

La modélisation est une approche adaptée à l'étude de processus complexes comme la dénitrification car elle permet de représenter le processus en prenant en compte les différents facteurs mis en jeu. De nombreux modèles ont déjà été appliqués pour étudier la dénitrification dans les eaux souterraines des plaines alluviales, à la fois à l'échelle du bassin versant (Hattermann et al., 2006; Almasri and Kaluarachchi, 2007) et à des échelles plus locales (Peyrard et al., 2011; Zarnetske et al., 2012). Cependant, les modèles utilisés à l'échelle locale (quelques km²) ne prennent pas en compte les spécificités des plaines alluviales, comme la dynamique des échanges nappe-rivière et les crues débordantes, qui sont pourtant déterminantes dans le fonctionnement biogéochimique de ces environnements (Junk et al., 1989; Tockner et al., 2000).

L'objectif principal de cette thèse est de développer une approche de modélisation à l'échelle locale, englobant la rivière et sa plaine alluviale, pour évaluer et mieux comprendre le processus de dénitrification et ses principaux facteurs de contrôle au sein des eaux souterraines des plaines alluviales. L'originalité de ce travail consiste à prendre en compte de façon détaillée l'hydrologie de la plaine alluviale (échanges nappe-rivière et épisodes de crue) dans la modélisation. Le modèle sera appliqué sur un site expérimental (Monbéqui, plaine alluviale de la Garonne) pour lequel de nombreuses données hydro-biogéochimiques acquises dans le cadre de ce travail sont disponibles. L'analyse de ces données permettra d'identifier les principaux facteurs de contrôle du processus de dénitrification qui seront intégrés dans la formulation du module calculant la dénitrification. Finalement, les résultats de l'application

du modèle sur trois autres sites expérimentaux seront analysés afin de valider l'utilisation du modèle et d'identifier les facteurs expliquant les différences potentielles quant à la capacité de dénitrification de chacun des sites étudiés.

Ce manuscrit s'articule autour de six chapitres :

- Le chapitre 1 définit le contexte de l'étude et est composé d'une revue de la littérature sur la dénitrification dans les plaines alluviales et sur les modèles existants. Les objectifs sont ensuite définis plus précisément.
- Le chapitre 2 présente le site expérimental de Monbéqui et les différentes données collectées. Le modèle MOHID Land utilisé au cours de ce travail est ensuite décrit.
- Le chapitre 3 présente l'analyse des données hydro-biogéochimiques récoltées sur le site d'étude dans le but d'améliorer la compréhension de la dynamique des nitrates dans la zone étudiée. Cette étude a permis d'identifier les principaux facteurs de contrôle de la dénitrification sur le site d'étude.
- Le chapitre 4 décrit l'application du modèle hydrologique (MOHID Land) sur le site expérimental. L'impact des crues débordantes sur les échanges nappe-rivière est analysé en détail.
- Le chapitre 5 porte sur l'implémentation du module de dénitrification au sein du modèle hydrologique (chapitre 4), basée sur l'analyse des données collectées sur le site (chapitre 3). L'application de ce modèle a permis de caractériser la dénitrification sur le site d'étude et d'analyser les facteurs contrôlant sa variabilité spatio-temporelle.
- Le chapitre 6 décrit l'application du modèle hydro-biogéochimique sur trois autres plaines alluviales possédant des caractéristiques contrastées. Ce chapitre a pour objectifs de valider la formulation du modèle et d'analyser les facteurs de contrôle de la dénitrification dans des contextes variés.

Chapitre 1 : Contexte scientifique et objectifs

Ce chapitre décrit les caractéristiques générales des plaines alluviales ainsi que leur fonctionnement hydrologique et biogéochimique. La dynamique des nitrates et les connaissances actuelles sur le processus de dénitrification sont présentées. Le concept de modélisation est ensuite introduit, suivi d'une revue de littérature sur les études de modélisation relatives à la dénitrification dans les plaines alluviales. Finalement les objectifs ainsi que l'approche méthodologique générale de la thèse sont détaillés.

1.1.Les plaines alluviales

1.1.1. Généralités

Les plaines alluviales (Figure 1-1) sont généralement définies comme *« les zones adjacentes aux rivières qui sont inondées lors des épisodes de crues »* (Goudie, 2004). En ce sens, leur surface peut être assimilée à celle du lit majeur du cours d'eau. Elles sont caractérisées par une surface topographique présentant de faibles pentes et sont plutôt situées à basse altitude, en aval des reliefs des bassins versants. Une caractéristique importante des plaines alluviales est d'être constituée par des alluvions déposées par le cours d'eau auxquel elles sont associées. La largeur des plaines alluviales varie de quelques dizaines de mètres à plusieurs dizaines de kilomètres et est proportionnelle au débit de la rivière. La plaine alluviale est délimitée latéralement par des terrasses qui peuvent correspondre à des reliques de plaines alluviales anciennes ou à la roche mère. Ces terrasses sont dites étagées lorsqu'elles sont séparées par la roche mère et emboitées le cas échéant. La superficie totale des plaines alluviales dans le monde est estimée à 2,2 10^6 km^2 (Bergkamp and Orlando, 1999).

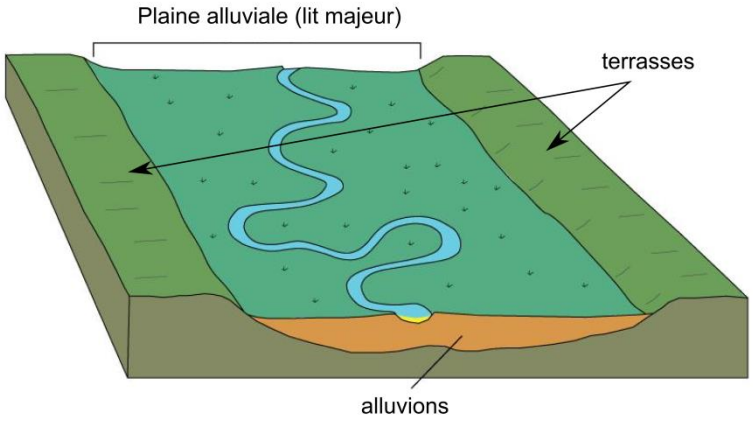

Figure 1-1 : Représentation schématique d'une plaine alluviale

1.1.2. Plaines alluviales, zones humides et zones ripariennes

D'après la convention de Ramsar signée en 1971 dont le titre officiel est « Convention relative aux zones humides d'importance internationale particulièrement comme habitats des oiseaux d'eau », les zones humides sont *«des étendues de marais, de fagnes, de tourbières ou d'eaux naturelles ou artificielles, permanentes ou temporaires, où l'eau est stagnante ou courante, douce, saumâtre ou salée, y compris des étendues d'eau marine dont la profondeur à marée basse n'excède pas six mètres»*. En France, selon le code de l'environnement, les zones humides sont des *« terrains, exploités ou non, habituellement inondés ou gorgés d'eau douce,*

salée ou saumâtre de façon permanente ou temporaire; la végétation, quand elle existe, y est dominée par des plantes hygrophiles pendant au moins une partie de l'année» (Art. L.211-1). Les zones humides couvrent une superficie estimée à 2% de la surface totale des terres émergées. Les plaines alluviales peuvent être considérées comme des zones humides et leur surface représentent 15% de la surface totale des zones humides (Bergkamp and Orlando, 1999).

Les zones ripariennes peuvent être définies comme l'interface (ou écotones) entre les écosystèmes aquatiques et terrestres (Gregory et al., 1991). La zone riparienne inclue le cours d'eau entre les basses et hautes eaux et le milieu terrestre où la végétation est influencée par un niveau élevé de la nappe, les inondations et la capacité du sol à retenir l'eau (Naiman et al., 1993). L'étendue d'une zone riparienne dépend de la taille et de la position du cours d'eau au sein du réseau hydrographique, du régime hydrologique et de la géomorphologie (Naiman and Décamps, 1997).

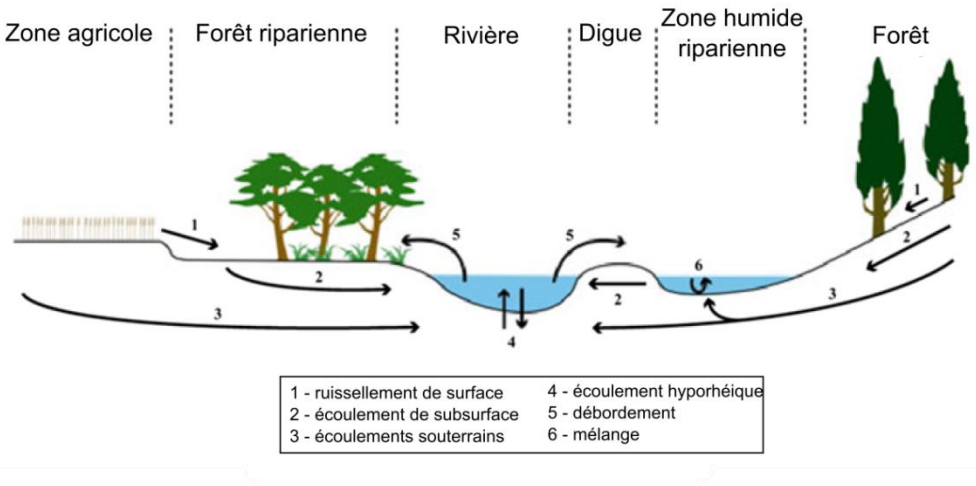

Figure 1-2 : Principaux écoulements au sein du continuum plateau - zone riparienne – rivière. Traduit de (Vidon et al., 2010)

Les plaines alluviales sont caractérisées par la surface inondée lors des crues et supportent une végétation adaptée à ces conditions (Figure 1-2). Les plaines alluviales naturelles peuvent donc être assimilées à des zones ripariennes qui correspondent elles-mêmes à un type de zones humides. Par exemple, aux États-Unis, la plaine alluviale délimitée par l'aire inondée lors d'une crue centennale (qui a une chance sur cent de se produire chaque année) est considérée comme une zone humide protégée par le Wetland Protection Act. En réalité les pressions exercées sur les plaines alluviales et notamment les changements d'usages des sols et les aménagements hydrauliques (digues, enrochements, barrages) peuvent considérablement modifier leurs caractéristiques (Tockner and Stanford, 2002). Au sein des

plaines alluviales, l'étendue des zones ripariennes se réduit pour faire place à des zones cultivées.

1.1.3. Une source de productivité

Les plaines alluviales constituent un système dynamique formé par la déposition successive de sédiments, soumis aux inondations et à de fortes interactions entre les eaux de surface et les eaux souterraines. Elles font partie des écosystèmes les plus productifs et les plus diverses du monde (Tockner and Stanford, 2002). Cette productivité est due à leur position basse dans les bassins versants et à leur enrichissement continuel en nutriments provenant de la zone amont et des apports latéraux. Par exemple, la production primaire moyenne des forêts ripariennes est estimée à 1 $kg.m^{-2}.an^{-1}$ (Mitsch and Gosselink, 2000). Les plaines alluviales constituent également des centres importants de biodiversité (Tockner 2002).

1.1.4. Services écosystémiques des plaines alluviales

Les plaines alluviales supportent de nombreux services écosystémiques et on estime qu'elles contribuent à plus de 25% des services écosystémiques terrestres alors qu'elles ne couvrent que 1,4 % des terres émergées (Mitsch and Gosselink, 2000). Ces services incluent entre autres la régulation des stocks d'eau, la recharge des aquifères, le contrôle des inondations et la rétention de carbone, nutriments, sédiments et polluants (Bergkamp and Orlando, 1999).

D'après la classification de (De Groot, 1992), les fonctions écologiques des écosystèmes peuvent être définies selon quatre catégories : (i) les fonctions de régulation, (ii) les fonctions d'habitat, (iii) les fonctions de production et (iv) les fonctions d'information. Les fonctions et services écosystémiques des zones ripariennes sont nombreux et concernent toutes les catégories (Soman et al., 2007). Parmi les services écosystémiques rendus par les zones ripariennes, l'élimination de l'azote est un des services principal avec des taux allant de 0,5 à 2,6 $kg\text{-}N.ha^{-1}.jour^{-1}$ (Tockner and Stanford, 2002).

1.1.5. Facteurs de dégradation

Les plaines alluviales sont des zones privilégiées pour l'agriculture et une partie importante des plaines alluviales a subi une transformation de l'usage de leurs des sols (90% des plaines alluviales d'Europe et d'Amérique du Nord sont cultivées). De plus, la dynamique hydrologique des grands fleuves est également impactée par la construction de barrages. Enfin les aménagements des cours d'eau (enrochements et digues) modifient la connectivité hydrologique entre la plaine alluviale et son fleuve ce qui tend à diminuer l'étendue des zones ripariennes au sein des plaines alluviales. On peut également citer comme facteurs de

dégradation des plaines alluviales l'augmentation de l'irrigation, la fertilisation et le nombre d'espèces invasives (Tockner and Stanford, 2002). Tous ces facteurs entrainent une dégradation des écosystèmes associée à une baisse de la biodiversité, une diminution des ressources en eau disponibles ainsi que d'importantes pollutions des masses d'eau alluviales souterraines.

1.2.Hydrologie des plaines alluviales

L'hydrologie est le principal facteur environnemental déterminant les propriétés des plaines alluviales (Keddy, 2010). C'est la dynamique fluviale qui, à travers l'expansion/contraction des eaux de surface, maintient une forte connectivité hydrologique dans la plaine alluviale (Junk et al., 1989; Tockner et al., 2000). La connectivité hydrologique est un processus clé dans ces environnements et correspond au transfert par l'eau de l'énergie, de la matière et des organismes entre les différents compartiments de l'écosystème (Tockner and Stanford, 2002). L'hydrologie des plaines alluviales se caractérise par une relation forte entre les eaux de surface et les eaux souterraines ainsi que par la présence de crues saisonnières.

1.2.1. Echanges nappe rivière

Les interactions entre les cours d'eau et les eaux souterraines sont contrôlées par la position des masses d'eau, les caractéristiques géologiques de leur lit et les conditions climatiques (Winter, 1999). Une caractérisation géomorphologique est également nécessaire afin de prendre en compte les échanges nappes-rivière à plus large échelle. Larkin and Sharp (1992) ont classé les systèmes nappes-rivières à partir de critères géomorphologiques (pente, sinuosité et ratio largeur/profondeur) en trois grandes catégories : (i) dominés par les écoulements de subsurface (les écoulements souterrains sont perpendiculaires à la rivière), (ii) dominés par les écoulements souterrains profond (les écoulements souterrains sont parallèles à la rivière) et (iii) mixtes.

En pratique, les échanges eaux de surface- eaux souterraines se font par infiltration des eaux de surface vers les eaux souterraines ou exfiltration dans le sens inverse. A l'échelle de la plaine alluviale, ces échanges sont contrôlés par (i) la répartition de la conductivité hydraulique au sein du cours d'eau et des dépôts alluviaux, (ii) la relation entre le niveau du cours d'eau et le niveau de la nappe adjacente et (iii) la géométrie et la position du cours d'eau au sein de la plaine alluviale (Woessner, 2000). En fonction de la différence de charge hydraulique entre le cours d'eau et la nappe, on distingue trois conditions principales (Figure 1-3). La plupart du temps, dans les régions tempérées, la charge hydraulique est plus

importante dans l'aquifère et l'eau souterraine s'écoule depuis la nappe alluviale vers la rivière. On dit que la rivière draine la nappe alluviale (Figure 1-3.a). Lorsque la charge hydraulique est plus importante dans le cours d'eau, l'eau s'infiltre dans les alluvions à travers les berges et recharge la nappe (Figure 1-3.b). Pendant les crues débordantes (lorsque le niveau du cours d'eau dépasse la hauteur des berges), l'eau s'écoule à travers la plaine alluviale et peut s'infiltrer dans les alluvions sur de grandes surfaces (Figure 1-3.c). Dans ce cas, la recharge de l'aquifère correspond au volume d'eau infiltré. Elle dépend de la durée et de l'intensité de la crue ainsi que de la conductivité hydraulique et de la capacité de stockage de l'aquifère (Sophocleous, 2002). Pendant les saisons sèches, le drainage de la nappe alluviale (précédemment rechargée pendant les épisodes de crues) compense la réduction du débit de la rivière. L'alternance des conditions de recharge et de drainage de la nappe a donc un effet tampon sur le régime hydrologique des rivières (Brunke and Gonser, 1997).

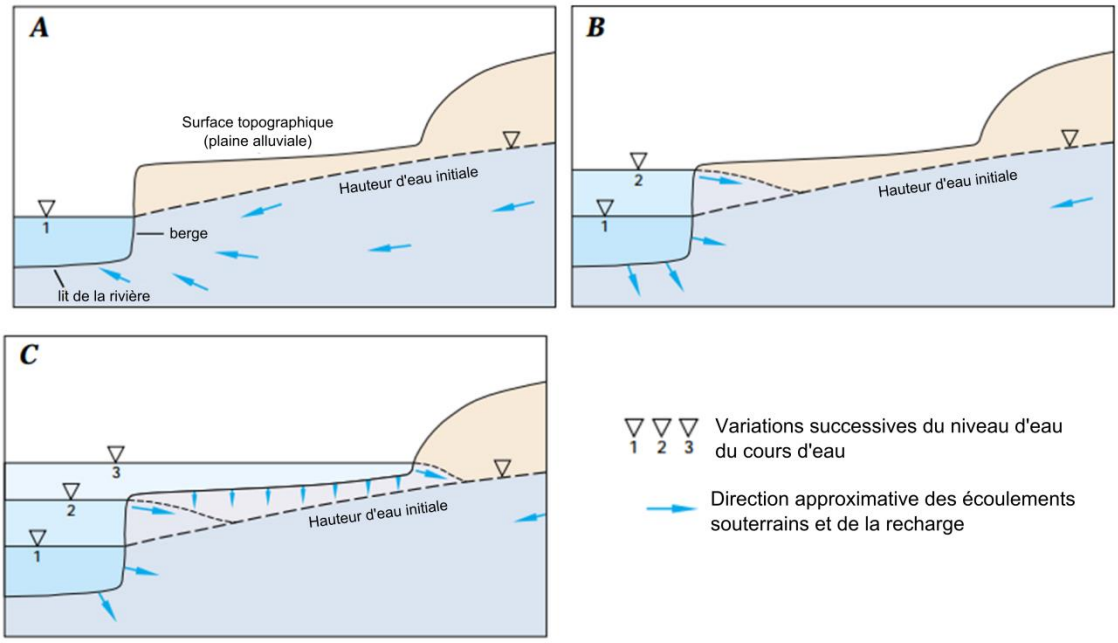

Figure 1-3 : Echanges nappe-rivière en condition drainante (A), en conditions de recharge lors de la montée du niveau d'eau dans la rivière (B) et lors de la crue débordante (C). Adapté de (Winter, 1998)

D'un point de vue quantitatif, le volume échangé entre la rivière et l'aquifère peut se résumer comme étant fonction de la différence de charge hydraulique entre les deux compartiments (Sophocleous, 2002). Une approche simplifiée consiste à appliquer la loi de Darcy, qui peut s'exprimer sous la forme suivante

$$q = k\Delta H$$

avec ΔH la différence entre la charge hydraulique de l'aquifère et de la rivière [L], q le débit entre la rivière et l'aquifère [$L^3.T^{-1}$] et k le coefficient d'infiltration du lit de la rivière [$L^2.T^{-1}$]. Cependant, cette relation linéaire représente les échanges de manière simplifiée et d'autres formulations non linéaires ont été proposées pour mieux rendre compte du phénomène.

1.2.2. La zone hyporhéique

Les échanges dans les deux directions entre la nappe et la rivière conduisent à créer une zone de mélange entre les eaux de surface et les eaux souterraines. Cette zone de mélange est appelée zone hyporhéique (Orghidan, 1959, Figure 1-4). Plus précisément elle peut être définie comme *« une zone de transition, spatialement et temporellement dynamique, située entre les masses d'eau de surface et souterraines et qui possède des caractéristiques physiques (température) et biogéochimique (forts gradients chimiques) spécifiques du fait du mélange eaux de surface - eaux souterraines et qui fournit un habitat dynamique et un potentiel refuge pour les espèces obligées et facultatives »* (Krause et al., 2011). La zone hyporhéique peut également être définie comme la partie de la zone saturée qui contient au moins 10% d'eau de surface (Triska et al., 1993; Lautz and Siegel, 2006).

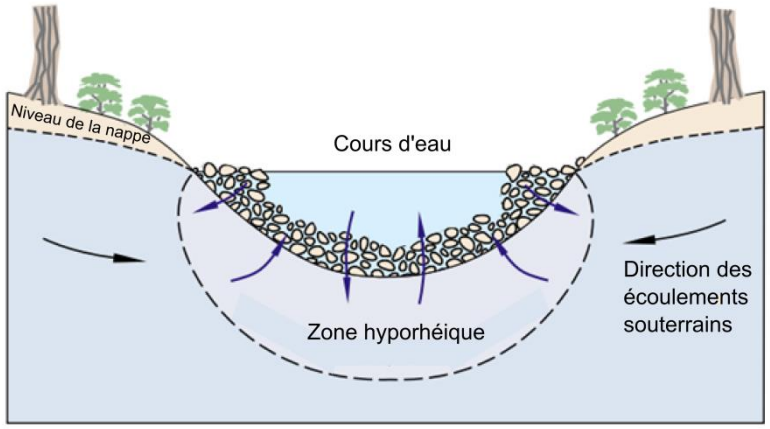

Figure 1-4 : Représentation schématique de la zone hyporhéique. Traduit de Winter (1998)

Les échanges au sein de la zone hyporhéique sont contrôlés par différents facteurs qui diffèrent en fonction de l'échelle considérée (Krause et al., 2011). A l'échelle du cours d'eau, les échanges hyporhéiques dépendent de la répartition de la charge hydraulique liée à la morphologie du lit de la rivière (Cardenas and Wilson, 2007) et à la perméabilité des sédiments (Packman and Salehin, 2003). A de plus larges échelles, les flux hyporhéiques sont

conditionnés par la largeur de la vallée, la profondeur de la roche mère et les propriétés de l'aquifère (Brunke and Gonser, 1997; Malcolm et al., 2005).

La zone hyporhéique est une zone d'échange dynamique importante pour l'écohydrologie des eaux souterraines et constitue un lieu d'une forte activité biogéochimique (Boulton et al., 1998; Krause et al., 2011; Sophocleous, 2002, Figure 1-5). De nombreuses études ont souligné l'importance de la zone hyporhéique sur les cycles biogéochimiques des nutriments et contaminants (Valett et al., 1996; Pinay et al., 1998; Lewandowski and Nützmann, 2010; Marmonier et al., 2012).

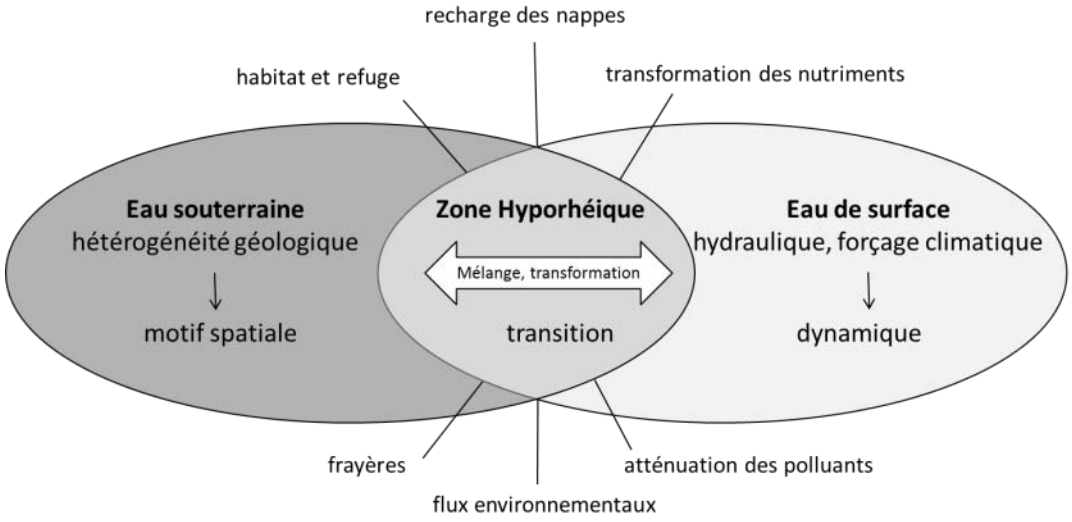

Figure 1-5 : Fonctions hydroécologiques et biogéochimiques de la zone hyporhéique en tant que zone de mélange et de transition entre les eaux de surface et les eaux souterraines. Traduit de Krause et al. (2011).

1.2.3. Les crues

Le *Flood Pulse Concept* (FPC, Junk et al., 1989) est un concept fondamental pour comprendre le fonctionnement des plaines alluviales qui intègre la rivière et sa plaine alluviale dans un système dynamique où elles sont liées entre elles par de fortes interactions entre les processus hydrologiques et écologiques. Dans ce système, les crues débordantes déterminent le degré de connectivité hydrologique et les échanges de matières et d'organismes le long du gradient rivière-plaine alluviale (Tockner et al., 2000). Ce concept initialement développé pour les grandes plaines alluviales tropicales a été étendu aux régions tempérées par Tockner et al. (2000) qui soulignent également le rôle des crues non débordantes comme facteur contrôlant les processus biogéochimiques dans les plaines alluviales (*Flow Pulse Concept*). Dans les plaines alluviales, la succession des crues entraine des cycles expansion-contraction qui façonne l'hétérogénéité des habitats et contrôle les processus écologiques et biogéochimiques.

1.3.Biogéochimie des plaines alluviales

1.3.1. Concept de *hot spot* et *hot moment*

Les zones ripariennes et notamment la zone hyporhéique sont des zones de transition entre les ecosystèmes terrestres et aquatiques où les cycles biogéochimiques sont très actifs et peuvent être considérés comme des *hots spots*, c'est à dire des zones où les taux de réaction sont disproportionnément plus intenses que dans les zones environnantes (McClain et al., 2003, Figure 1-6). Les *hots spots* résultent de la convergence des écoulements hydrologiques transportant un réactif avec d'autres écoulements ou substrats contenant des réactifs complémentaires. La définition des *hots spots* varie en fonction de l'échelle spatiale considérée de la colonne de sol au bassin versant (Groffman et al., 2009, Figure 1-7).

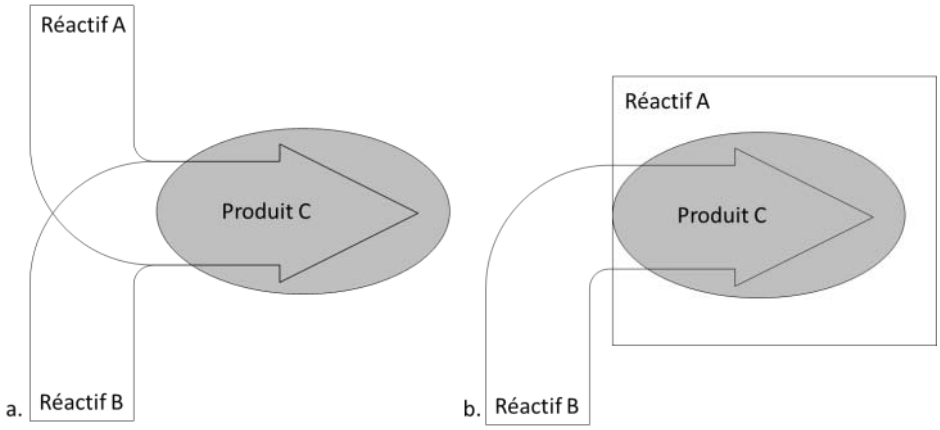

Figure 1-6 : Représentation schématique de la formation de hots spots par (a) convergence des écoulements souterrains transportant des réactifs complémentaires ou (b) lorsque les écoulements transportent un réactif A au contact d'un substrat qui contient le réactif B. Adapté de (McClain et al., 2003).

A l'échelle de la section de plaine alluviale (100-1000 m), les zones ripariennes en tant qu'espace de transition entre les eaux de surface et les eaux souterraines sont considérées comme des potentiels *hots spots* (McClain et al., 2003). C'est particulièrement le cas pour le processus de dénitrification lorsque les écoulements latéraux des eaux souterraines chargées en nitrates rencontrent des environnements anoxiques et riches en carbone organique. De la même manière, les *hots moments* correspondent aux épisodes hydrologiques mobilisant (ou remobilisant) une quantité importante de réactifs. Dans les zones ripariennes, les *hots moments* correspondent principalement aux épisodes de crue qui peuvent transporter des quantités importantes de nutriments et polluants et agissent fortement sur les écoulements au sein de la plaine alluviale. En plus des processus liés au cycle de l'azote, les zones ripariennes sont également des zones importantes pour d'autres éléments tels que le phosphore, la matière organique, les pesticides et le mercure (Vidon et al., 2010) .

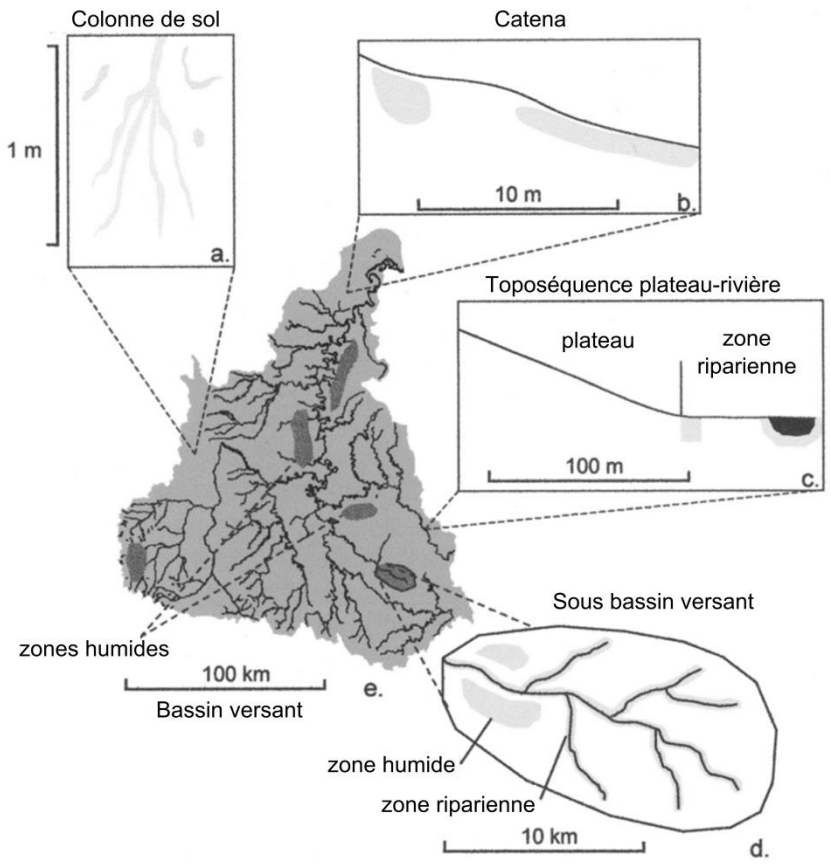

Figure 1-7 :Localisation des hots spots de dénitrification à différentes échelles spatiales. (a) Dans le sol, les hots spots sont situés autour des racines. (b) Le long du caténa, les dépressions topographiques accumulent la matière organique et retiennent l'humidité soutenant la dénitrification. (c) Le long de la séquence plateau-rivière, la zone riparienne, à l'endroit où les eaux souterraines riches en nitrates interceptent des sols riches en matière organique, constitue un hot spot. (d) A l'échelle du sous bassin, la répartition spatiale des hots spots est contrôlée par la localisation des zones humides et des zones riparienne. Le pourcentage de surface occupé par les zones humides détermine les hots spots de dénitrification à l'échelle du grand bassin versant. Traduit de (McClain et al., 2003)

1.3.2. Les réactions d'oxydoréduction dans les nappes alluviales

Dans les nappes alluviales, seule la partie supérieure est au contact de l'air. Il se produit donc une transition progressive d'un milieu aérobie vers un milieu anaérobie qui donne lieu à une séquence de réactions dites d'oxydoréduction. Les réactions d'oxydoréduction sont des réactions chimiques au cours desquelles se produit un transfert d'électrons d'un réducteur vers un oxydant. Dans le milieu naturel, ces réactions ont des cinétiques très lentes qui ne se produisent à une vitesse significative qu'n présence de bactéries qui jouent le rôle de catalyseurs (Atteia, 2005).

La réaction d'oxydoréduction majeure dans les eaux naturelles est la dégradation de la matière organique par les bactéries et autres micro-organismes qui vont utiliser cette matière organique pour leur respiration. Lorsque l'oxygène aura été entièrement consommé, les

bactéries utiliseront d'autres oxydants comme les nitrates, le manganèse, le fer ou encore les sulfates (Figure 1-8).

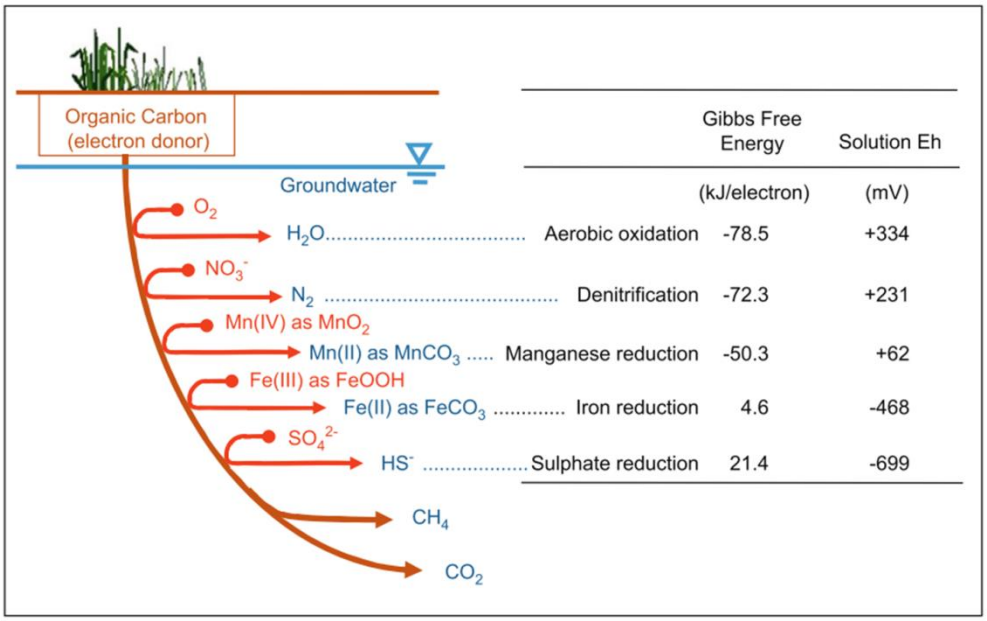

Figure 1-8 : Séquence redox des principaux accepteurs d'électron pour l'oxydation du carbone organique dans les eaux souterraines (Rivett, 2008)

1.3.3. Dynamique des nitrates

1.3.3.1. Cycle de l'azote

L'azote (N) est un élément chimique présent dans tous les organismes vivants. C'est un constituant de nombreuses biomolécules comme les protéines, l'ADN et la chlorophylle. En plus d'être présent dans l'atmosphère sous forme gazeuse (diazote N_2 et protoxyde d'azote N_2O), l'azote est présent dans l'environnement sous différentes formes à la fois inorganiques (principalement, ammonium NH_4^+, nitrate NO_3^- et nitrite NO_2^-) et organiques (dans les organismes vivant, l'humus et les différents produits de dégradation de la matière organique). L'azote passe d'une forme à l'autre à travers de nombreux processus souvent liés à l'activité des micro-organismes qui l'utilise pour leur besoin en énergie et leur croissance.

Le cycle de l'azote est représenté dans la Figure 1-9. L'azote, très abondant dans l'atmosphère sous forme de N_2 (78%), peut être assimilé par certaines bactéries lors du processus de fixation. Cependant, l'azote atmosphérique reste difficilement disponible pour les organismes vivants, c'est donc souvent un élément limitant la production primaire. Aussi, dans les zones

cultivées, une grande quantité d'azote est apportée par les engrais chimiques sous forme minérale et par les amendements sous forme organique.

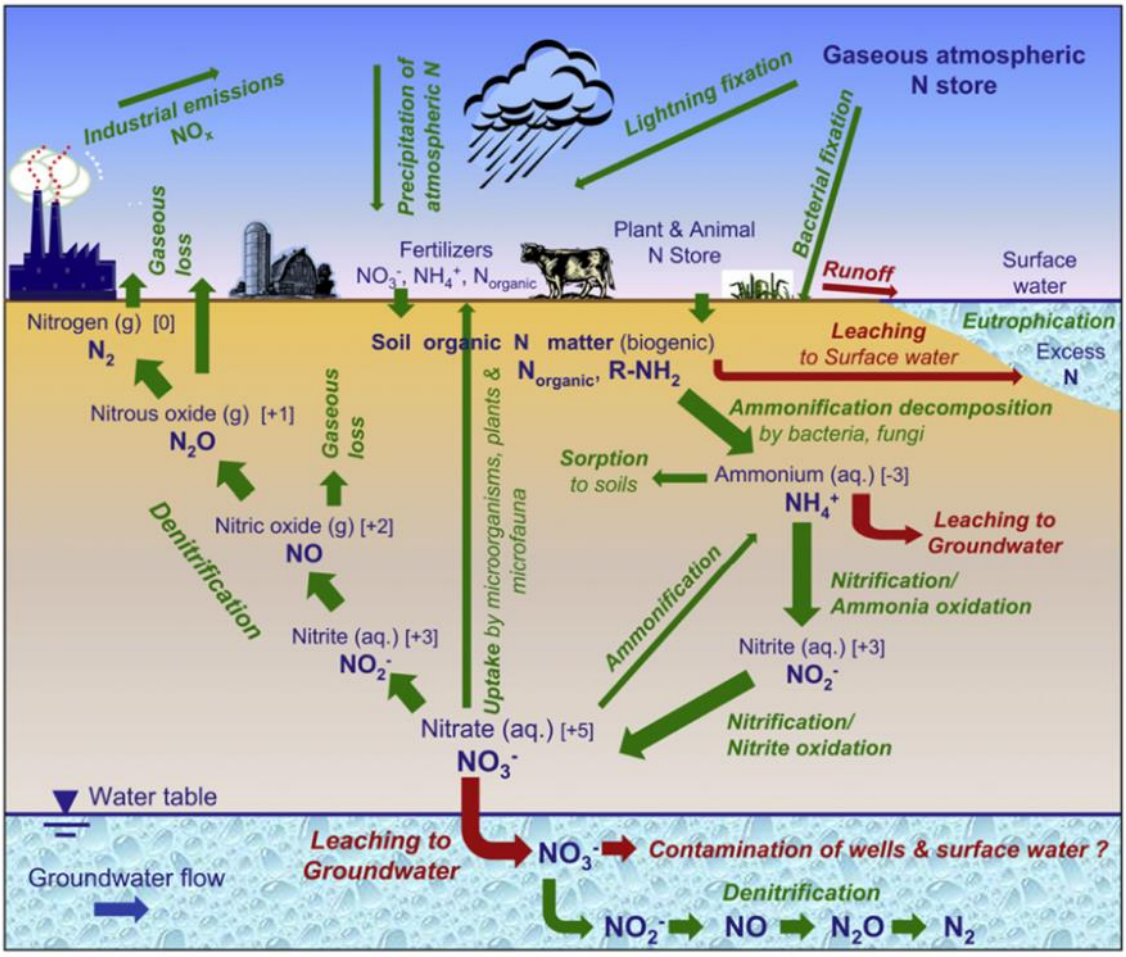

Figure 1-9 : Le cycle de l'azote et son influence sur les environnements aquatiques. Extrait de (Rivett et al., 2008).

Sous ses formes minérales (NH_4^+, NO_3^-, NO_2^-), l'azote dans le sol peut être prélevé par les plantes au niveau des racines, c'est le processus d'immobilisation. Sous forme organique, il est décomposé par les micro-organismes du sols et est transformé en NH_4^+, c'est le processus de minéralisation. A partir de sa forme NH_4^+, il est transformé en nitrites puis en nitrates par certaines bactéries en conditions oxygénées, c'est le processus de nitrification. L'azote sous forme de nitrate NO_3^- est très mobile dans les sols du fait de sa charge négative qui s'oppose à la charge négative du complexe argilo-humique du sol. Il est donc facilement entrainé par lixiviation et peut ainsi atteindre les eaux souterraines puis les eaux de surfaces. Finalement, l'azote sous forme nitrates (dans les sols ou les eaux souterraines) peut également retourner à l'atmosphère sous forme de N_2O et N_2 lors du processus de dénitrification.

1.3.3.2. Dynamique des nitrates dans les écosystèmes de plaine alluviale

Les activités agricoles, la présence d'une nappe peu profonde, la forte perméabilité des dépôts alluviaux et la forte connexion entre les eaux de surface et les eaux souterraines rendent les aquifères alluviaux particulièrement vulnérables à la pollution aux nitrates (Arauzo et al., 2011). L'utilisation de fertilisants azotés augmente la quantité de nitrates dans les sols qui sont ensuite entrainés par lixiviation vers la nappe peu profonde.

Les zones ripariennes sont reconnues comme étant des zones importantes de rétention des nitrates via différents mécanismes. Les principaux processus sont l'immobilisation par les plantes et les micro-organismes, la dénitrification et la dilution (Pinay et al., 1998; Craig et al., 2010; Ranalli and Macalady, 2010). L'importance des processus varie en fonction des saisons : pendant la saison de croissance de la végétation, il peut y avoir immobilisation par les plantes et les microbes et dénitrification alors que seuls les processus microbiens subsistent durant la période de dormance (Ranalli and Macalady, 2010). La nitrification peut également être importante dans les zones ripariennes. En général, dans les environnements peu chargés en nitrates, la zone hyporhéique fonctionne comme un réacteur oxydant et la nitrification prédomine, oxydant l'ammonium des eaux de surfaces. Dans le cas contraire, c'est la dénitrification des nitrates contenus dans les eaux souterraines qui prévaut (Krause et al., 2011).

Le phénomène de dilution des eaux souterraines chargées en nitrates avec les eaux de surface très peu chargées permet de diminuer la concentration en nitrates dans la zone de mélange (Pinay et al., 1998; Pfeiffer et al., 2006; Baillieux et al., 2014). Bien que ce phénomène puisse entrainer une diminution importante des concentrations en nitrates dans les aquifères alluviaux, ce n'est pas un processus de rétention d'azote car la quantité de nitrates ne varie pas (Pinay et al., 1998).

Parmi les différents processus qui affectent l'élimination des nitrates dans les zones ripariennes, la dénitrification est reconnue comme le plus important (Korom, 1992; Burt et al., 1999; Rivett et al., 2008).

1.3.3.3. La dénitrification

La dénitrification est une succession de réductions microbiennes des nitrates jusqu'au diazote (Knowles, 1982). Les organismes assurant la dénitrification sont omniprésents dans les eaux de surfaces, les sols et les eaux souterraines (Beauchamp et al., 1989). Il s'agit de bactéries anaérobies facultatives (capable de respiration aérobie et anaérobie) hétérotrophes (nécessitant

de la matière organique) qui obtiennent leur énergie et carbone de l'oxydation de la matière organique (Rivett et al., 2008). La réaction de dénitrification peut s'écrire sous la forme

$$4NO_3^- + 5CH_2O + 4H^+ \longrightarrow 2N_2(g) + 5CO_2(g) + 7H_2O$$

nitrate	matière organique	hydrogène	azote	dioxyde de carbone	eau

La dénitrification dans les zones ripariennes est connue pour éliminer efficacement les nitrates des eaux souterraines (Lowrance et al., 1984; Peterjohn and Correll, 1984; Pinay and Decamps, 1988; Osborne and Kovacic, 1993). La dénitrification est surtout importante dans les horizons supérieurs des sols ripariens riches en matière organique (Hill, 1996; Devito et al., 2000). Un fort gradient vertical est observé entre les zones profondes où les taux de dénitrification sont faibles toute l'année, et les horizons supérieurs plus riches en carbone organique et où les taux de dénitrification sont les plus élevés (Jacinthe et al., 1998; Clément et al., 2002; Puckett and Cowdery, 2002; Hill et al., 2004; Ranalli and Macalady, 2010). Néanmoins, le processus de dénitrification a également été observé dans les zones plus profondes des aquifères des zones ripariennes (Haycock and Burt, 1993; Starr and Gillham, 1993; Hill et al., 2000, 2004; Vidon and Hill, 2004).

D'après la revue de littérature de Rivett et al. (2008), les conditions nécessaires à la dénitrification dans les eaux souterraines sont :

- présence de nitrate, bactéries denitrifiantes et donneur d'électron (carbone organique)
- conditions anaérobiques (moins d'environ 1-2 $mg.L^{-1}$ d'oxygène dissout)
- conditions environnementales favorables (température, pH, éléments traces et nutriments)

Cependant, le facteur limitant principal est la disponibilité du carbone organique ; les effets des conditions environnementales sont généralement secondaires (Rivett et al., 2008). Bien que L'anoxie soit un facteur important, la dénitrification peut avoir lieu dans des environnements apparemment bien oxygénés dans des micro-sites localement anoxiques (Jacinthe et al., 1998).

Globalement, la dénitrification dans les eaux souterraines est limitée par la présence de carbone organique. Pfeiffer et al. (2006) indique que la variabilité temporelle des écoulements et que les épisodes de recharge permettent un apport en carbone organique dissous (COD)

supportant la dénitrification dans l'aquifère d'une plaine alluviale. Haycock and Burt (1993) relient la dénitrification dans un aquifère à la présence de sédiments de rivière contenant du carbone organique dans l'aquifère. De la même manière, Vidon and Hill (2004) ont observé le processus de dénitrification dans des couches profondes riches en carbone organique. Hill et al. (2000) ont observé de la dénitrification dans les eaux souterraines dans les zones d'interface sable-tourbière. Craig et al. (2010) ont déterminé que la dilution était le facteur principal de la diminution de la concentration en nitrates dans l'aquifère d'une plaine alluviale. Néanmoins, des zones de dénitrification ont été observées et reliées à la présence de COD et de carbone organique particulaire (COP) dans les sédiments. Le carbone organique peut être contenu dans les sédiments (végétation avec des racines profondes, lentilles de carbone enterrées). Il peut également provenir du lessivage des horizons supérieurs riches en matière organique ou être apporté par la rivière pendant les crues (Schade et al., 2001; Clinton et al., 2002; Gift et al., 2010; Peter et al., 2012).

Les caractéristiques géomorphologiques des aquifères entrainent des zones plus ou moins favorables à la dénitrification. Hill (1996) indique qu'un aquifère verticalement délimité par un niveau imperméable peu profond oblige les eaux à traverser les niveaux supérieurs des sols riches en matière organique et entraine une dénitrification efficace. L'efficacité de la dénitrification est donc liée aux caractéristiques géomorphologiques et hydrogéologiques en lien avec le temps de résidence et la vitesse des écoulements (Vidon and Hill, 2004). Les caractéristiques hydro-géomorphologiques des paysages peuvent donc être utilisées comme indicateurs de la dénitrification potentielle dans les zones ripariennes (Lowrance et al., 1997; Hill et al., 2000; Gold et al., 2001; Rosenblatt et al., 2001; Vidon and Hill, 2004). Par exemple, Ranalli and Macalady (2010) proposent d'évaluer la capacité de dénitrification des zones ripariennes en fonction de leurs caractéristiques topographiques et hydrologiques.

Enfin, la dénitrification est également contrôlée par la concentration en nitrates. En effet, les taux de dénitrification sont généralement plus hauts à l'interface plateau cultivé-zone riparienne qu'à l'interface zone riparienne-cours d'eau du fait d'une concentration en nitrates plus élevée (Groffman et al., 1992; McClain et al., 2003).

La dénitrification est donc un processus qui dépend de nombreux facteurs et est caractérisée par une forte variabilité spatiale et temporelle (McClain et al., 2003). C'est également un processus difficile à mesurer sur le terrain et dont l'extrapolation des mesures ponctuelles sur

de plus grandes surfaces est problématique (Groffman et al., 2006). Dans ce contexte, la modélisation peut s'avérer utile pour étudier le processus de dénitrification (Groffman, 2012).

La dénitrification peut également être effectuée par des bactéries autotrophes. Dans ce cas, le souffre et le fer jouent le rôle de donneur d'électron (réducteur) à la place du carbone organique. Cependant, ces réactions nécessitent des conditions spécifiques comme la présence de pyrite (FeS_2) dans l'aquifère (Korom, 1992; Atteia, 2005; Rivett et al., 2008).

1.4.Modélisation de la dénitrification dans les plaines alluviales

1.4.1. Concepts de modélisation

La modélisation consiste à établir un modèle qui est une représentation simplifiée de la réalité. L'objectif est d'identifier les variables et paramètres et les mécanismes clefs contrôlant le ou les phénomènes étudiés (physique, biologique, écologique, économique,…). Les modèles peuvent être utilisés pour prédire, décrire ou encore interpréter différents processus. La modélisation est particulièrement utile lors de l'étude de processus naturels qui nécessiteraient des expérimentations longues, couteuses et parfois impossibles à mettre en place.

En sciences environnementales, il existe une multitude de modèles qui diffèrent par leur façon de représenter les processus étudiés et qui sont adaptés à des échelles spatio-temporelles différentes. Les modèles sont généralement classés en trois grandes catégories selon leur façon de représenter les processus.

Les **modèles empiriques** sont construits à partir de données existantes et établissent le lien entre des variables explicatives et des variables à expliquer sans se préoccuper de représenter les mécanismes en action. C'est pourquoi ces modèles sont souvent appelés boites noires. Malgré un bon pouvoir prédictif dans leur plage de calibrage, ces modèles peuvent donner des résultats incorrects quand ils sont utilisés hors de leur plage de calibrage.

Les **modèles conceptuels** cherchent à représenter les processus étudiés à l'aide de relation simplifiées. Ils dépendent d'un certain nombre de paramètres auxquels il est parfois possible de donner un sens physique. Malgré tout, l'application de ces modèles nécessite des jeux de données conséquents afin de calibrer ces paramètres. C'est le cas par exemple des modèles hydrologiques constitués de réservoirs connectés entre eux et qui sont censés représenter les différents compartiments des bassins versants (eau de surface, eau souterraine, réseau hydrographique,…). Ces modèles sont adaptés à la simulation sur de grandes échelles (spatiales et/ou temporelles).

Enfin, les **modèles à base physique** (ou **mécanistiques**) représentent les processus étudiés en utilisant les lois de la physique. Ces modèles nécessitent généralement un grand nombre de paramètres représentant des grandeurs physiques qui peuvent parfois être mesurées *in-situ* ou en laboratoire. Ils sont adaptés à la représentation détaillée des processus sur de petites échelles et peuvent être appliqués en dehors de leur domaine de validation.

De plus, les modèles sont également différenciés en fonction de leur représentation de l'espace. Un modèle global considérera la zone modélisée (souvent le bassin versant en hydrologie) comme une entité unique et homogène. Cette représentation est particulièrement adaptée à la représentation empirique des processus (boîte noire). A l'opposé, un modèle distribué va représenter explicitement la variabilité spatiale du territoire modélisé, ce qui est nécessaire lors de l'implémentation d'un modèle à base physique. Il existe également des modèles semi-distribués dans lequel certains processus sont spatialisés dans différentes entités considérées comme homogènes.

La dimension temporelle est également importante à prendre en compte. En effet, la formulation des processus sera différente en fonction de l'échelle temporelle considérée. Un modèle destiné à simuler une longue période ne pourra pas représenter en détails les événements ponctuels. Par exemple, les modèles hydrologiques destinés à simuler des périodes de plusieurs décennies sont souvent opérés à pas de temps journalier ou supérieur et ne permettent pas de représenter correctement des épisodes comme les crues éclairs. Généralement les modèles empiriques et conceptuels sont adaptés aux échelles de temps plus grandes que les modèles à base physique.

Quoi qu'il en soit et malgré le type de modélisation utilisé, un modèle n'est jamais parfait et l'interprétation de ses résultats doit se faire en prenant en compte différents éléments comme les processus simulés par le modèle, les hypothèses réalisées lors de leur formulation et le domaine d'application du modèle. Aussi, le choix d'un modèle doit se faire en fonction des objectifs fixés au préalable.

1.4.2. Modélisation de la dénitrification dans les plaines alluviales

La modélisation est particulièrement adaptée à l'étude du processus de dénitrification dans les zones de plaine alluviale dont la forte variabilité spatio-temporelle couplée à la difficulté d'obtenir des mesures à grande échelle en font un processus difficile à représenter. La modélisation de la dénitrification dans les zones alluviales peut permettre de répondre à de multiples objectifs. Par exemple, la modélisation peut être utilisée pour évaluer le rôle des

zones ripariennes sur la dynamique des nitrates à l'échelle du bassin versant (Hattermann et al., 2006; Sun, 2015). Elle peut également permettre de prédire les sources et puits de nitrates au sein des zones hyporhéiques (Boano et al., 2010; Peyrard et al., 2011; Zarnetske et al., 2012).

Pour modéliser le processus de dénitrification dans les plaines alluviales, il existe différentes approches de modélisation, adaptées à différentes échelles et à différents objectifs. Cependant, la plupart des modèles associent (i) un modèle hydrologique incluant un module de transport afin de simuler les transferts d'eau et d'éléments associés (nitrates et carbone organique par exemple) et (ii) un modèle biogéochimique qui calcule les taux de dénitrification *in situ* en fonction de différents facteurs comme la concentration en nitrates et en COD. La différence entre les types de modèles utilisés dépend principalement de l'échelle spatiale considérée. Ainsi, on peut séparer les modèles qui intègrent la totalité du bassin versant de ceux appliqués à des échelles plus locales.

1.4.2.1. Approches de modélisation à l'échelle du bassin versant

Les modèles hydrologiques conceptuels semi-distribués (voire distribués) sont généralement appliqués pour la simulation des processus hydrologiques à l'échelle du bassin versant. Ces modèles considèrent les échanges entre différents réservoirs parmi ceux représentant les eaux de surfaces, le réseau hydrographique, le sol ou la zone non saturée et les eaux souterraines qui peuvent être séparées en aquifère peu profond et aquifère profond. Les processus simulés peuvent englober, les précipitations, l'évapotranspiration, le ruissellement de surface, l'infiltration, les écoulements souterrains et le réseau hydrographique. Le couplage entre différents modèles adaptés à chaque compartiment est également utilisé pour simuler le cycle hydrologique sur le bassin versant.

Les sources de nitrates prises en compte par ces modèles sont principalement les apports dus à la fertilisation mais peuvent également inclure la fixation atmosphérique et d'autres sources diffuses ou ponctuelles (Almasri and Kaluarachchi, 2007). Le transfert des nitrates à travers les sols est simulé grâce à un modèle de culture ou à des fonctions de transfert plus simplifiées. Des approches de bilan de masse sont généralement appliquées pour simuler le transfert des nitrates entre les différents compartiments simulés.

La dénitrification dans les eaux souterraines est généralement prise en compte de façon simplifiée par une équation différentielle du premier ordre qui peut s'écrire sous la forme

$$R = k.\mathrm{N}$$

avec R le taux de dénitrification $[M.L^{-3}.T]^{-1}$, k le coefficient de dégradation $[T]^{-1}$ et N la concentration en nitrates $[M.L^{-3}]$.

La dénitrification dépend donc de la teneur en nitrates dont le transfert est simulé dans le bassin versant et d'un unique paramètre k. Ce paramètre peut être estimé à partir de la géologie du réservoir avant d'être calibré. D'autres modèles incluent le rôle de la zone riparienne à travers un paramètre de rétention à calibrer (Ruelland et al., 2007). Plus récemment une approche consistant à prendre en compte les concentrations en carbone organique dissous et particulaire a été développée par Sun (2015).

Parmi les modèles hydrologiques conceptuels, on peut citer les modèles SWAT ou SWIM qui ont déjà été appliqués pour simuler, entre autres, le processus de dénitrification à l'échelle du bassin versant (Hattermann et al., 2006; Ferrant et al., 2011). Des approches intégrant le couplage entre différents modèles simulant les écoulements et la dynamique des nitrates dans les eaux de surfaces, la zone non saturée et la zone saturée ont été appliquées pour simuler la dynamique des nitrates dans les bassins versants (Almasri and Kaluarachchi, 2007; Krause et al., 2008).

L'utilisation des modèles développés pour les bassins versants est relativement simple mais nécessite de nombreuses données afin de calibrer les différents paramètres. Les résultats de ces modèles peuvent être interprétés à grande échelle mais sont peu exploitables à petite échelle. La dénitrification est donc considérée comme homogène au sein des zones ripariennes et la variabilité spatio-temporelle à l'intérieur de ces zones n'est pas représentée.

1.4.2.2. Approches de modélisation à l'échelle locale

Les applications de modèles qui prennent en compte la dénitrification à l'échelle du tronçon de la plaine alluviale (quelques km²) sont peu nombreuses. Ces études incluent des modèles de transport en une dimension (Peyrard et al., 2011; Zarnetske et al., 2012) et en deux dimensions (Boano et al., 2010) couplés à un modules calculant la dénitrification. Dans ces études, seuls les écoulements souterrains dans la zone hyporhéique sont pris en compte mais les autres compartiments du cycle hydrologique (évapotranspiration, précipitation, …) ne sont pas simulés. De plus, les échanges entre la nappe et la rivière se font uniquement au niveau du lit mineur et la simulation des échanges lors des crues débordantes n'est pas prise en compte.

Les sources de nitrates ne sont pas explicitement simulées mais sont imposées au travers des conditions aux limites qui nécessitent d'être connues. Dans ces modèles, la composante simulant le processus de dénitrification est plus complexe que dans les modèles utilisés à l'échelle des bassins versants. La dénitrification est fonction de la teneur en nitrates et en COD mais peut également prendre en compte la teneur en oxygène dissous, en COP et en ammonium. Le calcul de la dénitrification dans ces modèles est basé sur des équations de Monod modifiées de type :

$$R = R_{max} \left(\frac{C_1}{K_1 + C_1}\right)\left(\frac{C_2}{K_2 + C_2}\right)$$

avec R_{max} le taux de dénitrification maximal [$M.L^{-3}.T^{-1}$], C_1 et C_2 les concentration des espèces participants à la réaction [$M.L^{-3}$] et K_1 et K_2 les coefficients de demi saturation de chaque espèce [T^{-1}].

Le taux maximal de dénitrification R_{max} est souvent calculé dynamiquement en fonction de la dégradation du carbone organique dissous et particulaire (Peyrard et al., 2011; Zarnetske et al., 2012).

Ces modèles ont été appliqués à des zones d'études pour simuler la dynamique des nitrates et de la dénitrification dans un banc de graviers (Peyrard et al., 2011), au sein d'un méandre (Boano et al., 2010) ou utilisés pour déterminer théoriquement les facteurs contrôlant la distribution des zones de dénitrification et de nitrification au sein des zones hyporhéiques (Zarnetske et al., 2012). De tels modèles ont également été appliqués à l'échelle du lit de la rivière pour étudier le devenir des nitrates dans les sédiments des rivières (Marzadri et al., 2011; Briggs et al., 2014).

Ces modèles sont utiles pour quantifier et comprendre le processus de dénitrification à petite échelle. Cependant, dans les applications actuelles, l'hydrologie est simulée de manière simplifiée et ne prends pas en compte les épisodes de crue et les échanges nappe-rivière qui sont une caractéristique fondamentale des plaines alluviales où ils impactent la dénitrification bien que de nombreux modèles couplant eaux de surface et eaux souterraines soient développés (Furman, 2008; Maxwell et al., 2014; Pan et al., 2015).

Il existe également de nombreux modules permettant de simuler la dénitrification à l'échelle locale qui peuvent être classés en trois grands groupes : (1) les modèle de croissance

microbienne qui considèrent la dynamique des micro-organismes liés au cycle de l'azote, (2) les modèles de structure des sols qui considèrent la diffusion des gaz au sein des agrégats et où la dénitrification se produit dans les parties anoxiques, et (3) les modèles simplifiés qui calculent la dénitrification en fonction de paramètres faciles à obtenir (Heinen, 2006). Les modèles simplifiés sont plus facilement utilisables que les modèles complexes comme ceux basés sur la croissance des micro-organismes ou la diffusion des gaz qui nécessitent de nombreux paramètres et une discrétisation spatiales très fine. Dans son étude, Heinen (2006) compare une cinquantaine de modèles simplifiés qui sont basés sur la dénitrification potentielle ou considèrent la dénitrification comme une réaction du premier ordre. Et des facteurs limitant tels que la teneur en eau (utilisé comme un proxy pour la teneur en oxygène), la température et le pH. Cependant, la plupart de ses modèles sont utilisés pour simuler la dénitrification dans les horizons supérieurs des sols en réponse à différentes pratiques culturales et seule la dimension verticale du transfert d'azote est considérée.

1.5.Résumé de la problématique, objectifs et démarche méthodologique.

La contamination en nitrates des eaux souterraines des plaines alluviales est un problème environnemental majeur. La dénitrification est un processus naturel diminuant la teneur en nitrates dans les zones ripariennes. Cependant, ce processus complexe est spatialement et temporellement hétérogène et dépend de nombreux facteurs, ce qui le rend difficile à quantifier. Dans ce contexte, la modélisation s'appuyant sur des observations de terrain constitue une approche pertinente pour améliorer la compréhension et la quantification de la dénitrification dans les plaines alluviales. Bien que de nombreuses approches de modélisation aient déjà été développées pour simuler la dénitrification dans les eaux souterraines, peu de modèles permettent de rendre compte de la variabilité spatiale et temporelle de ce phénomène à l'échelle locale. De plus, ces modèles ne prennent pas en compte les caractéristiques majeures des plaines alluviales que sont les crues et les échanges nappe-rivière qui sont des éléments fondamentaux pour le fonctionnement biogéochimique de ces environnements.

L'objectif principal de cette thèse est de caractériser la variabilité spatio-temporelle du processus de dénitrification et d'identifier ses facteurs de contrôle dans les eaux souterraines des plaines alluviales, à travers une approche de modélisation à l'échelle locale.

L'originalité de ce travail est d'utiliser un modèle intégrant les processus hydrologiques importants pour le fonctionnement des processus biogéochimiques comme les crues

débordantes et leurs impacts sur les échanges nappe-rivière. De plus, la formalisation du processus de dénitrification et la validation du modèle s'appuient sur l'analyse de nombreuses données récoltées sur le terrain.

La démarche suivie dans ce travail combine une approche de terrain et de modélisation (Figure 1-10). Dans un premier temps, une analyse des données récoltées sur le site expérimental de Monbéqui (environ 6,6 km²) situé dans la plaine alluviale de la Garonne a été réalisée afin d'identifier les facteurs de contrôle de la dynamique des nitrates et du processus de dénitrification (chapitre 3). Puis, le modèle hydrologique distribué MOHID Land a été utilisé pour simuler le fonctionnement hydrologique sur le site d'étude en prenant en compte les échanges nappes-rivière et les épisodes de crue débordantes (chapitre 4). Ensuite, un module calculant la dénitrification et prenant en compte les facteurs identifiés dans le chapitre 3 a été ajouté au modèle MOHID Land afin de simuler la variabilité spatio-temporelle du processus de dénitrification sur le site de Monbéqui (chapitre 5). Finalement l'application du modèle à d'autres plaines alluviales a été analysé afin de tester la robustesse du modèle et d'identifier les facteurs de contrôle de la dénitrification dans des contextes variés (chapitre 6). Ce travail contribue à améliorer la modélisation du processus de dénitrification dans les plaines alluviales en identifiant ses principaux facteurs de contrôle et ouvre des perspectives quant à l'utilisation d'une telle approche pour étudier la problématique de la contamination en nitrates des eaux souterraines.

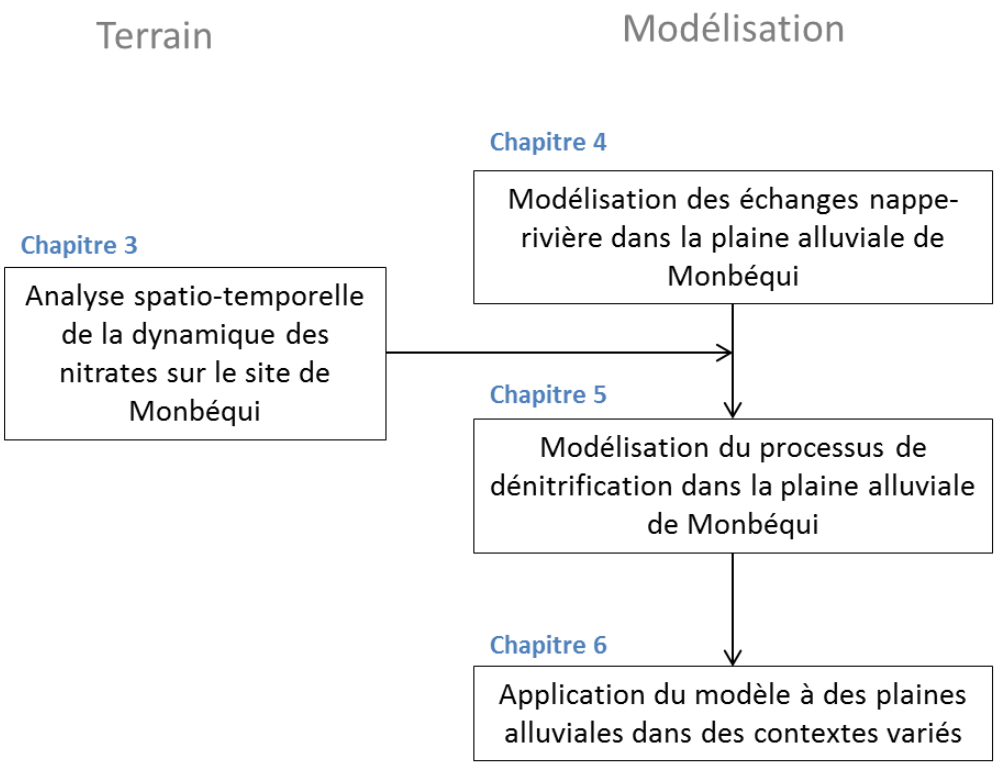

Figure 1-10 : Démarche méthodologique et organisation de la thèse

Chapitre 2 : Matériels et méthodes

Ce chapitre comporte la description du site d'étude et du travail de terrain réalisé, ainsi que la description du modèle utilisé. Dans un premier temps, le bassin versant de la Garonne, la moyenne Garonne toulousaine et le site instrumenté de Monbéqui sont présentés. Les différentes campagnes d'échantillonnages et les paramètres analysés sont détaillés. Puis, le fonctionnement du modèle MOHID Land utilisé dans cette étude est décrit. La modélisation des processus hydrologiques et le module destiné à simuler le processus de dénitrification sont abordés en détails.

2.1.Site d'étude

2.1.1. La Garonne et son bassin versant

La Garonne est un fleuve d'une longueur de 647 km qui prend sa source en Espagne et traverse le sud-ouest de la France pour se jeter dans l'océan Atlantique au niveau de l'estuaire de la Gironde. La majorité de son bassin versant qui s'étend sur 55 846 km² se situe en France et représente 10% du territoire français (Figure 2-1). Il draine les eaux de trois grandes zones géographiques que sont les Pyrénées, le Massif Central et le Bassin Aquitain. Le régime hydrologique de la Garonne peut être caractérisé de type pluvio-nival avec une période de hautes eaux de décembre à mai, résultant des précipitations atlantiques en hiver et complétée par la fonte des neiges pyrénéennes au printemps, et une période d'étiage de juillet à octobre (Figure 2-2).

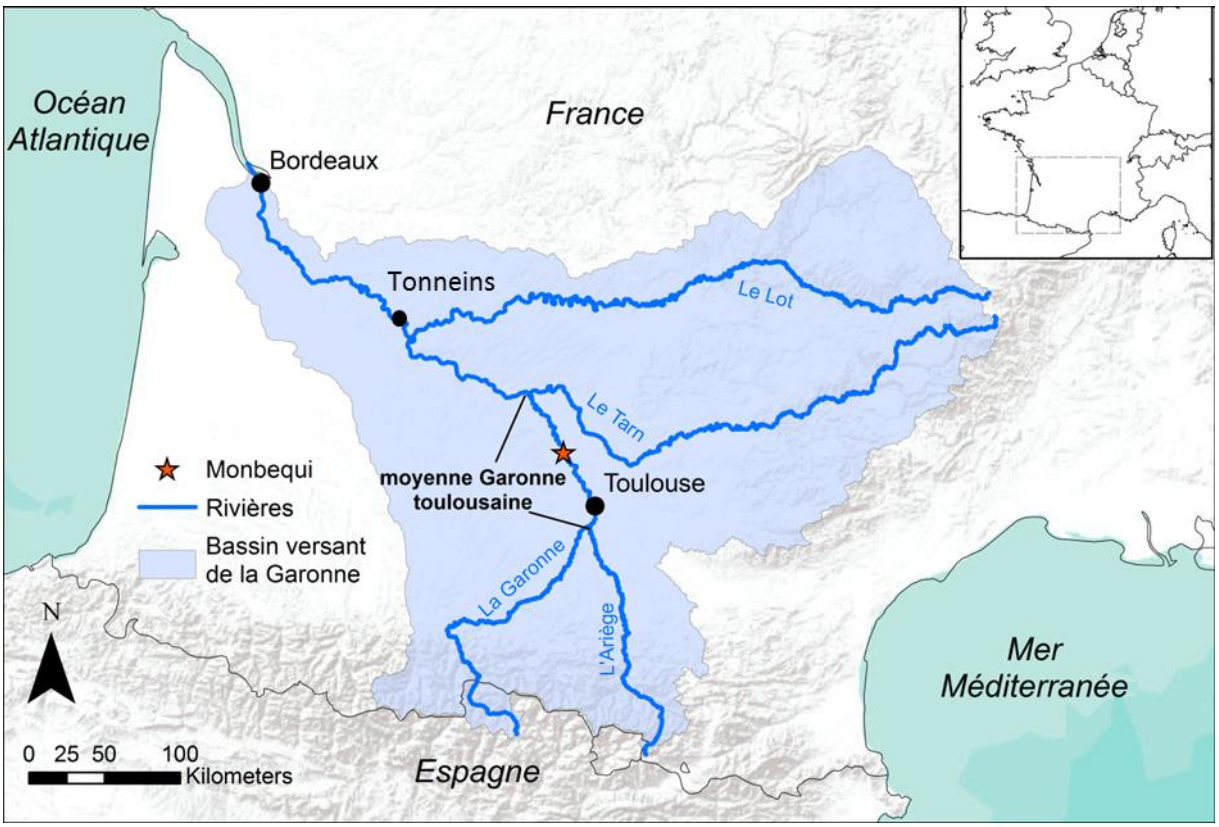

Figure 2-1 : Localisation du bassin versant de la Garonne

Le module hydrologique mesuré à la station hydrologique de Tonneins - la station localisée la plus en aval de la Garonne (BV de 51500 km²) – est de 601 $m^3.s^{-1}$. Le débit maximum enregistré depuis 1914 est estimé à 5700 $m^3.s^{-1}$ alors que le débit minimum enregistré est de 38 $m^3.s^{-1}$.

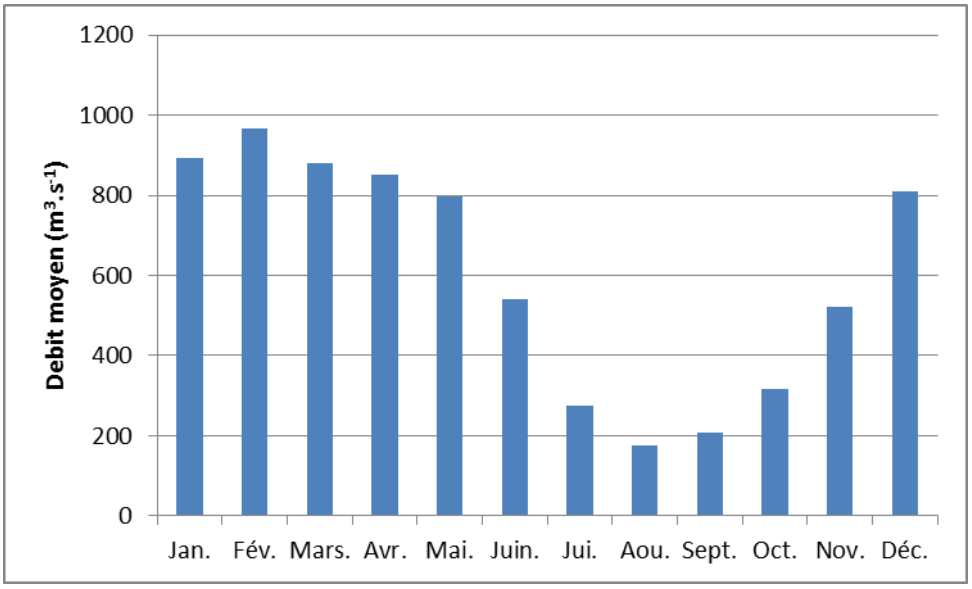

Figure 2-2 : Débit mensuels moyens enregistrés à la station hydrologique de Tonneins (BV : 51 500 km²) sur la période 1914 – 2015 (source : www.hydro.eaufrance.fr)

Le bassin versant de la Garonne est soumis à l'influence climatique atlantique et pyrénéenne, avec des précipitations annuelles variant de 600 mm près de Toulouse à plus de 1500 mm dans les Pyrénées. Du fait de cette configuration, la Garonne présente un système de crues complexe. Trois principaux types de crues ont été identifiés par Pardé (1935). Les crues entrainées par les précipitations dues au climat océanique pyrénéen sont fréquentes d'avril à juillet et touche principalement les zones en amont de la confluence Tarn-Garonne. Les crues dite méditerranéennes sont provoquées par des pluies orageuses intenses, généralement entre Septembre et début Novembre, et affectent surtout le Tarn et l'Agout dans la partie orientale du bassin versant. Enfin, les crues océaniques classiques qui se produisent en hiver (de fin novembre à fin mars) sont dues à des pluies de faible intensité mais de longue durée.

L'occupation des sols du bassin versant de la Garonne est constituée majoritairement de territoires agricoles (52%) et de forêt et milieux semi-naturel (44%), mais également de territoires artificialisés (3%) et de zones humides et surfaces en eau (1%) (Corine Land Cover, 2006, http://sia.eionet.europa.eu/CLC2006). La vallée de la Garonne concentre près de 2 millions d'habitants qui dépendent de la Garonne pour leur alimentation en eau potable. Pour l'agence de l'eau Adour-Garonne, la préservation de la ressource en eau potable reste donc l'objectif prioritaire du bassin Garonne. En effet, les masses d'eaux souterraines du bassin de la Garonne subissent des pressions en pollutions diffuses importantes (contaminations en nitrates issus de l'agriculture), ainsi qu'une forte pression de prélèvements principalement à

destination de l'irrigation (72% en 2010) mais aussi pour l'alimentation en eau potable (20%) et l'industrie (8%).

2.1.2. Plaine alluviale de la moyenne Garonne toulousaine

La Garonne peut être divisée en plusieurs secteurs en fonction de la morphologie de sa vallée et de son lit. Aussi, le secteur allant de la confluence avec l'Ariège à la confluence avec le Tarn (Figure 2-3) est appelé moyenne Garonne toulousaine (Lambert, 1988; Valette, 2002).

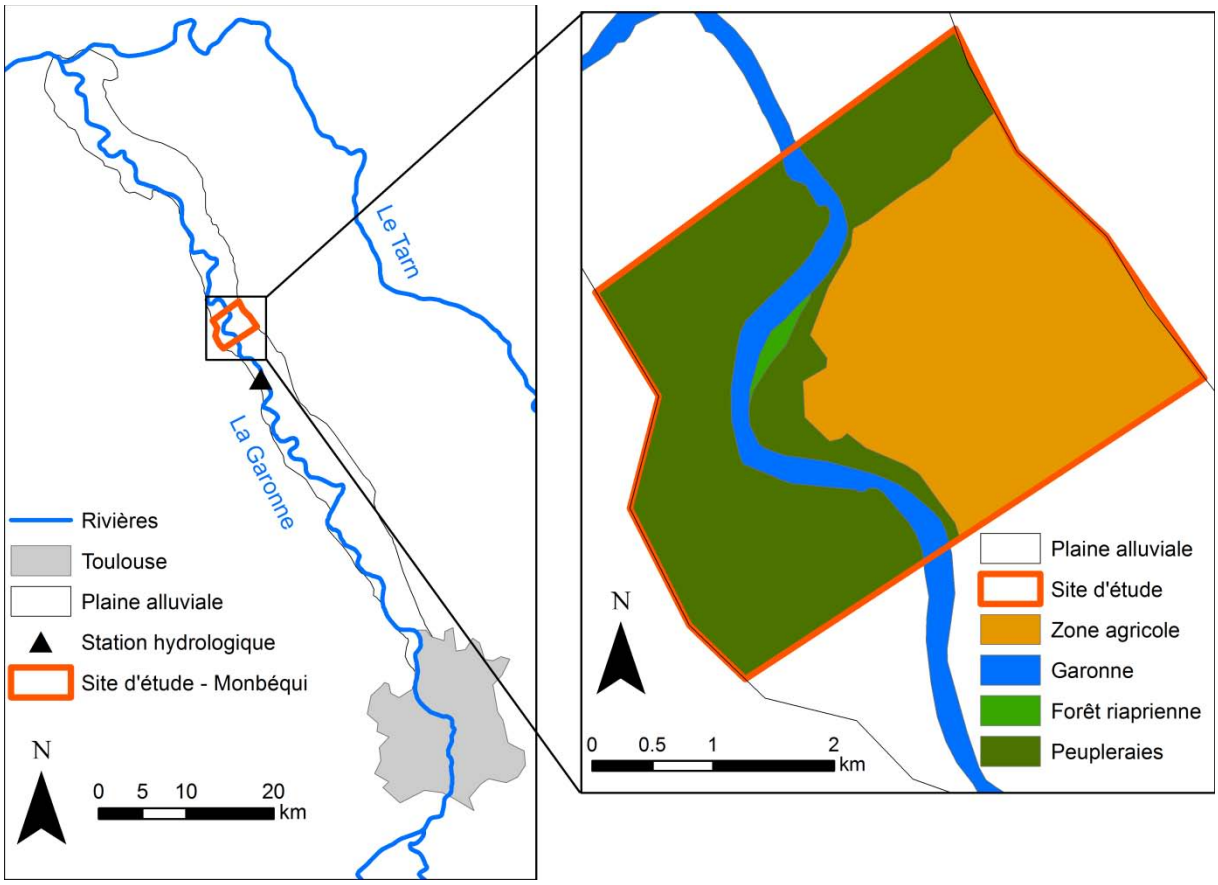

Figure 2-3 : Plaine alluviale de la moyenne Garonne toulousaine et localisation et occupation des sols du site d'étude de Monbéqui .

Sur ce secteur, long de 70 km, la pente de la Garonne est légèrement inférieure à 1‰. La plaine d'inondation s'élargit à l'aval de Toulouse pour s'étendre sur 2 à 4 km de large (Figure 2-3). La largeur moyenne du lit mineur est de 150 m et l'indice de sinuosité moyen est de 1,3 (Steiger and Corenblit, 2000). Dans cette zone, la plaine alluviale d'inondation est délimitée latéralement par une série de terrasses étagées et la Garonne s'écoule directement sur le substrat molassique imperméable (Figure 2-4). Alors que le fleuve à beaucoup bougé dans le passé, il est aujourd'hui très contraint suite aux aménagements de fixation de son lit (Valette et al., 2014).

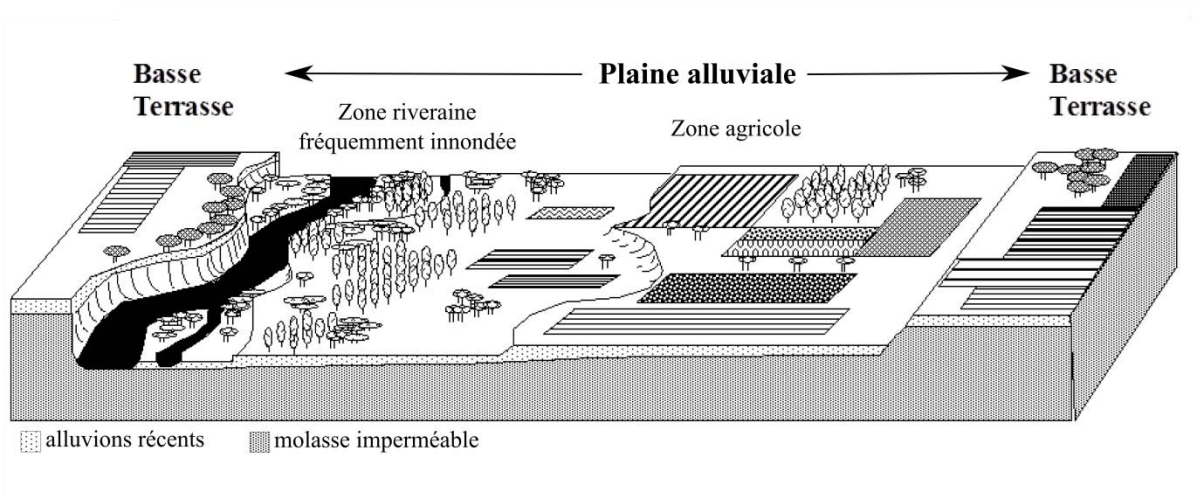

Figure 2-4 : Géomorphologie de la plaine alluviale de la moyenne Garonne toulousaine (adapté de Steiger and Corenblit, 2000)

Dans cette zone la pression agricole est très importante et les concentrations en nitrates mesurées dans la nappe alluviale peuvent dépasser les 50 mg-NO_3^-.L^{-1} (Pinay et al., 1998; J. M. Sánchez-Pérez et al., 2003) qui correspond, en Europe, à la limite fixée pour les eaux souterraines par la directive nitrate (91/676/CE) et la directive eaux souterraines (2006/118/CE). Ainsi, sur les 20 stations de surveillances de la masse d'eau alluviale intitulée « Alluvions de la Garonne moyenne et du Tarn aval, la Save, l'Hers mort et le Girou » (code européen : FRFG020), quatre stations présentent une moyenne supérieur à 50 mg-NO_3^-.L^{-1} et huit ont enregistrées des pics dépassant cette limite sur la période 2000-2007. Cette contamination n'est pas localisée et a été identifiée aussi bien en amont qu'en aval de la masse d'eau.

2.1.3. Site d'étude instrumenté de Monbéqui

Le site expérimental suivi dans cette étude est situé sur la commune de Monbéqui dans le Tarn-et-Garonne (Figure 2-3). Il s'agit d'un tronçon de la plaine alluviale de la moyenne Garonne toulousaine dont la largeur varie entre 2,5 et 3 km. Dans cette zone, la longueur de la Garonne est de 3,5 km et l'indice de sinuosité de 1,5. Le milieu poreux est constitué d'alluvions déposé sur le substrat molassique imperméable et d'épaisseur variant de 4 à 7 mètres (J. M. Sánchez-Pérez et al., 2003; Lancaster, 2005). Ils sont recouverts par des sols de type Fluviosol, d'une profondeur de 1,5 à 3 m avec une texture de type Limon sablo-argileux.

A cet endroit la Garonne draine une superficie de 13 730 km² et le débit annuel moyen mesuré 3 km en amont, à la station de Verdun sur Garonne est de 190 $m^3.s^{-1}$. Il a varié entre 98 (en 1989) et 315 $m^3.s^{-1}$ (en 1978) lors des 41 dernières années. Le mois le plus sec est le mois d'août avec 76 $m^3.s^{-1}$ et le plus humide est mai avec 343 $m^3.s^{-1}$ en moyenne. Le débit

journalier varie entre 10 $m^3.s^{-1}$ (étiage d'août 1991) et 2 930 $m^3.s^{-1}$ (crue du 6 Novembre 2000). Le débit instantané maximum enregistré a été estimé à 3780 $m^3.s^{-1}$ ce qui correspond à une crue de temps de retour estimé entre 10 et 20 ans. Les débits journaliers et instantanés et leur temps de retour associé sont présentés dans la

Table 2-1.

Table 2-1: Temps de retour et débits à la station de Verdun sur Garonne (www.hydro.eaufrance.fr)

Temps de retour (ans)	2	5	10	20	50
Débit journalier ($m^3.s^{-1}$)	1400	2100	2500	2900	3400
Débit instantané ($m^3.s^{-1}$)	1800	2700	3200	3700	4400

La plaine alluviale est totalement inondée lors de crues caractérisées par un temps de retour supérieur à 15 ans alors qu'une courte bande située le long de la rivière allant jusqu'à une centaine de mètres de largeur est inondée lors des événements plus fréquents (temps de retour annuel) (Figure 2-5).

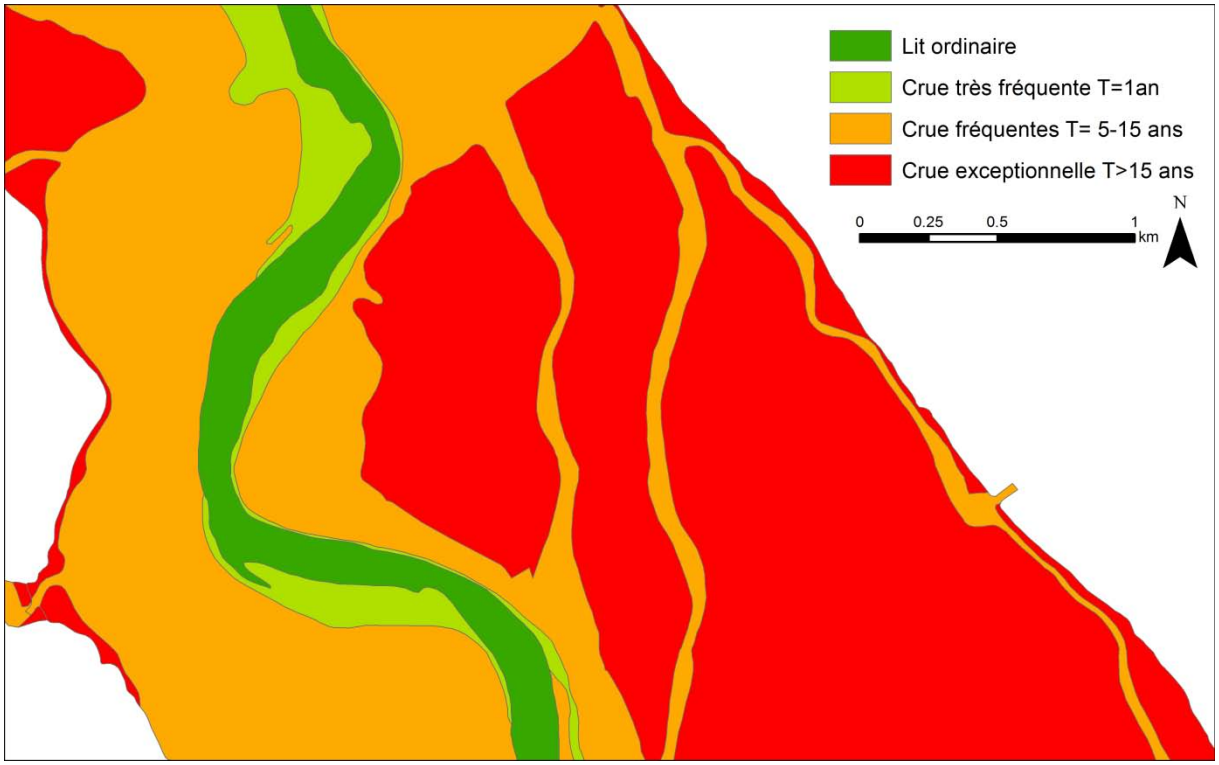

Figure 2-5: Emprise de la zone inondée par des crues de différents temps de retour sur le site étudié (source : CIZI, Carte Informative des Zones Inondables, DREAL Midi-Pyrénées)

Dans la zone d'étude le toit de la nappe alluviale se situe à une profondeur par rapport au sol variant entre 2 et 5,5 mètres pendant l'étiage, mais le niveau de la nappe peut rapidement augmenter pendant les crues. Les écoulement suivent la pente longitudinale de la vallée (1‰) mais sont également fortement impactés par les variations de débit de la Garonne (Weng et

al., 2003; Peyrard et al., 2008). Ainsi on passe d'une situation ou la Garonne draine la nappe pendant les périodes d'étiages à des situations ou la Garonne alimente la nappe pendant les épisodes de crue (Weng et al., 2003; Peyrard et al., 2008).

L'occupation des sols (Figure 2-3) est constituée d'une forêt riparienne (saules et frênes) le long de la Garonne (~0,5 km²), de plantations de peupliers (~2,5 km²) qui occupent la rive gauche et séparent sur la rive droite la forêt riparienne d'une zone agricole (~3,5 km²) qui comporte des cultures de maïs, blé, tournesol, soja et sorgho (Jégo, 2008).

Le site est équipé d'un réseau de 25 piézomètres principalement situés dans la partie intérieure du méandre (Figure 2-6), traversant les alluvions sur toute leur épaisseur.

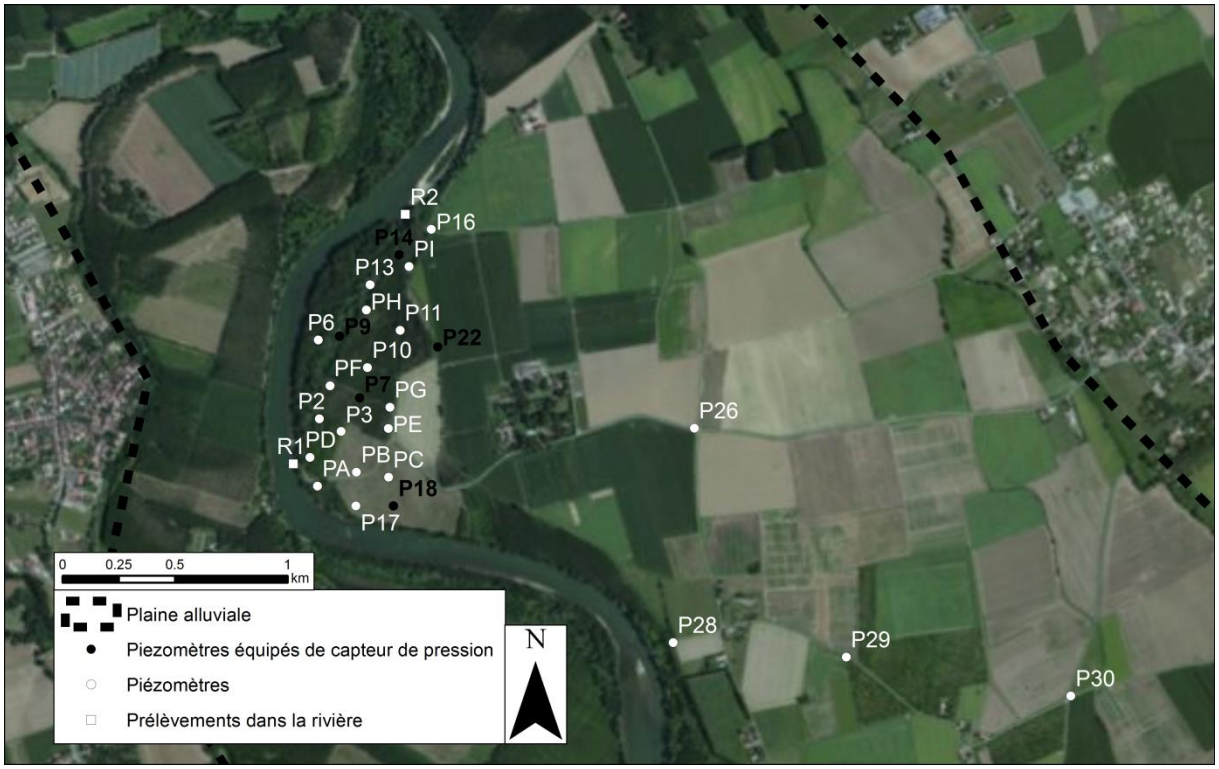

Figure 2-6 : Cartes de localisations des point d'échantillonnages du site d'étude (P : piézomètre, R : rivière).

De précédentes études ont déjà été menées sur ce site et ont permis d'améliorer la compréhension de son fonctionnement hydrologique et biogéochimique et notamment l'importance de la dénitrification sur la dynamique des nitrates (J. M. Sánchez-Pérez et al., 2003). L'importance des communautés bactériennes attachées au sédiment sur la dénitrification dans l'aquifère a également été mis en avant (Iribar et al., 2008). De plus, des études de modélisation ont mis en évidence l'importance des échanges nappe-rivière sur la composition chimique de l'aquifère (Weng et al., 2003; Peyrard et al., 2008; Sun et al., 2015)

et l'impact des pratiques agricoles sur le lessivage des nitrates dans l'aquifère (Jégo et al., 2012).

2.1.4. Echantillonnage

Le réseau de piézomètre a été suivi d'avril 2013 à mai 2014. Parmi les 25 piézomètres, 5 ont été équipés avec capteur de pression (CTD-Diver, Schlumberger) qui permettent l'enregistrement de la hauteur d'eau à un pas de temps de 5 minutes. L'ensemble du réseau a également été suivi lors de 12 campagnes mensuelles qui incluent des mesures physico-chimiques et des prélèvements d'échantillons d'eau souterraine. Des sédiments ont également été échantillonnés lors de quatre ces campagnes (Figure 2-7, Table 2-2). Pour chaque campagne, deux emplacements situés dans la rivière ont également été échantillonnés (Figure 2-6).

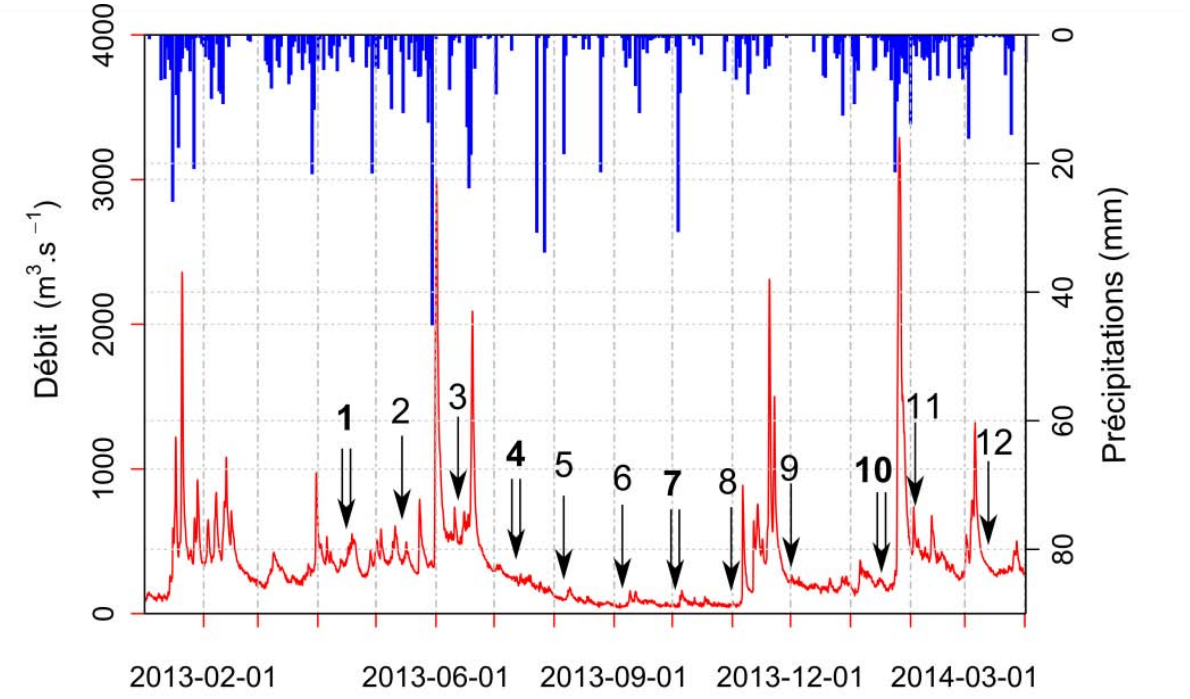

Figure 2-7 : Débits et précipitations journaliers sur la zone d'étude. La date des campagnes d'échantillonnage est indiquée. Les campagnes incluant le prélèvement de sédiment sont indiqué an gras avec une double flèche.

Pour chaque piézomètre, la profondeur de la nappe est mesurée à l'aide d'une sonde piézométrique. Deux paramètres sont utilisés pour décrire l'état de l'aquifère. La profondeur de la nappe (water depth, WD) correspond à la distance entre le toit de la nappe et la surface du sol alors que le niveau de la nappe (water level, WL) correspond à l'altitude du toit de la nappe par rapport à la référence (NGF, nivellement général de la France). Ensuite, l'eau est prélevée avec une pompe thermique et les principaux paramètres physico chimiques (oxygène dissous, température, pH et conductivité électrique) sont mesurés à l'aide d'un multi

paramètre portable (WTW Multi 3420) et de sondes spécifiques, et enregistrés lorsque les paramètres se stabilisent. Des échantillons d'eau sont ensuite prélevés. Une partie est filtrée sur le terrain à travers des filtres de 0,45 µm à membrane en acétate de cellulose et stockée dans des bouteilles en polyéthylène haute densité. Les échantillons destinés à l'analyse de la composition isotopique de l'oxygène sont stocké dans des flacons opaques.

Toutes les quatre campagnes, des prélèvements de sédiments ont été effectués. Il s'agit, après avoir prélevé les échantillons d'eau, d'augmenter le débit de pompage pendant 5 à 10 minutes en récupérant l'eau dans un bidon de 50 L où les sédiments se déposent avant d'être collectés (~300 mL) avec 100 mL d'eau dans des sacs plastiques stériles et étanches.

Lors de chaque campagne, deux points de prélèvement situés dans la rivière sont échantillonnés. Dans ce cas, la mesure des paramètres physico-chimique et le prélèvement de l'eau sont effectués directement dans le cours d'eau.

Table 2-2: Récapitulatif des prélèvements effectués et des conditions hydrologiques pour chaque campagne. Le débit correspond au débit enregistré à la station de Verdun sur Garonne moyenné sur la durée de chaque campagne (www.hydro.eaufrance.fr).

Campagne n°	Date	Physico-chimie & Prélèvement d'eau	Prélèvements sédiments	Débits moyens ($m^3.s^{-1}$)
1	8-10 avr. 2013	Oui	Oui	337
2	13-14 mai 2013	Oui		367
3	10-11 juin 2013	Oui		608
4	1-3 juill. 2013	Oui	Oui	314
5	29-30 juillet 2013	Oui		160
6	2-3 sept. 2013	Oui		49
7	30 sept. – 2 oct. 2013	Oui	Oui	53
8	4-5 nov.2012	Oui		83
9	2-3 déc. 2013	Oui		219
10	13-15 janv. 2014	Oui	Oui	209
11	3-4 févr. 2014	Oui		496
12	10-11 mars 2014	Oui		364

2.1.5. Analyses de l'eau

Les concentrations en ions (NO_3^-, Cl^-, SO_4^{2-}, PO_4^{3-}, Ca^{2+}, Mg^{2+}, K^+, Na^+ and NH_4^+) ont ensuite été mesurés au laboratoire par chromatographie ionique (Dionex ICS-5000$^+$ et DX-120).

La concentration en silice a été mesurée par spectrophotocolorimétrie (Alpkem) et l'alcalinité par titration acide.

Pour la détermination du carbone organique dissous (COD), les échantillons d'eau ont été filtré avec des filtres de 0,45 µm à membrane en acétate de cellulose préalablement rincés,

puis stockés dans des tubes en verre sans carbone, acidifiés avec de l'HCl et enfin analysés par combustion catalytique à 650°C (TOC 5000, Shimadzu).

La composition isotopique de l'oxygène a été mesurée par spectrométrie de masse après mise à l'équilibre CO_2-H_2O en utilisant la technique décrite par Epstein et Mayeda (1953). Les résultats sont exprimés relativement à un standard (V-SMOW, Gonfiantini, 1978) sous la forme :

$$\delta^{18}O = \frac{R\delta^{18}O_{échantillon} - R\delta^{18}O_{V-SMOW}}{R\delta^{18}O_{V-SMOW}}$$

où $R\delta^{18}O_{échantillon}$ et $R\delta^{18}O_{V-SMOW}$ sont les ratio $^{18}O/^{16}O$ respectivement de l'échantillon et du V-SMOW. $\delta^{18}O$ est généralement exprimé en ‰.

2.1.6. Analyses des sédiments

L'activité enzymatique dénitrifiante (denitrification enzyme activity, DEA) a été mesurée au laboratoire par la méthode de blocage à l'acétylène (Yoshinari and Knowles, 1976). Il s'agit de bloquer le stade final de la réaction de dénitrification par ajout d'acétylène et de doser le N_2O émit afin de quantifier la quantité d'azote dénitrifié lors de la réaction (Figure 2-8). Un mélange de 25 mL de sédiments humides et 50 mL d'une solution d'eau désoxygénée contenant 50 mg-C L^{-1} (ajout d'acétate de sodium) et 100 mg-N L^{-1} (ajout de nitrate de sodium) a été introduit dans des bouteilles de 150 mL pour mesurer une activité de production de N_2O en l'absence de limitation en substrat carboné et en nitrates (mesure du potentiel enzymatique).

L'oxygène a été éliminé en faisant buller de l'Hélium U 99,99% pendant 10 minutes. Après avoir fermé hermétiquement les bouteilles et fait le vide, la phase gazeuse des bouteilles est remplie avec de l'hélium. 15 mL d'acétylène (C_2H_2) ont ensuite été ajoutés pour inhiber la N_2O-reductase. Les bouteilles ont été incubées à l'obscurité à 14°C (température moyenne de l'aquifère). Après 30 min et 6 h 30 min d'incubation, 3 mL de gaz ont été prélevés dans la phase gazeuse (après agitation vigoureuse) et stockés dans des tubes vénoject (Terumo Scientific, NJ, USA). Le N_2O a ensuite été mesuré par chromatographie en phase gazeuse (Varian CP 3800). Les résultats de DEA sont exprimés en µg-N par gramme de sédiment sec par heure (µg-N.g-sed^{-1}.h^{-1}) et correspondent, pour chaque échantillon, à la moyenne de la production de N_2O pour les triplicats. La DEA représente le taux de dénitrification lorsque le carbone et l'azote ne sont pas limitants et est utilisé comme un proxy pour évaluer la capacité

de dénitrification du milieu aux différents emplacements endroits pour chaque date d'échantillonnage.

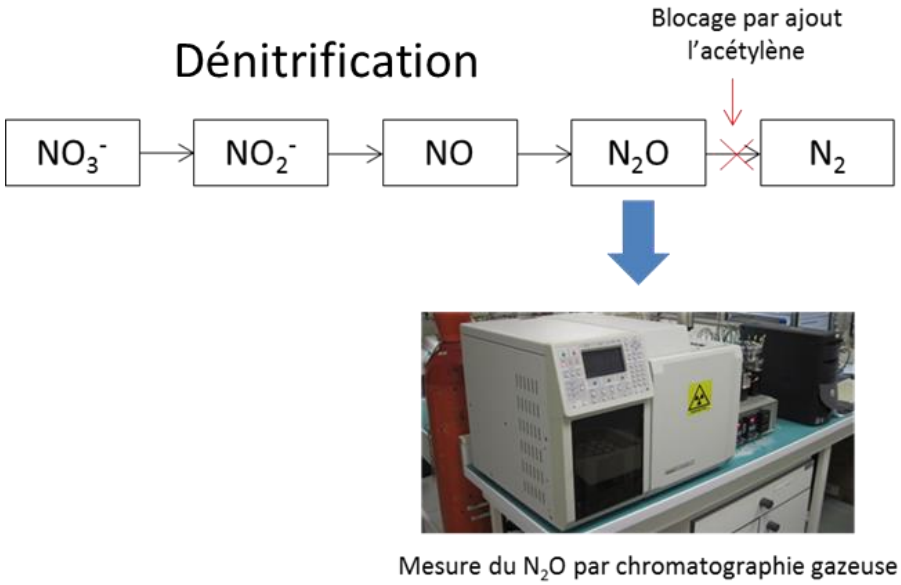

Figure 2-8 : Principe de mesure de la dénitrification potentielle par blocage à l'acétylène

Après incubation, chaque échantillon de sédiments est séché (105°C, 24 h) et brulé (550°C, 4 h) pour déterminer la quantité de matière organique du sédiment (organic matter, OM).

Le récapitulatif des paramètres analysés pour chaque échantillon d'eau et de sédiment est indiqué dans la Table 2-3. L'ensemble des données récoltées est présent dans l'Annexe 1.

Table 2-3 : Récapitulatif des analyses effectuées sur les échantillons d'eau et de sédiment

Echantillons		Paramètres analysés	Méthode
Eau	*Non filtrée*	Alcalinité	Titration acide
		Isotopie ($\delta^{18}O$)	Spectrométrie de masse
	Filtrée 0,45 µm	anions (NO_3^-, Cl^-, $SO_4^{2-}$and PO_4^{3-})	Chromatographie ionique
		cations (Ca^{2+}, Mg^{2+}, K^+, Na^+ and NH_4^+)	Chromatographie ionique
	Filtrée 0,45 µm après rinçage du filtre	Carbone organique dissous (COD)	Combustion
Sédiments		Activité enzymatique dénitrifiante (DEA)	Blocage à l'acétylène et dosage du N_2O
		Matière organique (MO)	Combustion

2.1.7. Analyses statistiques

La régression partielle au moindre carrés (partial least square régression, PLSR) est une méthode qui consiste en une régression linéaire maximisant la covariance entre la variable à expliquer et des composantes orthogonales calculées à partir de la matrice des variables

explicatives et qui permet de maximiser la variance des prédicteurs et de maximiser la corrélation entre les prédicteurs et la variable à expliquer. C'est une méthode très utile en écologie pour analyser des données avec de nombreux prédicteurs (Carrascal et al., 2009). Cette méthode a été utilisée pour expliquer les variations de concentrations en nitrates et de DEA en fonction des autres paramètres récoltés

2.2.Modélisation

2.2.1. Démarche de modélisation et choix du modèle

L'approche de modélisation de cette étude consiste à utiliser un modèle spatialement distribué à base physique afin de représenter en détails le fonctionnement hydrologique et biogéochimique du site d'étude. Les échanges entre la nappe et la rivière pendant les périodes de crue sont des caractéristiques importantes de l'hydrologie des plaines alluviales et doivent être inclus dans le modèle. Le modèle doit également permettre d'implémenter facilement un module biogéochimique pour simuler le processus de dénitrification. Les modèles conceptuels sont inadaptés à la modélisation détaillée des flux hydrologiques au sein des plaines alluviales car ils ne permettent pas une représentation explicite et détaillée de l'environnement modélisé.

Parmi les modèles à base physique couplant eaux de surface et eaux souterraines, MOHID Land a été choisi pour modéliser le système étudié dans cette étude car il permet la modélisation couplée des processus hydrologiques de surface et souterrains, la simulation des crues débordantes et contient un module de transport conservatif de solutés. Sa modularité a permis l'incorporation de module simulant le processus de dénitrification nécessaire à cette étude. Le modèle est décrit en détails dans les paragraphes suivants.

2.2.2. MOHID

MOHID Water Modelling System (Neves et al., 2013) est un logiciel libre, sous licence GPL (Général Public Licence), développé par le groupe MARETEC de l'IST (Instituto Superior Técnico) de Lisbonne et disponible sur www.mohid.com/. C'est un système de modélisation basé sur une approche orientée objet, ce qui permet l'intégration des différents processus physiques et biogéochimiques qui affectent le cycle de l'eau, de l'océan au bassin versant (Braunschweig et al., 2004; Trancoso et al., 2009; Brito et al., 2015). Le modèle est écrit en FORTRAN et utilise la méthode des volumes finis pour la résolution numérique des équations. Il se décline sous trois exécutables principaux destinés à la simulation de différents environnements : MOHID River Network (pour les réseaux hydrographiques), MOHID Land (pour les bassins versants) et MOHID Water (pour les masses d'eaux libres : océans,

estuaires, lacs). Dans cette étude, c'est MOHID Land qui est utilisé pour simuler l'environnement alluvial car il permet la prise en compte du milieu poreux souterrain et de l'environnement de surface. Le modèle inclut également de nombreux outils permettant le traitement et la mise en forme des données et qui sont accessibles depuis le logiciel d'interface utilisateur MOHID Studio.

2.2.2.1. Processus simulés

MOHID Land est un modèle à base physique, spatialement distribué, à pas de temps variable qui simule le cycle de l'eau et les processus biogéochimiques associés dans les milieux terrestres. Il est à l'origine destiné à la simulation hydrologique à l'échelle du bassin versant où les processus sont simulés dans 3 domaines qui sont (i) le réseau hydrographique, (ii) le milieu poreux (sols et aquifères) et (iii) les eaux de surface (ruissellement). Dans cette étude, le domaine modélisé est un tronçon de plaine alluviale ce qui implique un certain nombre d'ajustements afin de correctement représenter le domaine modélisé. La principale différence avec l'utilisation du modèle dans sa configuration originale, est que, dans ce cas, le domaine des eaux de surface contient à la fois les écoulements dans le lit mineur de la rivière et dans la plaine adjacente. En effet, dans la version originale de MOHID Land, la rivière est simulée à part et est connecté avec la plaine alluviale de façon simplifiée. Le choix d'intégrer la rivière dans le domaine des écoulements de surface permet de simuler de manière continue les écoulements entre la rivière et la plaine alluviale lors des épisodes de crues débordantes. Le module destiné à la modélisation du réseau hydrographique n'est donc pas utilisé et uniquement deux domaines sont modélisés : (i) les eaux de surface et (ii) le milieu poreux. Cela implique une représentation détaillée de la géométrie de surface et notamment de la géométrie du lit de la rivière.

De plus, MOHID Land permet la prise en compte de plusieurs processus hydro-biogéochimiques. Un module permettant la simulation des processus de dénitrification a notamment été ajouté dans le cadre de cette étude. Les principaux processus simulés et utilisés dans cette étude sont (Figure 2-9):

- Ecoulements 3D dans le milieu poreux
- Ecoulements 2D pour les eaux de surface
- Couplage entre le milieu poreux et les eaux de surface
- Transport des propriétés à travers les différents domaines
- Dénitrification dans le milieu poreux

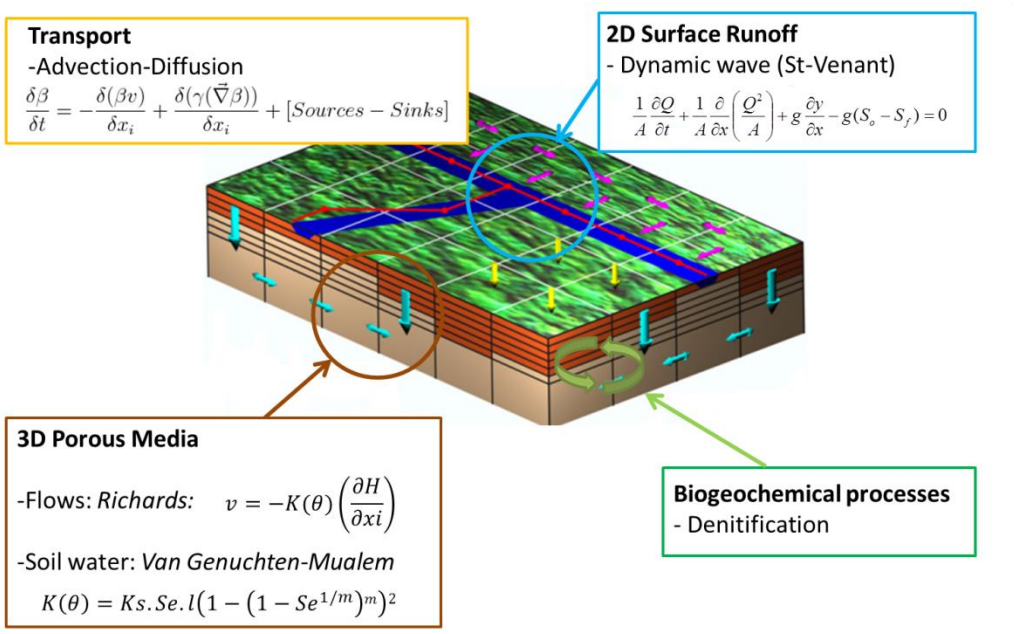

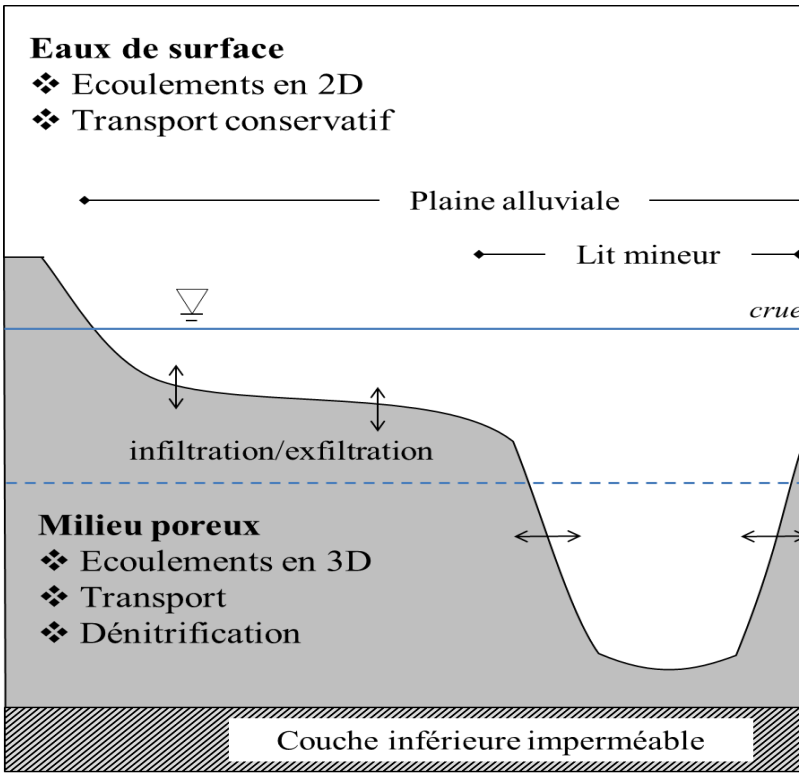

Figure 2-9 : Principaux processus simulés dans le modèle MOHID Land

2.2.2.2. Discrétisation spatiale

Pour les processus en 2 dimensions (2D) comme les écoulements de surface, la discrétisation spatiale horizontale est basée sur un maillage carré. Pour les processus en 3 dimensions (3D) comme les écoulements dans le milieu poreux, une dimension verticale est ajoutée. L'utilisateur indique le nombre et l'épaisseur des couches souhaités. Il faut également renseigner le modèle numérique de terrain (DTM) et la géométrie de la couche inférieure du domaine modélisé. Le modèle calcule ensuite, pour chaque cellule, le nombre de couches

verticales en fonction des paramètres de discrétisation indiqués par l'utilisateur (nombre et épaisseur des couches et altitude de la couche inférieure), afin de décrire au mieux la géométrie du milieu poreux.

2.2.2.3. Equations

2.2.2.3.1. Ecoulements en milieux poreux

La loi de Darcy exprime le débit d'un fluide incompressible s'écoulant à travers un milieu poreux saturé et est définie par l'équation 1.

$$Q = KA\frac{\partial H}{\partial x} \quad (1)$$

Avec :

- Q le débit ($m^3.s^{-1}$)
- K la conductivité hydraulique ($m.s^{-1}$)
- A l'aire de la section étudiée (m^2)
- $\partial H/\partial x$ le gradient hydraulique où ∂H représente la différence de charge hydraulique (m) entre deux points séparés par la longueur ∂x (m)

La charge hydraulique H est calculée par l'équation 2

$$H = h + p + z \quad (2)$$

Avec :

- H la charge hydraulique (m)
- h le potentiel matriciel (m)
- p la pression hydrostatique (m)
- z l'altitude (m)

La loi de Buckingham-Darcy décrit les écoulements dans les milieux poreux non saturés est une généralisation de la loi de Darcy pour le milieu non saturé, basée sur le fait que la conductivité hydraulique dépend du potentiel matriciel (équation 3)

$$q = -K(\theta)\nabla H \quad (3)$$

Avec :

- q la vitesse de Darcy ($m.s^{-1}$)
- K la conductivité hydraulique ($m.s^{-1}$)

- θ la teneur en eau ($m^3.m^{-3}$)

En combinant la loi de Darcy-Buckingham (équation 3) avec la loi de conservation de la masse (equation 4), on obtient l'équation de Richards qui décrit les écoulements dans le milieu non saturé (équation 5).

$$\frac{\partial Masse}{\partial t} = [Flux\ entrants - Flux\ sortants] + [Sources - Puits] \quad (4)$$

$$\frac{\partial \theta}{\partial t} = \frac{\partial}{\partial x}[K(\theta)\frac{\partial h}{\partial x}] + \frac{\partial}{\partial y}[K(\theta)\frac{\partial h}{\partial y}] + \frac{\partial}{\partial z}[K(\theta)(\frac{\partial h}{\partial z} + 1)] \quad (5)$$

Avec :

- x, y et z les trois directions de l'espace (z étant la direction verticale)

La résolution de l'équation de Richards nécessite de connaitre la valeur de la conductivité hydraulique K(θ) et donc de la teneur en eau θ. Dans MOHID Land, les équations de Van Genuchten (van Genuchten, 1980) est utilisée pour calculer la teneur en eau en fonction de la du potentiel matriciel h (équation 6 et 7).

$$h(\theta) = -\left|\left(S_E{}^{(-1/(1-1/N))} - 1\right)^{1/N}\right| / \alpha \quad (6)$$

$$S_E = \frac{\theta - \theta_r}{\theta_s - \theta_r} \quad (7)$$

Avec :

- S_E la saturation effective (sans dimension)
- θ_s la teneur en eau à saturation ($m^3.m^{-3}$)
- θ_s la teneur en eau résiduelle ($m^3.m^{-3}$)
- α, N les paramètres de formes de Van Genuchten

La conductivité hydraulique est ensuite calculée avec à la formule de Mualem (équation 8).

$$K(\theta) = K_s.S_E{}^{L}.\left(1 - \left(1 - S_E{}^{1/(1-\frac{1}{N})}\right)^{1-1/N}\right)^2 \quad (8)$$

Avec :

- L le paramètre de connectivité des pores (m)
- m= 1-1/N (sans dimensions)

Une fois les flux calculés, la teneur en eau θ de chaque cellule est mise à jour pour le nouveau pas de temps en faisant le bilan des flux entrants et sortants (équation 9).

$$\theta^{t+\Delta t} = \frac{\theta^t Vol + (Q_{in} - Q_{out})\Delta t}{Vol} \quad (9)$$

Avec :

- $\theta^{t+\Delta t}$ la teneur en eau à l'instant $t + \Delta t$ ($m^3.m^{-3}$)
- θ^t la teneur en eau à l'instant t ($m^3.m^{-3}$)
- Δt le pas de temps (s)
- Vol le volume de la cellule (m^3)
- Q_{in} la somme des flux entrants ($m^3.s^{-1}$)
- Q_{out} la somme des flux sortants ($m^3.s^{-1}$)

2.2.2.3.2. Eaux de surface

Les écoulements des eaux surfaces sont calculés en 2D avec les équations de Saint-Venant (shallow water equations en anglais). Les équations de Saint-Venants sont déduites des lois de conservation de la masse et de la quantité d'énergie et peuvent être écrites sous différentes formes selon les approximations effectuées. Sous la forme dite de l'onde dynamique, ces équations prennent en compte l'inertie, les forces de pression, de gravité et de friction. Dans les deux directions horizontales, x et y, elles s'écrivent selon les équations 10 et 11.

$$\frac{\partial Q_x}{\partial t} + v_x \frac{\partial Q_x}{\partial x} + v_y \frac{\partial Q_x}{\partial y} = -g.A\left(\frac{\partial H}{\partial x} + Sf\right) \quad (10)$$

$$\frac{\partial Q_y}{\partial t} + v_x \frac{\partial Q_y}{\partial x} + v_y \frac{\partial Q_y}{\partial y} = -g.A\left(\frac{\partial H}{\partial y} + Sf\right) \quad (11)$$

Avec :

- Q le débit ($m^3\ s^{-1}$) selon les directions x et y
- v la vitesse s'écoulement ($m.s^{-1}$) selon les directions x et y
- g l'accélération de la pesanteur ($m.s^{-2}$)
- A la section traversée (m^2)
- S_f la pente de l'écoulement ($m.m^{-1}$) définie par la formule de Manning (équation 12)

$$S_f = v^2 n^2 R_h^{-4/3} \quad (12)$$

Avec :

- n le coefficient de Manning ($s.m^{-1/3}$)
- R_h le rayon hydraulique (m)

2.2.2.3.3. Couplage eaux de surface-milieu poreux

Les flux d'eau entre le milieu poreux et les eaux de surface peuvent avoir lieu dans les deux directions : des eaux de surface vers le milieu poreux (infiltration) ou inversement du milieu poreux vers les eaux de surface (exfiltration). En effet, les eaux de surface peuvent s'infiltrer verticalement dans le milieu poreux quand celui est sous saturé ($\theta<\theta_s$). Ce processus est calculé avec l'équation de Darcy-Buckingham (équation 3). Le gradient hydraulique $\frac{\Delta H}{L}$ est calculé entre les eaux de surface et la couche supérieure du milieu poreux. Dans le cas où, après avoir effectué le bilan des flux entrants et sortants (équation 9), le milieu poreux est sur saturé ($\theta^{t+\Delta t}>\theta_s$), le volume excédentaire est exfiltré verticalement du milieu poreux vers les eaux de surface.

2.2.2.3.4. Transport de solutés

Le transport conservatif de solutés est calculé dans le milieu poreux avec l'équation d'advection-diffusion en négligeant la diffusion moléculaire (équation 13 et 14).

$$\frac{\partial \beta}{\partial t} = -\frac{\partial(\beta v)}{\partial x_i} + \frac{\partial\left(\gamma(\nabla \beta)\right)}{\partial x_i} \quad (13)$$

$$\gamma = \alpha v \quad (14)$$

Avec :

- β la concentration en soluté ($g.m^{-3}$)
- x_i la distance selon la direction i (m)
- γ le coefficient de diffusion ($m^2.s^{-1}$)
- α la dispersivité (m)

Pour les eaux de surface, le transport est considéré comme purement advectif (due au déplacement de l'eau) et la dispersion est nulle (effet de l'hétérogénéité des vitesses négligé).

2.2.2.3.5. Dénitrification

Un module pour simuler la dénitrification dans le milieu poreux a été ajouté pour cette étude. Il est inspiré de la formulation proposée par Peyrard et al. (2011). Le module calcule un taux de dénitrification en fonction de la concentration en carbone organique dissous (COD) dans les eaux souterraines, de la teneur en carbone organique particulaire (COP) du milieu poreux, de la concentration en nitrates et de la teneur en eau.

Dans ce modèle les consommations de COD et de COP sont représentées par une cinétique d'ordre 1 (équations 15 et 16). Le taux de dénitrification est représenté par une cinétique de type Michaelis-Menten ou le taux maximum de consommation en nitrates dépend de la concentration en COD et COP et de la teneur en eau (équation 17).

$$R_{POC} = -K_{POC}[POC] \quad (15)$$

$$R_{DOC} = -K_{DOC}[DOC] \quad (16)$$

$$R_{NO3} = -0{,}8\left(\rho\frac{1-\varphi}{\varphi}K_{POC}[POC]\frac{10^6}{M_C} + K_{DOC}[DOC]\right).\frac{[NO3]}{K_{NO3}+[NO3]}.f_{H2O} \quad (17)$$

Avec :

- R_{POC} le taux de consommation de COP ($mg.g^{-1}.jour^{-1}$)
- K_{POC} la constante de dégradation du COP ($jour^{-1}$)
- R_{DOC} le taux de consommation de COD ($\mu M.jour^{-1}$)
- K_{DOC} la constante de dégradation du COD ($jour^{-1}$)
- R_{NO3} le taux de consommation de NO_3^- ($\mu M.jour^{-1}$)
- K_{NO3} la constante de demi-saturation en NO_3^- (μM)
- ρ la densité du milieu poreux ($kg.m^{-3}$)
- φ la porosité du milieu poreux (-)
- M_c la masse molaire du carbone ($12\ g.mol^{-1}$)
- f_{H2O} le facteur lié à la teneur en eau (-)

En conditions non saturées, la dénitrification est limitée par la teneur en eau dans la cellule considérée à travers le facteur f_{H2O} (équation 18) extrait du modèle RZWQM (Root Zone Water Quality Model ; Ahuja et al., 2000)

$$f_{H2O} = 0{,}000304\ \exp(8{,}15\ \theta_{rel}) \quad (18)$$

Avec :

- θ_{rel} l'humidité relative qui correspond au rapport θ/θ_s

Dans ce modèle, le COP est une propriété du milieu poreux et est immobile. Il représente le carbone organique présent dans les sols et disponibles pour le processus de dénitrification. Le COD quant à lui est présent dans l'eau et est transporté au sein des eaux de surface et du milieu poreux, mais également échangé entre ces deux domaines. Il représente le carbone organique apporté par les flux hydrologique et la rivière. Aussi, plus qu'une séparation au

niveau de la taille comme communément admis, dans le modèle utilisé ici, COD et COP représentent deux sources différentes de carbone organique. En effet le COP représentant le carbone organique présent dans les sols dans le modèle, peut en réalité se dissoudre au contact de l'eau et fournir du DOC qui sera utilisé par les micro-organismes.

2.2.2.4. Pas de temps

Le pas de temps utilisé par le modèle varie en permanence. Dans le milieu poreux, l'utilisateur indique la variation maximale de la quantité d'eau autorisée par cellule pour chaque itération. Ce nombre permet de stabiliser le modèle et d'assurer la convergence des calculs en limitant les changements brutaux entre deux itérations. Si la condition [variation du volume d'eau dans la cellule] < [variation de volume maximale autorisée] est remplie dans chaque cellule, le pas de temps augmentera lors de la prochaine itération. Au contraire, le pas de temps sera réduit jusqu'à assurer le respect de cette condition. Pour le calcul des écoulements de surface, le pas de temps est contrôlé par le nombre de Courant qui permet de faire évoluer le pas de temps en fonction de la vitesse d'écoulement (équation 19).

$$C = \frac{v\Delta t}{\Delta x} \qquad (19)$$

Avec :

- v la vitesse dans la direction x ($m.s^{-1}$)
- Δt le pas de temps (s)
- Δx le pas spatial (m)

Le pas de temps utilisé par le modèle lors de l'itération suivante est le plus petit entre celui calculé dans le milieu poreux et celui calculé pour les eaux de surface. Globalement, le pas de temps diminue lors de changement de conditions hydrologiques et augmente quand les conditions sont stables. Le pas de temps utilisé par le modèle varie généralement entre 1 et 5 secondes.

2.2.2.5. Conditions initiales et conditions aux limites

Pour chaque domaine, les conditions initiales et conditions aux limites doivent être renseignées (Table 2-4, Figure 2-10). Dans le milieu poreux les conditions aux limites peuvent être une hauteur d'eau imposée dans l'aquifère ou un gradient nul en ce qui concerne l'hydrologie, et une concentration imposée ou un gradient nul pour la concentration en soluté. Pour les eaux de surfaces, les conditions aux limites peuvent être une hauteur d'eau imposée ou un gradient nul en ce qui concerne l'hydrologie, et une concentration imposée ou un

gradient nul pour la concentration en soluté. De plus, pour les eaux de surface, il est possible d'imposer un débit à un endroit donné avec une concentration en solutés donnée. Cela peut permettre par exemple de simuler le débit d'une rivière.

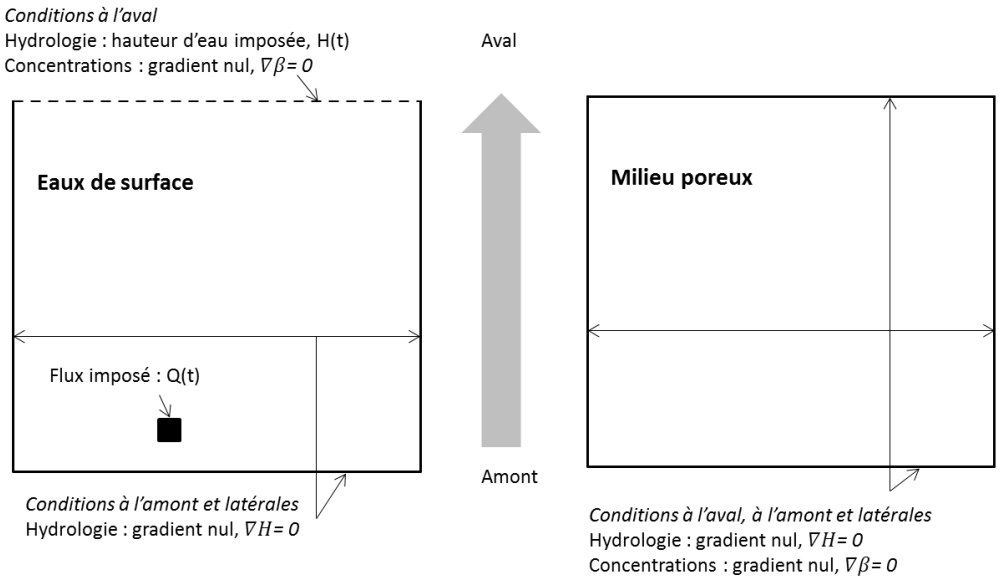

Figure 2-10 : Conditions aux limites pour les deux domaines (eaux de surface et milieu poreux)

Dans chaque domaine, les conditions initiales sont les hauteurs d'eaux et les concentrations en solutés. Ces valeurs correspondent la plupart du temps à des valeurs mesurées sur le terrain mais peuvent aussi être le résultat de simulations en conditions stationnaires (pour le niveau d'eau initial dans la rivière par exemple).

Table 2-4 : Récapitulatif des conditions initiales et des conditions aux limites possibles dans MOHID Land

Domaine	Conditions	Description
Milieux poreux	*Conditions initiales*	-Niveau d'eau dans l'aquifère -Concentration en soluté de l'aquifère
	Conditions aux limites	-Gradient nul ou valeur imposée (niveau de l'aquifère et concentration en soluté)
Ecoulement de surface	*Conditions initiales*	-Niveau d'eau en surface -Concentration en soluté
	Conditions aux limites	-Gradient nul ou valeur imposée (niveau de l'eau de surface concentration en soluté) -Débit imposé (à un endroit donné et à une concentration en élément donnée)

2.2.3. Application du modèle

MOHID Land étant un modèle à base physique, les paramètres qui contrôlent les processus simulés correspondent à des grandeurs physiques qui peuvent être mesurées. Dans cette étude le modèle est paramétré directement à partir de mesures ou de valeurs extraites de la littérature et ses performances sont ensuite évaluées. L'idée est de vérifier l'applicabilité du modèle dans

un contexte où la disponibilité des données servant à la calibrage et validation du modèle serait limitée. Pour ce faire, le modèle est utilisé à l'aide de données facilement disponibles dans un contexte de plaine alluviale, puis les performances du modèle sont évaluées grâce à un jeu de données important qui n'est pas disponible pour la majorité des sites ou le modèle pourrait potentiellement être appliqué. Les données nécessaires à la mise en œuvre du modèle ainsi que leurs sources sont détaillées dans la Table 2-5. Le jeu de données servant à la validation du modèle contient des chroniques mensuelles de niveau piézométrique et de concentrations en éléments dans 25 piézomètres ainsi que le suivi continu de la hauteur d'eau dans 5 piézomètres.

Table 2-5 : Récapitulatif des données nécessaires au fonctionnement de MOHID Land et de leurs sources

Domaine	Processus	Données nécessaires	Source
Général	Géométrie	*Modèle numérique de terrain (MNT)*	LiDAR - RGE ALTI (IGN)
		Géométrie de la couche inférieure	Forage et expertise locale
Milieux poreux	Hydrologie	*Paramètres de Van Genuchten-Mualem* (α, θ_s θ_r,*N,Ks*)	Texture du sol et fonction pédotransfert (Schaap et al., 2001)
	Transport de solutés	*Dispersivité horizontale/verticale* (α_h, α_v)	Extrait de la bibliographie (Peyrard et al., 2008)
	Dénitrification	*Paramètres de l'équation de dénitrification* (K_{POC}, K_{DOC}, K_{NO3}, ρ)	Extrait de la bibliographie (Sun et al., soumis.; Peyrard et al., 2011)
Eau de surface	Hydrologie	*Coefficient de manning (n)*	Extrait de la bibliographie (Chow et al., 1988)
		Débit (conditions aux limites)	Banque Hydro www.hydro.eaufrance.fr

Le modèle a été appliqué sur la période allant du 15/05/2013 au 1/10/2013. Cette période est intéressante d'un point de vue hydrologique car elle contient une crue décennale suivie par une période d'étiage. Compte-tenu de la complexité du modèle et du nombre important de cellules, le modèle est inadapté à des périodes de simulations plus longues car cela nécessiterait un temps de calculs très important (un mois simulé pour un jour de calcul). La mise en place du modèle sur le site d'étude est abordée plus en détail dans les chapitres 4 et 5.

2.2.4. Evaluation du modèle

L'évaluation des performances du modèles est réalisé par le calcul de plusieurs indicateurs qui comparent les i valeurs simulées par le modèles $X(i)_{sim}$ aux i valeurs observées $X(i)_{obs}$ correspondantes. Ces critères s'appliquent aussi bien pour les valeurs de charge hydraulique que pour des valeurs de concentrations en différents éléments. Les critères utilisés dans cette étude sont :

- le coefficient de détermination (R^2)

Le coefficient de détermination (R^2, équation 20) est une mesure qui se définit comme le ratio des écarts à la moyenne des valeurs simulées sur écarts à la moyenne des valeurs observées. Il varie entre 0 et 1 à mesure que la qualité du modèle augmente.

$$R^2 = \frac{\sum_{i=1}^{n}(X(i)_{sim} - \overline{X_{obs}})^2}{\sum_{i=1}^{n}(X(i)_{obs} - \overline{X_{obs}})^2} \quad (20)$$

- le coefficient de Nash (NS)

Le coefficient de Nash-Sutcliffe (N-S, Nash and Sutcliffe, 1970) est très utilisé en hydrologie pour évaluer la qualité des résultats d'un modèle (équation 21). Il varie entre -∞ et 1. Une valeur de 1 indique une parfaite concordance entre les valeurs modélisées et les valeurs observées alors que si la valeur est négative, cela signifie que la moyenne explique mieux les valeurs observées que les résultats du modèle.

$$NS = 1 - \frac{\sum_{i=1}^{n}(X(i)_{sim} - X(i)_{obs})^2}{\sum_{i=1}^{n}(X(i)_{obs} - \overline{X_{obs}})^2} \quad (21)$$

- le pourcentage de biais (PBIAS)

Le PBIAS (pour percentage bias en anglais) mesure la tendance moyenne des données simulées à être plus grande ou plus faible que les données observées (équation 22). La valeur optimale est 0 alors que des valeurs positives indiquent une surestimation par le modèle et les valeurs négatives une sous-estimation par le modèle.

$$PBIAS = 100\left(\frac{\sum_{i=1}^{n}(X(i)_{sim} - X(i)_{obs})}{\sum_{i=1}^{n}(X(i)_{obs})}\right) \quad (22)$$

- l'erreur quadratique moyenne (RMSE)

L'erreur quadratique moyenne (RMSE pour root mean square error en anglais) donne l'écart-type des différences entre les valeurs observées et simulées (équation 23). Plus la valeur est proche de zéro plus le modèle est performant.

$$RMSE = \sqrt{\frac{1}{N}\sum_{i=1}^{n}(X(i)_{sim} - X(i)_{obs})^2} \quad (23)$$

Chapitre 3 : Facteurs de contrôle de la variabilité spatio-temporelle de la dynamique des nitrates et de la dénitrification dans les eaux souterraines du site de Monbéqui

Ce chapitre a pour objectif l'identification des facteurs contrôlant la variabilité spatio-temporelle de la dynamique des nitrates et du processus de dénitrification dans la nappe alluviale de Monbéqui. Il est constitué d'un article publié dans le journal *Ecological Engieneering,* actuellement accepté sous révision, et intitulé « Spatio-temporal analysis of factors controlling nitrate dynamics and potential denitrification hot spots and hot moments in groundwater of an alluvial floodplain ». L'article est précédé d'un résumé en français et est suivi d'une synthèse qui replace les résultats obtenus dans le cadre de la thèse.

3.1.Résumé

La contamination en nitrates des eaux douces est un enjeu global. Dans les plaines alluviales, les zones ripariennes ont été identifiées comme efficaces pour la diminution de la pollution en nitrate. Dans cette étude, un jeu de données conséquent, collecté pendant un an à pas de temps mensuel dans un méandre de la Garonne (France), a été analysé afin de d'améliorer la compréhension de la dynamique des nitrates et du processus de dénitrification dans les plaines alluviales.

Les résultats ont montrés que la concentration en nitrates (50 mg-NO_3^-.L^{-1} en moyenne) est principalement contrôlée par les phénomènes de dilution des eaux souterraines par les eaux de surface (expliquant 54% de la variabilité des concentrations en nitrates), mais également par des processus biogéochimiques naturels reliés à la dénitrification (14% de la variabilité des concentrations en nitrates). La dilution est principalement contrôlée par le trajet des écoulements souterrains et le temps de résidence des eaux souterraines, en relation avec les échanges nappe- rivière. La dénitrification potentielle est principalement contrôlée par l'absence d'oxygène, de fortes concentrations en carbone organique dissous et une teneur importante en matière organique dans les sédiments (ces trois facteurs expliquant 31% de la variabilité de la dénitrification potentielle). Le carbone organique dissous (COD) peut provenir à la fois des apports direct de la rivière pendant les crues ainsi que de la dégradation de la matière organique (OM) *in situ*. La géomorphologie apparait comme un élément clé pour expliquer la localisation des *hots spots* de dénitrification. En effet, les zones où les berges sont les moins hautes correspondent à des zones humides où la dénitrification potentielle est plus forte qu'aux endroits où berges sont plus hautes. Finalement, l'hydrologie détermine l'apparition de *hots moments* qui apparaissent après les crues et dont l'intensité et reliée à l'intensité des crues. Ces résultats soulignent l'importance d'intégrer les interactions nappes rivières, la géomorphologie et les différentes sources de carbone organique (rivière et sédiment) pour comprendre la dynamique des nitrates et de la dénitrification dans les zones alluviales.

3.2. Spatio-temporal analysis of factors controlling nitrate dynamics and potential denitrification hot spots and hot moments in groundwater of an alluvial floodplain

Léonard Bernard-Jannin[1,2*], Xiaoling Sun[1,2], Samuel Teissier[1,2], Sabine Sauvage[1,2], José-Miguel Sánchez-Pérez[1,2*]

[1]*University of Toulouse; INPT, UPS; Laboratoire Ecologie Fonctionnelle et Environnement (EcoLab), Avenue de l'Agrobiopole, 31326 Castanet Tolosan Cedex, France*

[2]*CNRS, EcoLab, 31326 Castanet Tolosan Cedex, France*

[*]*Corresponding authors: Avenue de l'Agrobiopole, 31326 Castanet Tolosan Cedex, Franc; l.bernardjannin@gmail.com; jose-miguel.sanchez-perez@univ-tlse3.fr*

Abstract

Nitrate (NO_3^-) contamination of freshwater systems is a global concern. In alluvial floodplains, riparian areas have been proven to be efficient in nitrate removal. In this study, a large spatio-temporal dataset collected during one year at monthly time step within a meander area of the Garonne floodplain (France) was analysed in order to improve the understanding of nitrate dynamic and denitrification process in floodplain areas. The results showed that groundwater NO_3^- concentrations (average of 50 mg NO_3^- L^{-1}) were primarily controlled by groundwater dilution with river water (explaining 54% of NO_3^- variance) but also by nitrate removal process identified as denitrification (explaining 14% of NO_3^- variance). Dilution was controlled by hydrological flow paths and residence time linked to river-aquifer exchanges and flood occurrence, while potential denitrification (DEA) was controlled by oxygen, high dissolved organic carbon (DOC) and organic matter content in the sediment (31% of DEA variance). DOC can originate both from the river input and the degradation of organic matter (OM) located in topsoil and sediments of the alluvial plain. In addition, river bank geomorphology appeared to be a key element to explain potential denitrification hot spots location. Low bankfull height (LBH) areas corresponding to wetlands area exhibited higher denitrification rates than high bankfull height (HBH) areas less often flooded. Hydrology determined the timing of denitrification hot moments occurring after flood events. These findings underline the importance of integrating dynamic water interaction between river and aquifer, geomorphology, and dual carbon source (river and sediment) when assessing nitrate dynamics and denitrification patterns in floodplain environments.

Keyword: groundwater, denitrification, nitrate, wetland, floodplain

3.2.1. Introduction

Nitrate contamination of groundwater through point source and diffuse pollution has long attracted world-wide attention (Power and Schepers, 1989; Bijay-Singh et al., 1995; Zhang et al., 1996; Arrate et al., 1997; Carpenter et al., 1998; Jégo et al., 2012). Nitrate pollution from agricultural sources is considered to be the main cause of groundwater degradation in the European Union (Sutton et al., 2011). In Europe and North America, up to 90% of floodplain areas are cultivated (Tockner and Stanford, 2002). Agricultural land use, in combination with factors such as shallow groundwater, high permeability of alluvial deposits and interconnections with surface water, make alluvial aquifers particularly vulnerable to nitrate diffuse pollution (Arauzo et al., 2011). As a result, nitrate concentrations exceeding the limit of 50 mg–NO_3^- L^{-1} set for groundwater systems in Europe by the Nitrate Directive (91/676/EEC) and the Groundwater Directive (2006/118/EEC) have been reported for several shallow aquifers in floodplain areas (Baillieux et al., 2014; Sánchez-Pérez et al., 2003).

Floodplain environments are characterised by strong surface water-groundwater interactions that are important for aquifer water composition (Amoros et al., 2002; Sun et al., 2015). Nitrate contamination in shallow aquifers can therefore be mitigated by the dilution resulting from mixing with river water containing low nitrate concentrations (Pinay et al., 1998; Baillieux et al., 2014). Nitrate mass removal also occurs through natural biogeochemical processes such as plant uptake, denitrification, dissimilatory nitrate reduction to ammonium and microbial immobilisation, among which denitrification is reported to be the most important in groundwater (Korom, 1992; Burt et al., 1999; Rivett et al., 2008).

Denitrification is the anaerobic reduction of nitrate (NO_3^-) into gaseous compounds (nitrous oxide or dinitrogen) by microorganisms. Denitrification in groundwater is linked to: (i) presence of nitrate, denitrifying bacteria and organic carbon (OC) as electron donor, (ii) anaerobic conditions and (iii) favourable environmental conditions in terms of e.g. temperature and pH (Rivett et al., 2008). However, among all these factors, availability of OC has been identified as the major limiting factor in nitrate-contaminated groundwater (see Rivett et al. (2008) for a review).

Riparian zones are located at the interface between aquatic and terrestrial environments (Vidon et al., 2010). In these areas, where surface water rich in organic matter (OM) meets groundwater containing abundant nutrients, denitrification is promoted (Hill et al., 2000; Sánchez-Pérez et al., 2003). Therefore riparian areas have been shown to be efficient in nitrate

pollution mitigation (Vidon and Hill, 2006; Dosskey et al., 2010; Naiman et al., 2010). In these systems, the hydrological exchanges at the river/groundwater interface can have a significant impact on denitrification rates in the aquifer (Baker and Vervier, 2004, Lamontagne et al., 2005). Such exchanges recharge aquifer with river water rich in OM, stimulating denitrification in groundwater (Iribar, 2007; Sánchez-Pérez et al., 2003). The location of the denitrification process is driven by advective flux, where flow paths lead organic matter and nitrate to meet (Seitzinger et al., 2006), at points defined as hot spots by McClain et al. (2003). At the scale of the floodplain section, denitrification is usually triggered by NO_3^- input from upland areas and hot spots can be located at the interface between the upland and riparian zones, between the riparian zone and the stream or within the riparian zone (McClain et al., 2003). At this scale, the efficiency of the riparian area in nitrate removal is reported to be related to hydrogeomorphic characteristics associated with geological and hydrological settings (Groffman et al., 2009), such as water residence time (Seitzinger et al., 2006). In addition, the occurrence of hot spots may vary in time, especially in environments with strong temporal variations in hydrological conditions. For example, denitrification rates have been found to be higher in high flow conditions (Baker and Vervier, 2004; Iribar, 2007; Peter et al., 2011), within periods corresponding to hot moments (McClain et al., 2003). Therefore, studies on denitrification processes need to take into account both spatial and temporal scale with suitable resolution in order to accurately describe the processes at stake and their impact on nitrate dynamics.

The main objective of this study was to examine the occurrence of potential denitrification hot spots and hot moments and their relationship to environmental conditions, in order to improve knowledge on nitrate dynamics in floodplains. Based on a high spatial resolution dataset collected during 12 monthly sampling campaigns , we: (i) identified the factors best explaining nitrate concentrations variations and explored their spatio-temporal patterns; (ii) identified the factors best explaining potential denitrification rates measured in aquifer sediment samples; and (iii) analysed the occurrence of denitrification hot spots/hot moments according to the controlling factors in order to develop a conceptual diagram of denitrification process in floodplain environments.

3.2.2. Materials and methods

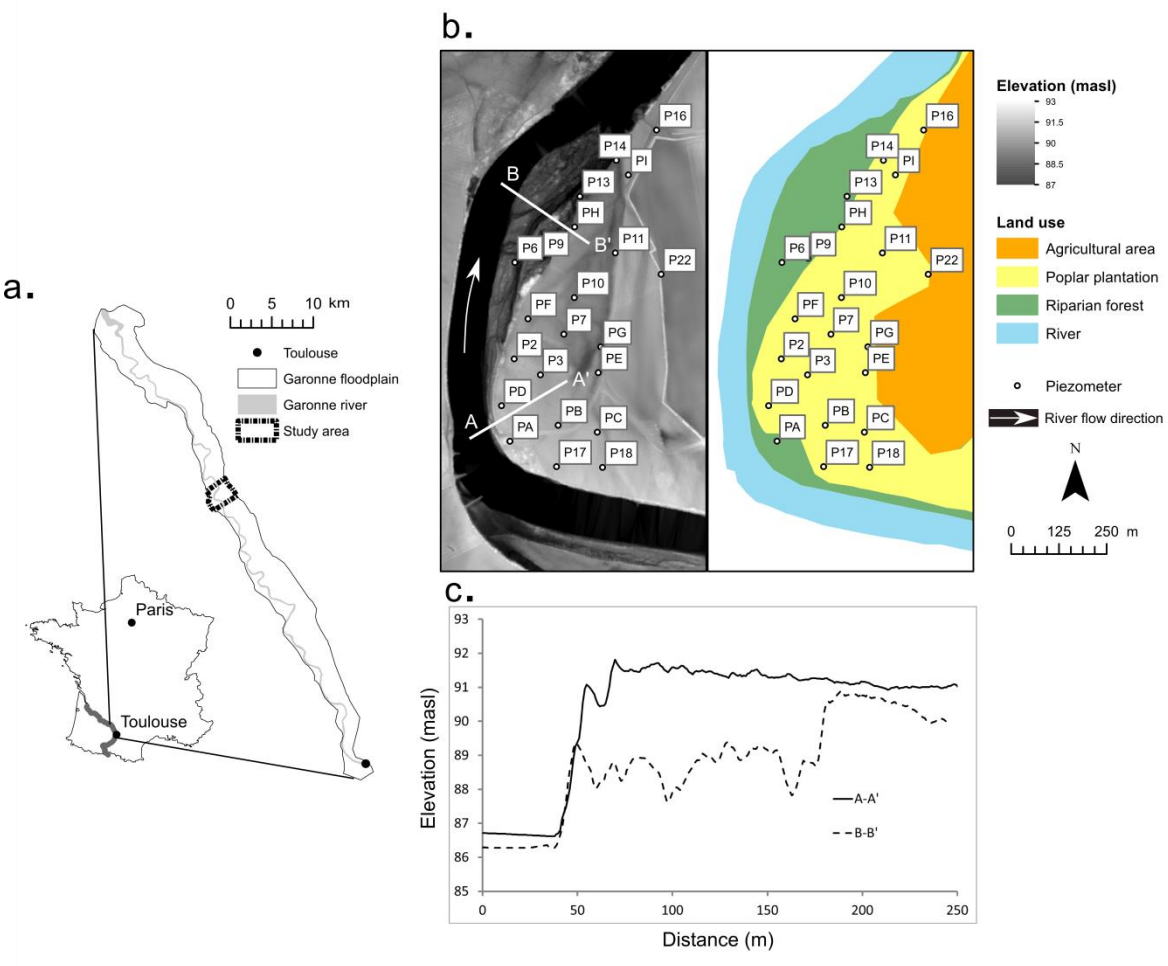

Figure 3-1: a) geographical location; b) digital terrain elevation and land use map of the study area, showing the network of piezometers (PA-P22) used in the present study and c) vertical profiles at two locations (A-A' and B-B')

3.2.2.1. Study site

The study area, which covers about 50 ha, is located within a 2 km long meander in the middle section of the Garonne river watershed, close to the village of Monbéqui in south-west France (Figure 3-1). Mean annual precipitation in the area is 660 mm. The drainage area of the Garonne watershed at the study site is about 13 730 km^2, with annual average flow of 190 $m^3\ s^{-1}$ and a range from 98 $m^3\ s^{-1}$ (1989) to 315 $m^3\ s^{-1}$ (1978) over the past 41 years. The driest month is August, with 76 $m^3\ s^{-1}$ on average, and the wettest is May, with 343 $m^3\ s^{-1}$ on average. The daily flow is highly variable, ranging from 10 $m^3\ s^{-1}$ during the severe drought in August 1991 to 2930 $m^3\ s^{-1}$ during the largest flood event recorded, on 6 November 2000 (www.hydro.eaufrance.fr). The two-year return period flood corresponds to daily flow of 1400 $m^3\ s^{-1}$. The floodplain comprises 4-7 m of quaternary sand and gravel deposits (mean saturated hydraulic conductivity 10^{-3} m s^{-1}), overlying impermeable molassic bedrock. In this area the Garonne River fully penetrates the alluvial formation, so that the riverbed lies on the

impermeable substratum. The alluvial deposits are covered with a silty soil layer 1-2 m deep and containing 1.5% OM on average (Jégo et al., 2012). The connection between aquifer and the Garonne river is strongly influenced by hydrological conditions (Sun et al., 2015). The floodplain is heavily cultivated (irrigated maize, sunflower, sorghum, wheat), leading to major nitrate influx into the groundwater. Concentrations of 100 mg-NO_3^- L^{-1} are common (Sánchez-Pérez et al., 2003). A small area of riparian forest, mainly composed of willow (*Salix alba*) and ash trees (*Fraxinus excelsior*), is located close to the river at a lower elevation than the rest of the study area, and is separated from the agricultural fields by plantations of poplar (*Populus alba*) (Figure 3-1). The geomorphology of the river bank on the right side of the river can be separated into two types: Low bankfull height type (LBH) corresponding to the profile A-A' (Figure 3-1), which is regularly flooded as the groundwater level is often close to the surface and can be designated as permanent wetland; and high bankfull height type (HBH), corresponding to the profile B-B', which is only flooded during the highest floods (greater than two-year return period flood events). Three piezometers (P6, P9 and P13) are located within a LBH area.

Previous studies carried out on this area have demonstrated the role of DOC borne by the river into the aquifer in denitrification (Sánchez-Pérez et al., 2003) and the importance of the sediment-attached bacterial community for aquifer denitrification (Iribar et al., 2008). In addition, modelling studies have shown the importance of river-aquifer exchanges for groundwater composition (Weng et al., 2003; Peyrard et al., 2008; Sun et al., 2015) and the impact of agricultural practices on nitrate leaching into the shallow aquifer (Jégo et al., 2012).

3.2.2.2. Sampling

A network of 22 piezometers (internal diameter 51 mm, with 1 mm slots) was installed throughout the study site between the Garonne river and the agricultural fields (Fig. 1). Water samples were collected within each piezometer during monthly sampling campaigns from April 2013 to March 2014, providing a high-spatial resolution dataset with around 50-100 m between sampling points. In four of these campaigns, called full campaigns, additional sediment sampling was performed (Figure 3-2).

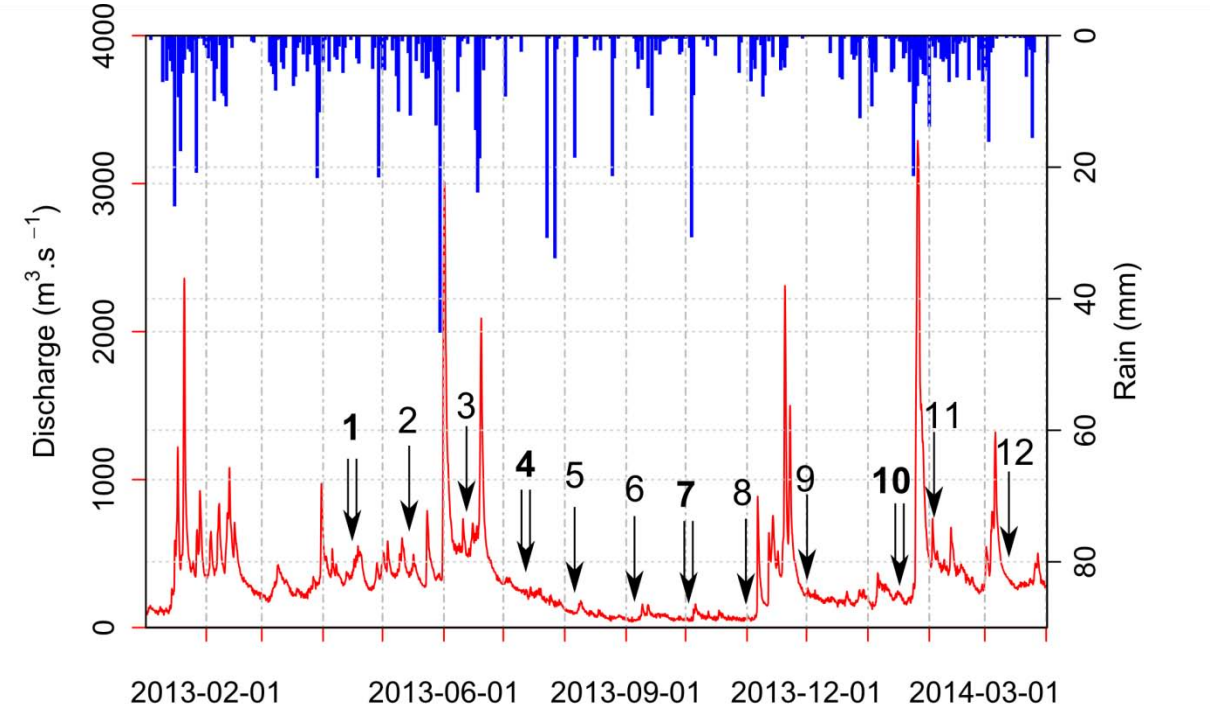

Figure 3-2: Water discharge (red) and rain (blue) in the study area. Arrows and numbers indicate sampling periods (simple arrows for regular sampling campaigns and double arrows with bold numbers for full campaigns).

After measuring water table depth (WD), as the distance between soil surface and water table surface, water was pumped with a thermal motor pump and physico-chemical parameters in water were measured once electrical conductivity (EC) has stabilized (Sánchez-Pérez, 1992). Dissolved oxygen (DO), temperature (T), pH and EC were measured using a portable meter (WTW Multi 3420) and specific probes. Water samples were then filtered through 0.45 µm cellulose acetate membrane filters. Anion concentrations, i.e. nitrate (NO_3^-), chloride (Cl^-), sulphate (SO_4^{2-}) and phosphate (PO_4^{3-}), and cation concentrations, i.e. calcium (Ca^{2+}), magnesium (Mg^{2+}), potassium (K^+), sodium (Na^+) and ammonium (NH_4^+), were determined by ion chromatography (Dionex ICS-5000$^+$ and DX-120). Silica concentration was determined by spectrophotocolorimetry (Alpkem) and alkalinity (Alk) by acid titration. Water samples collected for determination of DOC concentration were filtered through rinsed 0.45-µm cellulose acetate membrane filters, stored in carbon-free glass tubes, acidified with HCl and combusted using a platinum catalyser (Shimadzu, Model TOC 5000) at 650°C. For the four full campaigns, sediment was sampled after water sampling by increasing the pumping velocity for 5-10 minutes, with the water flowing into a 50-L tank where sediments settled before being collected together with 100 mL water in sealed sterile bags. In the river, *in situ*

physico-chemical measurements (DO, T and pH) were made and water was sampled directly within the stream. All the samples were immediately stored at 4°C after collection.

Oxygen isotope composition was measured by isotope ratio mass spectrometry after CO_2-H_2O equilibration using the technique described by Epstein and Mayeda (1953). The results were expressed relative to a standard (V-SMOW, Gonfiantini, 1978) using delta notation (δ), where $\delta^{18}O$ is given by :

$$\delta^{18}\mathrm{O} = \frac{\mathrm{R}^{18}O_{sample} - R^{18}O_{V-SMOW}}{R^{18}O_{V-SMOW}}$$

where $R^{18}O_{sample}$ and $R^{18}O_{V\text{-}SMOW}$ are the $^{18}O/^{16}O$ ratios for the sample and V-SMOW, respectively. As the difference between samples and standard is small, the 'δ-value' is usually expressed in parts per 1000 [‰].

*3.2.2.3. D*enitrifying enzyme activity (DEA)

Assessments of denitrifying enzyme activity (DEA) were conducted in the laboratory within the week following the sediment samples collection. Each sediment sample was analysed in triplicate. A 25 mL portion of wet sediment and 50 mL deoxygenated milliQ water containing KNO_3^- and sodium acetate, to give final concentrations of 100 mg-N L^{-1} and 50 mg-C L^{-1}, respectively, were added to a gas-tight 150-mL serum bottle. After complete deoxygenation (N_2 sparging), inhibition of N_2O reductases was achieved by injecting 15 mL C_2H_2. Incubations were performed in the dark at 14°C, corresponding to the average measured temperature of the groundwater in the study area. Atmospheric pressure in the serum bottles was ensured during incubation (removal of gas phase before C_2H_2 addition and addition of N_2 to compensated samples). Gas samples were taken from the gas phase of the serum bottles after vigorous shaking, at 30 min and 6 h 30 min after C_2H_2 injection. N_2O was determined by injection into a Varian CP 3800 gas chromatograph fitted with an electron capture detector. Calculations were performed with N_2O solubility coefficients taken from Weiss and Price (1980). The DEA results were expressed in µg of N per g of dry sediment per hour [µg-N $g\text{-}sed^{-1}$ h^{-1}] by averaging the rates of N_2O production for the triplicate samples. DEA represents the maximum rate of denitrification that can occur when C and N are freely available and was used in this study as a proxy for the denitrification capacity of the different sampling locations at the sampling times.

After incubation, each sediment sample was dried (105°C, 24 h) and combusted (550°C, 4 h) in order to determine sediment OM content, which was expressed as a percentage of dry sediment weight.

3.2.2.4. Bacterial richness

DNA was extracted after centrifugation of the sediment samples and PCR amplification of 16S rRNA genes was performed. Electrophoresis was used to produce T-RFLP profiles. Bacterial richness (BR) corresponded to the number of T-RF (corresponding to peaks on the T-RFLP pattern and defined hereafter as OTU, Operational Taxonomic Unit) per sample. Presence–absence data was used in our analyses. Details of the method can be found in Yao et al. (this issue).

3.2.2.5. Data analysis

Data treatment involved 20 parameters, including a descriptor of the hydrological condition (WD), physico-chemical parameters of the groundwater samples (DO, T, pH, DOC, Alk, SiO_2, NO_3^-, Cl^-, SO_4^{2-}, PO_4^{3-}, Ca^{2+}, Mg^{2+}, K^+, Na^+, NH_4^+, $\delta^{18}O$), biological parameters (BR and DEA) and a sediment-related parameter (OM). EC was used to ensure the stability of water characteristics during the sampling, but it was not used in data analysis as it was already represented through the major ions concentration data. Variables were transformed to ensure normality of their distribution when necessary. Partial least squares regression (PLSR) which is a very suitable method for ecological studies analysing a large array of related predictors (Carrascal et al., 2009), was performed here to relate NO_3^- and DEA to the others environmental factors. PLSR is a technique that combines features from principal component analysis and multiple regression to analysed the effects of linear combinations of several predictors X on a response variable Y. Associations are established with latent factors defined as linear combinations of predictor variables that maximize the explained variance of the dependent variable (Carrascal et al., 2009; Abdi, 2010). One of the interesting features of PLSR is that the relationships between the predictors and the response function can be inferred from the weights and regression coefficients of individual predictors in the most explanatory components (Yan et al., 2013). Leave-one-out (LOO) cross validation was performed to select the number of components and jack-knife estimation was used to test the signification of the coefficients (Mevik and Wehrens, 2007). For each PLSR, the percentage of variance explained for the response variable and the cross validated root mean square error (RMSECV) were calculated. After the pre-analysis of the data, NH_4^+ and PO_4^{3-} were not

selected for the statistical method because their concentrations were very low and below the limit of detection for more than, respectively, 25% and 66% of the measurements. PLSR was performed on the 14 parameters available for the 12 campaigns for NO_3^- (WD, DO, T, pH, DOC, Alk, SiO_2, Cl^-, SO_4^{2-}, Ca^{2+}, Mg^{2+}, K^+, Na^+, $\delta^{18}O$) and on the 17 parameters available for the four full campaigns for DEA (WD, DO, T, pH, DOC, Alk, NO_3^-, SiO_2, Cl^-, SO_4^{2-}, Ca^{2+}, Mg^{2+}, K^+, Na^+, $\delta^{18}O$, OM, BR). All statistical analyses were performed using R 3.1.1 software (R Core Team, 2012).

Interpolation of groundwater level, NO_3^-, DEA, DOC, OM, DO and PLSR components score values to produce maps was performed using the Inverse Distance Weight (IDW) method implemented on ArcGis 10.0 (ESRI, 2011).

3.2.3. Results

3.2.3.1. Hydrology of the study area

In all the sampling campaigns, the groundwater levels indicated groundwater flow from the alluvial plain to the river. Groundwater level for the four full sampling campaigns is shown in Fig. 3. In campaigns 1 and 10, which took place more than 50 days after the last peak flow (Q>1400 m^3 s^{-1}) and in relatively high flow conditions, the hydraulic gradient was smaller than for the other two full campaigns. Campaign 4 took place a few days after the largest flood recorded during the study period and the hydraulic gradient was the highest observed. Campaign 7 took place during a low water period, a few months after the same large flood before campaign 4 and the hydraulic gradient was lower (Figure 3-3, Table 3-1).

Table 3-1: Hydrological characteristics of the study area during the four full sampling campaigns

Campaign	Discharge [m^3 s^{-1}]	Time from last peak flow (Q>1400 m^3 s^{-1}) [days]	Sampling date
1	337	79	8-10 April 2013
4	314	13	1-3 July 2013
7	53	104	30 Sept-2 Oct 2013
10	209	54	13-15 Jan 2014

For all four campaigns the main water flow direction was from the centre of the meander to the north-west. However, some water flow to the west and south-west of the meander was detected in campaigns 4, 7 and 10 (Figure 3-3). Overall, the hydraulic gradient ranged from 1‰ to 6‰, which represents water flow velocities ranging from 0.09 to 0.52 m day^{-1}, considering a saturated hydraulic conductivity of 10^{-3} m s^{-1}. Depending on the location, the residence time of the water flowing from the agricultural field to the river was estimated to

vary from 100 days in the north of the meander (location A, Figure 3-3) to 3000 days in the south of the meander (location B, Figure 3-3).

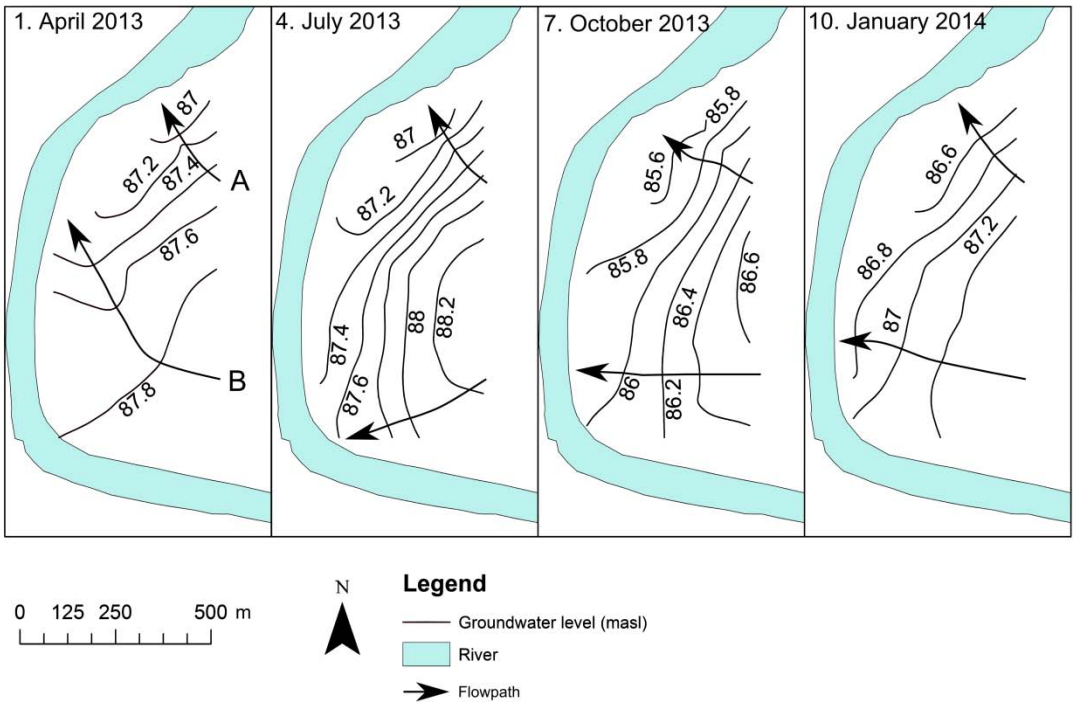

Figure 3-3: Groundwater level in the study area and groundwater flowpaths from two locations in the meander (one in the north, A, and one in the south, B) observed in the four full campaigns (1, 4, 7, and 10).

3.2.3.2. Biogeochemical characteristics of the study area

Mean values of the 20 parameters recorded during the 12 campaigns (four full campaigns for BR, DEA and OM) in the 22 piezometers and average river characteristics are summarised in Table 3-2. The average WD was typical of a shallow aquifer, 3.19 m on average, and ranged from 5.67 m to almost at the surface (0.16 m). Nitrate concentrations showed great variation, from 0.6 to 139 mg L^{-1} (coefficient of variation (CV) 73%). The Ca^{2+}, SO_4^{2-} and Cl^- concentrations were relatively high (>50 mg L^{-1} on average). The average NH_4^+ and PO_4^{3-} concentration were rather low (<0.1 mg L^{-1}), but on occasion reached higher concentrations. Biological and sediment-related parameters also exhibited strong variability. DEA values varied by several orders of magnitudes (2.42 x 10^{-4} to 1.83 x 10^{-1} µg-N g-sed^{-1} h^{-1}, CV=169%). Bacterial richness and OM were also very variable (CV 49% and 31%, respectively), while T, pH and $\delta^{18}O$ were the parameters with the smallest variability. Overall, DO, NO_3^-, DEA, PO_4^{3-} and NH_4^+ were the most variable parameters.

Table 3-2: Characteristic of the 20 parameters measured in the piezometers: Mean value, standard deviation (SD) minimum (Min), maximum (Max) and coefficient of variation (CV). Mean values for the parameters measured in the river are also presented (River mean). n indicates the number of campaign for which the parameter is available.

	Mean	SD	Min	Max	CV	River Mean	n
WD [m]	3.19	1.20	0.16	5.67	38%	-	12
DO [mg L^{-1}]	3.45	2.44	0.06	9.69	71%	10.6	12
T [°C]	13.72	1.12	10.70	16.00	8%	13.27	12
pH [-]	6.92	0.18	6.40	7.88	2%	7.92	12
DOC [mg L^{-1}]	1.03	0.65	0.26	4.87	63%	1.65	12
Alk [mg L^{-1}]	6.26	1.16	2.80	9.90	19%	2.26	12
NO_3^- [mg L^{-1}]	49.57	36.29	0.60	139.40	73%	8.06	12
Cl^- [mg L^{-1}]	53.77	29.62	7.57	196.63	55%	9.11	12
SO_4^{2-} [mg L^{-1}]	73.60	35.82	5.70	283.10	49%	19.96	12
SiO_2 [mg L^{-1}]	11.79	3.17	4.10	26.70	27%	4.90	12
Ca^{2+} [mg L^{-1}]	132.89	42.12	32.60	231.47	32%	48.66	12
Mg^{2+} [mg L^{-1}]	19.99	7.31	5.00	37.10	37%	4.93	12
K^+ [mg L^{-1}]	2.52	0.99	0.77	6.02	39%	1.50	12
Na^+ [mg L^{-1}]	24.84	10.32	7.40	65.00	42%	8.06	12
NH_4^+ [mg L^{-1}]	0.07	0.28	<d	2.78	368%	0.05	12
PO_4^{3-} [mg L^{-1}]	0.02	0.07	<d	1.16	352%	0.03	12
$\delta^{18}O$ [‰]	-8.88	1.02	-11.54	-5.62	12%	-10.81	12
BR [number of OTU]	13.15	6.50	2.00	36.00	49%	-	4
DEA [µg-N g-sed^{-1} h^{-1}]	2.15E-02	3.63E-02	2.42E-04	1.83E-01	169%	-	4
OM [%]	0.55	0.17	0.16	1.05	31%	-	4

3.2.3.3. Nitrate dynamic in the floodplain

Nitrate concentration maps showed a clear difference in concentration between north and south of the meander, with the north being highly concentrated and the south showing lower nitrate concentrations (Figure 3-4). However, the NO_3^- concentrations were lower in P6 and P13, both located in the low riparian area than in the north-west part of the meander, close to the agricultural fields, in full sampling campaigns 1, 4 and 10. On a temporal scale, NO_3^- were higher in campaign 7, after a long low water period. In addition, for this campaign, some points located close to the agricultural fields exhibit high nitrate concentrations (PG, PE, PC).

Table 3-3: Summary of the PLSR analysis on NO_3^-. RMSECV is the root mean square error of the cross validation.

Component	Cumulative % of explained variability in NO_3^-	% of explained variability in NO_3^-	RMSECV
1	56.44	56.44	0.668
2	70.82	14.38	0.545
3	72.65	1.83	0.543
4	74.19	1.54	0.537
5	75.90	1.71	0.525

The factors explaining the NO_3^- variations within the study area were investigated with a PLSR analysis (Table 3-3). The two first components were selected which explained respectively 56% and 14% of the variance of NO_3^- . The next component only added 2% of the explained variance and the decrease in RMSECV when using 3 components was relatively low compared to the RMSEC obtained with 2 components (<1%).

Table 3-4 : Results of the PLSR on NO_3^- with 14 predictors available for the 12 sampling campaigns. p-values are based on jack-knife estimate. W1 and W2 are the loadings weight of each predictor on components 1 and 2 (values greater than 0.3 are bolded and values lower than 0.1 are not shown).

	Estimate	p value	W1	W2
Mg^{2+}	0.16	<2.20E-16	**0.402**	
$\delta^{18}O$	0.25	<2.20E-16	**0.418**	0.288
Cl^-	0.16	<2.20E-16	**0.398**	
DO	0.23	1.91E-15	0.272	**0.458**
DOC	-0.15	4.27E-14	-0.113	**-0.407**
Na^+	0.06	6.72E-06	**0.304**	-0.268
K^+	0.10	9.66E-06	0.29	
T	0.10	4.20E-05	0.158	0.113
Alk	-0.09	1.94E-05		**-0.427**
SiO_2	0.09	1.02E-04	0.253	
SO_4^{2-}	0.05	3.95E-03	0.292	-0.257
pH	0.08	6.24E-03		**0.382**
Ca^{2+}	0.06	0.0129	0.248	-0.174
WD	0.03	0.134		0.146

Overall, the most significant predictor ($p<0.001$) were Mg^{2+}, $\delta^{18}O$, Cl^-, DO, DOC, Na^+, K^+, T, Alk and SiO_2, in decreasing order (Table 3-4). The less significant and only parameter with $p>0.1$ is WD. The correlation was positive between NO_3^- and the regression coefficients of all the variables but DOC and Alk. The most important predictors contributing to for the 1st component were Mg^{2+}, $\delta^{18}O$, Cl^- and Na^+ that accounted for 59% of the 1st component composition. SO_4^{2-} and K^+ were also important and when considering these variables, the

contribution to component 1 rose to 76%. All these variables had a positive weight on the 1st component. Considering the 2nd component, the most important variables contributing to the component were DO and pH (positive contribution) and DOC and Alk (negative contribution). These four variables contributed for 70% of the 2nd component. This value rose to 92% when adding $\delta^{18}O$ (positive contribution) and Na^+ and SO_4^{2-} (negative contribution).

The score of each component was positively correlated with NO_3^- and was calculated for each piezometer and for each campaign. The resulting interpolated maps for the four full campaigns are shown in Figure 3-4. Component 1 exhibited spatial differences between the north and the south of the meander, being higher in the north than in the south. In addition the 1st component scores were higher in summer after the drying stage phase (campaign 7) and the extent of the north area with high values was greater than for the other campaigns.

The 2nd component also displayed spatial differences but for this component, it is the north-west zone of the meander which had lower scores than the remaining area except for the campaign 7. For this campaign, the 2nd component had lower scores in the east and for two isolated piezometers in the south. Overall, the component score is lower after the large flood (campaign 4) than for the other sampling campaigns.

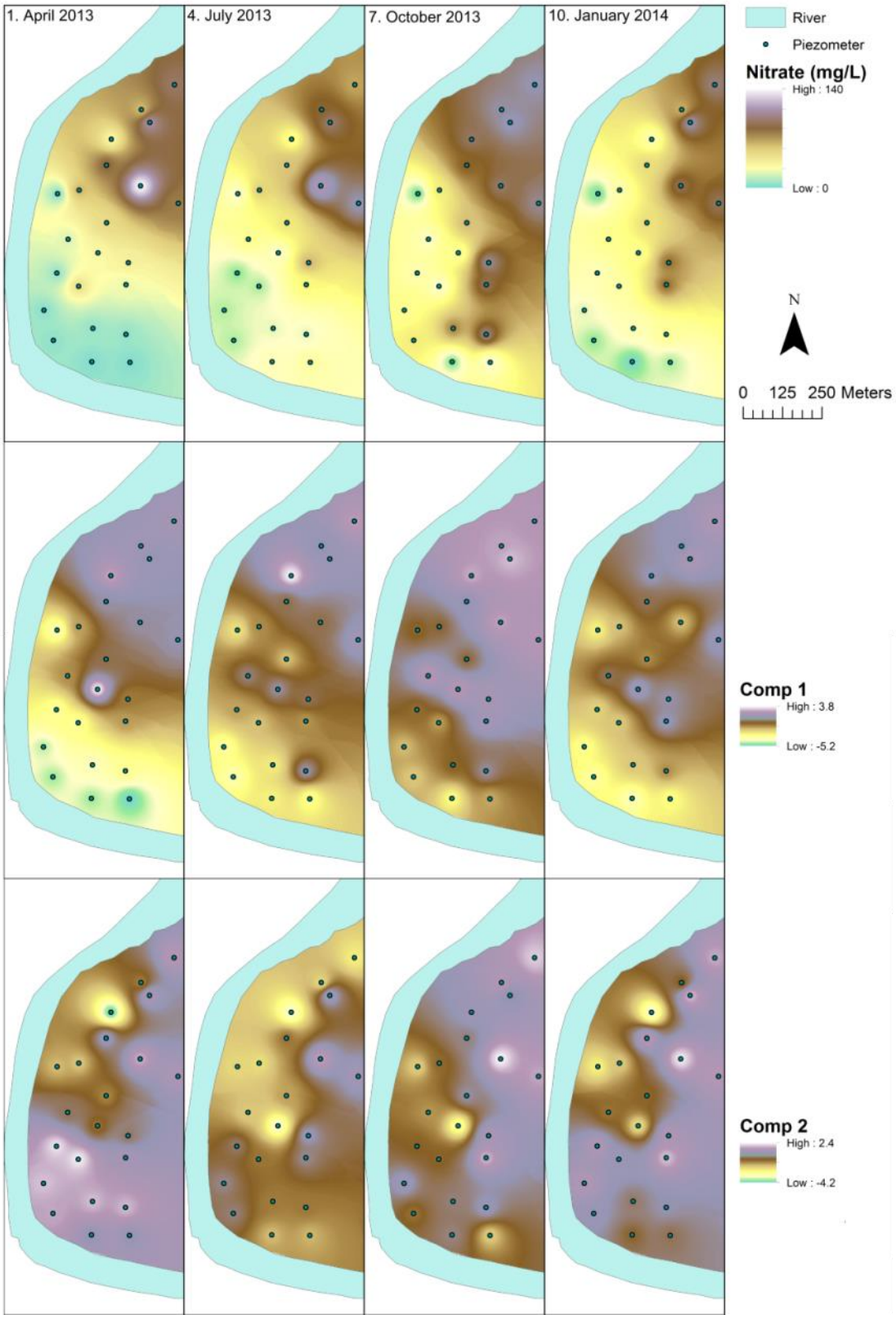

Figure 3-4: Maps of interpolated (IDW) nitrate concentrations and of the scores of the 1st (comp1) and 2nd components (comp2) of the PLSR performed on NO_3^- for the four full sampling campaigns.

3.2.3.4. Localisation and factor controlling DEA hot spots and hot moments

The spatial heterogeneity of DEA is clearly apparent from the maps in Figure 3-5. High DEA values greater than 0.1 µg-N g-sed^{-1} h^{-1} (corresponding to DEA hot spots) were observed in the LBH area (P6, P9 and P13) in campaigns 1, 4 and 7. In addition, relatively high values (greater than 0.05 µg-N g-sed^{-1} h^{-1}) were observed in the piezometers close to the river in campaign 4 (P3, P10, P14, P17, PD). In campaign 7, DEA remained high in piezometers located in the LBH area (especially P6 and P9). Finally, DEA appeared to be lower during campaign 10 and only P3 had a DEA greater than 0.05 µg-N g-sed^{-1} h^{-1}.

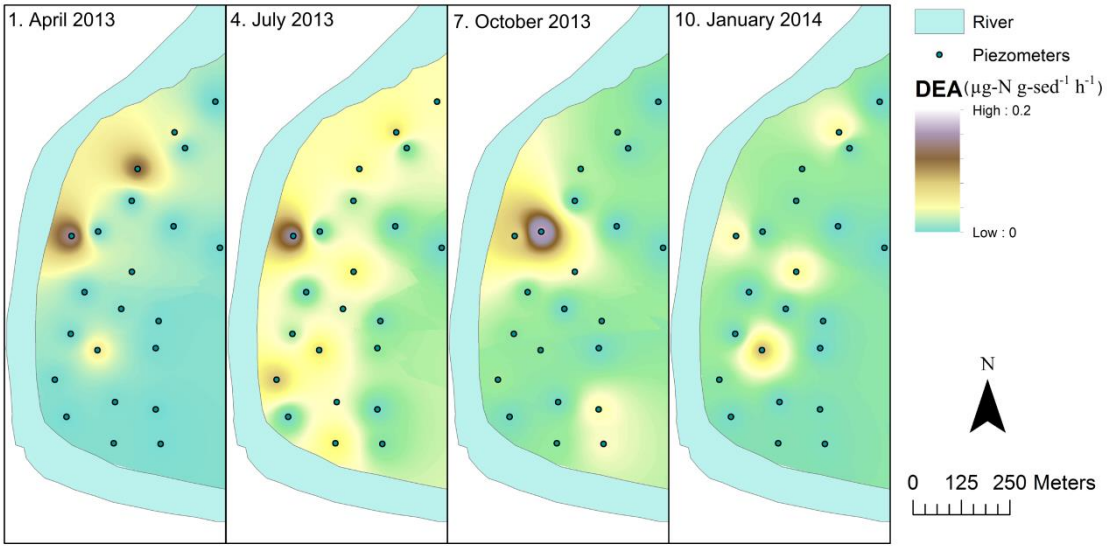

Figure 3-5: Maps of interpolated (IDW) denitrifying enzyme activity (DEA) for the four full campaigns.

Table 3-5: Summary of the PLSR analysis on DEA. RMSECV is the root mean square error of the cross validation

Component	Cumulative % of explained variability in DEA	% of explained variability in DEA	RMSECV
1	41.32	41.32	0.831
2	45.00	3.68	0.807
3	47.00	2.00	0.826
4	48.06	1.06	0.837
5	48.88	0.82	0.872

Table 3-6 : Results of the PLSR on DEA with 17 predictors available for the 4 full sampling campaigns. p-values are based on jack-knife estimate. W1 are the loadings weight of each predictor on component 1 (values greater than 0.3 are bolded and values lower than 0.1 are not shown).

	Estimate	p value	W1
DOC	0.20	2.33E-06	**0.494**
DO	-0.20	5.30E-06	**-0.493**
OM	0.20	2.13E-04	**0.489**
Alk	0.10	2.52E-03	0.246
NO_3^-	-0.11	0.018	-0.264
K^+	-0.11	0.036	-0.275
Ca^{2+}	0.06	0.19	0.148
$\delta^{18}O$	-0.05	0.29	-0.119
WD	-0.04	0.35	
Mg^{2+}	-0.04	0.41	
T	-0.03	0.50	
BR	0.03	0.59	
Na^+	0.02	0.67	
SiO_2	0.01	0.79	
Cl^-	-0.01	0.85	
SO_4^{2-}	0.01	0.86	
pH	0.00	0.91	

The factors explaining the DEA variations within the study area were investigated with a PLSR analysis. Only the first component was selected and explained 41% of DEA variance (Table 3-5). The next component only added 4% of the explained variance and the decrease in RMSECV when using 2 components was relatively low compared to the RMSEC calculated with 1 component (<4%).

The most significant predictors ($p<0.001$) were DOC, DO, and OM, in decreasing order (Table 3-6). DOC and OM were positively correlated with DEA while DO was negatively correlated with DEA. These three parameters contributed to 76% of the composition of the first components. Other parameters relatively important to explain DEA variance ($p<0.05$) were Alk (positive correlation), NO_3^- and K^+ (negative correlation).Parameters like WD, Mg^{2+},T, BR, Na^+, SiO_2, Cl^-, SO_4^{2-} and pH were the less important (weight<0.1).

3.2.3.5. DOC and OM dynamic in the floodplain

As OC is a key element for denitrification process, the variability in DOC and OM at the study site was investigated. The DOC maps showed strong temporal variations between sampling campaigns (Figure 3-6). The DOC concentrations were the over the entire meander in campaign 4, corresponding to the period after the largest flood event recorded during the

study period. Spatially, DOC concentrations were rather homogeneous over the meander except for one piezometer where values are higher (P13).

In addition, map of OM content of the sediment are also shown in Figure 3-6. In the first campaign, 2 piezometers exhibited high values (P3 and P11) while the others were relatively low compare to other campaign (especially camp 4 where OM values were higher than other campaigns). Overall OM was rather spatially and temporally homogenous (CV=31%), but some locations showed particulary high OM content (>0.8%; P3,P7,P11).

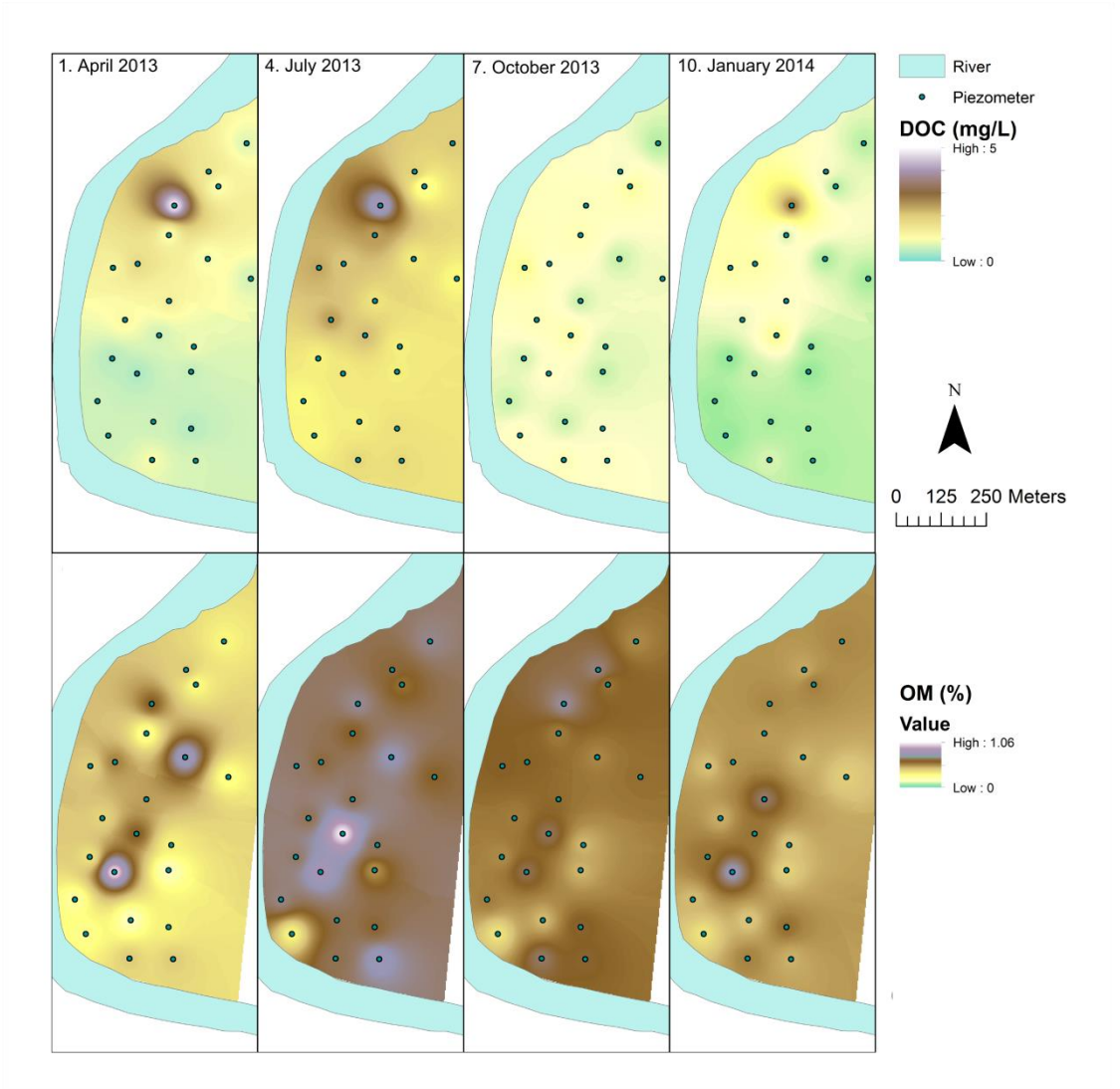

Figure 3-6: Maps of interpolated (IDW) DOC (top) and OM (bottom) for the four full campaigns.

3.2.3.6. Bank geomorphology effect on variable controlling denitrification

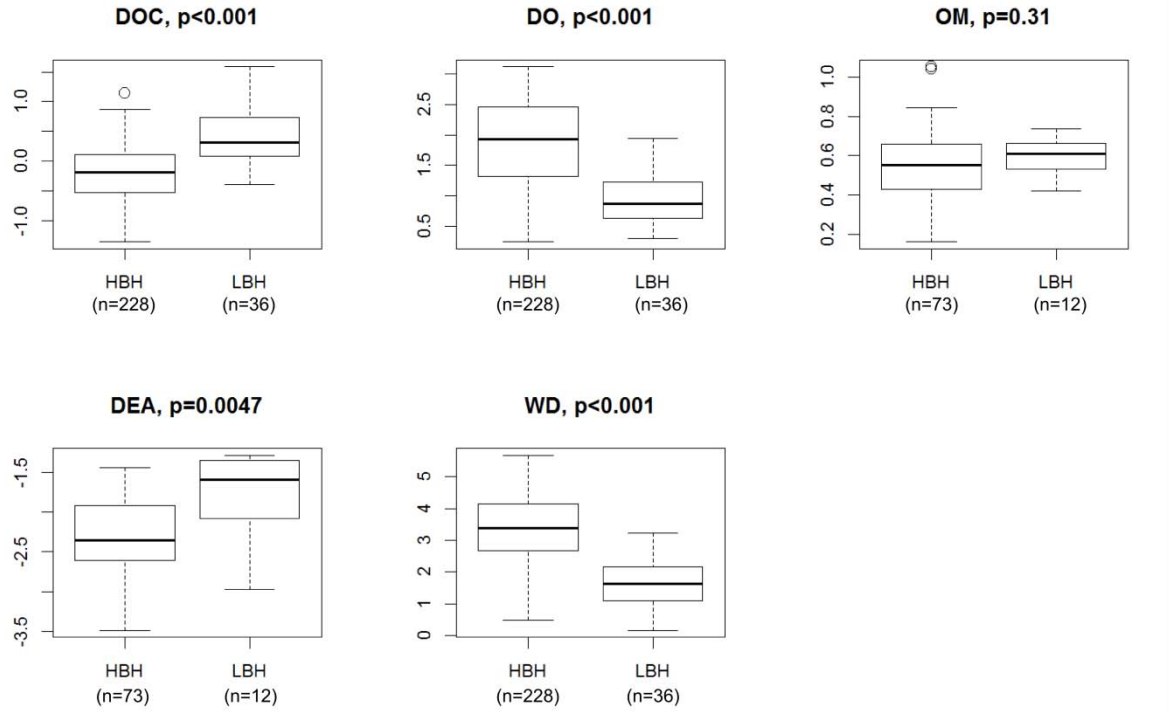

Figure 3-7: Boxplot of DOC, DO, OM, DEA and WD according to the two bank geomorphology types (LBH and HBH). DOC, DEA and DO were transformed to ensure normality of the data distribution. p-values are calculated with Student t-test.

Bank geomorphology in the study area can be distinguished between LBH and HBH areas. Boxplots of variables related to DEA and WD between LBH and HBH are shown in Figure 3-7. LBH areas have a greater DEA ($p<0.01$), a water table closer to the surface, lower DO values, higher DOC values ($p<0.001$) than HBH areas. However the OM content is not significantly different between the two bank geomorphology ($p=0.31$).

3.2.4. Discussion

3.2.4.1. Processes controlling spatio-temporal variations of nitrate concentrations at the study site

The PLSR performed on NO_3^- concentrations indicated that the two first components explained 56% and 14% of NO_3^- variance. The first component was mainly related to major ions concentrations especially Mg^{2+}, Cl^-, Na^+ but also to high $\delta^{18}O$ values. This component can be related to the degree of mixing between the groundwater characterised by high concentrations of ions (Cl^-, SO_4^{2-}, Ca^{2+}, Mg^{2+}, Na^{2+}) resulting from agricultural activities and

fertiliser input (Böhlke, 2002) and water-aquifer interactions, and the river water with lower ions concentrations. In addition $\delta^{18}O$ is also known to be a good tracer of different water bodies such as surface and subsurface water (Kendall and McDonnell, 2012). Therefore, the first component can be seen as an indicator of the intensity of mixing and of the connectivity between the river and the groundwater, primarily controlling nitrate concentration in the area, with high score representing high groundwater proportion and low score high river water proportion. Spatial mapping of the score of the first component for different campaigns indicated that the degree of mixing is linked to the hydrology of the area. According to the groundwater level (Figure 3-3), the dominant groundwater flow direction was from the agricultural area to north of the meander, and the water in this area has therefore a lower residence time than in the south of the area where groundwater flow velocities are lower. This is indeed in good agreement with high score of the 1st component in the north of the meander and the low score in the south of the meander. Therefore, the influence of the river was greater in the south of the meander, where the flooding occurrence could be higher than the residence time of the groundwater leading to an area of permanently low ions concentrations. In addition, temporal variations in the degree of mixing between groundwater and river water were observed. The influence of the groundwater affected a greater area in the campaign 7, more than three months after the last significant flood event, than for the others dates. This can be explained by the long groundwater draining period associated with the drying stage during which no river water enters the aquifer.

While previous studies have shown that mixing between the river and the groundwater mostly explain decrease in aquifer NO_3^- concentrations (Pinay et al., 1998; Baillieux et al., 2014), others studies have identified different sources leading to the NO_3^- dilution such as groundwater flowing upwards from the shallow bedrock aquifer (Craig et al., 2010) or from upland terraces recharge (Pfeiffer et al., 2006). In this study, the river-groundwater water exchanges were found to be essential to explain NO_3^- spatio-temporal patterns observed in the shallow aquifer of the study area which is mainly controlled by the residence time of the highly loaded groundwater flowing from the agricultural area to the river. Temporal variations in the degree of mixing can also been observed and are controlled by hydrological cycle, especially drying stage duration and flood occurrences.

The second component of the PLSR (14% of NO_3^- variance explained) is mainly related to DOC and alkalinity (negative contribution) and DO and pH (positive contribution). In riverine system , river water infiltrating through the hyporheic zone can provide groundwater with DO

(Boulton et al., 1998; Zarnetske et al., 2012). However, in the study area, the lower DO concentration areas are located along the river channel and therefore these low DO concentrations can more likely be linked to microbial activity consuming oxygen brought by the river water entering the hyporheic zone (Mermillod-Blondin et al., 2005). Alkalinity is a parameter that can be generated in riparian area through OC oxidation (Vidon et al., 2010) and denitrification process (Li and Irvin, 2007). In addition, DOC is a key element for heterotrophic micro-organisms growth and can be linked to heterotrophic activity. DOC is known to be related to heterotrophic activity (Wetzel, 1992) as well as relatively low pH that may be an indicator of high respiration level. The results could indicate that nitrate concentrations are affected by a biological process denoted by the 2nd component of the PLSR, and interacting with pH, fuelled by OC, consuming oxygen and producing alkalinity. Among all the biological processes affecting nitrate, this combination of parameters could be related to denitrification. Indeed, denitrification lead to nitrate removal under anaerobic condition and uses OC as electron donor (Rivett et al., 2008) and have been related to alkalinity production (Li and Irvin, 2007). Nitrification occurs in riparian area, but in this study, it is difficult to link the 2nd component with nitrification since groundwater in the study area exhibit low ammonium concentration. Another processes that could be considered is the assimilation of nitrate into microbial biomass but this process can only remove a small amount of nitrate and the rapid bacteria die-off may lead to N release as ammonium and then nitrate in groundwater (Rivett et al., 2008). In addition the probability that the second components is linked to denitrification is accentuated by the fact that riparian areas are known to be places where high denitrification rates can be measured (Pinay and Decamps, 1988; Hill et al., 2000; Ranalli and Macalady, 2010) and has already been observed in the study site (J. M. Sánchez-Pérez et al., 2003; Iribar et al., 2008). Denitrification had a lower impact on NO_3^- concentrations than water mixing but unlike mixing denitrification lead to effective N-removal from the groundwater (Pinay et al., 1998).

3.2.4.2. Environmental factors controlling DEA

In this study, DEA was used as an indicator of denitrification under optimal and standardised carbon and nitrate supply. While DEA measures the potential capacity of denitrifying communities under optimal conditions and does not represent actual *in situ* rate of denitrification, it has been related to the functional response (denitrification) of denitrifying communities (Iribar et al., 2008). DEA measured in the study area vary over several orders of magnitude. The average rate is 0.022 µg-N g-sed^{-1} h^{-1} which is consistent with the rates

reported by Peterson et al. (2013) for subsoil (0.015 µg-N g-sed^{-1} h^{-1}) and slightly higher than the rates they measured in deeper gravel layer (0.005 µg-N g-sed^{-1} h^{-1}) of an alluvial floodplain. However the highest rate recorded in the area (0.18 µg-N g-sed^{-1} h^{-1}) is lower than the rates measured in topsoils by Miller et al. (2008) that reached 1.3 µg-N g-sed^{-1} h^{-1} . Furthermore, results show that DEA rates in the study area could be very low (2.2 x 10^{-4} µg-N g-sed^{-1} h^{-1}).

In the present study, high DEA was related to high DOC concentration and OM content and to low DO concentrations, these factors explaining 31% of DEA variance over the study area. OM content has been linked to bacterial density and can be considered as a good proxy for bacterial biomass in sediment (Iribar, 2007). Therefore, the occurrence at the same spot of anoxia and high OM could indicate important bacterial activity. The above relationship can thus be explained by the fact that increased heterotrophic bacterial activity in the presence of DOC leads to anoxia (Arango et al., 2007) and growth of bacterial biomass (increasing OM), promoting conditions for denitrification to occur. In addition to be an indicator of bacterial biomass, OM can indicate patches located within sediment and be a source of OC fuelling denitrification process (Hill et al., 2000). Therefore, OC dynamic can be interpreted as a key factor explaining spatio-temporal variations in DEA and its source needs to be thoroughly investigated. Indeed carbon supply is often considered as the major limiting factor for denitrification (Starr and Gillham, 1993; Jacinthe et al., 1998; Devito et al., 2000; Rivett et al., 2008; Zarnetske et al., 2011; Peter et al., 2012). However bacterial richness which was the only variable describing the bacterial community was not related to DEA in this study. The total DEA variance explained by the others variables is relatively low. Others descriptors such as carbon bioavailability (Baker et al., 2000) or better descriptor of bacterial communities (Iribar et al., 2008) could have improve explained DEA variance.

OC in alluvial aquifer can originated to two sources: (i) degradation of the OM contained in the sediment and (ii) transported by water flows (Zarnetske et al., 2012). The first source includes the degradation of OM contained in the topsoil layer during high groundwater periods or leaching from leaf litter during inundation (Baldwin and Mitchell, 2000). Isolated OM patches such as buried channel deposit can also provide a source of OC within sediments (Hill et al., 2000). OC can also be related to the DOC brought by the river through lateral recharge and overbank flow infiltration during flood events (Peyrard et al., 2011; Zarnetske et al., 2012). The role of DOC coming from the river in the study area has been reported previously (Sánchez-Pérez et al., 2003), but recent modelling studies show that DOC input in

the riparian area through the river plays a small role in comparison with the *in-situ* sediment particulate organic carbon (POC) content (Sun et al., submitted). In this study DOC concentrations are higher near the river and in the period following a flood and can be linked to river transport. However, the DOC concentrations are not related to conservative tracer such as Cl^- suggesting that the DOC can also originate from another source being the sediment OM dissolution.

Differences in DEA and related factors were investigated for two different banks geomorphology, LBH and HBH. DEA, in relation with DOC and DO was more important in LBH than in HBH areas, making the LBH areas DEA hotspots. Geomorphology is known to affect denitrification in riparian area (Gold et al., 2001; Vidon and Hill, 2004; Ranalli and Macalady, 2010). Hill (1996) indicated that denitrification is promoted in riparian areas with an impermeable layer close to the surface forcing the groundwater to flow into area where conditions are optimum for denitrification. This setting corresponds to the LBH areas of this study. The lower water table, increasing the contact between water and top soil layer containing high OM content may explain the high DEA measured in LBH areas. In addition the OM content was not different between the two type of geomorphology and some high values could be found and related to DEA hotspots localized outside of LBH area.

3.2.4.3. Conceptual model of denitrification in alluvial floodplains

Analysis of the spatio-temporal variations in denitrification at the study site allowed a conceptual diagram of denitrification occurrence in alluvial floodplains to be shaped (Fig. 10). The two geomorphological configurations of the banks (LBH and HBH) showed differences in denitrification processes. To explain the dynamics of denitrification and nitrate in a floodplain, a typical temporal sequence starting from a flood event to the end of the drying stage has to be taken into consideration. During the flood, DOC coming from the river flow enters the aquifer through bank recharge in HBH and LBH. In addition, OC from the topsoil layer is incorporated into the groundwater in LBH, where the groundwater level reaches the surface and through leaching due to the infiltration of overbank flow (Figure 3-8 a). There is consequently more DOC in LBH due to its dual origin than in HBH. Then, following the flood, denitrification occurs at a significant rate in HBH and LBH, and nitrate flowing from the agricultural area to the river are consumed at both locations (Figure 3-8 b). After a drying stage period whose duration depends on the river floodplain geomorphological settings, DOC is entirely consumed in HBH and no longer supports denitrification. However, DOC

concentrations are higher at LBH than at HBH after the flood and the groundwater remains close to the surface for a longer period, making OC of the soil still available in LBH. Therefore, at LBH, denitrification remains active for a longer period during the drying stage (Figure 3-8 c). Denitrification in LBH will decrease as the drying stage continues and will stop eventually.

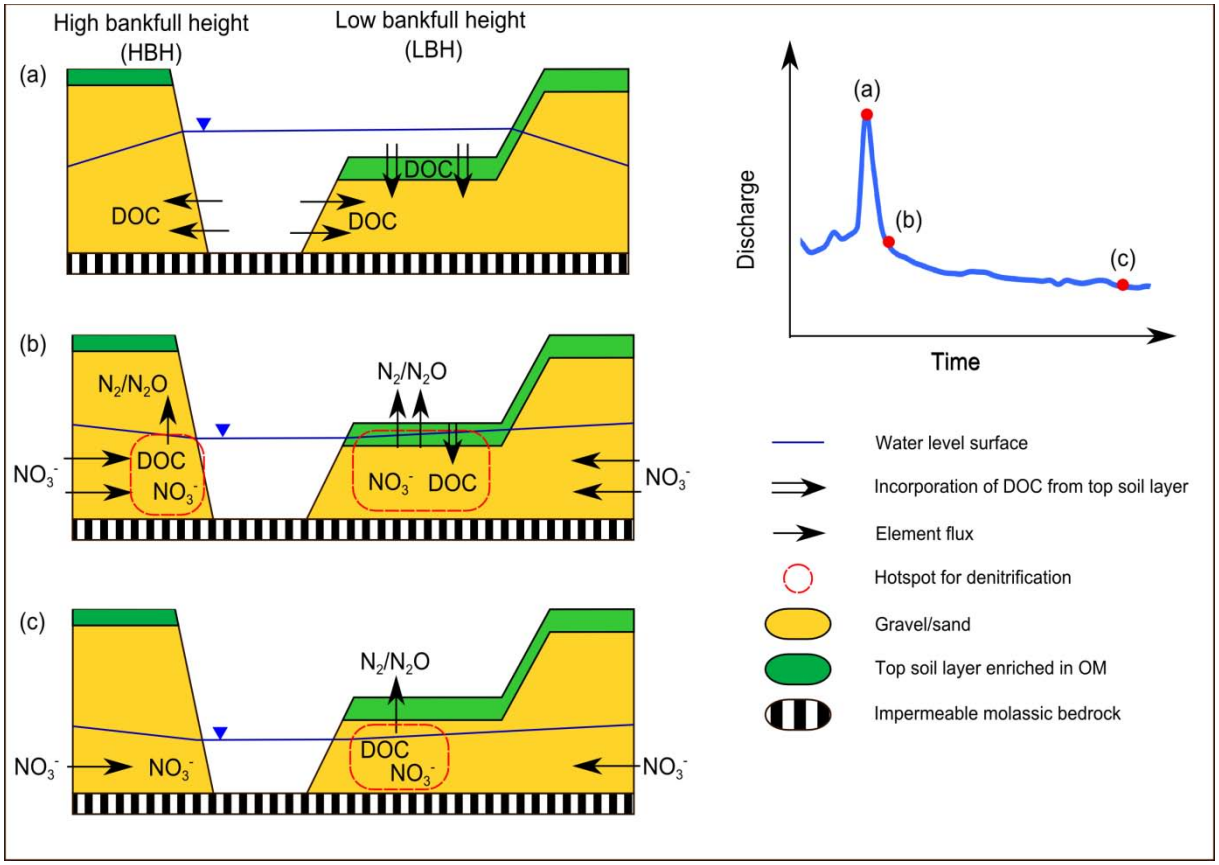

Figure 3-8: Conceptual diagram of denitrification process in the floodplain. High bankfull height (HBF) corresponds to the left bank and low bankfull height (LBF) to the right bank in the diagram. a) During the flood DOC enters the aquifer with river water and is degraded from OM of the top soil layer. b) after the flood denitrification hotspots occurs in HBF and LBF. c) after a long drying stage, denitrification is lower and only occurs in LBF area.

Some local deviations from the generalised nitrate dynamics described above were observed in the data and can be due to local heterogeneity of the substrate affecting flowing paths or local OM content. However, these observations were rather rare in view of the high density of sampling points, indicating that significant conclusions can be drawn from this study. This work was based on the hypothesis that denitrification is the most important process of nitrate removal, but the shallow water table in LBH area would allow plant uptake to occur (Pinay et al., 1998). This process would result in greater nitrate removal rates and should be included in further studies for better evaluation of nitrate removal potential of the riparian area.

3.2.5. Conclusions

This study examined the characteristics of processes occurring in a floodplain area, with the focus on denitrification patterns and nitrate dynamics. Based on a PLSR analysis, it was found that NO_3^- concentrations in groundwater were mainly controlled by the mixing between river water and groundwater and denitrification also played a significant role in nitrate removal. Potential denitrification rates were strongly linked to the presence of DOC, OM and anoxia. However, many factors, including geomorphology and hydrological cycle, appeared to control potential denitrification hot spot and hot moment patterns. The combination of these factors led to complex and heterogeneous nitrate dynamics in the study area. These findings show that accurate assessments of denitrification rates and nitrate loads in floodplain environments from field studies can be assessed from a detailed dataset. Due to the difficulty of getting a complete field dataset for every location, modelling work integrating all these factors might be a valuable tool in evaluating floodplain nitrate mitigation potential under different floodplain configurations.

Acknowledgments

This study was undertaken as part of the EU Interreg SUDOE IVB programme (ATTENAGUA - SOE3/P2/F558 project) and was funded by ERDF. It was carried out as part of “ADAPT’EAU” (ANR-11-CEPL-008), a project supported by the French National Research Agency (ANR) within the framework of the Global Environmental Changes and Societies (GEC&S) programme. We are grateful to various colleagues at ECOLAB for their help, especially to Ousama Chamsi with field data collection and Virginie Payré-Suc and Issam Moussa with laboratory analyses.

References

Abdi, H., 2010. Partial least squares regression and projection on latent structure regression (PLS Regression). Wiley Interdiscip. Rev. Comput. Stat. 2, 97–106.

Amoros, C., Bornette, G., Cedex, V., 2002. Connectivity and biocomplexity in waterbodies of riverine floodplains. Freshw. Biol. 47, 761–776. doi:10.1046/j.1365-2427.2002.00905.x

Arango, C.P., Tank, J.L., Schaller, J.L., Royer, T. V, Bernot, M.J., David, M.B., 2007. Benthic organic carbon influences denitrification in streams with high nitrate concentration. Freshw. Biol. 52, 1210–1222.

Arauzo, M., Valladolid, M., Martínez-Bastida, J.J., 2011. Spatio-temporal dynamics of nitrogen in river-alluvial aquifer systems affected by diffuse pollution from agricultural sources: Implications for the implementation of the Nitrates Directive. J. Hydrol. 411, 155–168. doi:10.1016/j.jhydrol.2011.10.004

Arrate, I., Sanchez-Perez, J.-M., Antiguedad, I., Vallecillo, M.A., Iribar, V., Ruiz, M., 1997. Groundwater pollution in Quaternary aquifer of Vitoria–Gasteiz (Basque Country, Spain). Environ. Geol. 30, 257–265.

Baillieux, A., Campisi, D., Jammet, N., Bucher, S., Hunkeler, D., 2014. Regional water quality patterns in an alluvial aquifer: Direct and indirect influences of rivers. J. Contam. Hydrol. 169, 123–31. doi:10.1016/j.jconhyd.2014.09.002

Baker, M.A., Valett, H.M., Dahm, C.N., 2000. Organic carbon supply and metabolism in a shallow groundwater ecosystem. Ecology 81, 3133–3148.

Baker, M.A., Vervier, P., 2004. Hydrological variability, organic matter supply and denitrification in the Garonne River ecosystem. Freshw. Biol. 49, 181–190. doi:10.1046/j.1365-2426.2003.01175.x

Baldwin, D.S., Mitchell, A.M., 2000. The effects of drying and re-flooding on the sediment and soil nutrient dynamics of lowland river–floodplain systems: a synthesis. Regul. Rivers Res. Manag. 16, 457–467. doi:10.1002/1099-1646(200009/10)16:5<457::AID-RRR597>3.0.CO;2-B

Bijay-Singh, Yadvinder-Singh, Sekhon, G.S., 1995. Fertilizer-N use efficiency and nitrate pollution of groundwater in developing countries. J. Contam. Hydrol. 20, 167–184. doi:10.1016/0169-7722(95)00067-4

Böhlke, J.-K., 2002. Groundwater recharge and agricultural contamination. Hydrogeol. J. 10, 153–179.

Boulton, A.J., Findlay, S., Marmonier, P., Stanley, E.H., Valett, H.M., 1998. The functional significance of the hyporheic zone in streams and rivers. Annu. Rev. Ecol. Syst. 29, 59–81. doi:10.1146/annurev.ecolsys.29.1.59

Burt, T.P., Matchett, L.S., Goulding, K.W.T., Webster, C.P., Haycock, N.E., 1999. Denitrification in riparian buffer zones: the role of floodplain hydrology. Hydrol. Process. 13, 1451–1463. doi:10.1002/(SICI)1099-1085(199907)13:10<1451::AID-HYP822>3.0.CO;2-W

Carpenter, S.R., Caraco, N.F., Correll, D.L., Howarth, R.W., Sharpley, A.N., Smith, V.H., 1998. Non point pollution of surface waters with phosphorus and nitrogen. Ecol. Appl. 8, 559–568. doi:10.1890/1051-0761(1998)008[0559:NPOSWW]2.0.CO;2

Carrascal, L.M., Galván, I., Gordo, O., 2009. Partial least squares regression as an alternative to current regression methods used in ecology. Oikos 118, 681–690. doi:10.1111/j.1600-0706.2008.16881.x

Craig, L., Bahr, J.M., Roden, E.E., 2010. Localized zones of denitrification in a floodplain aquifer in southern Wisconsin, USA. Hydrogeol. J. 18, 1867–1879.

Devito, K.J., Fitzgerald, D., Hill, A.R., Aravena, R., 2000. Nitrate dynamics in relation to lithology and hydrologic flow path in a river riparian zone. J. Environ. Qual. 29, 1075–1084.

Dosskey, M.G., Vidon, P., Gurwick, N.P., Allan, C.J., Duval, T.P., Lowrance, R., 2010. The Role of Riparian Vegetation in Protecting and Improving Chemical Water Quality in Streams1. JAWRA J. Am. Water Resour. Assoc. 46, 261–277. doi:10.1111/j.1752-1688.2010.00419.x

Epstein, S., Mayeda, T., 1953. Variation of O 18 content of waters from natural sources. Geochim. Cosmochim. Acta 4, 213–224.

ESRI, R., 2011. ArcGIS desktop: release 10. Environ. Syst. Res. Institute, CA.

Gold, A.J., Groffman, P.M., Addy, K., Kellogg, D.Q., Stolt, M., Rosenblatt, A.E., 2001. Landscape attributes as controls on groithd water nitrate removal capacity of riparian zones1.

Gonfiantini, R., 1978. Standards for stable isotope measurements in natural compounds.

Groffman, P., Butterbach-Bahl, K., Fulweiler, R., Gold, A., Morse, J., Stander, E., Tague, C., Tonitto, C., Vidon, P., 2009. Challenges to incorporating spatially and temporally explicit phenomena (hotspots and hot moments) in denitrification models. Biogeochemistry 93, 49–77. doi:10.1007/s10533-008-9277-5

Hill, A.R., 1996. Nitrate removal in stream riparian zones. J. Environ. Qual. 25, 743–755.

Hill, A.R., Devito, K.J., Campagnolo, S., Sanmugadas, K., 2000. Subsurface Denitrification in a Forest Riparian Zone: Interactions between Hydrology and Supplies of Nitrate and Organic Carbon. Biogeochemistry 51, 193–223.

Iribar, A., 2007. Composition des communautés bactériennes dénitrifiantes au sein d'un aquifère alluvial et facteurs contrôlant leur structuration: relation entre structure des communautés et dénitrification. Université de Toulouse III - Paul Sabatier.

Iribar, A., Sánchez-Pérez, J., Lyautey, E., Garabétian, F., 2008. Differentiated free-living and sediment-attached bacterial community structure inside and outside denitrification hotspots in the river–groundwater interface. Hydrobiologia 598, 109–121 LA – English. doi:10.1007/s10750-007-9143-9

Jacinthe, P.-A., Groffman, P.M., Gold, A.J., Mosier, A., 1998. Patchiness in microbial nitrogen transformations in groundwater in a riparian forest. J. Environ. Qual. 27, 156–164.

Jégo, G., Sánchez-Pérez, J.M., Justes, E., 2012. Predicting soil water and mineral nitrogen contents with the STICS model for estimating nitrate leaching under agricultural fields. Agric. Water Manag. 107, 54–65. doi:http://dx.doi.org/10.1016/j.agwat.2012.01.007

Kendall, C., McDonnell, J.J., 2012. Isotope tracers in catchment hydrology. Elsevier.

Korom, S.F., 1992. Natural denitrification in the saturated zone: A review. Water Resour. Res. 28, 1657–1668. doi:10.1029/92WR00252

Lamontagne, S., Herczeg, A.L., Dighton, J.C., Jiwan, J.S., Pritchard, J.L., 2005. Patterns in groundwater nitrogen concentration in the floodplain of a subtropical stream (Wollombi Brook, New South Wales). Biogeochemistry 72, 169–190. doi:10.1007/s10533-004-0358-9

Li, B., Irvin, S., 2007. The comparison of alkalinity and ORP as indicators for nitrification and denitrification in a sequencing batch reactor (SBR). Biochem. Eng. J. 34, 248–255. doi:10.1016/j.bej.2006.12.020

McClain, M.E., Boyer, E.W., Dent, C.L., Gergel, S.E., Grimm, N.B., Groffman, P.M., Hart, S.C., Harvey, J.W., Johnston, C.A., Mayorga, E., McDowell, W.H., Pinay, G., 2003. Biogeochemical Hot Spots and Hot Moments at the Interface of Terrestrial and Aquatic Ecosystems. Ecosystems 6, 301–312. doi:10.1007/s10021-003-0161-9

Mermillod-Blondin, F., Mauclaire, L., Montuelle, B., 2005. Use of slow filtration columns to assess oxygen respiration, consumption of dissolved organic carbon, nitrogen transformations, and microbial parameters in hyporheic sediments. Water Res. 39, 1687–98. doi:10.1016/j.watres.2005.02.003

Mevik, B.-H., Wehrens, R., 2007. The pls package: principal component and partial least squares regression in R. J. Stat. Softw. 18, 1–24.

Miller, M.N., Zebarth, B.J., Dandie, C.E., Burton, D.L., Goyer, C., Trevors, J.T., 2008. Crop residue influence on denitrification, N2O emissions and denitrifier community abundance in soil. Soil Biol. Biochem. 40, 2553–2562. doi:10.1016/j.soilbio.2008.06.024

Naiman, R.J., Decamps, H., McClain, M.E., 2010. Riparia: ecology, conservation, and management of streamside communities. Academic Press.

Peter, S., Rechsteiner, R., Lehmann, M.F., Brankatschk, R., Vogt, T., Diem, S., Wehrli, B., Tockner, K., Durisch-Kaiser, E., 2012. Nitrate removal in a restored riparian groundwater system: functioning and importance of individual riparian zones. Biogeosciences Discuss. 9, 6715–6750.

Peter, S., Rechsteiner, R., Lehmann, M.F., Tockner, K., Durisch-Kaiser, E., 2011. Denitrification hot spot and hot moments in a restored riparian system. IAHS-AISH Publ. 433–436.

Peterson, M.E., Curtin, D., Thomas, S., Clough, T.J., Meenken, E.D., 2013. Denitrification in vadose zone material amended with dissolved organic matter from topsoil and subsoil. Soil Biol. Biochem. 61, 96–104. doi:10.1016/j.soilbio.2013.02.010

Peyrard, D., Delmotte, S., Sauvage, S., Namour, P., Gerino, M., Vervier, P., Sánchez-Pérez, J.M., 2011. Longitudinal transformation of nitrogen and carbon in the hyporheic zone of an N-rich stream: A combined modelling and field study. Phys. Chem. Earth, Parts A/B/C 36, 599–611. doi:http://dx.doi.org/10.1016/j.pce.2011.05.003

Peyrard, D., Sauvage, S., Vervier, P., Sánchez-Pérez, J.-M., Quintard, M., 2008. A coupled vertically integrated model to describe lateral exchanges between surface and subsurface in large alluvial floodplains with a fully penetrating river. Hydrol. Process. 22, 4257–4273. doi:10.1002/hyp.7035

Pfeiffer, S.M., Bahr, J.M., Beilfuss, R.D., 2006. Identification of groundwater flowpaths and denitrification zones in a dynamic floodpain aquifier. J. Hydrol. 325, 262–272. doi:10.1016/j.jhydrol.2005.10.019

Pinay, G., Decamps, H., 1988. The role of riparian woods in regulating nitrogen fluxes between the alluvial aquifer and surface water: a conceptual model. Regul. Rivers 2, 507–516.

Pinay, G., Ruffinoni, C., Wondzell, S., Gazelle, F., 1998. Change in Groundwater Nitrate Concentration in a Large River Floodplain: Denitrification, Uptake, or Mixing? J. North Am. Benthol. Soc. 17, 179–189. doi:10.2307/1467961

Power, J.F., Schepers, J.S., 1989. Nitrate contamination of groundwater in North America. Agric. Ecosyst. Environ. 26, 165–187. doi:10.1016/0167-8809(89)90012-1

R Core Team, 2012. R: A language and environment for statistical computing. R Foundation for Statistical Computing, Vienna, Austria, 2012.

Ranalli, A.J., Macalady, D.L., 2010. The importance of the riparian zone and in-stream processes in nitrate attenuation in undisturbed and agricultural watersheds – A review of the scientific literature. J. Hydrol. 389, 406–415. doi:http://dx.doi.org/10.1016/j.jhydrol.2010.05.045

Rassam, D.W., Pagendam, D.E., Hunter, H.M., 2008. Conceptualisation and application of models for groundwater–surface water interactions and nitrate attenuation potential in riparian zones. Environ. Model. Softw. 23, 859–875. doi:http://dx.doi.org/10.1016/j.envsoft.2007.11.003

Rivett, M.O., Buss, S.R., Morgan, P., Smith, J.W.N., Bemment, C.D., 2008. Nitrate attenuation in groundwater: A review of biogeochemical controlling processes. Water Res. 42, 4215–4232. doi:http://dx.doi.org/10.1016/j.watres.2008.07.020

Sánchez-Pérez, J.M., 1992. Fonctionnement hydrochimique d'un écosystème forestier inondable de la Plaine du Rhin: la forêt alluviale du secteur de l'île de Rhinau en Alsace(France). Université Louis Pasteur, Strasbourg.

Sánchez-Pérez, J.M., Vervier, P., Garabétian, F., Sauvage, S., Loubet, M., Rols, J.L., Bariac, T., Weng, P., 2003. Nitrogen dynamics in the shallow groundwater of a riparian wetland zone of the Garonne, SW France: nitrate inputs, bacterial densities, organic matter supply and denitrification measurements. Hydrol. Earth Syst. Sci. 7, 97–107. doi:10.5194/hess-7-97-2003

Seitzinger, S., Harrison, J.A., Böhlke, J.K., Bouwman, A.F., Lowrance, R., Peterson, B., Tobias, C., Drecht, G. Van, 2006. Denitrification across landscapes and waterscapes: a synthesis. Ecol. Appl. 16, 2064–2090.

Starr, R.C., Gillham, R.W., 1993. Denitrification and organic carbon availability in two aquifers. Groundwater 31, 934–947.

Sun, X., Bernard-Jannin, L., Garneau, C., Arnold, J.G., Srinivasan, R., Sauvage, S., Sánchez-Pérez, J.M., n.d. Assessment of the denitrification process in alluvial wetlands at floodplain scale using SWAT model. Ecol. Eng.

Sun, X., Bernard-Jannin, L., Garneau, C., Volk, M., Arnold, J.G., Srinivasan, R., Sauvage, S., Sánchez-Pérez, J.M., 2015. Improved simulation of river water and groundwater exchange in an alluvial plain using the SWAT model. Hydrol. Process.

Sutton, M.A., Howard, C.M., Erisman, J.W., Billen, G., Bleeker, A., Grennfelt, P., van Grinsven, H., Grizzetti, B., 2011. The European nitrogen assessment: sources, effects and policy perspectives. Cambridge University Press.

Tockner, K., Stanford, J.A., 2002. Riverine flood plains: present state and future trends. Environ. Conserv. 29, 308–330.

Vidon, P., Allan, C., Burns, D., Duval, T.P., Gurwick, N., Inamdar, S., Lowrance, R., Okay, J., Scott, D., Sebestyen, S., 2010. Hot Spots and Hot Moments in Riparian Zones: Potential for Improved Water Quality Management1. JAWRA J. Am. Water Resour. Assoc. 46, 278–298. doi:10.1111/j.1752-1688.2010.00420.x

Vidon, P.G., Hill, A.R., 2006. A landscape-based approach to estimate riparian hydrological and nitrate removal functions. JAWRA J. Am. Water Resour. Assoc. 42, 1099–1112.

Vidon, P.G.F., Hill, A.R., 2004. Landscape controls on nitrate removal in stream riparian zones. Water Resour. Res. 40.

Weiss, R.F., Price, B.A., 1980. Nitrous oxide solubility in water and seawater. Mar. Chem. 8, 347–359. doi:10.1016/0304-4203(80)90024-9

Weng, P., Sánchez-Pérez, J.M., Sauvage, S., Vervier, P., Giraud, F., 2003. Assessment of the quantitative and qualitative buffer function of an alluvial wetland: hydrological modelling of a large floodplain (Garonne River, France). Hydrol. Process. 17, 2375–2392. doi:10.1002/hyp.1248

Wetzel, R.G., 1992. Gradient-dominated ecosystems: sources and regulatory functions of dissolved organic matter in freshwater ecosystems, in: Dissolved Organic Matter in Lacustrine Ecosystems. Springer, pp. 181–198.

Yan, B., Fang, N.F., Zhang, P.C., Shi, Z.H., 2013. Impacts of land use change on watershed streamflow and sediment yield: An assessment using hydrologic modelling and partial least squares regression. J. Hydrol. 484, 26–37. doi:10.1016/j.jhydrol.2013.01.008

Yao, J.M., Sánchez-Pérez, J.M., Sauvage, S., Teissier, S., Attard, E., Lauga, B., Durant, R., Julien, F., Bernard-Jannin, L., Ramburn, H., Gerino, M., n.d. Biodiversity, ecosystem purification function and service in alluvial wetlands. Ecol. Eng.

Zarnetske, J.P., Haggerty, R., Wondzell, S.M., Baker, M.A., 2011. Labile dissolved organic carbon supply limits hyporheic denitrification. J. Geophys. Res. Biogeosciences 116.

Zarnetske, J.P., Haggerty, R., Wondzell, S.M., Bokil, V.A., González-Pinzón, R., 2012. Coupled transport and reaction kinetics control the nitrate source-sink function of hyporheic zones. Water Resour. Res. 48.

Zhang, W.L., Tian, Z.X., Zhang, N., Li, X.Q., 1996. Nitrate pollution of groundwater in northern China. Agric. Ecosyst. Environ. 59, 223–231. doi:10.1016/0167-8809(96)01052-3

3.3.Synthèse

La première étape de cette thèse, préalable à la phase modélisation, consiste à analyser les données récoltées lors des douze campagnes mensuelles de terrains afin d'améliorer la compréhension de la dynamique des nitrates sur le site d'étude. En effet, en plus de servir pour la paramétrisation et la validation du modèle, l'analyse de ce jeux de données conséquent (12 campagnes, 25 piézomètres) a pour objectif d'améliorer la compréhension des processus à simuler et donc influencer la formulation du modèle pour améliorer la qualité des résultats la modélisation.

Cette étude avait pour objectif d'analyser la variabilité spatio-temporelle des teneurs en nitrates et de la dénitrification potentielle de l'aquifère du site de Monbéqui et d'identifier leurs facteurs de contrôle.

Les résultats de cette première partie indique que la géomorphologie, et notamment l'altitude des berges, est un facteur clé contrôlant la distribution spatiale de la dénitrification. Le carbone organique apporté par la rivière et originaire des sols joue un rôle important dans le processus de dénitrification. Les échanges nappe- rivière contrôlent également les flux de nitrates et de carbone organique dans l'aquifère alluvial. De plus, le rôle de l'hydrologie et des épisodes de crues est déterminant dans l'apparition de périodes de dénitrification plus intenses.

Afin de modéliser la dénitrification dans les zones alluviales, il est donc important de prendre en compte ces différents facteurs. Aussi, l'utilisation d'un modèle hydrologique distribué permettra de représenter la variabilité spatiale de la topographie du lieu et son rôle l'hydrologie et donc sur le processus de dénitrification. Les échanges nappes-rivière ainsi que le rôle des cures sur l'hydrologie devront également être pris en compte par le modèle. Finalement, le modèle devra intégrer les différentes sources de carbone organique (apporté par la rivière et présent dans les sols) lors du calcul de la dénitrification.

Chapitre 4 : Modélisation des échanges eaux de surface – eaux souterraines dans la plaine alluviale de la Garonne

Ce chapitre présente l'implémentation du modèle MOHID Land afin de simuler l'hydrologie sur le site de Monbéqui. Cette partie doit notamment permettre de valider la modélisation des processus hydrologiques incluant les échanges nappes-rivières et l'impact des crues débordantes qui sont des éléments importants pour le fonctionnement biogéochimique des plaines alluviales (chapitre 1), comme identifié lors de l'analyse des données récoltées sur le terrain (chapitre 3). Le modèle MOHID Land a donc été choisi pour sa capacité à simuler les échanges nappe-rivière et les crues débordantes. De plus, l'impact des crues débordantes sur les échanges nappe-rivière est également étudié.

Ce chapitre est constitué d'un article soumis au journal *Advances in Water Ressources*, actuellement accepté avec révisions, et intitulé «Spatially distributed modelling of surface water-groundwater exchanges during overbank flood events – a case study at the Garonne River». L'article est précédé d'un résumé en français et est suivi d'une synthèse qui replace les résultats obtenus dans le cadre de la thèse.

4.1.Résumé

Les échanges entre les eaux de surface et les eaux souterraines sont très importants pour les écosystèmes des plaines alluviales et leur fonctionnement biogéochimique. Les crues en particulier jouent un rôle clé dans le cycle hydrologique et les transferts et transformations des éléments. Cependant, ces échanges sont complexes et présentent une variabilité spatio-temporelle importante et la modélisation peut permettre d'améliorer les connaissances sur les processus qui s'opèrent à l'échelle du tronçon de rivière et de sa plaine alluviale adjacente.

Ce travail s'appuie sur l'utilisation d'un modèle distribué pour représenter les échanges eaux de surface – eaux souterraines dans la plaine alluviale de Monbéqui. Le modèle MOHID Land couple la modélisation des écoulements de surfaces en deux dimensions (équation de Saint-Venant) et la modélisation des écoulements souterrains en trois dimensions (équation de Richards). L'écoulement provoqué par le débordement lors des crues ainsi que les échanges entre les eaux de surface et les eaux souterraines sont simulés dans le modèle. Un module de transport conservatif est également présent, et la simulation du transport d'un traceur conservatif (chlorures) a été utilisée pour valider le mélange entre les eaux de surface et les eaux souterraines.

Le modèle a été appliqué sur le site d'étude de Monbéqui (6,6 km²) situé dans la plaine alluviale de la Garonne pour simuler une période de cinq mois (incluant des épisodes de crue) et a permis de représenter l'hydrologie sur la zone étudié. L'infiltration (eaux de surface vers les eaux souterraines) et l'exfiltration (eaux de souterraines vers les eaux de surface) ont été évaluées. Les résultats montrent que l'infiltration et l'exfiltration sur la plaine alluviale sont caractérisées par une forte variabilité spatio-temporelle. L'infiltration du ruissellement provoqué par les crues représente 88% de l'infiltration totale et se concentre sur de courtes périodes. Les résultats confirment que les épisodes de crues débordantes jouent un rôle prépondérant sur le bilan hydrique des plaines alluviales comparé aux épisodes de crues non débordantes. L'impact des crues sur le bilan hydrique est identique à partir d'un seuil correspondant à la crue de temps de retour quinquennal, en relation avec la topographie de la plaine alluviale de Monbéqui.

La simulation des crues débordantes est une spécificité nécessaire à prendre en compte pour évaluer précisément les échanges entre les eaux de surface et les eaux souterraines. La modélisation des échanges eaux de surface-eaux souterraines présentée ici constitue une base

pour l'intégration de processus biogéochimique sensible à l'hydrologie des plaines alluviales comme la dénitrification.

4.2. Spatially distributed modelling of surface water-groundwater exchanges during overbank flood events – a case study at the Garonne River

Léonard Bernard-Jannin[1,2,*], David Brito[3], Xiaoling Sun[1,2], Eduardo Jauch[3], Ramiro Neves[3], Sabine Sauvage[1,2], José-Miguel Sánchez-Pérez[1,2,*]

[1]*University of Toulouse; INPT, UPS; Laboratoire Ecologie Fonctionnelle et Environnement (EcoLab), Avenue de l'Agrobiopole, 31326 Castanet Tolosan Cedex, France*

[2]*CNRS, EcoLab, 31326 Castanet Tolosan Cedex, France*

[3]*MARETEC, Instituto Superior Tecnico, Universidade Tecnica de Lisboa, Av. Rovisco Pais, 1049-001 Lisboa, Portugal*

[*]*Corresponding authors: Avenue de l'Agrobiopole, 31326 Castanet Tolosan Cedex, Franc; l.bernardjannin@gmail.com; jose-miguel.sanchez-perez@univ-tlse3.fr*

Abstract

Exchanges between surface water (SW) and groundwater (GW) are of considerable importance to floodplain ecosystems and biogeochemical cycles. Flood events in particular are important for riparian water budget and element exchanges and processing. However SW-GW exchanges present complex spatial and temporal patterns and modelling can provide useful knowledge about the processes involved at the scale of the reach and its adjacent floodplain. This study used a physically-based, spatially-distributed modelling approach for studying SW-GW exchanges. The modelling in this study is based on the MOHID Land model, combining the modelling of surface water flow in 2D with the Saint-Venant equation and the modelling of unsaturated groundwater flow in 3D with the Richards' equation. Overbank flow during floods was also integrated, as well as water exchanges between the two domains across the entire floodplain. Conservative transport simulations were also performed to study and validate the simulation of the mixing between surface water and groundwater. The model was applied to the well-monitored study site of Monbéqui (6.6 km²) in the Garonne floodplain (south-west France) for a five-month period and was able to represent the hydrology of the study area. Infiltration (SW to GW) and exfiltration (SW to GW) were characterised over the five-month period. Results showed that infiltration and exfiltration exhibited strong spatiotemporal variations, and infiltration from overbank flow accounted for 88 % of the total simulated infiltration, corresponding to large flood periods. The results confirmed that overbank flood events played a determinant role in floodplain water budget and SW-GW exchanges compared to smaller (below bankfull) flood events. The impact of floods on water budget appeared to be similar for flood events exceeding a threshold corresponding to the five-year return period event due to the study area's topography. Simulation of overbank flow during flood events was an important feature in the accurate

assessment of exchanges between surface water and groundwater in floodplain areas, especially when considering large flood events.

Keywords: floodplain, flood, modelling, water exchanges, distributed model

4.2.1. Introduction

Exchanges at the interface between surface water (SW) and groundwater (GW) are known to play a key role in floodplain ecosystems (Amoros *et al.*, 2002; Sophocleous, 2002; Thoms, 2003). Areas of mixing between SW and GW are regions of intensified biogeochemical activity (Grimm and Fisher, 1984; McClain *et al.*, 2003). These processes include denitrification, which has been recognised as the most important nitrate removal process in GW (Rivett *et al.*, 2008) and can lead to significantly reduced nitrate concentrations in aquifers supporting agricultural activities (Correll et al., 1992; Sánchez-Pérez and Tremolières, 1997). Denitrification is known to be influenced by hydrological connectivity between SW and GW, and denitrification hotspots have been related to activation of the processes through the organic matter flux coming from surface water (J.-M. Sánchez-Pérez et al., 2003). This natural mitigation process is reinforced by the dilution of contaminant concentrations due to the mixing between SW and GW (Pinay *et al.*, 1998; Baillieux *et al.*, 2014). In floodplains, flood events are an important feature for ecosystems. The pulsing of river discharge is the major driving force determining the exchange processes of organic matter and organisms across river-floodplain gradients (Junk *et al.*, 1989; Tockner *et al.*, 1999). Furthermore it is recognised that the overbank flow component has to be included in SW-GW exchanges for a comprehensive water balance assessment (Rassam *et al.*, 2008). An accurate quantification and description of SW-GW exchanges, including overbank floods, is therefore a key factor when dealing with water quality in alluvial aquifers as it can help assess the patterns of activation of natural mitigation biogeochemical processes and dilution effects. However SW-GW interactions often present complex spatial and temporal patterns (Sophocleous, 2002; Krause et al., 2007) and a study at the scale of the stream and its adjacent floodplain (Woessner, 2000) is required to understand them fully.

As they allow characteristics of the environment to be taken into consideration on a detailed scale, physically-based, spatially-distributed models are valuable tools for improving knowledge of SW-GW exchanges and assessing the three-dimensional nature of the problem (Sophocleous, 1998; Bradford and Acreman, 2003). Numerous studies featuring distributed models and including SW-GW exchanges in floodplain areas have been carried out,

encompassing SW-GW exchange patterns and biogeochemical zonation induced by meander sinuosity (Boano et al., 2006, 2010), heat transport (Horritt *et al.*, 2006; Brookfield *et al.*, 2009), 3D-flow patterns in relation to river level variations (Derx *et al.*, 2010; Nützmann *et al.*, 2013), hydrofacies heterogeneity impact on SW-GW exchanges (Frei *et al.*, 2009), SW-GW exchange impact on floodplain water balance (Weng *et al.*, 2003; Krause and Bronstert, 2007; Krause *et al.*, 2007), solute transport through riparian areas (Weng *et al.*, 2003; Hoffmann *et al.*, 2006; Peyrard *et al.*, 2008) and contribution of GW to stream water (Partington *et al.*, 2011). While all these modelling studies integrate a surface and subsurface component as well as SW-GW exchanges, overbank flood events have not been included in the analysis. This can present a problem for assessing SW-GW exchanges in the floodplain accurately, especially during large flood events where infiltration from surface runoff can occur across the floodplain (Bates *et al.*, 2000) and inundated areas can drive aquifer recharge patterns (Helton *et al.*, 2014). Although overbank flood infiltration is not considered important when the river and aquifer are disconnected (Morin *et al.*, 2009), it is recognised that the lack of an overbank flow component in models leads to an underestimation of infiltration of river water into the aquifer (Doppler *et al.*, 2007; Engeler *et al.*, 2011). In another study, overbank flow during flooding has been simulated to study floodplain contamination, but only vertical infiltration has been taken into account to evaluate pollutant deposition and subsurface flows have not been simulated (Stewart *et al.*, 1998). In this case it is the simulation of subsurface flow returning to the river that is lacking in order to provide a comprehensive representation of SW-GW exchanges.

Overbank flood events are known to be very important for element processing and water budget in floodplain areas, but to the authors' knowledge they are not usually included in SW-GW studies. The main objective of this study was to assess the importance of overbank flood events on SW-GW interactions in a floodplain area. Using a distributed model, two domains – SW and GW – were simulated and coupled through infiltration/exfiltration processes. These processes were simulated across the entire floodplain area in order to include the impact of overbank flood events on SW-GW exchange dynamic. The model was applied to a well-monitored study site, providing a strong dataset for model validation, where SW-GW exchanges were analysed. A transport model was also included and the model was then used to evaluate SW-GW exchanges spatially and temporally for different flood conditions in the study area. This study is also a prerequisite for future work involving the simulation of biogeochemical processes such as denitrification in floodplain areas.

4.2.2. Materials and methods

4.2.2.1. Modelling approach

The modelling strategy for a complete surface-subsurface flow system should include surface and subsurface components and the coupling between them (Furman, 2008). Numerous models belong to this category that differ in terms of the formulation of the component governing equations (including dimensionality) and their coupling strategy and technical solution (Maxwell *et al.*, 2014). For subsurface flow, most of the models solve the Richards' equation (one, two or three dimensions) and solve a formulation of the Saint-Venant equation (kinematic, diffusive or dynamic wave in one or two dimensions) for the surface component (Furman, 2008). The models differ in terms of their coupling strategy involving asynchronous linking (e.g. Condon and Maxwell, 2013), sequential iteration (e.g. Dagès et al., 2012) or a globally implicit scheme (e.g. Kollet and Maxwell, 2006), and the technical solution involving boundary conditions (BC) switching (e.g. Dagès et al., 2012), first-order exchange (e.g. Panday and Huyakorn, 2004) or pressure continuity (e.g. Kollet and Maxwell, 2006) according to Maxwell *et al.* (2014). In a study comparing seven models with the different characteristics described above, it was found that the models demonstrate the same qualitative agreement although they use different approaches (Maxwell *et al.*, 2014).

Out of the open-source models able to simulate SW-GW exchanges, MOHID Land was applied in this study. This model includes all features required to simulate impact of flood events on SW-GW exchanges. Subsurface flow was computed with the three-dimensional Richard's equation needed to represent spatial variability of the flow in the unsaturated media of the floodplain area in detail. Surface flow was computed with the two-dimensional dynamic wave formulation of the Saint-Venant equation, allowing the correct representation of the rapidly changing stream stages during flooding. The coupling between the two components was produced through asynchronous linking and first-order exchange and realised across the entire modelled domain (*i.e.* not limited to the riverbed location). In addition, the model included a transport module. While these features are shared by several models, the novelty of the approach is to apply this type of model to simulate floodplain hydrology.

4.2.2.2. Overview of the MOHID model

MOHID Land is a part of the MOHID Water Modelling System (Neves et al., 2013, www.mohid.com). It is a physically-based, spatially-distributed model designed to simulate

the water cycle in hydrographic basins, including SW-GW interactions. It uses an object-oriented approach to facilitate the integration of different processes and modules, and a finite volume approach with a flux-driven strategy to facilitate the coupling of processes and verify the conservation of mass and momentum (Braunschweig et al., 2004; Trancoso et al., 2009; Brito et al., 2015).

Although it was originally designed to model river network systems and watersheds (Trancoso *et al.*, 2009), the modularity of MOHID Land allows the model to meet the specific features of a floodplain area. The model set-up used in this study consisted of two domains: the surface water (SW) domain and the porous media (PM) domain (Figure 4-1). The hydrology of the SW domain was calculated according to the two-dimensional Saint-Venant equation (dynamic wave). The river geometry was included in the SW domain to ensure the continuity of surface runoff simulation over the floodplain during overbank flood events. Water fluxes in the PM domain were calculated in three dimensions for saturated and unsaturated media using the Buckingham-Darcy equation. The spatially-distributed structure allowed interactions between the two domains – infiltration from SW to PM and exfiltration from PM to SW – to occur across the floodplain area at each time step. The possibility of imposing boundary conditions for the simulated domain in SW and PM was implemented in the model for the purposes of this study. Transport of chloride (Cl^-) as a conservative element was also simulated. Input data construction and output data visualisation were facilitated using the graphical user interface MOHID Studio. Due to its object-oriented modelling strategy, MOHID Land can provide a basis for further modelling studies in alluvial plains by facilitating the incorporation of modules designed to simulate biogeochemical processes for example.

4.2.2.2.1. Governing equations of MOHID Land

MOHID Land is a grid-based model with an Arkawa C-grid type (Purser and Leslie, 1988) in which flows and velocities are computed at the cell interfaces, while properties such as water content are computed at the centre of each cell. Unsaturated and saturated flows are computed in three dimensions in the PM domain, and surface flow in two dimensions (horizontal) in the SW domain where horizontal PM and SW grids are matching. Processes in each domain are calculated using a finite volume method to guarantee mass conservation, and solved with an explicit scheme. The model first computes PM processes, including infiltration/exfiltration, followed by SW processes.

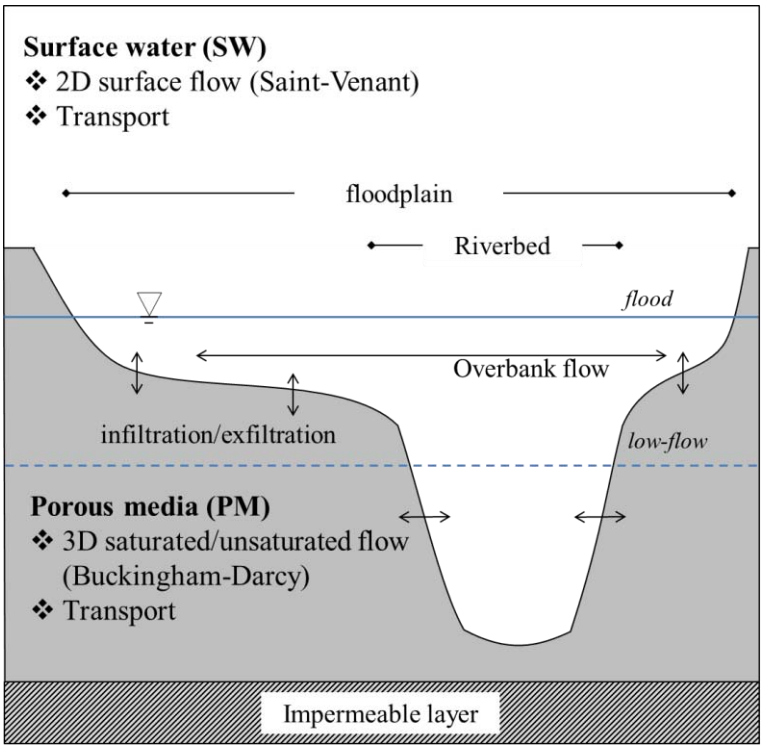

Figure 4-1: Presentation of the modelling approach. Water flows are modelled in and between PM and SW domains. Overbank flow is taken into account during flood events. Transport is considered in both domains

Porous media flow

First, water velocity is computed in each cell interface of the saturated and unsaturated medium using the Buckingham-Darcy equation (Swartzendruber, 1969) (1):

$$v_i = -K(\theta)\left(\frac{\partial H}{\partial x_i}\right) \tag{24}$$

where v_i [m s^{-1}] is the water velocity at the cell interface along direction i, x_i [m] is the distance along direction i, K [m s^{-1}] is hydraulic conductivity and θ [-] is the cell water content. H [m] is the hydraulic head computed in each cell centre as shown in equation 2:

$$H = h + \psi + z \tag{25}$$

where h [m] is the suction head, ψ [m] is the static pressure head and z [m] is the elevation of the centre of the cell.

The governing equation for flow in the porous media result from the combination of the Buckingham-Darcy equation (1) and the continuity equation and is known as the Richards' equation (Richards, 1931) (3).

$$\frac{\partial \theta}{\partial t} = \frac{\partial}{\partial x_i}\left[K(\theta)\frac{\partial H}{\partial x_i}\right] \quad (26)$$

The model uses the combination of the Mualem model (Mualem, 1976), which calculates the hydraulic conductivity in unsaturated soils (3 and 4), and the van Genuchten model (van Genuchten, 1980) for computing water retention in soils (5):

$$K(\theta) = K_s.{S_E}^L.\left(1-\left(1-{S_E}^{1/(1-\frac{1}{N})}\right)^{1-1/N}\right)^2 \quad (27)$$

$$S_E = (\theta - \theta_r)/(\theta_s - \theta_r) \quad (28)$$

$$h(\theta) = -\left|\left({S_E}^{(-1/(1-1/N))}-1\right)^{1/N}\right|/\alpha \quad (29)$$

where θ_r [-] is the residual water content, θ_s [-] is the saturated water content, α [cm^{-1}] is a term related to the inverse of the air entry pressure, N (dimensionless) is a measure of the pore-size distribution, S_E [-] is the effective saturation, L is an empirical pore-connectivity parameter and K_s [$m\ s^{-1}$] is the saturated hydraulic conductivity.

PM fluxes is calculated in the three-space direction, and vertical infiltration between SW and GW is then computed by applying the Darcy equation between SW and the top PM layer (Figure 4-3, eq. 6):

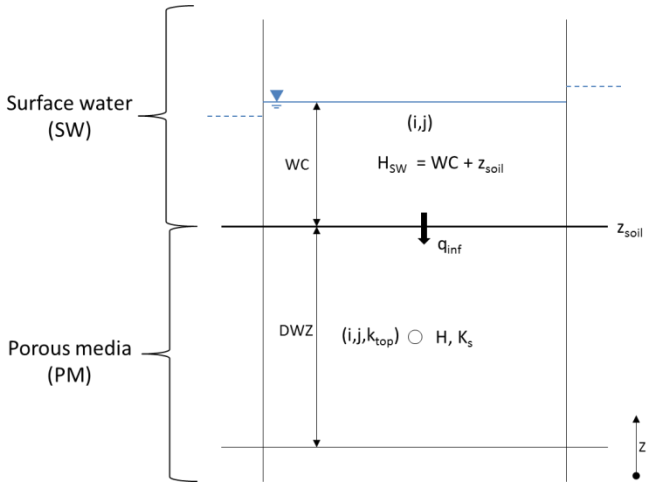

Figure 4-2: Schematic of the vertical infiltration flux (q_{inf}) calculation between SW cells (i,j) and the top PM cells (i,j,k_{top}). WC is the surface water column in SW and z_{soil} is the elevation of the soil surface. DWZ is the thickness, H is the hydraulic head and K_s is the saturated hydraulic conductivity of the top PM cell. i and j are the horizontal cell coordinates, k_{top} represents the vertical coordinate of the upper layer

$$q_{inf}(i,j) = K_s(i,j,k_{top})\, A(i,j) \left[\frac{H_{SW}(i,j) - H(i,j,k_{top})}{WC\ (i,j) + 0.5\ DWZ(i,j,k_{top})} \right] \qquad (30)$$

where q_{inf} is the vertical infiltration flux [$m^3\ s^{-1}$], A is the area of the cell [m^2], H_{SW} is the surface water elevation [m], WC is the surface water column [m], DWZ is the PM cell vertical height, i, j are the cell horizontal coordinates and k_{top} is the top PM layer coordinate.

To avoid negative volume in SW, the infiltration flux q_{inf} is limited to the available water volume in SW domain. Then θ^{t+dt} is updated in each cell of the PM domain according to the continuity equation (7):

$$\theta^{t+dt} = \left[\theta^t V + (q_x + q_y + q_z + q_{inf})dt\right]/V \qquad (31)$$

where θ^{t+dt} is the updated cell water content at time step t+dt [-], θ^t is the cell water content at time step t [-], V is the cell volume [m^3], dt is the time step [s], and q_x, q_y, q_z are the fluxes along the three space directions x,y and z [$m^3\ s^{-1}$].

Finally, for each cell the water content θ^{t+dt} is compared to the saturated water content θ_s. If $\theta^{t+dt} > \theta_S$ the excess of the cell water volume $(\theta^{t+dt} - \theta_S)$ is transferred first to the underlying cells if space is available and then to the upper cells. When all the cells of the column are saturated, the eventual remaining excess water volume is reallocated to the SW domain (exfiltration). This means that mass conservation is satisfied and $\theta^{t+dt} \leq \theta_S$ in every cell of the PM domain.

Surface water flow

Surface water flow is then computed, solving the 2D Saint-Venant equation (dynamic wave) in its conservative form, accounting for advection, pressure and friction forces (Chow *et al.*, 1988) for the two horizontal directions of the grid (8 and 9):

$$\frac{\partial Q_x}{\partial t} + v_x \frac{\partial Q_x}{\partial x} + v_y \frac{\partial Q_x}{\partial y} = -g.A\left(\frac{\partial H}{\partial x} + \frac{|Q|.Q_x.n^2}{A^2.R_h^{4/3}}\right) \quad (32)$$

$$\frac{\partial Q_y}{\partial t} + v_x \frac{\partial Q_y}{\partial x} + v_y \frac{\partial Q_y}{\partial y} = -g.A\left(\frac{\partial H}{\partial y} + \frac{|Q|.Q_y.n^2}{A^2.R_h^{4/3}}\right) \quad (33)$$

where Q [m^3 s^{-1}] is the flow at a cell face along the two horizontal directions of the grids x and y, v [m s^{-1}] is the flow velocity along the x and y directions, g [m s^{-2}] is the gravitational acceleration, A [m^2] is the cross-section of the water column, H is the water column [m], n [s $m^{-1/3}$] is the Manning coefficient, R_h [m] is the hydraulic radius, and x and y [m] are the distances along the two horizontal directions of the grid. The water volume and water column in each cell are then updated according to the continuity equation.

Transport

Transport of properties is computed in SW and PM through the advection-diffusion equations (10 and 11):

$$\frac{\partial \beta}{\partial t} = -\frac{\partial(\beta.v)}{\partial x_i} + \frac{\partial\left(\gamma\left(\vec{\nabla}\beta\right)\right)}{\partial x_i} \quad (34)$$

$$\gamma = \alpha_i.v_i \quad (35)$$

where β is the property concentration in [g m^{-3}], x_i [m] is the distance along the direction i, γ is the diffusivity [m^2 s^{-1}] and α_i is the dispersivity along the direction i [m].

4.2.2.2.2. Time step control and stability

MOHID Land uses an adaptive time step (Figure 4-3). Starting from an initial time step defined for the whole model (dt_{model}), an iterative process is performed within each domain (PM and SW) for which a stability criterion is defined. In PM, it corresponds to the maximum water volume variation allowed in a cell. In SW the time step is controlled by limiting the Courant number. In each domain the time step is reduced and the number of iterations increased until the criterion is met. The fluxes are then integrated for each domain over dt_{model}. At the end of the iterative process, a time step is calculated for each domain (dt_{PM} and dt_{PM}). This time step corresponds to an increased value of the dt_{model} if one iteration is enough to meet the stability criterion or a decreased value of the dt_{model} if more than one iteration is needed to compute domain processes. The dt_{model} is then updated, corresponding to the minimum between dt_{SW} and dt_{PM} and the next model iteration is computed. This procedure avoids negative volumes and optimises simulation time cost without compromising model stability. This is particularly important in explicit methods and to avoid numerical dispersion (Trancoso *et al.*, 2009).

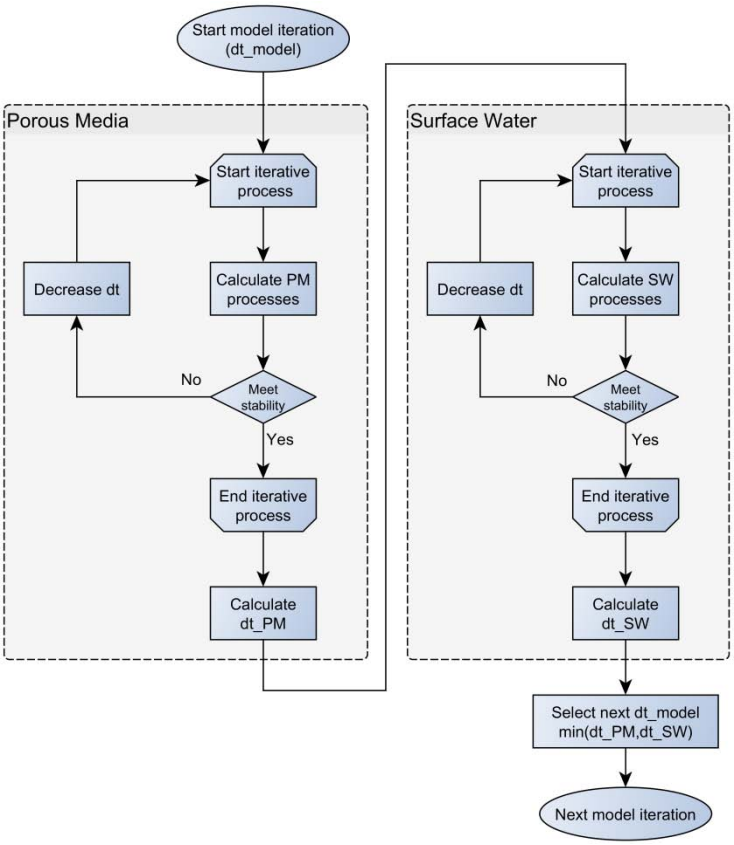

Figure 4-3: Schematic of time step management (see text for explanations)

4.2.2.3. Study site

The Garonne River is a 525 km-long river flowing from the Pyrenees in Spain to the Atlantic Ocean in the Gironde estuary in France. The flow regime is influenced by both the rainy season in the Massif Central and snow melting in the Pyrenean mountains. The middle section of the Garonne River is considered to be the 70 km long floodplain between the confluence with the Ariege River and the confluence with the Tarn River, north of the city of Toulouse. This area is characterised by a two to four kilometre-wide floodplain and a 150 m-wide river with a slope less than 0.1 % (Steiger *et al.*, 1998). The study reach is a 3.4 km-long meander-shaped channel in the middle section of the Garonne and its floodplain located near the village of Monbéqui, about 30 km downstream of Toulouse, covering an area of about 6.6 km^2 (Figure 4-4). The land cover is composed of a riparian forest close to the river (0.5 km^2), an agricultural area located on the right side of the river (3.5 km^2) and a poplar plantation (2.3 km^2) located between the riparian forest and the agricultural area on the left side of the river. Hourly discharge is recorded at the Verdun-sur-Garonne gauging station (www.hydro.eaufrance.fr) located 3.5 km upstream, with no major tributary between the station and the studied reach. At this location, the drainage area is about 13,730 km^2. Annual average flow is about 190 $m^3 s^{-1}$, ranging from 98 $m^3 s^{-1}$ in 1989 to 315 $m^3 s^{-1}$ in 1978, over the past 41 years. The driest month is August with 76 $m^3 s^{-1}$ on average and the wettest is May with 343 $m^3 s^{-1}$ on average. The daily flow is highly variable, ranging from 10 $m^3 s^{-1}$ during the severe drought in August 1991 to 2,930 $m^3 s^{-1}$ for the largest flood event recorded on 6 November 2000. The floodplain is filled with between four to seven metres of quaternary sand and gravel deposits overlying the impermeable molassic bedrock (Lancaster, 2005). In this area the Garonne River fully penetrates the alluvial formation, implying that the riverbed lies on the impermeable substratum (Weng *et al.*, 2003). Several studies have been conducted on this study site, including 3D groundwater modelling (Weng *et al.*, 2003), 2D SW-GW interaction modelling (Peyrard *et al.*, 2008), modelling of nitrate leaching under agricultural fields (Jégo *et al.*, 2012), and the relationship between the bacteria community structure and denitrification hotspots (Iribar *et al.*, 2008).

A network of 24 piezometers was installed in the inner part of the study meander (Figure 4-4). The available data consist of the hydraulic head measured at a monthly time step in each piezometer and 15 min water levels in five piezometers (P7, P9, P14, P18, P22) recorded by pressure sensor (CTD-Diver, Schlumberger) from April 2013 to March 2014.

In addition, monthly campaigns were conducted from April 2013 to March 2014, during which groundwater samples were taken in every piezometer and Cl^- concentrations, among other parameters, analysed. To ensure that the water sample corresponded to the aquifer and not to stagnant water accumulated in the piezometer, groundwater was extracted beforehand until in-situ measured electrical conductivity was constant (Sánchez-Pérez, 1992).

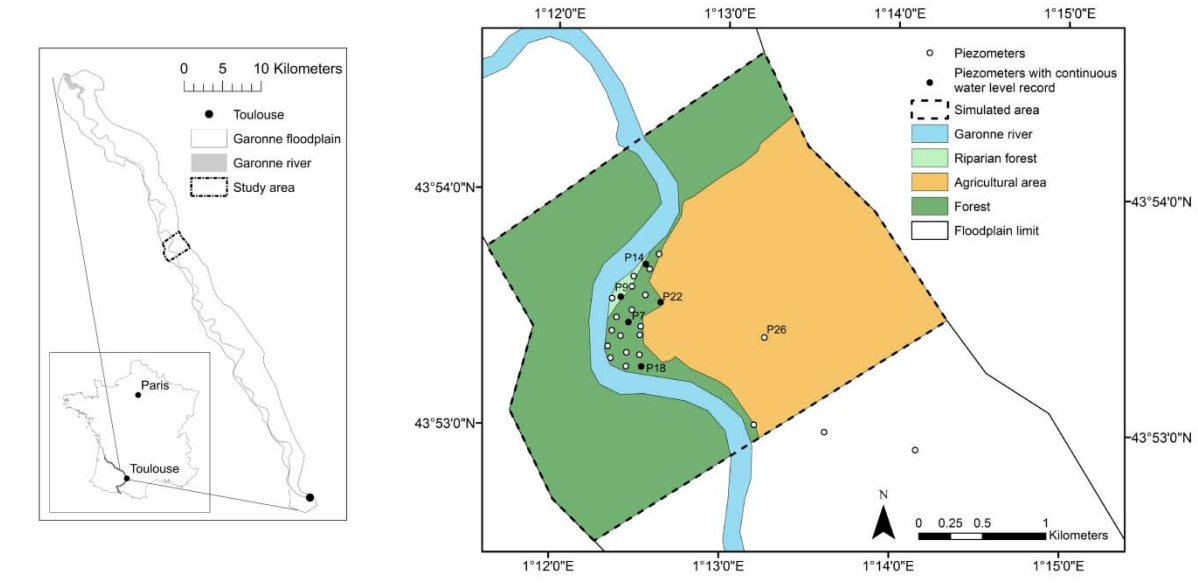

Figure 4-4: Study site location, simulated area and piezometer location

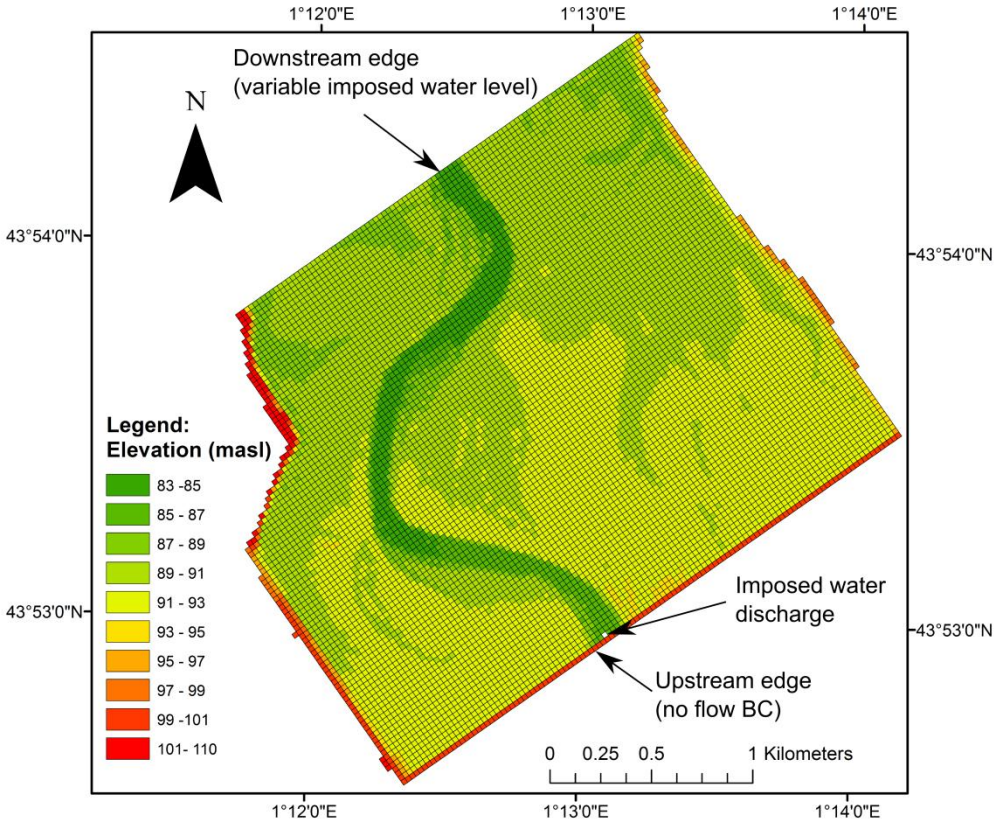

Figure 4-5: Digital terrain model (DTM) according to model grid resolution (25 m) and SW domain boundary conditions

4.2.2.4. Model implementation

4.2.2.4.1. Model geometry

The model geometry implemented for the study area involved a horizontal 2D grid with a 25 m cell side length for a total simulated area of 6.6 km^2. The PM domain has to be defined between the surface topography and a bottom layer. As the riverbed lies on impermeable molassic bedrock, the bottom layer was considered to be impermeable and located 20 cm under the riverbed. The geometry of the impermeable bottom layer followed the slope of the riverbed. The vertical layers were built from the surface to the bottom layer, with a fixed depth for each layer. The number of layers was adjusted in each cell to match as closely as possible the elevation difference between the surface and the bottom layers according to the vertical discretisation consisting of a maximum of ten layers 0.2, 0.3, 0.5, 1, 1, 1, 1, 1, 1 and 1 metre thick respectively from top to bottom.

The digital terrain model (DTM) required by the model was created by averaging the 1-m resolution LiDAR DTM (IGN) in the 25 m grid. According to the modelling strategy, the

river geometry needs to be defined in the DTM. As the original DTM did not provide the elevation of the riverbed, the river was manually dug according to available river profiles along the river (Sauvage, 1999). The 25-m resolution permitted a good representation of the riverbed geometry, with a minimum of three cells to represent the riverbed width (Figure 4-5).

4.2.2.4.2. Model parameterisation

Model parameterisation was undertaken *a priori* based on available data and knowledge to assess the ability of applying the model without a time-consuming calibration stage. The model parameters were Van Genuchten parameters (5) for the PM domain and the Manning coefficient for the SW domain (Table 1). Soil parameters used by the Van Genuchten model were obtained from pedotransfer functions (PTF) based on soil texture values, corresponding to a neural network developed and included in the ROSETTA software (Schaap *et al.*, 2001). N, α, θ_s and θ_r were derived from this PTF using a soil texture composed of 28 % sand, 52 % loam and 20 % clay, corresponding to measured field data (Jégo *et al.*, 2012). The saturated hydraulic conductivity Ks was set to 10^{-3} m s^{-1}, corresponding to the average of the measurements on the study site (Peyrard *et al.*, 2008) and matching the coarse texture of the floodplain aquifer. The Manning coefficients were different for the riverbed and the floodplain, and were extracted from Chow (1959) and reduced to 0.01 and 0.1 s $m^{-1/3}$ respectively for the riverbed (n_r) and the floodplain (n_f) since the Manning coefficient should be lower for 2D models (Néelz, 2009). Horizontal dispersivity α_H was set at 25 m in accordance with a previous simulation (Peyrard *et al.*, 2008) and vertical dispersivity α_V was set ten times lower at 2.5 m.

Table 4-1: Model parameters

Domain	Symbol	Unit	Signification	Value
Porous media (PM)	θ_s	-	Saturated water content	0.41
	θ_r	-	Residual water content	0.06
	N	-	Pore size distribution related term	1.62
	α	cm^{-1}	Air entry pressure related term	0.56
	Ks	m s^{-1}	Saturated hydraulic conductivity	10^{-3}
	α_H	m	Horizontal dispersivity	25
	α_V	m	Vertical dispersivity	2.5
Surface water (SW)	n_r	s $m^{-1/3}$	Manning riverbed	0.01
	n_f	s $m^{-1/3}$	Manning floodplain	0.1

4.2.2.4.3. Initial and boundary conditions of the model

Initial conditions included hydraulic heads in PM obtained through the interpolation of the observations in the piezometers. In the unsaturated zone, water content was set to be equal to

field capacity. Initial Cl^- concentrations in PM were also required. However, due to the lack of observation points in the agricultural area, knowledge of the spatial variability of Cl^- concentrations in this area is limited. Therefore two scenarios with different initial Cl^- concentrations for the agricultural area were tested and called IC80 and IC150, with a constant concentration in the agricultural area of 80 mg L^{-1} and 150 mg L^{-1} respectively, corresponding to the range of observed concentrations. For the rest of the area, the IC corresponded to the interpolation of observed concentrations for both scenarios. The initial water level in SW was defined according to a preliminary simulation run, with constant discharge corresponding to the first discharge value of the simulation period.

The boundary condition for PM was set to no flow conditions. This assumption was based on a previous simulation study which shows that lateral exchanges between the river and the groundwater are more important than groundwater recharge through the domain boundary (Peyrard *et al.*, 2008). This behaviour was confirmed by the low longitudinal hydraulic head gradient of 0.001 measured in the study area. The boundary condition for Cl^- concentrations was null gradient. The water level for the SW boundary condition on the downstream edge was imposed according to the river level recorded at the Verdun-sur-Garonne gauging station and transposed to the downstream edge of the modelled domain. Due to the higher elevation on the lateral edges resulting from the alluvial valley topography, the runoff could not exit through the sides. In the upstream edge, the boundary condition for SW was no flow (Figure 4-5). Furthermore in SW, the hourly water discharge recorded in the Verdun gauging station was imposed in the cell located in the middle of the river closest to the upstream boundary. The Cl^- concentration of the imposed discharge was set at a constant of 9 mg L^{-1}, corresponding to the average of the measured concentrations in the river.

The simulation period was from 15 May to 1 October 2013, characterised by a first flood with a five to 10-year return period, followed by a second smaller flood corresponding to a two to five-year return period, and a three-month drying stage period (Figure 4-6).

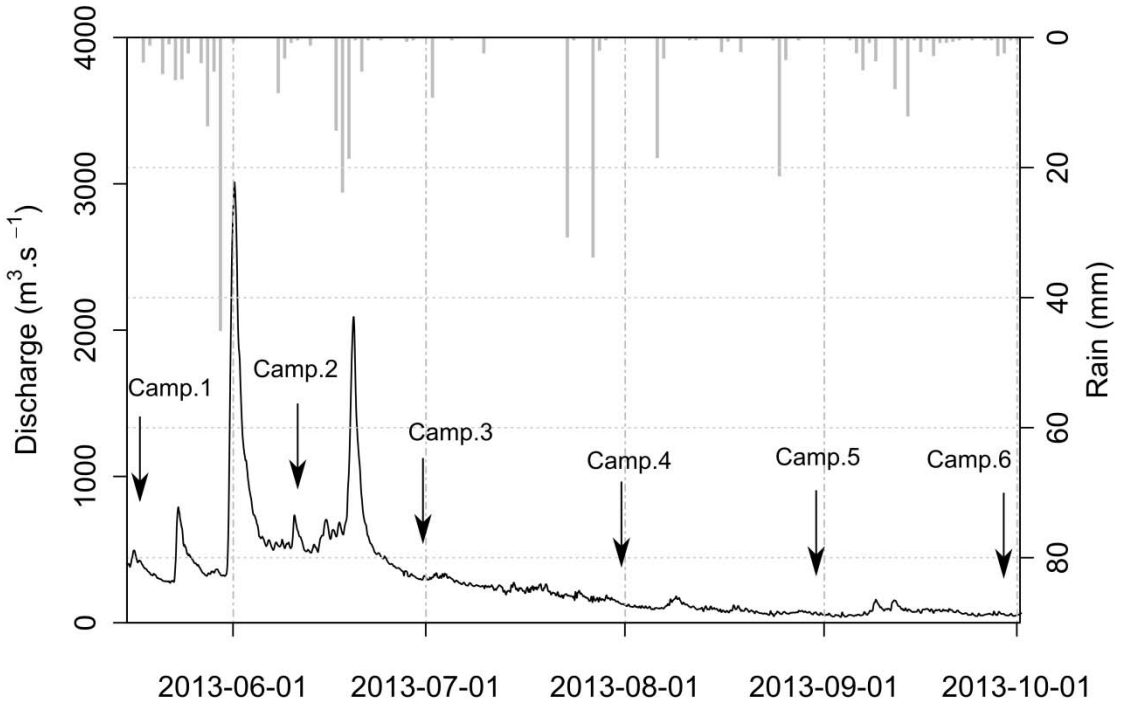

Figure 4-6: Daily discharge and rainfall during the simulated period. Arrows correspond to the sampling campaign periods (campaigns 1 to 6 from 15 May 2013 to 1 October 2013)

4.2.2.4.4. Model evaluation and analysis

The evaluation of the quality of the simulations included the calculation of the Nash-Sutcliffe coefficient (NS) (Nash and Sutcliffe, 1970), root mean square error (RMSE), percent bias between simulations and observations (PBIAS) as defined in Sorooshian *et al.* (1993), and coefficient of determination (R^2). The hydraulic head was continuously recorded by pressure sensors in five piezometers (P7, P9, P14, P18, and P22) and monthly manual records were also taken for all the piezometers. Observed hydraulic heads were compared to the hydraulic head simulated in the deeper cell corresponding to each piezometer location. Cl^- concentrations analysed monthly were compared to the average of the simulated Cl^- concentrations over the saturated area. Daily infiltration and exfiltration were separated between the area corresponding to the riverbed (including the banks) and the rest of the simulated domain corresponding to the floodplain. Positive values corresponded to infiltration (SW to PM) and negative value to exfiltration (PM to SW).

4.2.2.4.5. Application to different return period flood events

The model was applied to simulate water exchanges for two, five, 10 and 20-year return period floods according to the French Banque Hydro archives. The floods consist of a 16-day period equivalent to the linear transformation of the flow values observed during the flood recorded between 29 May 2013 and 7 June 2013, to match the instantaneous peak flow values corresponding to the return period (1800, 2700, 3200 and 3700 $m^3 s^{-1}$ for the two, five, 10 and 20-year return periods respectively).

4.2.3. Results

4.2.3.1. Hydraulic heads

The simulated hydraulic head and the observed hydraulic head for the 24 piezometers over the five campaigns from June to October 2013 (campaigns 2 to 6, Figure 4-6) are shown in Figure 4-7. Overall, the model was able to reproduce the observation correctly, with RMSE of 0.33 m, R^2 of 0.92 and NS of 0.90 for the hydraulic head recorded monthly in all the piezometers. However there was a slight overestimation of the simulated hydraulic head (PBIAS=0.2 %). This is especially true for P26, which is the furthest piezometer from the river (Figure 4-4). Figure 4-7 shows the temporal series of observed and simulated hydraulic heads for the five piezometers equipped with continuous water level-recording sensors. With regard to the scoring parameters, P9 and P18 hydraulic heads were the best simulated, with the highest NS (0.85, 0.88) and R^2 (0.89, 0.91) and the lowest RMSE (0.38 and 0.33 m) out of the five piezometers. However, differences were observed between the piezometers. P9 offered a good representation of the hydraulic head during the peak flow, while the hydraulic head in P18 was simulated more closely for the recession curve. P7 exhibited behaviour close to P9. Finally P22 and P14 were the least satisfactory (NS=0.71 and 0.65). Hydraulic heads during the first peak flow (1 June 2013) were generally well represented in the model, while the values for the second peak flow (19 June 2013) were overestimated. On the whole, the hydraulic heads at the end of the recession period were slightly overestimated. Water level greater than soil surface was recorded by the continuous sensors in three of the five piezometers (P9, P14 and P7) during the peak flow of the flood on 1 June 2013 and can be interpreted as flood overbank flow. However, the simulation results indicated that overbank flow occurred at all the piezometer locations.

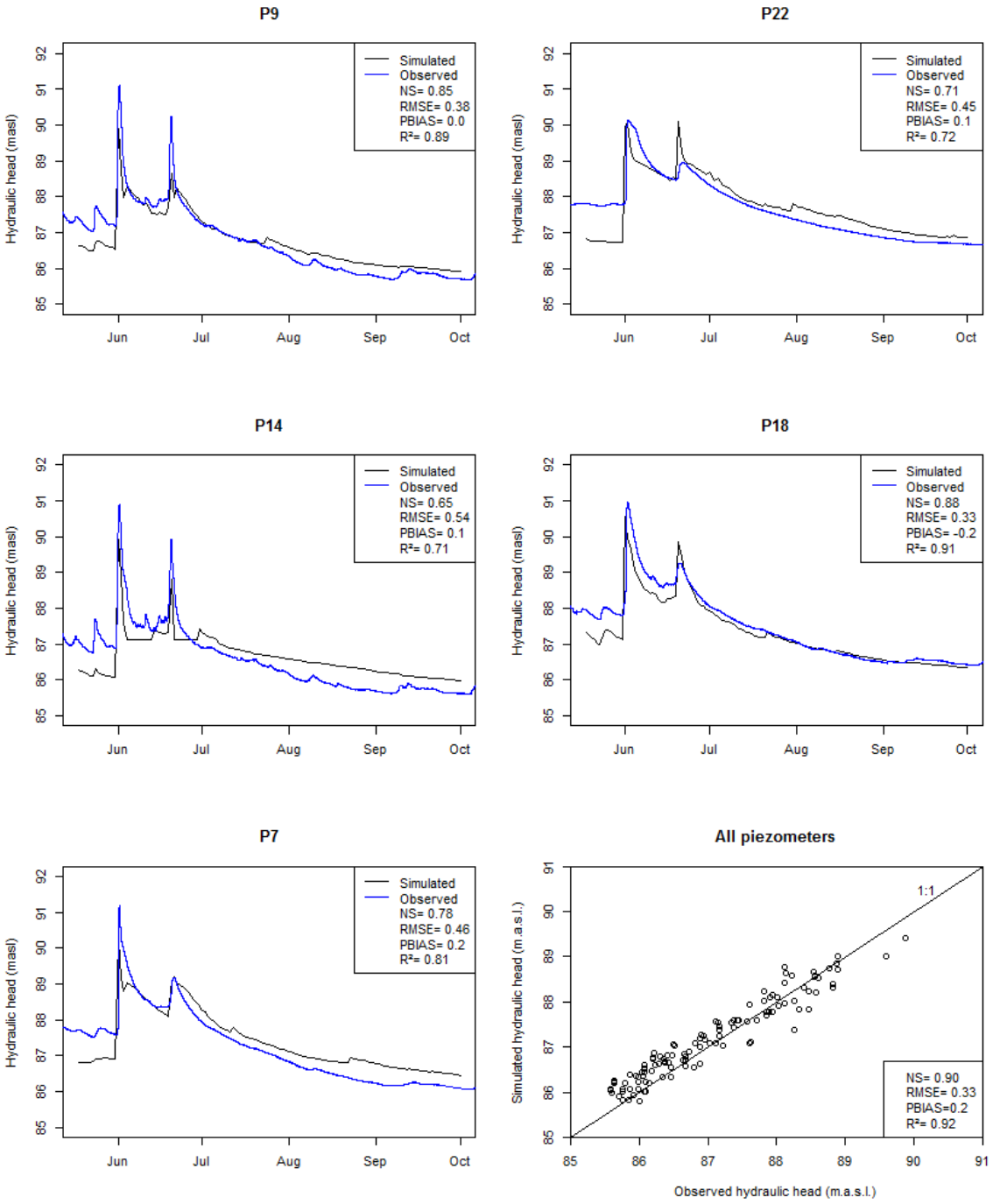

Figure 4-7: Simulated and observed hydraulic heads for the five piezometers with continuous records from 15 May 2013 to 1 October 2013, and observed *vs.* simulated hydraulic head in the 24 piezometers for sampling campaigns 1 to 5

4.2.3.2. SW-GW exchanges

Simulated daily exchanges between SW and PM across the entire simulated area are shown in Figure 4-8, together with river discharge. The total infiltration water volume of 3.46×10^6 m^3 corresponded to an average of 425 mm over the 6.6 km^2 simulated area and represented 49 % of the maximum aquifer water volume attained on 1 June 2013. During the simulated period, the infiltrated volume was 0.43×10^6 m^3 in the riverbed location and 3.04×10^6 m^3 in the

floodplain, while the exfiltrated volume was 1.68×10^6 m^3 in the riverbed location and 1.12×10^6 m^3 in the floodplain. Infiltration was therefore 23 % greater than exfiltration. Infiltration only occurred for a short period (64 % of the infiltration occurred over four days) compared to exfiltration (64 % of the exfiltration occurred over 41 days), but with greater intensity. The high infiltration periods corresponded to flood events. In contrast, exfiltration occurred at lower rates than infiltration, but during the entire recession period. Water exchanges were very small outside flood periods (only 9 % of exchanges where the daily discharge was below 250 m^3 s^{-1}, representing 61 % of the period length). Figure 4-9 represents the spatial distribution of accumulated infiltration and exfiltration during the simulated period. Infiltration occurred over most of the floodplain area, with higher infiltration in terrain depressions. Exfiltration mostly occurred at the riverbank location, but was also localised in terrain depressions. Indeed, 88 % of the infiltration and 40 % of the exfiltration occurred in the floodplain area. Both exfiltration and infiltration occurred at the same time at different locations. It was also observed that in the first few days immediately after the flood, exfiltration rates were similar in the floodplain and riverbed areas, but after a few days exfiltration occurred primarily in the riverbed area.

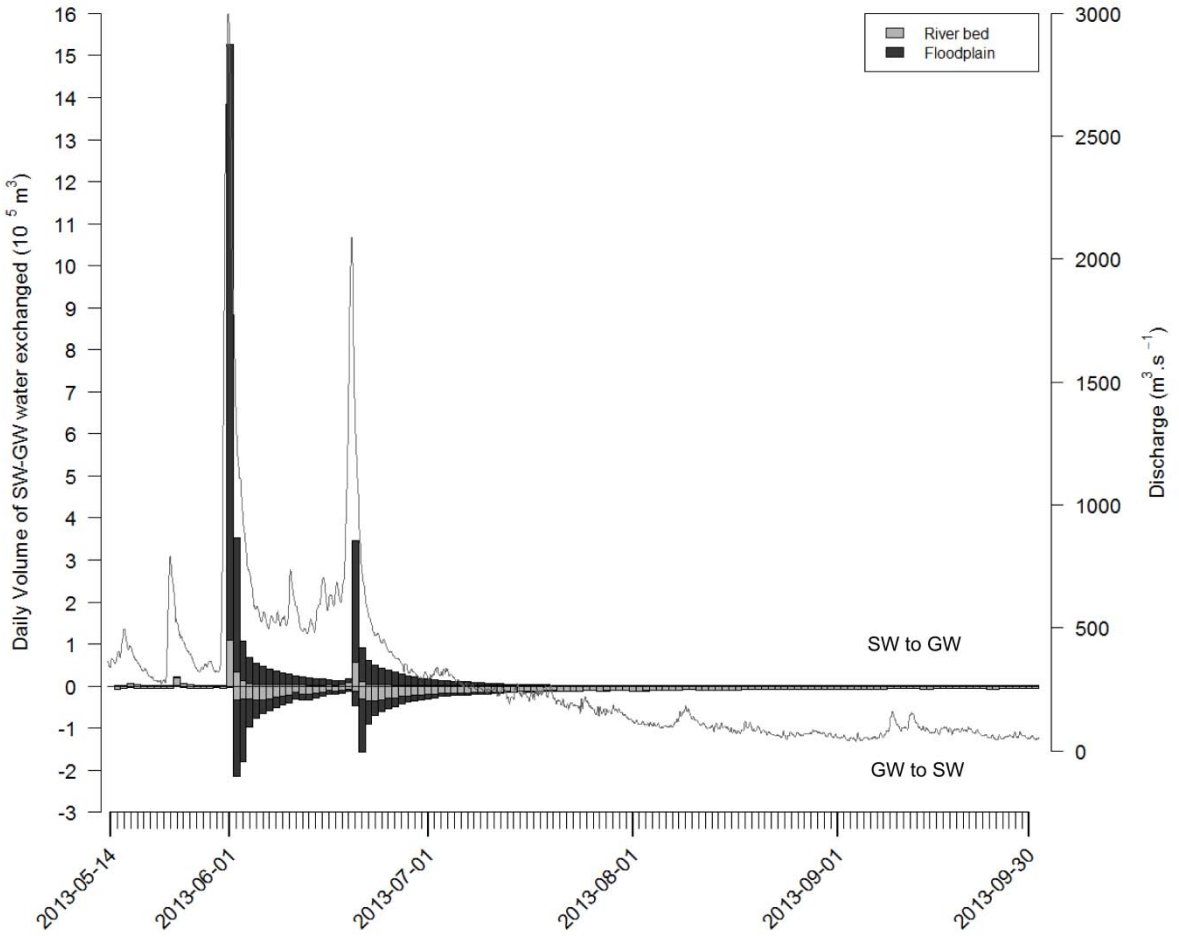

Figure 4-8: Daily exchanged water volume between SW and GW (positive values for infiltration, negative values for exfiltration). Dark grey represents exchanges for the plain area, and light grey for the riverbed area. Hourly discharge is shown by a black solid line.

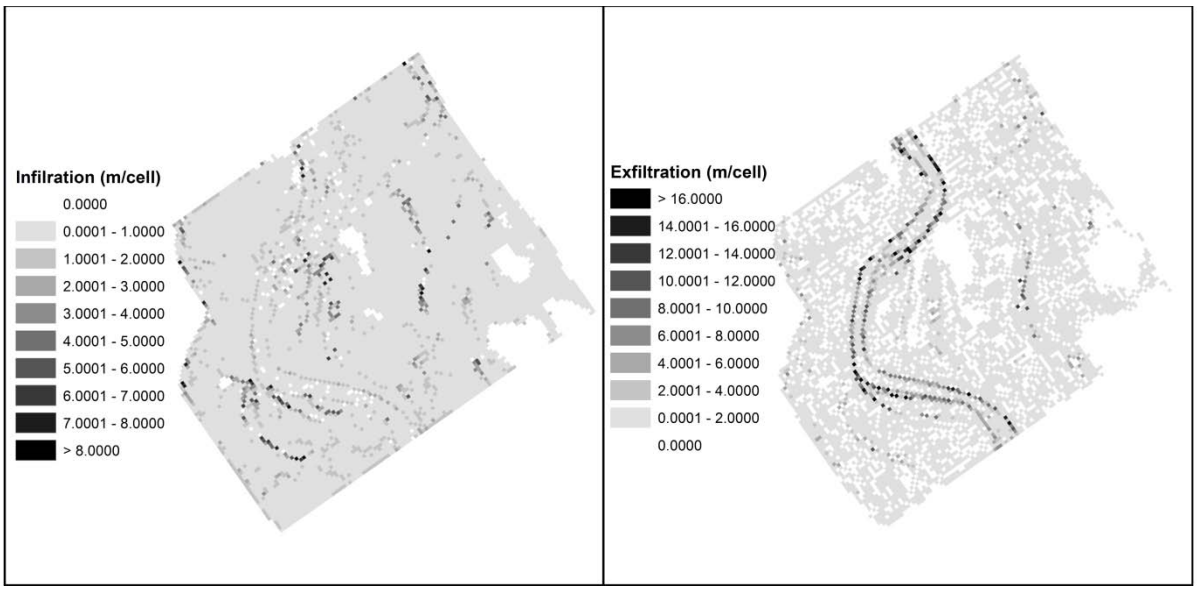

Figure 4-9: Spatial pattern of accumulated infiltrated water (left) and exfiltrated water (right) during the simulated period

In Table 4-2, exchanged volume is indicated for a below bankfull and an overbank flood event during the simulation period. The maximum discharge recorded for the overbank flood event was more than three times greater than the below bankfull flood event and was characterised by a 10-year return period while the below bankfull event return period was one year. In terms of water exchanged, infiltration was 77 times greater and exfiltration 85 times greater during the overbank flood event than during the below bankfull flood event.

Table 4-2: Instantaneous peak flow (Q max) and estimated return period associated to a below bankfull and an overbank flood event. Volume of water infiltrated (Inf.), exfiltrated (Exf.) and net exchanges (Net) during the period indicated

Flood event	Period	Q max [$m^3.s^{-1}$]	Return period [yr]	Inf [10^3 m^3]	Exf [10^3 m^3]	Net [10^3 m^3]
Below bankfull	23/05/2013-25/05/2013 [3 days]	790	1	30	-10	20
Overbank	1/06/2013-10/06/2013 [10 days]	3010	10	2327	-855	1472

4.2.3.3. Transport simulations

The simulated average Cl^- concentrations in the aquifer were performed with two different initial conditions corresponding to different Cl^- concentrations in the agricultural area (scenarios IC80 and IC150). RMSE between observed and simulated values was 28.8 $mg \cdot L^{-1}$ for both simulations, R^2 and PBIAS were 0.34 and -35.9 % respectively for IC80 and 0.46 and -21.3 % for IC150. Temporal series of simulated and measured Cl^- concentrations for the piezometers equipped with a continuous water level sensor are shown in Figure 4-10. Simulated concentrations were in good agreement with the observation for P9 for both scenarios. Simulated Cl^- concentrations for P14 and P22 showed differences between the two simulations, with better results for the IC150 scenario than for the IC80 scenario. Finally, simulated Cl^- concentrations for P7 and P18 had similar values for the IC80 and IC150 scenarios, but neither simulated concentration was able to represent the rise of Cl^- concentrations observed in August and September.

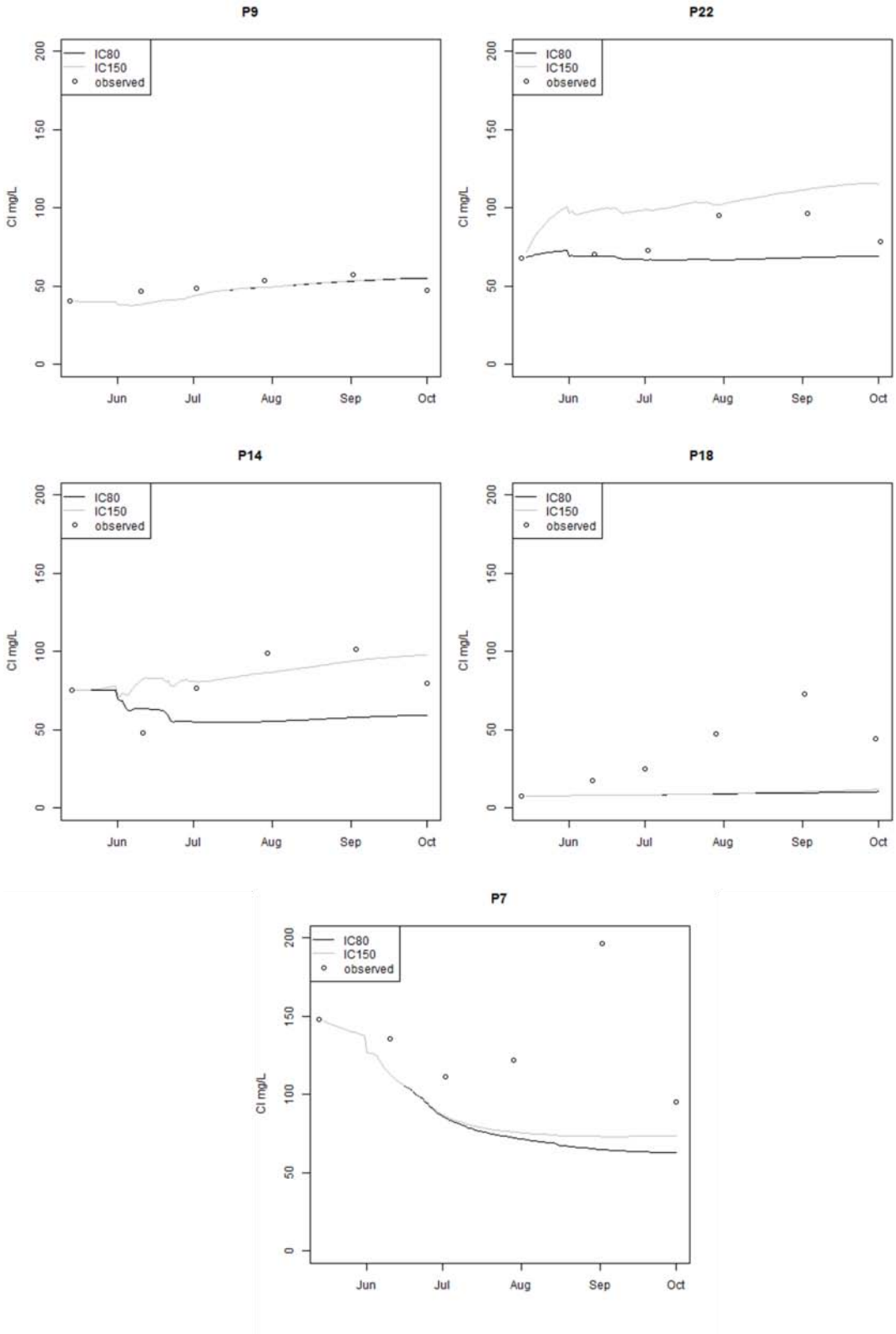

Figure 4-10 (a to e): Simulated and observed Cl^- concentrations for the five piezometers with continuous hydraulic head records. Black and grey lines correspond to the initial concentrations of 80 mg L^{-1} (scenario IC80) and 150 mg L^{-1} (scenario IC150) respectively in the agricultural area

4.2.3.4. Application to different return period flood events

Four different flood events corresponding to the two, five, 10 and 20-year return period maximum discharges were simulated. Exchanged volumes were calculated and separated into infiltration, exfiltration and net exchange for the riverbed, the floodplain and the whole area. The maximum flood extent, corresponding to the maximum area submerged during the simulations, was also computed (Table 3). The volume of SW-GW exchanges and flood extent area increased with the return period of the event. Only the exfiltration volume for the river area appeared to be limited to a threshold value for flood intensity above the five-year return period. The magnitude of the increase in water exchanges and flood extent area between the two and five-year return period was greater than the magnitude of the increase between the five and 20-year return period.

Table 4-3: Volume of water infiltrated (Inf.), exfiltrated (Exf.) and net exchanges (Net) in 10^6 m^3 and the flood extent in km^2 for the riverbed area (r), the floodplain area (f) and the whole area (tot). Results are given for each return period flood (T)

	Inf. f	Inf. r	Inf. tot	Exf. f	Exf. r	Exf. tot	Net f	Net r	Net tot	Flood extent
T=2 yr	0.81	0.15	0.96	-0.14	-0.28	-0.42	0.67	-0.13	0.54	3.2
T=5 yr	1.37	0.19	1.56	-0.35	-0.38	-0.72	1.02	-0.23	0.79	5.7
T=10 yr	1.46	0.22	1.68	-0.39	-0.38	-0.77	1.07	-0.16	0.91	6.1
T=20 yr	1.53	0.28	1.81	-0.43	-0.38	-0.82	1.10	-0.10	1.00	6.3

4.2.4. Discussion

The aim of the study was to assess SW-GW exchanges in a floodplain area using a model coupling a 3D flow in the porous media and 2D flow in the surface runoff including infiltration and exfiltration. The major feature included in this study was to capture overbank flow infiltration into the aquifer during large floods. To assess the relevance of the model's application in areas with limited knowledge and available data, the parametrisation was performed *a priori*. The main parameters were defined using accessible information that could be obtained for a large number of sites. In addition to the requirement for a DTM of the studied area, the use of the model requires hydraulic conductivity that was set homogenously and correspondingly for a coarse alluvial aquifer and field measurement data. Soil retention parameters were derived from widely-used PTF based on soil texture. Manning coefficients were chosen from the literature (Chow, 1959) and reduced, as advised when considering 2D models (Néelz, 2009). Finally, dispersivity was chosen based on previous modelling studies

(Peyrard *et al.*, 2008). However the model was validated against an extensive observation dataset to assess the applicability of the model in similar contexts to that studied here.

Modelling the surface runoff with the 2D Saint-Venant equation using a finite volume method has been successfully applied to simulate flooding in floodplains (Caleffi *et al.*, 2003; Horritt *et al.*, 2007). In this study, simulated hydraulic heads for all the piezometers indicated the presence of overbank flow, although it was only observed in four of the five piezometers in which the water level was being monitored continuously, indicating that the simulated flood extent was being overestimated. This has already been observed in a study using the same equation but a different numerical scheme method (Morales-Hernández *et al.*, 2014), and is related to an incorrect definition in levees. Indeed, the grid resolution complicated the representation of small structures such as dykes and ditches that could prevent flow from reaching certain areas or could locally accelerate the dewatering rate. The 2D finite volume model also shows greater sensitivity to grid resolution than topographic sampling (Horritt *et al.*, 2006). In addition, the flood extent is closely related to discharge input, and uncertainties in flood discharge evaluation can be a critical issue in this particular case (Baldassarre and Montanari, 2009). However a model using a finite volume method solving the 2D Saint-Venant equation has been shown to be less sensitive to the Manning parameter during high flow and especially the Manning coefficients for the floodplain (Horritt *et al.*, 2007).

Despite the overestimation of the extent of the flood, the simulated hydraulic heads were in good agreement with the observed data. The rapid hydraulic head increase in the piezometers close to the river during the flood was well represented (P9, P14 and P18). Generally, the hydraulic heads simulated for the first peak flow of the simulated period matched reality, while the model results tended to be overestimated for the second peak flow. The good representation of hydraulic heads indicated that the simplification of hydraulic conductivity over the domain, which is known to be heterogeneous and important for SW-GW exchanges (Frei *et al.*, 2009), did not appear to have a strong negative impact on the simulated hydraulic heads.

Modelling of conservative tracers (Cl^-) was performed for two scenarios representing two levels of aquifer contamination by agriculture to validate the simulation of water fluxes. The results showed RMSE of 28.8 mg L^{-1} for both scenarios, but the results were found to be heterogeneous between piezometers. The simulation results showed that simulated Cl^- concentrations for piezometers in locations under the influence of water-mixing between river

and groundwater (P14) differed between the two scenarios. Other locations seemed to be mainly under the influence of the initial conditions defined in the agricultural area only (P22), since differences in initial conditions led to an increase in Cl^- concentrations while no impact from dilution with river water was observed. Other locations were under the influence of the river alone (P9), since the simulated concentrations did not vary for different initial conditions, but dilution of Cl^- concentrations could be observed. Cl^- concentrations were well simulated for these piezometers when considering the scenario corresponding to the highest concentration in the agricultural area. This indicated that a good definition of initial concentrations in the agricultural zone was important for correctly simulating element concentrations in the monitored area. However, concentrations were not necessarily homogenous in the agricultural area and spatial and temporal variations could explain variations between observed and simulated concentrations. For other piezometers (P7 and P18), while simulated Cl^- concentrations were close to observations for the first two months of simulations, the observations showed a rise in Cl^- concentrations over the last three months which the model was unable to reproduce. Difficulties in representing Cl^- concentrations for these piezometers could be explained by the presence of sources of Cl^- that were not taken into account by the model. Indeed previous studies have shown that concentrations can rise when the water level reaches the higher soil layer (Ochoa-Salazar, 2008) and point source pollution might have occurred. For example in P7, Cl^- concentrations reached a level higher than initial conditions (around 200 mg L^{-1}). In this case, the observed concentrations cannot be explained by the mix between river water and groundwater, therefore other processes have to be taken into account. This might explain the overall underestimation of Cl^- concentrations by the model (PBIAS of -35.9 % and -21.1 % for the IC80 and IC150 scenarios respectively). These results indicate that consideration of processes other than conservative transport is required to improve Cl^- dynamic modelling. Nevertheless, the simulation could be considered satisfactory as the mixing processes near the river – where river water groundwater interactions are dominant – were well simulated, leading to a good representation of SW-GW exchanges in these area.

SW-GW exchanges were evaluated for the simulated period and exhibited strong spatial and temporal variations. Infiltration occurred mostly during the water-rising periods and in the days following the peak flow, and infiltration in the floodplain represented a large amount of the total water infiltrated. Exfiltration was occurring at a lesser intensity than infiltration, but throughout the entire recession period and mainly near the river location. Moreover, the two

processes can occur in the same location but at different times. The importance of flow dynamics and short-term variation of river flow on SW-GW exchanges has already been pointed out in similar studies (Derx *et al.*, 2010; Helton *et al.*, 2014) and SW-GW interactions are known to control the floodplain water balance (Helton *et al.*, 2014). The results indicated that during the simulation period, infiltration was greater than exfiltration. This showed that extensive floods can influence groundwater storage over a number of months. Furthermore, these findings underlined the importance of taking infiltration from overland flow into account to represent exchanges during flood events accurately. Indeed in the case of large flood events similar to the one presented here, the volume infiltrated in the floodplain was greater than infiltration at the river location and accounted for 29 % of the aquifer's maximum water volume. The importance of flooding on water exchanges and floodplain and water budget (Krause and Bronstert, 2007) is also confirmed by the results indicating that the exchanged water volume during a large overbank flood event (10-year return period) is more than 70 times greater than during an annual below bankfull flood event.

Modelling floods of different magnitudes according to the return period allowed conclusions to be drawn on the relationship between water exchange-related parameters and flood extent. The link between all water exchange parameters and water extent confirmed that accounting for overland flow during large floods is essential when assessing GW-SW exchanges. Exfiltration through the riverbank seemed limited to a certain threshold, meaning that the exfiltration volume would reach a limit in the areas close to the river while increasing in the floodplain for large floods. In addition major differences were found between the two-year return period flood and others of a higher magnitude. This showed that water exchanges in the floodplain can be very significant for the largest flood, and that exceptional events with a high return period flood might be of great importance in the mixing process in the floodplain compared to more common flood events with a lower intensity. However above a certain threshold (corresponding to the five-year return period in this study), the impacts of flooding on water exchanges were similar. Above this value, depending on the topography of the floodplain, the whole area of the floodplain is flooded and the porous media is fully saturated. This can have an impact on the residence time of surface water during floods that would decrease exponentially with river discharge due to a smaller percentage of surface water entering the subsurface (Helton *et al.*, 2014).

The modelling approach in this study allowed an assessment of the importance of overbank flow for SW-GW exchanges during a flood event at reach scale. However, to represent these

detailed SW-GW processes, the use of a distributed model of this kind required significant computation time and could only be applied at reach scale for a short time. In addition the results depended on the accuracy of the flood extent modelling, which requires a very detailed topography and considerable effort to incorporate topography features such as dykes and ditches in order to improve modelling results. Solute transport simulation was found to produce good results for some piezometers, while results for others were unsatisfactory. However this problem might be due to the use of a tracer (chloride) that not only reflects SW-GW mixing but can be influenced by other processes such as point source pollution and soil leaching that should be included in the model to improve simulation results. Furthermore, despite the good results with the actual parameterisation, a sensitivity analysis could be performed on key parameters such as hydraulic conductivity to provide a better assessment of the role of the parameters on model performance.

4.2.5. Conclusions

This study presented a modelling approach coupling physically-based 2D surface runoff and unsaturated 3D flows in porous media to assess the water-exchange dynamics between surface water and groundwater in floodplains. Using a basic knowledge of the study site for parameterisation, the results revealed the model's ability to reproduce the local hydrology effectively. The model highlighted the spatial and temporal variability of infiltration and exfiltration patterns over the floodplain. SW-GW exchange periods were limited to flood events and the following few days. The results particularly underlined the importance of infiltration from overbank flow in SW-GW interactions during large floods. However, the impact of flooding on the floodplain water budget appeared to be similar for events above a certain threshold of flood intensity. Efforts have to be made to accurately model the flood extent, which is very sensitive to surface topography and important for correctly evaluating water exchanges since infiltrated volume is closely related to flood extent.

As overbank flood events and hyporheic fluxes are key elements in floodplain ecology and hydrology (Tockner *et al.*, 1999; Krause *et al.*, 2011), the modelling of SW-GW including this feature is fundamental for studying the flood plain environment. The modularity of the model structure allows further modules to be developed easily, including biogeochemical processes occurring in floodplain areas such as denitrification. Following this first step of hydraulic validation, the model could then be used to study the impact of management practices and

different reach geomorphology on water exchange and associated biogeochemical cycles in floodplains.

Acknowledgements

This study was undertaken as part of the EU Interreg SUDOE IVB programme (ATTENAGUA - SOE3/P2/F558 project) and was funded by ERDF. This research was carried out as a part of "ADAPT'EAU" (ANR-11-CEPL-008), a project supported by the French National Research Agency (ANR) within the framework of the Global Environmental Changes and Societies (GEC&S) programme. This work was granted access to the HPC resources of CALMIP under allocation P13119. The 1m-digital terrain model was provided by the French National Geographical Institute (IGN) and the discharge data by DREAL. The source code for the model used in this study, MOHID LAND, is free of charge and is available from mohid.codeplex.com. The authors thank Claire Tarring for helping to improve the English.

References

Amoros, C., Bornette, G., Cedex, V., 2002. Connectivity and biocomplexity in waterbodies of riverine floodplains. Freshw. Biol. 47, 761–776. doi:10.1046/j.1365-2427.2002.00905.x

Baillieux, A., Campisi, D., Jammet, N., Bucher, S., Hunkeler, D., 2014. Regional water quality patterns in an alluvial aquifer: Direct and indirect influences of rivers. J. Contam. Hydrol. 169, 123–31. doi:10.1016/j.jconhyd.2014.09.002

Baldassarre, G. Di, Montanari, A., 2009. Uncertainty in river discharge observations: a quantitative analysis. Hydrol. Earth Syst. Sci. 13, 913–921.

Bates, P.D., Stewart, M.D., Desitter, A., Anderson, M.G., Renaud, J.-P., Smith, J.A., 2000. Numerical simulation of floodplain hydrology. Water Resour. Res. 36, 2517–2529. doi:10.1029/2000WR900102

Boano, F., Camporeale, C., Revelli, R., Ridolfi, L., 2006. Sinuosity-driven hyporheic exchange in meandering rivers. Geophys. Res. Lett. 33, 1–4.

Boano, F., Demaria, A., Revelli, R., Ridolfi, L., 2010. Biogeochemical zonation due to intrameander hyporheic flow. Water Resour. Res. 46, 1–13.

Bradford, R.B., Acreman, M.C., 2003. Applying MODFLOW to wet grassland in-field habitats: a casestudy from the Pevensey Levels, UK. Hydrol. Earth Syst. Sci. Discuss. 7, 43–55.

Braunschweig, F., Leitao, P.C., Fernandes, L., Pina, P., Neves, R.J.J., 2004. The object-oriented design of the integrated water modelling system MOHID, in: Science, C.T.M. and G.F.P.B.T.-D. in W. (Ed.), Computational Methods in Water Resources: Volume 2 Proceedings of the XVth International Conference on Computational Methods in Water Resources. Elsevier, pp. 1079–1090. doi:http://dx.doi.org/10.1016/S0167-5648(04)80126-6

Brito, D., Campuzano, F.J., Sobrinho, J., Fernandes, R., Neves, R., 2015. Integrating operational watershed and coastal models for the Iberian Coast: Watershed model implementation – A first approach. Estuar. Coast. Shelf Sci. 167, 138–146. doi:10.1016/j.ecss.2015.10.022

Brookfield, A.E., Sudicky, E.A., Park, Y.-J., Conant, B., 2009. Thermal transport modelling in a fully integrated surface/subsurface framework. Hydrol. Process. 23, 2150–2164. doi:10.1002/hyp.7282

Caleffi, V., Valiani, A., Zanni, A., 2003. Finite volume method for simulating extreme flood events in natural channels. J. Hydraul. Res. 41, 167–177. doi:10.1080/00221680309499959

Chow, V.T., 1959. Open channel hydraulics. McGraw-Hill, New-York.

Chow, V.T., Maidment, D.R., Mays, L.W., 1988. Applied Hydrology. McGraw-Hill, New-York.

Condon, L.E., Maxwell, R.M., 2013. Implementation of a linear optimization water allocation algorithm into a fully integrated physical hydrology model. Adv. Water Resour. 60, 135–147. doi:10.1016/j.advwatres.2013.07.012

Correll, D.L., Jordan, T.E., Weller, D.E., 1992. Nutrient flux in a landscape: effects of coastal land use and terrestrial community mosaic on nutrient transport to coastal waters. Estuaries 15, 431–442.

Dagès, C., Paniconi, C., Sulis, M., 2012. Analysis of coupling errors in a physically-based integrated surface water–groundwater model. Adv. Water Resour. 49, 86–96. doi:10.1016/j.advwatres.2012.07.019

Derx, J., Blaschke, A.P., Blöschl, G., 2010. Three-dimensional flow patterns at the river–aquifer interface — a case study at the Danube. Adv. Water Resour. 33, 1375–1387. doi:10.1016/j.advwatres.2010.04.013

Doppler, T., Hendricks Franssen, H.-J., Kaiser, H.-P., Kuhlman, U., Stauffer, F., 2007. Field evidence of a dynamic leakage coefficient for modelling river–aquifer interactions. J. Hydrol. 347, 177–187. doi:10.1016/j.jhydrol.2007.09.017

Engeler, I., Hendricks Franssen, H.J., Müller, R., Stauffer, F., 2011. The importance of coupled modelling of variably saturated groundwater flow-heat transport for assessing river–aquifer interactions. J. Hydrol. 397, 295–305. doi:10.1016/j.jhydrol.2010.12.007

Frei, S., Fleckenstein, J.H., Kollet, S.J., Maxwell, R.M., 2009. Patterns and dynamics of river–aquifer exchange with variably-saturated flow using a fully-coupled model. J. Hydrol. 375, 383–393. doi:10.1016/j.jhydrol.2009.06.038

Furman, A., 2008. Modeling Coupled Surface–Subsurface Flow Processes: A Review. Vadose Zo. J. 7, 741–756. doi:10.2136/vzj2007.0065

Grimm, N.B., Fisher, S.G., 1984. Exchange between interstitial and surface water: implications for stream metabolism and nutrient cycling. Hydrobiologia 111, 219–228.

Helton, A.M., Poole, G.C., Payn, R.A., Izurieta, C., Stanford, J.A., 2014. Relative influences of the river channel, floodplain surface, and alluvial aquifer on simulated hydrologic residence time in a montane river floodplain. Geomorphology 205, 17–26. doi:http://dx.doi.org/10.1016/j.geomorph.2012.01.004

Hoffmann, C.C., Berg, P., Dahl, M., Larsen, S.E., Andersen, H.E., Andersen, B., 2006. Groundwater flow and transport of nutrients through a riparian meadow – Field data and modelling. J. Hydrol. 331, 315–335. doi:http://dx.doi.org/10.1016/j.jhydrol.2006.05.019

Horritt, M.S., Bates, P.D., Mattinson, M.J., 2006. Effects of mesh resolution and topographic representation in 2D finite volume models of shallow water fluvial flow. J. Hydrol. 329, 306–314. doi:10.1016/j.jhydrol.2006.02.016

Horritt, M.S., Di Baldassarre, G., Bates, P.D., Brath, A., 2007. Comparing the performance of a 2-D finite element and a 2-D finite volume model of floodplain inundation using airborne SAR imagery. Hydrol. Process. 21, 2745–2759. doi:10.1002/hyp.6486

Iribar, A., Sánchez-Pérez, J., Lyautey, E., Garabétian, F., 2008. Differentiated free-living and sediment-attached bacterial community structure inside and outside denitrification hotspots in the river–groundwater interface. Hydrobiologia 598, 109–121 LA – English. doi:10.1007/s10750-007-9143-9

Jégo, G., Sánchez-Pérez, J.M., Justes, E., 2012. Predicting soil water and mineral nitrogen contents with the STICS model for estimating nitrate leaching under agricultural fields. Agric. Water Manag. 107, 54–65. doi:http://dx.doi.org/10.1016/j.agwat.2012.01.007

Junk, W.J., Bayley, P.B., Sparks, R.E., 1989. The flood pulse concept in river-floodplain systems. Can. Spec. Publ. Fish. Aquat. Sci. 106, 110–127.

Kollet, S.J., Maxwell, R.M., 2006. Integrated surface–groundwater flow modeling: A free-surface overland flow boundary condition in a parallel groundwater flow model. Adv. Water Resour. 29, 945–958. doi:10.1016/j.advwatres.2005.08.006

Krause, S., Bronstert, A., 2007. The impact of groundwater–surface water interactions on the water balance of a mesoscale lowland river catchment in northeastern Germany. Hydrol. Process. 21, 169–184. doi:10.1002/hyp.6182

Krause, S., Bronstert, A., Zehe, E., 2007. Groundwater–surface water interactions in a North German lowland floodplain – Implications for the river discharge dynamics and riparian water balance. J. Hydrol. 347, 404–417. doi:10.1016/j.jhydrol.2007.09.028

Krause, S., Hannah, D.M., Fleckenstein, J.H., Heppell, C.M., Kaeser, D., Pickup, R., Pinay, G., Robertson, A.L., Wood, P.J., 2011. Inter-disciplinary perspectives on processes in the hyporheic zone. Ecohydrology 4, 481–499. doi:10.1002/eco.176

Lancaster, R.R., 2005. Fluvial Evolution of the Garonne River, France: Integrating Field Data with Numerical Simulations.

Maxwell, R.M., Putti, M., Meyerhoff, S., Delfs, J.-O., Ferguson, I.M., Ivanov, V., Kim, J., Kolditz, O., Kollet, S.J., Kumar, M., Lopez, S., Jie, N., Paniconi, C., Park, Y.-J., Phanikumar, M.S., Shen, C., Sudicky, E.A., Sulis, M., 2014. Surface-subsurface model intercomparison: A first set of benchmark results to diagnose integrated hydrology and feedbacks. Water Resour. Res. 50, 1531–1549.

McClain, M.E., Boyer, E.W., Dent, C.L., Gergel, S.E., Grimm, N.B., Groffman, P.M., Hart, S.C., Harvey, J.W., Johnston, C.A., Mayorga, E., McDowell, W.H., Pinay, G., 2003. Biogeochemical Hot Spots and Hot Moments at the Interface of Terrestrial and Aquatic Ecosystems. Ecosystems 6, 301–312. doi:10.1007/s10021-003-0161-9

Morales-Hernández, M., Hubbard, M.E., García-Navarro, P., 2014. A 2D extension of a Large Time Step explicit scheme (CFL>1) for unsteady problems with wet/dry boundaries. J. Comput. Phys. 263, 303–327. doi:10.1016/j.jcp.2014.01.019

Morin, E., Grodek, T., Dahan, O., Benito, G., Kulls, C., Jacoby, Y., Langenhove, G. Van, Seely, M., Enzel, Y., 2009. Flood routing and alluvial aquifer recharge along the ephemeral arid Kuiseb River, Namibia. J. Hydrol. 368, 262–275. doi:10.1016/j.jhydrol.2009.02.015

Mualem, Y., 1976. A new model for predicting the hydraulic conductivity of unsaturated porous media. Water Resour. Res. 12, 513–522.

Nash, Je., Sutcliffe, J. V, 1970. River flow forecasting through conceptual models part I—A discussion of principles. J. Hydrol. 10, 282–290.

Néelz, S., 2009. Desktop review of 2D hydraulic modelling packages. Bristol: Environment Agency.

Neves, R., Mateus, M., Neves, R., 2013. The MOHID concept. Ocean Model. Coast. Manag. Stud. with MOHID 1–11.

Nützmann, G., Levers, C., Lewandowski, J., 2013. Coupled groundwater flow and heat transport simulation for estimating transient aquifer-stream exchange at the lowland River Spree (Germany). Hydrol. Process. 10.1002/hyp.9932

Ochoa-Salazar, B.-X., 2008. Etude conjuguée géochimique/hydrologique des relations nappes-rivière dans une zone humide : cas de la zone humide alluviale de Monbéqui, France. Université de Toulouse III - Paul Sabatier.

Panday, S., Huyakorn, P.S., 2004. A fully coupled physically-based spatially-distributed model for evaluating surface/subsurface flow. Adv. Water Resour. 27, 361–382. doi:10.1016/j.advwatres.2004.02.016

Partington, D., Brunner, P., Simmons, C.T., Therrien, R., Werner, A.D., Dandy, G.C., Maier, H.R., 2011. A hydraulic mixing-cell method to quantify the groundwater component of streamflow within spatially distributed fully integrated surface water–groundwater flow models. Environ. Model. Softw. 26, 886–898. doi:10.1016/j.envsoft.2011.02.007

Peyrard, D., Sauvage, S., Vervier, P., Sánchez-Pérez, J.-M., Quintard, M., 2008. A coupled vertically integrated model to describe lateral exchanges between surface and subsurface in large alluvial floodplains with a fully penetrating river. Hydrol. Process. 22, 4257–4273. doi:10.1002/hyp.7035

Pinay, G., Ruffinoni, C., Wondzell, S., Gazelle, F., 1998. Change in Groundwater Nitrate Concentration in a Large River Floodplain: Denitrification, Uptake, or Mixing? J. North Am. Benthol. Soc. 17, 179–189. doi:10.2307/1467961

Purser, R.J., Leslie, L.M., 1988. A Semi-Implicit, Semi-Lagrangian Finite-Difference Scheme Using Hligh-Order Spatial Differencing on a Nonstaggered Grid. Mon. Weather Rev. 116, 2069–2080. doi:10.1175/1520-0493(1988)116<2069:ASISLF>2.0.CO;2

Rassam, D.W., Pagendam, D.E., Hunter, H.M., 2008. Conceptualisation and application of models for groundwater–surface water interactions and nitrate attenuation potential in riparian zones. Environ. Model. Softw. 23, 859–875. doi:http://dx.doi.org/10.1016/j.envsoft.2007.11.003

Richards, L.A., 1931. Capillary conduction of liquids through porous mediums. J. Appl. Phys. 1, 318–333.

Rivett, M.O., Buss, S.R., Morgan, P., Smith, J.W.N., Bemment, C.D., 2008. Nitrate attenuation in groundwater: A review of biogeochemical controlling processes. Water Res. 42, 4215–4232. doi:http://dx.doi.org/10.1016/j.watres.2008.07.020

Sánchez-Pérez, J.M., 1992. Fonctionnement hydrochimique d'un écosystème forestier inondable de la Plaine du Rhin: la forêt alluviale du secteur de l'île de Rhinau en Alsace(France). Université Louis Pasteur, Strasbourg.

Sánchez-Pérez, J.-M., Tremolières, M., 1997. Variation in nutrient levels of the groundwater in the Upper Rhine alluvial forests as a consequence of hydrological regime and soil texture. Glob. Ecol. Biogeogr. Lett. 211–217.

Sánchez-Pérez, J.-M., Vervier, P., Garabétian, F., Sauvage, S., Loubet, M., Rols, J.-L., Bariac, T., Weng, P., 2003. Nitrogen dynamics in the shallow groundwater of a riparian wetland zone of the Garonne, SW France: nitrate inputs, bacterial densities, organic matter supply and denitrification measurements. Hydrol. Earth Syst. Sci. Discuss. 7, 97–107.

Sauvage, S., 1999. Modélisation hydrobiogéochimique de la Garonne à l'étiage estival: cas de l'azote entre Toulouse et Agen (120 kilomètres). Toulouse, INPT.

Schaap, M.G., Leij, F.J., van Genuchten, M.T., 2001. ROSETTA: a computer program for estimating soil hydraulic parameters with hierarchical pedotransfer functions. J. Hydrol. 251, 163–176.

Sophocleous, M., 2002. Interactions between groundwater and surface water: the state of the science. Hydrogeol. J. 10, 52–67. doi:10.1007/s10040-001-0170-8

Sophocleous, M.A., 1998. Perspectives on sustainable development of water resources in Kansas. Bull 239, Kansas Geologi- cal Survey, Lawrence, Kansas.

Sorooshian, S., Duan, Q., Gupta, V.K., 1993. Calibration of rainfall-runoff models: Application of global optimization to the Sacramento Soil Moisture Accounting Model. Water Resour. Res. 29, 1185–1194.

Steiger, J., James, M., Gazelle, F., 1998. Channelization and consequences on floodplain system functioning on the Garonne River, SW France. Regul. Rivers Res. Manag. 14, 13–23.

Stewart, M.D., Bates, P.D., Price, D.A., Burt, T.P., Bates, Y.Ã.P.D., 1998. Modelling the spatial variability in floodplain soil contamination during flood events to improve chemical mass balance estimates. Hydrol. Process. 12, 1233–1255. doi:10.1002/(SICI)1099-1085(19980630)12:8<1233::AID-HYP614>3.0.CO;2-2

Swartzendruber, D., 1969. The flow of water in unsaturated soils. Flow through Porous Media, Acad. Press. New York 215–292.

Thoms, M.C., 2003. Floodplain–river ecosystems: lateral connections and the implications of human interference. Geomorphology 56, 335–349. doi:10.1016/S0169-555X(03)00160-0

Tockner, K., Pennetzdorfer, D., Reiner, N., Schiemer, F., Ward, J. V, 1999. Hydrological connectivity, and the exchange of organic matter and nutrients in a dynamic river–floodplain system (Danube, Austria). Freshw. Biol. 41, 521–535. doi:10.1046/j.1365-2427.1999.00399.x

Trancoso, A.R., Braunschweig, F., Chambel Leitão, P., Obermann, M., Neves, R., 2009. An advanced modelling tool for simulating complex river systems. Sci. Total Environ. 407, 3004–3016. doi:http://dx.doi.org/10.1016/j.scitotenv.2009.01.015

van Genuchten, M.T., 1980. A closed-form equation for predicting the hydraulic conductivity of unsaturated soils. Soil Sci. Soc. Am. J. 44, 892–898.

Weng, P., Sánchez-Pérez, J.M., Sauvage, S., Vervier, P., Giraud, F., 2003. Assessment of the quantitative and qualitative buffer function of an alluvial wetland: hydrological modelling of a large floodplain (Garonne River, France). Hydrol. Process. 17, 2375–2392. doi:10.1002/hyp.1248

Woessner, W.W., 2000. Stream and Fluvial Plain Ground Water Interactions: Rescaling Hydrogeologic Thought. Ground Water 38, 423–429. doi:10.1111/j.1745-6584.2000.tb00228.x

4.3.Synthèse

La modélisation des échanges nappes-rivière constitue une étape préliminaire nécessaire à la simulation du processus de dénitrification dans les plaines alluviales. Le modèle MOHID Land a permis une représentation satisfaisante de l'hydrologie du site de Monbéqui en prenant en compte le rôle des épisodes de crues. Les résultats ont également permis de confirmer l'importance des crues sur le bilan hydrique des plaines alluviales, et donc sur les transferts des éléments qui sont importants pour les processus biogéochimiques dans ces environnements. Cependant, dans le cas de Monbéqui, la topographie de la zone conduit à un seuil d'infiltration maximal qui est identique pour toutes les crues plus exceptionnelles que la crue quinquennal. Les résultats des simulations du transport conservatif des chlorures ont donné des résultats contrastés et on mis en avant la nécessité de représenter précisément les conditions initiales (concentrations en chlorures) dans la zone agricole pour un résultat satisfaisant sur la zone riparienne. Néanmoins, les zones de mélange entre les eaux de surface et les eaux souterraines localisées à proximité de la rivière sont bien représentées par le modèle.

Le modèle MOHID Land constitue donc une modèle adapté à la modélisation hydrologique des environnements de plaine alluviale. L'application de ce modèle constitue une base pour l'intégration du processus de dénitrification dans la modélisation.

Chapitre 5 : Modélisation du processus de dénitrification dans la plaine alluviale de Monbéqui

A partir des observations réalisées dans le chapitre 3 et des modèles de dénitrification existants dans la littérature, un module simulant la dénitrification a été implémenté dans le modèle MOHID Land, utilisé au préalable pour simuler l'hydrologie de la zone (chapitre 4). Le module choisi est basé sur le modèle proposé par Peyrard et al. (2011) car il prend en compte à la fois le carbone organique dissous apporté par la rivière et la carbone organique particulaire présent dans les sols. En effet, ces deux sources de carbone organique jouent un rôle potentiel sur la dénitrification (chapitre 3).

Ce chapitre décrit l'application du modèle au site de Monbéqui avec comme objectif principal l'identification des facteurs contrôlant la variabilité spatio-temporelle de la dénitrification sur le site de Monbéqui. Il est constitué d'un article en préparation pour soumission au journal *Biogeochemistry,* et intitulé « Analysis of denitrification process in groundwater in a floodplain using a modelling approach. ». L'article est précédé d'un résumé en français et est suivi d'une partie décrivant l'analyse de sensibilité du module de dénitrification. Enfin, une synthèse replace les résultats obtenus dans le cadre de la thèse.

5.1.Résumé

La contamination en nitrates des eaux douces représente un enjeu global. Au sein des plaines alluviales, particulièrement vulnérables à la pollution en nitrates, les zones ripariennes constituent des lieux favorables à l'élimination des nitrates, à travers le processus de dénitrification. Cependant, la dénitrification est un processus complexe caractérisé par une forte variabilité spatio-temporelle et contrôlé par de nombreux facteurs dont le plus important est la présence de carbone organique. La modélisation permet de prendre en compte les différents facteurs de manière dynamique et est un outil adapté pour améliorer la caractérisation et compréhension de ce processus.

Dans cette étude, un modèle combinant i) un modèle hydrologique distribué à base physique couplant écoulements de surfaces et écoulements souterrains et incluant un module de transport (MOHID Land) avec ii) un module calculant la dénitrification de façon simplifiée et prenant en compte le carbone organique dissous (COD) apporté par la rivière et le carbone organique particulaire (COP) présent dans les sols, a été appliqué à la zone d'étude de Monbéqui (6,6 km²). Le modèle est capable de reproduire de façon satisfaisante, l'évolution des concentrations en nitrates dans l'aquifère. La dénitrification a été estimée à 28 kg $N\text{-}NO_3^-$ $.ha^{-1}.an^{-1}$, représentant 38% des apports en nitrates par les eaux souterraines en provenance de la zone agricole. Les zones de dénitrification les plus intenses ont été localisées dans la zone riparienne de faible altitude, et reliées à l'inondation des horizons supérieurs des sols, riche en matière organique alimentant la réaction de dénitrification. Néanmoins, une dénitrification importante a également été simulée dans toute la moitié aval du méandre qui correspond à la zone alimentée par l'eau souterraine chargée en nitrates en provenance des zones agricoles. Dans ces zones, même si l'activité de dénitrification n'est pas la plus importante, la plus grande épaisseur de l'aquifère fait que la dénitrification affecte de plus grands volumes, entrainant une quantité totale d'azote dénitrifié plus importante. Les caractéristiques hydro-géomorphologiques (topographie, écoulements souterrains) déterminent la variabilité spatiale de la dénitrification dans la zone étudiée. Les crues entrainent des périodes de plus forte dénitrification à travers l'inondation les horizons supérieurs des sols riches en COP alors que l'apport de COD par la rivière ne semble pas jouer un rôle majeur.

Le modèle est adapté à la simulation de la dénitrification dans les eaux souterraines des plaines alluviales. Les résultats peuvent également servir à la validation de modèle appliqué à de plus larges échelles ou encore permettre de tester différentes configurations (géomorphologiques et hydrologiques) sur la capacité de dénitrification des plaines alluviales.

5.2. Analysis of denitrification process in the groundwater of floodplains using a modelling approach

Léonard Bernard-Jannin[1,2,*], David Brito[3], Xiaoling Sun[1,2], Ramiro Neves[3], Sabine Sauvage[1,2], José-Miguel Sánchez-Pérez[1,2,*]

[1]*University of Toulouse; INPT, UPS; Laboratoire Ecologie Fonctionnelle et Environnement (EcoLab), Avenue de l'Agrobiopole, 31326 Castanet Tolosan Cedex, France*

[2]*CNRS, EcoLab, 31326 Castanet Tolosan Cedex, France*

[3]*MARETEC, Instituto Superior Tecnico, Universidade Tecnica de Lisboa, Av. Rovisco Pais, 1049-001 Lisboa, Portugal*

[*]*Corresponding authors: Avenue de l'Agrobiopole, 31326 Castanet Tolosan Cedex, Franc; l.bernardjannin@gmail.com; jose-miguel.sanchez-perez@univ-tlse3.fr*

Abstract

Nitrate (NO_3^-) contamination of freshwater systems is a global concern. In alluvial floodplains, highly vulnerable to nitrate pollution due to widespread agricultural activities, riparian areas have been proven to be efficient in nitrate removal through denitrification. However, denitrification presents complex spatio-temporal patterns and is controlled by many factors. Hence, modelling can provide useful knowledge about this biogeochemical process, by helping to identify key factors involved in denitrification process and its spatio-temporal variability. In this study, a modelling approach combining i) a distributed hydrodynamic model, coupling surface and subsurface flow (MOHID Land), with ii) a simplified denitrification calculation module including dissolved organic carbon (DOC borned by the river) and particulate organic carbon (POC present in soil) have been applied to a monitored meander area of the Garonne river (6.6 km²). The average denitrification rate was estimated to 28 kg $N.ha^{-1}.yr^{-1}$ representing 38% of the lateral nitrate input from the agricultural area. Denitrification was the highest in the low elevation riparian area in relation with inundated soils releasing topsoil organic carbon fueling denitrification. In addition high denitrification rates were simulated in downstream part of the meander in relation with the high nitrates flux coming from the agricultural area. Geomorphological settings and groundwater flows in the area play a major role in controlling denitrification in floodplain area. Flood events lead to high denitrification periods by increasing topsoil layer POC availability with higher water level in the aquifer. However, the role of DOC borne by the river seems restricted. The model can be applied to estimate nitrate removal capacity of riparian area and provide validation for larger scale modelling application.

Keyword: groundwater, denitrification, nitrate, modelling, floodplain

5.3.Introduction

Nitrate pollution of water system has been a global concern for decades (Power and Schepers, 1989; Bijay-Singh et al., 1995; Zhang et al., 1996; Arrate et al., 1997; Carpenter et al., 1998; Jégo et al., 2012; Boithias et al., 2014). In the European Union, nitrate contamination originating agricultural sources is considered to be the main cause of groundwater degradation (Sutton et al., 2011). In floodplain area, the agricultural land use, in combination with factors such as shallow groundwater, high permeability of alluvial deposits and strong interactions with surface water, make alluvial aquifers particularly vulnerable to nitrate diffuse pollution (Arauzo et al., 2011). As a result, nitrate concentrations exceeding the limit of 50 mg L^{-1} set for groundwater systems in Europe by the Nitrate Directive (91/676/EEC) and the Groundwater Directive (2006/118/EEC) have been reported for several European shallow aquifers in floodplain areas (Baillieux et al., 2014; Sánchez-Pérez et al., 2003).

There are different natural ways by which nitrate concentration in shallow alluvial aquifer can be reduced. First, nitrate contamination in shallow aquifers can be mitigated through the dilution resulting from the mixing with river water with low nitrate concentrations (Pinay et al., 1998; Baillieux et al., 2014). However, nitrates are not removed from hydrosytems when dilution occurs. Nitrate mass removal occurs through natural biogeochemical processes such as plant uptake, denitrification, dissimilatory nitrate reduction to ammonium and microbial immobilisation, among which denitrification is reported to be the most important in groundwater (Korom, 1992; Burt et al., 1999; Rivett et al., 2008).

Denitrification corresponds to the anaerobic reduction of nitrates (NO_3^-) into gaseous compounds (nitrous oxide NO_2 or dinitrogen N2) by microorganisms activity. Denitrification in groundwater is known to be associated to: (i) presence of nitrate, denitrifying bacteria and electron donor (organic carbon), (ii) anaerobic conditions and (iii) favourable environmental conditions in terms of e.g. temperature and pH (Rivett et al., 2008). However, among all these factors, availability of organic carbon has been identified as the major limiting factor in nitrate-contaminated groundwater (see Rivett et al. (2008) for a review). Riparian zones are interfaces between terrestrial and aquatic ecosystems and are known to be efficient for nitrate removal (Osborne and Kovacic, 1993; Lowrance et al., 1997; Dosskey et al., 2010). Denitrification is known to be more important in topsoil unsaturated layer but also occur in groundwater (Haycock and Burt, 1993; Hill et al., 2000; J. M. Sánchez-Pérez et al., 2003; Vidon and Hill, 2004). In riparian area, surface water-groundwater (SW-GW) interactions are important (Bernard-Jannin et al., submitted.; Sun et al., 2015) and denitrification rates are

highly variable in space and time due to the heterogeneity of flowpaths that lead nitrates and organic carbon to meet, promoting denitrification (Hill et al., 2000). Therefore denitrification is known to occur preferentially in given location during defined period (also referred as hot spots and hot moments, McClain et al., 2003). Hot spots occurrences in groundwater are known to be driven by the geomorphology and hydrological settings of the area (Vidon and Hill, 2005; Groffman et al., 2009; Bernard-Jannin et al., 2016). In addition subsurface hydrology and flood events have been related to subsurface hydrology and flood events occurence (Pfeiffer et al., 2006; Peter et al., 2011). However denitrification patterns and rates in groundwater remain difficult to extrapolate from field measurement to larger scales (Groffman, 2012).

As they allow characteristics of the environment to be taken into consideration on a detailed scale, physically-based, spatially-distributed models are valuable tools for improving knowledge on denitrification process in floodplain area. A large number of models including denitrification process simulation can be found in the literature and Heinen (2006) listed more than 50 existing models simulating denitrification. These models are often applied to the unsaturated area under agricultural plot to simulate nitrate leaching to the groundwater but are usually not apply to simulate denitrification occurring in the shallow aquifer itself. However, in agricultural floodplain, the major input of nitrate in the riparian area is not leaching from the forested covered soil but brought laterally through groundwater flowing from contaminated agricultural areas. Therefore, an interesting approach to model denitrification in shallow aquifer is the coupling of a hydrodynamic model to correctly reproduced element fluxes through the different flow paths together with a denitrification module calculating denitrification rates. The hydrodynamic model should be able to handle SW-GW exchanges and specific features of floodplain area such as overbank flood events that are important to assess SW-GW exchanges (Bernard-Jannin et al., submitted.). According to Heinen (2006), denitrification models can be separated in 3 groups by including (i) microbial growth model, (ii) soil structural models and (iii) simplified process models. While the two first categories of model require a great number of input data, simplified models are easier to use. These models are based on potential denitrification or consider denitrification as a first-order process and reduction functions to account for environmental conditions (anoxia, temperature, pH) and nitrates concentrations. When based on potential denitrification, the potential rates can be computed from carbon degradation dynamic. Peyrard (2011) developed a model taking into account both dissolved organic carbon (DOC) and particulate organic carbon (POC)

degradation as well as nitrate and oxygen content to compute denitrification rates. The biogeochemical module was implemented in a 1D advective transport model and successfully applied to simulate nitrate content in gravel bars but not included in a spatially distributed hydrodynamic model. Accounting for different sources of organic carbon is an important feature as a recent field and modelling studies underlined the importance of the dual origin of organic carbon, brought by the river and derived from the soil profile in denitrification process as well as geomorphology and hydrology of the area (Sun et al., submitted.; Peyrard et al., 2011). Therefore, modelling denitrification in shallow aquifer of floodplain area can be assessed when simulating i) the detailed hydrodynamic of the area, including SW-GW interactions and overbank flood event and ii) denitrification process with a simplified model taking into account the dual origin of organic carbon and its degradation rates to compute denitrification rates.

Current approaches involve coupling of a denitrification module with one dimensional transport model along gravel bar (Peyrard et al., 2011), or with a two dimensional hydrodynamic model simulating hyporheic flows induced by meander sinuosity (Boano et al., 2010). Zarnetske et al. (2012) used a one dimension transport model coupled with a biogeochemical process and conduct a Monte-Carlo analysis of model parameters to evaluate parameters controlling denitrification/nitrification processes in hyporheic zone. However the coupling of a denitrification module with a three dimensional surface- subsurface hydrodynamic model including overbank flow has never been conducted to the authors knowledge. The objective of this paper is to implement a model including these features in a alluvial floodplain in order to i) assess spatio-temporal patterns of denitrification rates and ii) identify factors controlling denitrification in an alluvial shallow aquifer.

5.4.Material and method

5.4.1. Study site

5.4.1.1. Description

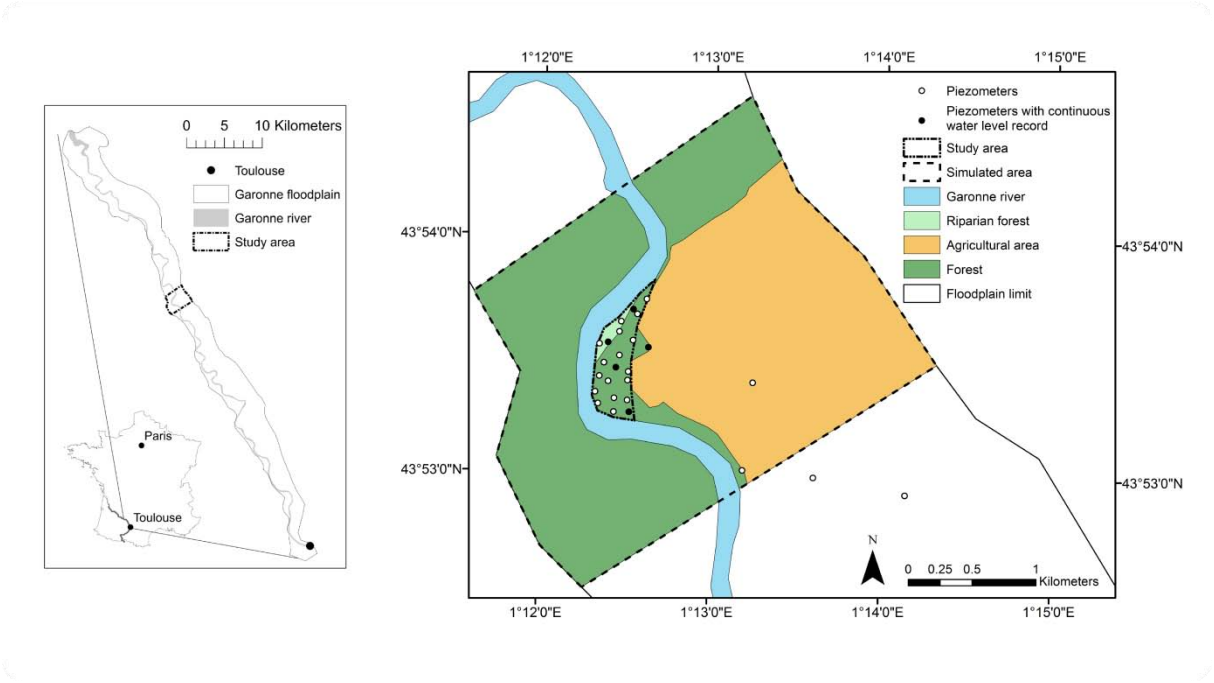

Figure 5-1: Geographical location and land use of the simulated and study area

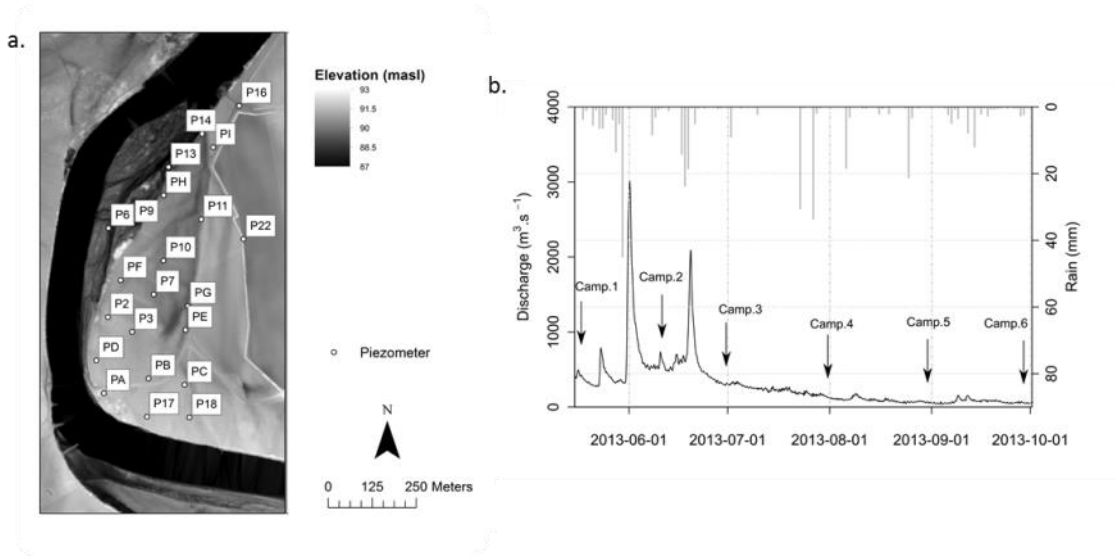

Figure 5-2: a) Digital terrain model and piezometer location in the study area and b) daily discharge and rainfall in the study area for the simulated period. Sampling campaigns are also indicated.

The study area, which covers about 29 ha, is located within a 2 km long meander in the middle section of the Garonne river watershed, close to the village of Monbéqui in south-west France (Figure 5-1). Mean annual precipitation in the area is 660 mm. The drainage area of

the Garonne watershed at the study site is about 13 730 km^2, with annual average flow of 190 $m^3\ s^{-1}$ and a range from 98 $m^3\ s^{-1}$ (1989) to 315 $m^3\ s^{-1}$ (1978) over the past 41 years. The driest month is August, with 76 $m^3\ s^{-1}$ on average, and the wettest is May, with 343 $m^3\ s^{-1}$ on average. The daily flow is highly variable, ranging from 10 $m^3\ s^{-1}$ during the severe drought in August 1991 to 2930 m3 s-1 during the largest flood event recorded, on 6 November 2000 (www.hydro.eaufrance.fr). The two-year return period flood corresponds to daily flow of 1400 m3 s-1. The floodplain comprises 4-7 m of quaternary sand and gravel deposits (mean saturated hydraulic conductivity 10^{-3} m s^{-1}), overlying impermeable molassic bedrock. In this area the Garonne river fully penetrates the alluvial formation, so that the riverbed lies on the impermeable substratum. The alluvial deposits are covered with a silty soil layer 1-2 m deep and containing 1.5% OM on average (Jégo et al., 2012). The connection between aquifer and the Garonne river is strongly influenced by hydrological conditions (Bernard-Jannin et al., submitted.; Sun et al., 2015). The floodplain is heavily cultivated (irrigated maize, sunflower, sorghum, wheat), leading to major nitrate influx into the groundwater. Concentrations of 100 mg L^{-1} NO_3^- are common (Sánchez-Pérez et al., 2003). A small area of riparian forest, mainly composed of willow (*Salix alba*) and ash trees (*Fraxinus excelsior*), is located close to the river at a lower elevation than the rest of the study area (Figure 5-2), and is separated from the agricultural fields by plantations of poplar (*Populus alba*) (Figure 5-1).

Previous studies carried out on this area have demonstrated the role of dissolved organic carbon (DOC) borne by the river into the aquifer in denitrification (Sánchez-Pérez et al., 2003) and the importance of the sediment-attached bacterial community for aquifer denitrification (Iribar et al., 2008). In addition, modelling studies have shown the importance of river-aquifer exchanges for groundwater composition (Bernard-Jannin et al., submitted.; Peyrard et al., 2008; Sun et al., 2015; Weng et al., 2003) and the impact of agricultural practices on nitrate leaching into the shallow aquifer (Jégo et al., 2012).

1.1.1.1. Sampling

A network of 24 piezometers was installed in the inner part of the study meander (Figure 5-2). Three of the piezometers (P6, P9 and P13) are located in the low elevation riparian area. The available data consist of the hydraulic head measured at a monthly time step in each piezometer and 15 min water levels in five piezometers (P7, P9, P14, P18, P22) recorded by pressure sensor (CTD-Diver, Schlumberger) from April 2013 to March 2014. In addition, monthly campaigns were conducted from April 2013 to March 2014 during which groundwater samples were taken in every piezometer and NO_3^- and DOC concentrations,

among other parameters, were analysed using ion chromatography and platinum catalyser. To ensure that the water sample corresponded to the aquifer and not to stagnant water accumulated in the piezometer, groundwater was extracted beforehand until in-situ measured electrical conductivity was constant (Sánchez-Pérez, 1992).

5.4.2. Model

The modelling strategy applied in this study combine a distributed hydrodynamic model with a simplified process denitrification model that takes into account the main factors influencing denitrification in alluvial floodplain aquifer. MOHID Land is an integrated model that has been successfully applied to simulate SW-GW exchanges during floods in the same study area (Bernard-Jannin et al., submitted.) and was chosen for simulating hydrodynamic in the study. The denitrification model was adapted from Peyrard et al. (2011). The advantage of this model is to take into account both POC and DOC degradation in denitrification rates calculation that were identified as control factors of the process in a previous field study (Bernard-Jannin et al., 2016). The modularity of MOHID Land model allowed to easily implement the denitrification module within its numerical code.

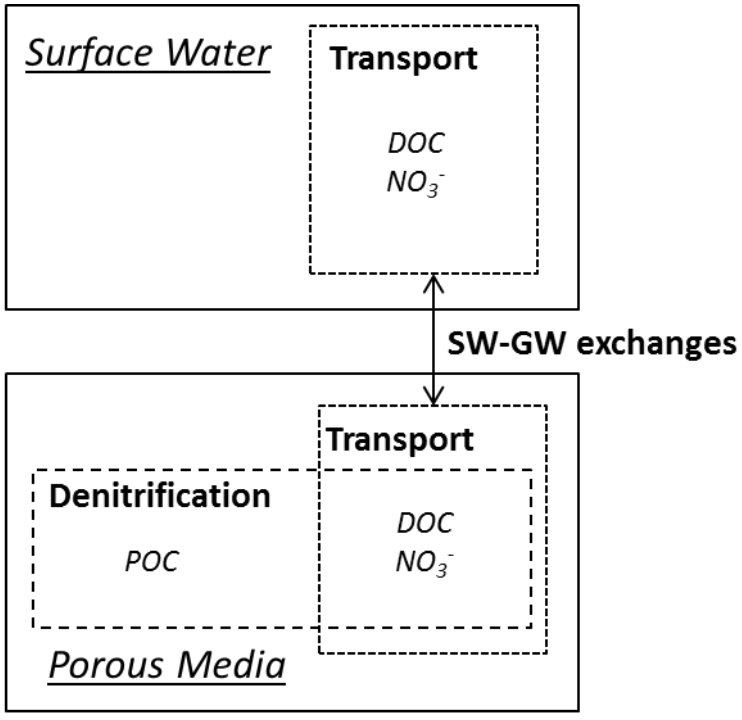

Figure 5-3: Processes involving dissolved organic carbon (DOC), particulate organic carbon (POC) and nitrates (NO_3^-) simulated in MOHID Land within and between Surface Water (SW) and Porous Media (PM) domains. DOC and NO_3^- are transported within and between the two domains while POC is static in PM. Denitrification is computed in PM according to DOC, NO_3^- and POC concentrations.

5.4.2.1. MOHID Land

MOHID Land is a distributed, physically based model simulating hydrodynamic in two domains: surface water (SW) and porous media (PM). In SW, two-dimensional surface water flows are computed with the dynamic wave of the Saint-Venant equations. In PM, three-dimensional unsaturated flow are computed with Richard's equation. Both domains interact through infiltration (SW to PM) and exfiltration (PM to SW). Equations are solved using a finite volume method. MOHID Land also includes a transport models for both PM and SW. The model has been applied successfully to simulate the hydrology in the study area and detailed information about the hydrological model set-up can be found in (Bernard-Jannin et al., submitted).

5.4.2.2. Denitrification module

A denitrification model was added to the MOHID Land model based on the model developed by Peyrard et al., (2011). The model can be considered as a simplify process model (*sensu* Heinen, 2006) and calculates a potential denitrification rates according to the first-order decay of both DOC and POC. This potential rate is limited by nitrate concentration according to a Michaelis-Menten kinetics and a function of PM H_2O saturation to account for oxygen content. In the original model, anoxia is taken into account through oxygen concentration. However oxygen dynamic in the porous media is a complex process to simulate and water content is often used as a complementary for oxygen (Heinen, 2006). A water content reduction function was then introduced and based on the RZQM model formulation (Ahuja et al., 2000) to replace oxygen computation. This model includes a DOC degradation function (1) a POC degradation function (2) and a nitrate degradation (denitrification) function (3 and 4).

$$R_{POC} = -K_{POC}[POC] \quad (1)$$

$$R_{DOC} = -K_{DOC}[DOC] \quad (2)$$

$$R_{NO3} = -0.8\left(\rho\frac{1-\varphi}{\varphi}K_{POC}[POC]\frac{10^6}{M_C} + K_{DOC}[DOC]\right).\frac{[NO3]}{K_{NO3}+[NO3]}.f_{H2O} \quad (3)$$

$$f_{H2O} = 3.04\times10^{-4}\exp(8.15\,\theta_{rel}) \quad (4)$$

R_{POC} is the POC degradation rate ($mg.g^{-1}.day^{-1}$), K_{POC} is the first-order POC decay constant (day^{-1}), R_{DOC} is the DOC degradation rate ($\mu M.day^{-1}$), K_{DOC} is the first-order DOC decay constant (day^{-1}), R_{NO3} is the denitrification rate ($\mu M.day^{-1}$), K_{NO3} is the half saturation for

nitrate limitation (µM), ρ is the PM density (kg.dm^{-3}), φ is the PM porosity and is equal to the saturated water content θ_s (-),M_c is the carbon molar mass (12 g.mol^{-1}), f_{H2O} is the water content reduction function (-), θ_{rel} is the relative water content (-). POC content in PM [POC] is expressed in mg.kg^{-1} and DOC concentration of water [DOC] in µM. [NO3] correspond to the nitrate concentration in µM.

In the model, DOC and NO_3^- transport within and between the two domains is computed. The POC is considered to be a motionless property of the PM and is not simulated in the SW and its transport in PM is not simulated. The denitrification is only computed in PM and depends on POC, DOC and NO_3^- concentrations (Figure 5-3).

5.4.2.3. Model set-up

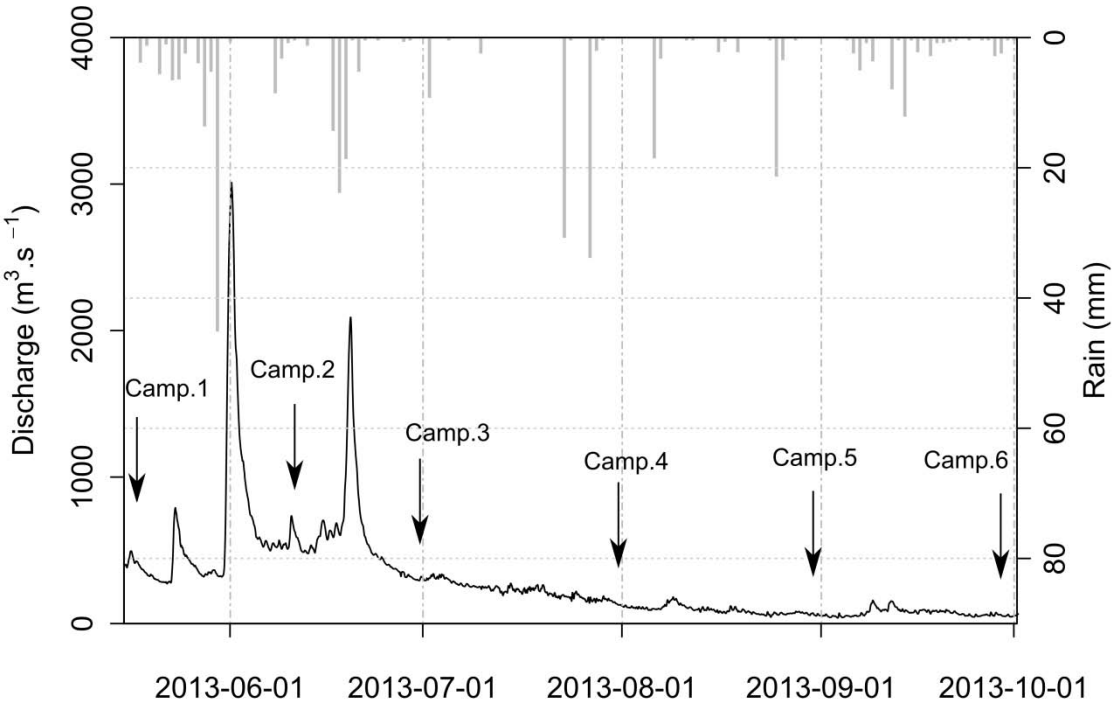

Figure 5-4: Daily discharge and rainfall in the study area for the simulated period. Sampling campaigns are also indicated.

The hydrodynamic model set-up is the same than described in Bernard-Jannin et al. (submitted). The discretization is based on a 3D grid with 25m horizontal resolution (covering 6.6 km²) and 10 vertical layers with variable thickness ranging from 0.2m in surface to 1m in depth. The number of layer is adjusted in each cell to match at best with the geometry of the impermeable layer. The surface DTM was manually dug to include riverbed geomorphology

according to available river profile. The parameters used in the model are summarized in the Table 5-1.

Table 5-1: Parameters of the hydrodynamic model set-up (Bernard-Jannin et al., submitted)

Domain	Symbol	Unit	Signification	Value
Porous media	θ_s	-	Saturated water content	0.41
(PM)	θ_r	-	Residual water content	0.06
	N	-	Pore size distribution related term	1.62
	α	cm^{-1}	Air entry pressure related term	0.56
	Ks	$m\ s^{-1}$	Saturated hydraulic conductivity	10^{-3}
	α_H	m	Horizontal dispersivity	25
	α_V	m	Vertical dispersivity	2.5
Surface water	n_r	$s\ m^{-1/3}$	Manning coefficient in riverbed	0.01
(SW)	n_f	$s\ m^{-1/3}$	Manning coefficient in floodplain	0.1

The parameters required for the new implemented denitrification module and their values are listed in the Table 5-2. The dry density was obtained with sample analysis. K_{POC} and K_{DOC} constant were manually calibrated. K_{NO3} was set to 30 µM according to the literature (Peyrard et al., 2011).

Table 5-2: Parameters of the denitrification module

Symbol	Unit	Signification	Value
$\boldsymbol{\rho}$	$kg.dm^{-3}$	Dry sediment density	1.45
$\mathbf{K_{POC}}$	day^{-1}	first-order POC decay constant	$1x10^{-6}$
$\mathbf{K_{DOC}}$	day^{-1}	first-order DOC decay constant	$1x10^{-3}$
$\mathbf{K_{NO3}}$	µM	half saturation for nitrate limitation	30

In PM, the initial POC content was defined according to measurements in soil profile (Jégo, 2008). The POC content was set different for the top PM layers (0 to 50 cm) with $1.5x10^3$ $mg.kg^{-1}$ and for the PM layers below 50 cm with $0.275x10^3$ $mg.kg^{-1}$. Initial concentration of NO_3^- and DOC were defined according to data from the piezometer water samples. However, the initial NO_3^- was set homogeneous to 150 $mg\text{-}NO_3^-.L^{-1}$ in the entire agricultural area. This value corresponds to the maximum concentration recorded in the piezometers located in the border of the agricultural field. Nitrate leaching under the agricultural area is variable (Jégo et al., 2012) and the available data did not allow for an accurate representation of this variability. Instead, initial conditions represent a scenario with high nitrate contamination of the

groundwater under the agricultural area. In the river DOC and NO_3^- concentration were set constant respectively to 1.5 $mg.L^{-1}$ and 8 $mg\text{-}N.L^{-1}$ according to measurements performed in river water samples. The values are summarized in Table 5-3.

Table 5-3: Initial condition in Porous Media (meander area and agricultural area) and boundary condition in river discharge for DOC, POC and NO_3^- concentrations

Element	Unit	Meander area	Agricultural area	River discharge
NO_3^-	$mg.L^{-1}$	Field observation (15/03/13)	150	8
DOC	$mg.L^{-1}$	Field observation (15/03/13)	1	1.5
POC	$mg.kg^{-1}$	0-50 cm : 1 500	0-50 cm : 1 500	not simulated
		50-max : 275	50-max : 275	

The model was applied to the study site for a period going from 15/05/2013 to 1/10/2013 during which 6 campaigns were performed. The first campaign helped to defined initial conditions and the 5 others were used for model evaluation compared to water level and nitrates concentrations. The evaluation of the quality of the simulations included the calculation of the Nash-Sutcliffe coefficient (NS, Nash and Sutcliffe, 1970), root mean square error (RMSE), percent bias between simulations and observations (PBIAS), as defined in Sorooshian et al. (1993), and coefficient of determination (R^2). Monthly measured NO_3^- concentrations in the piezometer were compared to the average of the simulated NO_3^- concentrations over the saturated area for the campaigns 2 to 6.

The denitrification rates were expressed in two different units. First, when expressed in $mg\text{-}N.L^{-1}.day^{-1}$ the denitrification rate refers to the intensity of the denitrification in the considered cell of the porous media and was called denitrification activity. To spatially represent this denitrification activity for the aquifer, the denitrification activity was averaged in each cell over the saturated aquifer. However the denitrification intensity has to be analyzed in regard to the water content to evaluate the total quantity of N removed by the process. Therefore, the denitrification was also expressed in $mg\text{-}N.ha^{-1}.day^{-1}$ and was referred to as integrated denitrification. The integrated denitrification corresponds to the vertical integration of the product of the denitrification intensity by the water content over the saturated aquifer.

5.5.Results

5.5.1. Nitrate simulation

The model was evaluated by comparing simulated and observed nitrate concentrations recorded during 5 campaigns over the 22 piezometers located in the forested area of the meander (poplar plantation and riparian forest) which are presented in the Figure 5-5. The overall trend between the observed and simulated nitrate concentration was correct (R^2=0.69). However simulated nitrates concentrations appears to be under estimated (PBIAS = -23.9 %). The quality of the simulated nitrate concentrations is not the same when considering different periods and locations (Table 5-4). The results are better for the campaign 2 and 3 (RMSE=18.27 mg $NO_3^-.L^{-1}$ and PBIAS= -8%) than for the remaining 3 campaigns (4 to 6) for which the nitrate concentrations are more underestimated (RMSE=29.8 mg $NO_3^-.L^{-1}$ and PBIAS= -30.9 %). The observed and simulated nitrate concentrations in the groundwater at the end of the simulation (140 days) are shown in (Figure 5-6). The underestimation of the data is especially true for the lower concentrations (< 40 mg $NO_3^-.L^{-1}$) corresponding to the piezometers located in the south of the meander. Among these piezometers the simulated nitrate concentrations is not satisfactory for three particular piezometers (P18, PB and PC).

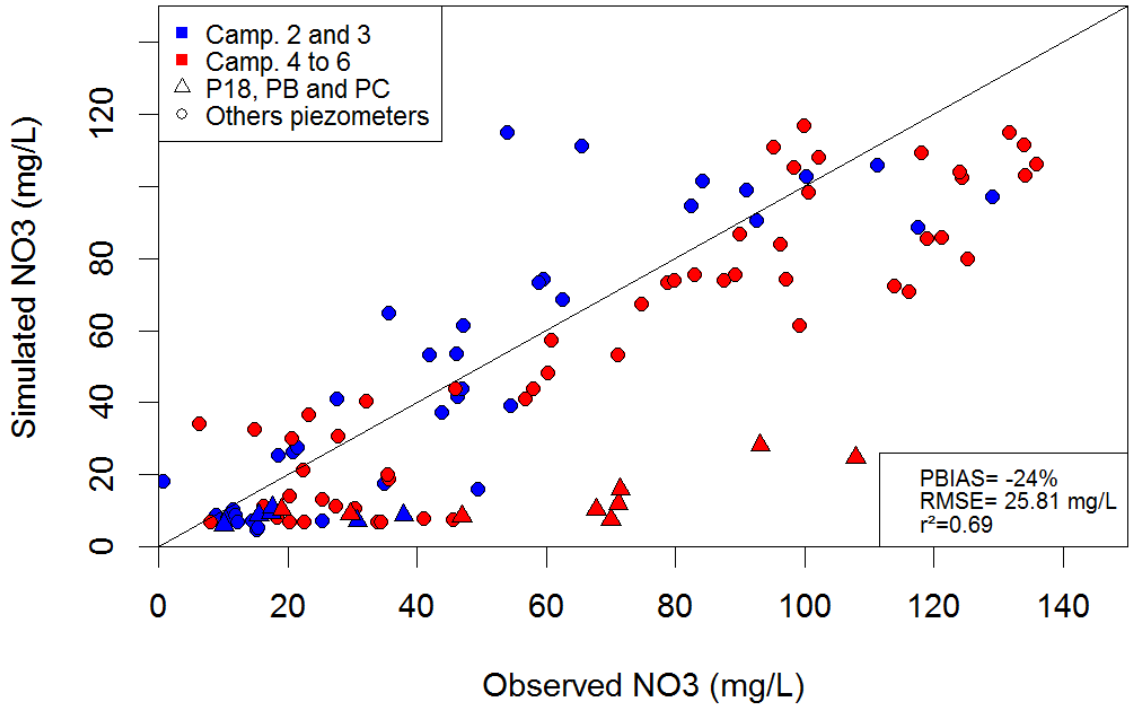

Figure 5-5: Observed and simulated nitrate concentrations. The results are separated for different campaigns (colors) and different locations (symbol).

Table 5-4: Evaluation of the model for different periods and different piezometers location.

	Campaigns 2 to 3	Campaigns 4 to 6	All campaigns
All piezometers	RMSE=18.27	RMSE=29.8	RMSE=25.8
	PBIAS=-8.1	PBIAS=-30.9	PBIAS=-23.9
	R^2=0.75	R^2=0.70	R^2=0.69
Without P18, PB, PC	RMSE=17.99	RMSE=22.7	RMSE=20.9
	PBIAS=-3	PBIAS=-23.2	PBIAS=-16.8
	R^2=0.75	R^2=0.84	R^2=0.78

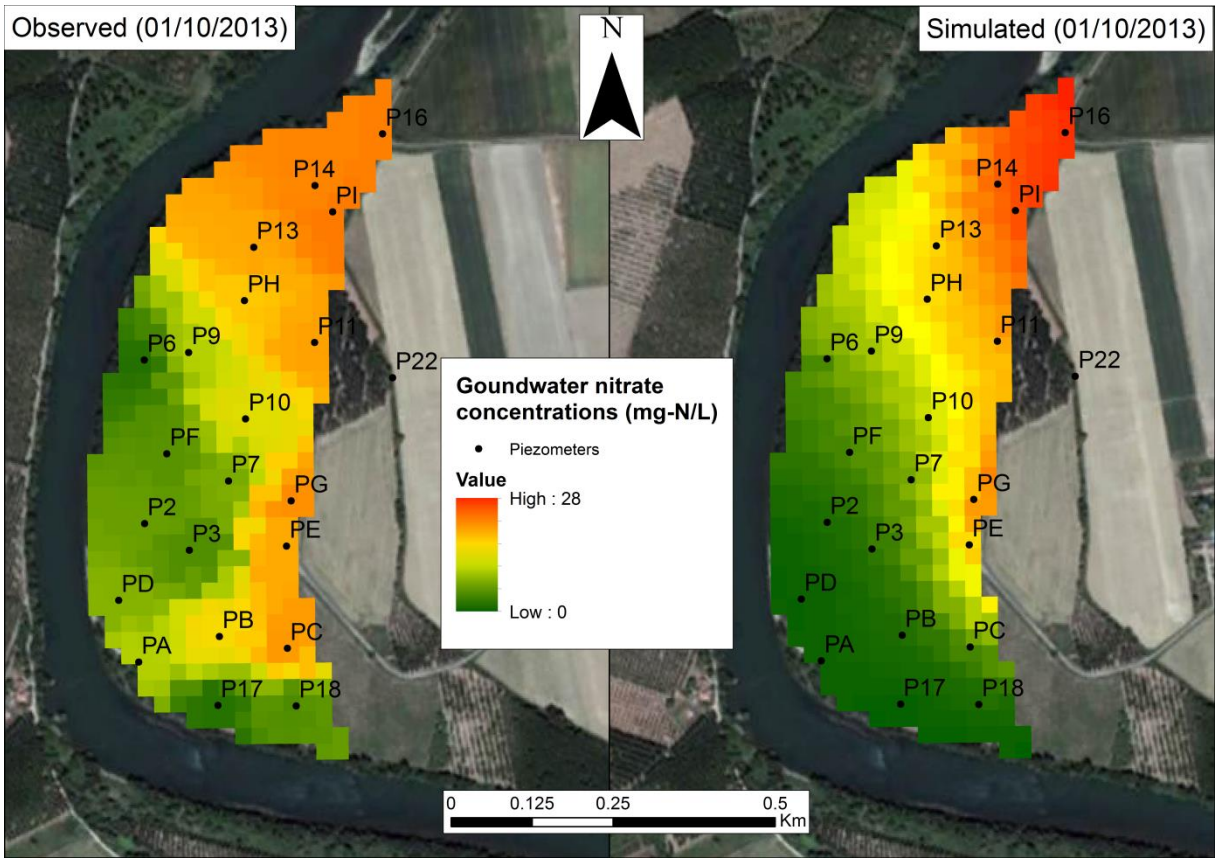

Figure 5-6: Observed (left) and simulated (right) groundwater nitrates concentration for the 1/10/2013 (after 140 days of simulation)

5.5.2. Denitrification rates

The integrated denitrification computed over the simulated period (140 days) and across the meander area is 10.6 kg-N.ha^{-1}, which represents 76 g-N.ha^{-1}.day^{-1} or 27.6 kg-N.ha^{-1}.yr^{-1}. The denitrification activity over the simulated period is 0.81 mg-N.L^{-1} which represents 6.10^{-3} mg-N.L^{-1}.day^{-1} or 2.11 mg-N.L^{-1}.yr^{-1}. The denitrification rates are heterogeneous in time. The Figure 5-7 represents the temporal evolution of the averaged integrated denitrification over the study area. Integrated denitrification ranges from 50 to 175 mg-N.ha^{-1}.day^{-1}. The denitrification temporal pattern is closely linked to the river discharge with two peaks in

denitrification corresponding to the two peaks flow. The temporal evolution of the averaged denitrification activity over the meander is similar to the one of the integrated denitrification (r^2=0.99, Figure 5-8).

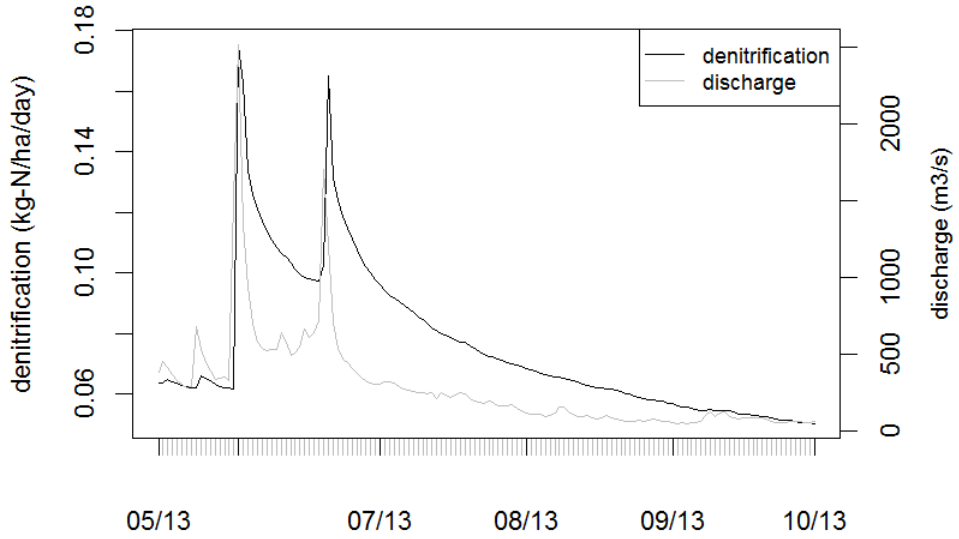

Figure 5-7: Temporal evolution of simulated integrated denitrification (average of the study area) and observed discharge.

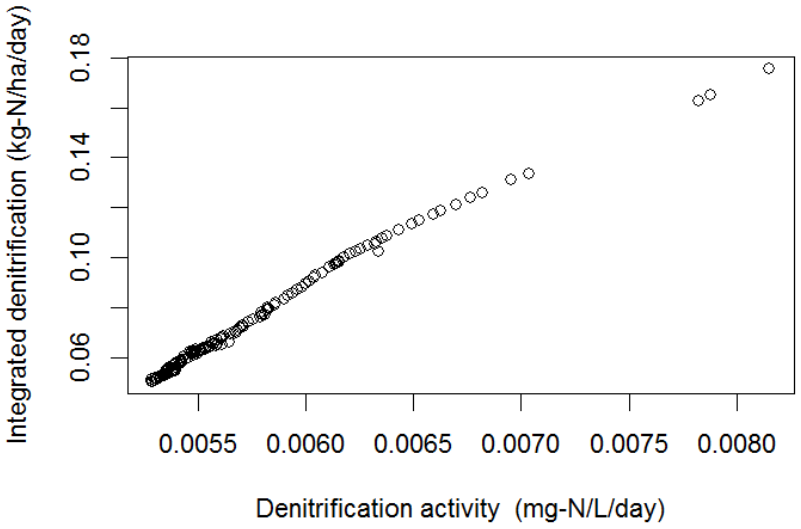

Figure 5-8: Relationship between daily integrated denitrification and denitrification activity (average of the study area)

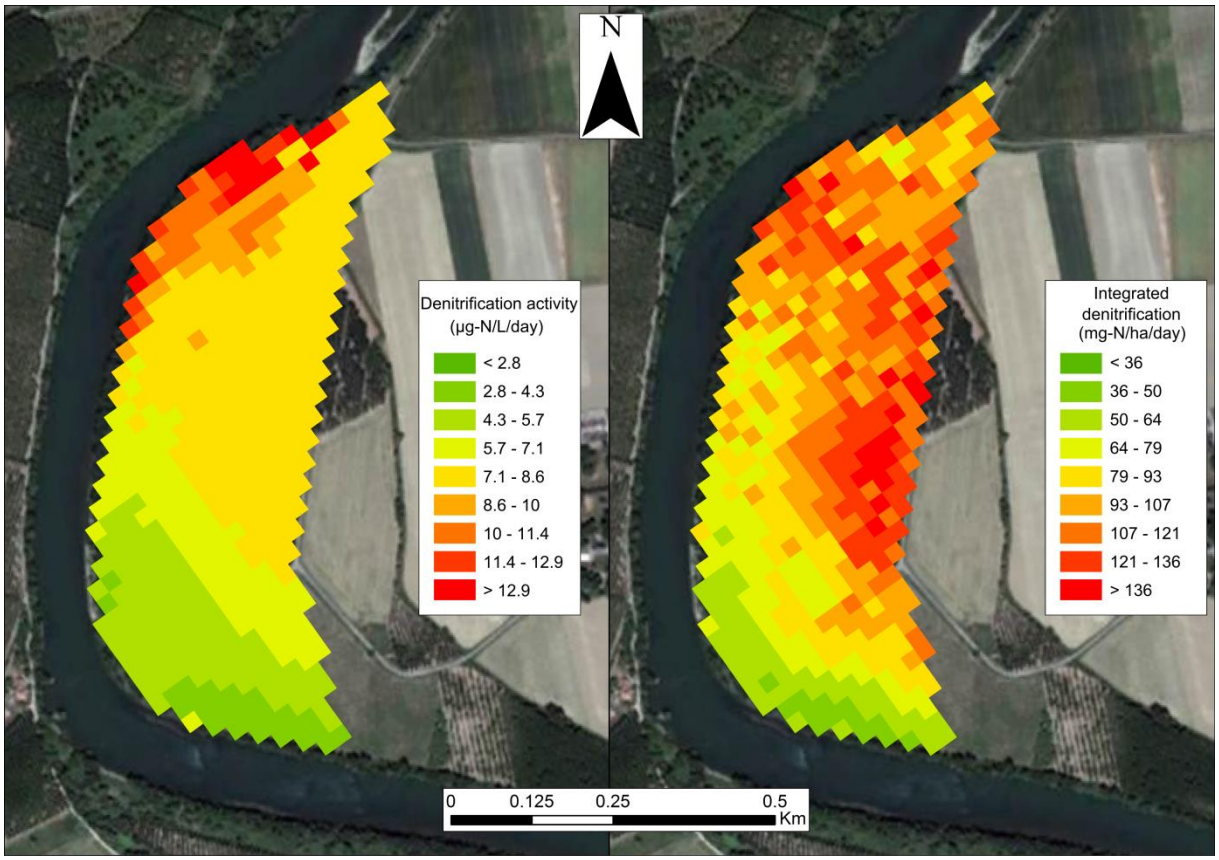

Figure 5-9: Average simulated denitrification intensity (left) and integrated denitrification (right) for the simulated period.

Spatial representation of the mean denitrification activity and integrated denitrification over the study period are shown in Figure 5-9. The denitrification activity map exhibits higher values in a narrow band located along the river in the north west of the area, corresponding to the low elevation riparian area, and lower values in the south of the meander. The integrated denitrification map presents a different pattern with high values in the center east and north east of the meander. However, like denitrification activity, integrated denitrification rates are lower in the south of the meander.

5.5.3. Factors controlling spatial denitrification pattern

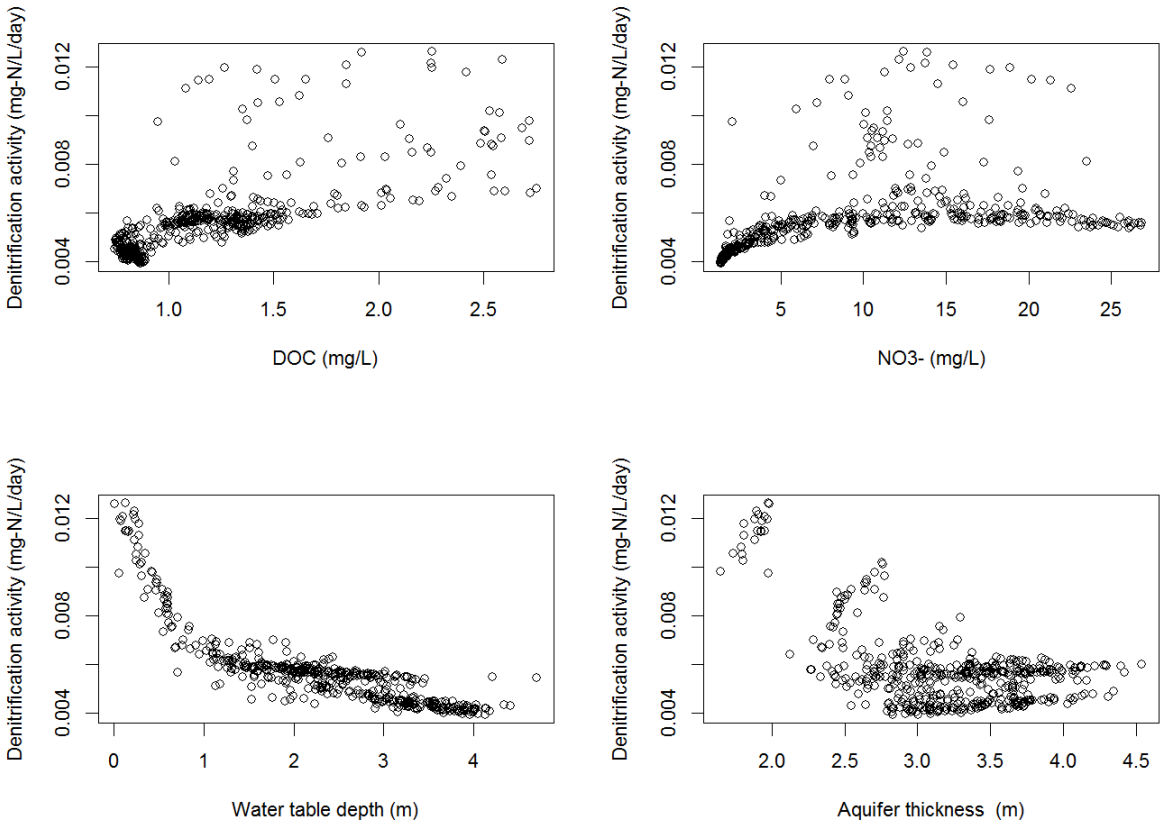

Figure 5-10: Spatial relationship between denitrification activity and DOC and nitrate groundwater concentrations, water table depth and aquifer thickness. The points represent the average of the values for each cell.

In order to investigate the factors controlling denitrification in the area, the average of denitrification activities in each cell for the simulated period was related with the average of DOC concentrations, NO_3^- concentrations, water table depth (distance soil groundwater table) and aquifer thickness (distance impermeable bottom – groundwater table) over the simulated periods (Figure 5-10). Pearson's correlation coefficient are 0.71 0.44 -0.83 and -0.56 for DOC, NO_3^- , water table depth, aquifer thickness, respectively (p-value <0.001 for all).The results show that the denitrification activity is strongly linked to the water table depth (negative correlation) especially for water table depth between 0 and 1 m. Denitrification activity was less related to the others parameters. In addition, the highest denitrification activity rates are related with the lowest aquifer thickness (less than 2 m) and DOC concentrations above 1 $mg.L^{-1}$ but not with particular values of DOC and NO_3^- concentrations. Denitrification activity increases with nitrate concentrations until a value of about 5 $mg\text{-}N.L^{-1}$.

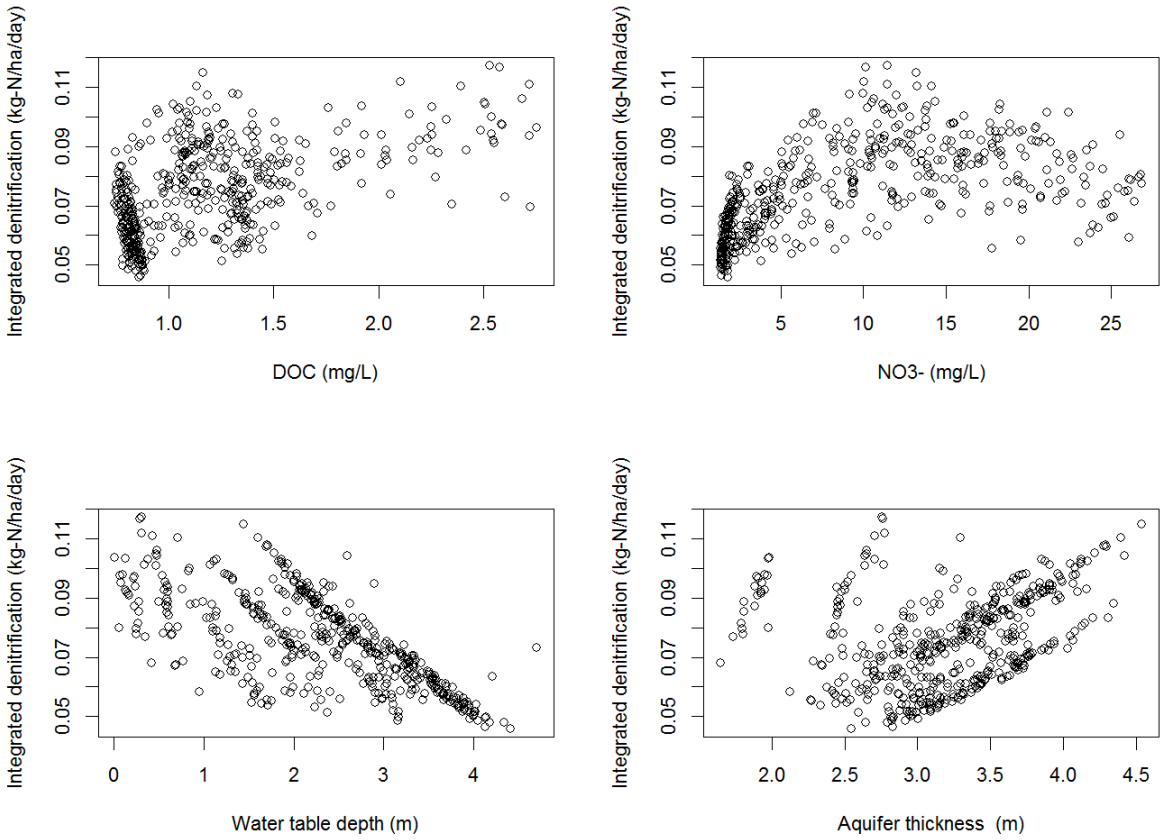

Figure 5-11 : Spatial relationship between integrated denitrification activity and DOC and nitrate (NO3) groundwater concentrations, water table depth and aquifer thickness. The points represent the average of the values for each cell.

Similarly, the average of the integrated denitrification for the simulated period for each cell was related with the same parameters than described than described above (DOC, NO_3^-, water table depth and aquifer thickness; Figure 5-11). Pearson's correlation coefficient are 0.52, 0.53, -0.68 and 0.56 for DOC, NO_3^-, water table depth, aquifer thickness, respectively (p-value <0.001 for all). However, it can be noticed that the highest denitrification rates are related with nitrates concentrations around 10-15 mg-N-NO_3^-.L^{-1} and water table depth below 2 m. The integrated denitrification is also the highest for aquifer thickness around 2.5 m and 4.5 m. The correlation between aquifer thickness and integrated denitrification is positive while it is negative between aquifer thickness and denitrification activity.

5.5.4. Spatio temporal pattern of denitrification activity

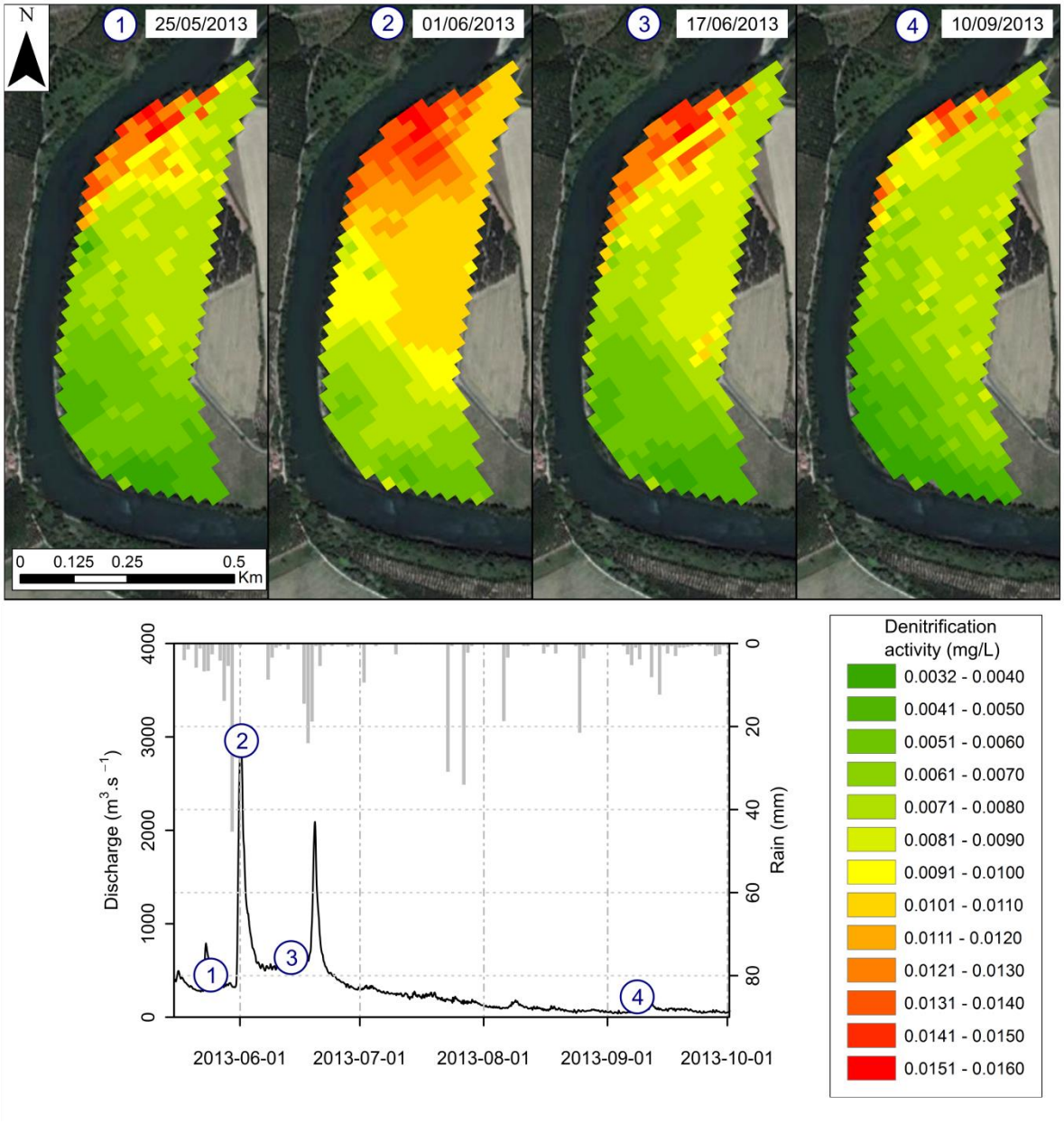

Figure 5-12: Denitrification activity maps at four different dates

Spatio-temporal variations of the denitrification activity have been investigated. Denitrification activity has been mapped for different dates corresponding to the period before the first flood peak, the day after the flood peak when the denitrification is maximal 17 days after the first peak and more than two months after the last flood (Figure 5-12). The results indicated that before the flood, denitrification activity is higher in the north west of the meander. The denitrification activity increases immediately after the flood peak in all the meander area and the area of high activity in the north west of the meander expands. Then, 17 days after the peak flow, the denitrification activity is similar than at the beginning of the

simulation. Finally, two months after the flood, the denitrification activity is overall less intense, but a small area of high denitrification activity remains in the north west of the meander.

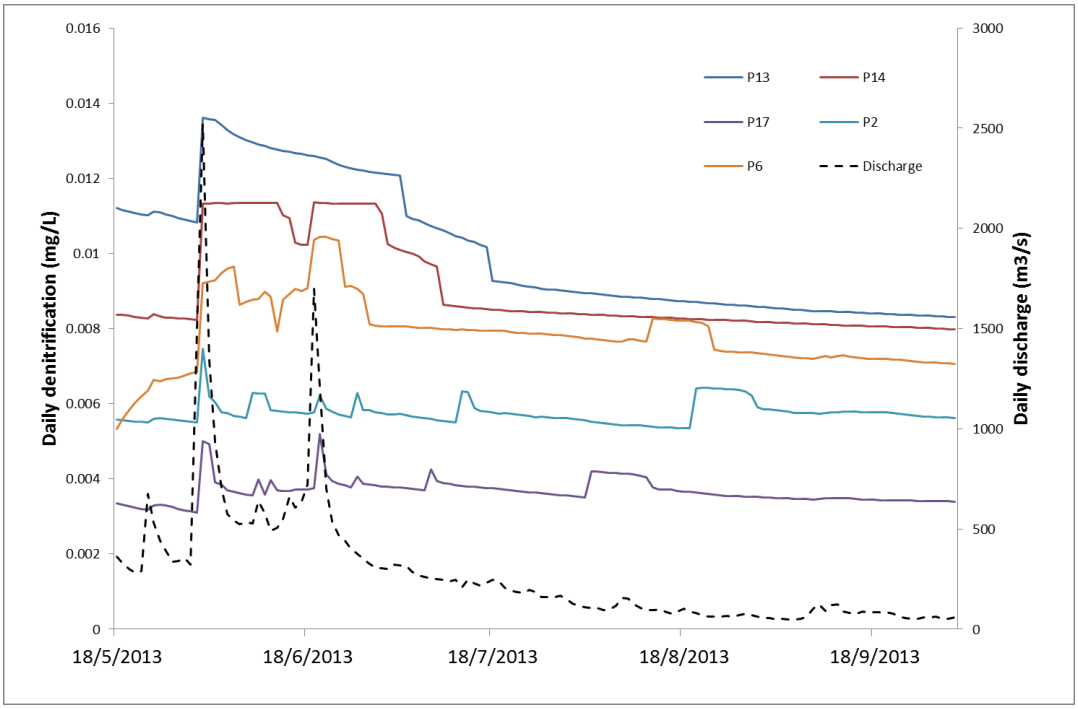

Figure 5-13: Daily denitrification activity and river discharge temporal evolution at 5 piezometers location

The temporal evolution of denitrification activity for some piezometers located in different areas is shown in Figure 5-13. The denitrification was higher for the piezometers located in the low elevation riparian area in the north west of the meander (P13 and P6) and in the piezometer the closest to this area (P14,) than in piezometer located in the south of the meander (P2 and P17). Among these piezometers the P6, located more in the south than P14 and P13, showed a relative lower denitrification activity than these two piezometers. P13 exhibited the highest denitrification rates. Denitrification activities increased when the first peak flow occurred for all the piezometers but with higher intensity in P6, P13 and P14. In addition the denitrification activity also increases during the second peak flow in all the locations but P13.

5.5.5. Nitrate balance in the shallow aquifer

During the simulated period, a simulated nitrate load of 200 g-N.ha^{-1}.day^{-1} entered in the study area groundwater, brought by groundwater flowing from the upland agricultural area. 30 g-N.ha^{-1}.day^{-1} were exported from the study area groundwater to the river. Finally,

according to the model results, 76 g-N.ha^{-1}.day^{-1} were removed through denitrification in the study area (Figure 5-14). The denitrification in the study area accounted for 38% of the incoming nitrates originating from the agricultural area. In addition the results indicated that 94 g-N.ha^{-1}.day^{-1} have accumulated in the groundwater of the study area during the simulated period.

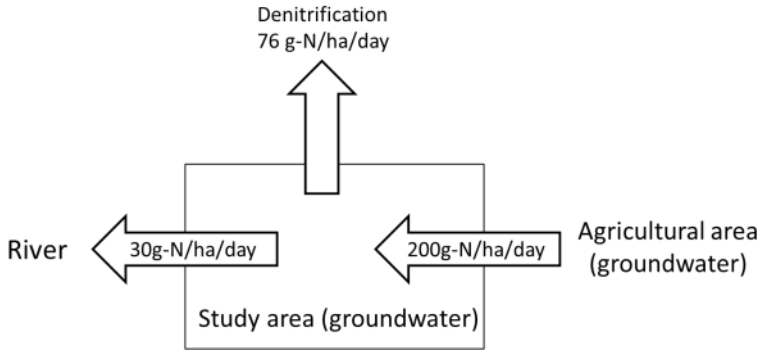

Figure 5-14: Nitrates mass balance of the study area groundwater for the simulated period. Groundwater fluxes from the agricultural area to the study area and from the study area to the river are shown as well as the N-removal through denitrification.

5.6.Discussion

5.6.1. Nitrate simulations

This work aims to study the factors controlling spatio-temporal variability of the denitrification process in a shallow aquifer of a floodplain area by using a modelling approach, combining a distributed hydrodynamic and transport model with a simplified denitrification module. Observed and simulated nitrate concentrations in the aquifer were compared to evaluate the quality of the model. Results were found to be heterogeneous with a better agreement for the first two months corresponding to the first flood event of the simulated period than for the following period where concentrations were underestimated. This can be related with an overestimation of the inundated area and SW-GW exchanges during the second peak flow that would dilute nitrate concentrations more than in reality. The underestimation of nitrate concentrations was especially significant for three piezometers located in the south of the meander close to the agricultural area. This problem can be related to the definition of initial concentrations in the agricultural area that influence the piezometers located close to this area. The initial concentrations in the agricultural area were defined homogeneous but could locally be higher because of practices highly variable in time and space and, therefore, explain the underestimation of the concentration. In addition the vertical leaching of nitrates was not taken into account in the model. However the estimated nitrate

load leaching in the meander area was estimated to 10 kg $N.ha^{-1}.yr^{-1}$ (Jégo, 2008; Sun, 2015) that would represent an increase of about 0.3 mg $N.L^{-1}$ when considering an aquifer thickness of three meters and would not significantly influence nitrate concentrations in the area during the period of the simulation. The poor fit of the simulated nitrates concentration in the south of the area could be more related to the transport process than to the denitrification calculation process. Indeed, nitrates concentrations area known to be primarily controlled by dilution process in the area (Bernard-Jannin et al., 2016) meaning that the transport is an important process to obtain good results of simulated nitrates concentration. Nevertheless, the model was able to correctly simulate nitrate concentration for the rest of the area and the results are satisfactory.

5.6.2. Source of organic carbon

The denitrification module includes POC and DOC as different sources of organic carbon for denitrification process to occur. This separation have been successfully applied in other modelling studies (Sun et al., submitted.; Peyrard et al., 2011; Zarnetske et al., 2012). In the model, POC should be seen as a source of organic carbon contained in the soil that become available for denitrifying bacteria when the water table reaches higher soil level and that would fuel denitrification. DOC in the model represents the organic carbon advected by the river through hyporheic exchanges or overbank infiltration during flood event. Taking into consideration both sources of organic carbon is essential since accounting only for the DOC would not be sufficient to support significant rates of denitrification as the aquifer contain low DOC concentrations (1.03 $mg.L^{-1}$ in average) as reported in other studies (Peyrard et al., 2011; Zarnetske et al., 2011). In addition, K_{DOC} and K_{POC} are two parameters representing the degradation of each carbon source and their availability for denitrification. In this study the two parameters were set homogenous in the PM domain. In reality, their value would differ according to the quality of organic matter and the spatial distribution of micro-organisms communities that could vary along the soil profile (Vilain et al., 2012). However, denitrifying bacteria are known to be ubiquitous in the subsurface environment while organic carbon was identified as the main limiting factors for denitrification (Rivett et al., 2008). Therefore, the modelling strategy used in this study was to capture the influence of hydrology and geomorphology on denitrification process through its influence on organic carbon availability controlling bacterial activity and denitrification rather than explicitly consider bacterial community variability itself.

5.6.3. Factors controlling denitrification

Simulated denitrification activity rate in the study area is 6.10^{-3} mg $N.L^{-1}.day^{-1}$ in average. This result is in accordance with the average potential denitrification values of 5.10^{-2} mg $N.L^{-1}.day^{-1}$ measured in the area (Bernard-Jannin et al., 2016) as potential denitrification rates are known to be 4 to 31 times more important than in situ denitrification in the area (Iribar, 2007). Denitrification removed 28 kg $N.ha^{-1}.yr^{-1}$ over the meander area. This is lower than results of a modelling study carried out in the same area with a catchment scale model reported denitrification rates ranging from 55 to 120 kg $N.ha^{-1}.yr^{-1}$ (Sun, 2015). In the Rhine river, Venterink et al. (2003) measured denitrification rates ranging from 96 to 131 kg $N.ha^{-1}.yr^{-1}$ in flooded sediment. Denitrification rates were spatially and temporally heterogeneous. The simulated denitrification in the study area accounted for 38% of the nitrate load brought through lateral groundwater flow coming from the agricultural area, underlying the importance of denitrification process in riparian area. However, these results were obtained considering the homogenous parametrization of the denitrification module parameter as discussed above and further work on the sensitivity of the model has to be carried out to better asses their significance.

High denitrification activities have been identified in the low riparian area and were related to low water table depth and aquifer thickness. Water table depth is directly linked to POC availability that rose when the topsoil layers, richer in POC than deeper layers, are submerged. This is more likely to happen in the area close to the river with low elevation and where the aquifer thickness is relatively low due to the geometry of the impermeable layer that is at the same elevation than the riverbed and can explain the results. Therefore, the high denitrification location can be explained by the geomorphological settings that lead to a favorable condition for top soil saturation making POC available for denitrification. In addition, within the low riparian area, denitrification activity was higher in the north than in the south area. This can be related to the hydrology of the area as the groundwater containing high nitrates concentrations flows from the agricultural area mostly in the north of the meander (Bernard-Jannin et al., 2016). This findings are in agreement with Hill et al. (2000) that identified denitrification hotspots location where flow path lead nitrate loaded groundwater to meet rich organic sediment layer. In addition, no clear relationship between DOC and denitrification could have been established meaning that the role of the DOC borne by the river into the groundwater is less important than the one of topsoil saturation. This can be expected as the concentration in the river (1.5 $mg.L^{-1}$) is only slightly higher than the DOC

concentration in the aquifer (1.03 $mg.L^{-1}$ in average). However the DOC concentration was set constant in the river according to the measurements while it could rise during flood events.

Unlike denitrification activity, integrated denitrification over the aquifer depth (28 $kg\ N.ha^{-1}.yr^{-1}$ in average) was higher in the north area of the meander with high denitrification and not only in the low elevation riparian area. Integrated denitrification has been related to water table depth below 2 m and aquifer thickness around 2.5 m and 4.5 m. However, unlike denitrification activity, integrated denitrification was positively correlated with aquifer thickness. This could explain the different spatial patterns between them. Even with lower denitrification activity, areas with thicker aquifer exhibit integrated denitrification similar to the low elevation riparian area where the aquifer is thinner. In both case nitrates concentration appears to be a limiting factor but only for extremely low concentrations. The geometry of the porous media is linked to two processes promoting denitrification being 1) low elevation area providing high organic carbon to fuel the denitrification but low water storage volume and 2) higher elevation area with less organic carbon and subsequent denitrification activity but affecting larger volume of water. The higher denitrification rates occur in the north area of the meander corresponding to the area of higher groundwater flow velocities (Bernard-Jannin et al., 2016). Thus, this hotspots of denitrification would be triggered by the higher nitrate flux coming from the agricultural area (Hill et al., 2000; McClain et al., 2003) while the south of the meander which is under the influence of river water exhibit lower nitrates concentrations and denitrification rates (Bernard-Jannin et al., 2016).

In addition, denitrification is also temporally heterogeneous. Unlike the spatial patterns, the temporal evolution of both integrated denitrification and denitrification activity is similar. Flood events triggered higher denitrification periods during which integrated denitrification increased by a factor 3 and denitrification intensity by a factor 1.5. Denitrification activity increase can only be related with an increase of organic carbon (DOC and POC) availability while integrated denitrification also depends on aquifer thickness. In both cases, the increase can be explained by the saturation of topsoil layers increasing POC availability and by the additional DOC brought by the river water infiltration. However the denitrification increase is more likely explained by the saturation of the top soil layer than by the DOC income since DOC concentration in the river is relatively low as already discussed. This results confirmed previous studies underlying the role of flood events and high water periods on denitrification (Baker and Vervier, 2004; Pfeiffer et al., 2006).

5.7.Conclusion

A modelling approach coupling a three dimensional hydrodynamic model with a simplified denitrification model was applied over a floodplain section area. The model was able to simulate nitrate concentrations and denitrification rates and allowed to identify keys parameters controlling denitrification. Denitrification was estimated to 28 kg $N.ha^{-1}.yr^{-1}$ representing 38% of the nitrates brought with the groundwater flowing from the agricultural area. High denitrification areas were identified in the low elevation riparian area and in the north of the area. In addition, the main factors controlling denitrification in the area were i) the geomorphology of the floodplain that controlled water table depth and subsequent POC availability and ii) the groundwater flows transporting nitrates from the agricultural area. In addition, aquifer thickness was also important when considering the total N removal (integrated denitrification) by increasing the volume of groundwater where denitrification occurred. Finally, flood events were found to trigger high denitrification episodes. The model can help to assess the potential of riparian area for nitrate removal in floodplain areas for different hydro-geomorphological settings (e.g. sinuosity, dam impact on river discharge). In addition the results can be used to evaluate the validity of larger scale model. However, further studies have to be carried out to assess the sensitivity of the model to the denitrification parameters to better assess the significance of the results.

Acknowledgements

This study was undertaken as part of the EU Interreg SUDOE IVB programme (ATTENAGUA - SOE3/P2/F558 project) and was funded by ERDF. This research was carried out as a part of “ADAPT’EAU” (ANR-11-CEPL-008), a project supported by the French National Research Agency (ANR) within the framework of the Global Environmental Changes and Societies (GEC&S) programme. This work was granted access to the HPC resources of CALMIP under allocation P13119. The 1m-digital terrain model was provided by the French National Geographical Institute (IGN) and the discharge data by DREAL. The source code for the model used in this study, MOHID LAND, is free of charge and is available at from www.mohid.codeplex.com.

References

Ahuja, L.R., Rojas, K.W., Hanson, J.D., Shaffer, M.J., Ma, L., 2000. Root zone water quality model. Water Resour. Publ., Highl. Ranch, CO.

Arauzo, M., Valladolid, M., Martínez-Bastida, J.J., 2011. Spatio-temporal dynamics of nitrogen in river-alluvial aquifer systems affected by diffuse pollution from agricultural sources: Implications for the implementation of the Nitrates Directive. J. Hydrol. 411, 155–168. doi:10.1016/j.jhydrol.2011.10.004

Arrate, I., Sanchez-Perez, J.-M., Antiguedad, I., Vallecillo, M.A., Iribar, V., Ruiz, M., 1997. Groundwater pollution in Quaternary aquifer of Vitoria–Gasteiz (Basque Country, Spain). Environ. Geol. 30, 257–265.

Baillieux, A., Campisi, D., Jammet, N., Bucher, S., Hunkeler, D., 2014. Regional water quality patterns in an alluvial aquifer: Direct and indirect influences of rivers. J. Contam. Hydrol. 169, 123–31. doi:10.1016/j.jconhyd.2014.09.002

Baker, M.A., Vervier, P., 2004. Hydrological variability, organic matter supply and denitrification in the Garonne River ecosystem. Freshw. Biol. 49, 181–190. doi:10.1046/j.1365-2426.2003.01175.x

Bernard-Jannin, L., Brito, D., Sun, X., Jauch, E., Neves, R.J.J., Sauvage, S., Sánchez-Pérez, J.M., n.d. A physically-based, spatially-distributed modelling approach coupling surface water and groundwater flows to evaluate water exchanges in an alluvial floodplain during flood events. Adv. Water Resour.

Bernard-Jannin, L., Sun, X., Teissier, S., Sauvage, S., Sánchez-Pérez, J.-M., 2016. Spatio-temporal analysis of factors controlling nitrate dynamics and potential denitrification hot spots and hot moments in groundwater of an alluvial floodplain. Ecol. Eng. doi:10.1016/j.ecoleng.2015.12.031

Bijay-Singh, Yadvinder-Singh, Sekhon, G.S., 1995. Fertilizer-N use efficiency and nitrate pollution of groundwater in developing countries. J. Contam. Hydrol. 20, 167–184. doi:10.1016/0169-7722(95)00067-4

Boano, F., Demaria, A., Revelli, R., Ridolfi, L., 2010. Biogeochemical zonation due to intrameander hyporheic flow. Water Resour. Res. 46, 1–13.

Boithias, L., Srinivasan, R., Sauvage, S., Macary, F., Sánchez-Pérez, J.M., 2014. Daily Nitrate Losses: Implication on Long-Term River Quality in an Intensive Agricultural Catchment of Southwestern France. J. Environ. Qual. 43, 46–54.

Burt, T.P., Matchett, L.S., Goulding, K.W.T., Webster, C.P., Haycock, N.E., 1999. Denitrification in riparian buffer zones: the role of floodplain hydrology. Hydrol. Process. 13, 1451–1463. doi:10.1002/(SICI)1099-1085(199907)13:10<1451::AID-HYP822>3.0.CO;2-W

Carpenter, S.R., Caraco, N.F., Correll, D.L., Howarth, R.W., Sharpley, A.N., Smith, V.H., 1998. Non point pollution of surface waters with phosphorus and nitrogen. Ecol. Appl. 8, 559–568. doi:10.1890/1051-0761(1998)008[0559:NPOSWW]2.0.CO;2

Dosskey, M.G., Vidon, P., Gurwick, N.P., Allan, C.J., Duval, T.P., Lowrance, R., 2010. The Role of Riparian Vegetation in Protecting and Improving Chemical Water Quality in Streams1. JAWRA J. Am. Water Resour. Assoc. 46, 261–277. doi:10.1111/j.1752-1688.2010.00419.x

Groffman, P., Butterbach-Bahl, K., Fulweiler, R., Gold, A., Morse, J., Stander, E., Tague, C., Tonitto, C., Vidon, P., 2009. Challenges to incorporating spatially and temporally explicit phenomena (hotspots and hot moments) in denitrification models. Biogeochemistry 93, 49–77. doi:10.1007/s10533-008-9277-5

Groffman, P.M., 2012. Terrestrial denitrification: challenges and opportunities. Ecol. Process. 1, 1–11.

Haycock, N.E., Burt, T.P., 1993. Role of floodplain sediments in reducing the nitrate concentration of subsurface runoff: A case study in the Cotswolds, UK. Hydrol. Process. 7, 287–295.

Heinen, M., 2006. Simplified denitrification models: Overview and properties. Geoderma 133, 444–463. doi:http://dx.doi.org/10.1016/j.geoderma.2005.06.010

Hill, A.R., Devito, K.J., Campagnolo, S., Sanmugadas, K., 2000. Subsurface Denitrification in a Forest Riparian Zone: Interactions between Hydrology and Supplies of Nitrate and Organic Carbon. Biogeochemistry 51, 193–223.

Iribar, A., 2007. Composition des communautés bactériennes dénitrifiantes au sein d'un aquifère alluvial et facteurs contrôlant leur structuration: relation entre structure des communautés et dénitrification. Université de Toulouse III - Paul Sabatier.

Iribar, A., Sánchez-Pérez, J., Lyautey, E., Garabétian, F., 2008. Differentiated free-living and sediment-attached bacterial community structure inside and outside denitrification hotspots in the river–groundwater interface. Hydrobiologia 598, 109–121 LA – English. doi:10.1007/s10750-007-9143-9

Jégo, G., 2008. Influence des activités agricoles sur la pollution nitrique des eaux souterraines. Analyse par modélisation des impacts des systèmes de grande culture sur les fuites de nitrate dans les plaines alluviales. Université de Toulouse III - Paul Sabatier.

Jégo, G., Sánchez-Pérez, J.M., Justes, E., 2012. Predicting soil water and mineral nitrogen contents with the STICS model for estimating nitrate leaching under agricultural fields. Agric. Water Manag. 107, 54–65. doi:http://dx.doi.org/10.1016/j.agwat.2012.01.007

Korom, S.F., 1992. Natural denitrification in the saturated zone: A review. Water Resour. Res. 28, 1657–1668. doi:10.1029/92WR00252

Lowrance, R., Altier, L.S., Newbold, J.D., Schnabel, R.R., Groffman, P.M., Denver, J.M., Correll, D.L., Gilliam, J.W., Robinson, J.L., Brinsfield, R.B., Staver, K.W., Lucas, W., Todd, A.H., 1997. Water Quality Functions of Riparian Forest Buffers in Chesapeake Bay Watersheds. Environ. Manage. 21, 687–712. doi:10.1007/s002679900060

McClain, M.E., Boyer, E.W., Dent, C.L., Gergel, S.E., Grimm, N.B., Groffman, P.M., Hart, S.C., Harvey, J.W., Johnston, C.A., Mayorga, E., McDowell, W.H., Pinay, G., 2003. Biogeochemical Hot Spots and Hot Moments at the Interface of Terrestrial and Aquatic Ecosystems. Ecosystems 6, 301–312. doi:10.1007/s10021-003-0161-9

Nash, Je., Sutcliffe, J. V, 1970. River flow forecasting through conceptual models part I—A discussion of principles. J. Hydrol. 10, 282–290.

Osborne, L.L., Kovacic, D.A., 1993. Riparian vegetated buffer strips in water-quality restoration and stream management. Freshw. Biol. 29, 243–258. doi:10.1111/j.1365-2427.1993.tb00761.x

Peter, S., Rechsteiner, R., Lehmann, M.F., Tockner, K., Durisch-Kaiser, E., 2011. Denitrification hot spot and hot moments in a restored riparian system. IAHS-AISH Publ. 433–436.

Peyrard, D., Delmotte, S., Sauvage, S., Namour, P., Gerino, M., Vervier, P., Sánchez-Pérez, J.M., 2011. Longitudinal transformation of nitrogen and carbon in the hyporheic zone of an N-rich stream: A combined modelling and field study. Phys. Chem. Earth, Parts A/B/C 36, 599–611. doi:http://dx.doi.org/10.1016/j.pce.2011.05.003

Peyrard, D., Sauvage, S., Vervier, P., Sánchez-Pérez, J.-M., Quintard, M., 2008. A coupled vertically integrated model to describe lateral exchanges between surface and subsurface in large alluvial floodplains with a fully penetrating river. Hydrol. Process. 22, 4257–4273. doi:10.1002/hyp.7035

Pfeiffer, S.M., Bahr, J.M., Beilfuss, R.D., 2006. Identification of groundwater flowpaths and denitrification zones in a dynamic floodpain aquifier. J. Hydrol. 325, 262–272. doi:10.1016/j.jhydrol.2005.10.019

Pinay, G., Ruffinoni, C., Wondzell, S., Gazelle, F., 1998. Change in Groundwater Nitrate Concentration in a Large River Floodplain: Denitrification, Uptake, or Mixing? J. North Am. Benthol. Soc. 17, 179–189. doi:10.2307/1467961

Power, J.F., Schepers, J.S., 1989. Nitrate contamination of groundwater in North America. Agric. Ecosyst. Environ. 26, 165–187. doi:10.1016/0167-8809(89)90012-1

Rivett, M.O., Buss, S.R., Morgan, P., Smith, J.W.N., Bemment, C.D., 2008. Nitrate attenuation in groundwater: A review of biogeochemical controlling processes. Water Res. 42, 4215–4232. doi:http://dx.doi.org/10.1016/j.watres.2008.07.020

Sánchez-Pérez, J.M., 1992. Fonctionnement hydrochimique d'un écosystème forestier inondable de la Plaine du Rhin: la forêt alluviale du secteur de l'île de Rhinau en Alsace(France). Université Louis Pasteur, Strasbourg.

Sánchez-Pérez, J.M., Vervier, P., Garabétian, F., Sauvage, S., Loubet, M., Rols, J.L., Bariac, T., Weng, P., 2003. Nitrogen dynamics in the shallow groundwater of a riparian wetland zone of the Garonne, SW France: nitrate inputs, bacterial densities, organic matter supply and denitrification measurements. Hydrol. Earth Syst. Sci. 7, 97–107. doi:10.5194/hess-7-97-2003

Sorooshian, S., Duan, Q., Gupta, V.K., 1993. Calibration of rainfall-runoff models: Application of global optimization to the Sacramento Soil Moisture Accounting Model. Water Resour. Res. 29, 1185–1194.

Sun, X., 2015. Modélisation des échanges nappe-rivière et du processus de dénitrification dans les plaines alluviales à l'échelle du bassin versant. Université de Toulouse III - Paul Sabatier.

Sun, X., Bernard-Jannin, L., Garneau, C., Arnold, J.G., Srinivasan, R., Sauvage, S., Sánchez-Pérez, J.M., n.d. Assessment of the denitrification process in alluvial wetlands at floodplain scale using SWAT model. Ecol. Eng.

Sun, X., Bernard-Jannin, L., Garneau, C., Volk, M., Arnold, J.G., Srinivasan, R., Sauvage, S., Sánchez-Pérez, J.M., 2015. Improved simulation of river water and groundwater exchange in an alluvial plain using the SWAT model. Hydrol. Process.

Sutton, M.A., Howard, C.M., Erisman, J.W., Billen, G., Bleeker, A., Grennfelt, P., van Grinsven, H., Grizzetti, B., 2011. The European nitrogen assessment: sources, effects and policy perspectives. Cambridge University Press.

Venterink, H.O., Hummelink, E., Van den Hoorn, M.W., 2003. Denitrification potential of a river floodplain during flooding with nitrate-rich water: grasslands versus reedbeds. Biogeochemistry 65, 233–244.

Vidon, P., Hill, A.R., 2005. Denitrification and patterns of electron donors and acceptors in eight riparian zones with contrasting hydrogeology. Biogeochemistry 71, 259–283.

Vidon, P.G.F., Hill, A.R., 2004. Landscape controls on nitrate removal in stream riparian zones. Water Resour. Res. 40.

Vilain, G., Garnier, J., Roose-Amsaleg, C., Laville, P., 2012. Potential of denitrification and nitrous oxide production from agricultural soil profiles (Seine Basin, France). Nutr. Cycl. Agroecosystems 92, 35–50.

Weng, P., Sánchez-Pérez, J.M., Sauvage, S., Vervier, P., Giraud, F., 2003. Assessment of the quantitative and qualitative buffer function of an alluvial wetland: hydrological modelling of a large floodplain (Garonne River, France). Hydrol. Process. 17, 2375–2392. doi:10.1002/hyp.1248

Zarnetske, J.P., Haggerty, R., Wondzell, S.M., Baker, M.A., 2011. Labile dissolved organic carbon supply limits hyporheic denitrification. J. Geophys. Res. Biogeosciences 116.

Zarnetske, J.P., Haggerty, R., Wondzell, S.M., Bokil, V.A., González-Pinzón, R., 2012. Coupled transport and reaction kinetics control the nitrate source-sink function of hyporheic zones. Water Resour. Res. 48.

Zhang, W.L., Tian, Z.X., Zhang, N., Li, X.Q., 1996. Nitrate pollution of groundwater in northern China. Agric. Ecosyst. Environ. 59, 223–231. doi:10.1016/0167-8809(96)01052-3

5.8. Résultats complémentaires : analyse de sensibilité du module de dénitrification

Le calcul de la dénitrification dépend de plusieurs paramètres (K_{POC}, K_{DOC}, K_{NO3}) et variables (POC, DOC, NO_3^-). Les paramètres liés à la dégradation du carbone organique (K_{POC}, K_{DOC}) peuvent variés dans le temps et l'espace car ils dépendent, entre autres, de l'activité des micro-organismes et de la qualité de la matière organique. Cependant, une des limites de l'application du modèle au site de Monbéqui est que la valeur de ces paramètres a été définie comme homogène dans le temps et l'espace car leur variabilité n'est pas connue. De plus, une valeur de DOC constante a été définie dans la rivière alors que la concentration en DOC peut augmenter pendant les crues. Bien que le modèle ait donné des résultats satisfaisants, évaluer l'impact de ces simplifications est important pour mieux analyser les résultats obtenus. Une analyse de sensibilité des facteurs liés au calcul de la dénitrification a donc été effectuée afin de mieux comprendre le rôle de chaque paramètre et variable sur le calcul de la dénitrification (chapitre 2, équation 17).

La méthode de Morris (Morris, 1991) a été utilisée pour évaluer la sensibilité su modèle aux six facteurs (paramètres et variables) que sont K_{POC}, K_{DOC}, K_{NO3}, POC, DOC et NO_3^-. La densité et la porosité ne sont pas incluses car leur valeur est considérée comme étant bien connue. La méthode est détaillée dans Garneau (2014) et consiste à prendre n jeux de paramètres à l'intérieur de bornes prédéfinies puis à perturber chaque facteur pour en calculer l'effet élémentaire. Les facteurs ont été normalisés selon une loi uniforme ou exponentielle pour que tous aient des effets élémentaires similaires. La moyenne μ^* et l'écart –type σ des effets élémentaires sont ensuite calculés pour chaque facteur. Une moyenne des effets élémentaires élevée est synonyme d'un facteur dominant tandis qu'un écart-type élevé indique que les interactions entre les paramètres sont importantes. Dans cette étude, 1000 jeux de paramètres ont été utilisés. Les valeurs minimales et maximales affectées à chaque facteur ainsi que la méthode d'échantillonnage sont présentées dans la Table 5-5.

Table 5-5: Facteurs inclus dans l'analyse de sensibilité. Inf. et Sup. indiquent les limites données aux facteurs. Le type d'échantillonnage uniforme (log=0) ou exponentiel (log=1) est indiqué.

Facteurs	Unités	Inf.	Sup	log
NO3	mg-N.L^{-1}	0	30	0
DOC	mg-N.L^{-1}	0	20	0
POC	mg.kg^{-1}	500	5000	0
K_{NO3}	mg-N.L^{-1}	1	30	0
K_{DOC}	jour^{-1}	1,00E-06	1,00E-01	1
K_{POC}	jour^{-1}	1,00E-08	1,00E-03	1

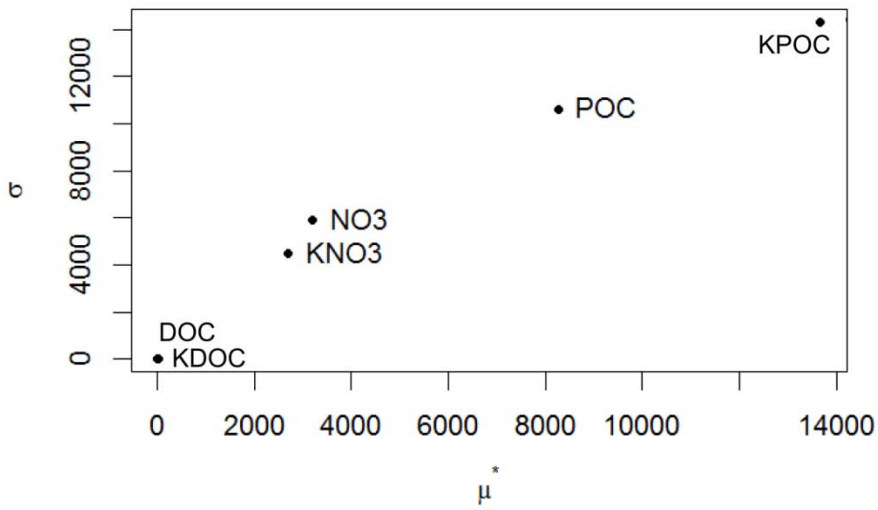

Figure 5-15 : Graphiques $\sigma - \mu^*$de la sensibilité du module de la dénitrification

La Figure 5-15 présente la moyenne et l'écart-type des effets élémentaires de chaque facteur. La dénitrification est très sensible aux facteurs liés au POC (K_{POC} et POC) alors qu'elle est très peu sensibles à ceux liés au DOC (K_{DOC} et DOC). La sensibilité aux facteurs liés aux nitrates (K_{NO3} et NO3) est intermédiaire.

La faible sensibilité de la dénitrification aux facteurs lié au DOC indique que le fait d'avoir défini une valeur de DOC constante dans la rivière n'impacte que très peu le calcul de la dénitrification. Au contraire, la plus forte sensibilité de la dénitrification aux facteurs liés au POC et aux nitrates indique que les résultats du modèle dépendent fortement des valeurs de POC et de K_{POC}.et, dans une moindre mesure, des valeurs de NO_3^- et K_{NO3}. Ces résultats indiquent que les résultats du modèle sont valables pour les valeurs de K_{POC} et de POC données. Aussi, malgré le fait que le paramètre K_{POC} ait été calibré, il est défini comme étant constant et sa potentielle variabilité (spatiale et temporelle) n'est pas prise en compte dans le modèle. La même conclusion s'applique au paramètre K_{NO3} auquel la dénitrification est

également sensible (moins que pour le K_{POC}). De même, la variabilité du POC (autre que la différenciation entre les 50 premier cm et les zones plus profondes telle que définie dans le modèle) n'est pas prise en compte dans le modèle. Finalement, la sensibilité de la dénitrification aux nitrates indique qu'il est important de représenter correctement la dynamique des nitrates dans le modèle. C'est le cas dans le modèle, car le transport des nitrates et leur transformation (dénitrification) sont pris en compte.

5.9.Synthèse

Le modèle MOHID Land a permis de simuler l'hydrologie de la plaine alluviale de Monbéqui (chapitre 4). Dans ce chapitre, un module de dénitrification a été ajouté au modèle MOHID Land, puis appliqué sur le même site expérimental de Monbéqui. La formalisation du processus de dénitrification a été influencée par les résultats obtenus à la suite de l'analyse d'un jeu de données conséquent (chapitre 3). La principale caractéristique du module implémenté est de prendre en compte la présence de carbone organique présent des sols et apportés par la rivière.

Le modèle est capable de représenter correctement les concentrations en nitrates dans l'aquifère. Les résultats montrent que les zones où la dénitrification est la plus importante sont en lien avec la géomorphologie et les écoulements souterrains alors que les périodes de forte dénitrification sont liées aux crues. Le principal processus identifiés expliquant les variations de dénitrification dans la zone de Monbéqui est relatif à la saturation des horizons supérieurs des sols, qui libèrent du carbone organique alimentant la réaction de dénitrification. Ceci se produit dans les zones les plus basses ou la profondeur de l'aquifère est faible et dans les zones inondées pendant les périodes de crue. Néanmoins, malgré des activités de dénitrification plus faibles, la quantité totale de nitrates éliminés peut être importante dans les zones ou l'aquifère est plus épais. La concentration en nitrates est également un facteur contrôlant la variabilité spatiale de la dénitrification. En effet, une plus forte dénitrification est simulée dans les zones les plus concentrées en nitrates. Dans la zone d'étude, la concentration en nitrates est contrôlée par les écoulements souterrains en provenance de la zone agricole.

Cependant, l'effet de l'apport du carbone organique par via les eaux de surface semble négligeable par rapport à la présence de carbone organique dans les sols. Ceci est confirmé par l'analyse de sensibilité qui montre que la dénitrification est peu sensible aux concentrations en COD. Au contraire, l'analyse de sensibilité à mis en avant la sensibilité du calcul de la dénitrification aux facteurs liés au COP (K_{POC} et POC), et dans une moindre

mesure, aux nitrates (K_{NO3} et NO3). Il faut donc prendre en compte que le fait d'avoir défini des paramètres de dégradation du COP (K_{POC}) comme étant constant dans le domaine modélisé ne permet pas de représenter l'effet de la variabilité des facteurs qui influent sur la vitesse de dégradation de la matière organique (par exemple, les communautés bactériennes et la qualité de la matière organique). Toutefois, les paramètres K_{POC} et K_{DOC} ont été calibrés et les résultats des simulations ont montrés que les concentrations en nitrates étaient bien représentées par le modèle. De plus, le taux de dénitrification calculé (28 kg $N.ha^{-1}.yr^{-1}$) est du même ordre de grandeur que ceux reportés par d'autres études menées dans des plaines alluviales. La dynamique générale de la dénitrification modélisée peut donc être considérée comme représentative de la réalité.

L'approche consistant à coupler observations de terrains et modélisation a donc permis de mettre au point un modèle adapté à la simulation de la dénitrification dans les plaines alluviales en prenant en compte l'effet des facteurs hydro-géomorphologiques. La prochaine étape consiste à appliquer le modèle pour d'autres sites d'études afin d'évaluer ses performances dans des conditions différentes.

Chapitre 6 : Etude du processus de dénitrification dans des plaines alluviales contrastées du territoire sud-ouest européen (SUDOE)

Le modèle MOHID Land a été appliqué avec succès sur le site de Monbéqui et a permis de simuler la dynamique spatio-temporelle du processus de dénitrification. Afin de vérifier la transposabilité du modèle à d'autres sites, et d'identifier les facteurs expliquant différentes capacités de dénitrification pour chaque site, ce dernier a également été appliqué sur trois autres plaines alluviales dans le cadre du projet européen ATTENAGUA (INTERREG SUDOE, http://www.attenagua-sudoe.eu/fr/). Les trois sites étudiés sont situés dans les plaines alluviales de l'Ebre (près de Saragosse, Espagne), de la Bidassoa (près de Irun, pays basque espagnole), et du Tage (près de Tolède, Espagne), et sont présentés dans la première partie de ce chapitre. Ces sites, ainsi que le site de Monbéqui, ont fait l'objet d'une étude comparative ayant pour but de caractériser leur capacité d'atténuation des contaminations en nitrates (Antiguedad et al., soumis) dont les principaux résultats sont décrits dans la deuxième partie de ce chapitre. Finalement, la troisième partie de ce chapitre présente l'application du modèle MOHID Land sur chacun des sites afin d'analyser le processus de dénitrification dans ces plaines alluviales.

6.1.Introduction

L'application du modèle MOHID Land au site de Monbéqui a mis en avant le rôle de l'hydro-géomorphologie dans la variabilité spatio-temporelle de la dénitrification. Sur ce site, c'est la saturation des horizons supérieurs des sols qui entraine des taux de dénitrification importants. La saturation des sols dépend de la géomorphologie du lieu (les zones les plus basses sont plus facilement inondées) et de la fréquence et de l'intensité des inondations. De plus, la concentration en nitrates des eaux souterraines est également reliée au taux de dénitrification. Dans ce chapitre, le modèle est appliqué à des sites de plaine alluviale possédant des caractéristiques variées, afin d'étudier les facteurs contrôlant la dénitrification entre les différents sites.

6.2.Description des sites d'études

Les sites étudiés dans ce chapitre sont, comme pour le site de Monbéqui, des tronçons de plaine alluviale agricole de différents fleuves situés dans le sud-ouest européens (Bidassoa, Ebre, Garonne et Tage ; Figure 6-1). Cependant, chaque site possède des caractéristiques différentes en termes d'hydrologie et de géomorphologie.

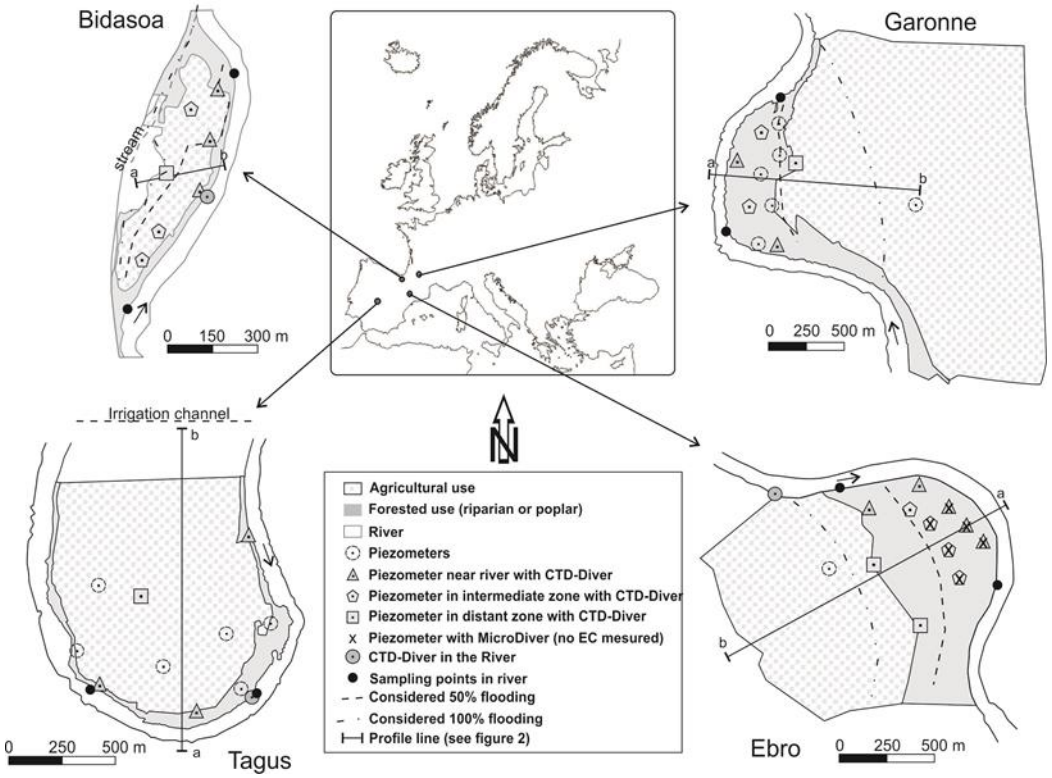

Figure 6-1 : Localisations des sites d'études des quatre plaines alluviales étudiées (extrait de Antiguedad et al., soumis)

6.2.1. L'Ebre

Le site d'étude est localisé dans un méandre situé à 12 km en aval de la ville de Saragosse (Espagne, Figure 6-1). L'agriculture est présente sur ce site avec principalement des cultures irriguées de maïs et de céréales. La zone comprend également une zone riparienne étendue composée de peupliers, saules blancs et tamarix. La pente de la plaine alluviale est de 0,13% dans la zone riparienne et de 0,04% dans la zone agricole plus distante de la rivière. L'incision de la rivière est la plus faible des sites étudiés, environ 1,5 m. La pluviométrie annuelle est de 380 mm et la température annuelle moyenne de 15°C.

L'aquifère alluvial est composé de dépôts quaternaires constitués principalement de gros graviers. Il s'étend sur une largeur de 7 km et une profondeur de 15 m. La profondeur moyenne du toit de la nappe alluviale est de 1,4 m dans la zone riparienne et de 4 m dans la zone agricole. Le régime hydrologique de l'Ebre (BV de 25 000 km² au site d'étude) est très irrégulier avec des pics de débit important en hiver et au printemps. Sur la période étudiée (2013-2014), le débit a varié de 40 à 1420 $m^3.s^{-1}$ (165 $m^3.s^{-1}$ en moyenne) avec un débit spécifique de 6,6 $L.s^{-1}.km^{-2}$.

6.2.2. La Bidassoa

Le site d'étude est localisé dans un méandre situé à 7 km en amont de la ville d'Irun dans le pays basque espagnol (Figure 6-1). La plaine alluviale supporte quasi exclusivement des activités agricoles, principalement des cultures de maïs, des prairies et de l'élevage. Une zone riparienne de faible étendue longe le cours d'eau. L'incision de la rivière est d'environ 5 m et la pente de la plaine alluviale est inférieure à 0,25%. L'hydrologie de l'aquifère est conditionnée par un affluent sur la rive gauche qui a entrainé la formation d'un cône alluvial. Une ferme est située dans la zone d'étude et constitue une source ponctuelle importante de pollution azotée. La pluviométrie annuelle est de 1870 mm et la température annuelle moyenne de 13°C.

L'aquifère alluvial peut atteindre une profondeur de 30 m et une largeur maximale de 300 m. L'aquifère constitue donc une réserve d'eau douce importante qui en fait un endroit intéressant pour l'abduction d'eau potable. L'aquifère est constitué de niveaux limoneux en surface qui recouvrent une zone graveleuse plus en profondeur. La zone imperméable est constituée de roche mère granitique. La profondeur moyenne du toit de la nappe alluviale se situe entre 4 m, proche de la rivière, et 4,5 m proche des terrasses. Le régime hydrologique (BV de 700 km² au site d'étude) est très irrégulier avec des pics de débits en hiver et au

printemps et une période d'étiage en été. Sur la période étudiée (2013-2014), le débit a varié de 9 à 630 $m^3.s^{-1}$ (35 $m^3.s^{-1}$ en moyenne) avec un débit spécifique de 49,3 $L.s^{-1}.km^{-2}$.

6.2.3. Le Tage

Le site d'étude est localisé dans un méandre situé à 40 km en aval de la ville de Tolède (Espagne, Figure 6-1). L'agriculture est l'activité dominante sur le site, avec principalement des cultures irriguées de céréales, du maraichage et des prairies. Un canal d'irrigation (dérivation de l'Ebre) est situé à l'intérieur du méandre et alimente la nappe alluviale. Une bande étroite de forêt riparienne longe le cours d'eau. L'incision de la rivière est d'environ 6 m. La pente est de 0,80% proche de la rivière et monte jusqu'à 1,60% proche des terrasses. La précipitation annuelle est de 375 mm et la température annuelle moyenne de 15°C.

L'aquifère alluvial est composé de dépôts quaternaires, principalement des graviers et des argiles, recouverts d'un horizon sableux. La profondeur de l'aquifère est supérieure à 9 m qui est la profondeur maximale des piézomètres installés dans la zone. La profondeur du toit de la nappe varie entre 1 m proche de la rivière à 5 m au centre du méandre. La connexion entre la rivière et la nappe est très faible en raison du fort contrôle exercé par des barrages et des déviations sur le débit qui est quasiment constant (BV de 25 000 km² au site d'étude). Sur la période étudiée (2013-2014), le débit a varié de 10 à 12 $m^3.s^{-1}$ (10 $m^3.s^{-1}$ en moyenne) avec un débit spécifique de 0,4 $L.s^{-1}.km^{-2}$.

6.2.4. La Garonne

Les principales caractéristiques du site de Monbéqui (Garonne, France), décrit en détails dans le chapitre 2, sont récapitulées ici. L'occupation des sols est constituée d'une forêt riparienne (saules et frênes) le long de la Garonne, de plantations de peupliers qui occupent la rive gauche et séparent sur la rive droite la forêt riparienne d'une zone agricole qui comporte des cultures irriguées de maïs, blé, tournesol, soja et sorgho. La pente moyenne est de 0,4% et l'incision de la rivière est d'environ 7 m et atteint la roche mère (molasse). La précipitation annuelle est de 710 mm et la température annuelle moyenne de 13,5°C.

L'aquifère alluvial est constitué de dépôts quaternaires constituée de sables et graviers. Il s'étend sur plus de 4 km et présente une profondeur qui varie de 4 à 7 m. La profondeur du toit de la nappe alluviale se situe entre 1 m dans la zone riparienne et 4 m dans la zone agricole. Le régime hydrologique (BV de 13 700 km² au site d'étude) est de type pluvio-nival avec des débits importants de Novembre à Mai et un étiage de Juin à Septembre. Sur la

période étudiée (2013-2014), le débit a varié de 40 à 2800 $m^3.s^{-1}$ (308 $m^3.s^{-1}$ en moyenne) avec un débit spécifique de 22 $L.s^{-1}.km^{-2}$.

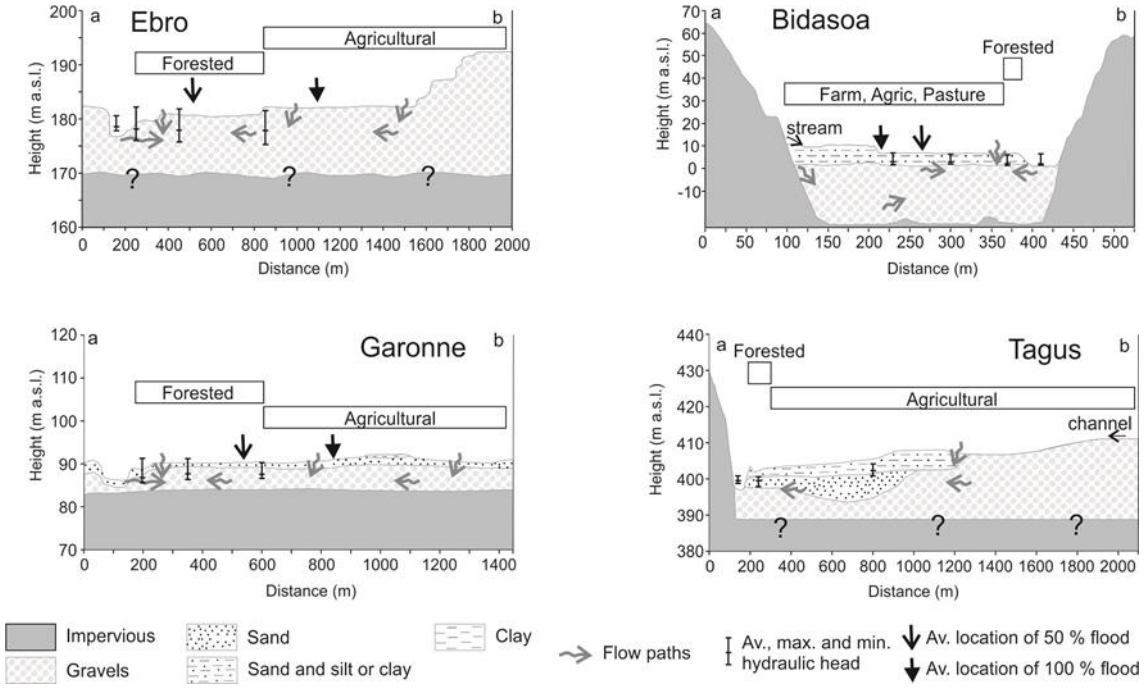

Figure 6-2 : Profils géologiques, occupation des sols et niveaux piézométriques des quatre plaines alluviales étudiées (extrait de Antiguedad et al., soumis).

6.2.5. Typologie des sites d'études

Les sites étudiés correspondent à des environnements variés (Figure 6-2), que ce soit en termes d'hydrologie (contrôle anthropique pour le Tage, régime naturel pour les trois autres) ; d'occupation des sols (forte pression agricoles sur le Tage, pollution ponctuelle sur la Bidassoa, présence d'une zone riparienne relativement étendue sur l'Ebre et la Garonne) ; d'hydrogéologie (aquifère peu épais sur la Garonne et plus épais sur les autres sites) ; de géomorphologie (vallée encaissée pour la Bidassoa, plaines alluviales plus étendues sur l'Ebre et la Garonne). L'objectif de ce chapitre est d'étudier l'impact de ces différentes caractéristiques sur le processus dénitrification.

6.3. Fonctionnement hydrologique et processus de dénitrification de quatre plaines alluviales du territoire SUDOE

La comparaison du fonctionnement hydrologique et son impact sur les processus d'atténuation des nitrates des différents sites sont étudiés dans une publication soumise à *Ecological Engeneering* par Antiguedad et al (soumis) intitulée « From hydrochemical observation to hydrological conceptualization: a multi-criteria assessment in four different riparian zones » à laquelle j'ai participé (Annexe 2) et dont les principaux résultats sont repris

ci-dessous. Ma contribution à ce travail inclue l'instrumentation du site de Monbéqui, la participation aux campagnes d'échantillonnage sur ce site, et l'analyse des données récoltées.

6.3.1. Données récoltées et méthodes d'analyse

Des données ont été récoltées pour chaque site dans un réseau comprenant entre 7 et 25 piézomètres et deux points d'échantillonnage dans la rivière (Figure 6-1). L'échantillonnage consiste en un suivi mensuel du réseau pendant une année (Avril/Mai 2013 à Mars/Avril 2014) des sites comprenant le prélèvement d'échantillons d'eau et la mesure *in situ* des caractéristiques physico chimiques (température T, conductivité électrique EC, pH, potentiel redox ORP et oxygène dissous O_2) et de la profondeur du toit de la nappe alluviale (dans les piézomètres uniquement). Les analyses des échantillons prélevés incluent la mesure des ions majeurs (Ca^{2+}, Mg^{2+}, Na^{+}, K^{+}, Cl^{-}, NO_3^{-} and SO_4^{2-}) et du carbone organique dissous (COD). En outre, le niveau piézométrique est mesuré en continue (toutes les 10 à 20 minutes) dans 5 à 8 piézomètres sur chaque site à l'aide de sondes de pression (CTD Divers, Schlumberger Water Services).

Pour chaque site, les piézomètres ont été séparés en trois groupes en fonction de leur distance à la rivière : les piézomètres proches de la rivière (NR), ceux situés dans la zone intermédiaire (IZ) et ceux dans la zone la plus éloignée de la rivière (DZ) (Figure 6-1). Les valeurs des principaux paramètres physico-chimiques de chacune de ces zones et de la rivière (R) pour chaque site sont présentées dans la Figure 6-3.

Un gradient de profondeur d'eau existe entre la zone distante (DZ) et la zone proche de la rivière (NR) pour l'Ebre et le Tage mais pas pour la Bidassoa et la Garonne. Les eaux souterraines du site de la Bidassoa et des zones intermédiaires (IZ) et DZ du Tage sont les plus profondes (toujours supérieure à 2,5 m).

La température dans les eaux souterraines est homogène sur les différentes zones de chaque site et présente une variabilité maximale de 8°C (IZ, Ebre). En revanche les variations de température sont plus marquées dans les eaux de surface (R). Les températures sont similaires pour les sites de l'Ebre, de la Bidassoa et de la Garonne et légèrement plus élevées sur le site du Tage.

.

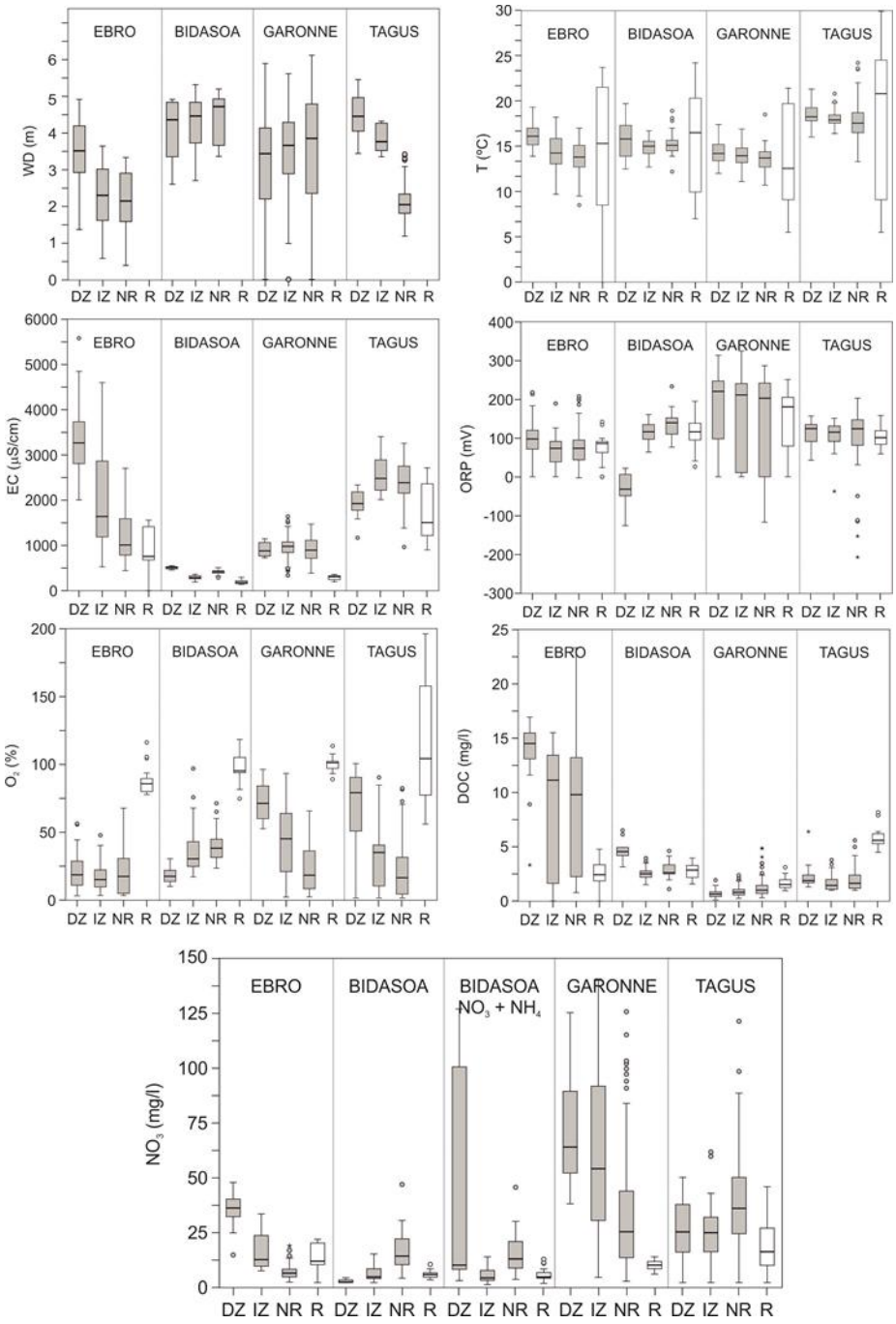

Figure 6-3 : Box plots des principaux paramètres physico-chimiques : profondeur de la nappe (WD), température (T), conductivité électriques (EC), potentiel d'oxydo-réduction (ORP), oxygène dissous (O_2), concentration en carbone organique dissous (DOC) et en nitrates (NO_3^-). La zone distante (DZ), intermédiaire (IZ) et proche de la rivière (NRZ) ainsi que la rivière (R) sont considérées séparément sur chaque site (extrait de Antiguedad et al., submitted).

On observe un gradient décroissant de conductivité électrique (EC) marqué entre la DZ et la rivière pour l'Ebre. Pour les autres sites l'EC est plus faibles dans la rivière mais il n'y a pas de gradient entre les différentes zones sauf entre l'IZ et la rivière pour le Tage. Globalement l'EC est plus faible sur la Bidassoa et la Garonne que sur les deux autres sites

Le potentiel d'oxydo-réduction (ORP) est stable sur tous les sites sauf pour le site de la Garonne ou il varie plus largement au sein de chaque zone. La DZ de Bidassoa et quelques mesures de la NR du Tage présentent des valeurs d'ORP particulièrement basse.

L'oxygène dissous (O_2) est logiquement plus important dans la rivière pour chaque site. On observe un gradient décroissant de la DZ vers la NR pour la Garonne et le Tage alors qu'on a un gradient croissant entre les mêmes zones de la Bidassoa.

En ce qui concerne le carbone organique dissous (COD), les concentrations dans les eaux souterraines sont les plus fortes sur le site de l'Ebre. Pour les trois autres sites, les concentrations moyennes en COD sont inférieures à 5 $mg.L^{-1}$ sauf pour la rivière du Tage.

Enfin, les concentrations en nitrates (NO_3^-) dans les eaux souterraines sont les plus importantes sur le site de la Garonne alors que celles dans la rivière sont plus importantes dans le Tage. Les concentrations en NO_3^- dans la rivière sont toujours plus faibles ou équivalentes aux concentrations des eaux souterraines sauf pour la NR de l'Ebre. Il existe un gradient de concentrations décroissant entre la DZ et la NR de l'Ebre et de la Garonne. Alors que les concentrations dans les eaux souterraines sont les plus importantes dans la NR pour la Bidassoa et le Tage. Pour la Bidassoa, les concentrations accumulées en ammonium (NH_4^+) et nitrates sont également indiquées afin de montrer l'impact de la ferme sur la quantité d'azote (sous forme d'ammonium) présent dans les eaux souterraines de la DZ.

Une analyse en composante principale (ACP) a été réalisée dans chaque site afin d'étudier les caractéristiques des eaux souterraines des différentes zones d'étude et pour identifier le degré de connectivité entre les eaux de surface et les eaux souterraines ainsi que les zones de mélanges et les processus hydrologiques de chaque site. Les résultats sont présentés dans la Figure 6-4. Pour chaque site les échantillons d'eau sont séparés entre les trois zones alluviales (DZ, IZ, NR) et la rivière (R). La connectivité entre la nappe alluviale et la rivière est représentée par un cadre pointillé englobant la rivière et la NR. Cela permet d'observer que la connectivité hydrologique est plus forte sur le site de l'Ebre que pour ceux de la Garonne et de la Bidassoa. Le cas du Tage est spécifique car les eaux de la rivière ont des caractéristiques plus proches de celle de la DZ. Ceci est en lien avec le canal d'irrigation qui alimente la DZ avec l'eau du Tage. De plus, les échanges entre les différentes zones sont représentés par des flèches. Les échanges entre la DZ et la NR, à travers la IZ, sont bien mis en avant pour le site de l'Ebre et de la Garonne. Pour la Bidassoa, la rivière est connectée avec la NR et l'IZ dont les eaux possèdent des caractéristiques similaires alors que les eaux de la DZ sont plus

distinctes. Enfin, pour le Tage, les eaux des différentes zones sont assez similaires et il est difficile de les différencier.

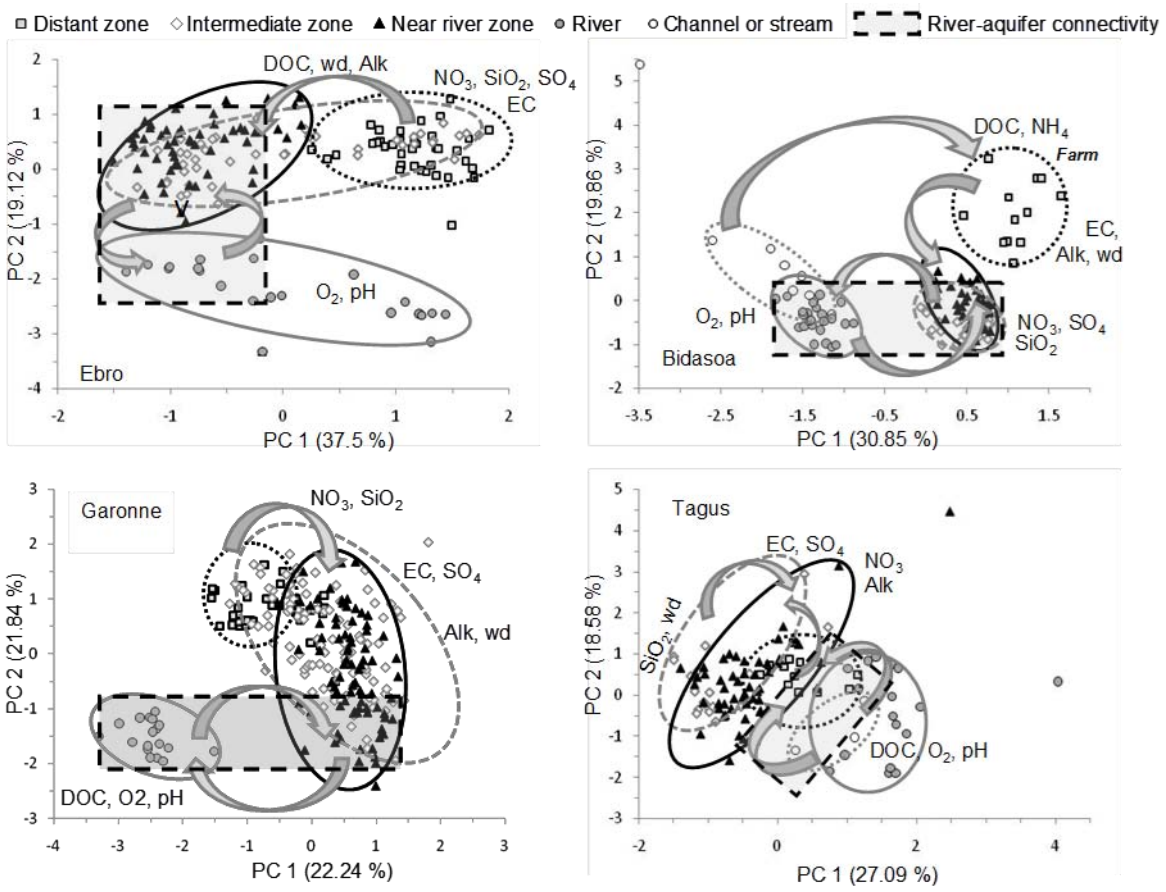

Figure 6-4 : Evolution spatiale des caractéristiques des eaux en fonction de leurs groupes (voir description dans le texte) dans le plan factoriel I-II de l'ACP effectuée pour chaque site. La connectivité entre la rivière et la zone proche de la rivière (NR) est également indiquée (cadre pointillé). Les flèches représentes les échanges entre les différents groupes (extrait de Antiguedad et al., submitted).

6.3.2. Fonctionnement hydro-biogéochimique des sites

6.3.2.1. Connectivité hydrologique

Les ACP effectuées ont permis d'évaluer le degré de connectivité hydrologique entre les différentes zones (R, NR, IZ, DZ) sur chaque site d'étude. Les plaines de l'Ebre et de la Garonne sont caractérisées par une séparation marquée entre la rivière (R), la zone riparienne proche de la rivière (NR) et la zone agricole distante (DZ). Cependant, la connectivité hydrologique entre la rivière et la zone riparienne est plus importante sur le site de l'Ebre que sur le site de la Garonne. Ceci est en lien avec l'hydrologie et la géomorphologie du site. En effet, la zone riparienne est plus étendue et plus souvent inondée sur l'Ebre que sur la Garonne, améliorant la connectivité hydrologique entre les deux zones. Au contraire, la

distinction entre la zone distante et la zone proche de la rivière est plus marquée sur l'Ebre que sur la Garonne.

Tout comme pour la Garonne, la plaine alluviale de la Bidassoa apparait être très peu connectée avec la rivière. Ceci s'explique par la faible étendue de la zone inondée lors des crues et une plus faible fréquence d'inondation. Les caractéristiques des eaux souterraines distantes (DZ) sont fortement marquées par la présence de la ferme (fuite d'azote et de COD) et sont différentes des eaux des NR et IZ qui présentent des caractéristiques similaires entre elles, et plus semblables à l'eau de la rivière que l'eau de la DZ.

Pour le site du Tage, les caractéristiques des trois zones sont assez similaires et hétérogènes. Ceci est représentatif de la faible connectivité entre les eaux de surface et la plaine sur ce site. En effet, le fort contrôle anthropique sur le débit du fleuve à travers les barrages conduit à un débit quasi-constant et à l'absence de connectivité hydrologique entre le fleuve et la plaine alluviale. Au contraire, on peut remarquer que l'eau de la zone distante (DZ) est la plus proche de celle de la rivière. Ceci s'explique par la présence du canal d'irrigation alimenté par l'eau du Tage dont l'infiltration affecte les eaux souterraines de la DZ.

Globalement, la connectivité hydrologique entre la rivière et l'aquifère dépend principalement de la géomorphologie de la plaine alluviale et de la dynamique hydrologique. La géomorphologie de la plaine alluviale contrôle l'étendue de la zone riparienne et des zones inondées lors des crues. Par exemple, le site de l'Ebre présente un lit de rivière peu profond et la zone riparienne est très faiblement pentue. Les inondations sont donc susceptibles d'y être plus fréquentes et d'affecter des zones plus grandes que sur d'autres sites ou le lit de la rivière est plus profond et le relief plus pentu (Bidassoa et Garonne). La dynamique hydrologique et notamment la fréquence et l'intensité des crues est primordiale pour avoir une forte connectivité entre la rivière et la plaine. En effet, lorsque les crues sont absentes, comme sur le site du Tage, la connectivité rivière-plaine est inexistante. La distribution de ces facteurs sur les quatre sites étudiés conduit à une connectivité hydrologique plus forte dans le site de l'Ebre (faible incision du cours d'eau, faible pente et crues fréquentes) suivi du site de la Garonne (incision et pente plus importante), puis du site de la Bidassoa (pente plus importante). Finalement le Tage apparait être complètement déconnecté de sa plaine alluviale du fait de l'absence de crues.

6.3.2.2. Capacité de dénitrification

La dénitrification dans les eaux souterraines dépend de nombreux facteurs et est hétérogène dans le temps et l'espace. Dans les zones ripariennes, les zones de dénitrification les plus intenses (*hots spots*) se situent aux endroits où les nitrates et les donneurs d'électrons (carbone organique) se rencontrent (McClain et al., 2003; Rivett et al., 2008). Dans la plupart des cas, les nitrates proviennent de la nappe alluviale sous l'influence des activités agricoles alors que le carbone organique est amené lors des crues par la rivière à travers la recharge latérale mais aussi via l'infiltration lors des crues débordantes. Une autre source de carbone est également la présence *in situ* de carbone organique généralement plus importante dans les horizons supérieurs des sols, et qui est remobilisé lorsque le niveau de la nappe alluviale augmente. Aussi, la connectivité entre la nappe alluviale et l'aquifère joue un rôle prépondérant dans la capacité de dénitrification des plaines alluviales en contrôlant les flux de nitrates et de COD et la disponibilité du COP dans la plaine alluviale. En fonction des caractéristiques de chaque site, la capacité de dénitrification sera donc différente. Il est ainsi nécessaire de prendre en compte la connectivité hydrologique (qui détermine le transfert d'éléments au sein de la plaine alluviale) ainsi que les sources de NO_3^- et de COD sur chacune des plaines alluviales étudiées pour identifier les zones propices à la dénitrification.

En analysant la connectivité ainsi que les différentes sources et trajets de COD et NO_3^-, les zones les plus propices à la dénitrification de chaque site étudié ont été identifiées (Figure 6-5).

Les sites de l'Ebre et de la Garonne sont caractérisés par une forte connectivité entre les eaux de surface (R) et les eaux souterraines au sein de la zone riparienne (NR). Dans cette zone, la présence de nitrates provenant de la zone agricole ainsi que la présence de carbone organique apporté par la rivière lors des crues et présent dans les sols induisent une zone de forte dénitrification (Figure 6-5). Toutefois, des différences existent entre les deux sites. La rivière qui est source de COD le cas de la Garonne est une source de NO_3^- dans le cas de l'Ebre. Pour ces deux plaines alluviales, la présence d'une zone riparienne caractérisée par une altitude plus faible que la zone agricole distante favorise la saturation des sols et la disponibilité du carbone organique qu'ils contiennent. Toutefois, des différences existent entre les deux sites. Les eaux souterraines du site de l'Ebre sont plus chargées en COD que sur le site de la Garonne (Figure 6-3) et la zone riparienne est plus étendue sur le site de l'Ebre (Figure 6-2). De plus, la connectivité hydrologique entre la rivière et la nappe est plus développée sur le

site de l'Ebre (Figure 6-4). Par conséquent, la capacité de dénitrification de la plaine alluviale de l'Ebre est censée être plus importante que pour la Garonne.

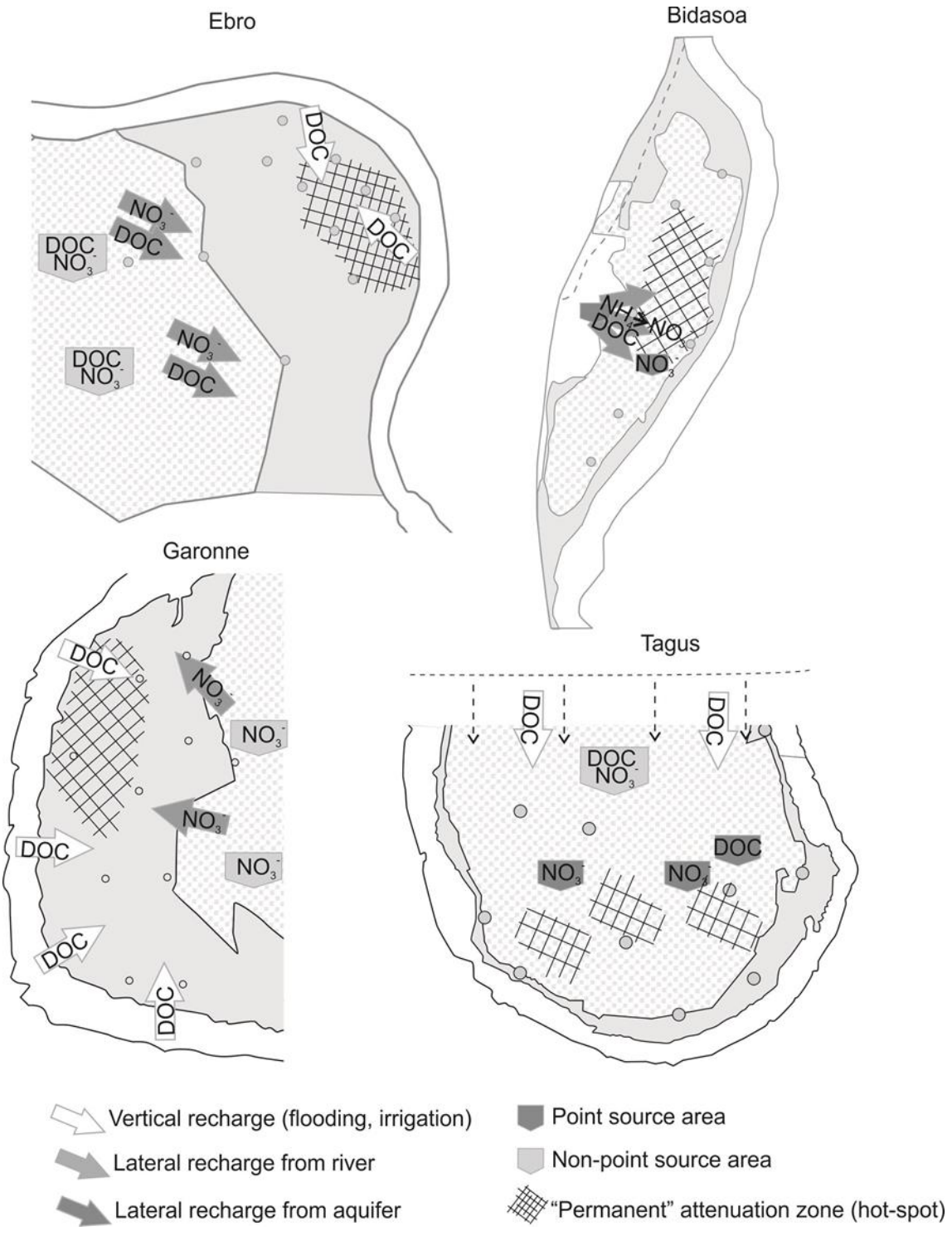

Figure 6-5 : Localisation des sources de NO_3^- et de COD, et des hot-spots de dénitrification pour chaque site d'étude.

Le site de la Bidassoa est caractérisé par une pollution en nitrates localisée autour de la ferme, à la fois source d'azote et de COD (Figure 6-3). C'est donc aux alentours de la ferme, sur les lignes de courant rejoignant la rivière, qu'est située la zone de forte dénitrification (Figure

6-5). La connectivité hydrologique étant limitée (Figure 6-4) sur ce site, la dénitrification reste faible dans la zone riparienne en comparaison avec les sites de l'Ebre et de la Garonne.

Enfin, sur le site du Tage, la nappe alluviale est soumise à des contaminations ponctuelles, sources de COD et NO_3^- dans les zones les plus proches de la rivière (NR et IZ). La nappe subie également une pollution diffuse en provenance du canal d'irrigation (COD et NO_3^-) dans la zone distante (DZ, Figure 6-3). Sur ce site, il très difficile d'identifier les zones potentielles de dénitrification qui dépendent fortement de la distribution spatiale des sources locales de contamination (Figure 6-5). Du fait de l'absence de zone riparienne et de connectivité hydrologique (Figure 6-4), la capacité de dénitrification attendue pour ce site est faible par rapport aux autres sites étudiés.

6.3.3. Conclusion

L'analyse comparative de données hydro-chimiques de quatre sites de plaine alluviale a permis de mettre en avant les facteurs contrôlant la connectivité hydrologique entre les eaux de surface et les eaux souterraines dans ces environnements qui sont la dynamique hydrologique et la géomorphologie impactant la fréquence et l'étendue des inondations. La connectivité hydrologique joue un rôle majeur dans le contrôle du processus de dénitrification en favorisant les zones de mélanges entre le COD et NO_3^-, principaux réactifs de cette réaction, au sein de la plaine alluviale. Cependant, il est également important de considérer la localisation des différentes sources de COD et de NO_3^- comme les apports de la rivière et les sources de pollution ponctuelle.

Les sites étudiés présentent des différences de géomorphologie, d'hydrologie et d'organisation de l'usage des sols et donc des différences en termes de connectivité hydrologiques et de sources de COD et NO_3^-. Il est possible de distinguer les sites présentant une bonne connectivité hydrologique et une source de contamination en nitrates de la nappe alluviale importante comme le site de l'Ebre, et dans une moindre mesure celui de la Garonne (connectivité nappe-rivière plus faible que pour l'Ebre), et les sites présentant une connectivité limitée et une source de nitrate localisée comme le site de la Bidassoa. Enfin le site du Tage est particulier et est caractérisé par une connectivité nappe-rivière inexistante et une pression agricole forte avec de multiples sources de nitrates. Il faut également souligner les différentes sources de COD qui provient de la rivière pour les sites de la Garonne et du Tage (à travers le canal d'irrigation) et des zones agricoles pour les sites de l'Ebre et de la Bidassoa. De plus, les sols des zones ripariennes constituent également une source de carbone

organique pour les sites de l'Ebre et de la Garonne. Finalement les sources ponctuelles de d'éléments azotés sur le site de la Bidassoa influent sur la localisation potentielle des zones de dénitrification. Aussi, il est possible de classer les sites étudiés en fonction de leur capacité de dénitrification potentielle, de la plus importante à la plus faible : l'Ebre, la Garonne, la Bidassoa et le Tage.

Le fait que la capacité de dénitrification soit différente pour chaque site mais dépendent des mêmes facteurs permet de considérer la modélisation comme un outil pertinent pour représenter le processus de dénitrification dans différentes configurations, en prenant en compte les facteurs de contrôle de la dénitrification.

6.4.Modélisation de l'hydrologie et du processus de dénitrification

Le modèle MOHID Land permet de modéliser le processus de dénitrification en prenant en compte les facteurs de contrôle et a donné des résultats satisfaisants sur le site de Monbéqui (chapitre 5). Afin de vérifier la validité et l'applicabilité du modèle MOHID Land pour simuler la dénitrification dans les environnements de plaines alluviales, le modèle a été appliqué sur les trois autres sites d'études par Brito (2014a, 2014b, 2014c, 2014d). Les résultats sont présentés et analysés dans cette partie. Ma contribution à ce travail inclue la formalisation du module de dénitrification, la participation aux phases de test lors de l'implémentation du module dans MOHID Land et l'application du modèle au site de la Garonne. Ce travail a été effectué en collaboration avec l'équipe MARETEC de l'Insituto Superior Técnico (IST) de Lisbonne.

6.4.1. Méthodologie générale

Le modèle MOHID Land a été appliqué sur chaque plaine alluviale (Garonne, Ebre, Bidassoa et Tage), en utilisant les données de terrains collectées sur chacun des sites. Le processus de dénitrification a été modélisé sur chaque site pendant une période de crue. De plus, différents scénarios incluant des modifications géomorphologiques et hydrologiques ont été testés. La description de l'implémentation du modèle ainsi que les résultats des simulations pour chaque site sont discutés ci-dessous et disponibles sur http://attenagua.actionmodulers.dtdns.net/ (Bernard-Jannin, 2014; Brito, 2014a, 2014b, 2014c, 2014d).

6.4.2. Modélisation des différente sites

6.4.2.1. La Garonne

Avant d'être appliqué sur tous les sites, le modèle a été testé sur le site de la Garonne. L'application du modèle et les résultats obtenus sont détaillés dans les chapitres 4 et 5. La première étape a été l'application du modèle hydrologique et de transport. Les résultats ont montrés que le modèle était capable de représenter l'hydrologie sur le site ainsi que le mélange entre les eaux de surface et les eaux souterraines. Les résultats ont montré que, malgré une paramétrisation effectuée de manière simplifiée (paramètres homogènes dans le milieu poreux), le modèle était capable de représenter l'influence des conditions hydro-géomorphologiques sur la dénitrification dans le site de Monbéqui. Les zones de dénitrification les plus intenses ont été identifiées dans la zone riparienne de basse altitude mais la quantité totale de nitrates éliminés par dénitrification est importante dans toute la partie aval du méandre, en relation avec les écoulements souterrains qui contrôlent les flux de nitrates dans l'aquifère.

6.4.2.2. L'Ebre

L'application du modèle sur le site de l'Ebre est détaillée dans Brito (2014b). La spécificité du site de l'Ebre est de présenter une forte connectivité hydrologique entre la rivière et la nappe alluviale ainsi que des sources multiples de COD et NO_3^-. Le COD provient à la fois de la zone agricole mais également des sols de la zone riparienne. Les sources de NO_3^- sont les zones agricoles distantes ainsi que la rivière elle-même qui contient des concentrations plus élevée en NO_3^- que la zone riparienne proche de la rivière (Figure 6-3).

Dans un premier temps, on remarque que le modèle est capable de reproduire l'hydrologie de la zone d'étude. L'étendue modélisée des zones inondées est différente pour des crues d'intensités variables (Figure 6-6) et le niveau piézométrique modélisé correspond au niveau mesuré dans différents piézomètres (Figure 6-7).

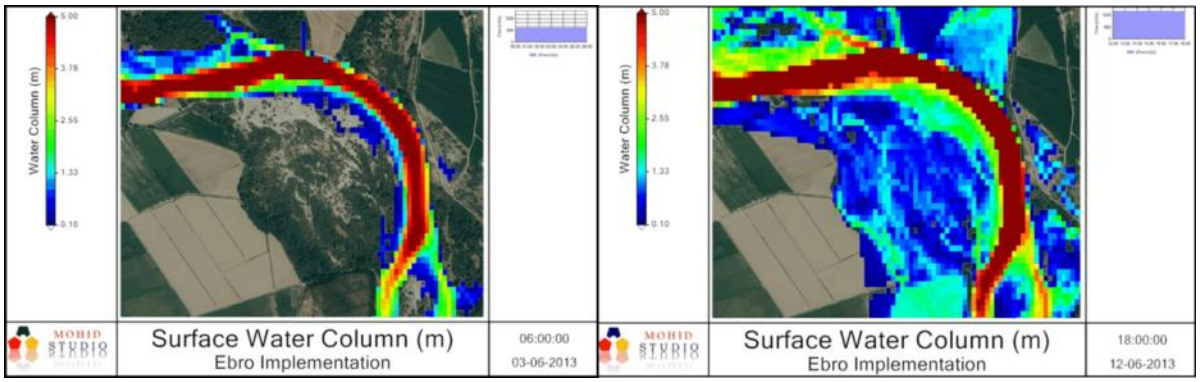

Figure 6-6: Hauteur d'eau simulée pour des crues de débits 650 m^3/s (gauche) et 1600 m^3/s (droite), http://attenagua.actionmodulers.dtdns.net/

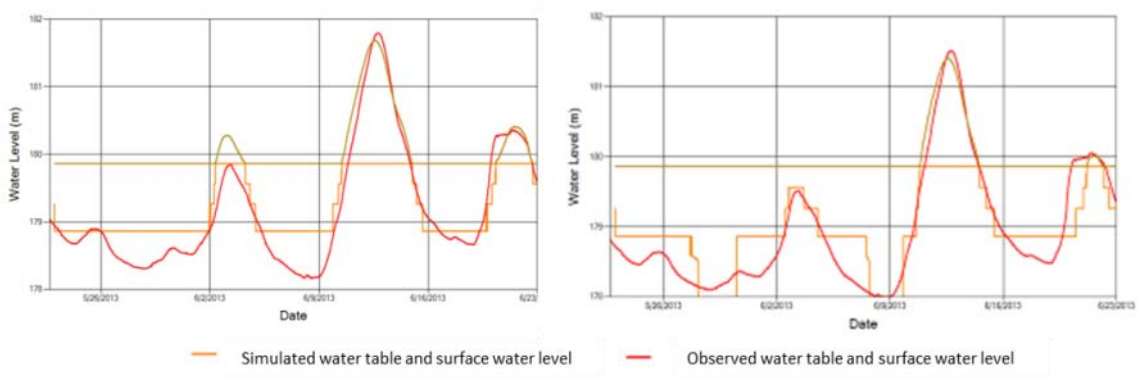

Figure 6-7 : Niveau piézométrique observé et simulé dans deux piézomètres situés dans le site de l'Ebre (Brito, 2014b)

Le modèle a permis de représenter les concentrations en nitrates dans l'aquifère (Figure 6-8). La concentration en nitrates dans la zone riparienne augmente lors des crues du fait de l'apport de la rivière. Dans le même temps, les taux de dénitrification augmentent également dans la zone riparienne lors des crues (jusqu'à trois fois plus importante en surface qu'en période d'étiage) en relation avec la saturation des horizons supérieurs des sols, riches en carbone organique particulaire. Cependant, la dénitrification reste la plus forte dans une zone située le long de la rivière aussi bien à l'étiage que pendant les crues (Figure 6-9). En effet, cette zone présente une plus forte saturation et de plus fortes concentrations en nitrates due à sa proximité avec la rivière. La dénitrification totale simulée pendant l'épisode de crue d'une durée de trois jours est de 2 $kg\text{-}N.ha^{-1}$.

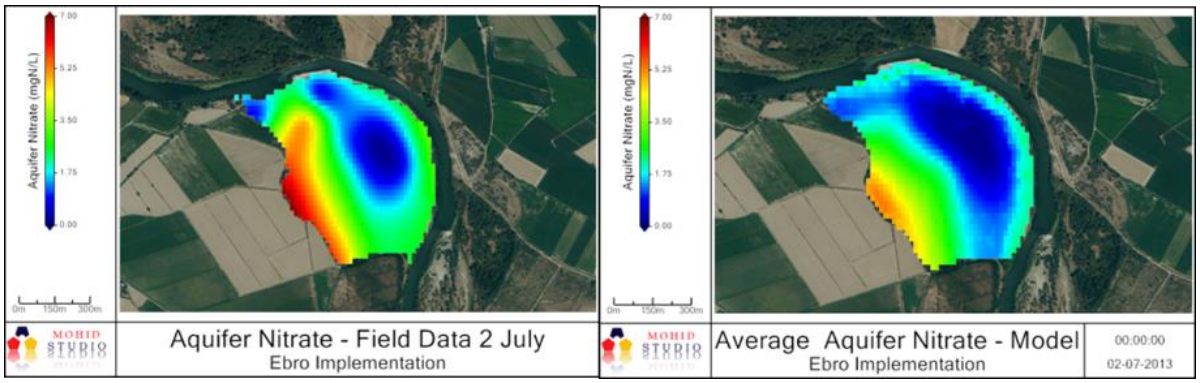

Figure 6-8 : Concentrations en nitrates observées (gauche) et simulées (droite) sur le site de l'Ebre après deux mois de simulation (Brito et al., 2014)

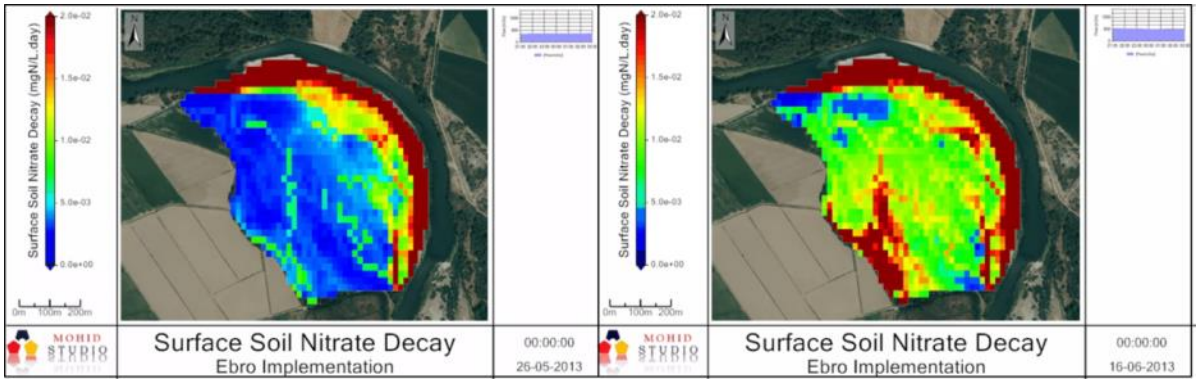

Figure 6-9 : Taux de dénitrification dans les horizons supérieurs des sols modélisés sur le site de l'Ebre à l'étiage (gauche) et après la crue de 1600 m^3/s (droite), http://attenagua.actionmodulers.dtdns.net/

6.4.2.3. La Bidassoa

L'application du modèle sur le site de l'Ebre est détaillée dans (Brito, 2014a). La spécificité du site est que la qualité des eaux de la nappe alluviale est fortement influencée par la présence d'une ferme sur le site. De plus, la connectivité hydrologique entre la rivière et la nappe est plus faible que sur les sites de l'Ebre et de la Garonne.

Sur ce site, l'hydrologie est également bien reproduite par le modèle, tant au niveau de l'étendue des zones inondées, que des niveaux piézométriques (Figure 6-10,Figure 6-11).

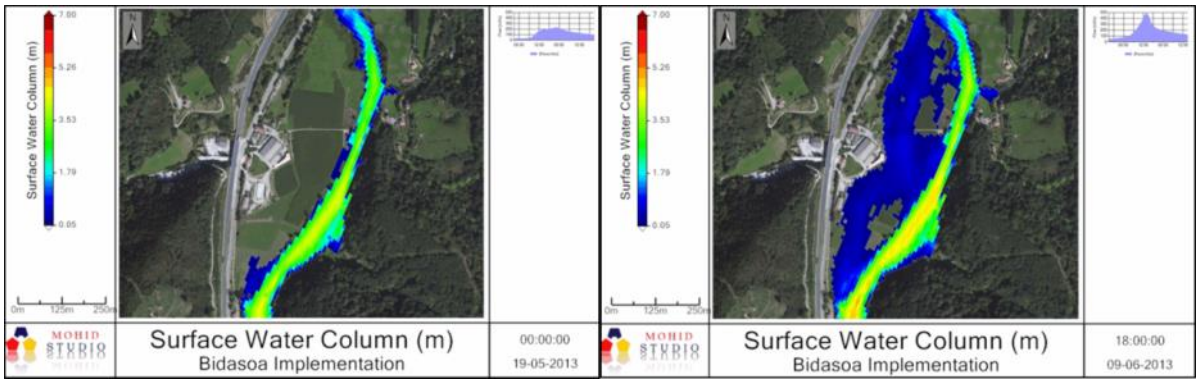

Figure 6-10 : Hauteur d'eau pour des crues correspondant à un débit de 200 m^3/s (gauche) et 500 m3/s (droite), http://attenagua.actionmodulers.dtdns.net/

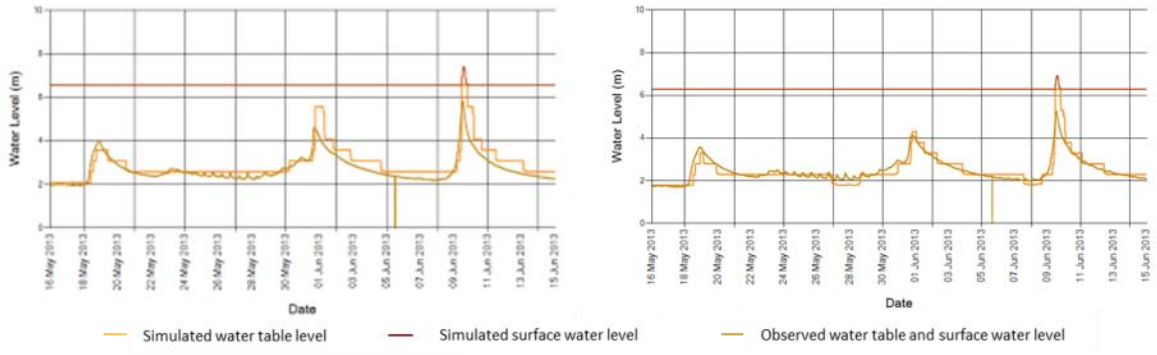

Figure 6-11 : Niveau piézométrique observé et simulé dans deux piézomètres situés dans le site de la Bidassoa (Brito, 2014a)

La concentration en nitrates est correctement simulée et l'impact de la ferme sur la concentration en nitrates ainsi que la dilution des concentrations lors des crues sont également bien reproduits par le modèle (Figure 6-12). Sur ce site, la dénitrification est assez homogène et varie peu, même pendant les crues (Figure 6-13). Ceci s'explique par la faible concentration en nitrates et en carbone organique dans la nappe. De plus, le toit de la nappe alluviale est assez profond sur ce site et atteint rarement les horizons supérieurs des sols riches en carbone organique, même pendant les périodes de crue, expliquant la stabilité de la dénitrification pour ces deux conditions. La dénitrification totale simulée pendant l'épisode de crue d'une durée d'un jour est de 0,5 kg-N.ha^{-1}.

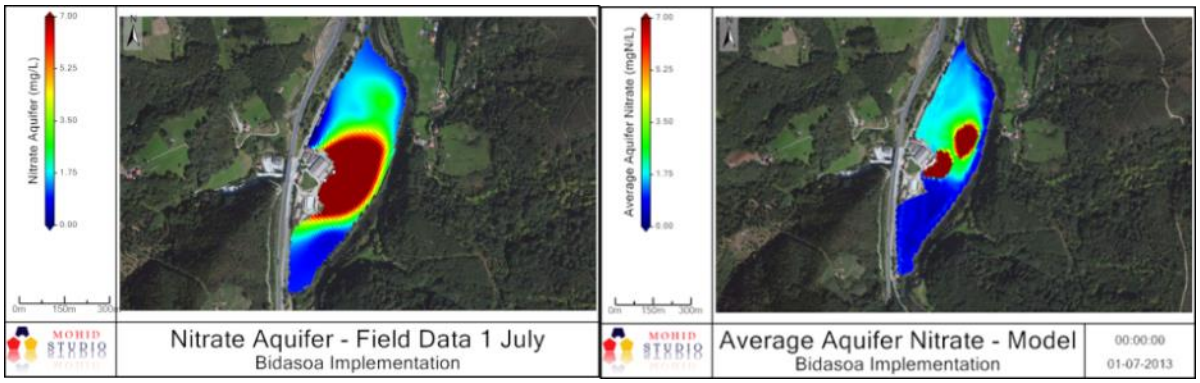

Figure 6-12 : Concentrations en nitrates observées (gauche) et simulées (droite) sur le site de la Bidassoa après deux mois de simulation

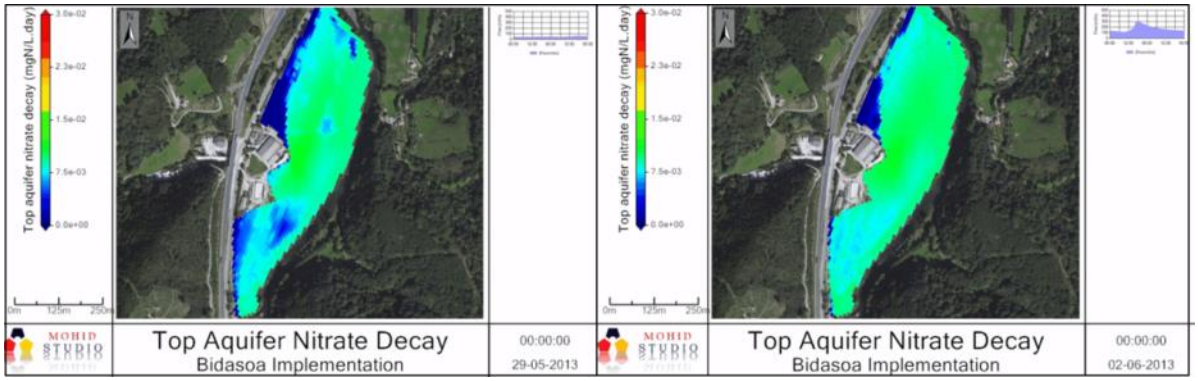

Figure 6-13 : Taux de dénitrification modélisé sur le site de la Bidassoa à l'étiage (gauche) et après une crue de 300 m^3/s (droite), http://attenagua.actionmodulers.dtdns.net/

6.4.2.4. Le Tage

L'application du modèle sur le site du Tage est détaillée dans(Brito, 2014c). La spécificité du site est un contrôle important de l'hydrologie du Tage par différents barrages, ce qui entraine un débit quasi-constant tout au long de l'année. De ce fait, la connectivité hydrologique entre la rivière et la nappe alluviale est inexistante. Cependant, la nappe alluviale est alimentée par un canal d'irrigation qui est une déviation du Tage et les eaux de la zone agricole sont donc influencées par une eau dont la composition est proche de celle du Tage.

L'hydrologie du site est très stable et le modèle arrive facilement à la reproduire. Cependant, on peut noter que le modèle réussit à représenter la hausse du niveau piézométrique dans les piézomètres sous influence du canal d'irrigation lors des périodes d'irrigation (Figure 6-14).

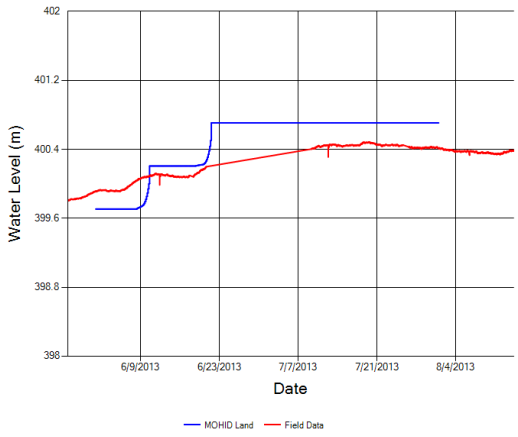

Figure 6-14 : Niveau piézométrique observé et simulé pour un piézomètres sous influences du canal d'irrigation situé dans le site de la Bidassoa (Brito, 2014c)

Les concentrations en nitrates simulées dans l'aquifère sont représentées dans la Figure 6-15. Les concentrations sont similaires aux conditions initiales du fait de la faible dynamique hydrologique sur le site. La dénitrification, quant à elle, est homogène sur le site et légèrement plus importantes dans certaines zones situées le long de la rivière, en lien avec la saturation des horizons superficiels (Figure 6-16).

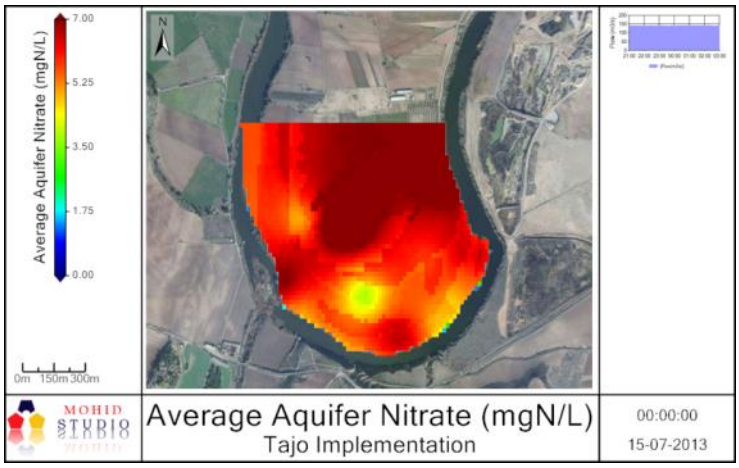

Figure 6-15: Concentrations en nitrates simulées sur le site du Tage après deux mois de simulation

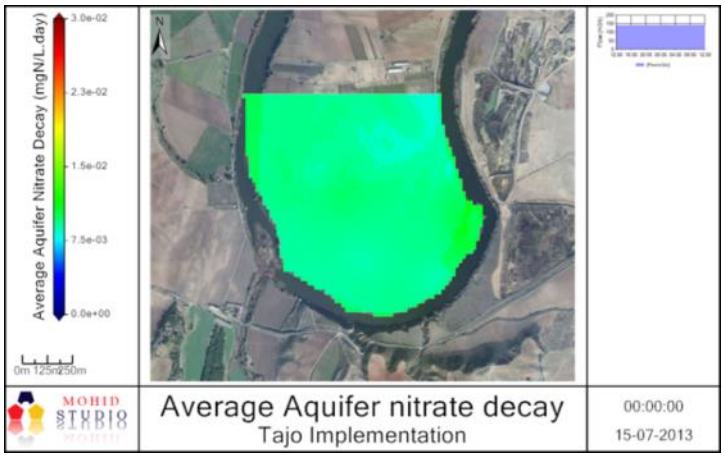

Figure 6-16 : Taux de dénitrification modélisé sur le site du Tage, http://attenagua.actionmodulers.dtdns.net/

6.4.3. Scénarios

Différents scénarios ont été appliqués afin de tester leur impact sur la capacité de dénitrification des plaines alluviales. Les scénarios impliquent des modifications de deux types : hydrologiques et géomorphologiques. Cette partie est constituée de résultats préliminaires destinés à évaluer le potentiel d'application du modèle pour tester différents scénarios et leur impact sur la dénitrification. La Figure 6-17 représente les variations de dénitrification par rapport aux scénarios originaux.

Les modifications hydrologiques ont été testées sur le Tage afin d'analyser l'impact d'un retour au système hydrologique naturel. Les résultats montrent une augmentation de la dénitrification proche de la rivière mais relativement faible (< à 1%). L'impact est plus faible qu'attendu mais de nouvelles simulations incluant différentes intensité de crues donneraient une meilleure indication des changements potentiels.

Des modifications géomorphologiques ont été testées sur l'Ebre et la Garonne. La zone riparienne caractérisée par une élévation par rapport au lit de la rivière plus faible que sur le reste de la zone a été étendue sur la Garonne. Les conséquences sont une augmentation de la dénitrification dans la zone riparienne due à une augmentation de la saturation dans cette zone. Sur l'Ebre, la suppression d'un obstacle dans le lit de la rivière a entrainé une augmentation du débordement lors des crues et donc une augmentation de la teneur en nitrates apportés par la rivière malgré une augmentation la dénitrification.

Finalement, un scénario représentant une contamination ponctuelle de la rivière a été modélisé à Bidassoa. Il est représenté par une augmentation de la concentration en nitrates dans la

rivière pendant un épisode de crue. Il y a très peu de changement car la connectivité hydrologique est limitée sur ce site.

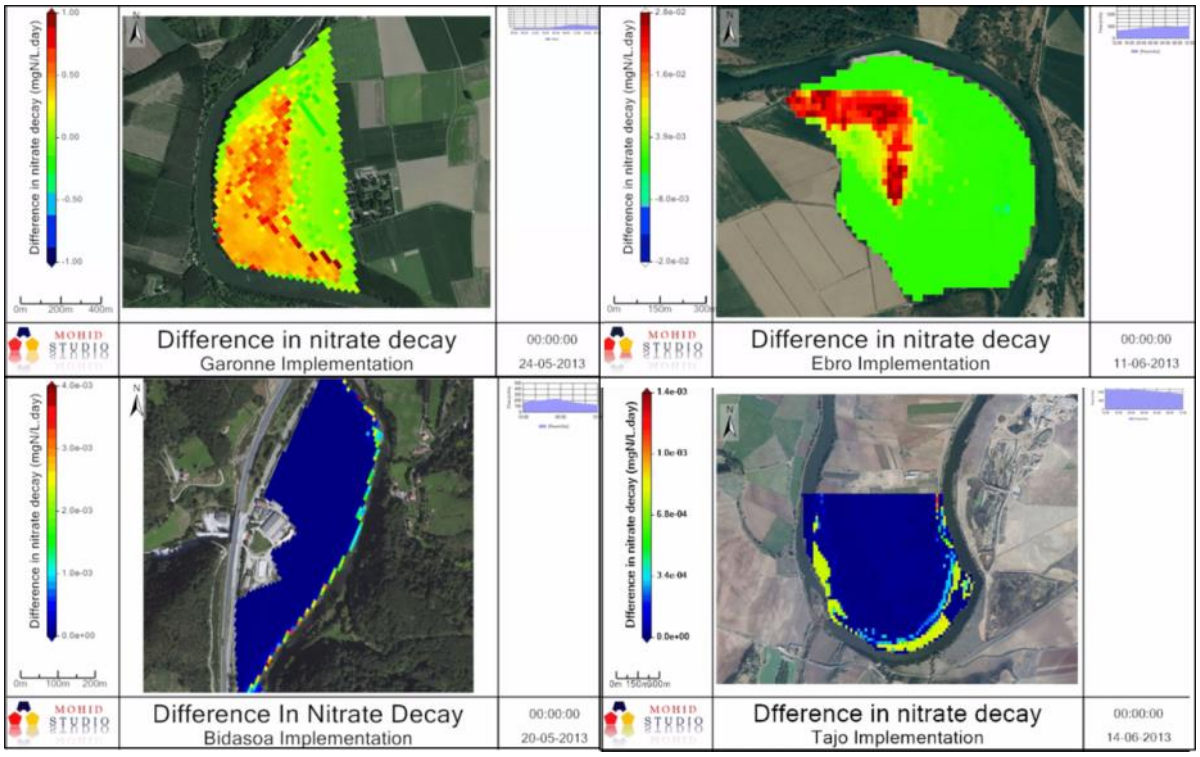

Figure 6-17 : Modifications des taux de dénitrification en fonction des différents scénarios appliqués sur chaque site

6.4.4. Apport de la modélisation à l'étude de la dénitrification

Au total, le modèle MOHID Land a été appliqué sur quatre sites de plaine alluviale d'une superficie de l'ordre du km². Ce modèle couple la modélisation de l'hydrologie et du transport, et de la dénitrification. Dans chacun des cas, le modèle a permis de reproduire correctement l'hydrologie des sites. La simulation des concentrations en nitrates est également satisfaisante. Le modèle a été utilisé pour caractériser le processus de dénitrification et ses facteurs de contrôle sur chacun des sites.

Dans le cas de la Garonne, les résultats (détaillés dans le chapitre 5) ont montré que le modèle identifiait des zones de plus forte dénitrification dans la zone riparienne de basse altitude, plus souvent inondée et alimentée par les flux de nitrates en provenance de la zone agricole. L'impact des crues a également été mis en avant.

Dans le cas de l'Ebre, les simulations indiquent que la zone riparienne présente de fort taux de dénitrification pendant les périodes de crues. Cependant, d'après les résultats du modèle, à l'étiage comme pendant les crues, c'est la zone qui longe la rivière qui présente les plus haut taux de dénitrification. Ceci peut s'expliquer par la plus forte concentration en nitrates dans la

rivière que dans les eaux souterraines proches de la rivière et par la présence d'horizons superficiels saturés et riches en carbone organique le long du fleuve.

Pour la Bidassoa, la zone située proche de la ferme avait été identifiée comme un potentiel *hot spot* de dénitrification lors de l'analyse des données. Cependant, ce résultat ne se reflète pas dans les simulations qui montrent que la dénitrification est assez homogène sur le site. D'après les résultats du modèle, l'apport de nitrates et de COD n'est pas suffisant pour réellement entrainer un *hot spot* de dénitrification. De plus, l'impact des crues sur les taux de dénitrification est faible comme attendu, du fait de la faible connectivité hydrologique entre la nappe et la rivière observée sur ce site.

Pour le site du Tage, les *hots spots* de dénitrification dépendent des sources ponctuelles de nitrates et de COD. Ces sources ponctuelles ne sont pas prises en compte dans le modèle car les informations ne sont pas disponibles à la résolution du modèle (25 m) et il est impossible d'identifier les *hots spots* de dénitrification liés à ce phénomène. Cependant, on remarque que la dénitrification simulée est sensiblement plus importante le long de la rivière que dans le reste de la zone en lien avec la géomorphologie et la saturation des horizons supérieurs des sols.

Les résultats de modélisation permettent de rendre compte de situations variées, notamment à travers des différences de connectivité hydrologique entre la nappe et la rivière. Le modèle permet également la prise en compte de sources ponctuelles de contamination (Bidassoa). De plus, la simulation de différents scénarios a permis de reproduire l'impact d'éventuelles modifications d'ordre géomorphologique, qui, en impactant la saturation des horizons supérieurs des sols et l'étendue des zones inondées entrainent des modifications qui peuvent être importante, surtout en période de crues. Des modifications d'ordre hydrologique ont également été testées à travers le rétablissement du régime hydrologique naturel sur le Tage, rétablissant la connectivité entre l'aquifère et la rivière sur le site du Tage. Dans ce cas, les résultats montrent une très faible augmentation des taux de dénitrification dans la zone proche de la rivière.

Les facteurs de contrôle hydro-géomorphologiques de la dénitrification identifiés sur le site de la Garonne (chapitre 5), qui sont i) le contrôle de la saturation des horizons supérieurs riche en carbone organique par la géomorphologie, ii) l'importance des épisodes de crues sont également mis en avant dans les trois autres plaines alluviales. Cependant, leur importance relative est différente selon les sites et dépend de la connectivité hydrologique et des sources

de carbone organique et de nitrates de chaque plaine alluviale étudiée. Ainsi, sur les sites à forte connectivité hydrologique, (Ebre et Garonne) la saturation des horizons supérieurs des sols affectera une plus grande surface pendant de plus longue période, entrainant une dénitrification plus importante que sur les sites ou la connectivité hydrologique est plus faible et où la dénitrification est relativement stable (Bidassoa et Tage). De la même manière, les sources de nitrates conditionnent la répartition spatiale de la dénitrification. Sur le site de la Garonne, les nitrates sont apportés par les eaux souterraines en provenance de la zone agricole et la dénitrification est plus importante dans la partie aval du méandre, où les concentrations en nitrates sont plus importantes. Dans le cas de l'Ebre, les nitrates sont également apportés par la rivière, et toute la zone située le long de cette dernière est caractérisée par de plus forts taux de dénitrification. Toutefois, la source ponctuelle d'azote identifiée dans le cas de la Bidassoa ne semble pas impacter la dénitrification sur ce site.

Le modèle est donc capable de prendre en compte les spécificités de chaque site étudié (hydrologie, géomorphologie, sources de nitrates et de carbone organique) et semble adapté à la modélisation de la dénitrification dans un contexte de plaine alluviale. Cependant, bien que l'application du modèle sur le site de la Garonne ait été discutée en détail dans le chapitre 5, l'analyse des résultats de modélisation pour les autres sites constitue une approche globale et une analyse plus approfondie des résultats sur chaque site permettrait d'obtenir des informations plus détaillées sur le fonctionnement de chaque site étudié.

6.5. Synthèse

Ce chapitre décrit l'analyse de la dénitrification sur quatre tronçons de plaine alluviale (incluant le site de Monbéqui) possédant chacun des caractéristiques différentes en termes de géomorphologie, d'hydrologie et d'usage des sols.

L'analyse des jeux de données récoltés sur chaque site a permis de mettre en avant le rôle de la connectivité hydrologique et des sources de nitrates et de carbone organique pour expliquer les différences en termes de dénitrification de chaque site. Le modèle MOHID Land a été appliqué sur chacun des sites afin de vérifier ses performances dans des conditions contrastées. Le modèle a permis de correctement reproduire l'hydrologie et les concentrations en nitrates sur chaque site malgré leurs différences. La modélisation a également permis de caractériser le processus de dénitrification sur chaque site. Les facteurs de contrôle identifiés dans le chapitre 5 conditionnent la dénitrification sur chaque site mais leur importance relative diffère entre les cas. Une plus forte connectivité hydrologique entraine une dénitrification plus

importante et présentant une plus forte variabilité temporelle qu'une connectivité hydrologique réduite. De plus, les différentes sources de nitrates peuvent conditionner la localisation des zones de forte dénitrification.

MOHID Land permet donc la prise en compte des facteurs contrôlant la dénitrification à l'échelle du tronçon de plaine alluviale (km²). Il permet de représenter la variabilité de la dénitrification au sein des zones étudiées mais également entre les différents sites. Le modèle semble donc adapté à la modélisation du processus de dénitrification dans les plaines alluviales.

Conclusion générale et perspectives

Contribution à l'étude de la dénitrification dans les aquifères des plaines alluviales

La dénitrification est un processus important permettant l'élimination des nitrates présents dans les aquifères des zones ripariennes (Pinay and Decamps, 1988; Lowrance et al., 1997; Ranalli and Macalady, 2010). Ce processus a fait l'objet de nombreuses études qui ont mis en avant son interaction avec de nombreux facteurs, expliquant sa forte variabilité spatio-temporelle (Groffman, 2012).

La dénitrification dans les eaux souterraines a été reliée à la présence de nitrates, de bactéries dénitrifiantes et de carbone organique (Rivett et al., 2008). Dans les zones ripariennes, le facteur limitant la dénitrification identifiée est généralement la présence de carbone organique (Haycock and Burt, 1993; Pfeiffer et al., 2006; Zarnetske et al., 2011). De plus, les caractéristiques géomorphologiques sont également reliées à la capacité de dénitrification des zones ripariennes (Hill, 1996; Vidon and Hill, 2004; Ranalli and Macalady, 2010).

La dénitrification étant un processus hétérogène dans l'espace et le temps, il est donc difficile d'extrapoler des mesures ponctuelles sur de plus larges zones. Par conséquent, la modélisation est une approche intéressante pour identifier les facteurs de contrôle majeurs de cette variabilité ainsi que pour quantifier les taux de dénitrification dans les plaines alluviales (Groffman, 2012).

L'objectif principal de cette thèse de caractériser la variabilité spatio-temporelle du processus de dénitrification dans les eaux souterraines des environnements de plaines alluviales en s'appuyant sur un travail couplant les mesures et la modélisation à l'échelle locale et l'étude de données récoltées sur le terrain.

L'originalité de ce travail de thèse consiste en la prise en compte des crues débordantes et des échanges nappes-rivières dans l'application d'un modèle destiné à simuler la dénitrification dans les aquifères des plaines alluviales à l'échelle du tronçon de quelques kilomètres. Ces éléments sont en effet absents des modèles utilisés jusqu'à présent pour simuler la dénitrification dans ces environnements.

Dans un premier temps, des données hydro-biogéochimiques récoltées sur le site expérimental de Monbéqui ont été analysées afin d'identifier les facteurs contrôlant la dynamique des nitrates et la dénitrification dans la zone (chapitre 3). Les résultats ont montré que, bien que le mélange entre les eaux de surface et les eaux souterraines explique majoritairement la variabilité des concentrations en nitrates dans l'aquifère alluvial de Monbéqui, le processus de

dénitrification n'est pas négligeable. La dénitrification a été reliée à la géomorphologie du site et aux conditions hydrologiques. Notamment, les zones ripariennes de faibles altitudes sont des zones propices à la dénitrification car les horizons supérieurs des sols, riches en matière organique sont plus souvent inondés et libèrent du carbone organique alimentant le processus de dénitrification. Les épisodes de crues sont également importants et entrainent des périodes de forte dénitrification. L'apparition de ces périodes est provoquée par l'apport de carbone organique dissous par la rivière dans l'aquifère et à la saturation des horizons supérieurs des sols riches en carbone organique suite aux inondations.

Les résultats des simulations ont mis en avant les facteurs expliquant la variabilité spatio-temporelle de la dénitrification dans les plaines alluviales. Il s'agit :

- de la géomorphologie, qui détermine le niveau de saturation des sols et notamment des horizons supérieurs riches en carbone organique ;
- des écoulements souterrains, qui contrôlent la distribution spatiale des nitrates provenant des zones agricoles ;
- de l'intensité et de la fréquence des épisodes de crues, qui entrainent des périodes favorables à la dénitrification à travers la saturation des horizons supérieurs des sols

Ces résultats sont en accord avec de nombreuses études qui ont déjà mis en avant le contrôle de la dénitrification à travers les paramètres reliés à l'hydro-géomorphologie des plaines alluviales (Hill, 1996; McClain et al., 2003; Vidon and Hill, 2004; Ranalli and Macalady, 2010). Cependant, bien que plusieurs études soulignent le rôle du COD apporté par les crues (Schade et al., 2001; Clinton et al., 2002; Gift et al., 2010; Peter et al., 2012), les résultats des simulations indiquent que son rôle apparait limité dans le cas des plaines alluviales étudiées au regard de l'importance du carbone organique libéré lors de la saturation des horizons supérieurs des sols. Cette observation est en accord avec les résultats de Sun (2015) qui a estimée à plus de 90% la contribution du carbone originaire des sols au processus de dénitrification sur la même zone d'étude. De plus, l'augmentation de la dénitrification dans les horizons supérieurs des sols est en accord avec de nombreuses études qui ont mis en évidence un gradient vertical avec une dénitrification plus importante en surface qu'en profondeur (Clément et al., 2002; Hill and Cardaci, 2004; Ranalli and Macalady, 2010). L'influence des épisodes de crue sur la dénitrification a été confirmée et elle semble être plus reliée à la saturation des horizons supérieurs des sols (due à la remontée de la nappe) qu'à l'apport de COD par la rivière.

Les résultats ont également mis en avant le fait que la quantité totale de nitrates éliminés par dénitrification n'est pas la plus importante dans les zones les plus propices à la dénitrification. En effet, la concentration en nitrates et la profondeur de l'aquifère jouent également un rôle important. Malgré une activité dénitrifiante plus faible, la dénitrification affecte un volume d'eau plus important dans les zones où l'aquifère est plus profond, ce qui conduit à une masse totale de nitrates éliminés plus importante.

Le modèle a également été appliqué sur trois autres sites de plaines alluviales avec des caractéristiques différentes en termes de géomorphologie, d'hydrologie et d'usage des sols. Les résultats ont permis de confirmer l'utilisation du modèle dans des plaines alluviales contrastées du sud-ouest européen. Les principaux facteurs expliquant les variations dans la dynamique de dénitrification entre les sites sont i) la connectivité hydrologique entre la nappe et la rivière et ii) les sources de nitrates et de carbone organique. En effet, le contrôle anthropique de l'hydrologie ou encore les différences en terme de géomorphologie des plaines alluviales influencent la connectivité hydrologique et notamment l'étendue et la fréquence des inondations. De plus, la distribution spatiale des sources de nitrates et de carbone organique va conditionner la localisation des zones préférentielles de dénitrification.

Finalement, les résultats obtenus au cours de ce travail permettent de valider l'approche de modélisation utilisée dans cette thèse. En effet, le rôle de l'hydrologie et des épisodes de crues et la géomorphologie des plaines alluviales apparaissent comme fondamentaux dans le contrôle de la variabilité spatio-temporelle de la dénitrification. Le choix d'utiliser un modèle distribué capable de représenter la topographie à fine échelle et de prendre en compte le débordement induit par les épisodes de crues est adapté à la simulation de la dénitrification dans un contexte de plaine alluviale.

Limites de l'approche de modélisation

Malgré les résultats satisfaisants obtenus dans le cadre de ce travail, l'utilisation de la modélisation implique un certain nombre de simplifications qui doivent être discutés pour interpréter correctement les résultats obtenus.

Modélisation hydrologique :

La modélisation de l'hydrologie ne prend pas en compte les processus comme les précipitations où l'évapotranspiration, ce qui peut constituer un frein quant à la qualité des résultats du modèle, notamment dans un contexte de changement d'échelle. Néanmoins, les

résultats montrent que le modèle permet de correctement représenter l'hydrologie sur le site d'étude laissant penser que ces processus ne sont pas très importants en comparaison de l'influence de la rivière sur la nappe alluviale à l'échelle concernée.

Modélisation de la dénitrification

La dénitrification est représentée de manière simplifiée dans le modèle bien que les principaux facteurs contrôlant la dénitrification (carbone organique et nitrates) soient inclus dans l'équation. Des facteurs environnementaux comme le pH, la température ne sont pas pris en compte. Néanmoins, ces facteurs peuvent être considérés comme secondaires par rapport à la présence de carbone organique car ils sont relativement stables dans les eaux souterraines (Rivett et al., 2008). Par ailleurs, dans une étude comparant une cinquantaine de module simulant le processus de dénitrification, Heinen (2006) a montré que le taux de dénitrification calculé était peu sensible à la température. De plus, ces facteurs ne sont pas ressortis dans l'analyse des données récoltées sur le terrain comme étant reliés au processus de dénitrification (chapitre 3). La teneur en oxygène est également absente du modèle alors que c'est un paramètre important pour l'apparition de la dénitrification. Toutefois, la dénitrification peut avoir lieu dans de nombreux microsites anoxiques présents dans des eaux en apparence bien oxygénées (Jacinthe et al., 1998) que la discrétisation spatiale du modèle ne permet pas de représenter. Afin de ne pas alourdir les calculs, l'oxygène a été introduit à travers une fonction basée sur la saturation du milieu poreux qui permet de prendre en compte la présence d'oxygène gazeux dans la zone non saturée.

De plus, les sources de nitrates comme le lessivage depuis les horizons de surface ne sont pas explicitement prises en compte dans le modèle. Cependant, ces apports ne semblent pas conséquents au regard de la quantité de nitrates présents dans l'aquifère. En effet, les apports annuels en nitrates par lessivage sur la zone riparienne ont été estimés à 10kg-N.ha^{-1} (Jégo, 2008; Sun, 2015). Si on considère un aquifère d'un mètre d'épaisseur, cela correspond à une concentration de seulement 1 mg-N.L^{-1}. L'apport principal en nitrates se fait via l'écoulement des eaux souterraines en provenance des zones agricoles qui sont fortement concentrées en nitrates et prise en compte dans la modélisation.

Paramétrisation du modèle

Un des problèmes majeurs relatifs à l'utilisation de modèles distribués, est la nécessité de renseigner les paramètres à l'échelle de la discrétisation spatiale du modèle. Dans ce travail, cela a été le cas pour la topographie qui était disponible avec une résolution de 1m, inférieure

à la résolution du modèle (25m). Ceci est important car la topographie joue un rôle majeur dans l'hydrologie de surface. Cependant, les paramètres affectant les écoulements souterrains (paramètres de Van Genuchten) sont définis comme étant homogène car leur variabilité spatiale n'est pas connue. Toutefois, cette approche combinant une représentation détaillée de la topographie et un sous-sol homogène a déjà été appliqué avec succès pour simuler les échanges hyporhéiques (Käser et al., 2014).

Le même problème se pose pour les facteurs inclus dans le calcul de la dénitrification. Une analyse de sensibilité du module de dénitrification a montré que la dénitrification était très sensible au teneur en COP et au paramètre K_{POC}. Dans le modèle, le paramètre K_{POC} est constant dans le temps et l'espace. Les teneurs en COP quant à elles sont définies en fonction de la profondeur du sol mais ne varient pas spatialement. De ce fait, les résultats du modèle sont valables pour des valeurs de COP et K_{POC} données et la variabilité spatio-temporelle potentielle du K_{POC} n'est pas prise en compte dans le modèle. En revanche, la dynamique générale de la dénitrification en lien avec les facteurs hydro-géomorphologiques (crues, échanges nappes-rivière, topographie, transport des nitrates) est bien représentée par le modèle.

Validation du modèle

La validation du modèle de dénitrification est difficile car il n'existe pas de données de dénitrification au sein de la zone d'étude. L'approche qui consiste à valider le modèle sur les concentrations en nitrates dans l'aquifère a été appliquée pour évaluer la qualité du modèle de dénitrification. Cependant, l'analyse des données a montré que les concentrations en nitrates sont fortement influencées par le mélange entre les eaux souterraines et les eaux de surface, ce qui peut masquer l'influence de la dénitrification. Malgré tout, la variabilité spatiale de la dénitrification simulée correspond à celle de la dénitrification potentielle mesurée sur le site, ce qui améliore la confiance dans les résultats des simulations.

Interprétation des résultats

La connaissance des limites liées à la modélisation évoquées ci-dessus influence l'interprétation des résultats obtenus lors des simulations. En effet, les valeurs de dénitrification simulées résultent de nombreuses simplifications. Il est impossible de quantifier les incertitudes, et, à cet égard, les taux de dénitrification doivent d'avantage être perçus comme des ordres grandeurs que des valeurs exactes. Bien que des différences locales entre les résultats des simulations et la réalité existent du fait de l'hétérogénéité du milieu

poreux qui n'est pas prise en compte par le modèle, la dynamique générale simulée sur le site est représentative de la réalité. La variabilité spatiale et temporelle simulée par le modèle peut être considérée comme correcte et le modèle réussit à identifier les zones et les périodes de dénitrification plus intense.

Perspectives

La mise en place d'un modèle destiné à simuler la dénitrification dans les plaines alluviales présentée dans cette thèse ouvre de nombreuses perspectives.

Perspectives d'amélioration du modèle

Tout d'abord, une analyse de sensibilité du modèle aux paramètres intervenant dans la simulation des écoulements (paramètres de Van Genuchten, coefficient de Manning) est une étape importante pour évaluer leur rôle et pour aller plus loin dans la caractérisation du processus de dénitrification et l'interprétation des résultats du modèle. Une telle analyse est coûteuse en temps de calculs et n'a pas pu être effectuée lors de cette thèse.

Le module de dénitrification est très sensible au paramètre de dégradation du COP (K_{POC}) et aux teneurs en COP qui sont pourtant définis constant dans le modèle. Une meilleure représentation de la variabilité ses facteurs permettrait d'améliorer la confiance dans les résultats, et de quantifier plus précisément la dénitrification dans la zone étudiée.

Toujours dans l'objectif d'améliorer la confiance dans les résultats du modèle, il pourrait être intéressant d'améliorer la validation du modèle en comparant les sorties du modèles avec des mesures de dénitrification *in situ*. De plus, un échantillonnage effectué à des profondeurs différentes permettrait de mieux exploiter la dimension verticale du modèle.

Enfin, il pourrait être intéressant d'ajouter certains éléments du cycle hydrologique comme les précipitations ou l'évapotranspiration pour évaluer leur impact sur les résultats. De la même manière, il est envisageable de complexifier le module calculant la dénitrification en ajoutant des paramètres tels que la température ou l'oxygène pour tester leurs influence sur la dénitrification.

Perspectives d'application du modèle

Le modèle a apporté des résultats prometteurs pour la simulation de la dénitrification à l'échelle du tronçon de la plaine alluviale. Toutefois, les résultats de cette étude restent préliminaires et les perspectives d'applications du modèle sont nombreuses. Elles

permettraient de répondre à plusieurs questions relatives à la caractérisation de la dénitrification dans les plaines alluviales. Les perspectives d'applications du modèle à l'échelle locale incluent la simulation de l'impact de mesures d'aménagement sur la dynamique des nitrates et de la dénitrification comme par exemple la restauration de bras morts, la modification du lit mineur ou encore des modifications de l'hydrologie du cours d'eau. D'une manière plus générale, le modèle permettrait de tester l'impact de nombreux scénarios relatifs à des modifications de la topographie et de l'hydrologie ou de tester l'impact des scénarios de changement globaux sur le processus de dénitrification et ses conséquences sur la teneur en nitrates des aquifères alluviaux. En effet, la simulation de scénarios simples effectuée sur différents sites d'études à donner des résultats prometteurs.

L'utilisation de MOHID Land pourrait également être étendue pour répondre à des problématiques autres que celle de la contamination des eaux par les nitrates. En étendant les processus simulés, il serait possible de prendre en compte la libération de N_2O engendrée par la dénitrification qui est un gaz à effet de serre notable et de quantifier l'impact, cette fois négatif, de la dénitrification sur l'environnement (Garnier et al., 2009). En appliquant une méthode similaire à celle présentée dans cette thèse, qui consiste à identifier des facteurs de contrôle d'un processus à travers des observations de terrains afin de construire des modèles adaptés à la problématique étudiée, il est possible d'envisager la modélisation du devenir d'autres contaminants. Une telle méthodologie serait adaptée à la modélisation du devenir des pesticides qui constituent une source de contamination importante des eaux souterraines des plaines alluviales. En allant plus loin, il serait même possible d'envisager la modélisation de l'effet des pesticides sur la dénitrification (Muñoz-Leoz et al., 2013).

Par ailleurs, les résultats du modèle peuvent contribuer à l'amélioration de la modélisation à plus grandes échelles, qui est nécessaire pour évaluer l'impact de la dénitrification dans les zones ripariennes sur la contamination des eaux de surface. En identifiant les facteurs de contrôle de la dénitrification à l'échelle locale, les résultats de cette thèse fournissent des pistes quant aux caractéristiques importantes à prendre en compte dans les modèles utilisés à l'échelle des bassins versants. Parmi les travaux récents, la thèse de Sun (2015) a montré qu'il était possible de représenter les échanges nappe-rivière et les épisodes de crues dans les plaines alluviales en utilisant une version modifiée du modèle SWAT, intitulé SWAT-LUD. Ces travaux sont présenté dans une publication à laquelle j'ai participé et incluse en annexe (Sun et al., 2015, Annexe 3). Dans SWAT-LUD, la dénitrification est simulée de la même manière que dans le modèle utilisé dans cette thèse mais la représentation de la

géomorphologie des plaines alluviales est simplifiée. Le modèle MOHID Land opéré à l'échelle locale pourrait permettre d'identifier les métriques relatives à la géomorphologie des plaines alluviales qui sont les plus influentes sur la dénitrification. Ces métriques, comme par exemple la sinuosité du cours d'eau, la profondeur du lit mineur ou la pente de la plaine alluviale, pourraient ensuite être intégrées dans les modèles utilisés à plus grande échelle.

MOHID Land est un modèle adapté à la simulation de nombreux processus liés au transfert et à la transformation des nutriments et contaminants à l'échelle de la plaine alluviale. A travers l'identification des facteurs contrôlant ces processus, son apport pour des modélisations à plus grande échelles s'inscrit dans une démarche générale qui permettrait d'évaluer les différents services écosystémiques rendus par les zones ripariennes à l'échelle du bassin versant.

Bibliographie

Abdi, H., 2010. Partial least squares regression and projection on latent structure regression (PLS Regression). Wiley Interdiscip. Rev. Comput. Stat. 2, 97–106.

Ahuja, L.R., Rojas, K.W., Hanson, J.D., Shaffer, M.J., Ma, L., 2000. Root zone water quality model. Water Resour. Publ., Highl. Ranch, CO.

Almasri, M.N., Kaluarachchi, J.J., 2007. Modeling nitrate contamination of groundwater in agricultural watersheds. J. Hydrol. 343, 211–229. doi:10.1016/j.jhydrol.2007.06.016

Amoros, C., Bornette, G., Cedex, V., 2002. Connectivity and biocomplexity in waterbodies of riverine floodplains. Freshw. Biol. 47, 761–776. doi:10.1046/j.1365-2427.2002.00905.x

Arango, C.P., Tank, J.L., Schaller, J.L., Royer, T. V, Bernot, M.J., David, M.B., 2007. Benthic organic carbon influences denitrification in streams with high nitrate concentration. Freshw. Biol. 52, 1210–1222.

Arauzo, M., Valladolid, M., Martínez-Bastida, J.J., 2011. Spatio-temporal dynamics of nitrogen in river-alluvial aquifer systems affected by diffuse pollution from agricultural sources: Implications for the implementation of the Nitrates Directive. J. Hydrol. 411, 155–168. doi:10.1016/j.jhydrol.2011.10.004

Arrate, I., Sanchez-Perez, J.-M., Antiguedad, I., Vallecillo, M.A., Iribar, V., Ruiz, M., 1997. Groundwater pollution in Quaternary aquifer of Vitoria–Gasteiz (Basque Country, Spain). Environ. Geol. 30, 257–265.

Atteia, O., 2005. Chimie et pollutions des eaux souterraines. Tec & doc.

Baillieux, A., Campisi, D., Jammet, N., Bucher, S., Hunkeler, D., 2014. Regional water quality patterns in an alluvial aquifer: Direct and indirect influences of rivers. J. Contam. Hydrol. 169, 123–31. doi:10.1016/j.jconhyd.2014.09.002

Baker, M.A., Valett, H.M., Dahm, C.N., 2000. Organic carbon supply and metabolism in a shallow groundwater ecosystem. Ecology 81, 3133–3148.

Baker, M.A., Vervier, P., 2004. Hydrological variability, organic matter supply and denitrification in the Garonne River ecosystem. Freshw. Biol. 49, 181–190. doi:10.1046/j.1365-2426.2003.01175.x

Baldassarre, G. Di, Montanari, A., 2009. Uncertainty in river discharge observations: a quantitative analysis. Hydrol. Earth Syst. Sci. 13, 913–921.

Baldwin, D.S., Mitchell, A.M., 2000. The effects of drying and re-flooding on the sediment and soil nutrient dynamics of lowland river–floodplain systems: a synthesis. Regul. Rivers Res. Manag. 16, 457–467. doi:10.1002/1099-1646(200009/10)16:5<457::AID-RRR597>3.0.CO;2-B

Bates, P.D., Stewart, M.D., Desitter, A., Anderson, M.G., Renaud, J.-P., Smith, J.A., 2000. Numerical simulation of floodplain hydrology. Water Resour. Res. 36, 2517–2529. doi:10.1029/2000WR900102

Beauchamp, E.G., Trevors, J.T., Paul, J.W., 1989. Carbon sources for bacterial denitrification, in: Advances in Soil Science. Springer, pp. 113–142.

Bergkamp, G., Orlando, B., 1999. Wetlands and climate change: exploring collaboration between the Convention on Wetlands (Ramsar, Iran, 1971) and the UN Framework Convention on Climate Change. IUCN, Gland. Switz.

Bernard-Jannin, L., 2014. Attenagua Project, Modelling in Garonne Site, MOHID Land Implementation. http://attenagua.actionmodulers.dtdns.net/files/GaronneModelling.pdf.

Bernard-Jannin, L., Brito, D., Sun, X., Jauch, E., Neves, R.J.J., Sauvage, S., Sánchez-Pérez, J.M., n.d. A physically-based, spatially-distributed modelling approach coupling surface water and groundwater flows to evaluate water exchanges in an alluvial floodplain during flood events. Adv. Water Resour.

Bernard-Jannin, L., Sun, X., Teissier, S., Sauvage, S., Sánchez-Pérez, J.-M., 2016. Spatio-temporal analysis of factors controlling nitrate dynamics and potential denitrification hot spots and hot moments in groundwater of an alluvial floodplain. Ecol. Eng. doi:10.1016/j.ecoleng.2015.12.031

Bijay-Singh, Yadvinder-Singh, Sekhon, G.S., 1995. Fertilizer-N use efficiency and nitrate pollution of groundwater in developing countries. J. Contam. Hydrol. 20, 167–184. doi:10.1016/0169-7722(95)00067-4

Billen, G., Garnier, J., 1999. Nitrogen transfers through the Seine drainage network: a budget based on the application of the "Riverstrahler"model, in: Man and River Systems. Springer, pp. 139–150.

Boano, F., Camporeale, C., Revelli, R., Ridolfi, L., 2006. Sinuosity-driven hyporheic exchange in meandering rivers. Geophys. Res. Lett. 33, 1–4.

Boano, F., Demaria, A., Revelli, R., Ridolfi, L., 2010. Biogeochemical zonation due to intrameander hyporheic flow. Water Resour. Res. 46, 1–13.

Böhlke, J.-K., 2002. Groundwater recharge and agricultural contamination. Hydrogeol. J. 10, 153–179.

Boithias, L., Srinivasan, R., Sauvage, S., Macary, F., Sánchez-Pérez, J.M., 2014. Daily Nitrate Losses: Implication on Long-Term River Quality in an Intensive Agricultural Catchment of Southwestern France. J. Environ. Qual. 43, 46–54.

Boulton, A.J., Findlay, S., Marmonier, P., Stanley, E.H., Valett, H.M., 1998. The functional significance of the hyporheic zone in streams and rivers. Annu. Rev. Ecol. Syst. 29, 59–81. doi:10.1146/annurev.ecolsys.29.1.59

Bradford, R.B., Acreman, M.C., 2003. Applying MODFLOW to wet grassland in-field habitats: a casestudy from the Pevensey Levels, UK. Hydrol. Earth Syst. Sci. Discuss. 7, 43–55.

Braunschweig, F., Leitao, P.C., Fernandes, L., Pina, P., Neves, R.J.J., 2004. The object-oriented design of the integrated water modelling system MOHID, in: Science, C.T.M. and G.F.P.B.T.-D. in W. (Ed.), Computational Methods in Water Resources: Volume 2 Proceedings of the XVth International Conference on Computational Methods in Water Resources. Elsevier, pp. 1079–1090. doi:http://dx.doi.org/10.1016/S0167-5648(04)80126-6

Briggs, M.A., Lautz, L.K., Hare, D.K., 2014. Residence time control on hot moments of net nitrate production and uptake in the hyporheic zone. Hydrol. Process. 28, 3741–3751. doi:10.1002/hyp.9921

Brito, D., 2014a. Attenagua Project, Modelling in Bidasoa Site, MOHID Land Implementation. http://attenagua.actionmodulers.dtdns.net/files/BidasoaModelling.pdf.

Brito, D., 2014b. Attenagua Project, Modelling in Ebro Site, MOHID Land Implementation. http://attenagua.actionmodulers.dtdns.net/files/EbroModelling.pdf.

Brito, D., 2014c. Attenagua Project, Modelling in Tagus Site, MOHID Land Implementation. http://attenagua.actionmodulers.dtdns.net/files/TagusModelling.pdf.

Brito, D., 2014d. Attenagua Project, Modelling Approach for Attenagua Alluvial Floodplains. http://attenagua.actionmodulers.dtdns.net/files/ModellingApproach.pdf.

Brito, D., Bernard-Jannin, L., Sauvage, S., Zabaleta, A., Comin, F.., Ladera, J., Neves, R., Sanchez-Pérez, J.M., 2014. Modeling the hydro-biogeochemistry functioning in alluvial wetlands, in: Wetlands 2014.

Brito, D., Campuzano, F.J., Sobrinho, J., Fernandes, R., Neves, R., 2015. Integrating operational watershed and coastal models for the Iberian Coast: Watershed model implementation – A first approach. Estuar. Coast. Shelf Sci. 167, 138–146. doi:10.1016/j.ecss.2015.10.022

Brookfield, A.E., Sudicky, E.A., Park, Y.-J., Conant, B., 2009. Thermal transport modelling in a fully integrated surface/subsurface framework. Hydrol. Process. 23, 2150–2164. doi:10.1002/hyp.7282

Brunke, M., Gonser, T., 1997. The ecological significance of exchange processes between rivers and groundwater. Freshw. Biol. 37, 1–33. doi:10.1046/j.1365-2427.1997.00143.x

Burt, T.P., Matchett, L.S., Goulding, K.W.T., Webster, C.P., Haycock, N.E., 1999. Denitrification in riparian buffer zones: the role of floodplain hydrology. Hydrol. Process. 13, 1451–1463. doi:10.1002/(SICI)1099-1085(199907)13:10<1451::AID-HYP822>3.0.CO;2-W

Caleffi, V., Valiani, A., Zanni, A., 2003. Finite volume method for simulating extreme flood events in natural channels. J. Hydraul. Res. 41, 167–177. doi:10.1080/00221680309499959

Cardenas, M.B., Wilson, J.L., 2007. Hydrodynamics of coupled flow above and below a sediment–water interface with triangular bedforms. Adv. Water Resour. 30, 301–313. doi:10.1016/j.advwatres.2006.06.009

Carpenter, S.R., Caraco, N.F., Correll, D.L., Howarth, R.W., Sharpley, A.N., Smith, V.H., 1998. Non point pollution of surface waters with phosphorus and nitrogen. Ecol. Appl. 8, 559–568. doi:10.1890/1051-0761(1998)008[0559:NPOSWW]2.0.CO;2

Carrascal, L.M., Galván, I., Gordo, O., 2009. Partial least squares regression as an alternative to current regression methods used in ecology. Oikos 118, 681–690. doi:10.1111/j.1600-0706.2008.16881.x

Chow, V.T., 1959. Open channel hydraulics. McGraw-Hill, New-York.

Chow, V.T., Maidment, D.R., Mays, L.W., 1988. Applied Hydrology. McGraw-Hill, New-York.

Clément, J.-C., Pinay, G., Marmonier, P., 2002. Seasonal dynamics of denitrification along topohydrosequences in three different riparian wetlands. J. Environ. Qual. 31, 1025–1037.

Clinton, S.M., Edwards, R.T., Naiman, R.J., 2002. Forest-river interactions: influence on hyporheic dissolved organic carbon concentrations in a floodplain terrace. J. Am. Water Resour. Assoc. 38, 619.

Condon, L.E., Maxwell, R.M., 2013. Implementation of a linear optimization water allocation algorithm into a fully integrated physical hydrology model. Adv. Water Resour. 60, 135–147. doi:10.1016/j.advwatres.2013.07.012

Correll, D.L., Jordan, T.E., Weller, D.E., 1992. Nutrient flux in a landscape: effects of coastal land use and terrestrial community mosaic on nutrient transport to coastal waters. Estuaries 15, 431–442.

Craig, L., Bahr, J.M., Roden, E.E., 2010. Localized zones of denitrification in a floodplain aquifer in southern Wisconsin, USA. Hydrogeol. J. 18, 1867–1879.

Dagès, C., Paniconi, C., Sulis, M., 2012. Analysis of coupling errors in a physically-based integrated surface water–groundwater model. Adv. Water Resour. 49, 86–96. doi:10.1016/j.advwatres.2012.07.019

De Groot, R.S., 1992. Functions of nature: evaluation of nature in environmental planning, management and decision making. Wolters-Noordhoff BV.

Derx, J., Blaschke, A.P., Blöschl, G., 2010. Three-dimensional flow patterns at the river–aquifer interface — a case study at the Danube. Adv. Water Resour. 33, 1375–1387. doi:10.1016/j.advwatres.2010.04.013

Devito, K.J., Fitzgerald, D., Hill, A.R., Aravena, R., 2000. Nitrate dynamics in relation to lithology and hydrologic flow path in a river riparian zone. J. Environ. Qual. 29, 1075–1084.

Doppler, T., Hendricks Franssen, H.-J., Kaiser, H.-P., Kuhlman, U., Stauffer, F., 2007. Field evidence of a dynamic leakage coefficient for modelling river–aquifer interactions. J. Hydrol. 347, 177–187. doi:10.1016/j.jhydrol.2007.09.017

Dosskey, M.G., Vidon, P., Gurwick, N.P., Allan, C.J., Duval, T.P., Lowrance, R., 2010. The Role of Riparian Vegetation in Protecting and Improving Chemical Water Quality in Streams1. JAWRA J. Am. Water Resour. Assoc. 46, 261–277. doi:10.1111/j.1752-1688.2010.00419.x

Engeler, I., Hendricks Franssen, H.J., Müller, R., Stauffer, F., 2011. The importance of coupled modelling of variably saturated groundwater flow-heat transport for assessing river–aquifer interactions. J. Hydrol. 397, 295–305. doi:10.1016/j.jhydrol.2010.12.007

Epstein, S., Mayeda, T., 1953. Variation of O 18 content of waters from natural sources. Geochim. Cosmochim. Acta 4, 213–224.

ESRI, R., 2011. ArcGIS desktop: release 10. Environ. Syst. Res. Institute, CA.

Fan, A.M., Steinberg, V.E., 1996. Health Implications of Nitrate and Nitrite in Drinking Water: An Update on Methemoglobinemia Occurrence and Reproductive and Developmental Toxicity. Regul. Toxicol. Pharmacol. 23, 35–43. doi:10.1006/rtph.1996.0006

Ferrant, S., Oehler, F., Durand, P., Ruiz, L., Salmon-Monviola, J., Justes, E., Dugast, P., Probst, A., Probst, J.-L., Sanchez-Perez, J.-M., 2011. Understanding nitrogen transfer dynamics in a small agricultural catchment: Comparison of a distributed (TNT2) and a semi distributed (SWAT) modeling approaches. J. Hydrol. 406, 1–15. doi:10.1016/j.jhydrol.2011.05.026

Frei, S., Fleckenstein, J.H., Kollet, S.J., Maxwell, R.M., 2009. Patterns and dynamics of river–aquifer exchange with variably-saturated flow using a fully-coupled model. J. Hydrol. 375, 383–393. doi:10.1016/j.jhydrol.2009.06.038

Furman, A., 2008. Modeling Coupled Surface–Subsurface Flow Processes: A Review. Vadose Zo. J. 7, 741–756. doi:10.2136/vzj2007.0065

Galloway, J.N., Aber, J.D., Erisman, J.W., Seitzinger, S.P., Howarth, R.W., Cowling, E.B., Cosby, B.J., 2003. The nitrogen cascade. Bioscience 53, 341–356.

Garneau, C., 2014. Modélisation du transfert des éléments traces métalliques dans les eaux de surface.

Garnier, J., Billen, G., Vilain, G., Martinez, A., Silvestre, M., Mounier, E., Toche, F., 2009. Nitrous oxide (N 2 O) in the Seine river and basin: observations and budgets. Agric. Ecosyst. Environ. 133, 223–233.

Gift, D.M., Groffman, P.M., Kaushal, S.S., Mayer, P.M., 2010. Denitrification potential, root biomass, and organic matter in degraded and restored urban riparian zones. Restor. Ecol. 18, 113–120.

Gold, A.J., Groffman, P.M., Addy, K., Kellogg, D.Q., Stolt, M., Rosenblatt, A.E., 2001. Landscape attributes as controls on groithd water nitrate removal capacity of riparian zones1.

Gonfiantini, R., 1978. Standards for stable isotope measurements in natural compounds.

Goudie, A., 2004. Encyclopedia of geomorphology. Psychology Press.

Gregory, S. V, Swanson, F.J., McKee, W.A., Cummins, K.W., 1991. An ecosystem perspective of riparian zones. Bioscience 540–551.

Grimm, N.B., Fisher, S.G., 1984. Exchange between interstitial and surface water: implications for stream metabolism and nutrient cycling. Hydrobiologia 111, 219–228.

Groffman, P., Butterbach-Bahl, K., Fulweiler, R., Gold, A., Morse, J., Stander, E., Tague, C., Tonitto, C., Vidon, P., 2009. Challenges to incorporating spatially and temporally explicit phenomena (hotspots and hot moments) in denitrification models. Biogeochemistry 93, 49–77. doi:10.1007/s10533-008-9277-5

Groffman, P.M., 2012. Terrestrial denitrification: challenges and opportunities. Ecol. Process. 1, 1–11.

Groffman, P.M., Altabet, M.A., Böhlke, J.K., Butterbach-Bahl, K., David, M.B., Firestone, M.K., Giblin, A.E., Kana, T.M., Nielsen, L.P., Voytek, M.A., 2006. METHODS FOR MEASURING DENITRIFICATION: DIVERSE APPROACHES TO A DIFFICULT PROBLEM. Ecol. Appl. 16, 2091–2122. doi:10.1890/1051-0761(2006)016[2091:MFMDDA]2.0.CO;2

Groffman, P.M., Gold, A.J., Simmons, R.C., 1992. Nitrate dynamics in riparian forests: microbial studies. J. Environ. Qual. 21, 666–671.

Hattermann, F.F., Krysanova, V., Habeck, A., Bronstert, A., 2006. Integrating wetlands and riparian zones in river basin modelling. Ecol. Modell. 199, 379–392. doi:http://dx.doi.org/10.1016/j.ecolmodel.2005.06.012

Haycock, N.E., Burt, T.P., 1993. Role of floodplain sediments in reducing the nitrate concentration of subsurface runoff: A case study in the Cotswolds, UK. Hydrol. Process. 7, 287–295.

Heinen, M., 2006. Simplified denitrification models: Overview and properties. Geoderma 133, 444–463. doi:http://dx.doi.org/10.1016/j.geoderma.2005.06.010

Helton, A.M., Poole, G.C., Payn, R.A., Izurieta, C., Stanford, J.A., 2014. Relative influences of the river channel, floodplain surface, and alluvial aquifer on simulated hydrologic residence time in a montane river floodplain. Geomorphology 205, 17–26. doi:http://dx.doi.org/10.1016/j.geomorph.2012.01.004

Hill, A.R., 1996. Nitrate removal in stream riparian zones. J. Environ. Qual. 25, 743–755.

Hill, A.R., Cardaci, M., 2004. Denitrification and organic carbon availability in riparian wetland soils and subsurface sediments. Soil Sci. Soc. Am. J. 68, 320–325.

Hill, A.R., Devito, K.J., Campagnolo, S., Sanmugadas, K., 2000. Subsurface Denitrification in a Forest Riparian Zone: Interactions between Hydrology and Supplies of Nitrate and Organic Carbon. Biogeochemistry 51, 193–223.

Hill, A.R., Vidon, P.G.F., Langat, J., 2004. Denitrification potential in relation to lithology in five headwater riparian zones. J. Environ. Qual. 33, 911–919.

Hoffmann, C.C., Berg, P., Dahl, M., Larsen, S.E., Andersen, H.E., Andersen, B., 2006. Groundwater flow and transport of nutrients through a riparian meadow – Field data and modelling. J. Hydrol. 331, 315–335. doi:http://dx.doi.org/10.1016/j.jhydrol.2006.05.019

Höring, H., Chapman, D. V, 2002. Nitrate and nitrite in drinking water. IWA.

Horritt, M.S., Bates, P.D., Mattinson, M.J., 2006. Effects of mesh resolution and topographic representation in 2D finite volume models of shallow water fluvial flow. J. Hydrol. 329, 306–314. doi:10.1016/j.jhydrol.2006.02.016

Horritt, M.S., Di Baldassarre, G., Bates, P.D., Brath, A., 2007. Comparing the performance of a 2-D finite element and a 2-D finite volume model of floodplain inundation using airborne SAR imagery. Hydrol. Process. 21, 2745–2759. doi:10.1002/hyp.6486

Iribar, A., 2007. Composition des communautés bactériennes dénitrifiantes au sein d'un aquifère alluvial et facteurs contrôlant leur structuration: relation entre structure des communautés et dénitrification. Université de Toulouse III - Paul Sabatier.

Iribar, A., Sánchez-Pérez, J., Lyautey, E., Garabétian, F., 2008. Differentiated free-living and sediment-attached bacterial community structure inside and outside denitrification hotspots in the river–groundwater interface. Hydrobiologia 598, 109–121 LA – English. doi:10.1007/s10750-007-9143-9

Jacinthe, P.-A., Groffman, P.M., Gold, A.J., Mosier, A., 1998. Patchiness in microbial nitrogen transformations in groundwater in a riparian forest. J. Environ. Qual. 27, 156–164.

Jégo, G., 2008. Influence des activités agricoles sur la pollution nitrique des eaux souterraines. Analyse par modélisation des impacts des systèmes de grande culture sur les fuites de nitrate dans les plaines alluviales. Université de Toulouse III - Paul Sabatier.

Jégo, G., Sánchez-Pérez, J.M., Justes, E., 2012. Predicting soil water and mineral nitrogen contents with the STICS model for estimating nitrate leaching under agricultural fields. Agric. Water Manag. 107, 54–65. doi:http://dx.doi.org/10.1016/j.agwat.2012.01.007

Junk, W.J., Bayley, P.B., Sparks, R.E., 1989. The flood pulse concept in river-floodplain systems. Can. Spec. Publ. Fish. Aquat. Sci. 106, 110–127.

Käser, D.H., Binley, A., Krause, S., Heathwaite, A.L., 2014. Prospective modelling of 3D hyporheic exchange based on high-resolution topography and stream elevation. Hydrol. Process. 28, 2579–2594. doi:10.1002/hyp.9758

Keddy, P.A., 2010. Wetland ecology: principles and conservation. Cambridge University Press.

Kendall, C., McDonnell, J.J., 2012. Isotope tracers in catchment hydrology. Elsevier.

Knowles, R., 1982. Denitrification. Microbiol. Rev. 46, 43.

Kollet, S.J., Maxwell, R.M., 2006. Integrated surface–groundwater flow modeling: A free-surface overland flow boundary condition in a parallel groundwater flow model. Adv. Water Resour. 29, 945–958. doi:10.1016/j.advwatres.2005.08.006

Korom, S.F., 1992. Natural denitrification in the saturated zone: A review. Water Resour. Res. 28, 1657–1668. doi:10.1029/92WR00252

Krause, S., Bronstert, A., 2007. The impact of groundwater–surface water interactions on the water balance of a mesoscale lowland river catchment in northeastern Germany. Hydrol. Process. 21, 169–184. doi:10.1002/hyp.6182

Krause, S., Bronstert, A., Zehe, E., 2007. Groundwater–surface water interactions in a North German lowland floodplain – Implications for the river discharge dynamics and riparian water balance. J. Hydrol. 347, 404–417. doi:10.1016/j.jhydrol.2007.09.028

Krause, S., Hannah, D.M., Fleckenstein, J.H., Heppell, C.M., Kaeser, D., Pickup, R., Pinay, G., Robertson, A.L., Wood, P.J., 2011. Inter-disciplinary perspectives on processes in the hyporheic zone. Ecohydrology 4, 481–499. doi:10.1002/eco.176

Krause, S., Jacobs, J., Voss, A., Bronstert, A., Zehe, E., 2008. Assessing the impact of changes in landuse and management practices on the diffuse pollution and retention of nitrate in a riparian floodplain. Sci. Total Environ. 389, 149–64. doi:10.1016/j.scitotenv.2007.08.057

Lambert, R., 1988. Atlas Géomorphologique de la Vallée de la Garonne.

Lamontagne, S., Herczeg, A.L., Dighton, J.C., Jiwan, J.S., Pritchard, J.L., 2005. Patterns in groundwater nitrogen concentration in the floodplain of a subtropical stream (Wollombi Brook, New South Wales). Biogeochemistry 72, 169–190. doi:10.1007/s10533-004-0358-9

Lancaster, R.R., 2005. Fluvial Evolution of the Garonne River, France: Integrating Field Data with Numerical Simulations.

Lautz, L.K., Siegel, D.I., 2006. Modeling surface and ground water mixing in the hyporheic zone using MODFLOW and MT3D. Adv. Water Resour. 29, 1618–1633.

Lewandowski, J., Nützmann, G., 2010. Nutrient retention and release in a floodplain's aquifer and in the hyporheic zone of a lowland river. Ecol. Eng. 36, 1156–1166. doi:10.1016/j.ecoleng.2010.01.005

Li, B., Irvin, S., 2007. The comparison of alkalinity and ORP as indicators for nitrification and denitrification in a sequencing batch reactor (SBR). Biochem. Eng. J. 34, 248–255. doi:10.1016/j.bej.2006.12.020

Lowrance, R., Altier, L.S., Newbold, J.D., Schnabel, R.R., Groffman, P.M., Denver, J.M., Correll, D.L., Gilliam, J.W., Robinson, J.L., Brinsfield, R.B., Staver, K.W., Lucas, W., Todd, A.H., 1997. Water Quality Functions of Riparian Forest Buffers in Chesapeake Bay Watersheds. Environ. Manage. 21, 687–712. doi:10.1007/s002679900060

Lowrance, R., Todd, R., Fail, J., Hendrickson, O., Leonard, R., Asmussen, L., 1984. Riparian forests as nutrient filters in agricultural watersheds. Bioscience 34, 374–377.

Malcolm, I.A., Soulsby, C., Youngson, A.F., Hannah, D.M., 2005. Catchment-scale controls on groundwater-surface water interactions in the hyporheic zone: implications for salmon embryo survival. River Res. Appl. 21, 977–989.

Marmonier, P., Archambaud, G., Belaidi, N., Bougon, N., Breil, P., Chauvet, E., Claret, C., Cornut, J., Datry, T., Dole-Olivier, M.-J., 2012. The role of organisms in hyporheic processes: gaps in current knowledge, needs for future research and applications, in: Annales de Limnologie-International Journal of Limnology. Cambridge Univ Press, pp. 253–266.

Marzadri, A., Tonina, D., Bellin, A., 2011. A semianalytical three-dimensional process-based model for hyporheic nitrogen dynamics in gravel bed rivers. Water Resour. Res. 47.

Maxwell, R.M., Putti, M., Meyerhoff, S., Delfs, J.-O., Ferguson, I.M., Ivanov, V., Kim, J., Kolditz, O., Kollet, S.J., Kumar, M., Lopez, S., Jie, N., Paniconi, C., Park, Y.-J., Phanikumar, M.S., Shen, C., Sudicky, E.A., Sulis, M., 2014. Surface-subsurface model intercomparison: A first set of benchmark results to diagnose integrated hydrology and feedbacks. Water Resour. Res. 50, 1531–1549.

Mayer, P.M., Reynolds, S.K., McCutchen, M.D., Canfield, T.J., 2007. Meta-analysis of nitrogen removal in riparian buffers. J. Environ. Qual. 36, 1172–1180.

McClain, M.E., Boyer, E.W., Dent, C.L., Gergel, S.E., Grimm, N.B., Groffman, P.M., Hart, S.C., Harvey, J.W., Johnston, C.A., Mayorga, E., McDowell, W.H., Pinay, G., 2003. Biogeochemical Hot Spots and Hot Moments at the Interface of Terrestrial and Aquatic Ecosystems. Ecosystems 6, 301–312. doi:10.1007/s10021-003-0161-9

Mermillod-Blondin, F., Mauclaire, L., Montuelle, B., 2005. Use of slow filtration columns to assess oxygen respiration, consumption of dissolved organic carbon, nitrogen transformations, and microbial parameters in hyporheic sediments. Water Res. 39, 1687–98. doi:10.1016/j.watres.2005.02.003

Mevik, B.-H., Wehrens, R., 2007. The pls package: principal component and partial least squares regression in R. J. Stat. Softw. 18, 1–24.

Miller, M.N., Zebarth, B.J., Dandie, C.E., Burton, D.L., Goyer, C., Trevors, J.T., 2008. Crop residue influence on denitrification, N2O emissions and denitrifier community abundance in soil. Soil Biol. Biochem. 40, 2553–2562. doi:10.1016/j.soilbio.2008.06.024

Mitsch, W.J., Gosselink, J.G., 2000. Wetlands (3rd edn).

Morales-Hernández, M., Hubbard, M.E., García-Navarro, P., 2014. A 2D extension of a Large Time Step explicit scheme (CFL>1) for unsteady problems with wet/dry boundaries. J. Comput. Phys. 263, 303–327. doi:10.1016/j.jcp.2014.01.019

Morin, E., Grodek, T., Dahan, O., Benito, G., Kulls, C., Jacoby, Y., Langenhove, G. Van, Seely, M., Enzel, Y., 2009. Flood routing and alluvial aquifer recharge along the ephemeral arid Kuiseb River, Namibia. J. Hydrol. 368, 262–275. doi:10.1016/j.jhydrol.2009.02.015

Morris, M.D., 1991. Factorial sampling plans for preliminary computational experiments. Technometrics 33, 161–174.

Mualem, Y., 1976. A new model for predicting the hydraulic conductivity of unsaturated porous media. Water Resour. Res. 12, 513–522.

Muñoz-Leoz, B., Garbisu, C., Charcosset, J.-Y., Sánchez-Pérez, J.M., Antigüedad, I., Ruiz-Romera, E., 2013. Non-target effects of three formulated pesticides on microbially-mediated processes in a clay-loam soil. Sci. Total Environ. 449, 345–354.

Naiman, R.J., Décamps, H., 1997. The ecology of interfaces: riparian zones. Annu. Rev. Ecol. Syst. 621–658.

Naiman, R.J., Decamps, H., McClain, M.E., 2010. Riparia: ecology, conservation, and management of streamside communities. Academic Press.

Naiman, R.J., Decamps, H., Pollock, M., 1993. The role of riparian corridors in maintaining regional biodiversity. Ecol. Appl. 3, 209–212.

Nash, Je., Sutcliffe, J. V, 1970. River flow forecasting through conceptual models part I—A discussion of principles. J. Hydrol. 10, 282–290.

Néelz, S., 2009. Desktop review of 2D hydraulic modelling packages. Bristol: Environment Agency.

Neves, R., Mateus, M., Neves, R., 2013. The MOHID concept. Ocean Model. Coast. Manag. Stud. with MOHID 1–11.

Nützmann, G., Levers, C., Lewandowski, J., 2013. Coupled groundwater flow and heat transport simulation for estimating transient aquifer-stream exchange at the lowland River Spree (Germany). Hydrol. Process. doi:10.1002/hyp.9932

Ochoa-Salazar, B.-X., 2008. Etude conjuguée géochimique/hydrologique des relations nappes-rivière dans une zone humide : cas de la zone humide alluviale de Monbéqui, France. Université de Toulouse III - Paul Sabatier.

Orghidan, T., 1959. Ein neuer Lebensraum des unterirdischen Wassers: der hyporheische Biotop. Arch. Hydrobiol 55, 392–414.

Osborne, L.L., Kovacic, D.A., 1993. Riparian vegetated buffer strips in water-quality restoration and stream management. Freshw. Biol. 29, 243–258. doi:10.1111/j.1365-2427.1993.tb00761.x

Packman, A.I., Salehin, M., 2003. Relative roles of stream flow and sedimentary conditions in controlling hyporheic exchange, in: The Interactions between Sediments and Water. Springer, pp. 291–297.

Pan, Y., Weill, S., Ackerer, P., Delay, F., 2015. A coupled stream flow and depth-integrated subsurface flow model for catchment hydrology. J. Hydrol. 530, 66–78.

Panday, S., Huyakorn, P.S., 2004. A fully coupled physically-based spatially-distributed model for evaluating surface/subsurface flow. Adv. Water Resour. 27, 361–382. doi:10.1016/j.advwatres.2004.02.016

Pardé, M., 1935. Le régime de la Garonne. Rev. Geogr. Pyren. Sud. Ouest. 6, 105–262.

Partington, D., Brunner, P., Simmons, C.T., Therrien, R., Werner, A.D., Dandy, G.C., Maier, H.R., 2011. A hydraulic mixing-cell method to quantify the groundwater component of streamflow within spatially distributed fully integrated surface water–groundwater flow models. Environ. Model. Softw. 26, 886–898. doi:10.1016/j.envsoft.2011.02.007

Peter, S., Rechsteiner, R., Lehmann, M.F., Brankatschk, R., Vogt, T., Diem, S., Wehrli, B., Tockner, K., Durisch-Kaiser, E., 2012. Nitrate removal in a restored riparian groundwater system: functioning and importance of individual riparian zones. Biogeosciences Discuss. 9, 6715–6750.

Peter, S., Rechsteiner, R., Lehmann, M.F., Tockner, K., Durisch-Kaiser, E., 2011. Denitrification hot spot and hot moments in a restored riparian system. IAHS-AISH Publ. 433–436.

Peterjohn, W.T., Correll, D.L., 1984. Nutrient dynamics in an agricultural watershed: observations on the role of a riparian forest. Ecology 65, 1466–1475.

Peterson, M.E., Curtin, D., Thomas, S., Clough, T.J., Meenken, E.D., 2013. Denitrification in vadose zone material amended with dissolved organic matter from topsoil and subsoil. Soil Biol. Biochem. 61, 96–104. doi:10.1016/j.soilbio.2013.02.010

Peyrard, D., Delmotte, S., Sauvage, S., Namour, P., Gerino, M., Vervier, P., Sánchez-Pérez, J.M., 2011. Longitudinal transformation of nitrogen and carbon in the hyporheic zone of an N-rich stream: A combined modelling and field study. Phys. Chem. Earth, Parts A/B/C 36, 599–611. doi:http://dx.doi.org/10.1016/j.pce.2011.05.003

Peyrard, D., Sauvage, S., Vervier, P., Sánchez-Pérez, J.-M., Quintard, M., 2008. A coupled vertically integrated model to describe lateral exchanges between surface and subsurface in large alluvial floodplains with a fully penetrating river. Hydrol. Process. 22, 4257–4273. doi:10.1002/hyp.7035

Pfeiffer, S.M., Bahr, J.M., Beilfuss, R.D., 2006. Identification of groundwater flowpaths and denitrification zones in a dynamic floodpain aquifier. J. Hydrol. 325, 262–272. doi:10.1016/j.jhydrol.2005.10.019

Pinay, G., Decamps, H., 1988. The role of riparian woods in regulating nitrogen fluxes between the alluvial aquifer and surface water: a conceptual model. Regul. Rivers 2, 507–516.

Pinay, G., Ruffinoni, C., Wondzell, S., Gazelle, F., 1998. Change in Groundwater Nitrate Concentration in a Large River Floodplain: Denitrification, Uptake, or Mixing? J. North Am. Benthol. Soc. 17, 179–189. doi:10.2307/1467961

Power, J.F., Schepers, J.S., 1989. Nitrate contamination of groundwater in North America. Agric. Ecosyst. Environ. 26, 165–187. doi:10.1016/0167-8809(89)90012-1

Puckett, L.J., Cowdery, T.K., 2002. Transport and fate of nitrate in a glacial outwash aquifer in relation to ground water age, land use practices, and redox processes. J. Environ. Qual. 31, 782–796.

Purser, R.J., Leslie, L.M., 1988. A Semi-Implicit, Semi-Lagrangian Finite-Difference Scheme Using Hligh-Order Spatial Differencing on a Nonstaggered Grid. Mon. Weather Rev. 116, 2069–2080. doi:10.1175/1520-0493(1988)116<2069:ASISLF>2.0.CO;2

R Core Team, 2012. R: A language and environment for statistical computing. R Foundation for Statistical Computing, Vienna, Austria, 2012.

Ranalli, A.J., Macalady, D.L., 2010. The importance of the riparian zone and in-stream processes in nitrate attenuation in undisturbed and agricultural watersheds – A review of the scientific literature. J. Hydrol. 389, 406–415. doi:http://dx.doi.org/10.1016/j.jhydrol.2010.05.045

Rassam, D.W., Pagendam, D.E., Hunter, H.M., 2008. Conceptualisation and application of models for groundwater–surface water interactions and nitrate attenuation potential in riparian zones. Environ. Model. Softw. 23, 859–875. doi:http://dx.doi.org/10.1016/j.envsoft.2007.11.003

Richards, L.A., 1931. Capillary conduction of liquids through porous mediums. J. Appl. Phys. 1, 318–333.

Rivett, M.O., Buss, S.R., Morgan, P., Smith, J.W.N., Bemment, C.D., 2008. Nitrate attenuation in groundwater: A review of biogeochemical controlling processes. Water Res. 42, 4215–4232. doi:http://dx.doi.org/10.1016/j.watres.2008.07.020

Rosenblatt, A.E., Gold, A.J., Stolt, M.H., Groffman, P.M., Kellogg, D.Q., 2001. Identifying riparian sinks for watershed nitrate using soil surveys. J. Environ. Qual. 30, 1596–1604.

Ruelland, D., Billen, G., Brunstein, D., Garnier, J., 2007. SENEQUE: a multi-scaling GIS interface to the Riverstrahler model of the biogeochemical functioning of river systems. Sci. Total Environ. 375, 257–273.

Sánchez-Pérez, J.M., 1992. Fonctionnement hydrochimique d'un écosystème forestier inondable de la Plaine du Rhin: la forêt alluviale du secteur de l'île de Rhinau en Alsace(France). Université Louis Pasteur, Strasbourg.

Sánchez-Pérez, J.-M., Tremolières, M., 1997. Variation in nutrient levels of the groundwater in the Upper Rhine alluvial forests as a consequence of hydrological regime and soil texture. Glob. Ecol. Biogeogr. Lett. 211–217.

Sánchez-Pérez, J.M., Vervier, P., Garabétian, F., Sauvage, S., Loubet, M., Rols, J.L., Bariac, T., Weng, P., 2003. Nitrogen dynamics in the shallow groundwater of a riparian wetland zone of the Garonne, SW France: nitrate inputs, bacterial densities, organic matter supply and denitrification measurements. Hydrol. Earth Syst. Sci. 7, 97–107. doi:10.5194/hess-7-97-2003

Sánchez-Pérez, J.-M., Vervier, P., Garabétian, F., Sauvage, S., Loubet, M., Rols, J.-L., Bariac, T., Weng, P., 2003. Nitrogen dynamics in the shallow groundwater of a riparian wetland zone of the Garonne, SW France: nitrate inputs, bacterial densities, organic matter supply and denitrification measurements. Hydrol. Earth Syst. Sci. Discuss. 7, 97–107.

Sauvage, S., 1999. Modélisation hydrobiogéochimique de la Garonne à l'étiage estival: cas de l'azote entre Toulouse et Agen (120 kilomètres). Toulouse, INPT.

Schaap, M.G., Leij, F.J., van Genuchten, M.T., 2001. ROSETTA: a computer program for estimating soil hydraulic parameters with hierarchical pedotransfer functions. J. Hydrol. 251, 163–176.

Schade, Jd., Fisher, S.G., Grimm, N.B., Seddon, J.A., 2001. The influence of a riparian shrub on nitrogen cycling in a Sonoran Desert stream. Ecology 82, 3363–3376.

Seitzinger, S., Harrison, J.A., Böhlke, J.K., Bouwman, A.F., Lowrance, R., Peterson, B., Tobias, C., Drecht, G. Van, 2006. Denitrification across landscapes and waterscapes: a synthesis. Ecol. Appl. 16, 2064–2090.

Soman, S., Beyeler, S., Kraft, S.E., Winstanley, D., 2007. Ecosystem Services from Riparian Areas: A Brief Summary of the Literature. Prep. Sci. Advis. Comm. Illinois River Coord. Counc.

Sophocleous, M., 2002. Interactions between groundwater and surface water: the state of the science. Hydrogeol. J. 10, 52–67. doi:10.1007/s10040-001-0170-8

Sophocleous, M.A., 1998. Perspectives on sustainable development of water resources in Kansas. Bull 239, Kansas Geologi- cal Survey, Lawrence, Kansas.

Sorooshian, S., Duan, Q., Gupta, V.K., 1993. Calibration of rainfall-runoff models: Application of global optimization to the Sacramento Soil Moisture Accounting Model. Water Resour. Res. 29, 1185–1194.

Starr, R.C., Gillham, R.W., 1993. Denitrification and organic carbon availability in two aquifers. Groundwater 31, 934–947.

Steiger, J., Corenblit, D., 2000. Dynamique fluviale de la Garonne toulousaine.

Steiger, J., James, M., Gazelle, F., 1998. Channelization and consequences on floodplain system functioning on the Garonne River, SW France. Regul. Rivers Res. Manag. 14, 13–23.

Stewart, M.D., Bates, P.D., Price, D.A., Burt, T.P., Bates, Y.Ã.P.D., 1998. Modelling the spatial variability in floodplain soil contamination during flood events to improve chemical mass balance estimates. Hydrol. Process. 12, 1233–1255. doi:10.1002/(SICI)1099-1085(19980630)12:8<1233::AID-HYP614>3.0.CO;2-2

Sun, X., 2015. Modélisation des échanges nappe-rivière et du processus de dénitrification dans les plaines alluviales à l'échelle du bassin versant. Université de Toulouse III - Paul Sabatier.

Sun, X., Bernard-Jannin, L., Garneau, C., Arnold, J.G., Srinivasan, R., Sauvage, S., Sánchez-Pérez, J.M., n.d. Assessment of the denitrification process in alluvial wetlands at floodplain scale using SWAT model. Ecol. Eng.

Sun, X., Bernard-Jannin, L., Garneau, C., Volk, M., Arnold, J.G., Srinivasan, R., Sauvage, S., Sánchez-Pérez, J.M., 2015. Improved simulation of river water and groundwater exchange in an alluvial plain using the SWAT model. Hydrol. Process.

Sutton, M.A., Howard, C.M., Erisman, J.W., Billen, G., Bleeker, A., Grennfelt, P., van Grinsven, H., Grizzetti, B., 2011. The European nitrogen assessment: sources, effects and policy perspectives. Cambridge University Press.

Swartzendruber, D., 1969. The flow of water in unsaturated soils. Flow through Porous Media, Acad. Press. New York 215–292.

Thoms, M.C., 2003. Floodplain–river ecosystems: lateral connections and the implications of human interference. Geomorphology 56, 335–349. doi:10.1016/S0169-555X(03)00160-0

Tockner, K., Malard, F., Ward, J. V, 2000. An extension of the flood pulse concept. Hydrol. Process. 14, 2861–2883.

Tockner, K., Pennetzdorfer, D., Reiner, N., Schiemer, F., Ward, J. V, 1999. Hydrological connectivity, and the exchange of organic matter and nutrients in a dynamic river–floodplain system (Danube, Austria). Freshw. Biol. 41, 521–535. doi:10.1046/j.1365-2427.1999.00399.x

Tockner, K., Stanford, J.A., 2002. Riverine flood plains: present state and future trends. Environ. Conserv. 29, 308–330.

Trancoso, A.R., Braunschweig, F., Chambel Leitão, P., Obermann, M., Neves, R., 2009. An advanced modelling tool for simulating complex river systems. Sci. Total Environ. 407, 3004–3016. doi:http://dx.doi.org/10.1016/j.scitotenv.2009.01.015

Triska, F.J., Duff, J.H., Avanzino, R.J., 1993. Patterns of hydrological exchange and nutrient transformation in the hyporheic zone of a gravel-bottom stream: examining terrestrial—aquatic linkages. Freshw. Biol. 29, 259–274.

Valett, H.M., Morrice, J.A., Dahm, C.N., Campana, M.E., 1996. Parent lithology, surface–groundwater exchange, and nitrate retention in headwater streams. Limnol. Oceanogr. 41, 333–345.

Valette, P., 2002. Les paysages de la Garonne: les métamorphoses d'un fleuve: entre Toulouse et Castets-en Dorthe.

Valette, P., Carozza, J.-M., Salles, D., David, M., Simonet, G., 2014. Construction géohistorique du" sauvage" de la Garonne toulousaine: quelle part de naturalisé dans les paysages fluviaux? part. 2. Développement durable Territ. 5, 22–p.

van Genuchten, M.T., 1980. A closed-form equation for predicting the hydraulic conductivity of unsaturated soils. Soil Sci. Soc. Am. J. 44, 892–898.

Venterink, H.O., Hummelink, E., Van den Hoorn, M.W., 2003. Denitrification potential of a river floodplain during flooding with nitrate-rich water: grasslands versus reedbeds. Biogeochemistry 65, 233–244.

Vidon, P., Allan, C., Burns, D., Duval, T.P., Gurwick, N., Inamdar, S., Lowrance, R., Okay, J., Scott, D., Sebestyen, S., 2010. Hot Spots and Hot Moments in Riparian Zones: Potential for Improved Water Quality Management1. JAWRA J. Am. Water Resour. Assoc. 46, 278–298. doi:10.1111/j.1752-1688.2010.00420.x

Vidon, P., Hill, A.R., 2005. Denitrification and patterns of electron donors and acceptors in eight riparian zones with contrasting hydrogeology. Biogeochemistry 71, 259–283.

Vidon, P.G., Hill, A.R., 2006. A landscape-based approach to estimate riparian hydrological and nitrate removal functions. JAWRA J. Am. Water Resour. Assoc. 42, 1099–1112.

Vidon, P.G.F., Hill, A.R., 2004. Landscape controls on nitrate removal in stream riparian zones. Water Resour. Res. 40.

Vilain, G., Garnier, J., Roose-Amsaleg, C., Laville, P., 2012. Potential of denitrification and nitrous oxide production from agricultural soil profiles (Seine Basin, France). Nutr. Cycl. Agroecosystems 92, 35–50.

Weiss, R.F., Price, B.A., 1980. Nitrous oxide solubility in water and seawater. Mar. Chem. 8, 347–359. doi:10.1016/0304-4203(80)90024-9

Weng, P., Sánchez-Pérez, J.M., Sauvage, S., Vervier, P., Giraud, F., 2003. Assessment of the quantitative and qualitative buffer function of an alluvial wetland: hydrological modelling of a large floodplain (Garonne River, France). Hydrol. Process. 17, 2375–2392. doi:10.1002/hyp.1248

Wetzel, R.G., 1992. Gradient-dominated ecosystems: sources and regulatory functions of dissolved organic matter in freshwater ecosystems, in: Dissolved Organic Matter in Lacustrine Ecosystems. Springer, pp. 181–198.

Winter, T.C., 1998. Ground water and surface water: a single resource. DIANE Publishing Inc.

Winter, T.C., 1999. Relation of streams, lakes, and wetlands to groundwater flow systems. Hydrogeol. J. 7, 28–45.

Woessner, W.W., 2000. Stream and Fluvial Plain Ground Water Interactions: Rescaling Hydrogeologic Thought. Ground Water 38, 423–429. doi:10.1111/j.1745-6584.2000.tb00228.x

World Health Organization, 2004. Guidelines for drinking-water quality: recommendations. World Health Organization.

Yan, B., Fang, N.F., Zhang, P.C., Shi, Z.H., 2013. Impacts of land use change on watershed streamflow and sediment yield: An assessment using hydrologic modelling and partial least squares regression. J. Hydrol. 484, 26–37. doi:10.1016/j.jhydrol.2013.01.008

Yao, J.M., Sánchez-Pérez, J.M., Sauvage, S., Teissier, S., Attard, E., Lauga, B., Durant, R., Julien, F., Bernard-Jannin, L., Ramburn, H., Gerino, M., n.d. Biodiversity, ecosystem purification function and service in alluvial wetlands. Ecol. Eng.

Yoshinari, T., Knowles, R., 1976. Acetylene inhibition of nitrous oxide reduction by denitrifying bacteria. Biochem. Biophys. Res. Commun. 69, 705–710.

Zarnetske, J.P., Haggerty, R., Wondzell, S.M., Baker, M.A., 2011. Labile dissolved organic carbon supply limits hyporheic denitrification. J. Geophys. Res. Biogeosciences 116.

Zarnetske, J.P., Haggerty, R., Wondzell, S.M., Bokil, V.A., González-Pinzón, R., 2012. Coupled transport and reaction kinetics control the nitrate source-sink function of hyporheic zones. Water Resour. Res. 48.

Zhang, W.L., Tian, Z.X., Zhang, N., Li, X.Q., 1996. Nitrate pollution of groundwater in northern China. Agric. Ecosyst. Environ. 59, 223–231. doi:10.1016/0167-8809(96)01052-3

Annexes

Annexe 1 : Données

Annexe 2 : Publication soumise à *Ecological Engineering* : From hydrochemical observation to hydrological conceptualization: a multi-criteria assessment in four different riparian zones

Annexe 3 : Publication parue dans *Hydrological Processes* : « Improved simulation of river water and groundwater exchange in an alluvial plain using the SWAT model »

Annexe 1: Données

Cette annexe contient les données récoltées dans les piézomètres installés à Monbéqui et dans la Garonne lors des 12 campagnes d'échantillonnage (avril 2013-mai 2014)

.

Piézomètre	Campagne	Date	Profondeur (m)	Charge hydraulique (m)	O2 (%)	O2_2 (mg/L)	T (°C)	pH	EC (µS/cm)	ORP (mV)	DOC (mg/L)	Alk (mg/L)	P-PO4 (µg/L)	NH4 (µg/L)	NO3 (mg/L)	NO2 (µg/L)	Cl (mg/L)	SO4 (mg/L)	Ca (mg/L)	Mg (mg/L)	Na (mg/L)	K (mg/L)	SiO2 (mg/L)	dO18 (‰)	DEA_sed (µg N-N2O / h/g sed sec)	DEA_OM (µg N-N2O / h/g MO)
P10	1	4/9/2013	2.75	87.61	21.8	2.32	12.2	7.02	1037		1.302	6.2	18.2	0	47.8		78.7	93.3	107.6	28	32.3	2.7	11.4	-9.62		
P11	1	4/9/2013	2.84	87.54	76.1	8.09	12.2	7.16	1034		0.923	5.3	27.2	7.4	139.4		63.3	73.5	114.2	28.1	30	2	11.7	-8.24	0.001160046	0.139603246
P13	1	4/9/2013	0.63	87.13	6.7	0.74	11	6.98	1307		4.87	8.3	45.4	0	32.5		96.7	151.8	191.8	31.7	56.5	1.4	23	-8.94	0.122730691	19.93522828
P14	1	4/10/2013	2.64	86.88	35	3.74	11.6	6.96	1208		1.469	7.6	31.9	0	59.7		86.6	106	97.9	23.1	37.3	1.5	16.7	-7.73	0.037985858	8.752085985
P16	1	4/10/2013	3.26	87.01	61	6.28	13.5	6.96	1076		0.783	6.1	6.6	0	94.4		70.7	93.7	110	22.7	28.4	3.8	14.7	-7.3	0.000242116	0.074574972
P17	1	4/8/2013	3.85	87.87	15.9	1.58	13.9	7.2	489		0.944	4.4	11.2	0	2.9		11.4	25.3	67.5	7.4	10.5	1.2	6.2	-10.66	0.004428303	1.040472971
P18	1	4/8/2013	3.71	87.88	6.5	0.68	13.3	7.08	337		0.698	2.9	0	211.9	2.9		8.7	19.4	61.4	7.6	8.8	1.3	6.1	-11.01	0.001409136	0.330683467
P2	1	4/8/2013	3.42	87.78	42.9	4.48	12.8	7.33	544		0.436	4.9	0	3.4	7.4		13.8	29.3	60	14.1	12	1.5	8	-9.84	0.002797421	0.762106286
P22	1	4/10/2013	2.33	87.72	53.1	5.68	12	7	989		0.672	5.9	16.3	3.5	78.2		66.5	72.1	125.6	22.2	27.3	2.6	13.8	-7.62	0.001051213	0.378387681
P26	1	4/10/2013	1.68	87.32	73	7.69	12.6	7.29	850		0.651	5.1	28	0	62.9		57.5	63.2	82.6	19.7	23.4	3.7	12.8	-8.11	0.000486843	0.120748964
P28	1	4/10/2013	4.34	89.04	64.1	6.59	13.7	7.25	876		0.692	5.9	3.5	185.9	42.4		52.2	67.8	72.2	19.7	28.2	2.5	12.1	-7.89		
P3	1	4/9/2013	3.24	87.62	51.3	5.38	12.7	7.25	600		0.394	5.2	0	4.3	44.1		16.1	5.7	65.5	15.8	14.2	1.6	8.8	-9.92	0.055344105	5.597302227
P30	1	4/10/2013	3.76	90.09	83	8.48	14.1	7.2	747		0.482	5.5	63.5	0	36.2		35.8	41	51.6	19.7	25.9	4	14	-8.72		
P6	1	4/9/2013	1.25	87.3	4.3	0.46	11.2	7.08	626		1.241	5.4	19.7	523.4	6		20.5	38.4	77.9	14.6	14.3	1.2	7.9	-10.01	0.151036967	35.54654666
P7	1	4/9/2013	2.6	87.6	34	3.64	12.1	6.92	1515		0.661	7.9	17.3	20.9	31.4		151.6	194.2	171.9	35.5	43.9	4.4	11.3	-8.29	0.007658349	1.25513687
P9	1	4/9/2013	1.72	87.23	19.7	2.11	11	6.95	924		1.703	6.5	2.4	1.4	60.7		38.1	68.2	140.1	21.8	21	2.4	9	-8.68	0.000696197	0.126821221
PA	1	4/8/2013	3.8	87.96	28	2.95	12.6	7.35	439		0.627	3.9	0	0	5.3		9.8	22.9	75.5	8.3	9.2	1.1	6.6	-10.64	0.001012322	0.37207561
PB	1	4/8/2013	3.39	87.78	68.6	7.17	12.7	7.11	471		0.625	4.4	0	0	6.8		9.2	20.6	76	10.5	8.7	1.2	7.5	-10.12	0.002636449	1.598268702
PC	1	4/8/2013	3.42	87.86	60	6.05	14.1	6.98	473		0.446	4.2	0	0	6.6		11.5	26.7	85.4	13.3	11.4	2	8.3	-10.43	0.000527136	0.157507707
PD	1	4/8/2013	3.71	87.63	47.9	5.14	11.7	7.28	429		0.636	3.6	0	0	5		11.4	22.3	64.2	9.7	8.9	1.1	7	-10.65	0.003070392	1.302174618
PE	1	4/8/2013	2.25	87.77	69.9	7.29	13	6.9	696		0.583	5.6	0	0	24.8		27.8	45.1	70.9	21.6	20	4.2	12.3	-9.46	0.001923411	1.204406492
PF	1	4/9/2013	3.32	87.48	39.2	4.12	13	7.06	896		1.105	6.8	34.7	154.6	20.6		46.7	67.1	73.5	23.5	21.9	2.9	10.9	-9.63	0.001847577	0.461457806
PG	1	4/9/2013	2	87.75	31.3	3.35	12.6	7.03	832		0.85	6	10.9	0	36		43.8	61.8	79.7	25	26	4.3	12.7	-9.47	0.001776398	0.538327364
PH	1	4/9/2013	2.95	87.14	53.9	5.72	12.2	7.09	1078		0.986	5.8	8.1	0	84.4		88.9	91.3	116.6	28.8	31.7	2.6	9.8	-8.71	0.001236739	0.48982585
PI	1	4/10/2013	3.52	87.23	61	6.34	13.3	6.98	1070		0.992	6	21.7	0	108.4		72.1	79.3	91.2	26.1	28.2	2.4	13.4	-7.8	0.005789197	1.604164175
R1	1	4/8/2013			96	10.89	9.1	8.26	311		1.843	2.8	380.7	194.5	7.9		8.2	16.9	56.9	7	6.4	1.2	4.8	-11.02	0.256691189	23.89694244
R2	1	4/10/2013			88	9.68	10	7.88	320		1.749	2.6	5.5	47.4	8.2		8.8	19	56.6	6.6	7.2	1.2	5	-10.73	5.123060981	90.38869526
P10	2	5/13/2013	2.68	87.68	4.9	0.52	12.8	6.94	1043		1.2	6.4	0	16.7	43.3	12.8	72.985	90.7	80.5		32.7	2.8	12.5	-8.94		
P11	2	5/13/2013	2.79	87.59	80.3	8.47	12.8	7.07	1012		1.062	5.4	0	7.7	112.8	0	63.28	70.3	102.6	22.7	29.2	2.1	10.3	-7.63		
P13	2	5/14/2013	0.65	87.11	3.4	0.35	12.3	6.88	1471		4.85	8.4	2.4	19.4	38.9	885.9	118.56	160.3	104.7	32.5	65	2.2	19.9	-7.84		
P14	2	5/14/2013	2.54	86.98	8.5	0.91	12.2	6.93	1150		1.433	7	0	10.7	59.5	463	75.262	89	98.3	25.3	34.6	1.5	17.5	-7.18		
P16	2	5/14/2013	3.12	87.15	60.3	6.26	13.2	6.88	1077		0.878	5.7	0	11.4	96.2	0	73.848	93.8	133	26.8	29.5	3.5	14.2	-7.37		
P17	2	5/13/2013	3.79	87.93	1.2	0.13	13.7	7.19	477		0.889	4.2	0	16.5	1.5	0	10.801	23.3	48.8	5.2	10	1.5	8.2	-10.53		
P18	2	5/13/2013	3.69	87.9	6.5	0.65	13.1	7.08	339		0.857	2.8	0	8.7	2.4	0	7.573	17.2	56.9	5	8.2	1.4	10.2	-10.32		
P2	2	5/13/2013	3.51	87.69	38.6	4.12	12.7	7.17	511		0.658	4.5	0	17.5	5.8	0	12.215	25.3	49.5	8.7	10.6	1.6	6.6	-10.59		
P22	2	5/13/2013	2.28	87.79	57.5	6.08	12.7	6.97	1010		0.846	5.9	0	9.5	80.7	0	67.932	74.2	110.1	24.1	28.2	2.6	14.7	-8.31		
P26	2	5/14/2013	1.58	87.42	72.8	7.54	13.2	7.08	848		1.11	4.9	0	14.5	63.6	0	58.561	60.8	109.2	20.1	24.6	3.8	13.3	-8.5		
P28	2	5/14/2013	4.31	89.07	66.5	6.87	13.3	6.96	959		1.031	6.1	0	12.1	53.3	0	60.739	75.1	72.1	21	30.8	2.7	15.3	-8.57		
P3	2	5/13/2013	3.06	87.8	36.7	3.86	12.9	7.13	548		0.695	4.9	0	8.4	5.2	0	12.684	28.2	95.3	10.1	12.4	1.8	12.1	-10.71		
P30	2	5/14/2013	3.59	90.26	88.8	9.1	13.6	7.14	754		1.383	5.4	0	8.5	37.2	0	36.874	42.6	106.4	19.3	27.7	4.2	15.5	-9.18		
P6	2	5/13/2013	1.15	87.4	0.9	0.09	11.7	7.08	507		1.134	4.6	11.8	413.8	0.6	0	13.37	23.5	57.7	8.2	11.1	1.3	11.4	-9.91		
P7	2	5/13/2013	2.47	87.7	26	2.77	12.3	6.83	1555		2.173	8.3	0	16.3	22.8	0	147.82	193.9	161.5	34	46.5	4.5	11.9	-9.46		
P9	2	5/13/2013	1.67	87.28	6.9	0.74	11.6	6.88	939		1.795	6.9	0	9.6	43	18.6	40.618	73.2	84.4	16.7	20.6	2.4	14	-9.12		
PA	2	5/13/2013	3.68	87.84	24	2.57	12.4	7.3	443		0.782	3.9	0	6.4	4.6	0	9.884	21.8	70.4		9.1	1.4	9.3	-10.91		
PB	2	5/13/2013	3.24	87.93	50.6	5.29	13	7.06	515		0.808	4.8	0	12	6.6	0	9.421	21.8	49.7	7.6	9.2	1.5	10.3	-10.89		
PC	2	5/13/2013	3.35	87.93	16.9	1.74	14	7.1	437		0.663	3.8	0	18.6	4.3	0	10.457	23.9	32.6	7.8	10.1	1.8	11	-11.05		
PD	2	5/13/2013	3.69	87.65	34.9	3.84	11.5	7.14	386		0.801	3.4	0	11.9	2.5	0	8.983	18	58	5.3	7.4	1.1	6.9	-11.54		
PE	2	5/13/2013	2.15	87.87	69.1	7.19	13.4	6.92	639		0.721	5.2	0	13.5	16	0	22.275	38	37.9	14.5	17	3.7	12.1	-9.74		
PF	2	5/13/2013	3.17	87.63	31.9	3.34	13.2	6.89	862		1.455	6.8	0	16	14.8	0	40.367	62	81.2	17.5	21.4	2.8	12	-10.47		
PG	2	5/13/2013	1.92	87.83	37.6	3.95	12.9	6.99	802		1.064	5.8	0	19	35.5	0	39.48	56.1	57.5	18.8	24.3	3.9	12.3	-9.56		
PH	2	5/14/2013	2.91	87.18	45.1	4.78	12.2	7.04	1126		1.329	6	0	12.1	74.7	24.1	89.12	98.4	87.2	24.5	34.7	2.6	13.2	-9.48		
PI	2	5/14/2013	3.44	87.31	62.7	6.53	13.3	6.95	1099		1.065	5.9	0	17.2	111.5	0	74.06	83.6	82.5	25.7	28.2	2.4	14.5	-8.13		
R1	2	5/13/2013			100.9	11.1	11.1	8.04	196.7		1.337	1.7	5.4	45.6	3.9	9.8	4.58	11.5	34.1	3	4	0.9	5.1	-12.54		
R2	2	5/14/2013			96.4	10.36	11.7	7.3	204		1.529	1.6	6.1	44.9	4.4	14.5	5.17	12.6	35.4	3.3	4.5	0.8	5.2	-12.21		

Piézomètre	Campagne	Date	Profondeur (m)	Charge hydraulique (m)	O2 (%)	O2_2 (mg/L)	T (°C)	pH	EC (µS/cm)	ORP (mV)	DOC (mg/L)	Alk (mg/L)	P-PO4 (µg/L)	NH4 (µg/L)	NO3 (mg/L)	NO2 (µg/L)	Cl (mg/L)	SO4 (mg/L)	Ca (mg/L)	Mg (mg/L)	Na (mg/L)	K (mg/L)	SiO2 (mg/L)	dO18 (‰)	DEA_sed (µg N-N2O / h/g sed sec)	DEA_OM (µg N-N2O / h/g MO)
P10	3	6/10/2013	1.75	88.61	15.6	1.64	13	6.98	923		1.172	6.2	0	15.3	46.3	0	48.898	61.7	107.2	20.5	26.5	2.7	11.8	-9.04		
P11	3	6/11/2013	1.83	88.55	84.5	8.81	13.2	7.04	948		1.544	5.3	0	3.8	129.1	0	38.275	51.2	105.4	20.9	22.2	1.9	12	-8.34		
P13	3	6/11/2013	0.16	87.6	9.4	0.98	12.4	6.86	1235		2.049	7.2	30.9	12.8	46.1	29.4	85.998	113.7	140.4	28	41.9	2.2	13.2	-8.4		
P14	3	6/11/2013	1.9	87.62	7.9	0.84	12.9	6.83	1116		1.923	7.5	0	5.5	92.5	429.5	48.023	68.7	135.6	25.9	27.1	1.4	19	-7.59		
P16	3	6/11/2013	2.41	87.86	28.9	3.01	13.2	6.78	1420		1.814	8	0	19.5	53.9	0	90.861	176.5	193.6	37.1	41.4	3.9	15.9	-8.76		
P17	3	6/10/2013	3.15	88.57	8.8	0.9	13.7	6.98	749		1.297	5.2	0	5.3	15.2	0	15.634	36	80.5	8.4	14.3	1.5	8.1	-9.93		
P18	3	6/10/2013	2.77	88.82	28.1	2.92	13.3	6.72	585		0.967	6.1	0	7.8	10.1	0	17.667	32.3	49.4	9.6	11.4	1.6	5.9	-9.86		
P2	3	6/10/2013	2.88	88.32	33.6	3.51	13.1	7.04	758		0.862	6.5	0	5	8.1	0	27.786	42.9	44.3	13.3	16.5	2	10.5	-10.17		
P22	3	6/11/2013	1.28	88.77	63.3	6.6	13.2	6.94	1106		1.016	6.1	1.6	8.1	111.3	0	70.235	82.3	116.3	26.3	30.9	2.6	14.1	-8.3		
P26	3	6/11/2013	1.15	87.85	76.4	7.8	14.2	7.05	808		0.862	4.7	0	8.4	53.8	0	48.098	52.5	82.9	18.7	24.2	3.5	8.2	-8.73		
P28	3	6/11/2013	3.5	89.88	59.9	6.25	13.2	6.88	1001		1.07	5.6	0	10.1	62.3	0	60.079	77.1	114.6	21	28.5	2.6	14.7	-8.75		
P3	3	6/10/2013	2.46	88.4	23.2	2.39	13.7	6.95	855		0.923	4.8	0	6.5	10.7	0	34.901	54	45.7	16.5	20.6	2.2	11.3	-9.43		
P30	3	6/11/2013	3.22	90.63	86.7	8.94	13.6	7.14	751		0.801	4.7	0	8.5	36.2	0	34.847	39.8	77.7	18.8	27.4	4.1	14.8	-8.78		
P6	3	6/10/2013	0.29	88.26	1.5	0.16	12.1	7.08	500		1.61	4.8	26.4	241.6	0.6	0	11.524	19.3	76.3	7.8	9.9	1.1	10.6	-10.9		
P7	3	6/10/2013	1.66	88.54	9.6	1.02	12.7	6.81	1509		1.99	8.4	0	11.4	18.5	0	135.9	183.3	104.6	33.2	51.9	4.3	12.1	-9.27		
P9	3	6/10/2013	1.06	87.89	7	0.75	12.2	6.84	962		1.67	6.7	0	8.6	43.9	0	46.938	69.8	139	18.3	21.8	2.5	13.8	-9.38		
PA	3	6/10/2013	3.05	88.47	35.9	3.78	12.6	7.13	668		1.577	4.6	0	4.4	14.4	0	20.412	52.5	110.1	9.1	11.7	1.5	8.5	-10.23		
PB	3	6/10/2013	2.62	88.55	32.2	3.34	13.5	6.9	727		0.96	5.2	0	7.6	15.5	0	23.678	42.1	76.5	12.4	14.6	1.8	9.6	-10.21		
PC	3	6/10/2013	2.39	88.89	31.2	3.21	13.6	6.82	1300		1.751	5.8	0	15.2	37.9	0	98.035	141.2	90.2	31.8	38.7	1.8	11.3	-9.94		
PD	3	6/10/2013	2.88	88.46	55.4	5.88	12.3	7.12	614		1.056	5	0	8	15.3	0	15.285	28.6	95.4	9.3	10.7	1.5	8.9	-8.57		
PE	3	6/10/2013	1.13	88.89	63.7	6.54	13.8	6.87	734		0.968	5.2	0	9.5	27.5	0	28.651	42.6	82.9	16.1	19.3	3.6	11.5	-9.2		
PF	3	6/10/2013	2.55	88.25	27.6	2.86	13.4	6.79	1232		3.133	3.4	0	13.6	49.4	0	79.407	109.3	125.2	25	31	3.3	12.8	-8.98		
PG	3	6/10/2013	0.88	88.87	63.7	6.6	13.3	7	869		1.092	3.4	0	11.2	47.2	0	44.9	60.5	133	21	26.4	3.9	12.9	-9.3		
PH	3	6/10/2013	2.24	87.85	43	4.53	12.8	7.03	1002		1.326	4.6	0	16.4	59.5	51.6	67.545	76.7	131	22.9	30.5	2.5	12.9	-9.42		
PI	3	6/11/2013	2.74	88.01	63.7	6.62	13.4	6.9	1033		0.743	6	0	9.1	84.1	0	67.056	77.8	109.9	24.9	29.7	2.5	8.7	-7.23		
R1	3	6/10/2013			99.7	10.5	12.6	7.97	253		2.564	2	8.8	59.9	6.4	19.3	6.78	13.7	41.2	4	5.2	1.4	5.5	-10.99		
R2	3	6/11/2013			100.8	10.69	12.5	7.95	249		3.12	2	6.8	72.3	6.4	17.9	6.546	13.1	43.1	4.3	5.2	1.4	5.9	-10.74		
P10	4	7/2/2013	2.46	87.9	10.5	1.07	13.8	6.98	859	198.5	1.735	6.5	0	25.4	46.9	3.5	38.708	49.9	98.4	17.4	19	2.4	12.2	-9.15	0.05909244	8.898385359
P11	4	7/2/2013	2.44	87.94	80.8	8.25	13.9	7.18	950	200.5	1.637	5.5	0	77.8	117.4	0	48.041	56.5	133.4	19.1	19.3	1.7	12.3	-7.9	0.002177428	0.267966679
P13	4	7/3/2013	0.74	87.02	5.7	0.59	13.2	6.86	1331	12.2	4.061	9	31	11	35.6	88.5	98.012	132.9	186.4	29	57.2	2	21.3	-6.75	0.048937929	6.66394396
P14	4	7/2/2013	2.62	86.9	6.7	0.69	13.6	6.91	1205	130.2	1.961	7.3	0	10.4	82.3	427.5	76.741	95	136	25	29.4	1.6	17.8	-8.53	0.071288004	11.53523367
P16	4	7/2/2013	3.1	87.17	19.8	2.04	13.4	6.84	1330	238.5	1.996	8.1	5	10.1	65.5	0	86.519	159.3	194.6	32.4	32.1	3.4	15.3	-8.65	0.03793688	5.252307284
P17	4	7/1/2013	4.01	87.71	10	1.02	14.1	7	850	247.4	1.862	7.2	0	15.2	25.3	0	23.541	50.4	145.1	9.3	15.1	1.4	6.7	-9.04	0.061237668	9.261406337
P18	4	7/1/2013	3.57	88.02	24.8	2.58	13.6	6.75	722	279.1	1.846	5.4	0	11.9	30.8	0	25.017	44.8	113.8	11.5	12.4	1.6	6.8	-10.25	0.009163743	1.156973763
P2	4	7/1/2013	3.75	87.45	28	2.91	13.4	7.01	898	243.8	1.561	7.2	0	8.6	8.9	0	42.328	57.5	111.5	12.1	13.9	1.6	8.7	-7.38	0.01621793	2.361921611
P22	4	7/2/2013	1.83	88.22	64.6	6.6	13.9	6.97	1064	243	1.464	5.4	0	7.4	100.2	0	73.082	79.9	150.4	23.9	25.2	2.4	14.4	-7.74	0.001163835	0.188383617
P26	4	7/3/2013	1.1	87.9	74.5	7.56	14.5	7.06	825	219.1	1.23	5	0	4.6	62.2	0	50.085	56.1	112.3	17.9	22.6	3.4	13.1	-6.54	0.000604986	0.083516323
P28	4	7/3/2013	3.79	89.59	72.2	7.5	13.4	6.91	1080	235	1.934	6.5	0	14.8	68.3	0	74.705	90.7	159.9	21.3	28	2.6	15.1	-7.18	0.000261247	0.039471671
P3	4	7/1/2013	3.26	87.6	20.5	2.07	14.5	6.94	957	185	1.643	6.3	0	18.8	11.4	0	45.424	64.7	100.1	14.9	17.4	1.8	9	-9.23	0.067447267	8.083485075
P30	4	7/3/2013	3	90.85	89.9	9.28	13.7	7.1	757	211.8	1.195	5.5	0	0	40.4	0	37.128	41.6	101.8	17.8	24.9	3.9	16.5	-7.92	0.000984612	0.128147494
P6	4	7/2/2013	1.33	87.22	2.2	0.24	12.7	6.98	808	-38.4	2.313	6.3	14.4	631.6	20.8	0	35.435	54.8	106.8	10.6	13.5	1.3	10.4	-8.28	0.144330847	21.01013388
P7	4	7/2/2013	2.39	87.81	3.1	0.31	13.2	6.84	1358	253.7	2.187	8.4	0	6.9	21.4	0	111.31	160.1	110.8	25.5	38.4	3.5	12.3	-9.5	0.024755854	2.364548389
P9	4	7/2/2013	1.79	87.16	11.7	1.22	12.8	6.9	993	247.7	2.094	7	0	0	54.4	0	48.845	71	117.3	16.3	18.9	2.2	15	-8.88	0.000977749	0.155431893
PA	4	7/1/2013	3.95	87.57	34.7	3.62	13.2	7.19	648	236.6	1.487	5.6	0	7.3	11.9	0	16.755	37.1	114.1	8.1	10.3	1.4	7.4	-10.15	0.00161236	0.509156359
PB	4	7/1/2013	3.36	87.81	21.8	2.22	14	6.95	774	248.9	1.597	6.5	0	18.1	17.4	0	27.029	45.7	88.3	12.9	15	1.9	8.9	-9.48		
PC	4	7/1/2013	3.16	88.12	33.2	3.4	13.9	6.85	1076	250.5	1.781	6.8	0	6.8	17.5	0	68.822	108.7	155.8	23.6	28.7	1.8	9	-7.86	0.002370314	0.381698689
PD	4	7/1/2013	3.99	87.35	49.3	5.15	12.9	7.09	661	251.1	1.452	5.7	0	91.4	12.1	0	16.807	32.3	93.4	9.9	11.2	1.6	8.3	-10.01	0.084119699	11.77730978
PE	4	7/1/2013	1.88	88.14	64.8	6.6	14.2	6.98	802	258.6	1.596	6	0	6.6	41.9	0	36.589	47.6	99.3	16.6	18.9	3.6	12.2	-9.13	0.013145529	2.503281218
PF	4	7/2/2013	3.37	87.43	21.1	2.18	13.7	6.85	1165	247.8	2.393	5.7	0	0	35	0	77.242	106.2	186.6	22.8	30.5	3	11.4	-9.36	0.002271335	0.343227866
PG	4	7/2/2013	1.63	88.12	60	6.15	14	7.04	887	244.8	1.601	5.7	0	6.9	62.4	0	49.791	58.2	132.6	19.8	22.7	3.4	13.2	-8.21	0.005562309	0.828409693
PH	4	7/2/2013	2.98	87.11	38.2	3.94	13.4	7.05	993	226	2.392	6.3	0	1.3	58.8	139.4	64.617	74.1	144	21.6	28.5	2.3	13	-9.1	0.017451079	2.888570351
PI	4	7/3/2013	3.38	87.37	65.8	6.78	13.6	6.95	1054	248.9	1.165	6	0	3.3	91	0	71.137	79.5	110.8	24.4	28	2.4	15.2	-7.93	0.006532049	1.135418008
R1	4	7/1/2013			101.1	9.65	17	7.92	240	203.7	1.992	1.7	6.8	38.7	5	16	5.599	15	36.1	3.2	5.1	1	4.6	-10.68	0.523927923	29.17952009
R2	4	7/2/2013			101.8	9.68	17.3	7.9	211	193.4	1.58	2	0	2.4	4.6	22.5	5.454	14.7	34.5	3.1	5.1	1	5.1	-11.74	3.844256956	60.45867211

Piézomètre	Campagne	Date	Profondeur (m)	Charge hydraulique (m)	O2 (%)	O2_2 (mg/L)	T (°C)	pH	EC (µS/cm)	ORP (mV)	DOC (mg/L)	Alk (mg/L)	P-PO4 (µg/L)	NH4 (µg/L)	NO3 (mg/L)	NO2 (µg/L)	Cl (mg/L)	SO4 (mg/L)	Ca (mg/L)	Mg (mg/L)	Na (mg/L)	K (mg/L)	SiO2 (mg/L)	dO18 (‰)	DEA_sed (µg N-N2O / h/g sed sec)	DEA_OM (µg N-N2O / h/g MO)
P10	5	7/29/2013	3.41	86.95	3.4	0.35	14.4	6.93	883	165.2	1.017	6.5	0	109.6	60.3	27.3	51.918	62.5	94.1	19.4	21.7	2.7	10.7	-8.74		
P11	5	7/29/2013	3.44	86.94	71.2	7.26	14.3	6.99	1030	202.7	0.51	5.9	0	85.4	121.2	8.1	75.785	81.7	111.8	23.2	26.2	2.3	12.3	-8.28		
P13	5	7/30/2013	1.47	86.29	5.3	0.55	14.5	6.84	1122	80	1.354	7.8	9.6	125	74.7	251.4	86.52	106.2	178.3	26.6	38.4	2.4	16.7	-7.5		
P14	5	7/30/2013	3.29	86.23	11.9	1.23	13.9	6.81	1160	192.6	0.659	6.6	0	80.1	100.6	363.4	98.82	112.2	121.4	27.5	33.5	2.3	14.7	-7.58		
P16	5	7/30/2013	3.86	86.41	59.2	6.12	13.8	6.86	1147	236.2	0.552	5.7	0	92.3	133.9	0	100.22	122.6	175	29.3	30.8	3.6	13.4	-6.06		
P17	5	7/29/2013	4.84	86.88	3.5	0.35	14	6.92	840	250.3	0.969	6.7	0	231.3	22.5	0	34.217	65.7	157.1	10.3	17.6	1.7	8.8	-10.4		
P18	5	7/29/2013	4.47	87.12	13.8	1.42	13.7	6.75	911	233.3	1.119	5.9	0	164.6	70	0	47.519	83.8	160.2	15.9	16.1	2.2	10.5	-9.29		
P2	5	7/29/2013	4.52	86.68	13.4	1.38	13.8	6.89	1006	250.8	1.328	8.4	0	114.2	16.5	0	61.881	85.9	79.5	18	23	2.4	11.3	-9.37		
P22	5	7/30/2013	2.68	87.37	61.5	6.22	14.9	6.94	1085	201.6	0.899	5.9	0	81.1	124	0	94.975	99.5	100.5	26.2	27	2.9	8.8	-6.64		
P26	5	7/30/2013	1.75	87.25	63.8	6.39	15.2	7.01	882	210.1	0.526	5	0	89.9	97	0	66.629	73.8	135.1	20.7	26.6	4.1	13.6	-8.75		
P28	5	7/30/2013	4.56	88.82	64.2	6.64	13.9	6.9	1094	234.2	0.652	6.5	0	169.4	83.5	0	96.222	113.3	92.8	23	31.4	3	12.8	-8.58		
P3	5	7/29/2013	4.13	86.73	7.7	0.79	14.3	6.92	863	76.6	1.036	7.1	0	58.2	16.3	510.4	36.794	63.9	136.7	16.6	18.9	2.3	9.1	-9.67		
P30	5	7/30/2013	3.3	90.55	89.9	9.26	14	7.06	751	223.3	0.549	5.6	0	56.9	50.3	0	44.692	51.6	72	19.2	27	4.3	14.9	-8.47		
P6	5	7/29/2013	2.08	86.47	1.9	0.18	14.1	6.87	912	-38.5	1.46	7.1	19.3	1691.4	20.6	53.8	53.023	71	119.2	14.5	19.7	2	13.4	-8.16		
P7	5	7/29/2013	3.32	86.88	1.4	0.15	13.9	6.81	1300	265.2	1.228	8.2	0	62.1	27.8	0	122.18	169.3	147.7	27.7	41.5	4.1	9.8	-9.57		
P9	5	7/29/2013	2.53	86.42	6.2	0.64	13.8	6.86	949	260.5	1.141	6.8	0	75	56.6	19.2	53.591	75.5	82	17.6	22.9	2.6	13.1	-8.97		
PA	5	7/29/2013	4.73	86.79	10.4	1.08	13.4	7.03	713	256.6	0.586	5.9	0	71.1	18.3	0	26.068	49	133.9	9.7	13.3	1.8	5	-10.19		
PB	5	7/29/2013	4.28	86.89	9.2	0.94	14	6.93	830	242.8	0.445	6.8	0	64.6	29.6	0	38.951	64.5	79.2	13.3	17.1	2.3	9.9	-7.81		
PC	5	7/29/2013	4.11	87.17	28	2.89	14	6.77	1086	215.5	0.881	6.5	0	80.4	71.5	0	71.71	114.6	91.2	21.1	28.3	2.7	10.6	-9.34		
PD	5	7/29/2013	4.67	86.67	29.4	3.07	13.3	7	752	240.5	0.536	6.2	0	118.3	22.6	0	31.268	51.5	138.9	12.5	14.3	2.1	9.7	-9.11		
PE	5	7/29/2013	2.86	87.16	78.2	7.98	14.3	7	896	244.2	0.325	5.3	0	67.2	99.2	0	64.246	70.7	142	21.4	21.9	5	11.6	-7.55		
PF	5	7/29/2013	4.17	86.63	11.4	1.16	14.3	6.81	1214	240.8	1.195	5.5	0	37.9	35.7	0	108.13	142.8	185.8	26.2	35.6	3.6	12	-9.16		
PG	5	7/29/2013	2.6	87.15	67.1	6.84	14.3	7	887	241.4	0.408	5.5	0	164.7	82.9	0	65.251	68.1	143.2	20.8	23.5	3.9	12.2	-8.57		
PH	5	7/30/2013	3.78	86.31	19.2	1.97	14	6.95	1011	191.5	0.74	6.5	0	40	78.8	31.1	76.793	87.7	163.7	22.9	30.5	2.6	12.8	-9.42		
PI	5	7/30/2013	4.08	86.67	63.4	6.52	13.9	6.91	1128	232.1	0.481	6	0	58.1	134.1	0	96.477	108.8	142.6	27.3	28	2.8	13.9	-8.17		
R1	5	7/29/2013			93.6	8.28	21.4	7.9	216	206.5	1.201	1.5	16.8	87.6	7.5	60.5	8.249	20.7	38.7	3.5	6.7	1.6	4.2	-11.6		
R2	5	7/30/2013			92.2	8.3	20.5	6.66	232	194.6	1.043	1.7	11.5	165	7.2	50.8	8.363	21.4	38.6	3.6	6.6	1.4	3.6	-11.76		
P10	6	9/2/2013	4.16	86.2	2	0.2	15.1	6.87	930	170	0.571	6.1	0	101.7	71	36.9	65.793	78.8	96.3	14.6	17.8	2.1	12.3	-8.77		
P11	6	9/3/2013	4.16	86.22	74.2	7.49	14.9	7.02	1059	229	0.257	6	0	52.6	119	0	86.981	91.5	181.2	27.9	33.6	2.7	12.5	-7.41		
P13	6	9/3/2013	2.13	85.63	16.7	0.77	15.3	6.89	1112	230	0.677	6.5	26	54.6	113.8	139.7	92.199	100.7	190.3	28	34.8	2.8	16.2	-9.2		
P14	6	9/3/2013	3.88	85.64	33.7	3.43	14.5	6.85	1151	208	0.401	6.2	2.9	102.4	124.4	0	101.34	120.1	180	30.1	33.2	2.6	14.5	-7.73		
P16	6	9/3/2013	4.4	85.87	61.2	6.21	14.8	6.93	1083	184	0.363	5.3	5.9	52.6	131.6	13.6	99.059	111.1	183	29.7	32.6	3.8	13.6	-8.01		
P17	6	9/2/2013	5.57	86.15	1.4	0.15	14.2	7.08	719	206	0.691	5.9	2	69.2	20.2	0	29.55	50.9	138.4	10.1	14.8	2	8.1	-10.29		
P18	6	9/2/2013	5.13	86.46	15.1	1.55	14.2	6.74	1062	225	1.301	5.6	3.1	76.8	46.9	0	72.58	143.4	187.2	19.6	24.5	2.8	11.3	-10.08		
P2	6	9/2/2013	5.22	85.98	16.7	1.72	14.1	6.92	995	219	0.6	5	0	65.5	30.3	0	67.466	91	136.5	22.2	29	3.1	11.8	-9.5		
P22	6	9/3/2013	3.23	86.82	60.4	2.98	15.8	6.97	1061	216	0.535	5.6	7	49.1	118.1	0	96.156	97.9	163.9	27.5	30.6	3.2	14.4	-7.64		
P26	6	9/3/2013	2.2	86.8	67	6.45	17	7.02	879	216	0.384	5	0	49.7	102.3	0	67.596	76.2	145	22.5	30.9	4.5	14.7	-8.67		
P28	6	9/3/2013	5.26	88.12	56	5.69	14.5	6.98	1087	240	0.609	6.2	0	122.9	88.2	0	103.06	119.8	175.3	26.1	37.5	3.3	15.4	-7.4		
P3	6	9/2/2013	4.81	86.05	3.4	0.33	15	6.95	853	217	0.443	7.3	0	59.7	25.3	0	42.449	68.2	165.6	19.4	22.9	2.7	10.9	-8.79		
P30	6	9/3/2013	3.67	90.18	92.8	9.38	14.8	7.14	752	230	0.162	5.2	0	99.9	59.6	0	46.841	55.3	121.8	20.5	29.9	4.6	16.1	-8.97		
P6	6	9/2/2013	2.79	85.76	1.3	0.13	15.1	6.7	911	-85	1.009	7.3	125.9	2778.4	14.8	0	59.3	69.9	177.3	17.3	24.6	2.4	14.5	-8.83		
P7	6	9/2/2013	4	86.2	5.6	0.57	14.9	6.64	1642	200	1.358	8.3	0	6	23.1	0	196.63	283.1	223.8	33.7	51.1	4.6	12.6	-8.82		
P9	6	9/2/2013	3.2	85.75	10.7	1.06	14.6	6.87	913	218	0.719	6.7	0	126.4	57.9	0	57.35	73.2	160.1	20.4	27.7	2.9	13	-9.34		
PA	6	9/2/2013	5.45	86.07	11.9	1.23	14.1	6.96	801	204	0.537	6.4	0	94.2	41	0	34.741	56.7	166.7	12.1	16	2	10.4	-9.99		
PB	6	9/2/2013	4.99	86.18	8.4	0.86	14.5	6.83	917	219	0.791	6.5	0	86.5	67.7	0	50.379	75.6	60.2	6.8	8.3	1.2	11.2	-9.62		
PC	6	9/2/2013	4.8	86.48	28.3	2.9	14.5	6.82	1019	199.5	1.01	6	0	107.9	107.9	0	71.614	99.5	166	21.8	24.8	3.4	11.3	-9.03		
PD	6	9/2/2013	5.48	85.86	28.2	2.93	13.6	7.01	793	220	0.726	6.4	2.6	16.6	33.9	0	37.363	55.6	117.8	14	16.8	2.2	10.4	-10.02		
PE	6	9/2/2013	3.51	86.51	70.3	7.03	15.3	7	1000	199	0.506	5.6	0	91.6	116.2	0	81.366	87.4	167.5	25.1	28	5.8	12.7	-8.49		
PF	6	9/2/2013	4.85	85.95	28	2.82	15	6.62	1182	215	0.964	5.8	0	69.7	35.5	0	107.85	140.8	212.5	27.2	37.5	4	13	-9.72		
PG	6	9/2/2013	3.26	86.49	69.3	6.99	14.9	7.04	1033	216.7	0.688	5.8	0	60.6	125.2	0	88.242	90.2	158.6	25.7	29.2	4.8	13.3	-8.37		
PH	6	9/3/2013	4.46	85.63	14.1	1.33	14.7	6.95	1036	223	0.862	6.5	0	84.1	97.1	0	78.442	87.2	179.1	25.6	33.8	2.9	13.9	-9.2		
PI	6	9/3/2013	4.67	86.08	59.4	6.03	14.6	6.88	1177	21	0.609	6.1	3.4	74.6	135.9	0	106.13	122.3	204.3	30.6	31.9	3.1	15.2	-8.22		
R1	6	9/2/2013			106.9	9.5	21.3	8.23	300	174	1.26	2.1	32.2	26.8	10.2	36.9	13.071	31.1	54.7	5.4	11	2.1	3.8	-10.88		
R2	6	9/3/2013			94.1	8.55	20.5	7.92	325	180	1.432	2.2	38.6	66.1	11.9	37	14.822	32.4	57.4	5.7	12.2	2.2	3.8	-11.05		

Piézomètre	Campagne	Date	Profondeur (m)	Charge hydraulique (m)	O2 (%)	O2_2 (mg/L)	T (°C)	pH	EC (µS/cm)	ORP (mV)	DOC (mg/L)	Alk (mg/L)	P-PO4 (µg/L)	NH4 (µg/L)	NO3 (mg/L)	NO2 (µg/L)	Cl (mg/L)	SO4 (mg/L)	Ca (mg/L)	Mg (mg/L)	Na (mg/L)	K (mg/L)	SiO2 (mg/L)	dO18 (‰)	DEA_sed (µg N-N2O / h/g sed sec)	DEA_OM (µg N-N2O /h/g MO)
P10	7	1/10/2013	4.32	86.04	1.8	0.18	15.7	6.99	937	169	0.512	5.9	0	0	60.7	0	51.46	58.3	168.058	23.953	28.073	3.26	7.7	-8.42		
P11	7	1/10/2013	4.3	86.08	65.9	6.48	15.3	7.04	1078	300	0.493	5.9	0	0	89.9	0	70.842	74	187.606	28.234	33.823	2.585	14	-7.74	0.000585394	0.108031876
P13	7	1/10/2013	2.17	85.59	16.6	1.64	15.6	6.94	1121	271	0.82	5.5	0	0	89.3	24.5	74.936	81.7	197.857	28.498	35.646	2.563	16.8	-7.25	0.016080157	2.184921567
P14	7	1/10/2013	3.92	85.6	43.2	4.28	14.8	6.92	1149	267	0.64	5.4	0	0	98.2	0	79.662	96.4	203.158	30.049	33.283	2.583	11.2	-7.64	0.013670934	1.927291679
P16	7	2/10/2013	4.48	85.79	62.8	6.23	15.2	6.96	1062	236	0.427	6.2	0	0	99.9	0	74.041	84	181.055	28.556	32.429	3.505	11.3	-8.13	0.001915412	0.355710064
P17	7	30/09/13	5.62	86.1	0.7	0.08	14.4	7.14	667	242	0.869	5.4	0	0	7.9	0	21.513	39	143.299	9.507	14.07	1.925	7.1	-8.87	0.012644709	1.855614554
P18	7	30/09/13	5.25	86.34	1.5	0.15	14.5	6.74	872	234	0.804	5.6	0	0	19.1	0	44.526	94.7	177.694	16.224	21.029	2.347	9.7	-10.36	0.028768331	4.64108759
P2	7	30/09/13	5.29	85.91	19.6	1.95	14.6	6.92	945	266	0.551	8.1	0	0	27.4	0	45.773	62.6	173.638	19.601	24.77	2.56	8.2	-9.57	0.011368989	2.064748052
P22	7	2/10/2013	3.39	86.66	56.6	5.54	15.8	6.9	1080	222	0.661	5.6	0	0	95.2	0	78.315	78.8	188.282	28.229	31.983	3.08	11.5	-7.92	0.002169106	0.406993415
P26	7	2/10/2013	2.3	86.7	74.2	7.02	17.4	7.13	855	270	0.364	4.9	0	0	69.9	0	49.35	56.6	143.894	22.348	30.801	4.381	11.7	-8.46	0.000478928	0.082590093
P28	7	2/10/2013	5.44	87.94	56.8	5.63	15.2	7	1080	265	0.567	6	0	0	66.5	0	77.907	90.9	190.083	25.672	38.021	3.107	16.6	-8.03	0.001157382	0.140696644
P3	7	30/09/13	4.87	85.99	2	0.2	15.3	6.94	870	240	0.783	5.8	0	0	20.2	0	34.202	54	168.714	19.181	22.111	2.533	10.5	-9.61	0.011908229	1.616210717
P30	7	2/10/2013	3.78	90.07	94.1	9.3	15.4	7.12	749	298	0.346	5	0	0	48.9	0	35.526	45.1	128.054	20.394	30.371	4.511	14	-8.69	0.003366681	0.511208241
P6	7	1/10/2013	2.8	85.75	1.4	0.14	15	6.87	1004	-105.7	1.223	5.8	0	1206.4	6.3	0	57.132	63.8	197.797	19.182	27.27	2.21	12.1	-9.71	0.076414664	12.47138673
P7	7	1/10/2013	4.12	86.08	12.5	1.24	15.1	6.4	1295	230	1.042	7.6	0	0	32.1	0	95.237	140.8	231.469	31.096	50.035	4.765	8.5	-9.54	0.001508678	0.226857033
P9	7	1/10/2013	3.24	85.71	18.4	1.84	14.8	6.88	947	234	0.735	6.6	0	0	45.9	0	47.516	58.8	177.518	20.611	27.814	2.826	11.7	-9.64	0.183093981	30.32686079
PA	7	30/09/13	5.52	86	6.7	0.67	14.5	6.97	868	213	0.816	6.6	0	0	45.5	0	32.372	50.8	205.899	13.006	17.284	1.99	8.7	-9.67	0.003109926	0.846506222
PB	7	30/09/13	5.08	86.09	8.6	0.84	15	6.86	984	226	0.51	6.3	0	0	71.2	0	46.748	67.1	190.701	17.916	21.848	2.563	8.6	-8.65	0.003351477	0.724127819
PC	7	30/09/13	4.91	86.37	29.7	2.93	15	6.82	1049	239.9	0.691	5.1	0	0	93.2	0	59.521	82.9	197.216	22.968	26.745	3.435	9.8	-8.64	0.038367173	6.176474783
PD	7	30/09/13	5.5	85.84	32.4	3.28	14	6.98	822	244	0.502	5.9	0	0	34.5	0	32.568	47.6	169.127	14.473	17.608	2.18	8.6	-9.75	0.015235819	2.739185786
PE	7	1/10/2013	3.65	86.37	63.5	6.18	15.8	6.89	1015	229	0.481	5.9	0	0	87.5	0	63.454	70.6	176.782	25.705	29.958	6.023	10.5	-8.18	0.001940166	0.411286434
PF	7	1/10/2013	4.93	85.87	37.7	3.71	15.3	6.65	1224	238	0.897	7.7	0	0	22.4	0	85.686	114.6	228.405	28.307	39.201	3.898	10.1	-8.97	0.009441767	1.702798761
PG	7	1/10/2013	3.4	86.35	69.2	6.83	15.3	7.02	1044	230	0.576	7.7	0	0	96.2	0	70.341	74.1	181.155	26.193	30.979	4.921	10.5	-8.34	0.011667627	2.48957569
PH	7	1/10/2013	4.5	85.59	22.4	2.21	15.2	6.96	1051	266	0.93	6.4	0	0	79.7	0	62.702	69	179.022	25.405	33.241	2.712	12.8	-8.7	0.001802187	0.324161741
PI	7	2/10/2013	4.77	85.98	61.1	6.06	15.1	6.93	1158	236	1.114	8.3	0	0	102.1	0	82.549	100.3	202.981	30.019	32.206	2.99	12.5	-7.61	0.004714706	0.82990359
R1	7	30/09/13			131.2	11.52	20.8	8.63	301	190	2.11	2	0	0	9.2	150.1	11.659	27.1	53.853	5.237	13.795	2.283	3.4	-10.88	1.16925362	56.97443557
R2	7	2/10/2013			106	9.66	20.3	8.1	321	193	1.942	2.3	0	0	9.1	0	12.657	27.9	58.453	5.65	14.33	2.22	2.2	-10.58	0.651176783	56.60249424
P10	8	5/11/2013	4.35	86.01	5.6	0.54	15.7	7.03	1014	215.1	0.844	6.6	0	0	78.5	0	66.331	70.8	160.283	24.1	27.79	3.12	11.1	-8.78		
P11	8	5/11/2013	4.32	86.06	61.7	6.07	15.4	6.96	1080	204.1	0.933	5.4	0	0	93.2	0	75.853	78.6	166.286	26.73	31.74	2.37	14.7	-8.39		
P13	8	5/11/2013	2.11	85.65	14.2	1.4	15.2	7.88	1126	203.8	0.914	6.4	7	0	95.7	47.4	80.97	87.8	168.246	26.84	33.41	2.31	16.6	-7.41		
P14	8	5/11/2013	3.86	85.66	43.8	4.35	14.8	6.86	1154	206.2	0.659	6.4	0	0	101.8	0	83.571	100.9	181.841	28.05	30.93	2.23	11	-6.01		
P16	8	5/11/2013	4.45	85.82	66.6	6.54	15.4	6.96	1042	221.8	0.719	5.1	0	0	100.5	0	73.887	84.8	159.498	25.84	30.14	3.22	13.4	-7.38		
P17	8	4/11/2013	5.67	86.05	1.1	0.1	14.7	7.03	546	196.5	0.688	4.4	0	0	2.5	0	17.555	35.4	100.532	6.79	11.38	1.51	4.9	-8.19		
P18	8	4/11/2013	5.29	86.3	0.6	0.06	14.6	6.73	490	188.9	0.536	5.9	0	0	5.6	0	20.073	49.5	87.2355	8.02	13.85	1.56	8.2	-9.74		
P2	8	4/11/2013	5.28	85.92	24.8	2.46	14.6	7	945	200.5	0.865	5.8	0	0	40.5	0	47.871	61.9	159.479	19	23.22	2.52	11.7	-8.82		
P22	8	5/11/2013	3.46	86.59	51.4	5	15.8	7	1073	207.6	0.655	5.9	0	0	94.2	0	77.962	80.6	165.425	26.34	29.95	2.81	7.9	-5.62		
P26	8	5/11/2013	2.35		77	7.3	16.9	7.06	842	205	0.359	4.7	0	0	65.9	0	48.647	56.9	123.358	20.32	27.91	3.96	15.6	-8.32		
P28	8	5/11/2013	5.46		53.8	5.26	15.5	7.02	1051	205.4	0.773	6.2	0	0	65.2	0	77.9	87.9	148.669	23.37	35.4	2.86	14.9	-7.94		
P3	8	4/11/2013	4.89	85.97	2.5	0.24	15.5	6.87	893	176.3	0.831	8.4	0	0	26.9	0	38.393	56.9	152.443	18.58	20.87	2.44	10.2	-8.58		
P30	8	5/11/2013	3.85	90	95.3	9.3	15.6	7.2	749	217.8	0.469	5	0	0	51.2	0	35.991	49	102.024	18.86	28.15	4.2	15.8	-8.75		
P6	8	4/11/2013	2.77	85.78	1.8	0.18	14.8	6.82	1083	-102.2	1.28	8.4	0	923.1	8.6	0	65.705	76.2	189.911	19.57	28.2	2.1	16.8	-8.79		
P7	8	4/11/2013	4.15	86.05	17.8	1.76	15	6.77	1121	195.6	0.771	7.2	0	0	56	0	74.892	95.7	179.447	25.03	36.87	4.17	7.8	-6.41		
P9	8	4/11/2013	3.22	85.73	13.1	1.29	14.7	6.91	984	188.6	1.143	6.7	0	0	52.7	0	56.977	68.1	160.45	20.33	26.63	2.61	11.1	-8.92		
PA	8	4/11/2013	5.53	85.99	14.4	1.41	14.6	7	910	210	0.808	6	0	0	40.7	0	38.116	62.8	168.131	12.58	16.85	1.72	4.1	-10.25		
PB	8	4/11/2013	5.11	86.06	11.3	1.1	15.3	6.52	1024	200	0.72	6.3	0	0	82.9	0	53.071	71.5	181.579	18.13	21.5	2.51	9.6	-8.28		
PC	8	4/11/2013	4.96	86.32	27.2	2.69	15.2	6.77	1080	199.4	0.63	7	0	0	96	0	60.952	87.2	178.812	22.16	25.45	3.24	9	-7.1		
PD	8	4/11/2013	5.44	85.9	35.3	3.53	14.1	6.91	882	200.4	0.555	6.3	0	0	50.8	0	38.871	54.4	127.662	13.94	17.08	1.95	11.1	-9.38		
PE	8	4/11/2013	3.7	86.32	61	5.88	16	6.88	1023	207	0.472	5	0	0	83.4	0	66.441	74.9	149.525	24.01	28.66	5.76	12.6	-6.73		
PF	8	4/11/2013	4.92	85.88	36.7	3.61	15.1	6.63	1227	206.2	1.116	6	0	0	26	0	82.049	110.6	193.08	26.48	37.04	3.63	12.9	-8.93		
PG	8	4/11/2013	3.35	89.9	65.5	6.39	15.5	7.02	1038	192.9	0.589	6	0	0	90.6	0	70.081	75.4	150.002	24	29.23	4.58	10.2	-7.19		
PH	8	5/11/2013	4.44	85.65	29.4	2.9	15.4	6.89	1044	201.4	0.568	6.1	0	0	86.2	0	66.801	72.3	154.362	23.73	30.76	2.36	11	-8.19		
PI	8	5/11/2013	4.75	86	63.8	6.27	15.3	7.05	1140	203.8	0.435	6	0	0	101.2	0	83.414	102.6	173.54	27	29.45	2.6	13.6	-6.49		
R1	8	4/11/2013		2.71	112.8	11.33	14.3	8.41	312	158.8	1.647	2.2	0	0	8.2	0	13.331	29.4	46.046	4.7	14.26	2.1	3	-9.45		
R2	8	5/11/2013		5.92	92.8	9.48	16.5	7.9	314	166.2	1.339	2.1	0	0	8.4	18.5	12.54	29.6	45.9597	4.68	13.77	2.03	3	-10.5		

Piézomètre	Campagne	Date	Profondeur (m)	Charge hydraulique (m)	O2 (%)	O2_2 (mg/L)	T (°C)	pH	EC (µS/cm)	ORP (mV)	DOC (mg/L)	Alk (mg/L)	P-PO4 (µg/L)	NH4 (µg/L)	NO3 (mg/L)	NO2 (µg/L)	Cl (mg/L)	SO4 (mg/L)	Ca (mg/L)	Mg (mg/L)	Na (mg/L)	K (mg/L)	SiO2 (mg/L)	dO18 (‰)	DEA_sed (µg N-N2O / h/g sed sec)	DEA_OM (µg N-N2O / h/g MO)
P10	9	2/12/2013	2.86	87.5	43.6	4.43	14.7	7.05	811	183.9	1.159	5.7	0	1.8	43.5	0	39.238	48.7	136.757	18.59	19.39	2.41	11.8	-8.38		
P11	9	3/12/2013	2.96	87.42	73.9	7.58	14.2	6.92	908	208.5	0.922	5.6	0	0	74.6	0	51.27	60.6	144.323	21.5	25.76	1.86	12.6	-8.54		
P13	9	3/12/2013	1.11	86.65	14.6	1.56	13	6.91	964	138.7	3.49	7.5	8.4	24.6	18.4	13.3	48.96	87.2	157.371	22.11	44.48	1.14	19.7	-9.28		
P14	9	3/12/2013	3	86.52	6.3	0.68	13.8	6.94	981	148.2	1.461	6.6	0	0	40	130.8	55.336	86.9	159.905	24.24	29.66	1.79	14.8	-8.99		
P16	9	3/12/2013	3.7	86.57	48.7	4.93	15.2	6.83	1084	198.2	0.961	5.8	0	4.9	69.3	10.3	52.693	97.3	174.385	28.24	28.08	3.2	15.2	-8.01		
P17	9	2/12/2013	4.62	87.1	17.1	1.73	15	7.01	585	218.2	0.866	5.1	0	1.6	4.6	0	11.096	35.9	108.662	6.93	12.89	1.28	7.5	-9.75		
P18	9	2/12/2013	3.96	87.63	14.2	1.46	14.6	6.81	518	238.3	0.9	6.1	0	0	7.4	0	16.295	39.9	86.128	8.19	12.06	1.49	8.5	-10.03		
P2	9	2/12/2013	3.13	88.07	49.5	5.03	14.5	7	690	202	0.844	5.5	0	9	17.1	0	21.778	46	120.96	12.45	15.01	1.79	10	-8.45		
P22	9	3/12/2013	2.41	87.64	52.6	5.3	15.2	6.88	1097	300.8	0.733	6.1	0	0	96.1	0	78.81	82.9	173.271	27.2	30.85	2.84	14.6	-7.47		
P26	9	3/12/2013	1.97	87.03	68.6	6.66	16.9	7.01	833	244.8	0.447	5.2	0	14.7	61.1	0	47.44	55.7	128.298	20.42	27.87	3.85	14.1	-8.07		
P28	9	3/12/2013	4.56	88.82	57.7	5.82	15.2	6.87	910	195.7	0.741	5.7	0	0	39	0	61.072	75.1	115.238	15.95	25.58	2.14	9.7	-8.68		
P3	9	2/12/2013	3.68	87.18	45.7	4.63	14.8	6.95	785	187.3	0.706	6.2	0	28	27.7	14.6	29.296	50.4	139.344	15.28	17.34	1.98	9.9	-9.53		
P30	9	3/12/2013	3.7	90.15	91.3	9.14	15.5	7.05	727	218.4	0.488	4.9	0	0	50.3	0	36.82	49.9	110.603	18.92	28.34	4.21	15.3	-8.91		
P6	9	2/12/2013	1.75	86.8	5.5	0.57	13.9	6.91	741	-117.2	1.615	6.2	0	2057.1	5.8	25.6	33.845	47.2	127.866	12.17	18.25	1.61	12.6	-9.36		
P7	9	2/12/2013	2.75	87.45	52.8	5.36	14.8	6.75	1182	267.3	1.193	8.4	0	3.6	36.9	0	75.929	110.2	197.525	27.33	39.26	3.76	12.4	-9.01		
P9	9	2/12/2013	2.16	86.55	36.8	3.79	14	6.9	865	241.9	1.447	6.6	0	2.3	28.2	0	40.594	68.7	150.361	17.84	21.78	2.28	12.9	-9.31		
PA	9	2/12/2013	4.43	87.09	46.9	4.82	14.4	7.1	552	200.3	0.906	6.5	0	1.8	11.4	0	14.674	37.7	108.036	7.59	11.13	1.36	8.9	-9.64		
PB	9	2/12/2013	3.79	87.38	61.7	6.2	15.2	6.83	718	195.3	0.639	5.6	0	0	23.1	0	21.674	45.2	130.581	11.96	14.57	1.76	10	-9.4		
PC	9	2/12/2013	3.64	87.64	22.5	2.28	14.6	6.9	773	200.7	1.053	6	0	0	21.1	0	27.954	62.1	132.15	15.85	18.23	2.61	10.2	-9.39		
PD	9	2/12/2013	4.37	86.97	61.8	6.46	13.8	7.11	489	163.3	0.597	4.1	0	2.1	12	0	12.472	28.8	86.927	7.23	9.92	1.34	8.2	-9.57		
PE	9	2/12/2013	2.38	87.64	49.8	5.02	14.9	6.83	930	264.8	0.926	7	0	3.2	54.9	0	45.712	65	150.808	21.87	22.8	4.89	11.3	-8.62		
PF	9	2/12/2013	3.74	87.06	37.2	3.76	15	6.82	962	286.9	1.128	6.6	0	0	22.5	0	47.3	79.5	161.646	19.78	26.7	2.93	12.1	-9.42		
PG	9	2/12/2013	2.1	87.65	26.4	2.68	14.8	6.92	953	265.2	1.244	6.6	0	2.2	44.8	0	51.498	74.1	147.863	21.95	27.67	4.1	10.4	-8.94		
PH	9	3/12/2013	3.39	86.7	59.7	5.56	14.9	7.01	807	223.4	0.986	5.7	0	0	43.3	77.9	40.243	58.4	124.576	17.91	24.15	2.04	12.8	-8.89		
PI	9	3/12/2013	3.78	86.97	52.4	5.31	15	6.89	1133	183.7	0.657	6.3	0	0	91	0	79.745	102.4	173.812	27.1	30.88	2.51	13.8	-7.13		
R1	9	2/12/2013			99.6	12.6	5.5	8.2	337	181.1	1.552	2.5	5.7	15.2	10.7	11.2	9.236	20.8	58.795	5.75	7.14	1.39	7	-10.35		
R2	9	3/12/2013			98.6	12.49	5.6	8.19	342	172	1.495	2.7	1.6	53.3	10.9	15	10	20.7	56.654	5.64	7.04	1.77	7	-9.68		
P10	10	14/01/14	3.33	87.03	6.4	0.66	13.6	6.96	958	177.6	0.752	6.3	0	6.1	49.7	0	52.563	64.3	77.3	21.41	25.95	3.09	12.7	-9.37	0.049041913	7.165112875
P11	10	14/01/14	3.4	86.98	77.3	7.84	13.9	6.97	1007	280	0.396	6.1	0	3.4	87.1	0	62.236	60.2	36	7.81	9	0.77	9.1	-8.67	0.000850223	0.179291565
P13	10	14/01/14	1.23	86.53	13.3	1.42	11.6	6.9	1187	142.6	2.595	8.1	25.4	10.5	27.1	0	72.04	100.8	152.7	26.51	52.8	1.82	17.5	-9.54	0.01275119	2.365639427
P14	10	14/01/14	3.1	86.42	13.9	1.43	13	6.9	1177	232.8	0.677	7.1	0	2.3	62.8	493.4	78.069	99.9	135.6	28.51	35.91	1.91	8.2	-8.23	0.048375348	9.87187948
P16	10	14/01/14	3.73	86.54	63.2	6.31	14.8	6.83	1007	325	0.45	5.7	0	2	92.7	0	69.673	86.7	149.6	25.56	31.22	3.33	14.8	-8.16	0.001458601	0.270802874
P17	10	13/01/14	4.62	87.1	1.5	0.15	14.5	6.97	601	192	0.545	5.4	0	1.5	1.6	0	13.846	36.1	112.9	7.15	13.68	1.43	7.8	-10.35	0.006124526	1.114120166
P18	10	13/01/14	4.35	87.24	5.6	0.56	14.4	6.74	610	216	0.392	4.6	0	8	11.9	0	22.292	53.1	94.5	9.79	14.07	1.79	9	-10.33	0.004790563	1.002516668
P2	10	13/01/14	4.32	86.88	36.5	3.72	14	6.96	757	256	0.31	6	0	4.1	24.1	0	23.253	39.7	88.2	13.95	16.13	2.16	10.6	-9.69	0.001295088	0.226360449
P22	10	15/01/14	2.75	87.3	51.6	5.32	13.4	6.86	1065	313.8	0.384	5.7	0	5	87.6	0	71.277	77.1	108	26.08	29.65	2.8	13.7	-8.33	0.001356208	0.31960561
P26	10	15/01/14	1.82	87.18	77.2	7.88	13.8	6.98	833	283.9	0.143	5.1	0	4.3	58.7	0	44.949	55.2	80.7	20.76	27.88	3.94	13.1	-8.89	0.000649832	0.124700262
P28	10	15/01/14	4.64	88.74	57.6	5.78	14.7	6.96	986	292.5	0.276	5.8	0	4.7	47.5	0	69.402	76	114.2	20.86	33.24	2.85	13.2	-8.8	0.000808752	0.137581588
P3	10	13/01/14	3.89	86.97	30.4	3.08	14.1	6.94	813	205.8	0.5	5.8	0	4.1	29.3	39.6	28.372	43.2	96.9	15.97	17.78	2.22	10.6	-9.69	0.087976423	10.84214809
P30	10	15/01/14	3.48	90.37	92.1	9.27	14.9	7.28	751	303.3	0.105	4.8	0	5.9	48.4	0	36.647	47.8	65.8	16.92	25.42	3.96	15.8	-8.65	0.002959992	0.377740599
P6	10	14/01/14	1.92	87.65	1.5	0.16	12.2	6.89	837	-91.5	1.037	6.9	0	881.1	5.3	0	34.906	52.1	98	14.99	21.56	1.87	7.6	-9.77	0.039378828	8.632286575
P7	10	14/01/14	3.17	87.03	22.2	2.28	13.4	6.66	1321	295	1.198	8	0	0	35	0	86.8	127.7	112.3	29.08	42.4	4.18	11.5	-8.57	0.002102976	0.366761089
P9	10	14/01/14	2.28	86.67	16.5	1.75	12.5	6.81	927	270.4	1.039	6.8	0	5.5	29.8	0	41.773	65.2	104.3	18.79	23.46	2.49	7.9	-9.54	0.004649554	0.891447926
PA	10	13/01/14	4.5	87.02	4.9	0.51	14	7.08	623	238	0.324	5.1	0	4.4	9.6	0	16.905	41.1	116.1	8.36	12.73	1.58	8.6	-10.3	0.002214599	0.601416232
PB	10	13/01/14	4.05	87.12	11.6	1.17	14.7	6.83	827	242	0.397	6.5	0	2.8	25.5	0	29.133	58.2	98.1	13.79	16.56	2.28	11	-9.53	0.001692684	0.383728304
PC	10	13/01/14	3.97	89.11	25.2	2.52	15	6.78	837	180	0.421	5.8	0	12.2	33.5	0	37.991	70.6	97.8	17.48	18.99	2.99	11.1	-9.59	0.004487306	0.769973559
PD	10	13/01/14	4.56	86.78	34.2	3.53	13.5	7.01	632	274	0.346	5	0	2.1	17.1	0	18.654	38.5	85.5	9.8	12.57	1.71	8.8	-10.3	0.009415264	2.036896504
PE	10	13/01/14	2.8	87.22	70.1	7.07	14.6	6.87	1007	279.6	0.317	6	0	6.2	76.1	0	57.414	71.1	113.3	24.17	26.6	5.82	14	-8.6	0.000331114	0.080994131
PF	10	14/01/14	3.97	86.83	25.7	2.6	14	6.79	1037	273.9	0.646	7.6	0	1.6	35	0	56.866	84.9	119.9	22.29	29.1	3.52	11	-9.2	0.001431221	0.299323363
PG	10	14/01/14	2.57	87.18	51	5.17	14	6.91	1019	254.3	0.394	6.4	0	5.9	75.4	0	63.456	72.1	96.4	23.76	28.87	4.86	13.5	-8.39	0.001640776	0.371711922
PH	10	14/01/14	3.56	86.53	54.7	5.58	13.7	6.97	886	252	0.552	5.4	0	7.3	51.1	0	52.305	64.2	116.1	20.29	25.99	2.33	11.4	-8.5	0.008849626	1.733815552
PI	10	14/01/14	4	86.75	58.9	5.91	14.5	7.04	1151	266.2	0.442	6.1	0	3.7	100	0	81.384	102.8	138.2	26.62	29.96	2.73	15.4	-8.43	0.002699882	0.485426454
R1	10	13/01/14			100	11.61	8.5	8.09	278	238	1.009	2.2	3	53.5	7.8	37.5	8.398	17.5	47.7	4.79	6.93	1.24	5.7	-10.82	0.141293722	17.87957193
R2	10	14/01/14			100.5	11.1	8.1	8.35	290	251	0.955	2.1	2.4	58.8	7.9	21.4	8.74	18.1	48.3	4.96	7.19	1.24	2.8	-10.95	21.88340476	300.8414492

Piézomètre	Campagne	Date	Profondeur (m)	Charge hydraulique (m)	O2 (%)	O2_2 (mg/L)	T (°C)	pH	EC (µS/cm)	ORP (mV)	DOC (mg/L)	Alk (mg/L)	P-PO4 (µg/L)	NH4 (µg/L)	NO3 (mg/L)	NO2 (µg/L)	Cl (mg/L)	SO4 (mg/L)	Ca (mg/L)	Mg (mg/L)	Na (mg/L)	K (mg/L)	SiO2 (mg/L)	dO18 (‰)	DEA_sed (µg N-N2O / h/g sed sec)	DEA_OM (µg N-N2O / h/g MO)
P10	11	4/2/2014	1.53	88.83	30.1	3.14	12.8	6.95	851	255	0.581	7.1	16.3	14.9	51.3	0	44.134	52.9	128.2	17.5	19.63	2.46	8.3	-6.9		
P11	11	4/2/2014	2.44	87.94	92.4	9.69	12.5	7	734	262	0.742	6	15.9	18.2	63.8	0	30.717	43.3	117.1	16.73	17.62	1.59	8.01	-8.83		
P13	11	4/2/2014	0.26	87.5	17.2	1.87	11.1	6.88	1203	219	2.407	5.2	24.2	15.5	34.9	26	76.765	92.9	182.8	26.82	48.98	2.05	17.22	-7.39		
P14	11	4/2/2014	2.2	87.32	35.8	3.87	11.1	6.88	1048	259.5	1.229	8.9	15.1	14.9	78.6	73.3	59.378	83.2	171.9	24.22	26.64	1.28	10.42	-8.38		
P16	11	4/2/2014	2.35	87.92	24.8	2.53	13.8	6.79	975	323	1.03	7.3	16.9	13.1	39.1	0	30.567	89.4	154.3	25.5	22.73	3	16.56	-8.86		
P17	11	3/2/2014	3.13	88.59	19.2	1.96	13.7	6.95	763	192.1	0.839	8.3	16.6	16.7	7.1	0	14.314	37.6	138.9	10.51	15.81	1.36	11.17	-9.42		
P18	11	3/2/2014	2.61	88.98	46.2	4.69	13.9	6.71	756	264.5	0.553	6.7	19.6	13.3	12.4	0	22.915	58.4	128.4	13.6	16.89	1.71	9.93	-8.65		
P2	11	3/2/2014	2.94	88.26	40.7	4.11	13.9	6.96	877	245	0.522	7.2	21.6	17.2	36	0	38.399	56.7	147	15.6	18.6	2.21	13.7	-8.2		
P22	11	4/2/2014	0.78	89.27	62.9	6.64	12.3	6.97	1129	250	0.846	6.5	14.5	13.8	108.3	12.1	77.068	93.8	174	27.47	29.66	2.71	15.64	-7.84		
P26	11	4/2/2014	0.3	88.7	71.7	7.4	13.4	7.07	761	275	0.394	5.7	15	15.3	45.9	0	40.28	50.7	111.3	18.24	23.75	3.35	14.78	-8.21		
P28	11	4/2/2014	2.87	90.51	80	8.3	13	6.93	965	282	0.641	6.5	14.5	14.4	52.9	0	64.242	74.9	153.4	19.44	28.45	2.96	15.55	-8.83		
P3	11	3/2/2014	2.37	88.49	46	4.72	13.2	6.89	977	265	0.579	7.2	15.3	13.5	40.4	0	46.946	66.8	162.8	18.42	22.36	2.14	7.61	-7.95		
P30	11	4/2/2014	1.67	92.18	92.6	9.33	14.3	7.11	763	265	0.156	5.5	16.9	14.9	53.8	0	40.988	51.2	112.5	18.88	27.39	4.14	17.23	-8.63		
P6	11	4/2/2014	0.9	87.65	6	0.64	12.1	6.85	782	-15	1.139	6.7	14.8	648.4	10	0	31.321	49.5	130.8	12.59	17.5	1.64	15.1	-9.37		
P7	11	3/2/2014	1.39	88.81	23.6	2.45	12.6	6.73	1349	252	1.311	6.7	13.8	14.4	40.9	0	89.123	145	186.1	29.9	45.95	3.98	10.89	-8.38		
P9	11	4/2/2014	1.18	87.77	22.9	2.42	12.1	6.85	898	260.1	1.005	9.4	21.3	25	36.4	0	40.887	63.3	147.6	17.64	21.42	2.25	17.38	-9.22		
PA	11	3/2/2014	3.14	88.38	39.5	4.09	13.2	6.94	735	240	0.831	6.9	14.4	14.6	11.5	0	19.321	54.5	142.9	9.78	13.26	1.45	12.26	-10.08		
PB	11	3/2/2014	2.47	88.7	44.2	4.56	13.2	6.81	895	240	0.513	7.4	16.8	16.1	34.1	0	35.95	62.7	154.1	15.86	18.29	1.82	7.88	-8.61		
PC	11	3/2/2014	2.17	89.11	34.4	3.51	13.3	6.69	1350	214.6	1.437	9.4	19.4	16.8	23.5	0	84.67	139.2	209	34.34	36.73	2.09	9.9	-8.83		
PD	11	3/2/2014	3.32	88.02	64.5	6.73	12.5	7.04	619	236	0.789	5.7	17	14.6	14.1	0	16.253	33.4	115.4	9.24	11.54	1.3	11.65	-10.08		
PE	11	3/2/2014	0.77	89.25	76.2	7.1	13.3	6.89	876	306	0.487	6.5	14.2	13.5	59.5	0	45.639	58.8	136	19.95	22.53	4.36	13.77	-8.64		
PF	11	3/2/2014	2.57	88.23	36.8	3.78	13.3	6.79	1109	275	1.482	8.6	16.5	16.7	34.8	0	60.256	94.9	192.3	23.61	30.65	3.29	15.64	-8.81		
PG	11	3/2/2014	0.48	89.27	84.5	8.64	13.4	6.95	955	278	0.426	6.4	16.4	14.5	77.4	0	58.585	67.2	150.3	21.91	23.53	3.81	12.94	-7.42		
PH	11	4/2/2014	2.42	87.67	59.7	6.24	12.5	6.97	773	221.7	0.762	6.1	17.1	14	38.5	40	36.058	49.5	125.3	17.89	20.92	1.86	13.25	-9.02		
PI	11	4/2/2014	2.57	88.18	62	6.31	14	6.89	1182	292	0.539	6.8	18.2	61.9	104	0	85.375	108.1	178.9	28.39	30.52	2.51	18.75	-7.77		
R1	11	3/2/2014			102	12.1	7.2	8.16	352	180.1	2.356	3.1	23.6	18.5	11.2	26.7	9.944	19.2	60.1	5.93	7.01	1.74	5.56	-10.19		
R2	11	3/2/2014			100.8	11.89	7.4	8.09	358	237.5	2.207	3.1	16.5	17.5	11.4	20.8	10.142	19.3	60.7	6.01	7.11	1.59	7.81	-9.86		
P10	12	10/3/2014	2.33	88.03	13.7	1.45	12.4	7.03	802	190	0.957	6.4	19.2	70.5	33	0	25.269	32.2	122.408	18.42	18.83	2.23	9.9	-7.89		
P11	12	11/3/2014	2.35	88.03	81.1	8.68	12.1	7.02	1087	220	0.689	6.4	12	51	98.7	0	66.698	70.1	156.914	25.48	28.14	1.87	15	-7.92		
P13	12	11/3/2014	0.63	87.13	10.4	1.15	10.7	6.92	1233	164.7	3.494	9.9	45	54.6	20.1	26.1	55.358	73	164.75	29.19	62.12	1.21	26.7	-8.86		
P14	12	10/3/2014	2.46	87.06	17	1.81	12.2	6.88	1198	275	1.002	7.1	14.5	53.6	77.9	432.1	72.799	90.3	178.902	28.22	34	1.47	17.8	-7.58		
P16	12	11/3/2014	2.84	87.43	50.8	5.34	13	6.97	1070	240	1.093	6.2	16.7	40.4	102.1	0	69.308	96.6	149.563	28.7	32.47	2.86	14.8	-7.48		
P17	12	10/3/2014	3.8	87.92	5	0.51	13.2	6.94	809	190	1.031	8	16.8	59.4	4	6.6	16.623	39.4	134.929	10.64	19.09	1.38	10.4	-9.97		
P18	12	10/3/2014	3.46	88.13	37.5	3.92	13.4	6.77	919	225	1.184	7.2	15.5	58.1	38.1	0	27.842	63.2	145.544	17.86	19.94	1.98	12.2	-8.92		
P2	12	10/3/2014	3.54	87.66	40.7	4.24	13.1	7.01	823	235	0.801	7.1	14.4	30.9	14.5	0	21.408	33.5	127.606	16.24	19.39	1.99	13.3	-9.26		
P22	12	11/3/2014	1.75	88.3	55.5	5.99	12.4	6.95	1146	221.9	0.622	6.6	16	90.6	99.8	0	77.311	84	162.705	29.63	30.2	2.52	17.6	-7.76		
P26	12	11/3/2014	0.47	88.53	81.4	8.63	12.5	7.22	768	227	0.443	5.2	11.6	35.6	56.2	0	40.155	47.7	104.141	19.4	25.97	3.39	12.1	-7.83		
P28	12	11/3/2014	3.26	90.12	83.3	8.81	12.7	7.03	986	232	0.95	6.4	10.2	36.8	41.7	0	48.471	55.5	141.372	20.38	31.59	3.76	16.5	-7.69		
P3	12	10/3/2014	2.95	87.91	38.1	4.02	12.8	6.93	892	230	0.895	7.7	19.9	29.6	23	0	28.64	45	143.07	18.78	20.27	2.14	10.9	-8.99		
P30	12	11/3/2014	1.89	91.96	94.7	9.75	13.8	7.18	785	226	0.381	5.5	18.2	45.6	51	0	40.351	44.9	96.1627	20.18	28.66	4.13	18.2	-8.63		
P6	12	10/3/2014	1.29	87.26	7	0.74	12.1	6.94	756	-40	1.376	6.4	23.2	1312.1	4.1	0	24.089	36.4	113.72	12.94	17.87	1.65	14.1	-9.8		
P7	12	10/3/2014	2.2	88	9	0.86	12.2	6.83	1214	198	1.585	8.8	12.7	21.8	42.2	0	77.771	130.7	179.121	29.41	43.3	3.55	14.8	-8.75		
P9	12	10/3/2014	1.57	87.38	21.4	2.28	12.1	6.9	881	245	1.274	7.2	13.1	209.1	38.4	0	34.405	51.1	136.926	18.75	22.14	2.21	16.7	-9.2		
PA	12	10/3/2014	3.75	87.77	34.2	3.58	13.2	6.96	815	248	0.691	7.1	12.2	29.3	19.2	0	29.353	57.6	133.488	11.43	16.21	1.47	11.6	-8.3		
PB	12	10/3/2014	3.16	88.01	53.5	5.63	12.8	6.89	901	255	0.817	7.4	18	55	35.3	0	38.621	62.6	139.459	17.89	21.08	2.18	12.3	-8.51		
PC	12	10/3/2014	3.07	88.21	50.6	5.29	13.3	6.82	860	250	0.99	6.5	10.7	53.5	30.8	0	30.718	50	127.412	18.69	20.97	2.25	12.6	-8.35		
PD	12	10/3/2014	3.9	87.44	55.3	5.89	12.4	7.05	643	255	0.754	5.6	17	57.2	14.2	0	17.145	29	106.965	10.2	13	1.39	10.8	-9.43		
PE	12	10/3/2014	1.81	88.21	85.3	8.93	13.2	7.05	809	225	0.67	5.7	18	56.7	53.3	0	35.151	43.7	118.992	19.31	19.57	4.37	14.2	-9		
PF	12	10/3/2014	3.13	87.67	38.3	4.03	12.7	6.89	1113	240	1.463	8.7	11.3	45.5	30.2	0	53.581	82.1	175.755	24.73	32.45	2.82	15.1	-8.83		
PG	12	10/3/2014	1.54	88.21	75.2	7.92	12.9	7.02	831	215	0.846	5.8	13.8	47.3	53.6	15	36.576	44.4	120.222	19.59	21.36	3.29	13.7	-9.63		
PH	12	11/3/2014	2.87	87.22	52.5	5.69	11.7	7.05	862	234.9	0.761	6.4	13.9	30.8	31.5	50.6	32.261	37.9	128.949	20.45	24.24	1.85	8.1	-7.92		
PI	12	11/3/2014	3.17	87.58	61.3	6.38	13.4	6.97	1214	247	0.588	6.5	14.6	44.3	97.1	0	76.862	92.1	179.261	30.61	29.81	2.5	17.6	-8.68		
R1	12	10/3/2014			101.1	11.57	9.4	8.17	341	210	1.247	3	25.4	83.2	5.9	34.8	6.93	11.7	50.8953	5.71	7.4	1.07	5.8	-10.27		
R2	12	11/3/2014			98.6	11.13	9.9	8.12	347	225	1.132	3	25.4	30.8	9.1	44.4	n.a.	15.7	53.0579	6.47	8.25	1.16	7.8	-9.9		

Annexe 2 : Publication soumise à *Ecological Engineering* : From hydrochemical observation to hydrological conceptualization: a multi-criteria assessment in four different riparian zones

Cette annexe contient la publication soumise par Antiguedad et al., à laquelle j'ai participé et dont les résultats sont discutés dans le chapitre 6.

From hydrochemical observation to hydrological conceptualization: a multi-criteria assessment in four different riparian zones

Iñaki Antiguedad[a], Ane Zabaleta[a], Miren Martinez-Santos[b], Estilita Ruiz[b], Jesus Uriarte[a], Tomas Morales[a], Francisco A. Comin[c], Fabian Carranza[c], Cecilia Español[c], Enrique Navarro[c], José Maria Bodoque[d], Julian Ladera[d], David Brito[e], Ramiro Neves[e], Léonard Bernard-Jannin[f,g], Xiaoling Sun[f,g], Samuel Teissier[f,g], Sabine Sauvage[f,g], José-Miguel Sanchez-Perez[f,g]

[a] *University of the Basque Country (UPV/EHU). Faculty of Science and Technology. Department of Geodynamics. 48940 Leioa. Basque Country (Spain).*

[b] *University of the Basque Country (UPV/EHU). Faculty of Engineering. Department of Chemical and Environmental Engineering. 48013 Bilbao. Basque Country (Spain).*

[c] *Pyrenean Institute of Ecology (IPE-CSIC). Avda Montañana 1005. 50050 Zaragoz,. Spain.*

[d] *University of Castilla-La Mancha (UCLM). Department of Geology and Mine Engineering. Avda Carlos III. 45071 Toledo. Spain.*

[e] *MARETEC, Instituto Superior Técnico. Universidade de Lisboa. Av. Rovisco Pais. 1049-001 Lisboa. Portugal.*

[f] *University of Toulouse; INPT, UPS; Laboratoire Ecologie Fonctionnelle et Environnement (EcoLab), Avenue de l'Agrobiopole. 31326 Castanet Tolosan Cedex, France.*

[g] *CNRS, EcoLab, 31326 Castanet Tolosan Cedex, France.*

Corresponding author: Iñaki Antiguedad. *inaki.antiguedad@ehu.eus*

Highlights

- A comparative study among four riparian areas of SUDOE region is conducted
- The approach is based on a one year monitoring: hydrochemistry and flow net
- River-floodplain-upland connectivity and C and N source-pathways are considered
- Indicators to map the attenuation zones are proposed

Abstract

This study is part of a research project funded by the European Regional Development Fund which aims to improve the knowledge on attenuation zones in riparian areas. Four contrasted meanders in the alluvial floodplain were selected in the European southwestern lowland area in order to have a wide representation of the typologies: the rivers Ebro, Bidasoa, Tagus (Spain) and the Garonne (France) were chosen. They have some common characteristics (alluvial aquifers, connectivity with the river to some extent, nitrate pollution) but differ in other important aspects (water table elevation and fluctuation, aquifer thickness, flooding dynamics, landscape control on hydrology, land use, agricultural practices, pollution sources, climate). Bearing that in mind a comparative study was conducted in order to highlight the influence of these factors on the processes controlling the nitrate removal capacity of the selected sites. We integrate hydrochemical and hydrological observations in order to establish an overall conceptualization of the functionality of the riparian areas. The observation was based on a detailed monthly monitoring during a year ensuring data at high and low water periods. A key point is the nitrogen and carbon sources and the way they interact in the riparian area. Since the objective of the project was to broadly identify the best location of good quality waters for supply purposes, the emphasis is put on the spatial delimitation of the main attenuation processes within the site, while the temporal evolution, and the processes themselves, are secondarily considered. Based on the results obtained in the study sites, indicators are proposed to map the areas of natural attenuation of pollution as regards of nitrate, depending on the hydrogeological and landscape characteristics of the aquifers and sources of contamination. These maps provide a good reference of the attenuation zones as hot spots. A methodology is defined that enables the identification of the optimal location of those areas of the riparian environment, where the water is of better quality. This methodology resulted for three of the four studied sites, indicating that in sites where agricultural practices are very heterogeneous more detailed monitoring is needed. Hence, the

study combines observation-conceptualization framework, previous to modelling, with river-riparian-upland connectivity and source-pathway-target continuity.

Keywords: Riparian areas, detailed monitoring, connectivity, flooding, attenuation zones mapping, nitrogen and carbon sources.

Introduction

Aquifers and rivers have traditionally been considered as independent compartments in the environment (Smith et al, 2009). Recent legislation, as the EU Water Framework Directive (WFD, 2000), emphasizes the need for an integrated management of hydrological catchments, including better understanding of water exchange between aquifers (GW) and rivers (SW). These exchanges are usual in riparian zones where GW-SW interface may extend several hundreds of meters from the river, depending on the site-specific conditions. The surface-groundwater interface supports the purification of water by attenuating nitrates in the vegetation-soil system and in the aquifer (Sánchez-Pérez et al., 1991a, 1991b; Takatert et al., 1999). The riparian landscape is unique among environments because it is a terrestrial habitat strongly affecting and affected by aquatic environments (Mander et al., 2005). Its role has been highlighted as ecotone or as corridor, depending on the authors, but in both the cases, the riparian zones can act as conduits, filters or barriers controlling flows of energy, matter and species in landscapes (Burt et al., 2013).

Riparian zone can be broadly defined as semi terrestrial area lying at the interface of the terrestrial and aquatic environment. Often the riparian zone is taken to be synonym for floodplain, formed mainly of river sediments and often influenced by overbank flooding events, so that it connects upland and river through surface and subsurface hydrologic flow paths (Naiman et al., 2005; Burt et al., 2013). Intersecting these flow paths produces dynamic moisture and biogeochemical conditions in which processes impacting on the fate and transport of solutes can occur (Korom, 1992; Cirmo and McDonell, 1997; Gold et al., 2001; Vidon and Hill, 2004; Burt el al., 2013). Taking into consideration that in these zones there is exchange of water between the river and the subsurface, some authors refer to them as Hyporheic Zone: “the water saturated transitional zone between surface water and groundwater” (Booker et al., 2008; Marmonier et al., 2012).

As the moisture and biogeochemical conditions are heterogeneous in both space and time “hot spots” and “hot moments” concepts have been developed (McClain et al., 2003) to describe

the function of riparian areas as buffer zones. The "hot" terms refer to a disproportionately high reaction rates relative to the surrounding area (spot) or to longer time periods (moment). Though the authors focused on N and C compounds these concepts may also apply for a wide variety of constituents (Vidon et al., 2010).

Vidon et al (2010) add a new step in this approach by distinguishing between transport-driven and biogeochemical process-driven hot spots and moments, which aims to highlight if the cause being behind the high reaction rate is a biogeochemical process or a transport event, although these phenomena should be considered simultaneously. As regarding denitrification (a microbial process common in riparian areas), biogeochemically active hot spots in aquifers of the riparian zones are formed where flow paths with high concentrations of electron acceptor species (mainly oxygen, nitrate) intersect flows, or patches, with high concentration of organic carbon. Sources (point or non-point) and pathways (surface water or groundwater) of these elements are site-specific, and therefore vary from one riparian area to another, but the most usual situation is where nitrate comes to the riparian aquifer through groundwater coming from agricultural areas. The hydrological conditions at the river-groundwater interfaces have been shown to have a significant impact on denitrifying processes in aquifers (Lamontagne et al., 2005; Rassam et al., 2008). In riparian areas where groundwater levels are lower than soil root zones, denitrification has been found to attenuate nitrate efficiently in groundwater. In these conditions, the recharged river water, rich in organic matter, has stimulated the occurrence of denitrification (Sánchez-Pérez et al., 2003b; Iribar et al. 2008, 2015).

Agricultural activities are known to be a significant source of nitrate in groundwater (Hamilton and Helsel, 1995; Almasri and Kaluarachchi, 2007; Liu et al., 2005). As alluvial plains support intensive agricultural activities, they often suffer from groundwater nitrate pollution (Arrate et al., 1997; Sánchez-Pérez et al., 2003a; Almasri and Kaluarachchi, 2007). As nitrate contamination of groundwater has become a significant environmental problem the ability of riparian buffers to remove agricultural contaminants has been studied extensively (McCarty et al., 2007; Rivett et al, 2008; Williams et al., 2014) and biological denitrification has been identified as a primary pathway for nitrate removal. Microbial "hot spots", with significant denitrification activity, have been found in patches of organic-rich soil and also at depths of several meters in zones near interfaces of different types of flows (McCarty et al., 2007). Among several factors controlling biological denitrification, hydrology and hydrogeology (Maître et al., 2003; Vidon and Hill, 2004; Lewandowski et al., 2009; Landon

et al., 2011; Williams et al., 2014), geomorphology (Gold et al., 2001), geology and land use (Dosskey et al., 2010; Español et al., this issue), all of them as a continuum, can influence nitrate removal capacity of the riparian areas. Classifications based on these attributes have been proposed in order to fulfill requirements of the Water Framework Directive (Dahl et al., 2007).

The hillslope-riparian-river connectivity (McGlynn and McDonnell, 2003; Klaus et al., 2015) is widely acknowledged as a fundamental property of all ecosystems (Kondolf et al., 2006) and has been taken as a primary element in conceptual model describing dynamics in riparian areas (Peyrard et al., 2008; Opperman et al., 2010). In rivers, hydrologic connectivity refers to the water-mediated fluxes of material, energy, and organisms within and among components, e.g., the channel, floodplain, alluvial aquifer, etc. This connectivity can be viewed as operating in longitudinal, lateral, and vertical dimensions and over time.

Lowrance et al (1997), among others, pointed out some of the most important multifunctional elements that riparian biotopes present (filtering pollutants, protecting riverbanks, regulating flows, improving microclimate, creating connectivity). Other authors (Opperman et al., 2010; Burt et al., 2013) emphasize floodplains as geomorphic features upon which ecosystems with immense ecological and economic value develop. Despite of this a lot of floodplains in the world have been disconnected from river flows and converted to agricultural or urban use. According to the abovementioned values, efforts must be made to identify and manage hot spots for a better attenuation of pollutants by acting on disturbed riparian zones. In this way restoring hydrologic connectivity (Kondolf et al., 2006) or recovering forest areas to enhance biogeochemical processes (Burt et al., 2013; Comin et al., this issue) have been proposed. Booker et al. (2008) establish a typology of Hyporheic Zones based on their pollutant attenuation capacity in order to a better consideration of the Water Framework Directive in a surface water body scale. According to the method employed the authors prioritize the available field data in order to determine the distribution and variability of environmental variables.

In this paper we are interested in the identification of hot spots in riparian areas. In fact, as pointed out by Vidon et al (2010) “developing monitoring techniques to map the distribution of biogeochemical hot spots in riparian areas is likely to remain a particular concern in the future because other relevant fine-scale data that reflect physical and biological soil heterogeneity are not yet readily available”. Our study has been carried out in the framework

of the Attenagua Project. It is a research project INTERREG IVB SUDOE (Southwest Europe) funded by the European Regional Development Fund (ERDF). The main objective of Attenagua is to develop a method to identify the best locations for the use of the riparian area groundwater to supply drinking water in the SUDOE space. This involves taking advantage of self-purification capacity in riparian floodplains, namely denitrification. The method is based on the integration of the knowledge on physical-biogeochemical interactions in four alluvial riparian areas (lowland of the rivers Ebro, Bidasoa, Garonne and Tagus). These sites were chosen because of their differences in hydrology, landscape, land cover and anthropogenic context representative of the SUDOE region.

In the Attenagua Project nitrate attenuation activity in riparian areas was characterized by using different methodological approaches based on water physicochemical characterization (Ochoa-Salazar et al., this issue; Bernard-Jannin et al., this issue), characterization of the invertebrate diversity and functionality (Español et al., this issue; Comin et al., this issue; Yao et al, this issue), characterization of the microalgae, analysis of denitrification potential, analysis of the bacterial community structure (Bodoque et al., this issue) and hydrobiochemical modelling (Sun et al., 2015). The present paper deals with the first approach mentioned, so that we take advantage of a high resolution dataset of physicochemical parameters to understand nitrates dynamics in relationship with water fluxes and carbon organic availability.

Based on the results obtained in the study sites, indicators are proposed to map the areas of natural attenuation of pollution, depending on the hydrogeological and landscape characteristics of the aquifers and sources of contamination. Thus, a methodology is defined that enables the identification of the optimal location of those areas of the riparian environment, where the water is of better quality. This paper does not aim to provide accurate spatial representations of the attenuation processes in riparian areas but to provide a good estimation of the hot spots with a simple method based on relative few field indicators. Furthermore this knowledge is essential to focus on the issues to be investigated in detail. Specific objectives are: i) To test a simple approach to delimitate attenuation zones (hot spots) in riparian areas as regards nitrate pollution. ii) To put in evidence the importance that site-specific attributes have on these spots. This study combines observation-conceptualization framework, previous to modelling, with river-riparian-upland connectivity and source-pathway-target continuity.

Materials and methods

Study sites description

For the study we selected four river meanders (figure 1) located in South-western Europe: the rivers Ebro, Bidasoa, Garonne and Tagus. These sites were selected in areas characterized by a combination of agricultural occupation and patches of natural riparian forest that might favour the potential degradation of agricultural pollutants. In order to favour the comparison of the study sites (figures 2 and 3) a wide variation of climatic and environmental conditions (land use, landscape, geology, hydrology and hydrogeology) were considered.

In order to better consider some processes occurring in the alluvial aquifer, piezometers were grouped according to the distance to the river (land use was not considered in this classification). So they were included in three different groups: Near River (NR), for those located next to the river, Intermediate Zone (IZ), that includes those located to a higher distance, and Distant Zone (DZ), for those located farther, usually in or near the pollution source area. This distribution has been used in many of the analysis incorporated in the present paper.

Ebro site

This study area (alluvial aquifer in Soto de Nis site, 78 ha) is a meander located 12 km downstream of Zaragoza, Spain (UTM 686179, 4607010), which is included in the "Los Galachos" natural reserve. It is mostly subjected to agricultural land use, mainly corn and irrigated cereals, but it shows an extensive riparian corridor dominated by white poplar (*Populus alba*), European black poplar (*Populus nigra*), white willow (*Salix alba*) and salt cedar (*Tamarix* spp.) (González et al., 2010). Near the river (forested zone) slope is around 0.13% and it is even smaller in a more distant zone (around 0.04%) which is located in a terrace 3 m above the near river zone (figure 2). River incision is the smallest one in this site, about 1.5 m. Mean annual precipitation and temperature is 380 mm and 15°C, respectively.

The aquifer comprises quaternary alluvial deposits consisting mainly of highly permeable big sized gravels. In the study area the aquifer has 7 km wide and over 15 m thick; in fact, previous wells drilled in the area up to this depth did not reach the bedrock, which is thought to be formed by impermeable evaporitic materials (figure 2). No data are available in this site

but hydraulic conductivity must be high due to the big sized gravel formation. The average water table is located at a depth of between 1.4 m (in the riparian zone) and 4 m in agricultural areas. The Ebro River (around 25.000 km^2 up to the study site) shows a very irregular hydrological regime with high peaks in winter and spring and very low discharge in summer (figure 3). No tributary stream is crossing the study area. Until 1980´s the Ebro River in this area could be defined as a meandering channel, but since them the river course has undergone important modifications which in turn have conditioned relationships with the aquifer. In fact, present near river zone was previously the water course.

In the framework of Attenagua Project a network of 12 piezometers was installed in the site up to 9 m depth. Sampling network was completed with 2 point in the river (figure 1). All these points were monitored during the study period (May 2013 - April 2014).

Garonne site

This study area (alluvial aquifer in Monbéqui site, 12 km^2) is located in a meander 50 km north of Toulouse in South-West France (UTM 355758, 4861267). The floodplain site (figure 1) consists of irrigated agricultural land (distant zone), mainly corn and sunflower, poplar plantations (intermediate zone) and riparian forest (near river zone), dominated by poplar (*Populus* spp.), ash (*Fraxinus* spp.) and oak (*Quercus* spp.). Topography is almost flat in all the floodplain area (4 km width) with slopes around 0.40%, and the river incision is about 7 m (figure 2). Mean annual precipitation and temperature is 710 mm and 13.5°C, respectively.

The aquifer comprises quaternary alluvial deposits on top of the impermeable molassic bedrock. They consist of highly permeable sand and gravel, 4 to 7 m thick, with high lateral continuity (Lancaster, 2005; Sánchez-Pérez et al., 2003b; Bernard-Jannin et al., this issue; Ochoa-Salazar et al., this issue). According to existing data, hydraulic conductivity in Garonne site is on average around 300 m/d in the river near zone but decreasing up to 100 m/d in distant zones (Sun et al., 2015). The average groundwater table is located at a depth of between 1 m (in the riparian zone) and 4 m in agricultural areas and rise rapidly up to soil profile during floods (Weng et al, 2003). The upper layers of the riverbed and the top soil layers of the floodplain are silty. The particularity of the Garonne River in this site (around 13.700 km^2 up to here) is that the water courses over an impermeable molassic bed (figure 2), with an annual average flow of about 200 $m^3.s^{-1}$ which ranges from 10 $m^3.s^{-1}$ to 2900 $m^3.s^{-1}$ (Banque Hydro, http://www.hydro.eaufrance.fr/). Therefore the exchanges between the river

and the alluvial aquifer are mainly horizontal and controlled by the river water level. The river course has undergone some changes during the last centuries. The river flow at the study site is very variable, peaking in winter and spring and declining in summer (figure 3). No tributary stream is crossing the study area.

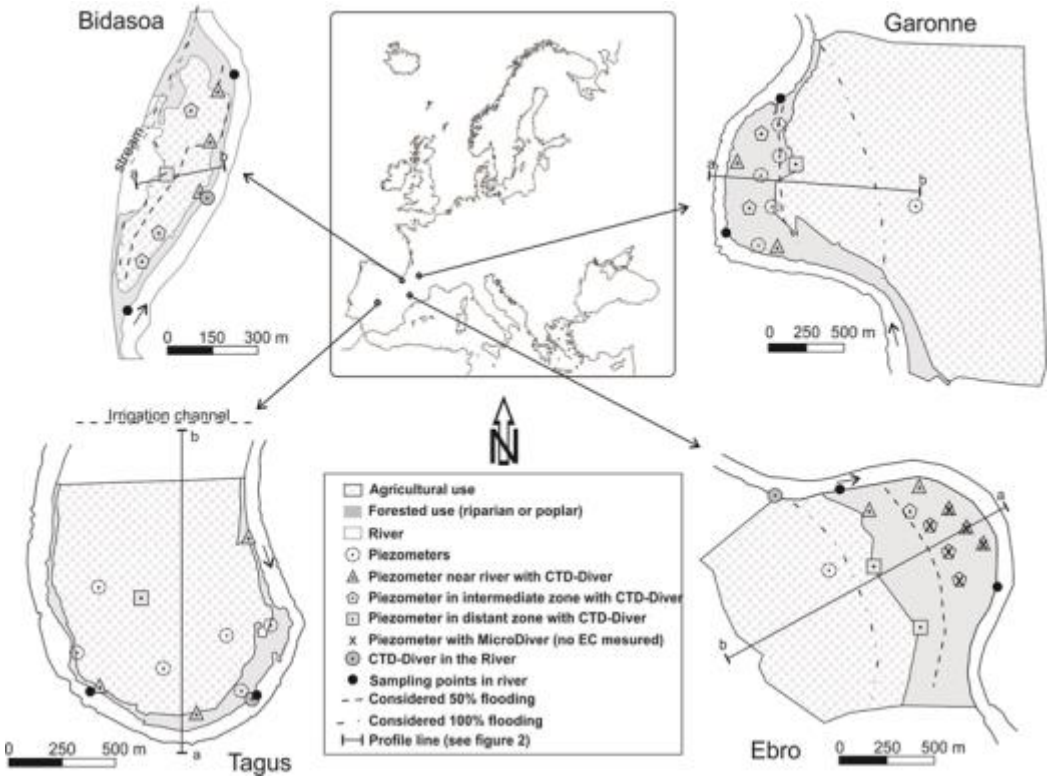

Figure 1: Four study sites location, land uses and monitoring network (modified from Español et al., this issue).

A network of about 50 piezometers has been installed in the site reaching up to the roof of the molassic bedrock. However, for the purposes of this work, in order to compare all the study sites with a similar set of points a network of 13 points (11 piezometers and 2 sample locations in the river, figure 1) was monitored during the study period (April 2013 - March 2014).

Bidasoa site

The study area (alluvial aquifer in Lastaola site, 22 ha) is located in a meander 7 km upstream of Irun, Basque Country, Spain (UTM 602190, 4797250). Agriculture, mainly corn and pasture, and livestock practically cover the entire floodplain surface, leaving a tight riparian corridor along the river shore (figure 1). Forest area is very small and dominated by white willow (*Salix alba*), alder (*Alnus glutinosa*) and ash (*Fraxinus excelsior*). Invasive species American pokeweed (*Phytolacca Americana*) is abundant. River incision is quite important (5

m) and the slope of the site is quite flat, less than 0.25% (figure 2), being bigger (more than 25%) in the west side where an alluvial fan related to a lateral stream can be observed. This stream, and the associated fan, seems to have a high control on the hydraulic response of the aquifer. On this fan a farm (dairy) is located, which represents an important point source of pollution. Mean annual precipitation in the site is very high, around 1870 mm, and temperature 13 °C.

Quaternary deposits in the alluvial aquifer can be up to 30 m thick but no more than 300 m width (figure 2). This thickness makes the area interesting from the hydrogeological point of view, as demonstrated by water extractions (for drinking water supply) carried out in the past during dry periods. The deposits consist of silty sands in the top and highly permeable gravels below. Hydraulic conductivity of the aquifer is between 10 and 100 m/d (model application, not published). The silty materials on top make this aquifer to show a semi-confined behavior. Under the alluvial aquifer, almost impervious materials, as granites or shales, are found. These materials can also be found in the western limit of the aquifer. The topography of the bedrock is quite irregular making groundwater upwelling near the river possible. The average water level depth in the aquifer ranges from 4 m, in the distant zone, to 4.5 m. The Bidasoa River (around 700 km^2 up to the study site) shows a very irregular regime peaking in winter and spring and declining in summer (figure 3).

A network of 7 piezometers, up to 9 m depth, was installed along the site. Sampling network was completed with 3 points to sample surface water, 2 of them in the river and the other in the lateral stream (figure 1). All these points were monitored during the study period (April 2013 - April 2014). Apart from these, 10 wells were installed in the past reaching the base of alluvial deposits, some of which has been used to complete geological information.

Tagus site

The study area (alluvial aquifer in El Soto Redondo site, 80 ha) is situated in a meander of the Tagus River, about 40 km west of the city of Toledo, Spain (UTM 380482, 4410115). This site is under extensive agriculture, mainly irrigated cereals, vegetables and pasture. Throughout the whole area is applied pig manure to fertilize. Only some isolated patches of riparian forest remain, in a narrow line near the river, being dominated by white poplar (*Populus alba*) and salt cedar (*Tamarix* spp.). River incision is quite important (6 m). Land

slope in the site is 0.80% in the lowland but slope increases toward upland reaching 1.60% in some terraces (figure 2). Mean annual precipitation and temperature is 375 mm and 15°C, respectively.

The aquifer is composed of unconsolidated quaternary alluvium, with a high lateral continuity, consisting mostly of gravel and clay size sediments that are overlain by deposits of sand. To the south, the aquifer is limited by materials mainly formed by sand and clay. Thickness of the aquifer is unknown but it has to be more than 9 m as the piezometers installed along the site have not reached the bedrock, which consists of impervious granitic rocks. In Tagus site hydraulic conductivity is around 10 m/d (Bodoque et al., this issue). The water table ranges from 1 m (near river banks) to 5 m inside the meander arc. The recharge of the aquifer is mainly due to irrigation (Castrejón channel derived from the river is located 2 km north), while the hydraulic connection between the river and the aquifer is insignificant because of the Tagus River is highly regulated by dams and water derivations, with a discharge that hardly varied (figure 3) (Bodoque et al., this issue).

In this site a network of 10 piezometers, up to 9 m depth, was installed in the framework of the project. Sampling network was completed with 2 points in the river (figure 1) and one point in the irrigation channel. All these points were monitored during the study period (May 2013 - April 2014).

Monitoring system

Observation phase was based on a detailed monitoring, with a similar system for all the study sites. Monitoring network (figure 1) was designed considering the floodplain surface and the land use and consists of between 7 and 12 piezometers along the site and 2 or 3 points in the river. All the piezometers are 8 to 9 meters long and 60 to 100 mm width (internal diameter); the 1.5 m top of the PVC pipe is blind (the space around was sealed with bentonite clay to prevent rainwater from seeping down the hole) while the rest of it is screened. The top of the piezometers was capped. In all the sites two sampling points were located in the river (upwards and downwards the meander). In Bidasoa and Tagus another control point was included for superficial water, in the lateral stream in the first site, and in the irrigation channel in the last site.

All of the control points were sampled in each site once a month during a year (April/May 2013 – March/April 2014) ensuring sampling at high and low water levels in both river and alluvial aquifer (figures 1 and 3). Four of the twelve campaigns included sediment and biota sampling (Español et al, this issue; Bodoque et al., this issue; Comin et al., this issue; Yao et al, this issue). Groundwater was sampled in the piezometers after pumping. To ensure that the water sample corresponded to the aquifer and not to stagnant water in the piezometer, water samples were not taken until electrical conductivity (EC) of the extracted groundwater was constant (Sánchez-Pérez, 1992). Samples were kept cold (< 4ºC) in 500 ml plastic bottles and immediately carried to the laboratory for their subsequent analysis. Dissolved oxygen, temperature, pH, ORP (oxidation / reduction potential) and EC were measured in the field, and mayor anions and cations were measured in laboratory. Data logger devices (CTD Divers, Schlumberger Water Services) were installed in some of the piezometers (between 5 and 8 in each site, one of them in the river) to carry out continuous measurements (at 10-20 minutes interval) of water level depth, EC and temperature. A Baro-Diver was also installed in each zone for atmospheric pressure control, which is needed to deduce the hydraulic head.

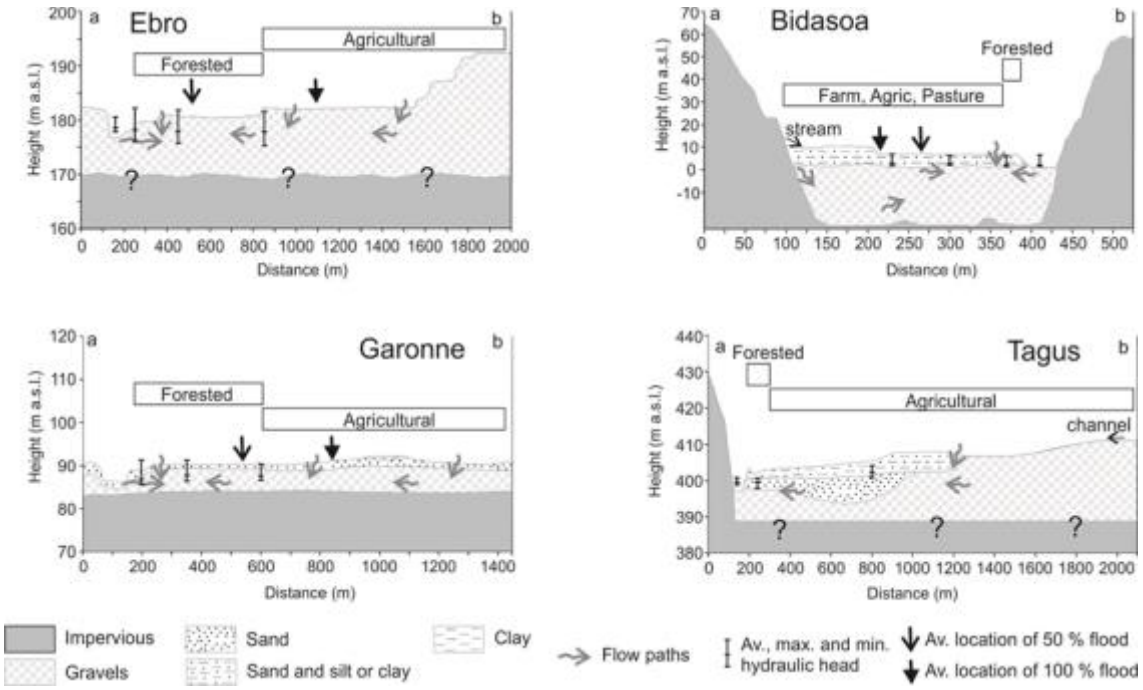

Figure 2: Four study sites geology and landscape. Hydraulic head variations along the site are also represented.

Water samples collected at all sampling points were filtered through 0.45 μm Milipore nitrocellulose filter. One replicate of each sample was acidified to pH<2 with HNO_3 (65%)

for base cations (Ca^{2+}, Mg^{2+}, Na^{+} and K^{+}) and silica analysis, which were measured using ICP-OES (Perkin Elmer Optima 2000). Major anions (Cl^{-}, NO_3^{-} and SO_4^{2-}) were measured in the non-acidified replicate using ion chromatography (DIONEX ICS 3000). DOC (dissolved organic carbon) and TOC (total organic carbon) were respectively analyzed in one filtered and one non-filtered replicate of each sample using a Total Organic Carbon Analyzer (TOC-L Shimadzu), while POC (particulate organic carbon) was calculated by the difference between TOC and DOC. Alkalinity was also determined in the unfiltered sample from the TIC (total inorganic carbon) values measured by the TOC-L Shimadzu. The analysis of the phosphate (PO_4^{3-}) was conducted using the ascorbic acid method (APHA-AWWA-WPCF, 1998) and determined by colorimetric method. Modified Berthelot reaction using salicytate and dichloroisocyanurate was used to determine the ammonium (NH_4^{+}) by colorimetric method. Analyses were performed on the spectrophotometer Jasco V-630 and all of them showed an Ion Balance Error (IBE) between 10% and -10%.

Hydrology and Hydrogeology

Discharge in the river is measured in every study site in gauging stations located in a relatively small distance (between 3.5 and 20 km) upstream from the studied sites. There are not significant tributaries or water entrances to the river in the river section between the gauging station and the studied floodplain. In those stations discharge is measured every 10 to 30 minutes. However, considering that for the objective of this paper a coarser time scale can be used, the average daily discharge was calculated and used for further analysis (figure 3).

In the analysed series discharge necessary to start flooding and to flood around 50% and 100% of the studied floodplains was established based on modelling results. MOHID Land (Neves, 1985; Braunschweig et al., 2004) was applied in the four study areas with satisfactory results for the simulations of discharge and water depth in the aquifer (http://attenagua.actionmodulers.dtdns.net/files/ModellingApproach.pdf, Brito et al., 2014). The beginning of the flood was considered as the moment when a very narrow line next to the river is flooded. A 100% flooding was considered when almost the whole area of the floodplain was covered by water; the 50% flooding was defined as the moment when a great part of the floodplain, more or less the half, was flooded. In order to compare the percentage of time that different areas of the four study sites were flooded, flood duration curves were constructed and evaluated taking those data obtained from the model into account.

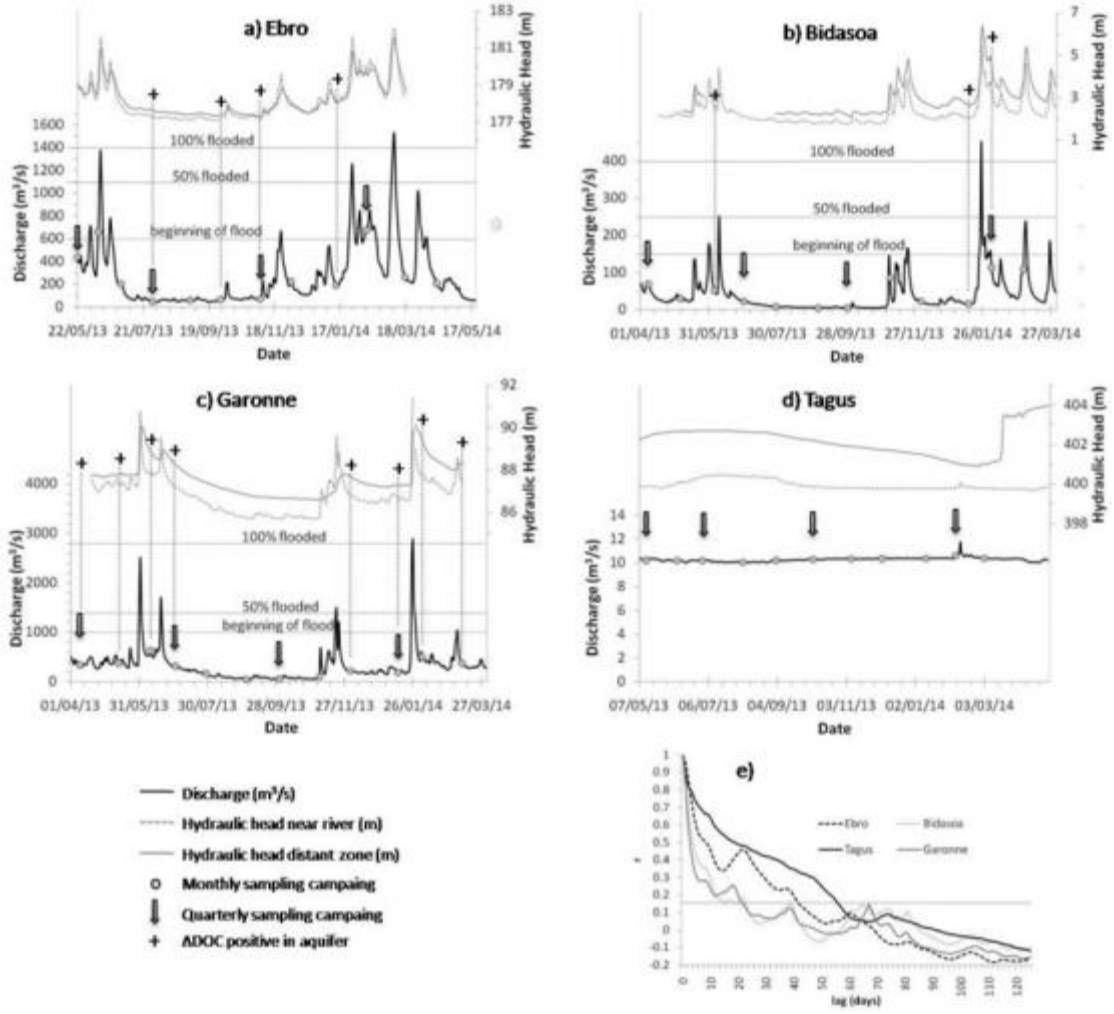

Figure 3: a-d) Hydrographs and piezographs registered in the studied sites (2013-2014). Sampling moments are also marked. e) Autocorrelation functions of the four rivers for the same period.

A correlation analysis was applied to daily discharge series from April-May 2013 to March-April 2014, in order to obtain the autocorrelation function for each discharge series. The mathematical development of the method, as applied in hydrology, is well known and can be found in Mangin (1984). In the case that data are of a nearly random nature the values of the autocorrelogram (r) fall quickly to values close to zero. On the contrary, when the events considered have a longer-term influence on time series under study, the slope of the autocorrelogram is gentler. This method can be used for the comparison of systems with different scales, as the autocorrelation function does not depend on the specific values of the runoff series but rather, on the shape of the time series, so the width and height of the runoff peaks are more important than the absolute values; as Grasso and Jeannin (1994) concluded, the sharper the hydrograph the more rapid the decrease in the runoff autocorrelogram.

With regard to groundwater, continuous water level data obtained from the Diver devices were transformed in continuous water depth series, considering terrain level and device

location. This enabled to analyze data in terms of water table fluctuation and also in terms of vertical distance from the top of soil/aquifer. In order to analyze those data in the same time step as discharge, mean daily water depth was calculated for each piezometer. After that, the percentage of time (days) that water level in the aquifer is below a certain depth was calculated (figure 4).

Additionally, water table manually measured during each sampling campaign was considered to obtain monthly flow net for each study site. For this purpose, spline analysis of interpolation was performed using ArcGIS 10.1 and flow direction arrows were manually drawn considering the obtained water table isolines. From those monthly maps two, one for high and another for low groundwater levels, were selected in order to obtain representative flow nets for those two situations in each studied site. Many of the results in the paper are based in those two different hydrological situations.

Statistical methods

In order to analyze field data variability boxplots were made with some of the parameters measured during the monthly sampling campaigns (water depth, temperature, EC, ORP, O_2, DOC and NO_3^-, and NH_4^+ for Bidasoa site only). Boxplots include median, 25th and 75th percentiles, 25th percentile minus and 75th percentile plus (1.5 x interquartile range) and upper and lower detached values.

Principal Component Analysis

Factor analysis is an effective way of interpreting and representing water chemical data. Such a multivariate statistical method yields the general relationship between measured chemical variables by showing multivariate patterns that may be help to classify the original data. It enables the geographical distribution of the resulting factors to be determined. The interpretation of factors yields insight into the main processes, which main govern the distribution of hydrochemical variables (Liu et al., 2003).

In this paper a Principal Component Analysis (PCA) was performed in each study site to give a general description of the sites in order to compare them and help identify the connectivity degree between surface water and groundwater as well as water mixing zones and processes. In fact, as pointed out by King et al (2014), among others, one of the most commonly used multivariate statistical analysis of hydrochemical data to assess alluvial aquifer-stream

connectivity is Principal Component Analysis (PCA). PCA is a mathematical manipulation that reduces a large number of parameters into fewer principal components (typically two or three), which can be often used to identify hydrological processes. PCA provides a visual representation of the hydrochemical characteristics of each studied zones. In addition data are displayed to highlight the hydrochemical evolution of groundwater.

In order to make the possible different groups of waters in each site visible a PCA analysis was performed on a subset of 13 selected variables (EC, Alk, SO_4^{2-}, SiO_2, DOC, ORP, NO_3^-, PO_4^{3-}, NH_4^+, K^+, O_2, Temperature, water depth) which represent the overall geochemical framework of the studies areas. Factor Analysis (Varimax Rotation) was conducted with the help of SPSS 19 software to extract the factors. The factors considered to be significant were those that showed eigenvalues equal or higher than 1 (Kim and Mueller, 1987). For discussion we consider parameter loadings classified as strong (values > 0.7) and moderate (0.5 - 0.7).

End-Members Mixing Analysis

With the objective of having more detailed information on the connectivity between river and aquifer an end-member mixing analysis (EMMA) was conducted to estimate the proportion of water from different sources in the mixed water of the aquifer. EMMA is a type of geochemical mixing model which solves mass balance equations for a number of tracers required to identify the likely runoff components. Basis of the method can be taken from Hooper et al (1990) or Christophersen and Hooper (1992) among others. Ochoa-Salazar et al (this issue) use this methodology in a geochemical way to evaluate the usage of metals to characterize hot spots in an alluvial area. Key assumptions for geochemical mixing models are: tracers behave conservatively, mixing process is linear, chemical composition of end-members does not change over the time-scale considered by the mixing model (time invariance) and chemical composition of end-members does not change with space (space invariance).

In the simplest form the contributions of the end-members can be computed by directly solving the mass balance equations for the selected tracers given the observed concentrations of the potential end-members. However, as pointed out by Inamdar (2011; Inamdar et al., 2013) this simple approach does not constitute a true EMMA. In fact, EMMA, as described by Hooper et al (1990), involves the use of a large number of tracers (more than the minimum

required to identify potential end-members and solve the mass balance equations) within a PCA framework.

We are conscious of what a deep application of EMMA method implies. However, we have applied this method in a simpler approach according to the objectives established for the study. In fact, in our sites uncertainties in the method application derive from the high temporal variability of the chemical composition of waters we can take as end-members. Our interest of applying such an analysis was not to provide accurate spatial representations of mixing spatial and temporal processes, but to provide an adequate estimation of them with few input parameters. Bearing this in mind, we tried to perform a mixing analysis with the least possible number of poles. In our sites the potential poles (end-members) we had according to available data are: river water, groundwater in agricultural areas, lateral stream water and irrigation channel water (rainfall water was not considered, soil water neither). We applied the method in a monthly scale, as it is the scale of the sampling. The results from PCA analysis and the site-specific attributes were used to choose the simplest end-member in each site. In this way special attention is paid to electrical conductivity (EC) as it can potentially differentiate end-members, namely river water and groundwater (Jencso et al., 2010).

Using the electrical conductivity of the end-members as a reference, the percentage of water coming from each of them in all the monitoring points of the aquifer was estimated. Taking the results obtained from the EMMA approach into account, the theoretical concentration of NO_3^- and DOC for each control point was calculated using the following equation:

$$[TC]i = (\%R*[C]R) + (\%Aq*[C]Aq)$$

where [TC] is the theoretical concentration of NO_3^- or DOC, % is the percentage of water from each end-member, and the subscripts i, R and Aq are the control point considered (i) and each of the end-members, respectively (usually the river and the aquifer). Once the theoretical concentrations of NO_3^- or DOC were calculated, they were compared with the real concentrations ([RC]), obtaining the rates of variation (depletion or enrichment), called Δ (delta), which can be mapped in the Δ-maps. These maps were made for each month of the sampling period in each site. For this purpose, spline analysis of interpolation was performed using ArcGIS 10.1.

$$\Delta C = ([RC]i - [TC]i)/[TC]i$$

In the places where Δ is negative there is a consumption/depletion of these compounds, meaning that attenuation processes might be taking place at these points. In the places where Δ is positive, there is an enrichment/increase of those compounds, so a point-source input might be contributing to higher concentrations.

Results

Hydrology

Figure 3a-d shows the daily average discharge measured in the gauging stations of each study site. Monthly and quarterly sampling campaigns were indicated in each hydrograph with circles and arrows respectively. In addition to measured one, discharge needed to start flooding and flood around the 50% and the 100% of the floodplains are shown for each study site. These data are not shown for the Tagus River as this is a highly regulated river where discharge barely shows any variation and flooding situations do not occur (Bodoque et al, this issue). Beginning of flooding was established in 600, 150 and 1000 m^3/s for the rivers Ebro, Bidasoa and Garonne, respectively, resulting in 10, 7 and 5 the events in which the water from the river starts flooding the forest next to the river (figures 1 and 2). For an event that would flood around the 50% of the floodplain area 1100, 250 and 1400 m^3/s thresholds were set, with 3, 2 and 4 events (figure 3) that flood a great part of the floodplain; mostly forest (riparian or poplar) in Ebro and Garonne sites and forest and agricultural areas in Bidasoa site (figure 1). From discharges of 1400, 400 and 2800 m^3/s upwards for the rivers Ebro, Bidasoa and Garonne, respectively, it is considered that almost all the floodplain area is flooded. Looking figure 3 only one event exceeded that threshold in each site reaching the agricultural area in all of them (figure 1). From these data it can be said that Ebro is the study site where the forest next to the river is flooded more often and Garonne the site where a great part of the floodplain is more frequently flooded.

In the figure 3e the autocorrelation functions of average daily discharge of the rivers Ebro, Bidasoa, Garonne and Tagus can be observed. The autocorrelation function for the Tagus River shows a very gentle decreasing slope due to the fact that this catchment is highly regulated. In the case of Ebro, this function shows a gentle decreasing slope which is related to a high dependency of eventual discharge on previous discharge and so, to a slower response of discharge during events (a certain level of regulation). This slower response would result on events of a longer duration. The autocorrelation function for daily average

discharge of Bidasoa and Garonne diminishes more rapidly and reaches the r = 1.5 level in half of the time than in Ebro. In these cases, a certain discharge has a lower influence on subsequent ones and flood events will last shorter.

Figure 4 shows the flow duration curve of the rivers Ebro, Bidasoa, Garonne and Tagus and represents the percentage of time that discharge is equal or higher than a certain value in each of the four study sites. The study period of one year between April-May 2013 and March-April 2014 is considered in the figure. Besides this, and based on MOHID model results (Brito et al., 2014; Bernard-Jannin et al., this issue; Bodoque et al., this issue), we have indicated in each graph the beginning of flood and the 50% and 100% flood thresholds and the percentage of time for which these three levels are exceeded. In Tagus site flooding did not happen owing to the fact this river is highly modified (Bodoque et al., this issue). It is clearly observed that Ebro site is partly flooded during a longer period than the other sites. Ebro is the site that shows a bigger area in the graph between the two lowest thresholds of flooding, related to the higher frequency of small floods and their longer duration. As observed in figure 2 the river in Ebro site shows the smallest incision, about 1.5 m, so it is relatively easy to have the area near the river flooded; the gentle slope of the floodplain near the river facilitates the flooding in a significant part of it. However, the flooding can hardly reach the more distant zone, which is located in a terrace.

Garonne site shows, in general, a lower flood duration but more than the half of the time floods cover a higher extension of the floodplain (around the 50 %) due to the flatter topography of the area. In this case higher increases in water level are needed to start flooding due to the higher incision of the river (about 7 meters). Finally, Bidasoa is the site that shows a lower duration and extension of floods as most of the time is only the forest line next to the river the flooded one. In this site the river incision is quite important so high water levels are needed to get water in the floodplain. However, once the first line of forest near the river is overflowed, the slope of the area is quite flat and a great part of it can be flooded.

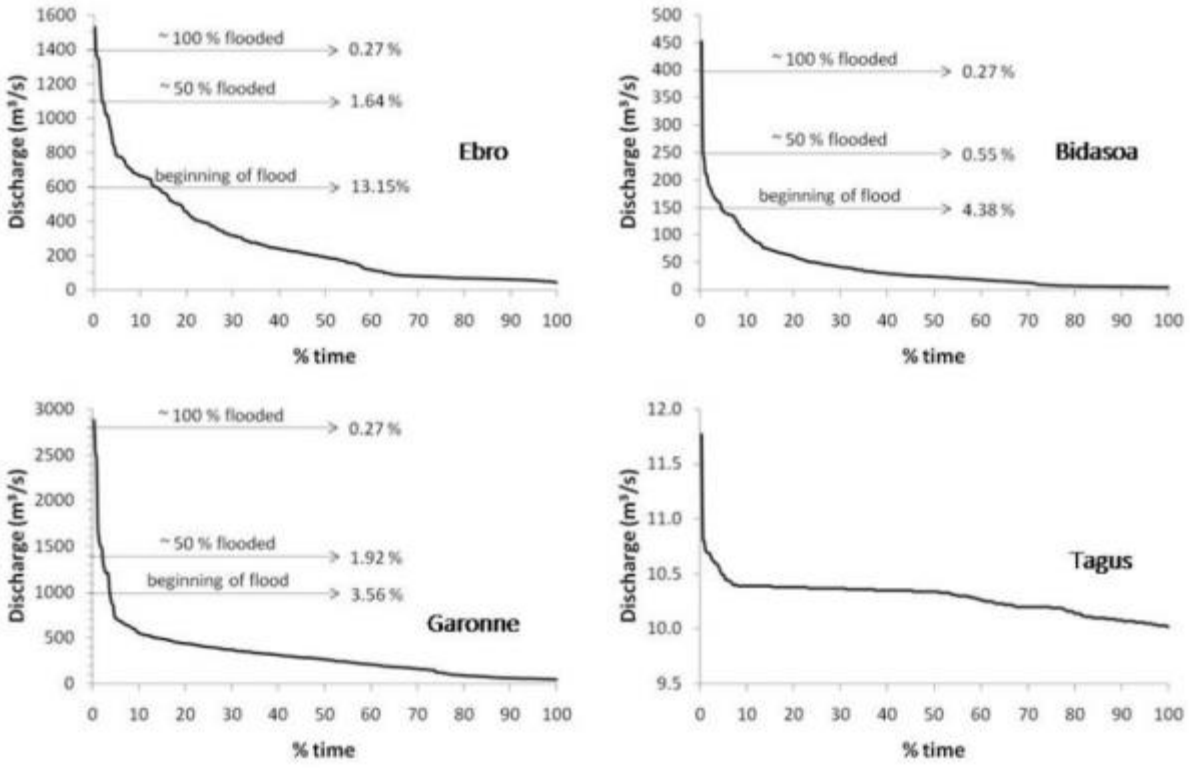

Figure 4: Flow duration curve of the four rivers. Different flooding level thresholds are marked.

Hydrogeology

In figure 2 some of the landscape differences between study sites have been represented. Recharge by irrigation in agricultural areas is important in all the sites except in Bidasoa. Recharge derived from flooding is also to be considered as mentioned previously. Discharge is always to the river. Two-ways water exchange between river and aquifer (connectivity) is clear mainly in Garonne (Sun et al., 2015) and Ebro sites. However, the Tagus River has hardly influence on the aquifer being a highly regulated river (Bodoque et al., this issue).

Additionally, the water level variations in both the river and the piezometers (near river, intermediate and distant zones) were indicated. Except in Tagus site, where water table only fluctuates during irrigation period, in the other studied sites water table temporal evolution in different piezometers is quite similar, as observed in figure 3, and similar also to the discharge evolution in the river. The average depth of the water table (figures 5, 6 and 7 wd) ranges from around 2 m (Ebro, Tagus) to 5 m (Bidasoa) being an increase in depth from the near river zone toward the distant zone in Ebro and Tagus sites. In the other two sites spatial distribution is more homogenous being the water table depth 4.5-5 m in Bidasoa site and 3.5-4 m in Garonne site, in this case with a high variation. In Garonne and Ebro sites water level in some piezometers is occasionally over the land surface, which happens in river flooding

moments. In Bidasoa site, however, water table does never reach the top of the soil when river floods neither, which is to be related to the semi-confined character of the aquifer.

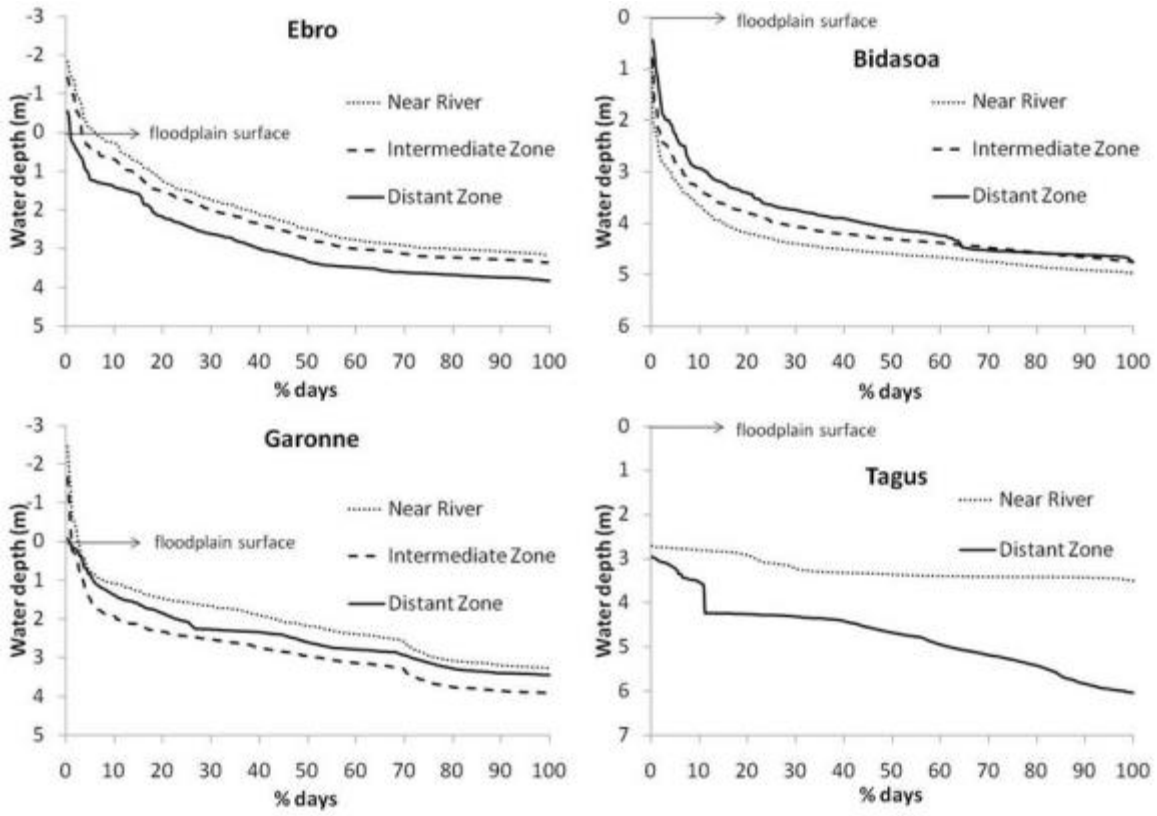

Figure 5: Percentage of time (days) that mean daily (continuously registered data) water depth in the aquifer is above a certain level (considering floodplain surface as 0) in piezometers of the near river, intermediate and distant zones of the study sites.

With regard to water table fluctuation boxplots in figure 7 show differences among the study sites. The biggest variation is observed in Garonne site where water level can fluctuate up to 6 m as much in the near river zone as in the distant zone. In Ebro site the fluctuation is also important, up to 3.5 m, being quite homogenous spatially. However, in Bidasoa site the variation is smaller, around 2-2.5 m, but homogenous also. Finally, the aquifer in Tagus site shows the smallest fluctuation, around 2 m in both extremes of the meander and 1 m in the middle part of it.

Figure 5 represents, for each site, the percentage of time (days) that water level in the aquifer is below a certain depth. All of the piezometers in each of the zones defined in the floodplains (near river, intermediate, distant) show similar responses of water level so one of the piezometers of each zone was selected for each site as an example in order to make the graphs in figure 5.

In Ebro site water level in the piezometers of the three zones is above terrain level in a small percentage of time (6% of the time in near river area, 3% in the intermediate zone and 0.7% in the distant zone), as it is shown by the negative water depths. This illustrates that there is a water level rise in the aquifer, above terrain level, during flooding. In the case of Garonne site the situation is similar but with lower percentages of flooding time in the near river, 2.5%, and the intermediate (0.9%) zones; for the distant zone the percentage is similar of that in Ebro site (0.6%). In Bidasoa site daily mean water depth did not reach terrain level during the studied period even if there were some events that flooded part or the entire floodplain area (figures 3 and 4). However, water level was eventually near the surface, to less than 1 meter 0.4 % of the time in the near river and intermediate zones and 0.7 % in the distant zone (according to Gold et al., 2001, substantial groundwater denitrification has been found where the water table was within 1 m of the surface). In Tagus site water level was more than 2.5 m deep from the terrain surface during the entire study period.

Figure 6 shows for each site the flow net of the aquifer in two hydrological situations which correspond to the usual low and high groundwater periods (flooding situations are not represented). An overall view of the figure allows making a distinction among the flow nets. The flow in Tagus site is radial with groundwater going from the internal part of the meander (more irrigated area) toward the river all along its course. However, in Ebro the flow is more or less parallel to the river with a clear influence of the river water in the aquifer. In the other two sites the flow presents an intermediate net, mainly in Bidasoa site where some flows change their direction depending on the hydrological situation (more radial from the alluvial fan in high level periods; more parallel in low level periods). Hydraulic gradient in a given situation hardly changes along the site. During low level periods is between 0.001 (Ebro) and 0.003 (Garonne and Bidasoa) and in high level periods between 0.002 (Ebro) and 0.004 (Garonne and Bidasoa). In Tagus site, due to its specificity, gradient is very low and practically constant in the river near zone (0.0002-0.0006) but increases greatly towards the center of the meander (0.007).

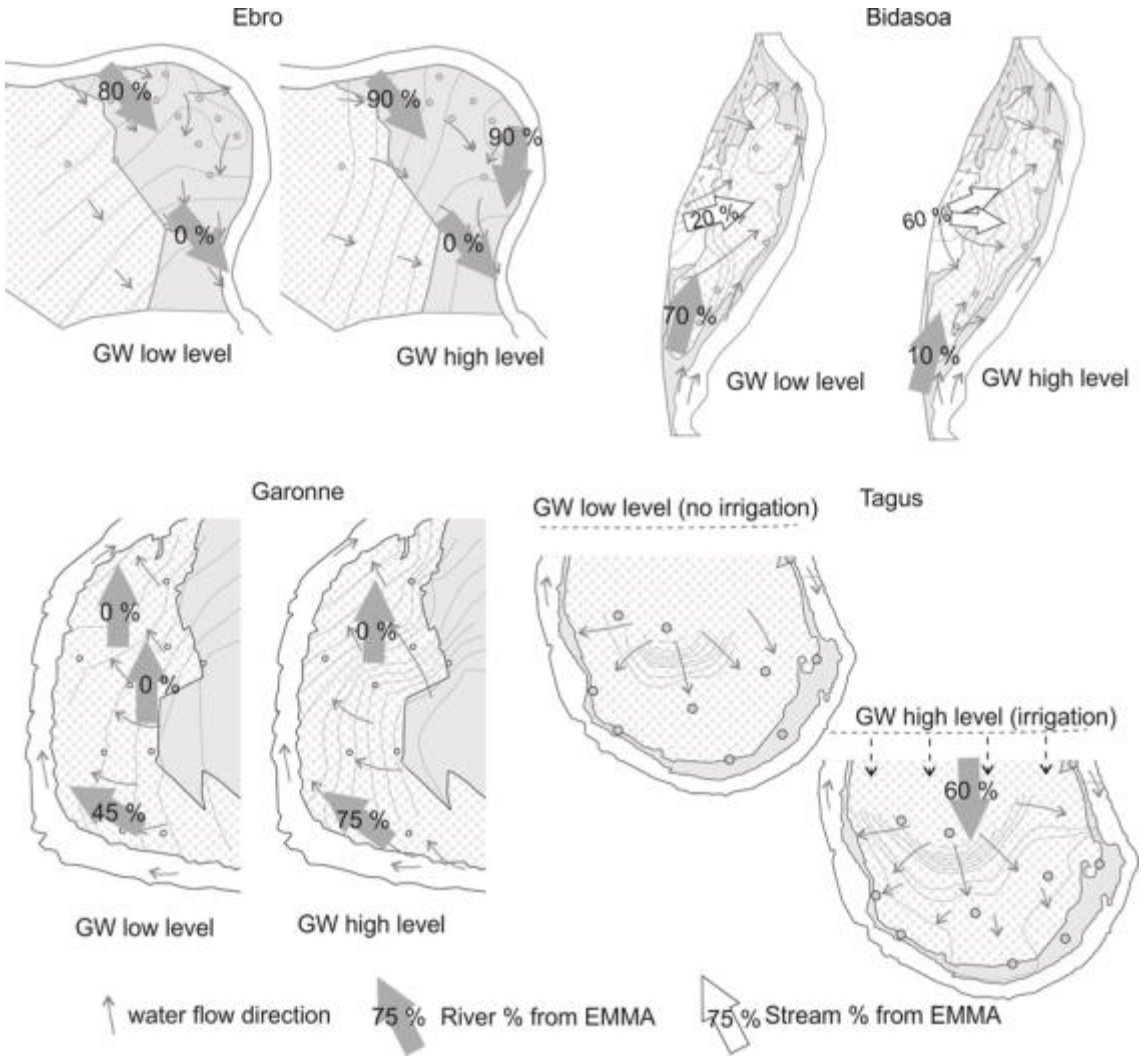

Figure 6: Flow nets of the study sites. Groundwater (GW) high and low level periods are considered separately. River water percentage in the aquifer is also shown.

Hydrochemical characterization

Figure 3 indicates on the hydrographs of the rivers the moment of the monthly (circles) and quarterly (arrows) sampling campaigns carried out, and figures 7 and 8 show the hydrochemical characterization of waters in each of the four study sites. In boxplots in figure 7 the variation range of the most significant parameters for the studied sites can be observed. Sulphate and alkalinity have not been included in the figure because, generally, their spatial evolution is similar to that of the electrical conductivity (EC). Sampling points in the aquifer have been grouped according to their distance to the river (near river, intermediate zone and distant zone) and results for those groups and for the river are shown separately in the figure.

Principal Component Analysis

In order to make visible the different groups of waters in each site a factor analysis was performed, separately for Ebro, Bidasoa, Garonne and Tagus sites. It was intended to better understand river-aquifer connectivity and mixing processes in the sites.

Considering the first four principal components (PCs) extracted from the analysis (eigenvalue exceeding one) all together between 70% (Tagus) and 76% (Ebro) of the variance of the data matrix is explained. In all the sites the highest positive loadings (>0.7) of the first component (22-37% of explained variance) are related to EC, Alkalinity and water depth (wd), except in Tagus site, and the most negative ones to dissolved oxygen (O_2) and pH, so that this component helps establishing differences between groundwater in the alluvial aquifer (positive loads) and river water (negative loads), except for Ebro site, where river shows a high hydrochemical variability. Aquifers are mainly affected by agricultural practices (sulphate load is moderate in this factor) in Ebro and Garonne sites, while in Bidasoa site it is affected by a point source pollution (farm). However, in Tagus site hydrochemistry of the aquifer is clearly impacted by superficial waters (irrigation channel), which have a strong load of dissolved organic carbon (DOC) and potassium (K^+). Concerning superficial waters Tagus and Bidasoa sites show a distinctive behavior due to the presence of a lateral stream generating recharge into the aquifer in Bidasoa site and of an irrigation channel, which is a diversion of the river, in Tagus site (figures 1 and 2).

The second component (19-22% of variance), is more variable and site-specific. This component shows better than the first one the differences of river water in Ebro site (with higher pH and O_2 values and lower DOC). In Bidasoa site PC2 is characterized by the high loading of DOC, K^+ and, in a lesser extent, ammonium (versus ORP) which clearly represents impact from the farm to the aquifer. In Tagus site, however, this component shows influence of intensive agriculture (high SO_4^{2-} level), with an excess of fertilizers (including uncontrolled application of manure and pig slurry). Finally, for Garonne site PC2 shows very clearly the influence of agricultural practices on the aquifer (NO_3^-, SO_4^{2-} with highly positive loadings). Third and fourth principal components (less than 16% of variance) are related to site-specific environmental conditions which affect biogeochemical processes controlling nitrogen compounds fate, oxidation-reduction conditions and temperature. Only in Bidasoa site PC3 (16%) shows a clear loading for nitrate and sulphate, which is indicating the influence of the limited (intermediate zone) agriculture activity in the site.

Principal Component meaning

Figure 7 can assist in interpreting the meaning of the PC axes. High EC, related mainly to sulphate variation and alkalinity (positive side of PC1) are clearly located in the agricultural area in Ebro site and values of these variables decrease towards the river. In Garonne and, mainly, in Tagus sites distribution is different, being the intermediate and near river zones the ones with the highest values of the mentioned parameters. This difference can be explained in Tagus site by the intense application of fertilizers in the lowland area of the meander; the distant zone, although it is also agricultural, is closer to the irrigation channel and directly affected by its waters, so that fertilizer loading is not as high as in the intermediate zone. In Garonne site explanation of this fact can be related to the biological activity in the floodplain which would be the source of an increase in alkalinity observed in this site. In Bidasoa site the highest values of EC and alkalinity are related to the farm (dairy); in any case values of EC, alkalinity and sulphate in Bidasoa site are always lower than those in the other sites.

Concerning dissolved oxygen (O_2) the highest contents (average higher that 85%) are always in river water, but also in the distant zone in Tagus (owing to the irrigation channel) and Garonne site (irrigation). In both cases the lowest contents are in groundwater in the near river zone (around 20% on average). Similar to those are the values that appear in the three defined zones of Ebro site. Slightly higher (30-37%) is the O_2 content in the riparian zone of Bidasoa site, except for groundwater near the farm where the content is lower (18%). With regard to the pH (no figure) its spatial distribution in the sites is quite similar to that of the dissolved oxygen, with the highest values in the rivers, between 7.7-8.7 in all the sites, and the lowest ones in groundwater in the riparian zone (6.0-6.8).

With respect to other variables involved in nitrate attenuation (DOC, ORP and N-compounds) factors controlling them are site-specific so that spatial distribution of these elements is quite different among sites. As can be observed in figure 5 the main DOC source in Bidasoa site is the farm (5 mg/l on average) and in Ebro site the agricultural input is very obvious, around 14 mg/l (in fact here DOC is in the positive side of PC1 as seen in figure 8), being in both cases the river the point where the lowest values are measured (2-3 mg/l). However, in the other two places the main source of dissolved organic carbon is the river (6 and 2 mg/l of DOC in Tagus and Garonne sites, respectively). In Tagus site, where DOC has a strong loading in PC1, there is a small increase in DOC in the distant zone which should be related to the influence of the irrigation channel. Rivett et al (2007) stated that DOC levels in most aquifers

are relatively low, typically < 5 mg/l, which is in accordance with our data except for Ebro site where intense irrigation makes the values to be higher anywhere in groundwater.

Regarding Oxidation Reduction Potential (ORP), presented in PC3 and PC4 (no figure), the highest values and the ones with a higher variation range are observed in Garonne site (figure 7) with average values between 180 and 230 mV and a decreasing trend from the agricultural area to the river. The other sites show a range between 75 and 150 mV without any significant spatial trend. It is to be pointed out the distant point in Bidasoa site, next to the farm, where groundwater shows negative values of ORP. These negative values of ORP come along with the highest values of alkalinity, DOC and ammonium and the lowest of dissolved oxygen. Negative values of ORP are also observed in some piezometers of Tagus site but only exceptionally.

N-compounds occur in different forms in the studied sites according to sources considered. In all the studied sites, except in Bidasoa, the majority of N is found as nitrate which is the more stable form when considering the physicochemical characteristics of waters in the studied aquifers. The highest concentrations of NO_3^- appear in groundwater of the agricultural area (32 mg/l in Ebro site and 62 mg/l in Garonne site, on average; in both nitrate comes along with high values of EC, SO_4^{2-}, K^+ and SiO_2 and is well represented in the first two components, figure 8) and the values decrease towards the river, mainly in Garonne site. In Tagus site spatial variation is not so evident but, nonetheless, a little higher concentration (35 mg/l) is observed in piezometers near the river as a result of the uncontrolled and intense use of chemical and organic fertilizers in this area.

In Bidasoa site the most significant source of organic pollution is the farm (a point source), being the principal N-form released ammonium (up to 36 mg/l NH_4^+ in piezometers near it, distant zone, and NO_3^- below 1 mg/l); in fact NH_4^+ shows a high loading in PC2 in Bidasoa site (figure 8). Another source of N to be considered in this site is related to agricultural practices though they are not very important and are limited to the intermediate zone; this is why a small increase in NO_3^- values (12 mg/l) is observed in piezometers near river. Nitrate in rivers range from 13, in Garonne, to 3 mg/l, in Bidasoa site.

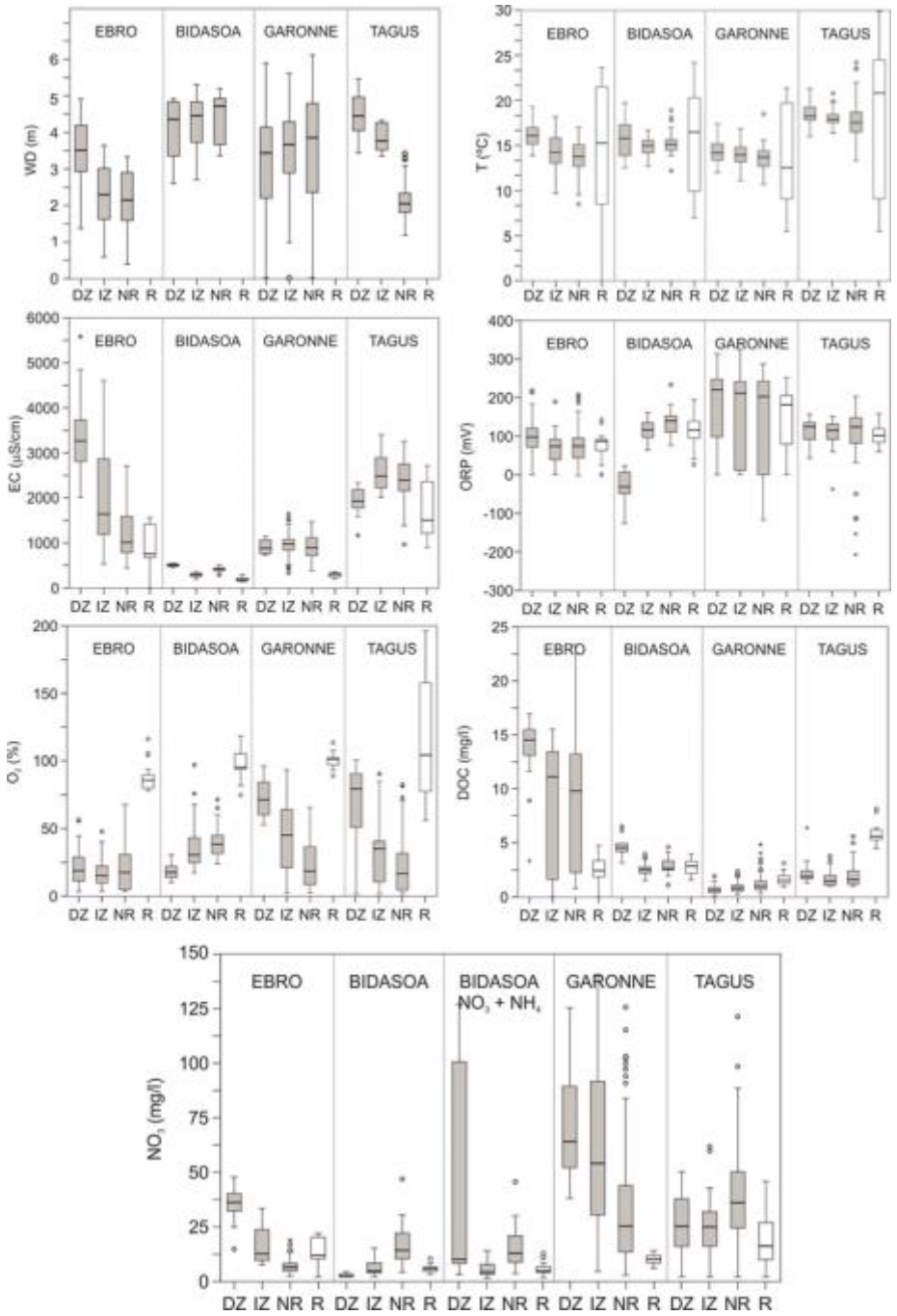

Figure 7: Boxplots of some important physicochemical indicators based on monthly sampling data. Distant zone (DZ), intermediate zone (IZ), near river zone (NR) and river (R) are considered separately.

Phosphate values are lower than 60 µg/l PO_4^{3-} in Garonne and Bidasoa sites being the highest values measured in the river (no figure). Values in Ebro site are also low on average but with a wide range in the river and near river waters (up to 122 µg/l PO_4^{3-} as usual values). A clear difference is observed in Tagus site where values in river and channel waters are around 1030 µg/l PO_4^{3-} on average but can reach more than 1800 µg/l (phosphate is represented in the first component); these high values are to be related to the many sewage treatment plants located

upstream. It can be concluded that in these sites phosphate is coming from the superficial waters.

Silica shows a similar pattern (no figure) in all the sites with values ranging from 10-20 mg/l of SiO_2 in groundwater (mainly in the distant zone) and up to 4-6 mg/l in rivers. This element is thought to be a lithological signature of groundwater due to the significant positive correlation with EC, sulphate, alkalinity and water depth and negative one with dissolved oxygen and pH. Silica is also well related to nutrients as nitrate and potassium in Garonne and Ebro sites where agricultural practices in distant zones are well defined; however, such a relation does not appear in the other two sites because these practices are either limited (Bidasoa) or quite uncontrolled (Tagus).

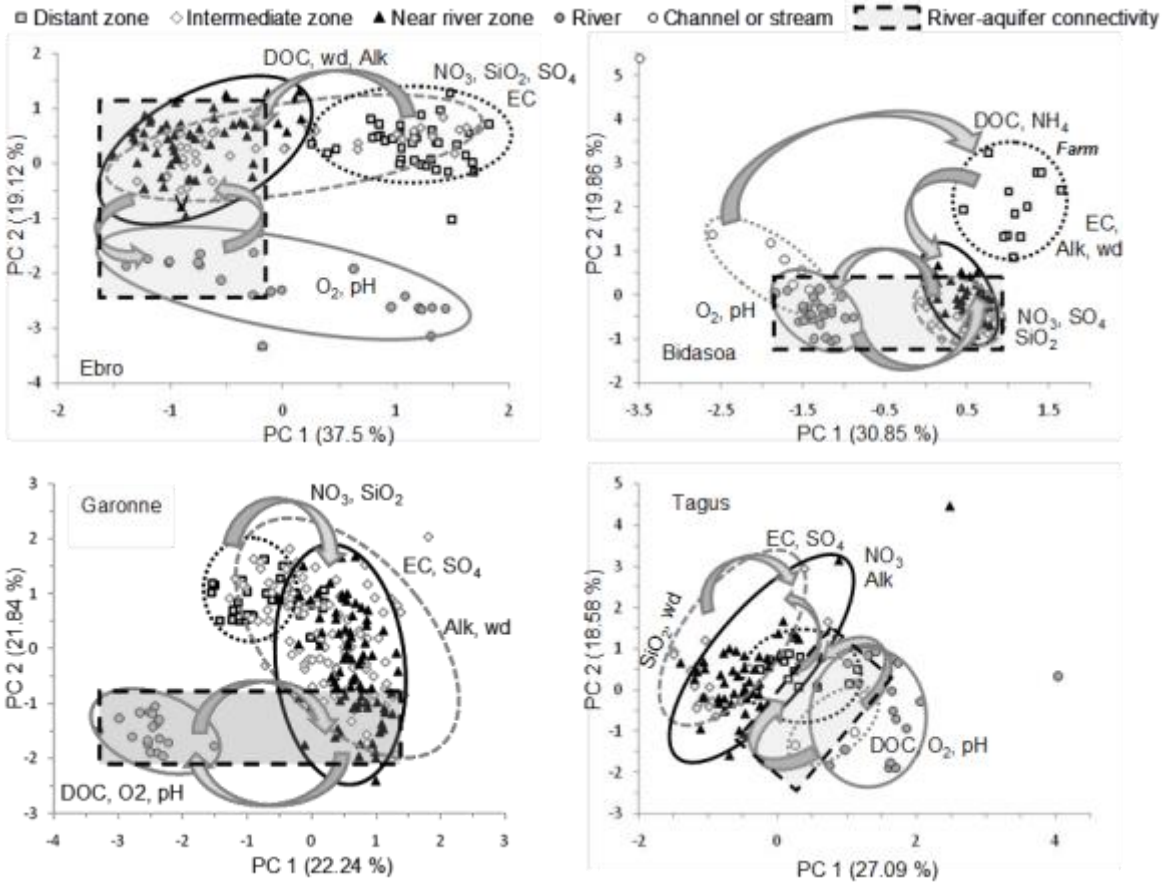

Figure 8: Water characteristics spatial evolution according to water groups location in the I-II factorial plane of the Principal Component Analysis performed in each site. Connectivity is also marked.

Groundwater average temperature ranges between 13 and 16°C in Ebro, Garonne and Bidasoa sites (figure 7) being the temperature in piezometers near the river in the lowest part of that range. In Tagus site temperature is a little higher (around 18°C) with slight differences between piezometers. River water average temperature is around 13.5-15°C, except in Tagus

site where it is higher (21°C) and more variable along the year (25°C fluctuation) as a result of being an extremely regulated river.

Hydrochemical spatial evolution

In figure 8 waters of different zones (river, near river, intermediate zone and distant zone) are gathered, for each site, according to their location in the I-II factorial plane of the PCA. Arrows on the graphs show groundwater flow from distant zones to the river as well as connection between aquifer and river. Diagrams of Garonne and Ebro sites depict similar hydrochemical evolution. In both places groundwater in agricultural area (distant zone) is characterized by NO_3^-, EC, SO_4^{2-}, Alk, and SiO_2, being in this zone where the water is deeper (wd). In Ebro site DOC content is also significantly high in the agricultural zone. Moving towards the river values of those elements in groundwater significantly decrease in Ebro site, whereas in the Garonne site they slightly increase. In both sites concentrations in water are the lowest in the river, except for O_2, pH and phosphate (also DOC in Garonne). Groundwater in intermediate zone of both sites occupies a broad space in the graph showing important hydrochemical variability ranging from hydrochemical composition of waters in distant zone to that of waters in near river zone. In Ebro site near river zone waters and distant zone waters appear more separated that in Garonne site, showing a clearer trend along the flow direction (figure 6). In any case, river waters always appear sharply separated from groundwater but close to the near river waters indicating a probable connectivity.

In Bidasoa site the farm (distant zone) significantly influences hydrochemical evolution of waters along the flow direction (figure 8) so that waters near the farm are clearly separated from the others in the graph. These waters are characterized by high values of DOC, ammonium, EC and alkalinity (usually with negative values of ORP). In this area the water level in the aquifer is quite deep. Downward nitrate and sulphate contents increase due to nitrification and to leaching of fertilizers applied in a reduced agricultural area in the intermediate zone so that the effects are more relevant near river. Also SiO_2 shows an increase towards the river what is to be related to water coming from the lateral small stream that drains granites and shales; in fact this lateral water enters into the aquifer deeply (bedrock below the alluvial is roughly 25 m deep, with a very irregular surface) and flows upward near the river (figure 2). Finally, river waters are characterized mainly by high values of dissolved oxygen and pH (as are the ones in the stream), and in a lesser extent by phosphate. As a result waters in this site are well distributed along the flow pathway.

Surface water lateral flow is also present in Tagus site where a channel derived from the river is used for irrigation purposes. So waters in both river and channel show similar hydrochemical characterization with high values of DOC, O_2 and pH (also PO_4^{3-}). From the channel downward there is a progressive increase in EC, SO_4^{2-}, alkalinity, SiO_2 and NO_3^- as fertilization is very intense, diverse and uncontrolled (Bodoque et al, this issue). The broad spatial variety of agricultural practices in this site makes practically impossible to establish a suitable relation between causes and effects on the basis of available data, which derive from a monitoring design that has been satisfactory to assess the main hydrochemical aspects in the other sites. Even though flow net in this site is very simple (figure 6), with a radial flow in the meander toward the river and without practically connectivity between aquifer and river, there is not a clear hydrochemical pattern being the groups in the graph (figure 8) quite mixed. Thus, river water group is not clearly separated, as it is the case in the other sites, despite the lack of influence of the river into the aquifer.

EMMA application

A simple end-member mixing analysis was performed in each study site to estimate the proportion of water from different sources in the mixed water of the aquifer. Our approach is based on the PCA results, being the main goal, as mentioned previously, to provide an adequate estimation of the mixing with few input parameters. Having this in mind, we tested the potential use of the electrical conductivity (EC) as a simple good indicator of water mixing. In fact, EC has a strong loading in the PC1 of the PCA performed in each of the study sites. Using this indicator the percentage of water coming from each of the end-members in all the campaigns and all the monitoring points of the aquifer was estimated. Δ-maps commented in the discussion have been derived from the EMMA results in order to localize the attenuation zones.

As observed in figure 7, EC can help separating well groundwater in agricultural zones and surface water in both river and stream (Bidasoa site) or channel (Tagus site). According to spatial hydrochemical evolution shown in figure 8 a mixing analysis with two end-members was applied: surface water (SW) and groundwater (GW). In Garonne site SW and GW sources were clearly identified (on average 250 and 1000 μS/cm, respectively), as well as in Ebro site (750 and 3200 μS/cm, respectively). In Tagus site (1900 μS/cm in the channel water and 2500 in agricultural areas) the situation is more complex being multiples fertilizers, including pig slurry, poured uncontrollably in the intermediate and near river zones, in spite

of this an attempt was made considering the irrigation channel as the SW source. This simple approach does not work in Bidasoa site owing to the disturbance created in EC by the point-source of pollution, so that in this case we were obliged to use three poles and, consequently, two physicochemical indicators (alkalinity and silica). In fact, in Bidasoa site apart from the river water pole (the lowest values) water spreading from de farm (high alkalinity, around 5 m/l), in a quite radial flow net, and water coming from the lateral rocks (granites, shales; high silica, around 10 mg/l) are also considered.

Figures 2, 3 and 6 help showing the river-aquifer relationship. In Garonne site during flood events, which only happens for a few days, the river water level increases rapidly and the water flows from the river into the floodplain allowing the lateral (water infiltrating through the river bank) and vertical (flooded water percolating through the surface) recharge of the alluvial aquifer. During the drying stage the water flows back into the river. Despite there being no observations during the flood itself, the part of the river water in the meander a few days after the flood ranges from 75% upstream next to the river to 0% towards the north and in the agricultural area. During the drying stage the water flows back from the aquifer to the river, and three months after the flood the percentage of water from the river in the meander is only between 45% in a small area near the river and 0% in more than half of the aquifer area. The fact that this proportion of river water is lower downstream to the north of the aquifer is in accordance with the hydraulic heads showing a more significant flow of water from the aquifer to the river in the northern area. Finally it seems that the water in the aquifer always contains a proportion of river water in the upstream part of the aquifer (southern part of the meander) where the flux of water flowing back from the aquifer is very small.

In Ebro site during the low waters period the river and the aquifer have similar water levels, and their water flow direction is quite parallel. There is a backflow entrance of water in the aquifer from the river that matches its previous course. Otherwise, during the high water period this backflow is compensated with the entrance of river water at the meander head, and the role of the previous river course is switched to a preferential path for the groundwater. During flooding situations the aquifer receives lateral and vertical recharge. The river water in the floodplain aquifer is always very high, up to 80% in near river zone and a part of intermediate zone during low level periods, and up to 90% in high level ones.

In Bidasoa site, during high flow periods surface water coming laterally from the small catchment located in the west part prevails. This water enters the aquifer mainly through the

alluvial fan (the highest hydraulic head), where the point-source of contamination is located, and it moves mainly towards the north part of the meander where its contribution can reach a 60% of water in the aquifer. In these periods the Bidasoa River contribution to the aquifer is small (10%) and spatially limited to the south part of the meander. However, during low flow periods there is a higher entrance of water from the river in this part, up to 70%, going this percentage decreasing from south to north at the same time that lateral contribution goes increasing. The floodplain is rarely occupied by the river but even in this case the water level in the aquifer does not reach the level of river water on the soil, which is due to the semi-confined character of the aquifer. In fact, the main recharge of the aquifer is water coming laterally from both river and stream, being the vertical recharge very reduced and delayed after flooding.

As previously mentioned in Tagus site there is not a two-way water exchange between the river and the aquifer. The entrance of surface water in the aquifer is addressed with the irrigation from the channel which is, in fact, an upstream diversion of the river. Water coming from he channel can represent up to 60% in some mixing areas but is very variable form one point to another.

Discussion

Some studies, reviewed by Burt et al (2013), point to the high degree of variability of factors accounting for the attenuation processes among sites in a riparian zone and a limited predictive capacity based upon broad-scale drivers. Now we discuss the results obtained from one year monitoring in order to delimit the places where attenuation processes are more evident along the water year and try to justify their spatial location.

Delta maps

Delta maps were obtained, in a monthly scale, from the comparison between theoretical concentrations of NO_3^- and DOC (EMMA analysis) and real concentrations. Negative rates of variation indicate a consumption of these compounds, meaning that attenuation might be taking place at these points. Positive rates, however, indicate an enrichment of those compounds. We discuss the results obtained emphasizing the spatial dimension of the attenuation processes. Figure 9 shows for each study site the places where usually attenuation

processes regarding nitrates happen along the year. N and C main sources are also shown for a better understanding of the involved dynamic.

In **Garonne** site the results show that negative ΔNO_3^- was observed in groundwater all along the floodplain, which could be related to attenuation processes by denitrification. However, it appears that the most active nitrate attenuation area is located in the central part of the floodplain (figure 9), with rates usually higher than 60% (even higher in high level periods). Attenuation processes in this area can be enhanced by the most important nitrate flux from the aquifer and by high DOC availability due to the low topography which makes flooding easier. Dissolved organic carbon has two main sources in this site: the river (figure 7) and the organic matter-rich top layers of soil. In fact, as observed in figure 3, positive ΔDOC appears in groundwater during and just after important rising of the water table (mainly in winter and spring) during which the table reaches topsoil. Water level evolution in the aquifer is similar to that in the river so that the highest rising situation coincides with flooding in the area. Indeed a half of the site is flooded during a percentage of time (2%, around 7 days a year) similar to the time during which the water table remains over the land surface in the near river and intermediate zones (figures 4 and 5), covered by forest. Despite the low duration of floods, they cover a high extension of the floodplain due to the flat topography of the area (figure 2).

Flooding enables the percolation of DOC from soil and its rapid incorporation to the aquifer due to the high permeability of the alluvial deposits. Therefore, DOC enters the aquifer both laterally from the river (when river discharge is rising) and vertically when flooding (occasionally). Nitrate input is guaranteed by the high lateral continuity of the alluvial deposits, with a continuous flow from the agricultural area (distant zone). In this area it is not expected to be high attenuation of nitrate as low DOC and high O_2 concentrations in groundwater are far from required. Water table fluctuation, which is very high (figure 7), is controlled by the river (horizontal exchange of water) due to the important river incision and the limited thickness of the deposits. Figure 9 summarizes the main sources and pathways of nitrate and carbon. Continuous input to the marked attenuation zone is guaranteed by both the aquifer (N) and the river (C), though the attenuation processes become most important in flooding situation when these processes could take place also in the north half of the site.

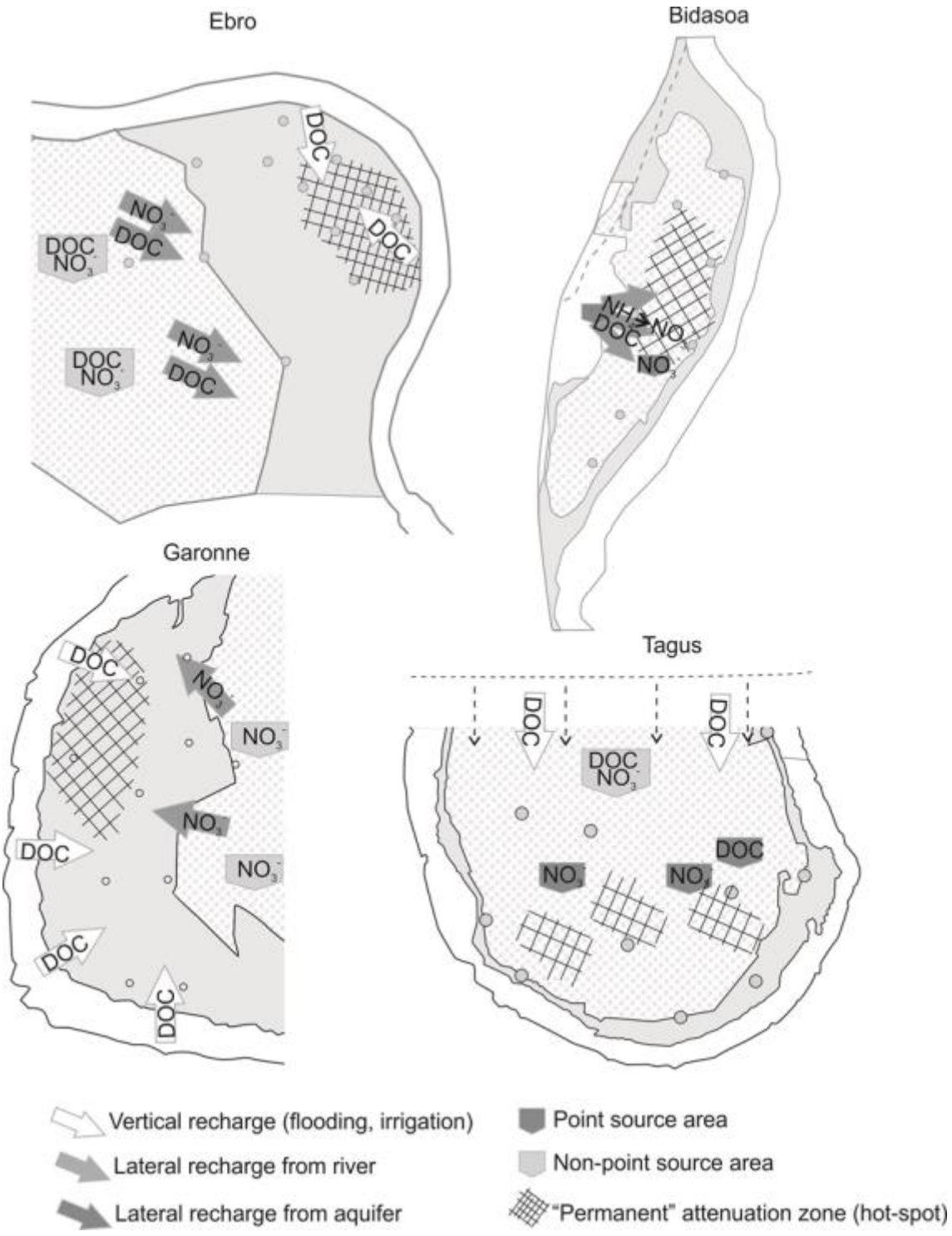

Figure 9: Main sources of N and C in the study sites. Most usual attenuation places along the year according to the EMMA results (negative delta). See figure 1 for information about land use.

In **Ebro** site negative ΔNO_3^- was observed in groundwater anywhere along the riparian area. Attenuation rate is high any time in the near river zone (up to 90%) but it is also important in the intermediate zone (up to 50% in high level periods). This fact has to be partly related to the river water presence in the aquifer (figure 6) which is always very high in these zones,

supported by the prevailing flow net in the site, parallel to river. The old course of the river, filled of coarse gravels, helps this pattern. The river is one of the sources of nitrate in the riparian zone as the concentration in the river water is relatively important, higher than in the Garonne and Bidasoa rivers (figure 7). Anyway, the most important source of N is the agricultural area (distant zone). According to the mentioned flow net, nitrate-rich groundwater flows towards the down part of the meander. On the other hand, the main source of DOC in this site is also the agricultural area, so that nitrate and dissolved organic carbon share the same source. Furthermore, concentration of DOC is quite high compared with the values in the agricultural areas of the other study sites (figure 7). This fact is to be related with an intense irrigation and a high content of organic matter in the soils of the area. Therefore it could be thought of the possibility for nitrate attenuation processes to take place in the agricultural area before groundwater reaches the riparian zone (dissolved oxygen content in the agricultural area is low, figure 7, and could help these processes). Unfortunately the monitoring piezometers of the agricultural area were located just in the limit with the riparian zone, so that we cannot consider processes potentially occurring in the distant zone itself.

Anyway, another DOC source to take into account is the vertical input to the aquifer from the topsoil when flooding. In fact, the small river incision (the smallest among the study sites) and the gentle slope of the floodplain make the flooding to occur (figure 4) more frequently and with a longer duration than in the other sites. At the same time, the extensive riparian corridor is dominated by forest. Both aspects favor DOC to enter the aquifer and flow downward adding dissolved organic carbon to the groundwater coming from agricultural land. Figure 3 shows periods when ΔDOC is positive in the aquifer. This occurs mainly in low level situations when the river water input to the riparian zone is lower and, comparatively, groundwater input is higher. The increase of DOC expected when flooding could be exported rapidly as not positive ΔDOC are observed, in general after this situation.

Water table in the riparian corridor (near river and intermediate zones) remains over the land surface around a 5% of time (18 days per year), longer than flooding time of the 50% of the site which is 2% (figures 4 and 5). Apart from this, water table fluctuation is relatively small (compared to Garonne site; figure 7) and similar in all the zones of the site. It means water table dynamics is mainly controlled by the aquifer, which has a high lateral continuity and a big thickness. As observed in figure 9 the most permanent attenuation zone is located in the near river and intermediate zones downstream in the meander where favorable conditions take place. The figure gives a general explanation of the processes considered. N and C inputs,

from the agricultural areas, converge in this spot of shallow water table where additional DOC supply could be expected during flooding events.

In **Bidasoa** site the most important source of nitrogen is a point one (the farm) where an important amount of NH_4^+ is introduced into the aquifer and transported according to the flow net in the site (figure 6). Most of this ammonium is transformed to nitrate when travelling towards oxidizing environments. In fact dissolved oxygen in groundwater near the farm is very low, the lowest among the observation points in all study sites (figure 7). This is the reason why total inorganic nitrogen (NO_3^- + NH_4^+) was considered when calculating ΔNO_3^- in this site. Attenuation is evident in groundwater all along the site with rates usually around 50-75%. Nitrate enrichment is observed punctually after high water table periods but only in piezometers near the limited agricultural area (a part of the intermediate zone). Concerning DOC the main source is also the farm, so that the highest amount of N and C are entering the aquifer from the same point source. In general, there is no positive ΔDOC along the riparian area as groundwater in the farm has been considered as an end-member in the EMMA analysis. Nevertheless, occasionally in time and punctually in space, positive ΔDOC were observed after the occurrence of some important floods in the river (figure 3), which means that the EMMA analysis, as we applied it, cannot be used to understand specific situations. Negative rates, ΔDOC up to 75%, are placed mainly along the flow lines from the farm.

As mentioned for Garonne and Ebro sites, in Bidasoa it has to be also considered the input of DOC into the aquifer by percolation from soil when flooding, even though the forest area is just a narrow strip along the river course. Such an event occurs occasionally in this zone, with lower duration and extension than in the previous sites (figure 3). Despite it, the water table remains deep and hardly reaches the topsoil (2 days a year) never rising above soil surface (figure 4). This is due to the semiconfined character of the aquifer, with a thick silty formation overlying the highly permeable gravel deposits. However, this situation can help the upper part of the terrain maintain high water content for a long period of time. Consequently, water percolation from the soil, including DOC, is limited and delayed in time, so that the most important input of DOC to the aquifer is the lateral from the farm area according to the flow net. On the other hand, water table fluctuation is quite similar in different strips from the river (figure 7), being the more distant where the table is shallower. Taking also the important incision of the river into account it can be concluded that the water table in this riparian area is mainly controlled by the lateral stream conducting its water into the aquifer, in a radial way in high level periods (figure 6).

Figure 9 shows the location of the most permanent attenuation zone. This spot is totally conditioned by the position of the farm and the flow pattern. In fact, all the zones of the aquifer which are not in the flow path from the farm show quite good quality water since surface water entering the aquifer (from both the river and the lateral stream) are of relatively good quality. We cannot refer to the potential attenuation processes in these zones as not mixing with water coming from the farm occurs there. But we can at least delimit the attenuation zone regarding the actual pollution source.

In **Tagus** site the obtained Δ-maps are difficult to understand because of the complexity of the performed EMMA analysis itself. Information gathered on this site has been treated by Bodoque et al. (this issue) showing the difficulty to integrate different approaches (hydrochemical, potential denitrification, taxonomic and functional composition of macroinvertebrates, bacterial community structure, hydrological modeling). Focusing on our interest, punctual patches of positive ΔNO_3^- appear during the irrigation period, which is related to the uncontrollable use of different fertilizers and the broad spatial variety of agricultural practices. This makes it practically impossible to establish suitable cause-effect relationships with our monitoring data. In fact, unlike in the previous sites in this one N inputs to the aquifer can occur everywhere as the agricultural practices cover the entire site from the distant zone to just the river line. High spatial continuity of the alluvial deposits allows a continuous lateral input of N.

In general, negative ΔNO_3^- predominate with values between 20 and 60% showing a high irregular spatial distribution. This fact is also visible when mapping ΔDOC. Only some enrichment patches of dissolved organic carbon are observed, without any temporal trend. Negative ΔDOC can reach up to 50% in the internal area of the meander, during irrigation period, without any spatial pattern. As observed in figure 7 the main source of DOC is the river. However, almost no river water enters the alluvial aquifer according to the hydraulic head distribution (figure 2) and no flooding situations occur (figure 4) being the river extremely regulated and very incised. Consequently, no DOC percolation from the soil is expected, moreover being the forest just a very narrow and disconnected strip along the river course. However, water used for irrigation in this site is tapped from a channel which in fact is a river diversion (figure 6). This allows DOC to reach the aquifer by irrigation.

Figure 9 shows the location of attenuation spot, which in this site is much more doubtful than in the previous ones. It is limited to some patches in the intermediate and near river zones.

Water table fluctuation is small and limited to the irrigation periods (figures 5 and 7). In any case water table is deep enough everywhere and any time. Bodoque et al. (this issue) have shown the importance that the recovery of flooding situations will be in order to activate again ecological functionality of the site.

Methodological aspects

Except for Tagus site, due to the site-specific complexity (Bodoque et al., this issue), the approach applied in this study resulted in a useful tool for the spatial delimitation of the zones where permanent attenuation processes take place in riparian areas. A monthly based one year monitoring, in both the river and the aquifer, in increasing distances from the river, allowed having an overall conceptualization of the attenuation processes, assuming that usual high and low level periods were monitored. Due to the inherent difficulty for sampling during short flooding events the continuous monitoring of the water level in the river and the aquifer becomes very helpful for further knowledge.

A key point is the connectivity upland-river-aquifer. Hydrochemical data can help us understand hydrological information. So, figure 8 shows the spatial evolution (from the distant zone to the river) of water characteristics based on PCA analysis of available data in each study site. Such a distribution allows tracking the main processes taking places in the sites. We have roughly marked on the figure the domain where surface water (SW) should be affecting groundwater (GW) chemistry. The fact that some points of SW remain out of this domain indicates specific time situations when such affection is not happening. Nevertheless our interest is in the overall conceptualization.

Diagrams of Garonne and Ebro sites depict similar evolution from the agricultural area to the river. This is a result of being the land use zoning of these sites very clear with the agricultural practices being limited to the distant zone. In Ebro site near river zone and distant zone (agricultural area) waters appear more separated than in Garonne site which can be explained by the flow net prevailing in each site (figure 6). In fact, in Ebro site river water enter the aquifer and flow all along the near river and intermediate zones making characteristics of waters in these zones to be closer to those in the river water. However, in Garonne site the groundwater flow is more radial from the distant zone so that characteristics of groundwater in the riparian zone are more homogeneous and they are clearly separated from the river water

even though the entrance from the river become very important in some periods in the upstream part of the meander.

Also in Bidasoa site surface waters and aquifer waters are clearly separated. As in Garonne site the more radial character of the flow net does not allow the river water presence in the aquifer to be continuously significant along the riparian area. Entrance of water from the lateral stream becomes relatively more abundant in some periods, nevertheless groundwater show very different characteristics as this water intersects the pollution point source. Consequently, waters of different distances from the river occupy different positions in the graph (figure 8) making very evident the influence of the farm on the overall hydrochemical behavior in the site. Water samples positions in the graph shows a messed spatial distribution for Tagus site which is in agreement with the different types of agricultural practices, some of them very localized in space and time, and with an uncontrolled use of a great variety of fertilizers. In this site surface waters appear near aquifer waters in distant zones from the river, but without really indicating direct connectivity with it. Irrigation with waters from the channel derived from the river explains this proximity.

Finally, Principal Component Analysis provides a good overview of the different types of waters in the river-aquifer system of a riparian area, being considered it is based on a detailed monitoring in both space and time. However, interpretation of the spatial evolution along the system may not be so obvious to do, as site-specific factors need to be taken into account. Similarity of hydrochemical characteristics can lead to an erroneous understanding of the connectivity with the river. On the other hand, a certain degree of connectivity may remain hided if collected data are not adequate to represent site-specific factors. In any case, hydrochemical data have to be interpreted together with hydrological observations.

Conclusions

A comparative study of the characteristics of four riparian areas in the SUDOE region (Southwest Europe) was conducted in the framework of the Attenagua Project, regarding their capacity for nitrate attenuation. The main goal was to develop a simple approach for the spatial delimitation of zones where the best conditions leading to favor attenuation processes (hot spots) are guaranteed along the time. The project wanted to identify these zones to take advantage of the processes in order to supply drinking water of good quality. This goal in mind we focused on several site-specific factors controlling these processes: flooding events,

water table fluctuations, flow net, N and C sources, mainly. The sites we chose present important differences in these factors and are representative of common situations in the SUDOE region.

Our approach was based on a detailed monitoring of chemical constituents, in both the river and the aquifer, once a month during a year, including a continuous measurement of water level. Based on a simple PCA and EMMA analysis, data treatment showed that such a monitoring can provide an accurate spatial representation of the attenuation places for three (Garonne, Ebro, Bidasoa) of the four studied sites. In the fourth one (Tagus), the vast heterogeneity of agricultural practices makes the representation to be inaccurate so that a more detailed monitoring would have been needed.

Once the attenuation zones were spatially delimited an attempt was made to validate them by considering site-specific attributes that can justify the processes leading to the attenuation of nitrate. Sources of N and C are different in each case, as they are the flow net and the flooding dynamics. As it has been observed, attenuation processes can occur in a riparian area even though connectivity with the river is temporally limited, given other factors favoring these processes take place in that area. It leads us to conclude that a general conceptual model cannot capture all the factors needed to understand the nitrate removal dynamics of a riparian zone. Site-specific study is necessary. However, the methodology followed in this project enables the delimitation of the attenuation zones in a site, as regards to nitrate, and this helps specify a more focused research in those zones.

Acknowledgements

This study was performed as part of the EU Interreg SUDOE IVB programme (ATTENAGUA - SOE3/P2/F558 project, http://www.attenagua-sudoe.eu) and funded by the European Regional Development Fund (ERDF). For the Garonne site the research has been carried out as a part of "ADAPT´EAU" (ANR-11-CEPL-008), a project supported by the French National Research Agency (ANR) within the framework of The Global Environmental Changes and Societies (GEC&S) programme.

References

Almasri, M.N., Kaluarachchi, J., 2007. Modeling nitrate contamination of groundwater in agricultural watersheds. J. Hydrol 343, 211-229. Doi:10.1016/j.jhydrol.2007.06.016

APHA-AWWA-WPCF. 1998. Standard Methods for the Examination of Water andWastewater. American Public Health Association: Washington, DC.

Arrate, I., Sanchez-Perez, J.M., Antiguedad, I., Vallecillo, M.A., Iribar, V., Ruiz, M., 1997. Groundwater pollution in Quaternary aquifer of Vitoria: Gasteiz (Basque Country, Spain): Influence of agricultural activities and water-resource management. Environ. Geol 30, 257-265. Doi:10.1007/s002540050155

Bernard-Jannin, L., Brito, D., Sun, X., Jauch, E., Neves, R.J.J., Sauvage, S., Sánchez-Pérez, J.M. A physically-based, spatially-distributed modelling approach coupling surface water and groundwater flows to evaluate water exchanges in an alluvial floodplain during flood events. Submitted in Advances in Water Resources.

Bernard-Jannin L., Sun X., Teissier S., Sauvage S., Sanchez-Pérez J.M. Spatio-temporal analysis of potential denitrification hot spots and hot moments in groundwater and their impact on nitrate dynamics in an alluvial floodplain. Submitted to Ecological Engineering.

Bodoque, J.M., Ladera, J., Yela, J.L., Alonso-Azcárate, J., Brito, D., Antiguedad, I., Comin, F.A., Duran, R., Attard, E., Lauga, B., Sánchez-Pérez, J.M. Recovering hydromorphological functionality to improve natural purification capacity of a highly man-modified wetland. Submitted to Ecological Engineering.

Booker, D., Goodwin, T., Griffiths, J., Old, G., Smith, J.W.N., Young, A. 2008. A classification scheme for pollutant attenuation potential at the groundwater - surface water interface. Science Report – SC030155/SR7. Environment Agency. ISBN: 978-1-84432-937-3

Braunschweig, F., Leitao, P.C., Ferdandes, L., Pina, P., Neves, R.J.J. 2004. The object-oriented design of the integrated water modelling system MOHID. Proceedings of the XV international conference on computational methods in water resources 2, Chapel Hill, NC, USA. 1079-90.

Brito, D., Bernard-Jannin L, Sauvage, S., Zabaleta, A., Comin, F., Bodoque J.M., Neves R., Sánchez-Pérez J.M. 2014. Modeling the hydro-biogeochemistry functioning in alluvial wetlands. International Conference Wetlands 2014. The alluvial system as a framework for physical-biogeochemical interactions. Huesca, Spain, 14-18 September 2014.

Burt, T., Pinay, G., Grimm, N., Harms, T. 2013. Between the land and the river: River conservation and the riparian zone. In: River Conservation: Challenges and Opportunities (Editors: Sabater, S. and Elosegi, A.), Chapter 9. Fundación BBVA, 217-241. ISBN: 978-84-92937-47-9

Christophersen, N., Hooper, R.P. 1992. Multivariate analysis of stream water chemical data: the use of principal component analysis for the end-member mixing problem, Water Resour Res 28, 99-107.

Cirmo, C.P., McDonell, J.J. 1997. Linking the hydrologic and biogeochemical controls of nitrogen transport in near-stream zones of temperate-forested catchments: a review. J Hydrol 199, 88-120.

Comin, F.A., Sánchez-Pérez, J.M, Español, C., Carranza, F., Sauvage, S., Antiguedad, I., Zabaleta, A., Martínez-Santos, M., Ladera, J., Gerino, M., Yao, J.M., Bernard-Jannin, L., Sun, X., Teissier, S., Bodoque, J.M., Neves, R., Brito, D., Ruiz, E., Uriarte, J., Navarro, E., Jiménes, J.J., García, M., Barcos, A. A conceptual model to characterize floodplain´s capacity for natural depollution of water in relation with the structure of their biological communities. Submitted to Ecological Engineering.

Dahl, M., Nilsson, B, Langhoff, J.H., Refsgaard, J.C. 2007. Review of classification systems and new multi-scale typology of groundwater–surface water interaction. J Hydrol 344, 1-16. Doi: 10.1016/j.jhydrol.2007.06.027

Dosskey, M., Vidon, P., Gurwick N.P., Allan. C.J., Duval, T.P., Lowrance, R. 2010. The Role of Riparian Vegetation in Protecting and Improving Chemical Water Quality in Streams. Journal of the American Water Resources Association 46(2), 261-277. Doi: 10.1111/j.1752-1688.2010.00419.x

Español, C., Comín, F., Gallardo, B., Yao, J., Yela, J.L., Carranza, F., Zabaleta, A., Ladera, J., Martínez-Santos, M., Gerino, M., Sauvage, S., Sánchez-Pérez, J.M. Does land use impact on groundwater invertebrate diversity and functionality in alluvial wetlands? Submitted to Ecological Engineering.

Gold, A.J., Groffinan, P.M., Addy, K., Kellogg, D.Q., Stolt, M., Rosenblatt, A.E. 2001. Landscape attributes as controls on groundwater nitrate removal capacity of riparian zones. Journal of the American Water Resources Association 37(6), 1457-1464.

González, E., González-Sanchis, M., Cabezas, A., Comín, F.A., Muller, E. 2010. Recent changes in the riparian forest of a large regulated Mediterranean river: Implications for management. J Environ Manage 45, 669-681. Doi: 10.1007/s00267-010-9441-2

Grasso, D.A., Jeannin P. 1994. Etude critique des méthodes d'analyse de la réponse globale des systèmes karstiques. Application au site de Bure (JU, Suisse), Bulletin d'hydrogéologie 13, 87-113.

Hamilton, P.A., Helsel, D.R. 1995. Effects of Agriculture on Ground-Water Quality in Five Regions of the United States. Ground Water 33, 217-226. doi:10.1111/j.1745-6584.1995.tb00276.x

Hooper, R.P., Christophersen, N., Peters, J. 1990. End-member mixing analysis (EMMA): an analytical framework for the interpretation of streamwater chemistry, J Hydrol 116, 321–345.

Inamdar, S.P. 2011. The use of geochemical mixing models to derive runoff sources and hydrologic flow paths in watershed studies (invited chapter), in Forest Hydrology and Biogeochemistry: Synthesis of Past Research and Future Directions, edited by D. Levia, D. Carlyle-Moses, and T. Tanaka, Ecological Studies 216, 163–183, Springer, NY. Doi: 10.1007/978-94- 1365-5-8.

Inamdar, S., Dhillon, G., Singh, S., Dutta, S., Levia, D., Scott, D., Mitchell, M., Van Stan, J., McHale, P. 2013. Temporal variation in end-member chemistry and its influence on runoff mixing patterns in a forested, Piedmont catchment. Water Resour Res 49, 1828-1844. Doi: 10.1002/wrcr.20158

Iribar, A., Sánchez-Pérez, J.M., Lyautey, E., Garabétian, F. 2008. Differentiated free-living and sediment-attached bacterial community structure inside and outside denitrification hotspots in the river–groundwater interface. Hydrobiologia 598, 109-121. Doi:10.1007/s10750-007-9143-9

Iribar, A., Hallin, S., Sánchez-Pérez, J.M., Enwall, K., Poulet, N., Garabétian, F. 2015. Potential denitrification rates correlation with nosZ genotypes colonization pattern in an alluvial wetland. Ecol Eng (In press).

Jencso, K.G., McGlynn, B.L., Gooseff, M.N., Bencala, K.E., Wondzell, S.M. 2010. Hillslope hydrologic connectivity controls riparian groundwater turnover: Implications of catchment structure for riparian buffering and stream water sources. Water Resour Res 46, W10524. Doi:10.1029/2009WR008818

Kim, J.O., Mueller, C.W. 1987. Introduction to Factor Analysis: What it is and How to do it. Quantitative Applications in the Social Sciences Series. Sage University Press, Newbury Park.

King, A.C., Raiber, M., Cox, M.E. 2014. Multivariate statistical analysis of hydro-chemical data to assess alluvial aquifer-stream connectivity during drought and flood: Cressbrook Creek, southeast Queensland, Australia. Hydrogeol J 22, 481-500. Doi: 10.1007/s10040-013-1057-1

Klaus, J., McDonnell, J.J., Jackson, C.R., Du, E., Griffit, N.A. 2015. Where does streamwater come from in low-relief forested watersheds? A dual-isotope approach. Hydrol Earth Syst Sci 19, 125–135. Doi: 10.5194/hess-19-125-2015

Kondolf, G.M., Boulton, A.J., O'Daniel, S., Poole, G.C., Rahel, F.J., Stanley, E.H., Wohl, E., Bång, A., Carlstrom, J., Cristoni, C., Huber, H., Koljonen, S., Louhi, P., Nakamura1, K. 2006. Process-based ecological river restoration: visualizing three dimensional connectivity and dynamic vectors to recover lost linkages. Ecology and Society 11(2): 5. [online] URL: http://www.ecologyandsociety.org/vol11/iss2/art5/

Korom, S.F. 1992. Natural denitrification in the saturated zone: a review. Water Resour Res 28(6), 1657-1668.

Lamontagne, S., Herczeg, A.L., Dighton, J.C., Jiwan, J.S., Pritchard, J.L. 2005. Patterns in groundwater nitrogen concentration in the floodplain of a subtropical stream (Wollombi Brook, New South Wales). Biogeochemistry 72, 169-190. Doi: 10.1007/s10533-004-0358-9

Lancaster R.R. 2005. Fluvial Evolution of the Garonne River, France: Integrating field data with numerical simulations. (Masterthesis) Louisiana State University, Baton Rouge, LA.

Landon, M.K., Green, C.T., Belitz, K., Singleton, M.J., Esser, B.K. 2011. Relations of hydrogeologic factors, groundwater reduction-oxidation conditions, and temporal and spatial distributions of nitrate, Central-Eastside San Joaquin Valley, California, USA. Hydrogeol J 19, 1203–1224.

Lewandowski, J., Lischeid, G., Nützmann, G. 2009. Drivers of water level fluctuations and hydrological exchange between groundwater and surface water at the lowland River Spree (Germany): field study and statistical analyses. Hydrol Process 23, 2117-2128. Doi: 10.1002/hyp.7277

Liu, C.W., Lin K.H., Kuo, Y.M. 2003. Application of factor analysis in the assessment of groundwater quality in a blackfoot disease area in Taiwan. Sci Total Envir 313, 77-89.

Liu, G.D., Wu, W.L., Zhang, J. 2005. Regional differentiation of non-point source pollution of agriculture-derived nitrate nitrogen in groundwater in northern China. Agric Ecosyst Environ 107, 211-220. Doi:10.1016/j.agee.2004.11.010

Lowrance, R., Altier, L.S., Newbold, J.D., Schnabel, R.R., Groffman, P.M., Denver, J.M., Correll, D.L., Gilliam, J.W., Robinson, J.L., Brinsfield, R.B., Staver, K.W., Lucas,W., Todd, A.H. 1997. Water quality functions of riparian forest buffers in Chesapeake Bay watersheds. Environ Manage 21, 687–712.

Maître, V., Cosandey, A.C., Desagher, E., Parriaux, A. 2003. Effectiveness of groundwater removal in a river riparian area: the importance of hydrogeological conditions. J Hydrol 278, 76-93.

Mander, U., Kuusemets, V., Hayakawa, Y. 2005. Purification processes, ecological functions, planning and design of riparian buffer zones in agricultural watersheds. Editorial. Ecol Eng 24, 421–432. Doi: 10.1016/j.ecoleng.2005.01.015

Mangin, A. 1984. Pour une meilleure connaissance des systèmes hydrologiques à partir des analyses corrélatoires et spectrales, J Hydrol 67, 25-43.

Marmonier, P., Archambaud, G., Belaidi, N., Bougon, N., Breil, P., Chauvet, E., Claret, C., Cornut, J., Datry, T., Dole-Olivier, M-J., Dumont, B., Flipo, N., Foulquier, A., Gérino, M., Guilpart, A., Julien, F., Maazouzi, C., Martin, D., Mermillod-Blondin, F., Montuelle, B., Namour, Ph., Navel, S., Ombredane, D., Pelte, T., Piscart, C., Pusch, M., Stroffek, S., Robertson, A., Sanchez-Pérez, J.M., Sauvage, S., Taleb, A., Wantzen, M., Vervier, P. 2012. The role of organisms in hyporheic processes: gaps in current knowledge, needs for future research and applications. Annales de Limnologie, International Journal of Limnology 48, 253-266.

McCarty, G.W., Mookherji, S., Angier, J.T. 2007. Characterization of denitrification activity in zones of groundwater exfiltration within a riparian wetland ecosystem. Biol Fertil Soils 43, 691-698. Doi: 10.1007/s00374-006-0151-0

McClain, M.E., Boyer, E.W., Dent, C.L., Gergel, S.E., Grimm, N.B., Groffman, P.M., Hart, S.C., Harvey, J.W., Johnston, C.A., Mayorga, E., McDowell, W.H., Pinay, G. 2003. Biogeochemical hot spots and hot moments at the interface of terrestrial and aquatic ecosystems. Ecosystems 6, 301-312.

McGlynn, B.L., McDonnell, J.J. 2003. Quantifying the relative contributions of riparian and hillslope zones to catchment runoff. Water Resour Res 39, 1310–1330.

Naiman, R.J., Decamps, H., McClain, M.E. 2005. Riparia: Ecology, Conservation, and Management of Streamside Communities. Elsevier Academic Press, London, United Kingdom, 430 pp

Neves, R.J. 1985. Etude expérimentale et modélisation des circulations transitoire et résiduelle dans l´Estuaire du Sado. PhD Thesis. University of Liege.

Ochoa-Salazar, X., Sánchez-Pérez, J.M., Baque, D., Dandurand, J.L., Loubet, M. Identification and quantification of biogeochemical and physico-chemical processes in an alluvial wetland zone along the Garonne River, SW France, using mixing diagrams. Submitted to Ecological Engineering.

Opperman, J., Luster, R., McKenney, B., Roberts, M., Meadows, A.W. 2010. Ecologically functional floodplains: Connectivity, flow Regime, and scale. Journal of the American Water Resources Association 46(2), 211-226. Doi: 10.1111/j.1752-1688.2010.00426.x

Peyrard, D., Sauvage, S., Vervier, P., Sánchez-Pérez, J.M. Quintard, M. 2008. A coupled vertically integrated model to describe lateral exchanges between surface and subsurface in large alluvial floodplains with a fully penetrating river. Hydrological Processes 22, 4257-4273

Peyrard, D., Delmotte, S., Sauvage, S., Namour, Ph, Gerino, M., Vervier, P., Sánchez-Pérez, J.M. 2011. Longitudinal transformation of nitrogen and carbon transport and in the hyporheic zone of an N-reach stream: a combined modeling and field study. Physics and Chemistry of the Earth 36, 599-611.

Rassam, D.W., Pagendam, D.E., Hunter, H.M. 2008. Conceptualisation and application of models for groundwater–surface water interactions and nitrate attenuation potential in riparian zones. Environ Model Softw 23, 859-875. Doi:10.1016/j.envsoft.2007.11.003

Rivett, M.O, Smith, J.W.N., Buss, S.R., Morgan, P. 2007. Nitrate occurrence and attenuation in the major aquifers of England and Wales. Quarterly Journal of Engineering Geology and Hydrogeology 40, 335-352.

Rivett, M.O., Buss, S.R., Morgan, P., Smith, J.N., Bemment, C. D. 2008. Nitrate attenuation in groundwater: a review of biogeochemical controlling processes. Water Res 42, 4215-4232.

Sanchez-Perez, J.M., Tremolieres, M., Carbiener, R. 1991a. Une station d'épuration naturelle des phosphates et nitrates apportés par les eaux de débordement du Rhin : la forêt alluviale à frêne et orme. Comptes Rendus Académie Sci. Sér. 3 Sci. Vie 312, 395-402.

Sanchez-Perez, J.M., Tremolieres, M., Schnitzler, A., Carbiener, R. 1991b. Evolution de la qualité physico-chimique des eaux de la frange superficielle de la nappe phréatique en fonction du cycle saisonnier et des stades de succession des forêts alluviales rhénanes (Querco-Ulmetum minoris Issl. 24). Acta Oecologica 12, 581-601.

Sánchez-Pérez, J.M. 1992. Fonctionnement hydrochimique d'un ecosysteme forestier inondable de la plaine du Rhin. La foret alluviale du secteur de l'île de Rhinau en Alsace (France). PhD, Universite Louis Pasteur, Strasbourg, 176 pp.

Sánchez-Pérez, J.M., Antiguedad, I., Arrate, I., García-Linares, C., Morell, I. 2003a. The influence of nitrate leaching through unsaturated soil on groundwater pollution in an agricultural area of the Basque country: a case study. Sci Total Environ 317, 173-187. Doi:10.1016/S0048-9697(03)00262-6

Sánchez-Pérez, J.M., Vervier, P., Garabétian, F., Sauvage, S., Loubet, M., Rols, J.L., Bariac, T., Weng, P. 2003b. Nitrogen dynamics in the shallow groundwater of a riparian wetland zone of the Garonne, SW France: nitrate inputs, bacterial densities, organic matter supply and denitrification measurements. Hydrol Earth Syst Sci Discuss 7, 97-107.

Smith, J.W.N., Surridge, B.W.J., Haxton, T.H., Lerner, D.N. 2009. Pollutant attenuation at the groundwater–surface water interface: A classification scheme and statistical analysis using national-scale nitrate data. J Hydrol 369, 392-402. Doi: 10.1016/j.jhydrol. 2009.02.026

Sun, X., Bernard-Jannin, L., Garneau, C., Volk, M., Arnold, J.G., Srinivasan, R., Sauvage, S., Sánchez-Pérez, J.M. 2015. Improved simulation of river water and groundwater exchange in an alluvial plain using the SWAT model. Hydrol Process. Doi: 10.1002/hyp.10575

Takatert, N., Sanchez-Pérez, J.M., Trémolières, M. 1999. Spatial and temporal variations of nutrient concentration in the groundwater of a floodplain: effect of hydrology, vegetation and substrate. Hydrol Process 13, 1511-1526. Doi: 10.1002/(SICI)1099-1085(199907)13:10<1511::AID-HYP828>3.0.CO;2-F

Vidon P., Hill A.R. 2004. Landscape controls on the hydrology of stream riparian zones. J Hydrol 292, 210-228. Doi: 10.1016/j.jhydrol.2004.01.005

Vidon, P., Allan, C., Burns, D., Duval, T.P., Gurwick, N., Inamdar, S., Lowrance, R., Okay, J., Scott, D., Sebestyen, S. 2010. Hot spots and hot moments in riparian zones: Potential for improved water quality management. Journal of the American Water Resources Association 46(2), 278-298. Doi: 10.1111/j.1752-1688.2010.00420.x

Water Framework Directive (WFD), 2000. Directive 2000/60/EC of the European Parliament and of the Council of 23 October 2000 establishing a framework for community action in the field of water policy. Official Journal of the European Communities, L327/1.

Weng, P., Sánchez-Pérez, J.M., Sauvage, S., Vervier, P., Giraud, F. 2003. Assessment of the quantitative and qualitative buffer function of an alluvial wetland: hydrological modelling of a large floodplain (Garonne River, France). Hydrol Process 17, 2375–2392. Doi: 10.1002/hyp.1248

Williams, M.R., Buda, A.R., Elliott, H.A., Hamlett, J., Boyer, E.W., Schmidt, J.P. 2014. Groundwater flow path dynamics and nitrogen transport potencial in the riparian zone of an agricultural headwater catchment. J Hydrol 511, 870-879. Doi: 10.1016/ j.jhydrol. 2014.02.033

Yao J., Sanchez-Pérez J.M., Sauvage S., Teissier S., Attard E., Lauga B., Duran R., Julien F., Bernard-Jannin L., Ramburn H., Gerino M. Biodiversity and ecosystem purification service in alluvial wetlands. Submitted to Ecological Engineering.

Annexe 3 : Publication parue dans *Hydrological Processes* : « Improved simulation of river water and groundwater exchange in an alluvial plain using the SWAT model »

Cette annexe contient une publication soumise par (Sun et al., 2015), à laquelle j'ai participé et qui présente l'intégration de la simulation de l'hydrologie des plaines alluviales dans le modèle SWAT opérant à l'échelle du bassin versant.

HYDROLOGICAL PROCESSES
Hydrol. Process. (2015)
Published online in Wiley Online Library
(wileyonlinelibrary.com) DOI: 10.1002/hyp.10575

Improved simulation of river water and groundwater exchange in an alluvial plain using the SWAT model

X. Sun,[1,2] L. Bernard-Jannin,[1,2] C. Garneau,[1,2] M. Volk,[3] J. G. Arnold,[4] R. Srinivasan,[5] S. Sauvage[1,2] and J. M. Sánchez-Pérez[1,2]*

[1] *INPT, UPS; Laboratoire Ecologie Fonctionnelle et Environnement (EcoLab), University of Toulouse, Avenue de l'Agrobiopole, Castanet Tolosan, Cedex, 31326, France*
[2] *EcoLab, CNRS, Castanet Tolosan, Cedex, 31326, France*
[3] *Department of Computational Landscape Ecology, UFZ Helmholtz Centre for Environmental Research, Permoserstr. 15, Leipzig D-04318, Germany*
[4] *Grassland, Soil & Water Research Laboratory, USDA-ARS, Temple, TX, 76502, USA*
[5] *Spatial Science Laboratory in the Department of Ecosystem Science and Management, Texas A&M University, College Station, TX, 77845, USA*

Abstract:

Hydrological interaction between surface and subsurface water systems has a significant impact on water quality, ecosystems and biogeochemistry cycling of both systems. Distributed models have been developed to simulate this function, but they require detailed spatial inputs and extensive computation time. The soil and water assessment tool (SWAT) model is a semi-distributed model that has been successfully applied around the world. However, it has not been able to simulate the two-way exchanges between surface water and groundwater. In this study, the SWAT-landscape unit (LU) model – based on a catena method that routes flow across three LUs (the divide, the hillslope and the valley) – was modified and applied in the floodplain of the Garonne River. The modified model was called SWAT-LUD. Darcy's equation was applied to simulate groundwater flow. The algorithm for surface water-level simulation during flooding periods was modified, and the influence of flooding on groundwater levels was added to the model. Chloride was chosen as a conservative tracer to test simulated water exchanges. The simulated water exchange quantity from SWAT-LUD was compared with the output of a two-dimensional distributed model, surface–subsurface water exchange model. The results showed that simulated groundwater levels in the LU adjoining the river matched the observed data very well. Additionally, SWAT-LUD model was able to reflect the actual water exchange between the river and the aquifer. It showed that river water discharge has a significant influence on the surface–groundwater exchanges. The main water flow direction in the river/groundwater interface was from groundwater to river; water that flowed in this direction accounted for 65% of the total exchanged water volume. The water mixing occurs mainly during high hydraulic periods. Flooded water was important for the surface–subsurface water exchange process; it accounted for 69% of total water that flowed from the river to the aquifer. The new module also provides the option of simulating pollution transfer occurring at the river/groundwater interface at the catchment scale. Copyright © 2015 John Wiley & Sons, Ltd.

KEY WORDS SWAT model; landscape unit; water exchange; floodplain; Garonne River

Received 27 October 2014; Accepted 10 June 2015

INTRODUCTION

In recent decades, numerous studies have been carried out on the hydrological linkage between surface and subsurface water (SW–GW) systems (Grannemann and Sharp, 1979; Harvey and Bencala, 1993; Wroblicky *et al*., 1998; Malard *et al*., 2002). One of the most promising linkage concepts has been the development of what is known as the hyporheic zone. It was first presented by Orghidan (1959) as a special underground ecosystem, but numerous different definitions by ecologists, hydrologists and biogeochemists have since been proposed (Sophocleous, 2002; Hancock *et al*., 2005). In all the definitions, the most important characteristic of hyporheic zones is the area of mixing between surface and subsurface water (White, 1993; Wondzell, 2011). As surface water contains rich oxygen and organic matter, and groundwater contains abundant nutriment elements, the water mix between those two systems has a significant impact on water quality, ecosystems and biogeochemistry cycling (Brunke and Gonser, 1997; Boulton *et al*., 1998; Sánchez-Pérez and Trémolières, 2003; Vervier *et al*., 2009; Krause *et al*., 2013; Marmonier *et al*., 2012).

The processes occurring at the river/groundwater interface are particularly important for the alluvial plains.

*Correspondence to: J. M. Sánchez-Pérez, Laboratoire d'Ecologie Fonctionnelle et Environnement (ECOLAB), UMR 5245 CNRS-UPS-INPT Ecole Nationale Supérieure Agronomique de Toulouse (ENSAT), Avenue de l'Agrobiopole BP 32607, Auzeville Tolosane, Castanet Tolosan, Cedex 31326, France.
E-mail: jose-miguel.sanchez-perez@univ-tlse3.fr

One of the important features of the alluvial plains is deposited sediment. Their depositional structure leads to higher hydraulic conductivity in the aquifer region than in adjacent upland (Woessner, 2000). As they support important agricultural activities, groundwater in alluvial plains often suffers from nitrate pollution (Arrate *et al*., 1997; Sánchez-Pérez *et al*., 2003a; Liu *et al*., 2005; Almasri and Kaluarachchi, 2007). Several studies show that the surface–groundwater interface contributes to nitrogen retention and/or transformation of the land-surface water continuum (Sabater *et al*., 2003; Weng *et al*., 2003). This interface supports the purification of water by its ability to eliminate nitrates during their infiltration through the vegetation–soil system to groundwater, and also through diffusion from groundwater to surface water (Sanchez-Perez *et al*., 1991a,b; Takatert *et al*., 1999) Hence, an understanding of the processes occurring in the surface–groundwater interface could offer considerable insight for the purposes of water management on a catchment scale.

SW–GW interactions are complex processes driven by geomorphology, hydrogeology and climate conditions (Sophocleous, 2002). In addition, it has been stated that overbank flow is a key hydrological process affecting riparian water table dynamics and ecological processes (Naiman and Decamps, 1997; Rassam and Werner, 2008). Models have been developed to simulate the hydrological conditions of the surface water, groundwater and river/groundwater interface. Rassam and Werner (2008) reviewed models at different complex levels that represented the surface and subsurface processes that have influence on the SW–GW exchange. The simulation of the SW–GW exchange is mainly carried out by using three types of models: (i) models developed for subsurface water, (ii) models developed for surface water and (iii) models that integrated the interface of the two domains. To account for complex geometry, hydrological conditions and materials composition, most of the models developed for subsurface water are distributed models, such as MODFLOW (Storey *et al*., 2003; Lautz and Siegel, 2006) or HYDRUS (Langergraber and Šimůnek, 2005). These models usually require spatial inputs in high resolution and numerous parameters and are characterized by a significant computation time that inhibits their application on large scales. Models that are developed for surface water include QUAL2K (Park and Lee, 2002) and OTIS (Morrice *et al*., 1997). In these models, the lateral floodplain operates as a storage pool to keep the upstream and downstream channel water balance. Loague and VanderKwaak (2004) and Kollet and Maxwell (2006) reviewed models that coupled surface and subsurface domains, and FSTREAM (Hussein and Schwartz, 2003) and surface–subsurface water exchange model (2SWEM) (Peyrard *et al*., 2008) are examples for this type of model. Most of these models are still too complicated to apply at a large scale.

Large-scale hydrological models have been developed to simulate hydrological conditions at a catchment or regional scale. Examples of such models include SWIM (Krysanova *et al*., 1998), TOPMODEL (Franchini *et al*., 1996) and MODHYDROLOG (Chiew and McMahon, 1994). However, the river/groundwater interface is mostly not included in these models. To overcome this issue, the incorporation of conceptual and distributed models has been suggested, as in SWAT-MODFLOW (Sophocleous and Perkins, 2000; Kim *et al*., 2008), WATLAC (Zhang and Li, 2009) and WASIM-ETH-I-MODFLOW (Krause and Bronstert, 2007). However, these developments have still been unable to reflect the impacts of land use management on groundwater quantity or are not applicable in large watersheds. The soil and water assessment tool (SWAT) model is a deterministic, continuous, semi-distributed, watershed-scale simulation model that allows a number of different physical processes to be simulated in a watershed. SWAT can simulate a large watershed with readily available data and has been used successfully all over the world (Jayakrishnan *et al*., 2005; Romanowicz *et al*., 2005; Fohrer *et al*., 2014). To reflect the hydrological connection between upslope and downslope parts of a landscape, a catena approach including divide, hillslope and floodplain landscape units (LUs) has been developed and included in SWAT (Volk *et al*., 2007; Arnold *et al*., 2010; Rathjens *et al*., 2015). The catena approach in the modified model (SWAT-LU) represents an effort to impose a systematic upscaling from a topographic position to a watershed scale. Within the catena, a more detailed downslope routing of surface runoff, lateral flow and groundwater can be accomplished, and the impact of upslope management on downslope landscape positions can be assessed (Arnold *et al*., 2010; Bosch *et al*., 2010). However, the hydrological processes are still single tracks in SWAT-LU, and the function of SW–GW exchange in both directions is not included. Furthermore, the flooded distance during flooding events is fixed at five times the width of the top channel, and the influence of flooding on groundwater levels is not taken into account.

In this study, a new module was developed to simulate the SW–GW exchange in the river/groundwater interface. The modified model was called SWAT-LUD. The SWAT-LUD model was tested on the example of the floodplain of the Garonne River, which has a typical alluvial plain starting from its middle section. Several distributed models (MODFLOW, MARTHE and 2SWEM) were applied to simulate the hydrological and biogeochemical processes in this area (Sánchez-Pérez *et al*., 2003b; Weng *et al*., 2003; Peyrard *et al*., 2008). Groundwater levels and water exchanges between

SW–GW were simulated in the present study. The simulated groundwater levels were then compared with the groundwater levels measured by the piezometers, and the simulated water exchanges verified by detecting the concentration of conservative tracer and undertaking a comparison with the simulated results of a two-dimensional (2D) distributed model – 2SWEM.

METHODOLOGY

SWAT model

The SWAT model (Arnold *et al*., 1998) is a semi-distributed, watershed-scale simulation model. It was developed to simulate the long-term impact of management on water, sediment and agricultural chemical yields in large river basins. It is a continuous time model that is operating on a daily time step. To represent the spatial heterogeneity, the watershed is first divided into subbasins. The subbasins are then subdivided into hydrological response units (HRUs), which are particular combinations of land cover, soil type and slope. SWAT is a process-based model; the major components include hydrology, nutrients, erosion and pesticides. In the SWAT model, processes are simulated for each HRU and then aggregated in each subbasin by a weighted average (Arnold *et al*., 1998; Neitsch *et al*., 2009).

Model development

LU structure. In the HRU delineation method of the usual SWAT model, flow is summed at the subbasin scale and not routed across the landscape. For this application, the watershed was divided into three LUs: the divide, the hillslope and the valley bottom. A representative catena was selected, and flow was routed across the catena as shown in Figure 1 (Volk *et al*., 2007). LUs represent additional units that take place between a subbasin and an HRU. Each subbasin is composed of three LUs, and HRUs are distributed across the different LUs (Volk *et al*., 2007; Arnold *et al*., 2010; Bosch *et al*., 2010; Rathjens *et al*., 2015). To represent the SW–GW exchanges occurring in the alluvial plain, a new type of subbasin called subbasin-LU was developed. Subbasin-LU corresponds to the subbasin delimited by the floodplain, and the LU structure was applied in subbasin-LU. Processes in the upland area of floodplain were calculated according to the original SWAT model. Processes were simulated for each HRU and aggregated to the river. Upland and subbasin-LU were connected through the river. The definition of the widths of LUs was made according to the surface of floodplain

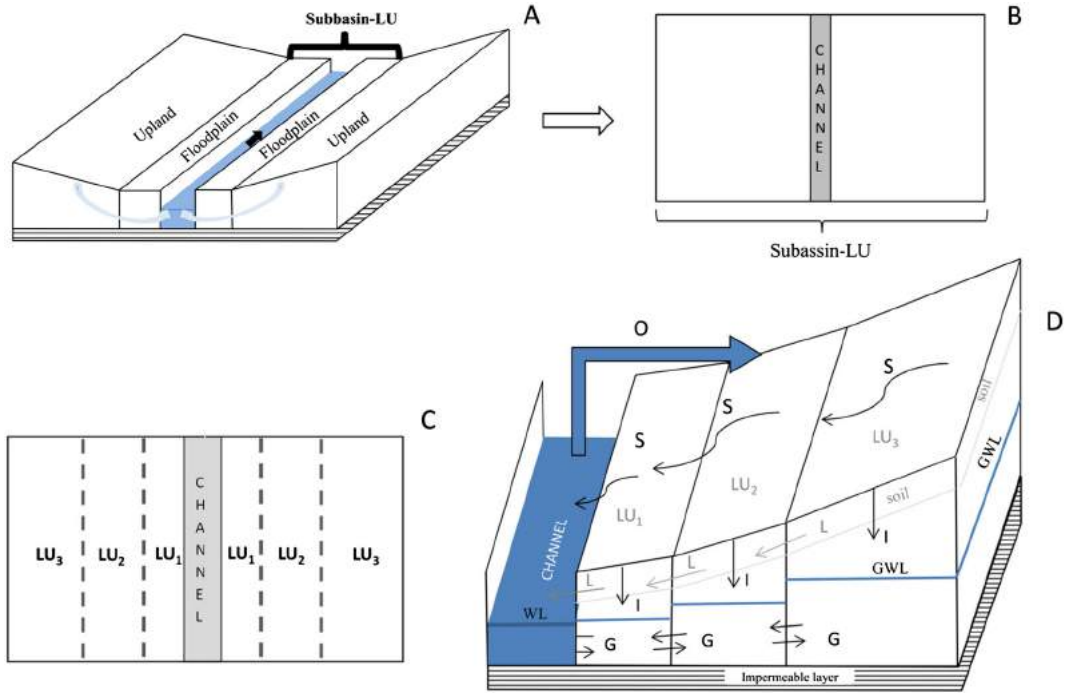

Figure 1. The catena method and its landscape unit (LU) structure in the soil and water assessment tool (SWAT)-LUD model. The figure shows the location of subbasin-LU, the LU structure in the SWAT-LUD model and the hydrologic processes: 'A' represents the location of subbasin-LU, 'B' represents subbasin-LU, 'C' represents the distribution of LUs in the subbasin-LU (plane) and 'D' represents the hydrologic processes in the LUs, where 'S' is surface flow, 'L' is lateral flow, 'I' is infiltration, 'G' is groundwater flow, 'O' is overbank flow, 'GWL' is groundwater level and 'WL' is river water level [according to Volk *et al*. (2007) and Arnold *et al*. (2010)]

covered by the flood return period: LU_1 represented the 1-year return flood area, LU_2 represented the 2- to 5-year return flood area and LU_3 corresponded to the 10 or more years' return flood area. LUs were located parallel to the channel and were defined by their widths and slopes. As LUs were located on both sides of the channel, the width of each side of LU was half its total width. All three LUs in one subbasin were considered as being of the same length, which was the length of the channel. Processes in each HRU were still computed separately and then summed at LU scale. The length was defined based on the river's hydromorphological structure. Finally, the processes were computed between LUs. With the catena method, surface runoff and lateral flow from LU_3 (which was furthest from the channel) were routed through LU_2 to LU_1 (which was nearest to the channel) and then entered the channel (Figure 1). A detailed description of the catena method can be found in Volk *et al.* (2007) and Arnold *et al.* (2010).

SW–GW interaction with LU structure. Darcy's (1856) equation (Equation (2.2.2.1)) was applied to calculate groundwater flow between the LUs and water exchanges between the river and the aquifer. Each LU had a unique groundwater level. The altitude of the riverbed in each subbasin was assumed to be the referenced value of the hydraulic head used to compute groundwater and surface water levels. HRUs were assumed to be homogenous inside, with no additional differentiation in soil and material underneath, and lateral flow was not simulated:

$$Q = K \times A \times \frac{\Delta H}{L} \tag{2.2.2.1}$$

where Q is water flow ($m^3\,day^{-1}$), A is the cross-sectional area between two units (m^2), K is saturated hydraulic conductivity ($m\,day^{-1}$), H is hydraulic head difference between two units (m) and L is the distance between two units through which the water is routed (m).

As the river is filled by water, two implementations of Darcy's equation were required:

(1) Groundwater flow between two LUs:

$$K = \frac{(K_{lua} \times W_{lua}) + (K_{lub} \times W_{lub})}{(W_{lua} + W_{lub})} \tag{2.2.2.2}$$

$$W = (W_{lua} + W_{lub})/4 \tag{2.2.2.3}$$

$$Q = 2 \times K \times A \times \frac{(H_{lua} - H_{lub})}{W} \tag{2.2.2.4}$$

where K represents the averaged hydraulic conductivity values of the two LUs (K_{lua}, K_{lub}) based on their widths ($m\,day^{-1}$), W_{lua} and W_{lub} are the widths of the two LUs (m), H_{lua} and H_{lub} are the hydraulic heads of the two LUs (m) and W is the distance between the centres of these two LUs on one side of channel. Because LUs are located in two sides of the channel, each side obtained half of its width, and W is a quarter of the total width of these two LUs (m). As groundwater flow occurs on both sides of the river, the flow was multiplied by two.

(2) Groundwater flow between LU_1 and the river:

$$K = K_{lu} \tag{2.2.2.5}$$

$$W = (W_{lu})/4 \tag{2.2.2.6}$$

$$Q = 2 \times K \times A \times \frac{(H_{lu} - H_{ch})}{W} \tag{2.2.2.7}$$

where K is the hydraulic conductivity value of LU_1 (K_{lu}) ($m\,day^{-1}$); W is the quarter width of LU_1 (W_{lu}) (half of the width of one side of the channel) (m); and H_{lu} and H_{ch} are hydraulic heads of LU_1 and the river (m).

Influence of flooding to surface water and groundwater level. The original algorithm for flooding events in the SWAT model only assumes that the flooded distance is five times the top channel width (Neitsch *et al.*, 2009). The influence of floodplain geometry and the influence of flooded water on groundwater are not considered. The new algorithm was based on the water volume during a flood event:

$$U_f = (v - v_{max}) \times T \tag{2.2.3.1}$$

where U_f is the flood volume (m^3), v is the discharge ($m^3\,s^{-1}$), v_{max} is the maximum discharge value at which water could stay in the channel ($m^3\,s^{-1}$) and T is the travel time of water passing through the channel (s).

During a flood, the surface water level is the sum of the riverbank height and the water depth on the surface relative to the height of riverbank:

$$A_f = L_{ch} * \left(W_{ch} + L_f\right) \tag{2.2.3.2}$$

$$H_{ch} = D_{ch} + \frac{U_f}{A_f} \tag{2.2.3.3}$$

where A_f is the flooded area (m^2), L_{ch} is the length of the channel (m), W_{ch} is the width of the channel (m), L_f is the flood distance on one side of the riverbank (m), H_{ch} is the surface water level and D_{ch} is the height of the riverbank (m).

With regard to groundwater levels in the LUs during flood periods (if flood water arrives at a LU), the groundwater of this LU was assumed to be the same level as the surface water:

$$H_{luf} = H_{ch} \tag{2.2.3.4}$$

where H_{luf} is the groundwater level of LU during the flood (m).

The infiltrated flood water was calculated as follows:

$$V_{in,f} = \left(H_{luf} - H_{lu}\right) \times A_{lu} \times p_{lu} \quad (2.2.3.5)$$

where $V_{in,f}$ is the infiltrated flood water volume in LU (m^3), A_{lu} is the surface area of the LU (m^2) and p_{lu} is the porosity of the LU (%).

The overbank flow would return back to the river the next day after flooding, and discharge of river water was recalculated:

$$IN = IN + U_f \quad (2.2.3.6)$$

$$v = IN/86\ 400 \quad (2.2.3.7)$$

where IN is the input water volume (m^3)

Transfer of dissolved elements. The transfer of dissolved elements between LUs and between LUs and surface water was calculated based on the water flow volume and concentration of the elements:

$$M_{lu} = M_{lu} + M_{in} - M_{out} \quad (2.2.4.1)$$

$$M_{in} = \sum(V_{in} * C_{in}) \quad (2.2.4.2)$$

$$M_{out} = \sum(V_{out} * C_{lu}) \quad (2.2.4.3)$$

$$C_{lu} = M_{lu}/V_{lu} \quad (2.2.4.4)$$

where M_{lu} is the mass content of the element in LU (g), M_{in} is the input mass (g) and M_{out} is the output mass (g). V_{in} is input water volume (m^3), C_{in} is the concentration of the elements in the input water ($mg\,l^{-1}$), V_{out} is the output volume (m^3), C_{lu} is the concentration of the element in calculated LU ($mg\,l^{-1}$) and V_{lu} is the water volume storage in LU (m^3).

Study area

The Garonne River is the third longest river in France. Its hydrology is influenced by Mediterranean climate and melting snow from the mountainous areas. The typical alluvial plain starts from the middle section of the Garonne River. It contains between 4- and 7-m coarse deposits (quaternary sand and gravel) eroded from the Pyrenees Mountains during the past glacial periods that overlie the impermeable layer of molassic substratum (Lancaster, 2005). The Verdun gauging station is located at about 4 km upstream of the study site Monbéqui. It is the nearest gauging station to the study site at the Garonne River. At the Verdun gauging station, the Garonne has a watershed size of 13 730 km^2 and an annual average flow of about 200 $m^3\,s^{-1}$. The monthly average flow ranges from about 75 $m^3\,s^{-1}$ in August to about 340 $m^3\,s^{-1}$ in May (Banque Hydro, http://www.hydro.eaufrance.fr/). The greatest discharges occur twice a year, in the spring as a result of snow melt and in late autumn following intense rainfalls (Sánchez-Pérez *et al*., 2003c). Previous studies in the Garonne river basin have shown that the river/groundwater interface plays an important role at the reach scale, both in the retention of nitrogen and phosphorous (Vervier *et al*., 2009) and in controlling aquifer water quality (Iribar *et al*., 2008). The study area is characterized by high nitrate pollution caused by agriculture (Jégo *et al*., 2008, 2012).

The study site is located in a meander of the alluvial plain of the Garonne River (Monbéqui), and the width of the floodplain in the area is about 4 km. The mean annual precipitation is about 690 mm in this area. The alluvium thickness ranges from 2.5 to 7.5 m, with an arithmetic mean of 5.7 m (Sánchez-Pérez *et al*., 2003c). The groundwater table varies from 2 to 5 m in low water periods and rises rapidly up to soil profile during floods (Weng *et al*., 2003). The first 50–200 m of the riverbank is covered by riparian forest and poplar plantations, surrounded by agricultural land. Several terraces exist in this area, generated by sediment deposition and washing out by flooding events. Artificial dykes have been constructed in the region to protect the agricultural land (Figure 2).

Measurements. Twenty-nine piezometers were installed in the study area, nine of which were equipped with water-level sensors [Orphimedes, OTT (in 1999–2000) and CTD-diver, Schlumberger, Germany (in 2013)] to record changes in groundwater level every 10 min. In addition, groundwater samples were taken monthly for analysis of physicochemical parameters. While pH, redox potential, electrical conductivity, oxygen content and temperature were measured in the field, other parameters such as nitrate, dissolved organic carbon and chloride were analysed in the laboratory.

In 1999–2000, the groundwater levels of six piezometers (P9, P15, P19, P22, P23 and P30) were recorded with water-level sensors, while groundwater samples were not taken; therefore, physicochemical parameters were not analysed during this period. In 2013, 25 piezometers (all the piezometers in Figure 2 except P15, P19, P23 and P29) and two river sites (R1 and R2) were sampled monthly, and groundwater-level sensors fitted in five piezometers (P7, P9, P14, P18 and P22). Piezometers that were recorded in both periods are P9, P22 and P30 (Figure 2).

LU parameters

For the purposes of simplification, only one subbasin-LU was simulated in this study, and each LU only contained one HRU. The daily discharge data of the Verdun gauging station were used as input data. Based on the flooded area of the Garonne River during different

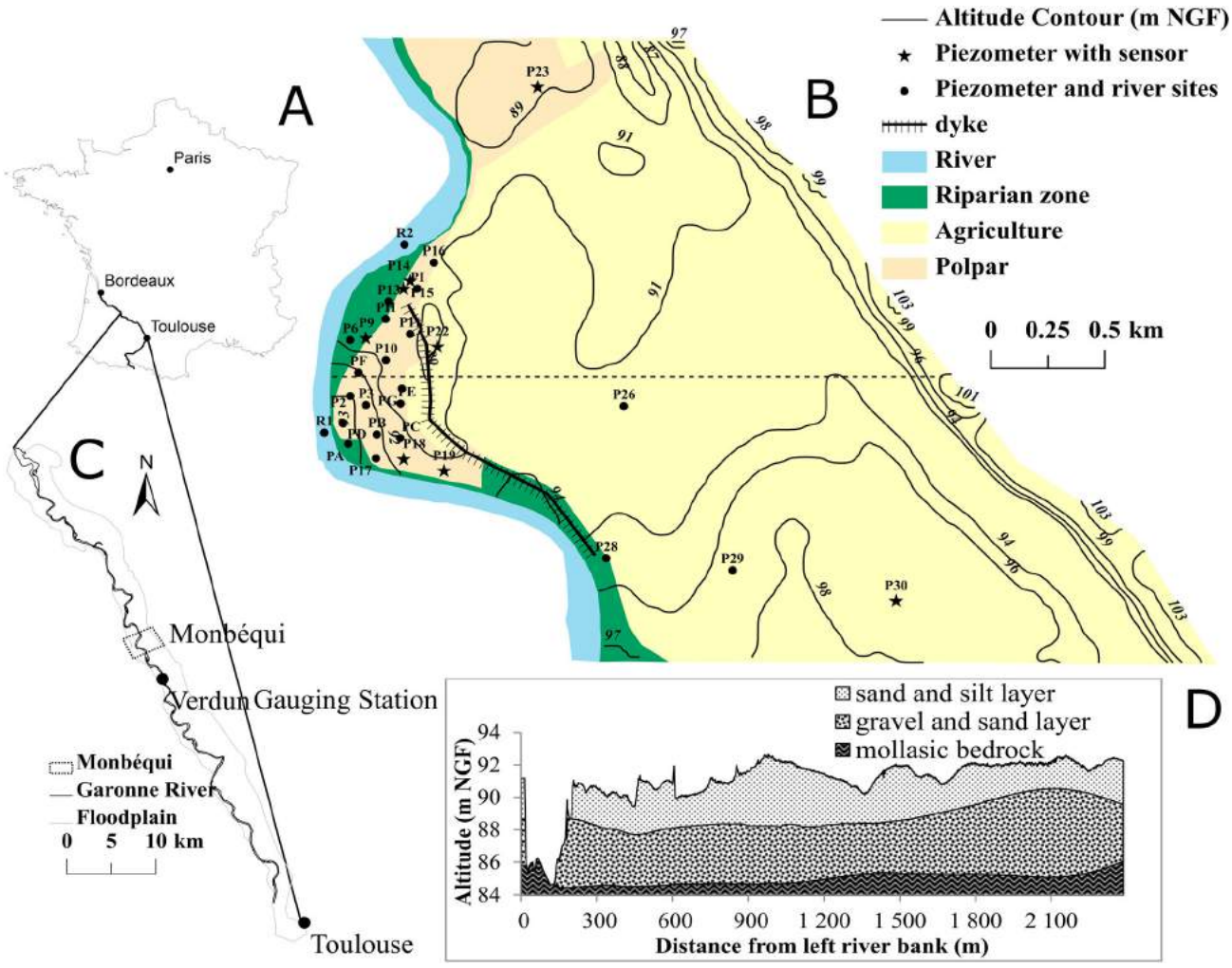

Figure 2. The Garonne River and the Monbéqui study site. 'A' represents the location of the Garonne River, 'B' represents the location of the alluvial plain and Monbéqui, 'C' represents the piezometers in Monbéqui and 'D' represents the cross-section profile of the floodplain correspondence to the dash line in 'C'. NGF, National Geographique Français

periods, the LU parameters are presented in Table I; the values of porosity were given based on the study of Seltz (2001) and Weng *et al.* (2003). The distributions of piezometers with installed sensors in the three LUs were as follows: five piezometers were located in LU_1: P9, P14, P15, P18 and P19; two piezometers, P22 and P23, were located in LU_2; and P30 was located in LU_3.

Table I. Parameters of LUs and channel

	LU_1	LU_2	LU_3	Channel
Width (km)	0.4	0.8	3.0	0.22
Length (km)	6.374	6.374	6.374	6.347
Slope (lateral)	0.002	0.005	0.005	—
Slope (vertical)	—	—	—	0.001
Porosity	0.1	0.1	0.1	—
Depth (m)	—	—	—	4.0

LUs, landscape units.

In the model, each LU had one groundwater-level value. With Darcy's equation, the altitude of the riverbed in each subbasin-LU was assumed to be the referenced hydraulic head. As the river sloped, the altitude of the riverbank was variable within one subbasin-LU. One referenced value had to be chosen for comparison with the measured groundwater levels in each subbasin-LU. At the study site, P9 was the only piezometer with groundwater-level sensors fitted during 1999–2000 and 2013 in LU_1. The groundwater level of LU_1 was more important to the calculation of the SW–GW exchange than that of the other two LUs. The altitude of the riverbed was set at 84.75 m National Geographique Français (NGF: the general levelling of France, with 'zero level' determined by the tide gauge in Marseille). It was calculated based on the altitude of the soil surface of P9 (88.95 m NGF) minus 4 m, corresponding to the height of the riverbank minus 0.2 m and the slope of LU_1 that was 0.002.

Calibration and validation

Groundwater levels. The calibration of the groundwater levels was performed manually. Because the flood that occurred in 2000 was the largest event in the recent 20 years, and the groundwater-level sensors were installed in all the three LUs in the period of 1999–2000, the observed groundwater levels in this period were used as calibration data. The observed data from 2013 were taken as validation data. The simulated groundwater levels of the LUs (average value) were compared with corresponding piezometers (point value). To limit the error caused by the vertical slope, piezometers were chosen for comparison with the simulated groundwater levels in each LU based on their location relative to P9. In LU_1, P15 and P9 had similar observed values in the calibration period (1999–2000), but P15 had a longer available time series than P9. In LU_2, P22 was closer to P9 than P23. P30 was located upstream of P9 but was the only piezometer with a groundwater-level sensor installed in LU_3. Therefore, the observed groundwater levels of P15, P22 and P30 during the calibration period (1999–2000) and P9, P22 and P30 during the validation period (2013) were used for comparison with the simulated results of LU_1, LU_2 and LU_3, respectively.

SW–GW exchanged water. Chloride as a well-known groundwater conservative tracer (Harvey *et al*., 1989; Cox *et al*., 2007) was chosen to verify the simulated water exchange between the river and LU_1. Because the concentrations of chloride were measured monthly, there are a lack of continuous observed data as input values of the model. However, the variations of the chloride concentrations in surface water and groundwater in LU_2 as well as in LU_3 were only slight; constant concentration values were given for the river, LU_2 and LU_3 during simulation. Concentration values were set based on the measured data in 2013 (Table II), because this was the only year in which surface water and groundwater samples were taken and analysed. The concentration values in LU_1 were simulated based on the mix of surface water and LU_2. The comparison of simulated and observed chloride concentrations in LU_1 could be used to verify the simulated SW–GW exchange in LU_1. Because the transport of chemistry elements was more complicated than water flow, it would be more difficult to match the simulated data for a LU with the observation from a certain piezometer. The chloride concentrations measured in all the 16 piezometers in LU_1 were compared with the simulated data.

Surface–subsurface water exchange model is a 2D hydraulic model. Horizontal 2D Saint Venant equations for river flow and a 2D Dupuit equation for aquifer flow were coupled in the model to simulate the dynamic variation of aquifer water level. It was originally developed to simulate water exchange occurring in the river/groundwater interface (Peyrard *et al*., 2008). Peyrard (2008) simulated surface water and groundwater exchange on the right side of the riverbank in the Monbéqui study area. The simulation was carried out for a 3.1-km length of the riverbank using the 2SWEM at a daily time step. The result of the SWAT-LUD simulation was adjusted [total exchanged volume divided by the length of channel (6.374 km) multiplied by 3.1 km] to match the distance of 3.1 km and then divided by 2 to compare it with the output of the 2SWEM.

The coefficient of determination (R^2), Nash–Sutcliffe efficiency (NSE), percent bias and root-mean-square error observations standard deviation ratio were chosen as evaluating parameters.

Table II. Detected values (in 2013) and constant values of chloride of river water and groundwater of LU_3 and LU_2

Zone		Chloride (mean ± SE) ($mg\,l^{-1}$)	Constant chloride ($mg\,l^{-1}$)
River	R1	8.97 ± 1.05	
	R2	9.38 ± 1.14	9.00
LU_2	P22	78.22 ± 3.60	75.00
LU_3	P26	54.88 ± 2.67	50.00
	P30	38.28 ± 1.45	

LU, landscape unit; SE, standard error.

RESULTS

Calibrated parameters

Hydraulic conductivities were determined by pumping tests and slug tests, varying from 10^{-2} to $10^{-5}\,m\,s^{-1}$ (Weng *et al*., 2003; Peyrard *et al*., 2008). Because the simulations with the SWAT-LUD model were carried out at a daily step, the converted daily hydraulic conductivities varied from 860 to $1\,m\,day^{-1}$. Calibrated parameters are given in Table III.

Groundwater levels

Figure 3 shows the shallow water tables in the study site based on the measured data of all the piezometers in two periods in 2013.

Table III. Manually calibrated parameters

Parameters	Default value	Calibrated values
Manning roughness coefficient	0.014	0.070
Hydraulic conductivity (LU_1) ($m\,day^{-1}$)	Undefined	300
Hydraulic conductivity (LU_2) ($m\,day^{-1}$)	Undefined	200
Hydraulic conductivity (LU_3) ($m\,day^{-1}$)	Undefined	100

LU, landscape unit.

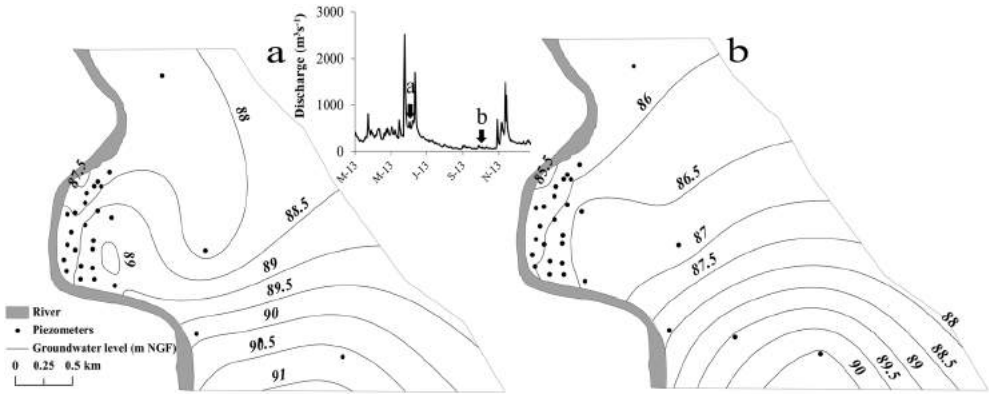

Figure 3. Contour maps of groundwater level in two periods: 'a' represents the groundwater levels in flood period and 'b' represents the groundwater levels in low hydraulic period. NGF, National Geographique Français

It shows that in the period between two floods, the direction of groundwater flow in the meander is from river to floodplain, and groundwater flowed from the floodplain to river in the stable low flow period.

The comparison of observed and simulated groundwater levels in the three LUs is shown in Figure 4.

The results demonstrated that observed and simulated values matched very well in LU_1, especially in 2013 when simulated and observed values almost overlapped ($R^2 = 0.96$, $NSE = 0.95$). There was considerable variation in the observed and simulated well heights in LU_2. The lower water-level values of the simulations were under the observations, and LU_2 was flooded too often compared with the observed data. For LU_3, the result showed that simulated values were much lower than the observed data in LU_3, but the two curves had the same variation trend ($R^2 = 0.94$) (Table IV). The graph also showed that with an increase in distance from the river, there was a decrease in the fluctuation in groundwater.

Water exchange between surface water and groundwater

Water exchange – verified with conservative elements. To verify simulated exchanged water, simulated concentration values of chloride (Cl^-) were compared with the mean values from the 16 piezometers. The simulated groundwater level in LU_1 was compared with P15 and P9, but only P9 was sampled in 2013. The detected values of Cl^- of P9 were also compared with the simulated data (Figure 5).

Figure 5 shows large variations in observed values within LU_1, matching the mean values more closely than P9.

Comparison with simulations by the 2SWEM. Figure 6 shows the comparison between the results of the SWAT-LUD model and the results of the 2SWEM. The models produced reasonably close results given the R^2 of 0.62 and *NSE* of 0.51 (Figure 6). In the period before May 2005, SWAT-LUD predicted less surface water entering the aquifer than the 2SWEM, and the lag time of groundwater flow to the river was greater in 2SWEM than in SWAT-LUD. After a large peak in May 2005, the results of the two models were almost identical.

Surface water and groundwater exchange. The water quantity exchanged annually between the river and the aquifer throughout the entire period simulated (1993–2013) is shown in Figure 7. Water flow can occur in two directions: from the river to the aquifer and from the aquifer to the river. It was found that the dominant net flow direction was from the aquifer to the river and that water exchange quantities varied annually. Water flowing from the river to the aquifer can be separated into two parts: (1) water infiltrating through the riverbank and (2) flooded water percolating through the surface of the LUs. Flooded water percolating through the soil surface accounted for 69% of water flowed from the river to the aquifer. The annually flooded water volume and flooded days are shown in Figure 8.

To understand the influence of river water discharge on the SW–GW exchanged water volumes, three river water discharge measurements were correlated with four simulated exchanged water volume components. The discharge measurements were annual mean discharge (Q_m), annual maximum discharge (Q_{max}) and annual discharge variation $\left(\Delta Q = \sqrt{\sum (Q - Q_m)^2}\right)$. The exchanged water volumes were the annual absolute exchanged water volume flowing in two directions (from river to aquifer and from aquifer to river), net exchanged water volume and total absolute exchanged volume. Results are shown in Figure 9. This demonstrated that river water discharge had a significant impact on the exchanged water quantities between the river and the aquifer. Along with the increase of Q_m, Q_{max} and ΔQ, the water volumes flowing from the river to the aquifer and from the aquifer to the river also increased. Water flow from the aquifer to the river is better correlated with ΔQ. Q_{max} played the most significant role in water flowing

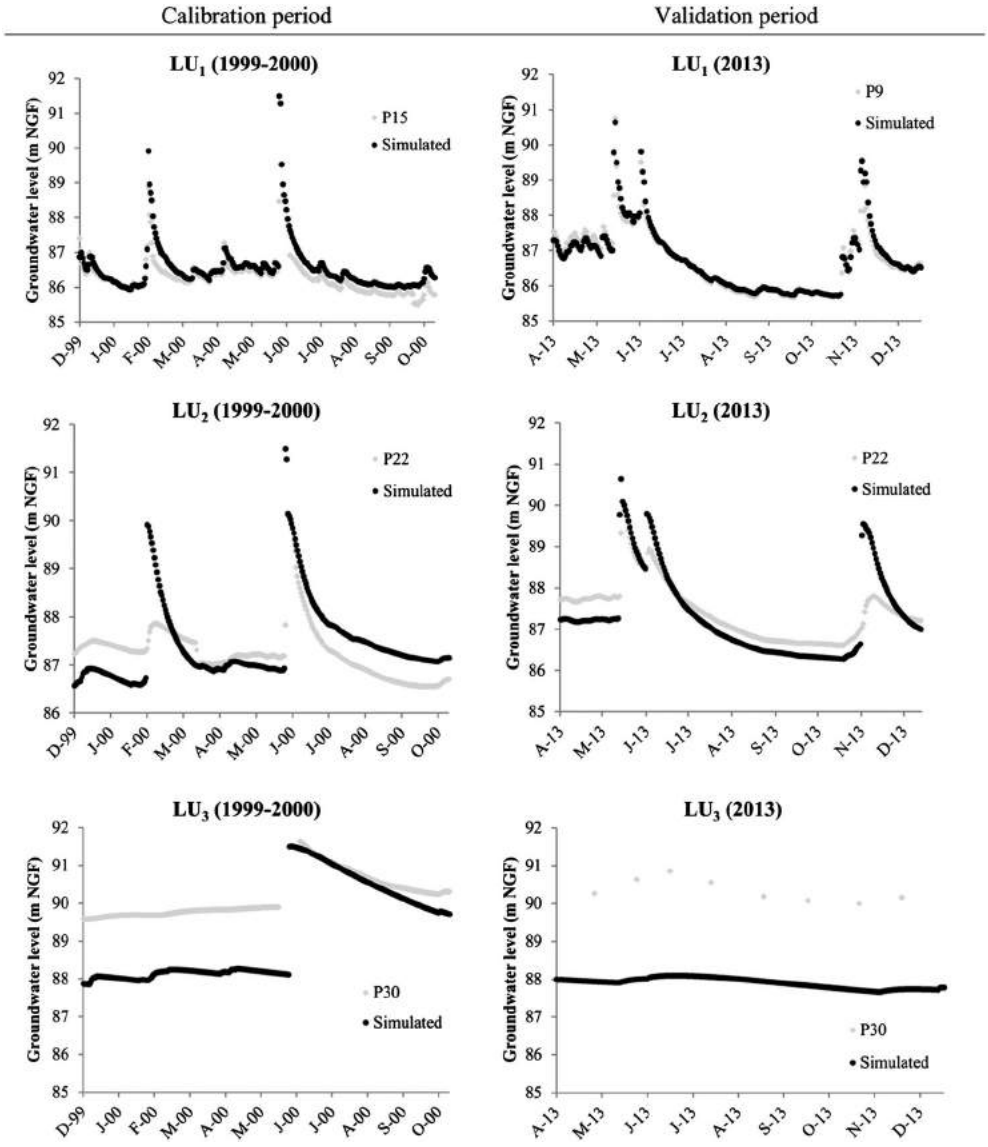

Figure 4. Observed and simulated groundwater levels in the calibration (1999–2000) and validation (2013) periods. LU, landscape unit; NGF, National Geographique Français

Table IV. Parameters for evaluating the accuracy of groundwater levels simulated by the SWAT-LUD model

		R^2	*NSE*	*PBIAS*	*RSR*
LU_1	Calibration	0.79	0.25	−0.27	0.87
	Validation	0.96	0.95	−0.05	0.22
LU_2	Calibration	0.38	−0.42	−0.15	1.19
	Validation	0.78	0.48	0.09	0.72
LU_3	Calibration	0.94	−4.14	1.12	2.27
	Validation	0.75	−72.3	2.68	8.56

LU, landscape unit; NSE, Nash–Sutcliffe efficiency; PBIAS, percent bias; RSR, root-mean-square error observations standard deviation ratio; SWAT, soil and water assessment tool.

from the river to the aquifer and total exchanged water volume. However, net exchanged water volumes were not significantly influenced by the discharge.

Based on the discharge values, simulated data were separated into two parts: low hydraulic period and high hydraulic period. The bound discharge value was set at $200\,m^3\,s^{-1}$, which is the long-term mean discharge of the Verdun gauging station (http://www.hydro.eaufrance.fr/). The results are given in Table V. During the entire simulation period, the water that flowed from the aquifer to the river accounted for 65% of the total exchanged water volume (exchanged water volume in two directions). The low hydraulic period contributed 57% of the water that flowed from the aquifer to the river. The main water flow from the river to the aquifer occurred during the high hydraulic period, which amounted to 97% of the total flow in this direction.

In the low hydraulic period, the main water flow direction was from the aquifer to the river, which was

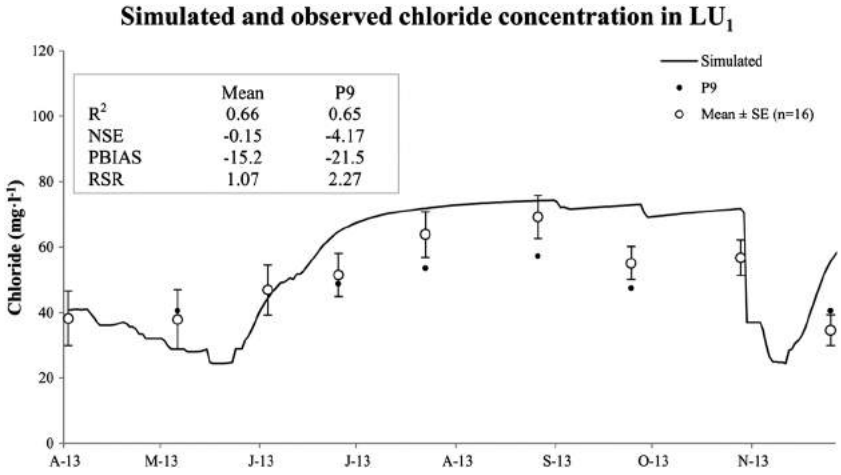

Figure 5. Comparison of concentration of chloride in LU_1 between the SWAT-LUD model's simulation and values detected from field sampling in 2013. LU, landscape unit; SE, standard error; NSE, Nash–Sutcliffe efficiency; PBIAS, percent bias; RSR, root-mean-square error observations standard deviation ratio; SWAT, soil and water assessment tool

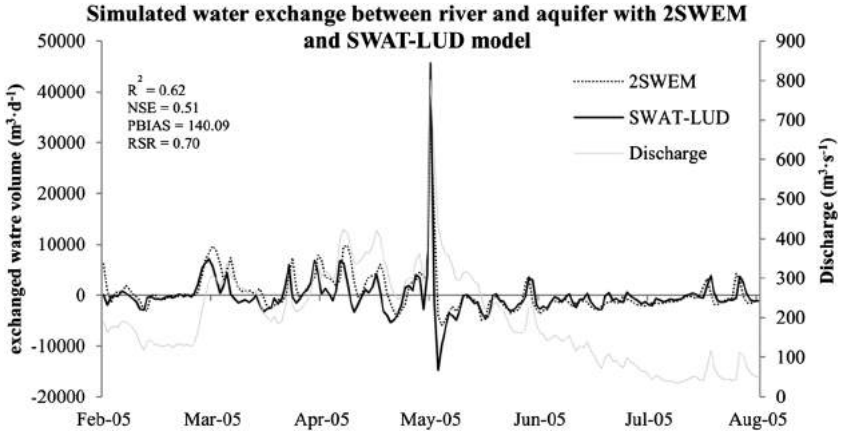

Figure 6. Comparison of the simulated water exchange between the SWAT-LUD model and the surface–subsurface water exchange model (2SWEM). NSE, Nash–Sutcliffe efficiency; PBIAS, percent bias; RSR, root-mean-square error observations standard deviation ratio; SWAT, soil and water assessment tool

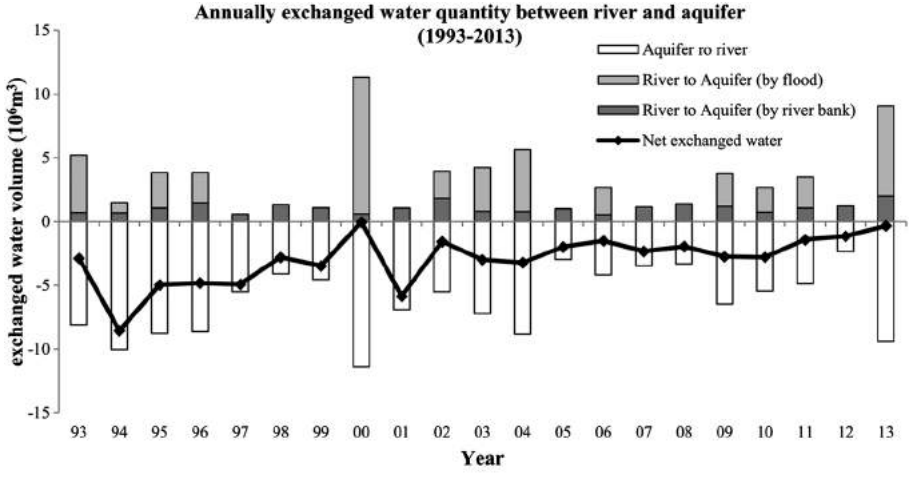

Figure 7. Annually exchanged water quantity between the river and the aquifer during the entire simulated period (1993–2013)

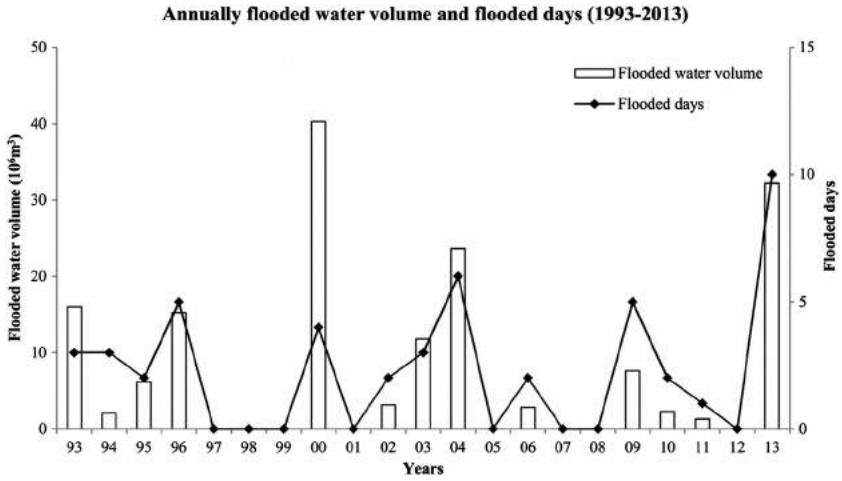

Figure 8. Annually flooded water volume and flooded days during the entire simulated period (1993–2013)

98% of the total water exchange in this period. The low flow period represented 70% of the simulated days, but the amount of exchanged water was only 38% of the total volume.

During the high hydraulic period, more water flowed from the river to the aquifer than from the aquifer to the river (54:46). However, the difference between those two flow directions was not as high as it was during the low flow period. The daily average flow in this period ($5.40 \times 10^4\,m^3\,day^{-1}$) was much greater than during the low water period ($1.43 \times 10^4\,m^3\,day^{-1}$).

DISCUSSION

The SWAT-LU model was modified by adding in the floodplain area the module simulating SW–GW water exchange at the river/groundwater interface. The algorithms calculating surface water and groundwater levels during flooding were also modified in agreement with the module. The comparison of simulations and observations proved that the modified model was able to reflect accurately the actual hydrological dynamics in the aquifer of the floodplain of the Garonne River. Darcy's equation was used to calculate water exchanges caused by the difference in hydraulic heads between the channel water and groundwater levels in LU_1 – hydraulic conductivities are important parameters for calculating the SW–GW interaction (Sophocleous, 2002). The comparison of simulations and observed groundwater levels confirmed that the model can accurately simulate groundwater levels. Moreover, the simulated SW–GW exchange was verified by comparing it with the detected values of tracer from field samples and the simulated water exchange with a 2D distributed model: the 2SWEM. The results demonstrated that the SWAT-LUD model was able to simulate SW–GW water exchange accurately in terms of fluxes.

The model was able to reproduce the two-way interactions occurring in SW–GW exchanges. The contribution of surface water to subsurface flow is not considered in most of the existing catchment-scale models such as SWIM (Krysanova *et al.*, 1998), TOPMODEL (Franchini *et al.*, 1996) or MODHYDROLOG (Chiew and McMahon, 1994). However, the results from this study showed its importance, because it accounted for 35% of total SW–GW exchanges over a long period. The two-way interaction that controls water mixing in the river/groundwater interface is an important driver in biogeochemical reactions occurring in this area (Amoros and Bornette, 2002). The SWAT-LUD model presented here provides a solid basis for further model development aiming at the simulation of biogeochemical processes in floodplain areas at catchment scale.

Previous research and this study have proven that discharge in the channel is the main driving factor of the SW–GW exchange in the study site (Peyrard *et al.*, 2008). As the main water flow direction during low hydraulic periods is from the aquifer to the river, the water mixing in river/groundwater interface occurs mainly during high hydraulic periods. Flooding has been proven to influence the plant communities of wetlands, in terms of both soil nitrate reduction and groundwater flow (Hughes, 1990; Casanova and Brock, 2000; Brettar *et al.*, 2002; Alaoui-Sossé *et al.*, 2005). In the present study, flooded water was found to be important for the SW–GW exchange process, which needs further investigation in future. As a daily step model, SWAT-LUD could not reflect the detailed processes occurring during flooding events. In this study, during flood periods, the groundwater levels of LUs reached by floodwater were considered to have the same value as the river water levels. The time lag of water infiltration was not taken into account, and as the LU has a unique groundwater level, the risk of overestimating infiltrated flooded water increased along with the increase

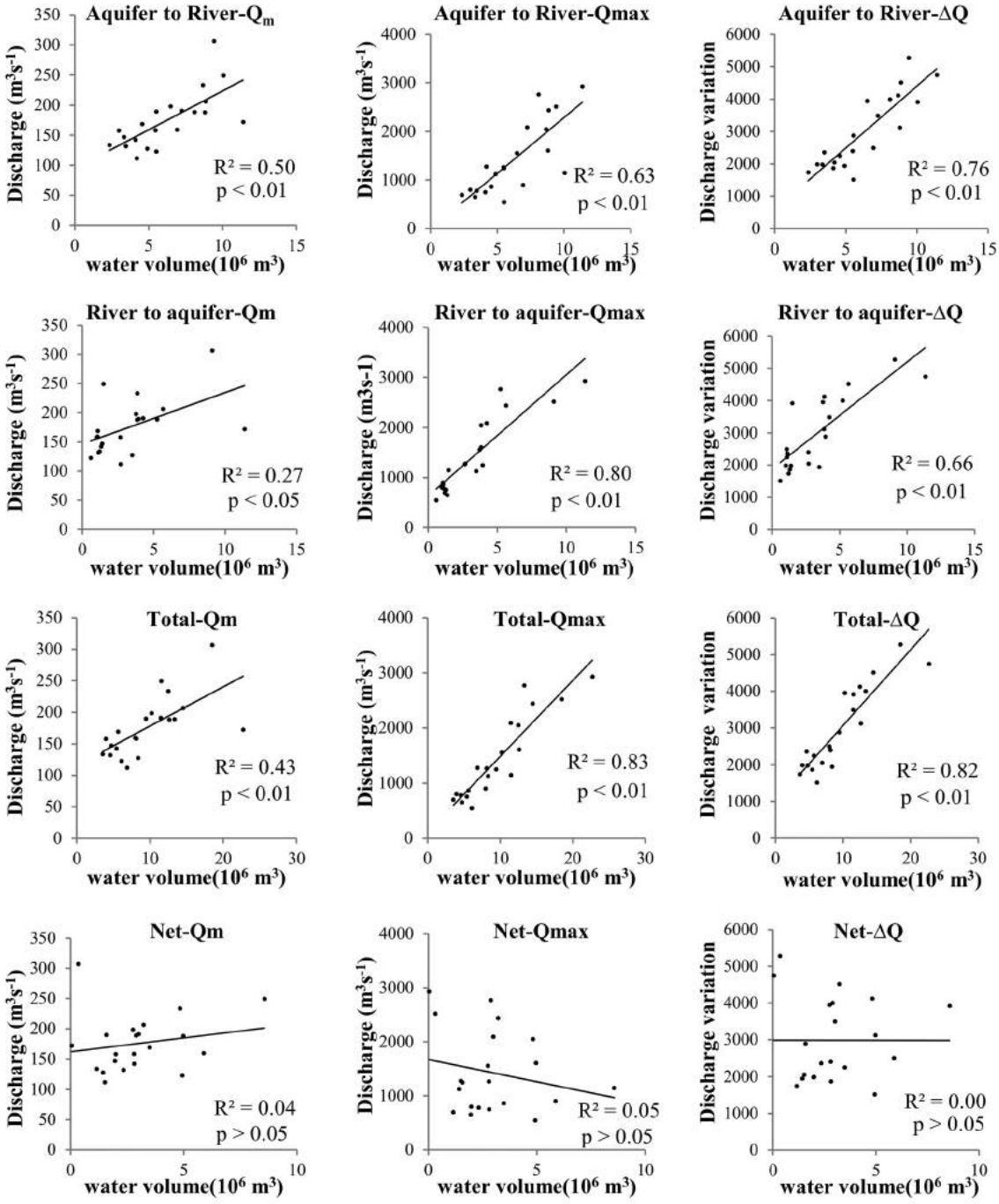

Figure 9. Correspondence between river water discharge and exchanged water volume between the river and the aquifer

of the width of LUs. Because the surface area of LU_3 is much larger than the two other LUs, if flooded water arrives in LU_3, the infiltrated flooded water could be more easily overestimated. The large flood that occurred during the calibration period reached LU_3. This probably explained the high simulated groundwater levels in LU_2 and LU_1 after the flooding event. The algorithm is still simple, and the simulated exchanged water volume should be compared with the results of a distributed model or observed data in a future study.

The water loss caused by plant evapotranspiration, especially in the riparian forest zones, was stated in many

Table V. Simulated exchanged water quantity between river and aquifer in two hydraulic periods (low water period and high water period) throughout the simulated period (1993–2013)

	All		Low ($<200\,m^3\,s^{-1}$)			High ($>200\,m^3\,s^{-1}$)		
Discharge	Value	%	Value	Total (%)	Period (%)	Value	Total (%)	Period (%)
Number of days	7670		5348	0.70		2322	0.30	
Exchanged water (A to R) ($10^7\,m^3$)	13.21	0.65	7.47	0.57	0.98	5.74	0.43	0.46
Exchanged water (R to A) ($10^7\,m^3$)	6.98	0.35	0.18	0.03	0.02	6.80	0.97	0.54
Total ($10^7\,m^3$)	20.19		7.65	0.38		12.54	0.62	
Daily average ($10^4\,m^3\,day^{-1}$)	2.63		1.43			5.40		

A to R means from aquifer to river, and R to A means from river to aquifer.

studies (Boronina *et al*., 2005; Butler *et al*., 2007; Gribovszki *et al*., 2008). However, because the groundwater table is usually beneath the root zone in the study site except during flood period, water uptake by plants is negligible and was not stated in this study. The influences of pumping on groundwater and river water flow were stated also in some researches (Hunt, 1999; Cooper *et al*., 2003; Rassam and Werner, 2008). This process was not included in the model yet, but it could be easily added to the model as an output source of groundwater in the future study. Because of the chosen model philosophy, the pumped water in each LU would be summed together, and influence of pumping on groundwater-level fluctuation would be simulated at LU scale (in contrast to more complex procedures in physically based models).

As a semi-distributed model, the SWAT-LUD model cannot consider detailed topographic information. In the model, each LU has a unique slope value and mean hydraulic conductivity. Because the model was applied at floodplain scale, the impermeable layer was considered to be flat in the model, and the complex topography of channel and adjacent floodplain was only considered to be mean slope for each LU. Channel processes and SW–GW water exchange were calculated at subbasin scale. Moreover, the groundwater was assumed to be flowing in a horizontal direction (perpendicular to the river flow). The vertical gradient of the groundwater hydraulic heads shown in Figure 10 was not considered. The existence of the vertical gradient was explained by the height difference between simulated groundwater levels and the observed values of P30 in LU_3. In LU_2, piezometer P22 was located just behind an artificial dyke, which was built to protect agricultural land from flooding. Flooded water has to move to the top of the dyke before it arrives at P22. As the model could not consider this local detailed information, LU_2 was oversaturated compared with the observation from P22. In addition, the simulated groundwater levels represented the average situations of all the LUs, so it would be difficult for the output of the model to match data from one piezometer closely. Moreover, hydraulic conductivity was a mean value in each LU. However, in reality, hydraulic conductivities are extremely heterogeneous (Weng *et al*., 2003), so the uncertainties of water-level simulations as a result of mean values linked to the mean values of hydraulic conductivities could be important when compared with local piezometers. To evaluate the uncertainties, a sensitivity analysis of hydraulic conductivity would be required.

The SWAT-LUD was not able to provide a detailed spatial distribution of hydraulic heads of the kind provided by physically based models [MODFLOW (Sánchez-Pérez *et al*., 2003b), MARTHE model (Weng *et al*., 2003) and 2SWEM (Peyrard *et al*., 2008)]. However, the objective of the study was not to provide accurate spatial representations of groundwater levels like the physically based models but to provide a good estimation of SW–GW interactions over a long timescale with a simple model. The model aimed to simulate large catchment sizes to support river basin water management. Therefore, the complexity of physically based models leading to long computation times for the simulation of small-scale areas (Helton *et al*., 2014; Lautz and Siegel, 2006) is not suitable. Moreover, physically based models need very detailed input information that can be difficult to collect, while this model needs only basic parameters. Nevertheless, SWAT-LUD gave similar results for SW–GW interactions when compared with the physically based 2SWEM (Peyrard *et al*., 2008). Although the shapes of the channels and LUs in the SWAT model were assumed to be straight and homogeneous, the values for exchanged water between river and aquifer simulated by the SWAT-LUD model were identical to the physically based 2SWEM. This showed that the SWAT-LUD model could accurately reflect the actual water exchange occurring at reach scale. SWAT-LUD was able to reproduce the spatial and temporal patterns of SW–GW exchanges at reach scale in a simple way, which means that it can be used for large catchment simulation and to support river basin management studies.

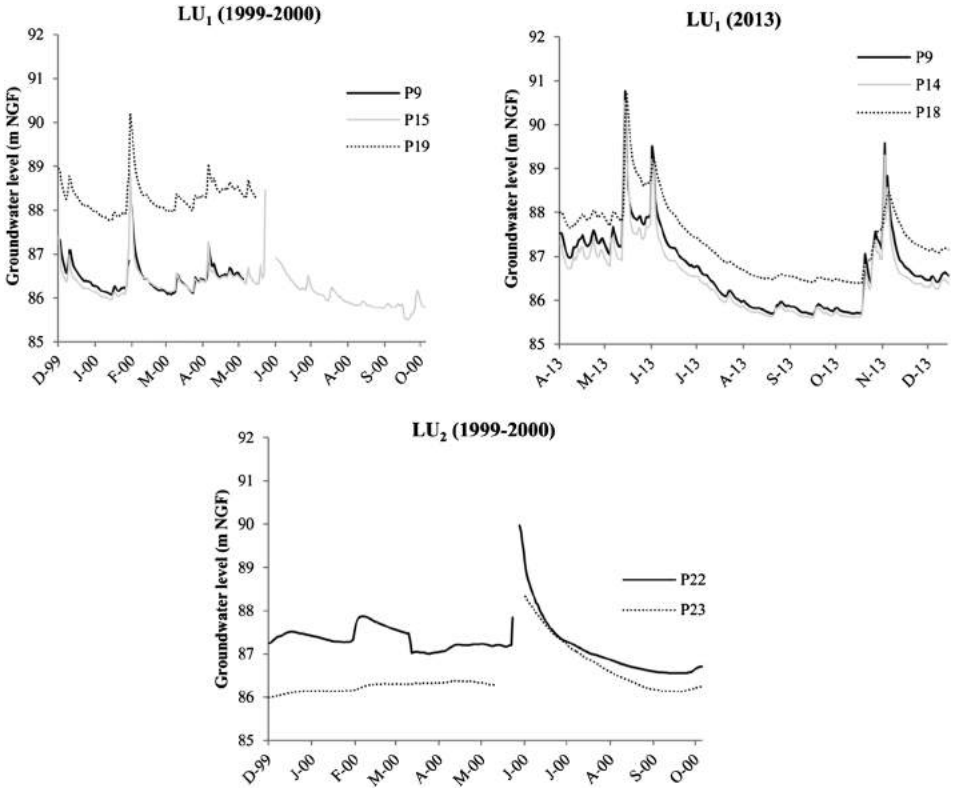

Figure 10. Observed groundwater levels in landscape units (LUs) with more than one piezometer equipped with a water-level sensor. NGF, National Geographique Français

CONCLUSIONS

This paper has described the new module of the SWAT-LUD model created to simulate surface water and floodplain groundwater. Darcy's equation was introduced to the model to simulate groundwater flow and SW–GW exchange occurring through the riverbank. The algorithms of river water and groundwater levels during flooding events were also modified. This new module was tested in a meander of the floodplain of the Garonne River in France. Comparisons between simulation results with observations from piezometers illustrated that the SWAT-LUD model could satisfactorily simulate groundwater levels near the area of the bank. Conservative tracer measured from field samples was used to validate the simulations, and SW–GW exchange modelling results with this approach corresponded well with the results obtained by a complex hydraulic model. This model was able to reflect accurately the actual water exchange between surface and subsurface systems of the alluvial plain of the Garonne River. River water discharge was found to have a great influence on the SW–GW exchange process. The main water flow direction was from groundwater to river; water that flowed in this direction in the river/groundwater interface accounted for 65% of the total exchanged water volume. The water mixing occurs mainly during high hydraulic periods. Flooded water was important for the SW–GW exchange process; it accounted for 69% of total water flowed from the river to the aquifer. As a catchment-scale model, SWAT-LUD could easily be applied to a large catchment with basic available data. The SWAT-LUD model enabling simulation of GW–SW exchange processes at catchment scale would be a useful tool for evaluating the role of river buffer strips and wetlands in improving water quality. Future work should include (i) an application of the modified model in a larger catchment with multiple subbasins and (ii) the simulation of land management operations and biogeochemical processes in the river/groundwater interface.

ACKNOWLEDGEMENTS

We are grateful to N. B. Sammons for her help with developing the module. This study was performed as part of the EU Interreg SUDOE IVB programme (ATTENAGUA – SOE3/P2/F558 project, http://www.attenagua-sudoe.eu) and funded by ERDF. This research has been carried out as a part of 'ADAPT'EAU' (ANR-11-CEPL-008), a project supported by the French National Research Agency (ANR) within the framework of 'The Global Environmental Changes and Societies

(GEC&S) programme'. X. Sun is supported by a grant from the China Scholarship Council (CSC).

REFERENCES

Alaoui-Sossé B, Gérard B, Binet P, Toussaint M-L, Badot P-M. 2005. Influence of flooding on growth, nitrogen availability in soil, and nitrate reduction of young oak seedlings (*Quercus robur* L.). *Annals of Forest Science* **62**: 593–600. DOI:10.1051/forest:2005052.

Almasri MN, Kaluarachchi JJ. 2007. Modeling nitrate contamination of groundwater in agricultural watersheds. *Journal of Hydrology* **343**: 211–229. DOI:10.1016/j.jhydrol.2007.06.016.

Amoros C, Bornette G. 2002. Connectivity and biocomplexity in waterbodies of riverine floodplains. *Freshwater Biology* **47**: 761–776. DOI:10.1046/j.1365-2427.2002.00905.x.

Arnold JG, Allen PM, Volk M, Williams JR, Bosch DD. 2010. Assessment of different representations of spatial variability on SWAT model performance. *Transactions of the ASABE* **53**: 1433–1443.

Arnold JG, Srinivasan R, Muttiah RS, Williams JR. 1998. Large area hydrologic modeling and assessment part I: model development 1. *JAWRA Journal of the American Water Resources Association* **34**: 73–89. DOI:10.1111/j.1752-1688.1998.tb05961.x.

Arrate I, Sanchez-Perez JM, Antiguedad I, Vallecillo MA, Iribar V, Ruiz M. 1997. Groundwater pollution in quaternary aquifer of Vitoria: Gasteiz (Basque Country, Spain): influence of agricultural activities and water-resource management. *Environmental Geology* **30**: 257–265. DOI:10.1007/s002540050155.

Boronina A, Golubev S, Balderer W. 2005. Estimation of actual evapotranspiration from an alluvial aquifer of the Kouris catchment (Cyprus) using continuous streamflow records. *Hydrological Processes* **19**: 4055–4068. DOI:10.1002/hyp.5871.

Bosch DD, Arnold JG, Volk M, Allen PM. 2010. Simulation of a low-gradient coastal plain watershed using the SWAT landscape model. *Transactions of the ASABE* **53**: 1445–1456.

Boulton AJ, Findlay S, Marmonier P, Stanley EH, Valett HM. 1998. The functional significance of the hyporheic zone in streams and rivers. *Annual Review of Ecology and Systematics* **29**: 59–81. DOI:10.1146/annurev.ecolsys.29.1.59.

Brettar I, Sanchez-Perez J-M, Trémolières M. 2002. Nitrate elimination by denitrification in hardwood forest soils of the Upper Rhine floodplain – correlation with redox potential and organic matter. *Hydrobiologia* **469**: 11–21. DOI:10.1023/A:1015527611350.

Brunke M, Gonser T. 1997. The ecological significance of exchange processes between rivers and groundwater. *Freshwater Biology* **37**: 1–33. DOI:10.1046/j.1365-2427.1997.00143.x.

Butler JJ, Kluitenberg GJ, Whittemore DO, Loheide SP, Jin W, Billinger MA, Zhan X. 2007. A field investigation of phreatophyte-induced fluctuations in the water table. *Water Resources Research* **43**: W02404. DOI:10.1029/2005WR004627.

Casanova MT, Brock MA. 2000. How do depth, duration and frequency of flooding influence the establishment of wetland plant communities? *Plant Ecology* **147**: 237–250. DOI:10.1023/A:1009875226637.

Chiew F, McMahon T. 1994. Application of the daily rainfall–runoff model MODHYDROLOG to 28 Australian catchments. *Journal of Hydrology* **153**: 383–416. DOI:10.1016/0022-1694(94)90200-3.

Cooper DJ, D'amico DR, Scott ML. 2003. Physiological and morphological response patterns of *Populus deltoides* to alluvial groundwater pumping. *Environmental Management* **31**: 0215–0226. DOI:10.1007/s00267-002-2808-2.

Cox MH, Su GW, Constantz J. 2007. Heat, chloride, and specific conductance as ground water tracers near streams. *Ground Water* **45**: 187–195. DOI:10.1111/j.1745-6584.2006.00276.x.

Darcy H. 1856. *Les fontaines publiques de la ville de Dijon: exposition et application*. Valmont V (ed). Paris; 590–594.

Fohrer N, Dietrich A, Kolychalow O, Ulrich U. 2014. Assessment of the environmental fate of the herbicides flufenacet and metazachlor with the SWAT model. *Journal of Environment Quality* **43**: 75. DOI:10.2134/jeq2011.0382.

Franchini M, Wendling J, Obled C, Todini E. 1996. Physical interpretation and sensitivity analysis of the TOPMODEL. *Journal of Hydrology* **175**: 293–338. DOI:10.1016/S0022-1694(96)80015-1.

Grannemann NG, Sharp JM Jr. 1979. Alluvial hydrogeology of the lower Missouri River valley. *Journal of Hydrology* **40**: 85–99. DOI:10.1016/0022-1694(79)90089-1.

Gribovszki Z, Kalicz P, Szilágyi J, Kucsara M. 2008. Riparian zone evapotranspiration estimation from diurnal groundwater level fluctuations. *Journal of Hydrology* **349**: 6–17. DOI:10.1016/j.jhydrol.2007.10.049.

Hancock PJ, Boulton AJ, Humphreys WF. 2005. Aquifers and hyporheic zones: towards an ecological understanding of groundwater. *Hydrogeology Journal* **13**: 98–111. DOI:10.1007/s10040-004-0421-6.

Harvey JW, Bencala KE. 1993. The effect of streambed topography on surface–subsurface water exchange in mountain catchments. *Water Resources Research* **29**: 89–98. DOI:10.1029/92WR01960.

Harvey RW, George LH, Smith RL, LeBlanc DR. 1989. Transport of microspheres and indigenous bacteria through a sandy aquifer: results of natural- and forced-gradient tracer experiments. *Environmental Science & Technology* **23**: 51–56. DOI:10.1021/es00178a005.

Helton AM, Poole GC, Payn RA, Izurieta C, Stanford JA. 2014. Relative influences of the river channel, floodplain surface, and alluvial aquifer on simulated hydrologic residence time in a montane river floodplain. *Geomorphology* **205**: 17–26. DOI:10.1016/j.geomorph.2012.01.004.

Hughes FMR. 1990. The influence of flooding regimes on forest distribution and composition in the Tana River Floodplain, Kenya. *The Journal of Applied Ecology* **27**: 475. DOI:10.2307/2404295.

Hunt B. 1999. Unsteady stream depletion from ground water pumping. *Ground Water* **37**: 98–102. DOI:10.1111/j.1745-6584.1999.tb00962.x.

Hussein M, Schwartz FW. 2003. Modeling of flow and contaminant transport in coupled stream–aquifer systems. *Journal of Contaminant Hydrology* **65**: 41–64. DOI:10.1016/S0169-7722(02)00229-2.

Iribar A, Sánchez-Pérez JM, Lyautey E, Garabétian F. 2008. Differentiated free-living and sediment-attached bacterial community structure inside and outside denitrification hotspots in the river–groundwater interface. *Hydrobiologia* **598**: 109–121. DOI:10.1007/s10750-007-9143-9.

Jayakrishnan R, Srinivasan R, Santhi C, Arnold JG. 2005. Advances in the application of the SWAT model for water resources management. *Hydrological Processes* **19**: 749–762. DOI:10.1002/hyp.5624.

Jégo G, Martínez M, Antigüedad I, Launay M, Sanchez-Pérez JM, Justes E. 2008. Evaluation of the impact of various agricultural practices on nitrate leaching under the root zone of potato and sugar beet using the STICS soil-crop model. *The Science of the Total Environment* **394**: 207–221. DOI:10.1016/j.scitotenv.2008.01.021.

Jégo G, Sánchez-Pérez JM, Justes E. 2012. Predicting soil water and mineral nitrogen contents with the STICS model for estimating nitrate leaching under agricultural fields. *Agricultural Water Management* **107**: 54–65. DOI:10.1016/j.agwat.2012.01.007.

Kim NW, Chung IM, Won YS, Arnold JG. 2008. Development and application of the integrated SWAT–MODFLOW model. *Journal of Hydrology* **356**: 1–16. DOI:10.1016/j.jhydrol.2008.02.024.

Kollet SJ, Maxwell RM. 2006. Integrated surface–groundwater flow modeling: a free-surface overland flow boundary condition in a parallel groundwater flow model. *Advances in Water Resources* **29**: 945–958. DOI:10.1016/j.advwatres.2005.08.006.

Krause S, Bronstert A. 2007. The impact of groundwater–surface water interactions on the water balance of a mesoscale lowland river catchment in northeastern Germany. *Hydrological Processes* **21**: 169–184. DOI:10.1002/hyp.6182.

Krause S, Tecklenburg C, Munz M, Naden E. 2013. Streambed nitrogen cycling beyond the hyporheic zone: flow controls on horizontal patterns and depth distribution of nitrate and dissolved oxygen in the upwelling groundwater of a lowland river. *Journal of Geophysical Research, Biogeosciences* **118**: 54–67. DOI:10.1029/2012JG002122.

Krysanova V, Müller-Wohlfeil D-I, Becker A. 1998. Development and test of a spatially distributed hydrological/water quality model for mesoscale watersheds. *Ecological Modelling* **106**: 261–289. DOI:10.1016/S0304-3800(97)00204-4.

Lancaster RR. 2005. Fluvial Evolution of the Garonne River, France: integrating field data with numerical simulations. Available at: http://etd.lsu.edu/docs/available/etd-11172005-131031/ [Accessed 30 June 2014]

Langergraber G, Šimůnek J. 2005. Modeling variably saturated water flow and multicomponent reactive transport in constructed wetlands. *Vadose Zone Journal* **4**: 924. DOI:10.2136/vzj2004.0166.

Lautz LK, Siegel DI. 2006. Modeling surface and ground water mixing in the hyporheic zone using MODFLOW and MT3D. *Advances in Water Resources* **29**: 1618–1633. DOI:10.1016/j.advwatres.2005.12.003.

Liu A, Ming J, Ankumah RO. 2005. Nitrate contamination in private wells in rural Alabama, United States. *Science of the Total Environment* **346**: 112–120. DOI:10.1016/j.scitotenv.2004.11.019.

Loague K, VanderKwaak JE. 2004. Physics-based hydrologic response simulation: platinum bridge, 1958 Edsel, or useful tool. *Hydrological Processes* **18**: 2949–2956. DOI:10.1002/hyp.5737.

Malard F, Tockner K, Dole-Olivier M-J, Ward JV. 2002. A landscape perspective of surface–subsurface hydrological exchanges in river corridors. *Freshwater Biology* **47**: 621–640. DOI:10.1046/j.1365-2427.2002.00906.x.

Marmonier P, Archambaud G, Belaidi N, Bougon N, Breil P, Chauvet E, Claret C, Cornut J, Datry T, Dole-Olivier M-J, Dumont B, Flipo N, Foulquiera A, Gérino M, Guilpart A, Julien F, Maazouzi C, Martin D, Mermillod-Blondin F, Montuelle B, Namour P, Navel S, Ombredane D, Pelte T, Piscart C, Pusch M, Stroffek S, Robertson A, Sanchez-Pérez J-M, Sauvage S, Taleb A, Wantzen M, Vervier P. 2012. The role of organisms in hyporheic processes: gaps in current knowledge, needs for future research and applications. *Annales de Limnologie - International Journal of Limnology* **48**: 253–266. DOI:10.1051/limn/2012009.

Morrice JA, Valett HM, Dahm CN, Campana ME. 1997. Alluvial characteristics, groundwater–surface water exchange and hydrological retention in headwater streams. *Hydrological Processes* **11**: 253–267. DOI:10.1002/(SICI)1099-1085(19970315)11:3<253::AID-HYP439>3.0.CO;2-J.

Naiman RJ, Decamps H. 1997. The ecology of interfaces: riparian zones. *Annual Review of Ecology and Systematics* **28**: 621–658.

Neitsch SL, Arnold JG, Kiniry JR, Williams JR. 2009. Soil and water assessment tool, Theoretical Documentation, Version 2009

Orghidan T. 1959. Ein neuer lebensraum des unterirdischen Wassers: Der hvporheische Biotop. *Archiv für Hydrobiologie* **55**: 392–414.

Park SS, Lee YS. 2002. A water quality modeling study of the Nakdong River, Korea. *Ecological Modelling* **152**: 65–75. DOI:10.1016/S0304-3800(01)00489-6.

Peyrard D. 2008. Un modèle hydrobiogéochimique pour décrire les échanges entre l'eau de surface et la zone hyporhéique de grandes plaines alluviales.phd, Université de Toulouse, Université Toulouse III – Paul Sabatier. Available at: http://thesesups.ups-tlse.fr/549/ [Accessed 28 February 2014]

Peyrard D, Sauvage S, Vervier P, Sanchez-Perez JM, Quintard M. 2008. A coupled vertically integrated model to describe lateral exchanges between surface and subsurface in large alluvial floodplains with a fully penetrating river. *Hydrological Processes* **22**: 4257–4273. DOI:10.1002/hyp.7035.

Rassam DW, Werner A. 2008. Review of groundwater–surfacewater interaction modelling approaches and their suitability for Australian conditions. eWater Cooperative Research Centre. Available at: http://www.ewater.com.au/uploads/files/Rassam_Werner-2008-Groundwater_Review.pdf [Accessed 16 March 2015]

Rathjens H, Oppelt N, Bosch DD, Arnold JG, Volk M. 2015. Development of a grid-based version of the SWAT landscape model. *Hydrological Processes* **29**(6): 900–914. DOI:10.1002/hyp.10197.

Romanowicz AA, Vanclooster M, Rounsevell M, La Junesse I. 2005. Sensitivity of the SWAT model to the soil and land use data parametrisation: a case study in the Thyle catchment, Belgium. *Ecological Modelling* **187**: 27–39. DOI:10.1016/j.ecolmodel.2005.01.025.

Sabater S, Butturini A, Clement J-C, Burt T, Dowrick D, Hefting M, Matre V, Pinay G, Postolache C, Rzepecki M, Sabater F. 2003. Nitrogen removal by riparian buffers along a European climatic gradient: patterns and factors of variation. *Ecosystems* **6**: 0020–0030. DOI:10.1007/s10021-002-0183-8.

Sánchez-Pérez JM, Trémolières M. 2003. Change in groundwater chemistry as a consequence of suppression of floods: the case of the Rhine floodplain. *Journal of Hydrology* **270**: 89–104. DOI:10.1016/S0022-1694(02)00293-7.

Sánchez-Pérez JM, Antiguedad I, Arrate I, García-Linares C, Morell I. 2003a. The influence of nitrate leaching through unsaturated soil on groundwater pollution in an agricultural area of the Basque country: a case study. *Science of the Total Environment* **317**: 173–187. DOI:10.1016/S0048-9697(03)00262-6.

Sánchez-Pérez JM, Bouey C, Sauvage S, Teissier S, Antiguedad I, Vervier P. 2003b. A standardised method for measuring *in situ* denitrification in shallow aquifers: numerical validation and measurements in riparian wetlands. *Hydrology and Earth System Sciences* **7**: 87–96. DOI:10.5194/hess-7-87-2003.

Sanchez-Perez JM, Tremolieres M, Carbiener R. 1991a. Une station d'épuration naturelle des phosphates et nitrates apportés par les eaux de débordement du Rhin: la forêt alluviale à frêne et orme. *Comptes rendus de l'Académie des sciences. Série 3, Sciences de la vie* **312**: 395–402.

Sanchez-Perez JM, Tremolieres M, Schnitzler A, Carbiener R. 1991b. Evolution de la qualité physico-chimique des eaux de la frange superficielle de la nappe phréatique en fonction du cycle saisonnier et des stades de succession des forêts alluviales rhénanes (Querco-Ulmetum minoris Issl. 24). *Acta oecologica: (1990)* **12**: 581–601.

Sánchez-Pérez JM, Vervier P, Garabétian F, Sauvage S, Loubet M, Rols JL, Bariac T, Weng P. 2003c. Nitrogen dynamics in the shallow groundwater of a riparian wetland zone of the Garonne, SW France: nitrate inputs, bacterial densities, organic matter supply and denitrification measurements. *Hydrology and Earth System Sciences Discussions* **7**: 97–107.

Seltz R. 2001. Analyse et modélisation d'une zone humide riveraine de la Garonne. l'Ecole de Physique du Globe de Strasbourg 1,81pp.

Sophocleous M. 2002. Interactions between groundwater and surface water: the state of the science. *Hydrogeology Journal* **10**: 52–67. DOI:10.1007/s10040-001-0170-8.

Sophocleous M, Perkins SP. 2000. Methodology and application of combined watershed and ground-water models in Kansas. *Journal of Hydrology* **236**: 185–201. DOI:10.1016/S0022-1694(00)00293-6.

Storey RG, Howard KWF, Williams DD. 2003. Factors controlling riffle-scale hyporheic exchange flows and their seasonal changes in a gaining stream: a three-dimensional groundwater flow model. *Water Resources Research* **39**: 1034. DOI:10.1029/2002WR001367.

Takatert N, Sanchez-Pérez JM, Trémolières M. 1999. Spatial and temporal variations of nutrient concentration in the groundwater of a floodplain: effect of hydrology, vegetation and substrate. *Hydrological Processes* **13**: 1511–1526. DOI:10.1002/(SICI)1099-1085(199907)13:10<1511::AID-HYP828>3.0.CO;2-F.

Vervier P, Bonvallet-Garay S, Sauvage S, Valett HM, Sanchez-Perez J-M. 2009. Influence of the hyporheic zone on the phosphorus dynamics of a large gravel-bed river, Garonne River, France. *Hydrological Processes* **23**: 1801–1812. DOI:10.1002/hyp.7319.

Volk M, Arnold JG, Bosch DD, Allen PM, Green CH. 2007. Watershed configuration and simulation of landscape processes with the SWAT model. In MODSIM 2007 International Congress on Modelling and Simulation. Modelling and Simulation Society of Australia and New Zealand, Canberra, Australia 74–80. Available at: http://www.mssanz.org.au.previewdns.com/MODSIM07/papers/43_s47/Watersheds47_Volk_.pdf [Accessed 1 September 2014]

Weng P, Sánchez-Pérez JM, Sauvage S, Vervier P, Giraud F. 2003. Assessment of the quantitative and qualitative buffer function of an alluvial wetland: hydrological modelling of a large floodplain (Garonne River, France). *Hydrological Processes* **17**: 2375–2392. DOI:10.1002/hyp.1248.

White DS. 1993. Perspectives on defining and delineating hyporheic zones. *Journal of the North American Benthological Society* **12**: 61–69. DOI:10.2307/1467686.

Woessner WW. 2000. Stream and fluvial plain ground water interactions: rescaling hydrogeologic thought. *Ground Water* **38**: 423–429. DOI:10.1111/j.1745-6584.2000.tb00228.x.

Wondzell SM. 2011. The role of the hyporheic zone across stream networks. *Hydrological Processes* **25**: 3525–3532. DOI:10.1002/hyp.8119.

Wroblicky GJ, Campana ME, Valett HM, Dahm CN. 1998. Seasonal variation in surface–subsurface water exchange and lateral hyporheic area of two stream–aquifer systems. *Water Resources Research* **34**: 317–328. DOI:10.1029/97WR03285.

Zhang Q, Li L. 2009. Development and application of an integrated surface runoff and groundwater flow model for a catchment of Lake Taihu watershed, China. *Quaternary International* **208**: 102–108. DOI:10.1016/j.quaint.2008.10.015.

Résumé :

Les eaux souterraines des plaines alluviales agricoles sont particulièrement vulnérables à la contamination en nitrates en raison d'une fertilisation importante, et de la faible profondeur des aquifères. Au sein de ces plaines alluviales, les zones ripariennes, caractérisées par des échanges importants entre les eaux de surface et les eaux souterraines, constituent des environnements propices à l'atténuation des nitrates via le processus de dénitrification. Ce processus naturel dépend de nombreux facteurs et est caractérisé par une forte variabilité spatio-temporelle. La modélisation est une approche intéressante pour étudier la dénitrification au sein des zones ripariennes car elle permet d'intégrer les différents facteurs contrôlant le processus de manière dynamique.

L'objectif de cette thèse est d'améliorer la caractérisation et la quantification du processus de dénitrification et d'identifier ses facteurs de contrôle dans les plaines alluviales à travers une approche de modélisation à l'échelle du tronçon de plaine alluviale. L'analyse d'un jeu de données collectées dans un réseau de 25 piézomètres installés dans un méandre de la Garonne (Monbéqui, 6,6 km²) lors de 12 campagnes mensuelles a permis, dans un premier temps, d'identifier les facteurs contrôlant la dynamique des nitrates et le processus de dénitrification. Les données ont ensuite servi à la mise en place et à la validation de l'application du modèle distribué MOHID Land pour simuler l'hydrologie de la zone d'étude. Puis, un module permettant de simuler la dénitrification et prenant en compte les facteurs identifiés au préalable, a été introduit dans le modèle.

L'analyse des données récoltées sur le terrain a montré que la dénitrification dans la zone d'étude est contrôlée par la géomorphologie, l'hydrologie et la présence de carbone organique. L'application du modèle hydrologique distribué MOHID Land a permis de simuler correctement l'hydrologie du site étudié en prenant en compte la géomorphologie de la plaine alluviale, les échanges eaux de surface - eaux souterraines et les épisodes de crues. Un module de dénitrification incluant à la fois le carbone organique dissous apporté par la rivière et le carbone organique particulaire présent dans l'horizon supérieur des sols a été implémenté dans le modèle hydrologique. Les résultats indiquent une dénitrification moyenne de 28 kg-N.ha^{-1}.an^{-1} sur la période simulée dans la zone riparienne de Monbéqui. La dénitrification est plus importante dans les zones ripariennes de basses altitudes et plus globalement dans la partie aval du méandre, caractérisée par de fortes concentrations en nitrates. Les facteurs contrôlant la dénitrification au sein des plaines alluviales ont été identifiés et sont i) la géomorphologie qui détermine la saturation des horizons supérieurs des sols et la disponibilité du carbone organique ; ii) les écoulements souterrains qui contrôlent la répartition spatiale des nitrates, et iii) l'intensité et la fréquence des épisodes de crues qui entrainent des périodes favorables à la dénitrification. Finalement, les résultats obtenus dans la zone d'étude ont été comparés avec des applications du modèle dans des plaines alluviales possédant des caractéristiques contrastées, validant ainsi l'utilisation du modèle dans les environnements de plaine alluviale variés. Les résultats ont mis en avant l'importance de la connectivité hydrologique entre la rivière et la nappe alluviale ainsi que la distribution spatiale des sources de nitrates et de carbone organique comme facteurs expliquant les différences de capacité de dénitrification entre les sites. Ces travaux ouvrent des perspectives pour évaluer l'impact des modifications induites par le changement global sur le processus de dénitrification ainsi que sur leur modélisation à plus large échelle.

Abstract :

Groundwater systems in cultivated floodplains are vulnerable to nitrate contamination due to extensive fertilisation and the shallow depth of the groundwater. Within the floodplain environment, riparian areas, characterised by significant exchanges between surface water and groundwater, are a favourable site for nitrate removal through denitrification. Denitrification is a natural process influenced by numerous factors and characterised by a high spatio-temporal variability. Modelling is an interesting approach for the study of denitrification within riparian areas because it means that floodplain spatial heterogeneity can be taken into account and many of its control factors integrated.

The main objective of this thesis was to enhance knowledge of the denitrification process in floodplains and to identify its control factors using a modelling approach at the scale of the floodplain reach. First, a dataset collected at a monthly time step over the course of a year within a 25-piezometer network of a meander area (Monbéqui, 6.6 km²) was analysed in order to identify factors controlling nitrate and denitrification patterns. The data were then used to set up and validate the MOHID Land model to simulate the hydrology in the study area. A module designed to simulate the denitrification process, taking the main denitrification control factors into account, was then integrated into the MOHID Land model.

The analysis of the dataset collected from the study area showed that denitrification was controlled by geomorphology, hydrology and organic carbon presence. The application of the MOHID Land model allowed the hydrology of the study area to be reproduced correctly, particularly the surface water – groundwater exchanges and the influence of flood events. A denitrification module integrating dissolved organic carbon borne by the river and particulate organic carbon from soil was added to the model. The results indicated that denitrification in the modelled riparian area was an average of around 28 kg-N.ha-1.yr-1 over the simulated period. High denitrification areas were located within the low elevation riparian area and, more generally, in the downstream area of the meander where the nitrate concentrations were highest. The factors controlling denitrification that were identified in the study area were i) geomorphology, which controlled topsoil layer saturation and organic carbon availability; ii) groundwater flowpaths, which controlled the variability in nitrate concentrations over the study area; and iii) flood event frequency and intensity, leading to high denitrification periods. Finally, the results were compared with other applications of the model in contrasting floodplains in order to assess the model's performance in various floodplain environment. The results indicated that hydrologic connectivity between the river and groundwater and the spatial location of sources of nitrates and organic carbon were the major factors behind differences in the denitrification process between floodplains. This study provides insight for an assessment of the impact of modifications that could be brought about by global changes to the denitrification process and for the modelling of denitrification at larger scales.